Lecture Notes in Civil Engineering

P. V. Timbadiya
Vijay P. Singh
Priyank J. Sharma *Editors*

Climate Change Impact on Water Resources

Proceedings of 26th International Conference on Hydraulics, Water Resources and Coastal Engineering (HYDRO 2021)

Springer

Lecture Notes in Civil Engineering

Volume 313

Lecture Notes in Civil Engineering (LNCE) publishes the latest developments in Civil Engineering—quickly, informally and in top quality. Though original research reported in proceedings and post-proceedings represents the core of LNCE, edited volumes of exceptionally high quality and interest may also be considered for publication. Volumes published in LNCE embrace all aspects and subfields of, as well as new challenges in, Civil Engineering. Topics in the series include:

- Construction and Structural Mechanics
- Building Materials
- Concrete, Steel and Timber Structures
- Geotechnical Engineering
- Earthquake Engineering
- Coastal Engineering
- Ocean and Offshore Engineering; Ships and Floating Structures
- Hydraulics, Hydrology and Water Resources Engineering
- Environmental Engineering and Sustainability
- Structural Health and Monitoring
- Surveying and Geographical Information Systems
- Indoor Environments
- Transportation and Traffic
- Risk Analysis
- Safety and Security

To submit a proposal or request further information, please contact the appropriate Springer Editor:

– Pierpaolo Riva at pierpaolo.riva@springer.com (Europe and Americas);
– Swati Meherishi at swati.meherishi@springer.com (Asia—except China, Australia, and New Zealand);
– Wayne Hu at wayne.hu@springer.com (China).

All books in the series now indexed by Scopus and EI Compendex database!

P. V. Timbadiya · Vijay P. Singh · Priyank J. Sharma
Editors

Climate Change Impact on Water Resources

Proceedings of 26th International Conference on Hydraulics, Water Resources and Coastal Engineering (HYDRO 2021)

Springer

Editors
P. V. Timbadiya
Department of Civil Engineering
Sardar Vallabhbhai National Institute of Technology
Surat, India

Priyank J. Sharma
Department of Civil Engineering
Indian Institute of Technology Indore
Indore, India

Vijay P. Singh
Department of Biological and Agricultural Engineering, Zachry Department of Civil and Environmental Engineering
Texas A&M University
College Station, TX, USA

ISSN 2366-2557 ISSN 2366-2565 (electronic)
Lecture Notes in Civil Engineering
ISBN 978-981-19-8523-2 ISBN 978-981-19-8524-9 (eBook)
https://doi.org/10.1007/978-981-19-8524-9

This Springer imprint is published by the registered company Springer Nature Singapore Pte Ltd.
The registered company address is: 152 Beach Road, #21-01/04 Gateway East, Singapore 189721, Singapore

Preface

Climate change is a big challenge to water and food security in the twenty-first century. A notable increase in greenhouse gas emissions and the global surface temperature has led to modifications in the global and regional hydrological cycles. The changes in the hydrological cycle and intensification of climate extremes have exacerbated stresses on the water systems. In recent decades, a significant rise in climate-related disasters, such as heatwaves, floods, droughts, cyclones, has been noticed. Such events are likely to amplify in a warming climate. Rising sea levels and related extremes due to climate change make coastal communities more vulnerable. The anthropogenic influences in the form of land use changes, river regulation, excessive groundwater extraction, and others have put additional stress on water availability. The Coupled Model Intercomparison Project phase 6 (CMIP6) models project a robust intensification of the Indian Summer Monsoon Rainfall (ISMR) under climate change. The ISMR is a major source of water supply for agricultural production in India, accounting for a 19.9% share of GDP. Thus, assessing the impact of climate change on water resources is vital for food and water security, affordable energy and sustainable living, and disaster mitigation and resilient communities. This book covers several aspects of climate change ranging from its detection, attribution, adaptation, and mitigation in different contexts through real-world case studies.

This book covers the broader theme of the impact of climate change on water resources while dealing with several sub-topics such as downscaling techniques, assessment of global circulation models (GCMs), trends in hydroclimatic extremes, crop water requirements, and stationarity assessment. Several applications of downscaling of climate data are presented using statistical and machine learning techniques such as artificial neural networks, deep learning, long short-term memory, kernel regression, and time-varying downscaling model for various river basins in India. The GCM datasets are adopted for analysing future projections of rainfall and temperature over the Western Ghats, the Godavari, and Tapi basins. The uncertainty due to climate change is also addressed in this study. Trend detection in several hydroclimatic variables, viz., rainfall, temperature, streamflow, and groundwater levels, has also been reported. The historical and projected trends in precipitation over Northeast India, Rajasthan, Himachal Pradesh, Brahmaputra basin, Savitri basin, and Swarna

basin have been discussed. The streamflow trends are reported for the Godavari, Mahanadi, Wainganga, and Cauvery River basins. The trends and variability in rainfall and temperature are detected in the Bardoli, Damoh, and Bharuch regions of Gujarat state in India. Lastly, the spatiotemporal changes in groundwater levels are assessed for Vishakhapatnam in Andhra Pradesh. The impact of climate change on crop water requirements is investigated for the Tapi basin, Seonath, Sehore, and Amreli districts of Gujarat state. A few studies dealing with stationarity assessment, development of fog index, hydrological resilience, extreme precipitation modelling, regionalization, and intensity–duration–frequency (IDF) curve development are also presented. In addition, two review studies focusing on climate change impact assessment and adaptation are also included in this book. This book will help the readers to gain an overview of the regional variations due to climate change impacts and their statistical modelling through various case studies and review articles.

Surat, India P. V. Timbadiya
College Station, TX, USA Vijay P. Singh
Indore, India Priyank J. Sharma

Acknowledgements

The editors are grateful for the support provided by the technical advisory committee and local organizing committee of the 26th International Conference on Hydraulics, Water Resources and Coastal Engineering (HYDRO 2021) held at Sardar Vallabhbhai National Institute of Technology (SVNIT) Surat during December 23–25, 2021. The editors thank the Indian Society for Hydraulics (ISH) Pune, India, its office bearers, and executive council members for their support in conducting the HYDRO 2021 International Conference. The editors wish to thank all the authors for their support and contribution to this book. The editors duly acknowledge the timely and sincere efforts of the reviewers in providing their valuable comments and suggestions to maintain the quality of the book. The editors would like to thank the keynote speakers, the session chairs and co-chairs, participants, and student volunteers for their contribution to the successful conduct of the conference. The editors are also thankful to the administrators of Sardar Vallabhbhai National Institute of Technology, Surat (SVNIT), India, for supporting the HYDRO 2021 International Conference. Lastly, the editors are sincerely thankful to the publishing team of Springer Nature for their support and cooperation at various steps since the beginning of the book project.

P. V. Timbadiya
Vijay P. Singh
Priyank J. Sharma

Contents

About the Editors

P. V. Timbadiya is an Associate Professor in the Water Resources Engineering section, Department of Civil Engineering, Sardar Vallabhbhai National Institute of Technology (SVNIT), India. He secured his doctoral degree and post-graduation in Water Resources Engineering from SVNIT Surat in 2012 and 2004, respectively. He did his under graduation in civil engineering from SVNIT. He has guided three doctoral thesis and 29 master's dissertations. He has more than 110 research papers to his credit, including 30 articles in peer-reviewed journals. He served as Dean (Alumni and Resources Generation), and currently serving as Sectional Head, Water Resources Engineering Section at SVNIT. He played an instrumental role in setting up infrastructure facilities in the Centre of Excellence on 'Water Resources and Flood Management' such as the Experimental Hydraulics Lab, Computational Hydraulics Lab, Water Circulation System, and others. He is appointed as 'National Consultant' for Kalpsar Project by Narmada, Water Resources, Water Supply and Kalpsar Department of the Government of Gujarat. He is a recipient of 'Young Engineers Award' by the Institution of Engineers (India) in 2015. He received 'Prof. R. J. Garde Research Award' in 2020 by the Indian Society for Hydraulics. He has awarded DST-SERB Core Research Grant for the project on 'Local Scouring around tandem and staggered bridge piers on Non-uniform mobile bed' in 2021. He is active in various professional bodies and organized numerous conferences, workshops, and short-term training programmes in his academic career.

Vijay P. Singh is a University Distinguished Professor, a Regents Professor, and Caroline and William N. Lehrer Distinguished Chair in Water Engineering at Texas A&M University. He received his B.S., M.S., Ph.D., and D.Sc. in engineering. He is a registered professional engineer, a registered professional hydrologist, and an Honorary Diplomate of ASCE-AAWRE. He is a Distinguished Member of ASCE, a Distinguished Fellow of AGGS, an Honorary Member of AWRA, and a Fellow of EWRI-ASCE, IAH, ISAE, IWRS, and IASWC. He has published extensively in the areas of hydrology, irrigation engineering, hydraulics, groundwater, water quality, and water resources (more than 1320 journal articles, 31 textbooks, 75 edited reference books, 110 book chapters, and 315 conference papers). He has received

over 95 national and international awards, including three honorary doctorates. He is a member of 11 international science/engineering academies. He has served as President of the American Institute of Hydrology (AIH), Chair of the Watershed Council of the American Society of Civil Engineers and is currently President of the American Academy of Water Resources Engineers. He has served/serves as Editor-in-Chief of three journals and two book series and serves on editorial boards of more than 25 journals and three book series. His Google Scholar citations include 64073, h-index: 115, and I10-index: 903.

Priyank J. Sharma is an Assistant Professor in the Department of Civil Engineering at the Indian Institute of Technology (IIT) Indore, India. He previously worked as an Assistant Professor at the Punjab Engineering College, India. He worked as a post-doctoral scholar in Hydrosystems Research Laboratory at Florida Atlantic University, USA. He completed his Ph.D. in Civil Engineering with a specialization in Water Resources Engineering from Sardar Vallabhbhai National Institute of Technology (SVNIT), India in 2020. He is a recipient of the 'INSPIRE Fellowship' by the Department of Science and Technology, Government of India and 'Institute Gold Medal' at SVNIT Surat. He also worked as an Assistant Manager at Essar Projects (India) Limited from 2010-2012. He has received several awards and accolades for his academic and research performance, the prominent being 'Prof. U. C. Kothyari Best Ph.D. Thesis Award 2020' from the Indian Society for Hydraulics. He has authored forty-seven research publications, including fifteen articles in peer-reviewed high-impact factor journals and five book chapters. His research interests are hydro-climatology and climate extremes, climate change impact assessment, streamflow prediction, and reservoir operation.

Temporal Networks: A New Approach to Model Non-stationary Hydroclimatic Processes with a Demonstration for Soil Moisture Prediction

Riya Dutta and Rajib Maity

Abstract Interactions between different components of the hydrologic cycle show a time-varying characteristic due to the impact of climate change that lead to the non-stationarity in many hydroclimatic variables. In fact, a lack of stationarity in most of the hydroclimatic processes is realized in many cases. In such situation, alternative methodologies that can effectively learn (adapt) from the changing climate will help in development of effective and efficient hydroclimatic models. This study presents the potential of a recently developed approach, namely *temporal networks.* These time-varying network structures help in hydroclimatic modelling by (i) identifying the complex association (dependence structure) among the large pool of influencing variables and (ii) identifying the temporal variability of the dependence structure to capture the time-varying characteristics in the association among the hydroclimatic variables. The approach helps to improve the accuracy of the model performance under a changing climate. As a demonstration, we picked out the slowly changing soil moisture regime at a location and attempted to capture its time-varying characteristics through *temporal networks* based time-varying modelling framework. Our target is to predict the monthly soil moisture with one-month to one-season (three months) in advance. The performance of the *temporal networks* based model is contrasted with the time-invariant modelling philosophy. Towards this, (i) time-invariant network model, as the closest counterpart, and (ii) Support Vector Regression (SVR) based models, Machine Learning (ML) technique commonly implemented in the field of hydroclimatology, are used. We established that the *temporal networks* satisfactorily capture the soil moisture variability over time.

R. Dutta · R. Maity (✉)
Department of Civil Engineering, Indian Institute of Technology Kharagpur, Kharagpur, West Bengal 721302, India
e-mail: rajib@civil.iitkgp.ac.in

P. V. Timbadiya et al. (eds.), *Climate Change Impact on Water Resources*, Lecture Notes in Civil Engineering 313, https://doi.org/10.1007/978-981-19-8524-9_1

Keywords Temporal networks · Time-varying characteristics · Non-stationary processes · Soil moisture

1 Introduction

The spatio-temporal variation of hydrologic variables under climatic change is typically governed by multiple hydroclimatic processes. For any system, temporal change does not necessarily imply non-stationarity of the system and, on the other hand, stationarity does not always imply an unchanging process [28]. In hydroclimatic studies, the stationarity assumption has been compromised in many cases because substantial change has been noticed to alter the mean as well as extreme events of many hydrologic variables, like temperature, precipitation, evapotranspiration, soil moisture, and river discharge [2, 26, 33]. Milly et al. [26] stated that the "stationarity is dead". While the need to deal with such issues related to underlying changes is not new to the hydrologic community, many approaches inherently assumes stationarity in the underlying processes [26, 31]. However, such assumptions may not hold good in many cases under a changing climate since the dependence structure among the associated hydroclimatic variables within the system is no longer time-invariant [33]. In such non-stationary environments, a model trained under the false stationarity assumption may fail over time or give subpar performance [9].

Learning in non-stationary environments can be divided into two sub-categories, namely active and passive approach [9, 36], where the active approach identifies the change in dependence structure [4, 6, 11, 12, 17, 18, 25, 27]. The time-variability of such *dependence structures*, leading to a time-varying prediction model, is a major concern in the field of hydroclimatology. Many systems, including the hydroclimatic systems, composed of multiple interacting elements can be represented as *conditional independence structures*. Different methods like Graphical Modelling (GM), Bayesian Networks (BNs), and Vine Copula can be effectively used to identify such network structures among the associated variables [20]. In general, considering the hydroclimatic system, multiple variables are associated with each other in complex ways, and GM helps to identify such associations [20, 22].

Another, important aspect is that most of the existing modelling frameworks focus on static networks, that is network structures with connections/edges that are permanent in nature. However, considering a non-stationary environment, the association between two variables, and thereby, the dependence structure may also change over time. Here comes the concept of temporal networks, also known as time-varying networks, that are characterized by temporal links between variables that may change over time [3, 12, 13, 23].

The objective of this study is to present the potential of a recently developed temporal network-based approach for modelling time-varying hydroclimatic system. A detailed network structure among all the variables is identified in order to obtain the directly associated/influencing input variables and a parsimonious prediction model is developed using these inputs. The network structure and the parameters of the

model may reflect a slow change over time, and thus, are updated after a fixed time interval to capture the time variability in the association among the variables. As an illustrative application, the proposed model is applied for modelling the time-varying association between soil moisture and other influencing hydrologic variables in order to develop a predictive model for soil moisture at monthly scale.

2 Methodological Approach in Temporal Networks

The overall framework for development of the proposed model is given in Fig. 1. Firstly, a network structure (compete conditional independence structure) is identified using the GM-based approach that provides the association between the input variables and the target variable. The primary goal of GM is to describe the complex relationship and to explain the dependence structure by conditioning and controlling other factors. It is a probabilistic model that facilitates the identification of conditional independence relations among the variables. Only the direct interactions, as identified from the network structure, are of interest to develop the conditional probabilistic model for the target variable. Conditioning is the key theoretical concept that forms the foundation for GM and leads to an explicit set of rules for interpreting the conditional independence structure. GM approach uses the concept of graphs that can be defined as mathematical objects consisting of nodes/vertices (V) and edges (E). The nodes represent the variables used in the analysis, and the edges represent the association between a pair of nodes. The edges can be shown as lines or directed arrows. Based on the type of edges, the graph structures are either directed, undirected, or bi-directed. Presence of an edge between two nodes shows that the variables are directly associated, and absence of an edge shows that the variables are either independent or conditionally dependent [34].

Secondly, the time-varying association between the input and target variables is identified using a series of such network structures [11, 23]. The input variables and model parameters are updated after a fixed time-interval, i.e., the model is re-calibrated to capture the time-varying characteristics. A detailed description on the development of the model including the mathematical formulations is presented in Dutta and Maity [12] and Dutta et al. [14].

3 Application of the Temporal Network-Based Approach

The potential of the TNTV model is demonstrated for modelling the slowly changing monthly soil moisture regime at a location to capture its time-varying characteristics. It is well established that large number of input variables influence the variation in soil moisture to different extent. The role of these influencing variables varies with both space and time. In the recent decades, many regions have experienced

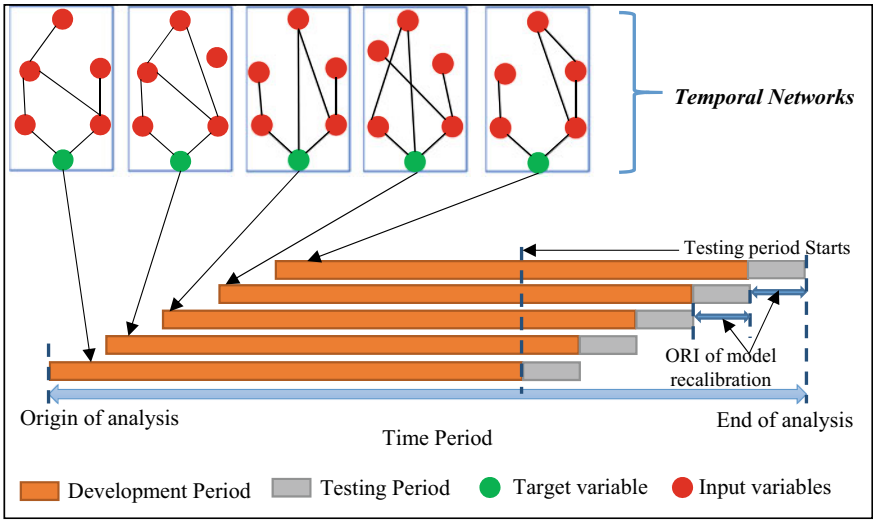

Fig. 1 Methodological outline for the development of the Temporal Network based Time-Varying (TNTV) model, adapted from Dutta and Maity [12]

significant wetting or drying trends, triggering serious socio-economic and environmental problems [5, 10, 16]. One of the important aspects for strategic management of water resources including possible change in future agricultural practices is development of reliable models for prediction of soil moisture month(s) or season ahead. Plethora of models have been explored over the years for simulation/prediction of soil moisture at different spatio-temporal scale [7, 24, 29, 32, 35], and these models have their own merits and demerits. Most of the modelling frameworks establish the association between soil moisture and different influencing variables, such as rainfall, temperature, and evaporation, initial moisture content, to name a few, and develop the simulation/prediction model based on the identified association among the variables [1, 8, 15, 19, 21, 30]. However, not considering the time variability in the association among the variables is a major drawback. This study utilizes the TNTV model to study the temporal change in the association of soil moisture and the large pool of influencing variables. These temporal networks are utilized for soil moisture prediction at a location with a lead time one to three months.

3.1 Study Area and Data Source

The observed soil moisture datasets for six different depths and multiple stations located across entire Indian mainland are procured from India Meteorological Department (IMD). The observed data is available once every week (every Wednesday) for the time period of 1991–2016, however, the data length varies from one station

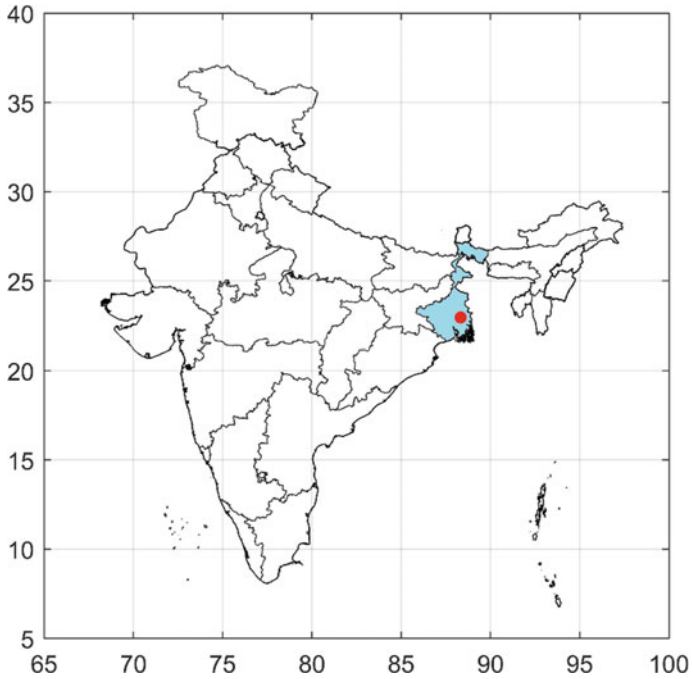

Fig. 2 Location of the soil moisture monitoring station at Kalyani

to another. For the demonstration of the model efficacy, one such station, namely Kalyani (lying within the state of West Bengal) with a sufficiently long data length from September 1993 to December 2015 (including a few missing data) is selected for this study (Fig. 2). The geographical location of this station is 22°05' N (latitude) and 88°20' E (longitude). The station data is converted into monthly series by taking the average of all the weekly values for that particular month and used for validating the developed model.

For development of the TNTV based model, current month's volumetric soil moisture (0–7 cm) is used as the target variable and lagged information of different hydro-meteorological variables, namely Soil moisture layer 1 (*s1*), Skin reservoir content (*wr*), Total precipitation (*tp*), Evaporation (*et*), Potential evaporation (*pe*), Skin temperature (*sk*), Soil temperature layer 1 (*t1*), Soil temperature layer 2 (*t2*), Temperature (*te*), Dewpoint temperature (*td*), Surface pressure (*sp*), Zonal wind (*uw*), Meridional wind (*vw*), Leaf area index high (*lh*), and Leaf area index low (*ll*), are used as input variables. These data are obtained from ERA5-Land. Further details on the target and input variables used for the analysis is provided in [14]. The gridded data from ERA5-Land is available at a spatial resolution of $0.1° \times 0.1°$. In order to obtain the values of each variable at the station, Inverse Distance Weighting (IDW) method is utilized. Based on the availability of the reanalysis data the model is developed

and tested for the period of 1981 to 2020 and validated over the period of 1993 to 2015 based on the availability of the observed station data.

3.2 Model Performance and Discussion

Figure 3 shows the time-varying association between the hydroclimatic variables and the target variable considering the lead time of one-month for the two model development periods (1981–2010 and 1986–2015). The results clearly indicate a gradual change in the association between the surface soil moisture and the other influencing variables.

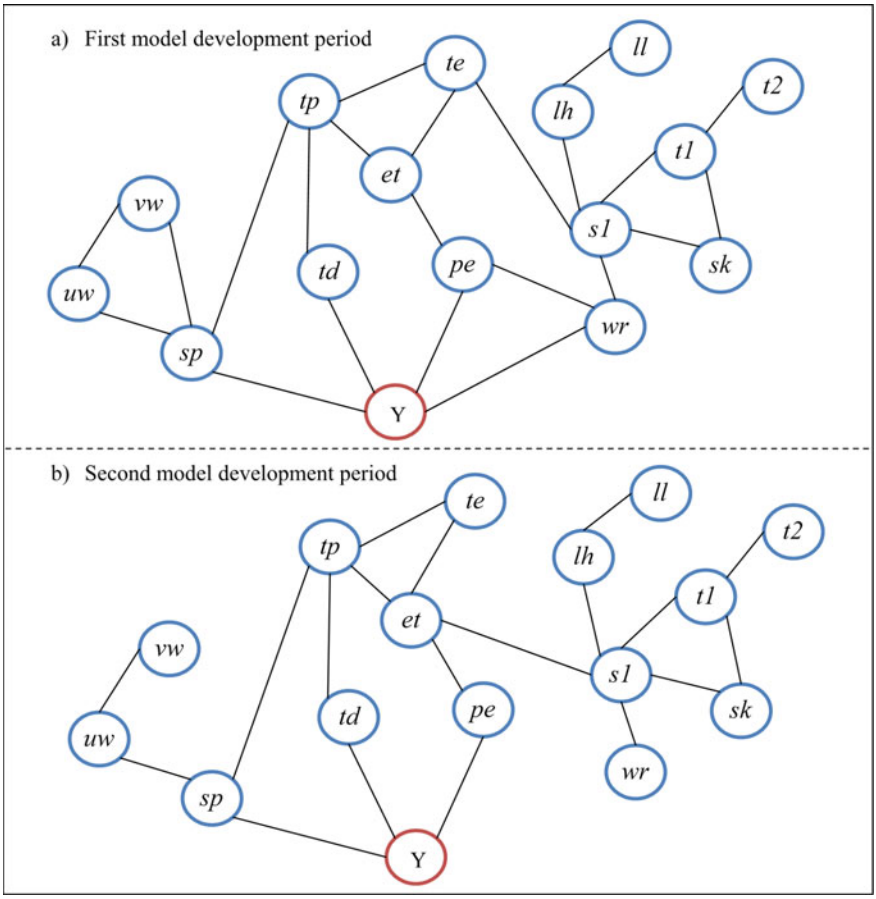

Fig. 3 Time-varying association between the input variables (15 variables with one-month lag) and the target variable designated as *Y*. The details on the input variables are provided in Table 1

Considering the first model development period (1981–2010), surface soil moisture shows direct association with previous month's skin water content (*wr*), potential evaporation (*pe*), dew point temperature (*td*), and surface pressure (*sp*). For the second model development period (1986–2015), the direct association between surface soil moisture and previous month's skin water content becomes insignificant given other input variables. It is interesting to note that the strength of association between surface pressure and surface soil moisture increases over time. The overall network structure remains almost the same compared to the first and second model development period, however certain edges appear/disappear over the time.

Next, the directly associated input variables are used to develop the prediction model. The different performance statistics obtained using the TNTV model, for the lead time of one-month, are as follows: $R = 0.885$, $R^2 = 0.788$, RMSE = 4.056, NSE = 0.759, and Dr = 0.787 (Table 1). Given the complexity associated with surface soil moisture and the large pool of influencing variables, the model successfully predicts the surface soil moisture one-month in advance. It may be further noted that the model performance deteriorates considering a time-invariant network-based model. That is the model developed for the first model development period (1981–2010) is used for prediction considering the entire testing period (2011–2020). The performance statistics obtained using the time-varying SVR-based model, for the lead time of one-month, are as follows: $R = 0.751$, $R^2 = 0.554$, RMSE = 4.421, NSE = 0.684 and Dr = 0.697. Similar results are observed for one-season ahead prediction of soil moisture. Overall, the ability of the TNTV model to capture the detailed dependence structure among a large pool of influencing variables and capture the time variability in the association among the variables helps to provide improved prediction performance for complex secondary hydrologic variables like soil moisture.

Lastly, the model validation is carried out by comparing the reanalysis product with the station data obtained from IMD. The overlap period between the two data sets considering the entire time period of the study is from September 1993 to December 2015. Figure 4 compares the observed soil moisture data as obtained from IMD with the reanalysis product and the modelled soil moisture data (lead time of one-month)

Table 1 Performance of the prediction models for the lead times of one-month and one-season

Lead time	Model	Performance statistics				
		R	R^2	RMSE	NSE	Dr
1-month	Temporal network	0.885	0.788	4.056	0.759	0.787
	Time-invariant network	0.674	0.472	5.146	0.533	0.556
	Time-varying SVR	0.751	0.554	4.421	0.684	0.697
	Time-invariant SVR	0.610	0.382	5.923	0.491	0.514
1-season	Temporal network	0.812	0.665	4.824	0.671	0.710
	Time-invariant network	0.598	0.384	6.186	0.537	0.618
	Time-varying SVR	0.704	0.462	5.391	0.590	0.624
	Time-invariant SVR	0.522	0.280	7.013	0.461	0.416

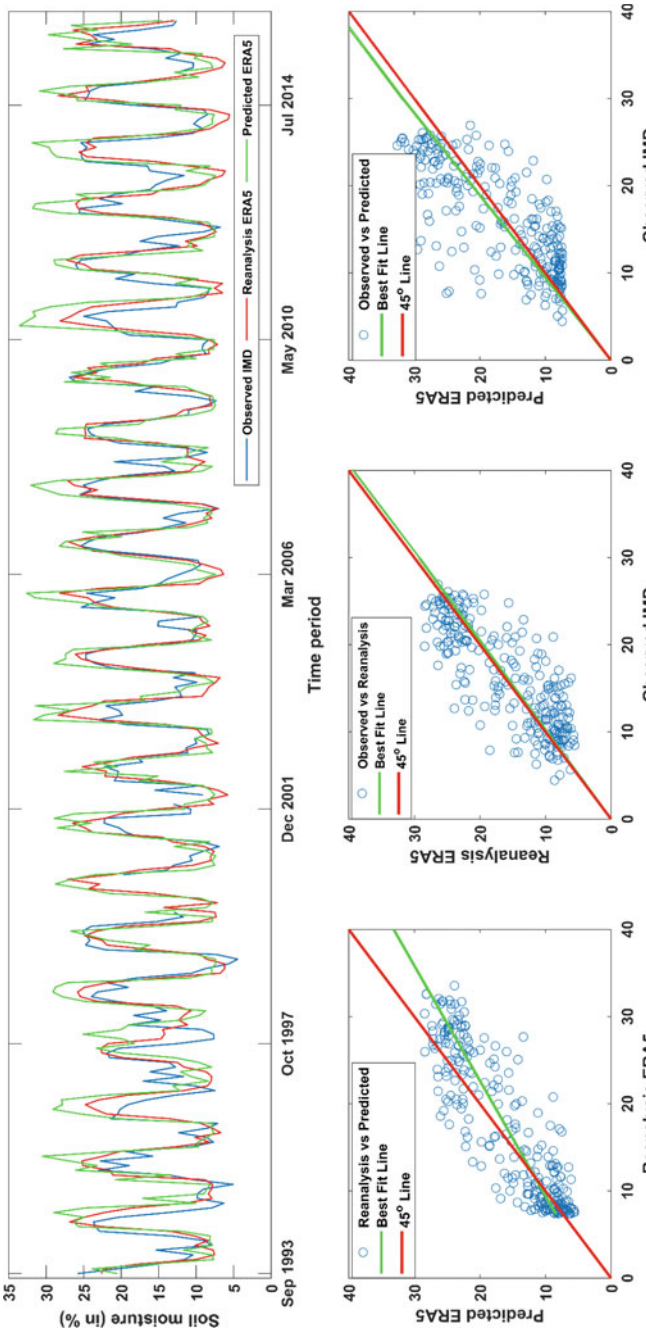

Fig. 4 Comparison of the soil moisture data obtained from ERA5-Land (a reanalysis product) and IMD (observed station data). The one-month ahead prediction of the soil moisture data as obtained using the TNTV are also presented and compared with the observed station data and the reanalysis product

during the first model development period and the following testing period. It is interesting to note that the reanalysis product very well agrees with the observed monthly soil moisture data at the selected location (Kalyani, West Bengal, India). Furthermore, comparison of the observed data (IMD) and predicted values obtained from the model developed using the reanalysis product shows that the proposed model very well captures the soil moisture values one-month and one-season in advance. The performance statistics obtained by comparing these two data sets, for the lead time of one-month, are as follows: $R = 0.813$, $R^2 = 0.651$, RMSE = 5.321, NSE = 0.584, and Dr = 0.344. Thereby, as the soil moisture data obtained from ERA5-Land shows good agreement with the IMD station data, the reanalysis product can be effectively utilized for modelling of soil moisture data for the entire Indian continent. Furthermore, the ability of the proposed model to capture the temporal variation in different hydroclimatic variables makes it an efficient approach for the prediction of such variables for different (long/short) lead times.

4 Concluding Remarks

The TNTV approach is highly potential in modelling under a changing climate. Considering the hydroclimatic processes to be stationary is an existing short-coming of many modelling approaches. The non-stationarity induced by changing climate and other dynamic factorscalls for exploration of alternative approaches that can perform efficiently in non-stationary environment. The proposed approach can be effectively utilized as one such alternative to capture the time-varying characteristics of the hydrologic system. The network structures identified using GM-based approach are updated after a fixed time interval to capture the temporal change in the association among the variables. Thereby, the prediction model is re-calibrated, in terms of model inputs and parameters, in order to incorporate the time-varying characteristics. As a demonstration, soil moisture prediction is carried out for a station at monthly scale. The results indicate a change in the network structures over time as the structure is updated after 5 years. The proposed model successfully captures the soil moisture values one-month to one-season in advance; however, while using its time-invariant counterpart, the model performance deteriorates. Advantage of identifying the complete conditional independence structure is also observed on comparing the results of the network-based models with the SVR-based models. Finally, as a future scope, the potential of the temporal network based approach can be explored for other hydroclimatic variables that are influenced by many interacting variables in complex ways and exhibit a temporal change/variability under climate change.

Acknowledgements This study is partially supported by a research project sponsored by Space Application Centre (SAC), Indian Space Research Organization (ISRO), Govt. of India through sponsored project (Ref No.: IIT/SRIC/R/SMT/2021/101).

References

1. Adeyemi O, Grove I, Peets S, et al (2018) Dynamic neural network modelling of soil moisture content for predictive irrigation scheduling. Sensors (Switzerland) 18. https://doi.org/10.3390/s18103408
2. Betterle A, Radny D, Schirmer M, Botter G (2017) What do they have in common? drivers of streamflow spatial correlation and prediction of flow regimes in ungauged locations. Water Resour Res 53:10354–10373. https://doi.org/10.1002/2017WR021144
3. Bracken C, Holman KD, Rajagopalan B, Moradkhani H (2018) A Bayesian hierarchical approach to multivariate nonstationary hydrologic frequency analysis. Water Resour Res 54:243–255. https://doi.org/10.1002/2017WR020403
4. Caroni C, Panagoulia D (2016) Non-stationary modelling of extreme temperatures. REVSTAT—Stat J 14:217–228
5. Dai A (2013) Increasing drought under global warming in observations and models. Nat Clim Chang 3:52–58. https://doi.org/10.1038/nclimate1633
6. Das S, Das J, Umamahesh NV (2021) Nonstationary modeling of meteorological droughts: application to a region in India. J Hydrol Eng 26:05020048. https://doi.org/10.1061/(asce)he.1943-5584.0002039
7. Das SK, Maity R (2013) Probabilistic simulation of surface soil moisture using hydrometeorological inputs. ISH J Hydraul Eng 19:227–234. https://doi.org/10.1080/09715010.2013.798907
8. Das SK, Maity R (2015) A hydrometeorological approach for probabilistic simulation of monthly soil moisture under bare and crop land conditions. Water Resour Res 51:2336–2355. https://doi.org/10.1002/2014WR016043
9. Ditzler G (2015) Learning in nonstationary environments: a survey. IEEE Comput Intell Mag 10:12–25. https://doi.org/10.1109/MCI.2015.2471196
10. Donat MG, Lowry AL, Alexander LV et al (2016) More extreme precipitation in the world's dry and wet regions. Nat Clim Chang 6:508–513. https://doi.org/10.1038/nclimate2941
11. Dutta R, Maity R (2018) Temporal evolution of hydroclimatic teleconnection and a time-varying model for long-lead prediction of Indian summer monsoon rainfall. Sci Rep 8:10778. https://doi.org/10.1038/s41598-018-28972-z
12. Dutta R, Maity R (2020a) Temporal networks-based approach for nonstationary hydroclimatic modeling and its demonstration with streamflow prediction. Water Resour Res 56:1–21. https://doi.org/10.1029/2020WR027086
13. Dutta R, Maity R (2020b) Spatial variation in long-lead predictability of summer monsoon rainfall using a time-varying model and global climatic indices. Int J Climatol, 1–16. https://doi.org/10.1002/joc.6556
14. Dutta R, Maity R, Patel P (2021) Short and medium range forecast of soil moisture for the different climatic regions of India using temporal networks. Water Resour Manag. https://doi.org/10.1007/s11269-021-03025-9
15. Gill MK, Asefa T, Kemblowski MW, McKee M (2006) Soil moisture prediction using support vector machines. J Am Water Resour Assoc 42:1033–1046. https://doi.org/10.1111/j.1752-1688.2006.tb04512.x
16. Greve P, Orlowsky B, Mueller B et al (2014) Global assessment of trends in wetting and drying over land. Nat Geosci 7:716–721. https://doi.org/10.1038/NGEO2247
17. Hao W, Shao Q, Hao Z et al (2019) Non-stationary modelling of extreme precipitation by climate indices during rainy season in Hanjiang River Basin, China. Int J Climatol 39:4154–4169. https://doi.org/10.1002/joc.6065
18. He B, Chang J, Wang Y et al (2021) Spatio-temporal evolution and non-stationary characteristics of meteorological drought in inland arid areas. Ecol Indic 126:107644. https://doi.org/10.1016/j.ecolind.2021.107644
19. Hummel JW, Sudduth KA, Hollinger SE (2001) Soil moisture and organic matter prediction of surface and subsurface soils using an NIR soil sensor. Comput Electron Agric 32:149–165. https://doi.org/10.1016/S0168-1699(01)00163-6

20. Ihler AT, Kirshner S, Ghil M et al (2007) Graphical models for statistical inference and data assimilation. Phys D Nonlinear Phenom 230:72–87. https://doi.org/10.1016/j.physd.2006.08.023
21. Jackson SH (2003) Comparison of calculated and measured volumetric water content at four field sites. Agric Water Manag 58:209–222. https://doi.org/10.1016/S0378-3774(02)00078-1
22. Jordan MI (2004) Graphical models. Stat Sci 19:140–155. https://doi.org/10.1214/088342304000000026
23. Li A, Cornelius SP, Liu YY, et al (2017) The fundamental advantages of temporal networks. Science 80(358):1042–1046. https://doi.org/10.1126/science.aai7488
24. Liang X, Wood EF, Lettenmaier DP (1996) Surface soil moisture parameterization of the VIC-2L model: Evaluation and modification. Glob Planet Change 13:195–206. https://doi.org/10.1016/0921-8181(95)00046-1
25. Machado MJ, Botero BA, López J et al (2015) Flood frequency analysis of historical flood data under stationary and non-stationary modelling. Hydrol Earth Syst Sci 19:2561–2576. https://doi.org/10.5194/hess-19-2561-2015
26. Milly PCD, Betancourt J, Falkenmark M, et al (2008) Stationarity is dead: Whither water management? Science 80(319):573–574. https://doi.org/10.1126/science.1151915
27. Mondal A, Mujumdar PP (2015) Modeling non-stationarity in intensity, duration and frequency of extreme rainfall over India. J Hydrol 521:217–231. https://doi.org/10.1016/j.jhydrol.2014.11.071
28. Montanari A, Koutsoyiannis D (2014) Modeling and mitigating natural hazards: stationarity is immortal! Water Resour Res 50:9748–9756. https://doi.org/10.1002/2014WR016092
29. Pan F, Peters-Lidard CD, Sale MJ (2003) An analytical method for predicting surface soil moisture from rainfall observations. Water Resour Res 39. https://doi.org/10.1029/2003WR002142
30. Ronghua J, Shulei Z, Lihua Z, et al (2017) Prediction of soil moisture with complex-valued neural network. In: Proc 29th Chinese Control Decis Conf CCDC 2017, 1231–1236. https://doi.org/10.1109/CCDC.2017.7978706
31. Sivapalan M, Takeuchi K, Franks SW et al (2003) IAHS Decade on Predictions in Ungauged Basins (PUB), 2003–2012: Shaping an exciting future for the hydrological sciences. Hydrol Sci J 48:857–880. https://doi.org/10.1623/hysj.48.6.857.51421
32. Todini E (1996) The ARNO rainfall-runoff model. J Hydrol 175:339–382. https://doi.org/10.1016/S0022-1694(96)80016-3
33. Wagener T, Sivapalan M, Troch PA et al (2010) The future of hydrology: an evolving science for a changing world. Water Resour Res 46:1–10. https://doi.org/10.1029/2009WR008906
34. Whittaker J (2009) Graphical models in applied multivariate statistics. Hoboken, NJ: Wiley Publishing.
35. Wigneron JP, Calvet JC, Olioso A et al (1999) Estimating the root-zone soil moisture from the combined use of time series of surface soil moisture and SVAT modelling. Phys Chem Earth, Part B Hydrol Ocean Atmos 24:837–843. https://doi.org/10.1016/S1464-1909(99)00090-8
36. Zambon D, Member S, Alippi C, Livi L (2018) Concept drift and anomaly detection in graph streams. IEEE Trans Neural Networks Learn Syst 29:5592–5605. https://doi.org/10.1109/TNNLS.2018.2804443

Downscaling of GCM Output Using Deep Learning Techniques

Chandra Prakash Tamang, Subir Paul, and Dasika Nagesh Kumar

Abstract General circulation models (GCMs) provide the data to study climate change under different scenarios, but they operate on a coarse scale. Therefore, to assess the hydrological impacts of global climate change on a regional scale, the output from a GCM must be downscaled to finer resolution. Moreover, regional precipitation simulations can be improved by using physically relevant variables from GCMs at different pressure levels as predictors. In this study, we have explored different deep learning techniques for multi-site downscaling of daily precipitation over the Mahanadi basin using large-scale hydroclimate variables as predictors. Hydroclimatic variables from NCEP reanalysis data (available at 2.5° × 2.5° resolution) are used to downscale the daily precipitation product at observational grid-scale (i.e., 1° × 1° spatial resolution). Different deep learning architectures, viz., deep neural network (DNN), 2D- and 3D-convolutional neural network (CNN), and hybrid-DNN are trained on these spatio-temporal variables. The results show that deep learning models have the ability to use the spatial information from predictor variables over the Indian subcontinent to capture monsoon patterns and downscale daily precipitation. The 2D-CNN model is able to learn the spatial features from high-dimensional predictor variables over continental sized domains. 3D-CNN further reduces the number of parameters and is able to learn from the stacked high-dimensional spatio-temporal datasets at different vertical pressure levels with

Disclaimer: The presentation of material and details in maps used in this chapter does not imply the expression of any opinion whatsoever on the part of the Publisher or Author concerning the legal status of any country, area or territory or of its authorities, or concerning the delimitation of its borders. The depiction and use of boundaries, geographic names and related data shown on maps and included in lists, tables, documents, and databases in this chapter are not warranted to be error free nor do they necessarily imply official endorsement or acceptance by the Publisher or Author.

C. P. Tamang (✉) · D. N. Kumar
Department of Civil Engineering, Indian Institute of Science, Bengaluru 560012, India
e-mail: chandraprakashtamang@gmail.com

D. N. Kumar
e-mail: nagesh@iisc.ac.in

S. Paul
Interdisciplinary Centre for Water Research, Indian Institute of Science, Bengaluru 560012, India

P. V. Timbadiya et al. (eds.), *Climate Change Impact on Water Resources*, Lecture Notes in Civil Engineering 313, https://doi.org/10.1007/978-981-19-8524-9_2

comparative ease. The hybrid-DNN is employed to make use of spatial structure of the predictor datasets as well as the information from the GCM precipitation outputs of neighboring grid points of the observation grids. The 2D-CNN, 3D-CNN, and hybrid-DNN perform better than the DNN showing the usefulness of exploiting the spatial gridded structure of the predictors. This study highlights the potential of deep learning techniques in learning precipitation patterns from coarse-resolution climate model outputs and in downscaling daily precipitation.

Keywords Deep learning · Statistical downscaling · Daily precipitation · Convolution neural networks

1 Introduction

General circulation models (GCMs) simulate the Earth's climate by mathematical equations that describe atmospheric and oceanic interactions and feedbacks. There are numerical atmospheric and oceanic models for climate and weather predictions based on solving time-dependent 3D geophysical fluid dynamics equations on the sphere including governing model physics (e.g., long-and short-wave atmospheric radiation, turbulence, convection and large-scale precipitation processes, clouds, interactions with land and ocean processes, etc.) and chemistry (constituency transport, chemical reactions, etc.). They provide global-scale climate information and are used to understand present climate and future climate under different emission scenarios and increased greenhouse gas concentrations. But due to their coarse resolution, they cannot account for fine-scale climate variability and are not suitable for hydrological impact assessments, as regional hydrological impact assessments depend on a much smaller scale data variability. The relevant regional scale variables are important for decision makers who require information about potential impacts on crop production, hydrology, species distribution, etc., at spatial scales of 10–50 km.

Downscaling techniques are applied to provide climate projections at higher resolutions. Downscaling methods can be categorized into statistical and dynamical downscaling [1]. Dynamical downscaling relies on the use of a regional climate models (RCM), which are derived similar to a GCM in its principles but with high resolution. RCM's high computational requirements limits its widespread use. The second approach, statistical downscaling aims to learn a statistical relationship between coarse-scale climate variables and high-resolution observations. A key advantage of statistical downscaling is its computational efficiency. It involves the establishment of empirical relationships between historical and/or current large-scale atmospheric and local climate variables. Once a relationship has been determined and validated, future atmospheric variables that GCMs project are used to predict future local climate variables. Statistical downscaling can produce site-specific climate projections, as relationship is developed specific to the data of the given region. Statistical downscaling has been performed by constructing a parametric/nonparametric

and/or linear/nonlinear relationship between large-scale atmospheric predictor variables and the regional climate variable(s) of interest (predictand) in order to simulate future scenarios [2]. The idea is that there is a relation between large-scale climate phenomena and local climatic/meteorological conditions.

Machine learning techniques are an increasingly popular way to automatically extract information without the need to construct explicit physical or statistical models. Support vector machine was used to downscale monthly precipitation from GCM [3]. Random forests have been used for rainfall downscaling [4, 5]. Dibike and Coulibaly [6] used temporal neural networks for extreme precipitation downscaling. The field of machine learning has further been boosted by the major deep learning (DL) breakthroughs in the field of neural networks. Conventional machine learning modeling process have a pre-engineered way to extract features, and hence captures little information beyond our prior knowledge. This issue is particularly severe for high-dimensional problems, where it is difficult to have much foresight in the data structures. The major advantage of deep neural networks (DNN) is that they offer an "end-to-end" modeling workflow: The feature extraction process is integrated into the modeling process, which allows the model to learn customized features rather than subject to the pre-engineered features. Recent advances in DL techniques and computational abilities have promoted their use in wide range of applications. Convolutional neural network (CNN) models, a type of DL model, were used to learn precipitation-related dynamical features from the simulated fields of geopotential heights [7, 8]. CNNs can better process structured high-dimensional data.

The spatial structure along with very high dimensionality of climate data on a continental scale justifies downscaling with modern DL methods. This present study shows the applicability of different DL techniques in downscaling daily precipitation over Mahanadi basin with hydroclimatic predictor variables.

2 Study Area and Datasets

2.1 Mahanadi Basin

The Mahanadi River basin, a major river basin with an area of 141,589 sq.km, is chosen as the study area for this work. Location of the Mahanadi basin is shown in Fig. 1. Eight grid points with spatial resolution of 1 degree are considered as observation data. These grid points are presented through a spatial map of the Mahanadi basin in Fig. 1.

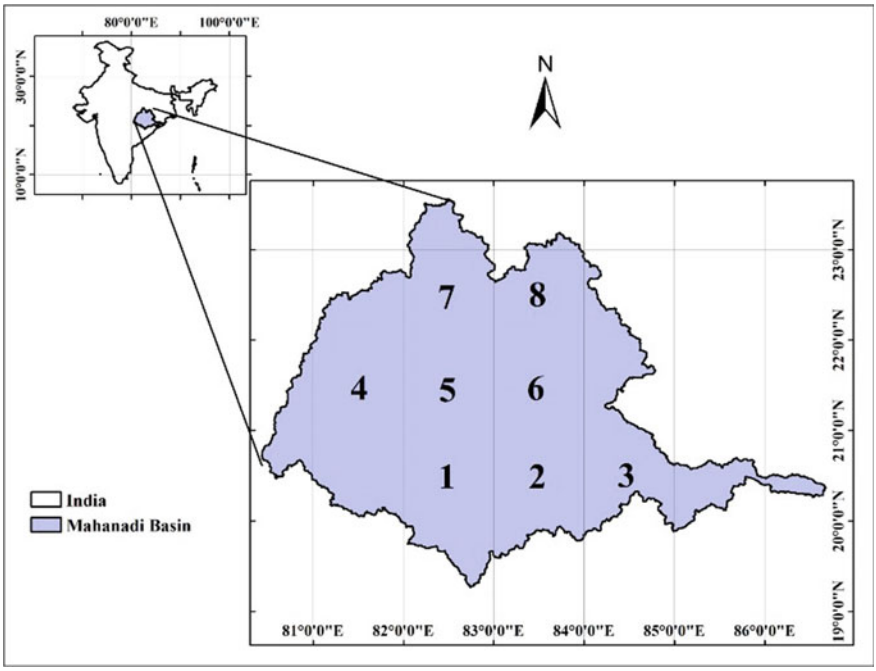

Fig. 1 Eight observation station grid points in Mahanadi Basin

2.2 NCEP Reanalysis Datasets

The predictors were obtained from the National Center for Environmental Prediction (NCEP) reanalysis dataset. The uncertainties and biases that occur in GCM datasets try to mitigate through data assimilation, and hence these reanalysis datasets are often used as proxies to GCMs for statistical downscaling. These datasets are assimilated with the help of comprehensive ocean–atmosphere datasets that comprise a collection of surface marine data, aircraft data, surface land synoptic data, satellite sounder data, special sensing microwave/imager surface wind speeds, and satellite cloud drift winds [9]. Based on the Indian summer monsoon activity and following the work by Kannan and Ghosh [10], a wide surrounding aerial region spanning latitudes of 7.5°–35.0° N and longitudes of 70.0°–97.5° E is selected (Fig. 2), which contains 144 reanalysis grid points, for downscaling. Daily climate data for the 144 grid points is extracted from the NCEP/NCAR datasets.

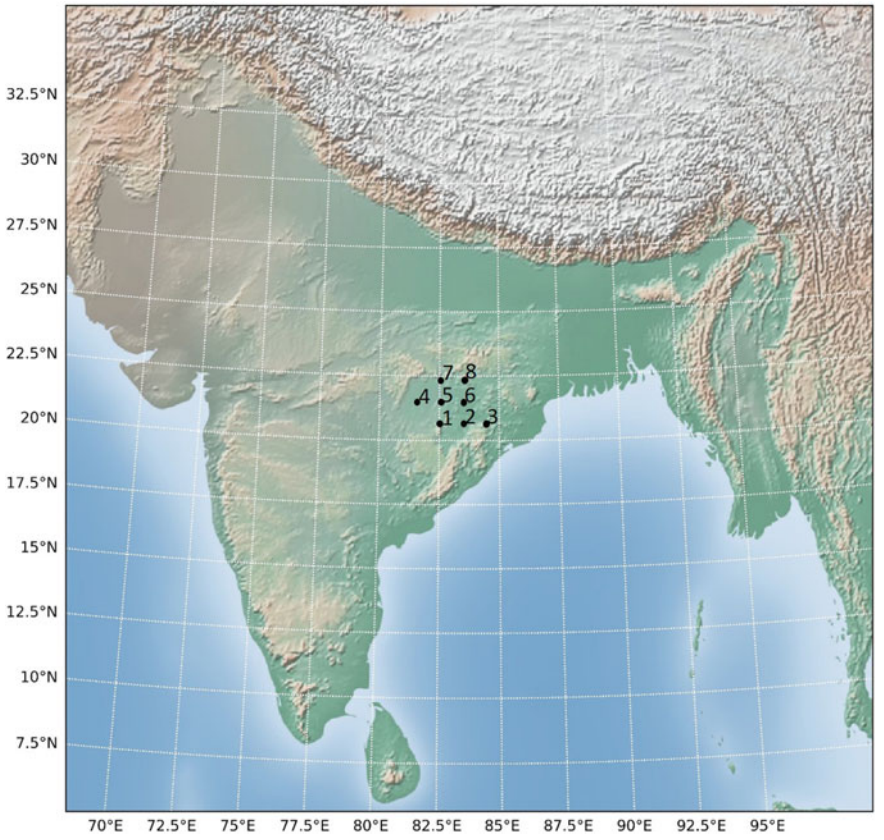

Fig. 2 Extent of area under the region between latitudes 7.5° N–35° N and longitudes 70° E–97.5° E which consists of 144 grid points of predictor variables (following Kannan and Ghosh [10]) and the 8 stations to which the precipitation is downscaled

2.3 Predictors Selection for Precipitation Prediction

The assumptions made by statistical downscaling methods for selection of predictors are: (I) They assume that the chosen predictors credibly represent the variability in the predictands; (II) It requires the statistical attributes of predictands and predictors to be valid outside the data used for statistical modeling; and (III) The climate change signal must be incorporated in the predictors through GCMs.

Because of these requirements, predictors must be carefully selected in order to obtain credible results. Same events can be driven by completely different physical processes depending on the region and many other factors. The predictor variables considered for trials and analysis in our study are presented in Table 1.

However, only nine variables (which are highlighted in Table 1) among these 20 predictor variables are selected for further analysis. These nine predictors are

Table 1 Predictor variables selected for analysis

air500	**Air temperature at 500 mb pressure level**
air700	Air temperature at 700 mb pressure level
hgt1000	Geopotential height at 1000 mb pressure level
hgt850	**Geopotential height at 850 mb pressure level**
hgt500	**Geopotential height at 500 mb pressure level**
hgt200	Geopotential height at 200 mb pressure level
pr_wtr	**Total precipitable water**
shum925	Specific humidity at 925 mb pressure level
shum850	**Specific humidity at 850 mb pressure level**
shum500	Specific humidity at 500 mb pressure level
Slp	**Mean sea level pressure**
uwnd850	**Horizontal component of wind at 850 mb pressure level**
uwnd200	Horizontal component of wind at 200 mb pressure level
vwnd850	**Vertical component of wind at 850 mb pressure level**
vwnd200	Vertical component of wind at 200 mb pressure level
prate	Precipitation rate
airsurface	**Mean daily air temperature at surface level**
rhumsurface	Relative humidity at surface level
uwndsurface	Horizontal component of wind at surface level
vwndsurface	Vertical component of wind at surface level

shortlisted after performing numbers of trials with different combinations of all the predictors.

2.4 APHRODITE Datasets

The APHRODITE (Asian Precipitation-Highly-Resolved Observational Data Integration Towards Evaluation) daily gridded precipitation is a continental-scale daily product that contains a dense network of daily rain-gauge data for Asia. These datasets have been used in many studies in India [11].

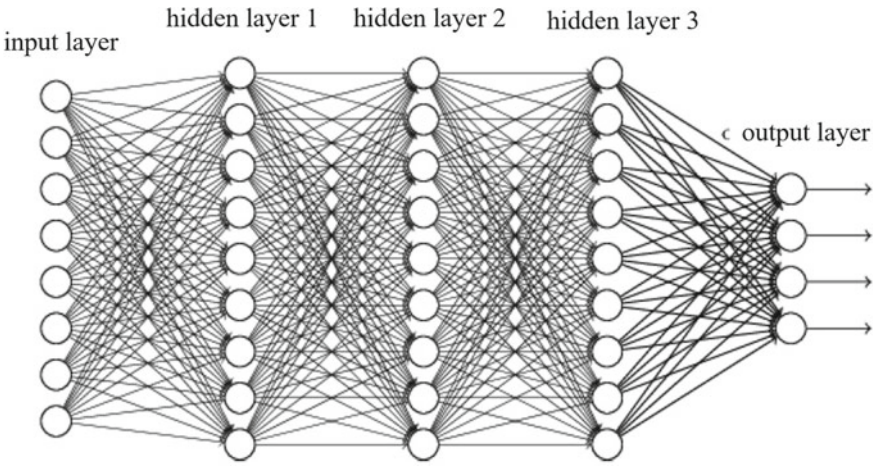

Fig. 3 A deep neural network (DNN) architecture

3 Methodologies

3.1 Deep Neural Network (DNN)

Neural networks are biologically inspired programming paradigm which enables computer to learn from observational data. Modern DNNs involve numerous network architecture variations, training algorithms and tricks, and regularization methods.

In case of DNN architecture used in this study (Fig. 3), the total dimension of the predictors is $144 \times 9 = 1296$. To reduce the dimension and remove multicollinearity from the data, a single hidden layer autoencoder is trained on the standardized predictor data in the training period. It has 500 nodes in the bottleneck layer. So, it reduced the dimension to 500. The inputs to the DNN network are the 500-dimension encoded features for the present day and lag-1 day. The lag-1 day features are also included in order to incorporate the temporal evolution of the precipitation event. The outputs of the network have eight nodes, and the outputs are compared with the observed precipitations of the eight stations of the Basin via the loss function of mean squared error.

3.2 Convolutional Neural Network (CNN)

CNN is a special type of DNN. CNN architectures involve two special matrix operators, viz., a convolutional layer and a pooling layer in one or more layers, which is different from simple matrix multiplication of fully connected DNN [12]. Convolution operation improves statistical efficiency with three important ideas,

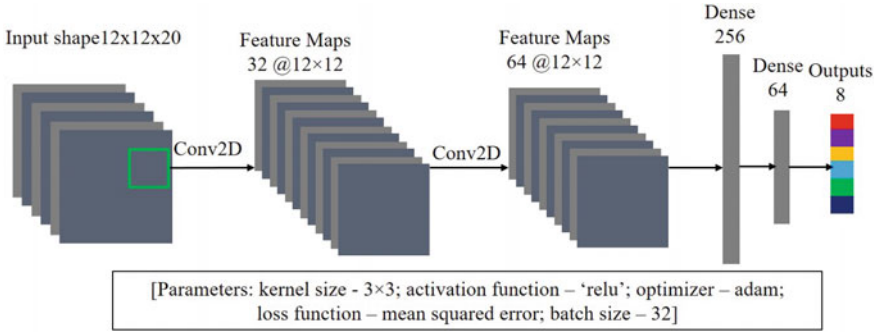

Fig. 4 Architecture used for 2D convolutional neural network (2D CNN) network

viz., sparse interactions, parameter sharing, and equivariant representations, and reduces the memory requirements of the machine learning system [12]. CNN models can be designed using one-dimensional (1D), 2D, and 3D CNN. If only spatial or temporal features are important then 2D or 1D CNN can be implemented, respectively. However, in case of spatio-temporal feature extraction, 3D CNN is best suited, which performs convolution in both spatial and temporal dimension. Here, we have implemented both 2D and 3D CNN architectures for downscaling of precipitation.

3.3 2D CNN

Ten predictor variables of the current day and lag-1 day over the 12 × 12 grid points (i.e., total 144 grids) are utilized as input in the 2D CNN architecture. 12 × 12 grids are considered as a single image, and such 10 images are available for 10 predictors of current-day. Similarly, another ten images are available for the lag-1 day predictors. All these images are stacked in a data cube with dimension of 12 × 12 × 20, which is used as input data in the 2D CNN architecture. The 2D CNN architecture used in our work is presented in Fig. 4.

3.4 3D CNN

A 3D convolution performs convolution operation over a volume. A 3D CNN performed successfully in classification of hyperspectral images [13]. The temporal dimension can be taken into account easily as stacks of images of present-day variables and lag-1 day variables can be fed into the network as two volumes. The present-day and lag-1 day standardized 12 × 12 gridded predictor variables which were used in 2D CNN network are fed into the 3D CNN as two stacked volumes of

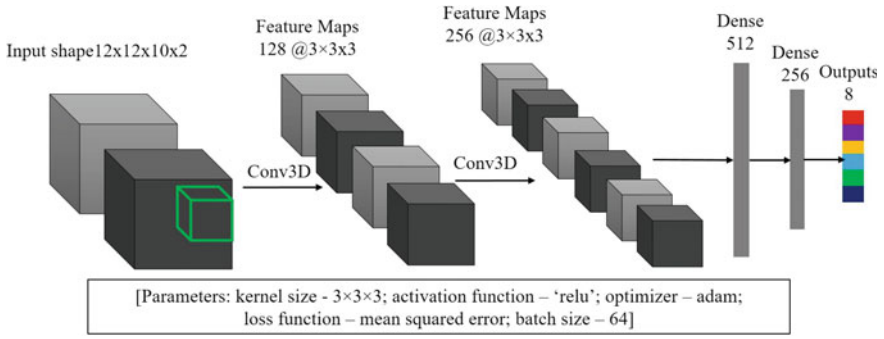

Fig. 5 3D convolutional neural network (3D CNN) architecture used

$(12 \times 12 \times 10)$ size. The network specification used in our experiment is as shown in the Fig. 5.

3.5 Hybrid Deep Neural Network (Hybrid-DNN)

To use the information given by the precipitation rate (prate) variable from the NCEP Reanalysis Data, 3×3 nearest grid points surrounding the basin were used as inputs to the network as well. The 12×12 gridded inputs of the other predictor variables used in the CNN network earlier were fed into a CNN, while the eight grid points' reanalysis precipitation rate variable was fed into a dense DNN. Both the networks were then concatenated as shown in the Fig. 6, and further two-layer dense network was added to the concatenated network. This technique allowed the network to learn spatial features from the predictor variables as well as the information of the reanalysis data of precipitation rates at the nearest grids. The network specification used in our experiment is as shown in the Fig. 6.

3.6 Performance Evaluation Metrics

The Pearson correlation coefficient (r) between simulated and observed daily precipitation is used as supplementary skill metric for measuring model performance in this study. Normalized mean squared error (NMSE) is used as an error metric.

$$\mathrm{NMSE} = \frac{\frac{1}{N}\sum_{i=1}^{N}\left(y_i - \hat{y}_i\right)^2}{\left(S_{\mathrm{obs}}\right)^2},$$

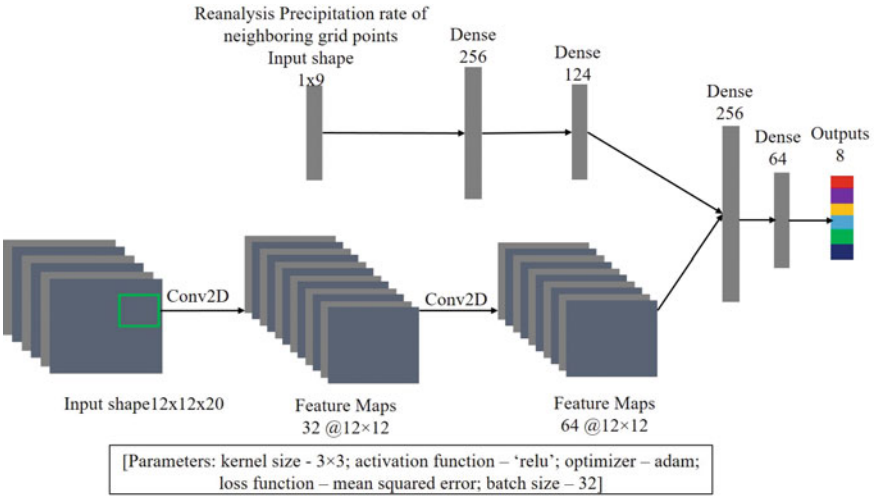

Fig. 6 Hybrid deep neural network (Hybrid-DNN) architecture used in this study

where $(S_{\text{obs}})^2$ is the variance of the observed precipitation, and on the numerator is the mean squared error of the predicted values with respect to the observed.

4 Results and Discussion

The models are trained using 40 years of data from 1954 to 1994 and are tested on data from 1994 to 2004. Performance evaluation metrics are calculated with four different model predictions for the test datasets and presented in Tables 2, 3, 4, and 5. The mean rainfall values are predicted best by the Hybrid-DNN with least variance on the mean bias%. This result is with the use of the reanalysis precipitation outputs as well in the inputs to the model. The standard deviation (SD) of the predicted rainfall is lesser than the observed rainfall for all networks. The extremes are not fully captured by the models as there are more uncertainties around the extreme values. The daily rainfall correlations are better for the networks that used the spatial structure of the predictor data than the DNN. Monthly mean rainfall is very well simulated by all the networks.

On comparing the average NMSE over the eight stations of the different architectures used, the 2D CNN performs slightly better than the rest and the 3D CNN and Hybrid-DNN have also performed quite well (Table 6). The DNN architecture, which did not use the spatial structure of the gridded predictor datasets, has not performed as well as the other networks. Thus, accounting for the spatial nature of the predictor data leads to better representation of the precipitation patterns.

A 2D CNN architecture is comparatively providing better performance. Hence, the time series plot of observed and predicted (from 2D CNN) rainfall and the scatter plot between them are presented for Station 1 data in Fig. 7. The precipitation patterns are well captured on the test set.

Table 2 Results of the DNN network

Station no.	RMSE (mm)	Actual mean (mm)	Predicted mean (mm)	Mean bias %	Actual SD (mm)	Predicted SD (mm)	SD bias %	Rainfall correlation	Monthly mean correlations	NMSE
1	7.57	5.64	5.50	−2.44	9.49	8.53	−10.1	0.65	0.90	0.64
2	7.57	5.81	5.58	−4.02	10.1	8.70	−13.4	0.68	0.89	0.57
3	7.32	5.90	5.12	−13.3	9.69	7.03	−27.4	0.66	0.86	0.57
4	6.92	4.97	4.41	−11.3	8.38	6.22	−25.8	0.59	0.98	0.68
5	6.00	5.19	4.86	−6.32	7.99	6.80	−14.8	0.68	0.99	0.56
6	8.51	6.49	5.70	−12.2	10.8	7.87	−26.9	0.63	0.96	0.62
7	7.31	6.13	6.01	−2.03	9.54	7.86	−17.5	0.66	0.98	0.59
8	7.56	6.60	6.29	−4.71	9.75	7.82	−19.8	0.65	0.97	0.60

Table 3 Results of the 2D CNN network

Station no.	RMSE (mm)	Actual mean (mm)	Predicted mean (mm)	Mean bias %	Actual SD (mm)	Predicted SD (mm)	SD bias %	Rainfall correlation	Monthly mean correlations	NMSE
1	6.61	5.64	5.62	0.24	9.49	7.02	−25.9	0.72	0.91	0.48
2	7.05	5.81	5.96	−2.55	10.1	7.25	−27.9	0.71	0.89	0.49
3	6.98	5.9	4.89	17.2	9.69	5.76	−40.5	0.71	0.81	0.52
4	6.1	4.97	5.15	−3.69	8.38	6.28	−25.0	0.69	0.98	0.53
5	5.55	5.19	5.81	−11.9	7.99	7.14	−10.6	0.74	0.98	0.48
6	7.94	6.49	6.57	−1.23	10.8	8.33	−22.7	0.68	0.96	0.54
7	6.82	6.13	7.14	−16.5	9.54	8.72	−8.52	0.73	0.96	0.51
8	6.73	6.6	7.15	−8.28	9.75	8.02	−17.7	0.73	0.95	0.48

Table 4 Results of the 3D CNN

Station no.	RMSE (mm)	Actual mean (mm)	Predicted mean (mm)	Mean bias %	Actual SD (mm)	Predicted SD (mm)	SD bias %	Rainfall correlation	Monthly mean correlations	NMSE
1	6.66	5.64	5.51	−2.29	9.49	6.6	−30.4	0.71	0.91	0.49
2	7.24	5.81	5.53	−4.97	10.1	7.05	−29.8	0.69	0.85	0.52
3	7.05	5.91	5.08	−13.9	9.69	6.19	−36.1	0.69	0.75	0.53
4	6.03	4.97	5.03	1.25	8.38	5.86	−30.1	0.69	0.98	0.52
5	5.42	5.19	5.1	−1.7	7.99	5.94	−25.7	0.74	0.98	0.46
6	8.02	6.5	5.76	−11.4	10.8	7.1	−34.2	0.67	0.94	0.55
7	6.7	6.13	5.63	−8.23	9.54	6.43	−32.6	0.71	0.98	0.49
8	7.11	6.6	5.49	−16.8	9.75	6.11	−37.3	0.7	0.97	0.53

Table 5 Results of the hybrid-DNN

Station no.	RMSE (mm)	Actual mean (mm)	Predicted mean (mm)	Mean bias %	Actual SD (mm)	Predicted SD (mm)	SD bias %	Rainfall correlation	Monthly mean correlations	NMSE
1	6.72	5.64	5.36	−4.91	9.49	6.83	−28.0	0.71	0.97	0.50
2	7.31	5.81	5.40	−7.00	10.1	6.91	−31.2	0.69	0.88	0.53
3	6.85	5.90	5.74	−2.75	9.69	7.45	−23.1	0.71	0.89	0.50
4	6.44	4.97	4.83	−2.74	8.38	6.91	−17.6	0.66	0.99	0.59
5	5.79	5.19	5.12	−1.29	7.99	7.18	−10.2	0.71	0.99	0.53
6	8.24	6.49	6.25	−3.67	10.8	8.81	−18.3	0.66	0.97	0.58
7	6.87	6.13	5.91	−3.64	9.54	7.75	−18.7	0.70	0.98	0.52
8	6.99	6.60	6.33	−4.16	9.75	7.69	−21.2	0.70	0.99	0.51

Table 6 Average NMSE values over the 8 stations

Network architectures	NMSE values
DNN	0.603
2D CNN	0.503
3D CNN	0.51
Hybrid-DNN	0.53

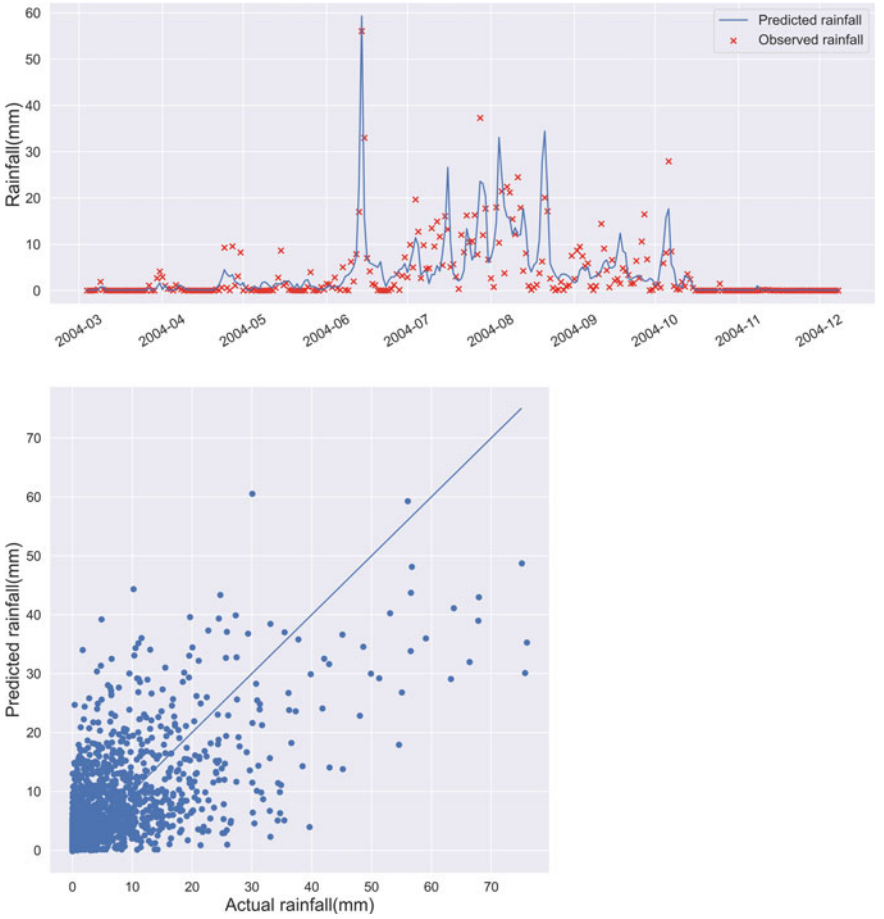

Fig. 7 (**Top**) Time series plot of observed rainfall and predicted rainfall for 2004, and (**Bottom**) Scatter plot of daily observed rainfall and rainfall predicted by 2D CNN for 1994–2004 for Station 1

5 Conclusions

In this study, we explored different DL approaches viz., DNN, 2D CNN, 3D CNN, and Hybrid-DNN to downscale daily precipitation for eight locations in the Mahanadi Basin. Our study shows the ability of DL models to process large continental scale datasets, learn features that can predict precipitation, and with consideration of the hydroclimatic variables as images we can further exploit the spatial structure of these datasets. These methods have an advantage over other statistical downscaling techniques as it solves the problem of high dimensionality by automatically selecting the features from the predictors by learning spatial information in the form of feature maps. The models performed well based on the statistics of normalized mean squared error, and the CNN network performed best.

Our study shows promise for further study of deep learning models with GCM datasets to capture the precipitation trends in future scenarios over the Indian subcontinent. Higher resolution predictor datasets can be used so that the potential of our models to learn spatial features can be better explored to simulate extreme scenarios in GCM datasets.

References

1. Trzaska S, Schnarr E (2014) A review of downscaling methods for climate change projections. United States Agency for International Development by Tetra Tech ARD, 1–42
2. Wilby RL, Wigley T, Conway D, Jones P, Hewitson B, Main J, Wilks D (1998) Statistical downscaling of general circulation model output: a comparison of methods. Water Resour Res 34(11):2995–3008
3. Tripathi S, Srinivas V, Nanjundiah RS (2006) Downscaling of precipita-tion for climate change scenarios: a support vector machine approach. J Hydrol 330(3–4):621–640
4. He X, Chaney NW, Schleiss M, Sheffield J (2016) Spatial downscaling of precipitation using adaptable random forests. Water Resour Res 52(10):8217–8237
5. Pham QB, Yang T-C, Kuo C-M, Tseng H-W, Yu P-S (2019) Combing random forest and least square support vector regression for improving extreme rainfall downscaling. Water 11(3):451
6. Dibike YB, Coulibaly P (2006) Temporal neural networks for downscaling climate variability and extremes. Neural Netw 19(2):135–144
7. Larraondo PR, Renzullo LJ, Inza I, Lozano JA (2019) A data-driven approach to precipitation parameterizations using convolutional encoder-decoder neural networks. arXiv preprint arXiv:1903.10274. 8.
8. Pan B, Hsu K, AghaKouchak A, Sorooshian S (2019) Improving precipitation estimation using convolutional neural network. Water Resour Res 55(3):2301–2321
9. Kalnay E, Kanamitsu M, Kistler R, Collins W, Deaven D, Gandin L, Woollen J (1996) The NCEP/NCAR 40-year reanalysis project. Bull Am Meteorolo Soc 77(3):437–472
10. Kannan S, Ghosh S (2013) A nonparametric kernel regression model for downscaling multisite daily precipitation in the Mahanadi basin. Water Resour Res 49(3):1360–1385
11. Sushama L, Said SB, Khaliq M, Kumar DN, Laprise R (2014) Dry spell characteristics over India based on IMD and APHRODITE datasets. Clim Dyn 43(12):3419–3437
12. Goodfellow I, Bengio Y, Courville A (2016) Deep learning. Book in preparation for MIT Press. http://www.deeplearningbook.org
13. Li Y, Zhang H, Shen Q (2017) Spectral–spatial classification of hyperspectral imagery with 3D convolutional neural network. Remote Sens 9(1):67

Application of TVDM in Modeling the Observed Precipitation Over Godavari River Basin, India

Subbarao Pichuka, Srikanth Bhoopathi, and Siva Sai Syam Nandikanti

Abstract The benefit of the time-varying downscaling model (TVDM) in downscaling the historical precipitation (1951–2015) data is explored in this study. The Godavari River Basin (GRB) is considered for demonstrating the results. The General Circulation Model (GCM) outputs from Canadian Earth System Model, version-2 (CanESM2) are considered for the analysis. The observed precipitation is obtained from India Meteorological Department (IMD), Pune. Firstly, the TVDM is calibrated using 40 years (1951–1990) of historical data and then validated for the remaining 15 years (1991–2005) in the historical period. Secondly, the downscaled data are analyzed with the observed precipitation data using different statistical measures. The results have shown a good association between observed and downscaled precipitation during both calibration and validation periods across the GRB. For instance, the correlation coefficient (R) ranges between 0.71 and 0.89 at various locations in the GRB. Further, the extreme events are also assessed using 90th and 95th percentiles and found a better match between the observed and TVDM downscaled data. Overall, the TVDM shows a promising result in modeling the precipitation. Hence, the TVDM can be used to downscale the future precipitation of GRB under the changing climate scenario, and the outputs can be used for many local-scale impact assessment studies.

Keywords Climate change · TVDM · Downscaling · GCM · Godavari River Basin

S. Pichuka (✉) · S. S. S. Nandikanti
Department of Civil Engineering, National Institute of Technology Andhra Pradesh, Tadepalligudem 534101, India
e-mail: subbarao@nitandhra.ac.in

S. Bhoopathi
Department of Civil Engineering, National Institute of Technology Warangal, Warangal, Telangana 506004, India

P. V. Timbadiya et al. (eds.), *Climate Change Impact on Water Resources*, Lecture Notes in Civil Engineering 313, https://doi.org/10.1007/978-981-19-8524-9_3

1 Introduction

Finer resolution products which are having spatial resolution below 20 km are not being presently provided by the general circulation models (GCMs) [1]. To assess the consequences of changing climate on a variety of human and natural systems, such as water resource management, agriculture, ecosystems, and so on, finer resolution representations of climate variables are necessary. As a result, downscaling GCM results to a finer spatial resolution that allows researchers to assess the regional-level consequences of future climate change [2]. Downscaling is a technique for transferring large-scale climate variables (causal variables) changes which are simulated by GCMs to regional meteorological records (target variable). There are different approaches for precipitation downscaling that have been widely used in various regions [3–5]. Dynamical downscaling [6–9] and statistical downscaling [10–14] are two types of downscaling methods. A nested regional climate model, finer resolution meteorological variables with coarse GCM data as the inceptive and boundary conditions, or a variable-resolution global model can also be used for dynamical downscaling [15, 16], but it needs a lot of computation and parameterization of the model. On the other hand, statistical downscaling is a computationally less demanding approach. It establishes statistical relationships, i.e., multiple linear regression analysis between predictor and predict and variables [17]. In this study, the time-varying downscaling model (TVDM) is employed for downscaling the rainfall data for Godavari River Basin (GRB). Further, the efficacy of the downscaling model in representing the observed data is also assessed. The model is calibrated and validated using the historical data (1951–2005). In this paper, the effectiveness of the TVDM is tested using various statistical parameters.

2 Study Area and Data Source

2.1 Godavari River Basin

The Godavari River is the largest east-flowing river in peninsular India. The catchment area of the basin is 312812 km^2 and shares almost 10% of the Indian geographical area. It is extended over seven states in India. The average annual rainfall of the basin is about 1110 mm. The basin lies between latitudes of 16°16′ 0″ N and 23°43′ 0″ N and longitudes of 73°26′ 0″ E and 83°07′ 0″ E. The Pravara and Manjeera are the primary tributaries joining on the right side of bank of the river, while the Purna, Pranhita, Indravati, and Sabari are the primary tributaries joining on the left side of the river bank. The basin map and its position within India are presented in Fig. 1.

Godavari begins its ascent in the Sahyadris which is nearby Triambakeswar, about 80 km from the Arabian Sea's coast, in the Maharashtra (Nasik district), at a height of 1067 m. Godavari enters the Bay of Bengal at Antarvedi after traveling approximately 1465 km in a general south-eastern direction across Maharashtra and Andhra Pradesh.

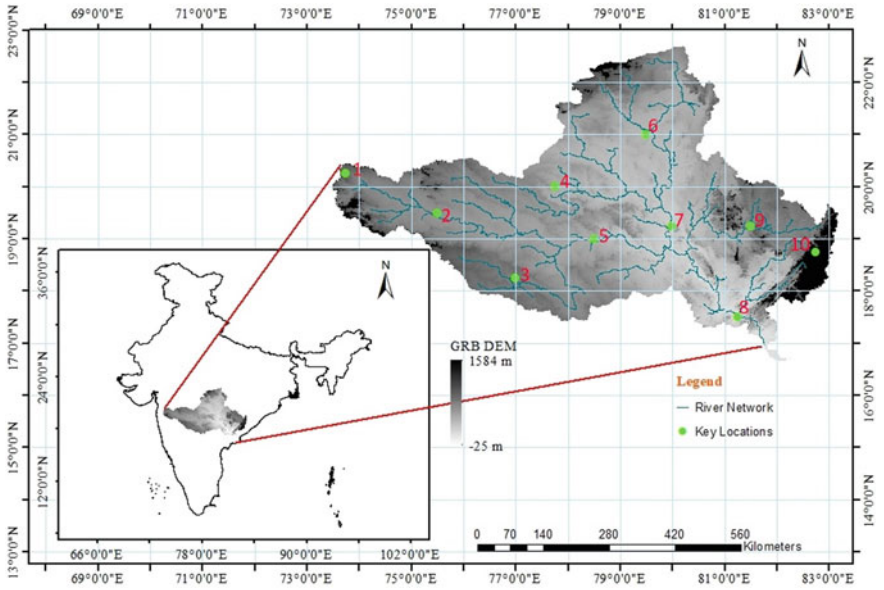

Fig. 1 Study area map

The efficacy of TVDM is tested at 10 key locations of GRB as shown in Fig. 1. These locations are well spread over the GRB and represent its characteristics. The first three locations (numbered 1, 2, and 3) are representing the Upper Godavari region, locations numbered 4 to 7 are falling under the Middle Godavari, and the locations 8, 9, 10 are falling in the Lower Godavari region.

2.2 Data Used

The daily rainfall data at 0.25° × 0.25° resolution for the Godavari basin is obtained from India Meteorological Department (IMD), Pune [18], and converted it into monthly data. Further, the data is divided into calibration period (40-years, i.e., 1951–1990) and validation period (15-years, i.e., 1991–2005. The World Meteorological Organization (WMO) recommended 30-years of data to effectively understand the anomalies of any meteorological variable due to climate change. Hence, 40-years of data is sufficient for the model development.

The causals data from CanESM-2 GCM are downloaded from the Coupled Model Intercomparison Project—Phase5 (CMIP-5) web portal. The mean sea level pressure, surface specific humidity, meridional and zonal winds, and temperature are found to be the potential causal variables (based on their correlation) to downscale the precipitation in this study basin.

2.3 Canadian Earth System Model–Version2 (CanESM2)

The CanESM-2 model GCM outputs are considered as the large-scale atmospheric variables (causal data) for this study. The CanESM2 is developed by the Canadian Centre for Climate Modeling and Analysis (CCCMA). It is the advanced version to CanESM series [19]. It has a resolution of 2.81° × 2.81° and also has 22 pressure levels in the atmosphere (altitude), i.e., vertical resolution. Further details of CanESM2 can be found from [20]. The causal data are downloaded from the CMIP5 web portal available at http://www.ipcc-data.org/sim/gcm_monthly/AR5/Reference-Archive.html, accessed in September 2021.

3 Methodology

3.1 Time-Varying Downscaling Model (TVDM)

The Bayesian technique is used to update the parameters that were previously used in the Bayesian dynamic linear model to create TVDM [21]. Numerous hydrological studies, including those that involve in quantifying uncertainty, water quality modeling, hydroclimatic analysis, etc., apply the Bayesian technique [22–28]. The goal of TVDM is to capture the dynamic relationship over time between pertinent (atmospheric) causative variables and the downscaled target variable.

The first step in the TVDM is to **standardize** all the variables (Causal and target) involved in the process to transform them into a similar range. It is achieved by subtracting the mean (μ) and dividing the difference with the standard deviation (σ) of each variable. Next step is to set-up **system equations** for successive update. Further step is **model initialization;** the model is initialized using the assumed information for the first time-step, and the downscaled value is computed. After computing the downscaled value, the error is evaluated with respect to observed value, and then posterior and prior distributions are calculated using system equations. The detailed methodology of TVDM model can be found in [29]. The downscaling expression used in this study for the target variable (Y_t) using the information of causal variables at tth time-step is expressed as

$$Y_t = F^T \Theta_t + v_t$$

where

F^T is the transpose of the vector of the causal variables at the tth time-step;

Θ_t is the parameter vector at the tth time-step;

v_t is the difference or error between the target variable's observed and the downscaled values.

4 Results and Discussions

The analysis has been carried out for the GRB using TVDM for the calibration period (1951–1990) and validation period (1991–2005) at each selected location in GRB. Several statistical parameters, i.e., correlation coefficient (R), unbiased Root Mean Square Error (uRMSE), and degree of agreement (D_r) are calculated to test the efficacy of the model in representing the observed rainfall for both the time periods. To understand the distribution and extremities of the rainfall, mean, standard deviation, 90th percentile, and 95th percentiles are computed.

The ability of TVDM in simulating the observed data is checked using the mean and standard deviation values shown in Table 1. The mean is well modeled by TVDM in almost all the key locations used in this study. For instance, the observed mean corresponding to the low rainfall location (location 2) is 53.50 mm, and the corresponding value of TVDM is 54.70 mm during the calibration period. The maximum observed (TVDM) mean is noticed as 137.4 mm (148.0 mm) at location 1. The standard deviation is also better modeled by TVDM. For instance, the observed and TVDM modeled standard deviation values at location 6 are 143.4 mm and 134.7 mm, respectively. The similar kind of results are found during the validation period (see Table 1). Further, the ability of TVDM in identifying the extreme values is assessed using the 90th and 95th percentile values as parameters. The good association between observed and TVDM is detected in this aspect also. For instance, the observed (TVDM modeled) 90th and 95th percentile values (in mm) during the calibration period at the upper GRB location (location 1) are noted as 451.90 (505.40) and 608.50 (628.60), respectively. The same values (in mm) at the lower GRB location (Location 10) are spotted as 278.60 (280.10) and 341.40 (322.30), respectively. More or less similar observations are noted during the validation period (refer to Table 1).

Furthermore, the effectiveness of TVDM is also tested using three vital statistical parameters (R, uRMSE and D_r), and the results are shown in Table 2. It is observed that the $\boldsymbol{R}$ value is ranging between 0.71 (location 2) and 0.86 (location 1) during the calibration period and the same is noticed as 0.72 and 0.75 during the validation period corresponding to the same locations. These results imply the good performance of TVDM in simulating the observed data over GRB. The degree of agreement (D_r) values ranges between 0.72 and 0.82 (see Table 2) during the calibration period, and the same is ranges between 0.68 and 0.79 during the validation period.

The visual variation of the observed and TVDM downscaled data is shown as scatter plot in Fig. 2. In this figure, the 45° line is represented with blue line, and the least square (best fit) line is identified with a red line. A 45° line or reference line is used to observe the correlation of the data; the nearer the points are to the reference line, the higher the correlation between the observed and the modeled data. A least square regression line or best fit line is the line that represents the best fit of the linear relationship between the variables. This line decreases the remoteness of the data from the regression line. The good association between observed and TVDM downscaled precipitation can be depicted in Fig. 2. The left panel is corresponding

Table 1 Performance metrics of observed and TVDM downscaled precipitation during Calibration period (1951–1990) and Validation period (1991–2005)

Period	Loc. no	Latitude (°N)	Longitude (°E)	Mean (mm)		Standard deviation (mm)		90th percentile (mm)		95th percentile	
				Observed	TVDM	Observed	TVDM	Observed	TVDM	Observed	TVDM
Calibration (1951–1990)	1	20.25	73.75	137.4	148.0	231.2	215.1	451.9	505.4	608.5	628.6
	2	19.50	75.50	53.5	54.7	76.8	68.0	165.5	139.6	212.3	159.4
	3	18.25	77.00	64.2	67.1	83.4	72.8	197.8	180.7	237.6	200.6
	4	20.00	77.75	80.2	82.2	117.4	106.7	248.2	253.9	325.3	287.0
	5	19.00	78.50	80.0	79.1	116.4	101.4	254.8	245.2	303.9	284.9
	6	21.00	79.50	98.6	99.1	143.4	134.7	326.3	331.8	395.7	368.5
	7	19.25	80.00	110.1	109.8	161.3	139.5	362.7	385.5	463.1	409.1
	8	17.50	81.25	101.2	100.4	123.9	101.1	281.0	274.9	338.1	310.3
	9	19.25	81.50	121.8	123.5	190.4	161.3	363.8	405.0	451.7	430.7
	10	18.75	82.75	107.6	113.8	117.3	101.7	278.6	280.1	341.4	322.3
Validation (1991–2005)	1	20.25	73.75	75.9	96.9	114.8	129.4	243.0	235.8	344.4	371.2
	2	19.50	75.50	69.1	56.1	106.1	94.1	234.1	225.4	285.9	255.7
	3	18.25	77.00	46.5	66.0	69.2	63.0	144.0	165.2	204.9	190.5
	4	20.00	77.75	73.3	82.0	115.2	92.4	226.7	243.7	322.3	258.0
	5	19.00	78.50	61.5	69.3	85.0	89.7	183.3	195.9	217.1	250.5
	6	21.00	79.50	71.5	88.7	104.2	110.3	241.5	314.1	307.0	330.2
	7	19.25	80.00	64.8	89.9	95.9	108.6	193.8	249.4	272.5	300.1
	8	17.50	81.25	61.6	79.4	83.6	101.2	183.4	196.9	239.1	268.9
	9	19.25	81.50	64.8	85.8	95.9	115.1	193.8	259.1	272.5	288.0
	10	18.75	82.75	56.8	76.9	77.6	94.1	182.4	266.6	215.8	278.2

Table 2 Performance measures during Calibration (1951–1990) and Validation (1991–2005) periods over the GRB

Location no.	R		uRMSE		D_r	
	Calibration	Validation	Calibration	Validation	Calibration	Validation
1	0.86	0.75	120.23	119.06	0.82	0.79
2	0.71	0.72	54.28	76.34	0.72	0.75
3	0.74	0.69	56.38	52.13	0.72	0.68
4	0.78	0.80	74.21	69.33	0.76	0.76
5	0.79	0.73	70.59	64.37	0.78	0.72
6	0.84	0.85	78.12	59.76	0.80	0.74
7	0.86	0.73	83.00	94.41	0.80	0.75
8	0.80	0.70	73.96	73.13	0.77	0.69
9	0.78	0.74	118.11	122.16	0.79	0.75
10	0.81	0.71	68.24	66.53	0.77	0.74

to the calibration period, and the right panel is a representation of the validation period. It is visually clear that the lower rainfall values have been overestimated by the TVDM and the higher values are slightly underestimated. A better version of these results can be expected after applying the bias correction. Overall, a good association between observed and TVDM downscaled precipitation is identified for the selected study area.

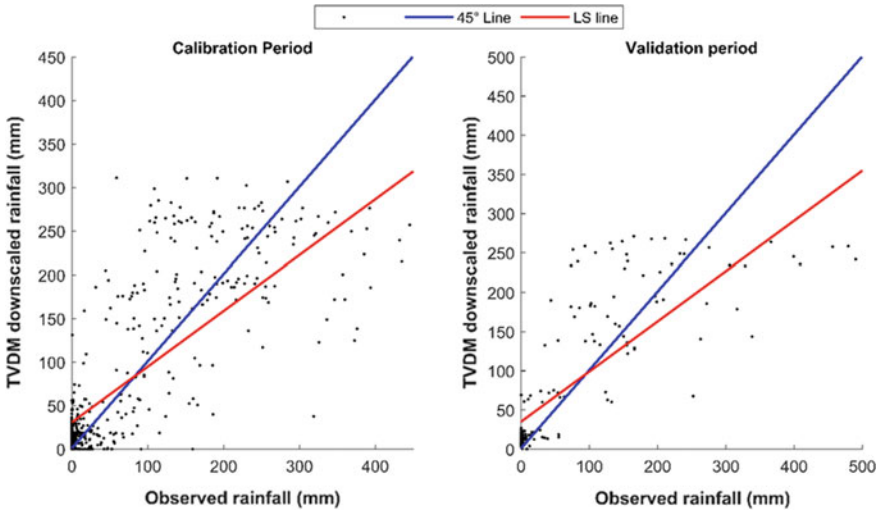

Fig. 2 Scatter plot between observed and TVDM downscaled precipitation during calibration and validation periods at location 4 in the study area map

5 Conclusions

The following conclusions are derived from this study-

(i) It is concluded that the Time-Varying Downscaling Model (TVDM) was found beneficial in downscaling the rainfall over the Godavari River Basin (GRB). It is confirmed through rigorous statistical checks.
(ii) The efficacy of TVDM in simulating the extreme events (90th and 95th percentiles are used in this study) is also demonstrated.
(iii) The ability of the model is tested using various statistical parameters, e.g., the ***R*** value ranges between 0.71 and 0.86.
(iv) The developed model can be used for downscaling the future precipitation, and the outputs can be used as an input in any rainfall-runoff model for modelling the future runoff/streamflow.
(v) The methodology of this study is general enough and can be applied for any other basin/region in the world for downscaling any hydroclimatic variable(s).

Acknowledgements The authors acknowledge the financial support received from Department of Science and Technology (DST), Startup Research Grant (SRG) Scheme, Ministry of Science and Technology, Government of India **(Ref No. DST/SRG/2020/000823)** to carry out present work. The authors are also thankful to India Meteorological Department (IMD) for providing the necessary data to conduct the present study.

References

1. Meehl GA, Covey C, Delworth D, Latif M, Mcavaney B, Mitchell JFB, Stouffer RJ, Taylor KE (2007) The WCRP CMIP3 multimodel dataset a new era in climate change research. Bull Am Meteorol Soc 88(9):1389–1394. http://cera-www.dkrz.de/IPCC_DDC
2. Pichuka S, Maity R (2018) Development of a time-varying downscaling model considering non-stationarity using a Bayesian approach. Int J Climatol 38(7):3157–3176. https://doi.org/10.1002/joc.5491
3. Linderson M-L, Achberger C, Chen D (2004) Statistical downscaling and scenario construction of precipitation in Scania, Southern Sweden. https://doi.org/10.2166/nh.2004.0019
4. Fowler HJ, Blenkinsop S, Tebaldi C (2007) Linking climate change modelling to impacts studies: recent advances in downscaling techniques for hydrological modelling. Int J Climatol 27(12):1547–1578. https://doi.org/10.1002/joc.1556
5. Maraun D et al (2010) Precipitation downscaling under climate change: recent developments to bridge the gap between dynamical models and the end user. Rev Geophys 48(3):003–037. https://doi.org/10.1029/2009RG000314
6. Druyan LM, Fulakeza M, Lonergan P (2002) Dynamic downscaling of seasonal climate predictions over Brazil. J Clim 15(23):3411–3426
7. Schmidli J et al (2007) Statistical and dynamical downscaling of precipitation: an evaluation and comparison of scenarios for the European Alps. J Geophys Res Atmospheres 112(4):105–125. https://doi.org/10.1029/2005JD007026
8. Orskaug E et al (2011) Evaluation of a dynamic downscaling of precipitation over the Norwegian mainland. Tellus, Series A: Dyna Meteorology Oceanography 63(4):746–756. https://doi.org/10.1111/j.1600-0870.2011.00525.x

9. de Sales F, Xue Y (2013) Dynamic downscaling of 22-year CFS winter seasonal hindcasts with the UCLA-ETA regional climate model over the United States. Clim Dyn 41(2):255–275. https://doi.org/10.1007/s00382-012-1567-x
10. Bates BC, Charles SP, Hughes JP (1998) Stochastic downscaling of numerical climate model simulations. Environ Model Softw 13(3–4):325–331. https://doi.org/10.1016/S1364-8152(98)00037-1
11. Goubanova K et al (2011) Statistical downscaling of sea-surface wind over the Peru-Chile upwelling region: diagnosing the impact of climate change from the IPSL-CM4 model. Clim Dyn 36(7):1365–1378. https://doi.org/10.1007/s00382-010-0824-0
12. Clark PU et al (2012) Global climate evolution during the last deglaciation. National Acad Sci 109(19):E1134–E1142. https://doi.org/10.1073/pnas.1116619109/-/DCSupplemental
13. Sun C, Monahan AH (2013) Statistical downscaling prediction of sea surface winds over the global ocean. J Clim 26(20):7938–7956. https://doi.org/10.1175/JCLI-D-12-00722.1
14. Paschalis A, Molnar P, Fatichi S, Burlando P (2013) A stochastic model for high-resolution space-time precipitation simulation. Water Resour Res 49(12):8400–8417. https://doi.org/10.1002/2013WR014437
15. Rummukainen M et al (2001) A regional climate model for northern Europe: model description and results from the downscaling of two GCM control simulations. Clim Dyn 17(5–6):339–359
16. Seibert J, Halldin S (1996) 211±236) and NOPEX data
17. Guan L (2009) Preparation of future weather data to study the impact of climate change on buildings. Build Environ 44(4):793–800. https://doi.org/10.1016/J.BUILDENV.2008.05.021
18. Pai DS, Sridhar L, Rajeevan M, Sreejith OP, Satbhai NS, Mukhopadyay B (2014) Development of a new high spatial resolution (0.25° × 0.25°) Long Period (1901-2010) daily gridded rainfall data set over India and its comparison with existing data sets over the region. MAUSAM 65(1):1–18
19. Chylek LA et al (2011) Guidelines for visualizing and annotating rule-based models †. Mol Biosyst 7(10):2779–2795. https://doi.org/10.1039/b000000x
20. Christian JR et al (2010) The global carbon cycle in the Canadian Earth system model (CanESM1): Preindustrial control simulation. J Geophys Res Biogeosci 115(3):014–034. https://doi.org/10.1029/2008JG000920
21. Saatloo SME, Siosemarde M, Hosseini SA, Rezaei H (2020) Variability assessment of simulated recharge resulted from precipitation using different GCMs, case study: west shore of Lake Urmia, Iran. Arab J Geosci 13(14):610. https://doi.org/10.1007/s12517-020-05567-5
22. Freni G, Mannina G (2010) Bayesian approach for uncertainty quantification in water quality modelling: the influence of prior distribution. J Hydrol 392(1–2):31–39. https://doi.org/10.1016/j.jhydrol.2010.07.043
23. Maity R, Kumar DN (2006) Bayesian dynamic modeling for monthly Indian summer monsoon rainfall using El Niño-Southern Oscillation (ENSO) and Equatorial Indian Ocean Oscillation (EQUINOO). J Geophys Res Atmospheres 111(7):104–116. https://doi.org/10.1029/2005JD006539
24. Kumar DN, Maity R (2008) Bayesian dynamic modelling for nonstationary hydroclimatic time series forecasting along with uncertainty quantification. Hydrol Processes 22(17):3488–3499. https://doi.org/10.1002/hyp.6951
25. Sarhadi A, Burn DH, Ausín MC, Wiper MP (2016) Time-varying nonstationary multivariate risk analysis using a dynamic Bayesian copula. Water Res Research 52(3):2327–2349. https://doi.org/10.1002/2015WR018525
26. Tyralis H, Koutsoyiannis D (2014) A Bayesian statistical model for deriving the predictive distribution of hydroclimatic variables. Clim Dyn 42(11–12):2867–2883. https://doi.org/10.1007/s00382-013-1804-y
27. Vrugt JA, ter Braak CJF, Gupta H, Robinson BA (2009) Equifinality of formal (DREAM) and informal (GLUE) Bayesian approaches in hydrologic modeling?" Stochastic Environm Res Risk Assess 23(7):1011–1026. https://doi.org/10.1007/s00477-008-0274-y

28. Yang J, Reichert P, Abbaspour KC (2007) Bayesian uncertainty analysis in distributed hydrologic modeling: a case study in the Thur River basin (Switzerland). Water Resour Res 43(10):401–414. https://doi.org/10.1029/2006WR005497
29. Pichuka S, Maity R (2017) Spatio-temporal downscaling of projected precipitation in the 21st century: indication of a wetter monsoon over the Upper Mahanadi Basin, India. Hydrol Sci J 62(3):467–482. https://doi.org/10.1080/02626667.2016.12418

Assessment of Kernel Regression Based Statistically Downscaled Rainfall Over Tapi River Basin, India

Lalit Kumar Gehlot, P. L. Patel, and P. V. Timbadiya

Abstract The downscaling of coarser scale general circulation model (GCM) variables, preferably the rainfall and temperature, to finer resolution followed by estimation of uncertainty/bias in the downscaled outcomes are essentially required prior to their application for hydrological assessments and decision-making. The kernel regression-based statistical downscaled (KRSD) rainfall data of five GCM models, from Coupled Model Intercomparison Project Phase-5 (CMIP-5), have been assessed to ascertain their ability to simulate the magnitude, variability, and extremes of Indian summer monsoon rainfall (ISMR) over the Tapi River basin (TRB) in India. The KRSD rainfall of GCMs is compared with gridded rainfall data obtained from India Meteorological Department-Pune (IMD) for the period 1951–2005 on annual and monsoon months (JJAS). The GCMs underestimate annual rainfall (PRCPTOT) on average by 21.7–28.4% over the TRB. Further, GCMs overestimate the number of rainy days (RD) and longest spell of consecutive rainy days (CWD) at an annual scale vis-à-vis IMD gridded rainfall dataset. The four-to seven-fold overestimation of CWD and RD is observed during September month compared to June, July, and August months. Also, one-day (Rx1D), five-day (Rx5D), and rainfall extremes above 95th percentile value (R95) from GCMs observed underestimation of the parameters ranging from 46.4 to 52.7%, 41.4 to 44.1%, and 45.0 to 48.8%, respectively. The present investigation concludes that the GCM fails to account for the seasonality of

L. K. Gehlot (✉) · P. L. Patel · P. V. Timbadiya
Department of Civil Engineering, Sardar Vallabhbhai National Institute of Technology Surat, Surat 395007, India
e-mail: gehlot.lalit1994@gmail.com

P. L. Patel
e-mail: plpatel@ced.svnit.ac.in

P. V. Timbadiya
e-mail: pvtimbadiya@ced.svnit.ac.in

P. V. Timbadiya et al. (eds.), *Climate Change Impact on Water Resources*, Lecture Notes in Civil Engineering 313, https://doi.org/10.1007/978-981-19-8524-9_4

ISMR over TRB. Overall, KRSD rainfall underestimates the PRCPTOT and rainfall extremes while overestimating the RD and CWD over the TRB. Thus, rainfall intensities are significantly underestimated for the historical period over TRB.

Keywords General circulation models (GCMs) · CMIP-5 · Kernel regression based statistical downscaling (KRSD) · Rainfall-indices · Tapi Basin

1 Introduction

The increasing greenhouse gas emission and local-scale anthropogenic changes have altered hydroclimatic variability, in general, and rainfall patterns across India, in particular [1]. Also, their consequential effects on regional hydrology have drawn the attention of governments, academic/climate researchers, and field agencies [2]. The general circulation models (GCMs) are widely used to understand the effects of various forcing conditions on current and future climate; however, their applicability is at the global scale. Therefore, they cannot be used directly for regional hydrologic estimations [3]. Downscaling, statistical or dynamic, is a technique by which the large-scale GCM predictors can be transformed to local-/regional-scale hydro-meteorological variables [2]. Statistical downscaling, being more accessible and computationally efficient, has been widely used by climate researchers. It is employed to establish a statistical relationship between large-scale climate variables/atmospheric patterns to the variable of interest at the local scale. These relationships are assumed to be valid for downscaling of future rainfall data. This assumption is one of the limitations of statistical downscaling techniques [5]. Broadly, statistical downscaling methods are classified as weather generator, weather typing, and regression or transfer function model [4, 5]. The details of various statistical downscaling techniques can be found in Lee and Singh [5]. The daily scale downscaling of rainfall at multiple sites is often very challenging. A rainfall event is a complex interaction of numerous climatic variables, oceanic circulation patterns, etc., and varies primarily over space. Kannan and Ghosh [2] developed a rainfall state-based method to overcome this problem, further extended by Salvi and Ghosh [4] for daily rainfall projections for seven meteorologically homogeneous regions of India using the kernel regression. Shashikant et al. [6] have emphasized on the downscaled rainfall extremes over India. The scientific advancements in atmospheric science help us understand the likely climate scenarios in the near future. The hydrologic response to these future climate scenarios is the fundamental interest of hydrologists for suitable measures/policies to be brought into practice.

The Tapi River Basin (TRB) is the second-largest west-flowing river of India, with a basin area of approximately 2% of the geographical area of India. TRB is climatologically heterogeneous, and the monsoon season is the primary source of water availability in the basin. The decreasing annual total rainfall and rising rainfall extremes in TRB lead to increased water stress conditions, thus widely affecting the socio-economic and agricultural activities in the basin. An attempt to understand the

climate scenarios over TRB is made in the present investigation; however, it is limited to ascertaining the efficacy of the kernel regression-based statistical downscaled (KRSD) rainfall over TRB. The outcomes of the present study will help to understand the accuracy of long-term historical predictions over TRB, and future estimates can be interpreted accordingly.

2 Study Area and Data Source

2.1 Tapi River Basin

The Tapi River is the sixth-largest river of Peninsular India and the second-largest westward flowing river draining into the Arabian Sea. The TRB, in west-central India, has a drainage area of 65,145 km^2, which is about 2% of the geographical area of India. The Tapi River originates at an elevation of 752 m near Multai in Betul district of Madhya Pradesh state and traverse a total distance of 724 km through three different states, viz, Madhya Pradesh (282 km), Maharashtra (228 km), and Gujarat (214 km), before falling into the Gulf of Khambhat near Surat city. The Tapi basin is subdivided into Upper Tapi basin (UTB $\approx$ 29,430 km^2), Middle Tapi basin (MTB $\approx$ 32,925 km^2), and Lower Tapi basin (LTB $\approx$ 2,790 km^2), wherein UTB, MTB, and LTB extend from the origin of Tapi River to the Hatnur dam, from the Hatnur dam to the Ukai dam, and from the Ukai dam to the Arabian sea, respectively (Fig. 1).

The average rainfall of the Tapi basin has been reported to be 815.7 mm, while corresponding values for UTB, MTB, and LTB are 839.2 mm, 742.9 mm, and 1284.6 mm, respectively. The Indian Summer Monsoon Rainfall (ISMR) primarily governs the availability of freshwater in TRB and the significant portion of India. The ISMR has been classified into four different seasons, viz. monsoon (Jun–Sept), post-monsoon (Oct–Nov), winter (Dec–Feb), and pre-monsoon (Mar–May). The south-west monsoon in the basin, on average, onsets by mid-June and withdraws by the first week of October. The Tapi basin receives approximately 90% of annual rainfall during the monsoon season, followed by post-monsoon (7.0%), pre-monsoon (1.6%), and winter (1.4%) seasons. The rainfall during June, July, August, and September months is 16.4%, 29.0%, 26.5%, and 18.1%, respectively of annual rainfall. From the global maps of the Köppen-Geiger climate classification, at spatial resolution of 0.5° for the period 1951–2000, it is found out that nearly 48.5% of the basin area is classified as semi-arid region (BSh), while remaining 51.5% region experiences sub-humid climate (tropical dry savannah-As, and tropical wet savannah-Aw).

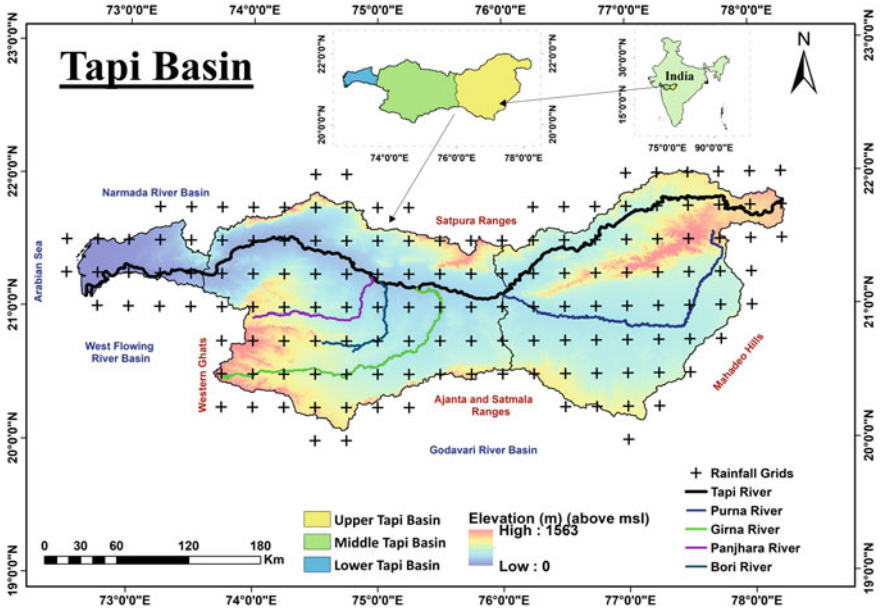

Fig. 1 Index map of Tapi basin showing rainfall grids at 0.25° resolution

2.2 Data Used

The rainfall of five GCM models (see Table 1) statistically downscaled using the kernel regression method [5, 7] has been used in the present study. The downscaled data at the spatial resolution of 0.25° has been obtained from the research project "Statistical Downscaling for Hydroclimatic projections with CMIP5 simulations to assess Impact of Climate Change" funded by the Indian National Committee on Climate Change (INCCC), Ministry of Jal Shakti, Department of Water Resources, River Development & Ganga Rejuvenation, Government of India. The gridded rainfall data of India Meteorological Department (IMD), Pune, at a similar spatial resolution, has been used as a reference dataset for statistical comparison of the downscaled data. The rainfall data of IMD and GCM historical period is analyzed from 1951 to 2005.

Table 1 Global climate models used in the present analysis

GCM model	Details
BMU ESM	Beijing Normal University Earth System Model, China
CCCma-CanESM2	Canadian Centre for Climate Modelling and Analysis-Second generation Canadian Earth System Model
CNRM CM5	Centre National de Recherches Meteorologiques, France
MPI ESM LR	Max Planck Institute for Meteorology (Germany) Earth System Model running on low resolution grid
MPI ESM MR	MPI ESM running on mixed resolution grid

The GCM models are denoted/cited/named as BNU, CCCma, CM5, MPI-LR and MPI-MR respectively

3 Results and Discussions

3.1 Rainfall Characteristics

The coarser scale GCM data for the five GCM models statistically downscaled using kernel regression is used for its performance assessment in representing the Indian Summer Monsoon Rainfall (ISMR) over the TRB. The various characteristics of ISMR, i.e., magnitude, duration, frequency, and extremes, have been used to quantify the performance of KRSD rainfall data w.r.t. IMD gridded rainfall data. The six indices representing different characteristics of ISMR and used in the present study are tabulated in Table 2. The percentage deviations in the index obtained from GCM data have been estimated as $\frac{I_{\text{IMD}} - I_{\text{GCM}}}{I_{\text{IMD}}} * 100$ where I_{IMD} and I_{GCM} represents the index value calculated using IMD data and KRSD rainfall data, respectively. Since the water availability in TRB is monsoon driven, the percentage deviations in the aforesaid rainfall characteristics have been estimated for June, July, August, and September months along with annual estimates.

The normal PRCPTOT of TRB ranges from 519.0 to 1460.0 mm with large scale spatial variability. The headwater region of Tapi River and LTB usually receives more rainfall than the basin mean rainfall of 796.5 mm indicating non-homogeneity of ISMR over TRB. The historical simulations of rainfall obtained from five GCM models, downscaled to 0.25° spatial resolution are analyzed, and their percentage deviations are shown in Fig. 2. From Fig. 2, it is apparent that the PRCPTOT for June month is underestimated by all the GCM models. The average (and variability range) error (in %) over TRB for June month is 18.8 (40.2–19.2) for BNU ESM, 47.1 (64.7–17.7) for CanESM2, 55.7 (78.9–24) for CNRM CM5, 18.7 (45.5–12.9) for MPI ESM LR, and 33.3 (53.6–4.7) for MPI ESM MR GCM models. The respective error (in %) estimates for July, August, and September month are 19.6 (41.5–9.7), 41.6 (73–23.4), 33.0 (54.5–2.6), 19.4 (45.3–0.1) and 19.8 (41.9–6.8); 21.0 (51.3–17.8), 14.6 (35.7–18.4), 28 (61.4–44.9), 24.7 (43.0–10.5) and 20.6 (37.8–25.0); and

Table 2 Rainfall indices used in present study

Indicator	Indicator name	Indicator definitions	Units
PRCPTOT	Total annual rainfall	Annual rainfall from days ≥ 2.5 mm	mm
RD	Rainy days	Number of days when rainfall ≥ 2.5 mm	days
Rx1D	Maximum 1-day rainfall	Annual maximum 1-day rainfall	mm
Rx5D	Maximum 5-day rainfall	Annual maximum consecutive 5-day rainfall	mm
R95	Very wet days	Annual total rainfall from days > 95th percentile	mm
CWD	Consecutive wet days	Maximum number of consecutive days when rainfall ≥ 2.5 mm	days

The 95th percentile threshold at individual grid point is calculated using monsoon rainfall for the period 1951–2005

31.2 (61.9–6.0), −4.8 (49.3–64.2), −5.5 (35.7–65.2), 17.6 (57.6–9.3), and 9.1 (52.3–42.7), respectively. However, on annual scale the percentage error (%) estimates for aforesaid GCM models are 23.1 (44.3–0.9); 23.1 (50.8–33.1), 28.4 (50.5–12.9), 21.7 (37.6–7.8), and 22.7 (38.5–3.5), respectively. It can also be seen that the GCM rainfall estimates are more in LTB particularly during August and September months. From the error estimates during monsoon months and annual time scale, it can be stated that the monsoonal rainfall has been underestimated while the non-monsoonal rainfall has been overestimated. In other words, the monsoon/seasonal cycles of ISMR over TRB have not been simulated well. Overall, based on the error estimates, the MPI ESM LR model can be considered better that the remaining GCM models.

The number of days having rainfall more than 2.5 mm, defined as a rainy day (RD), may be considered important from the hydrological perspective in conjunction to the prevailing wet soil conditions in the area. The number of RDs obtained from KRSD rainfall data and their relative deviations w.r.t. IMD data are shown in Fig. 3. The mean (variability range) RDs for TRB ranges from 36 to 74.5 days (8.0–14.6 days)

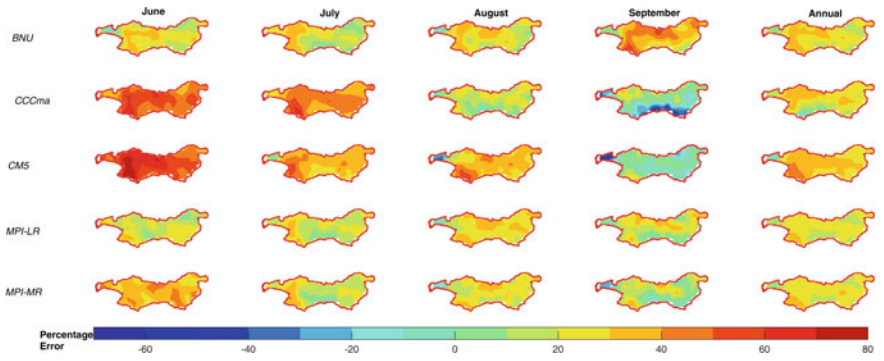

Fig. 2 Percentage error in PRCPTOT derived from KRSD-Historical period rainfall

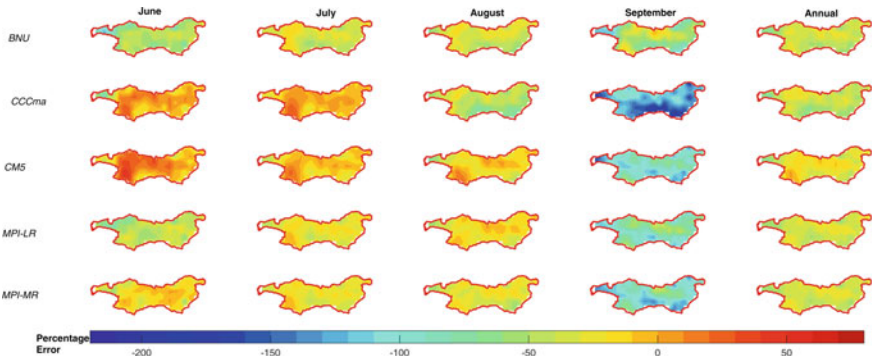

Fig. 3 Percentage error in RD derived from KRSD-Historical period rainfall

with maximum RDs in headwater regions of TRB. The error estimates for GCM RDs with reference to IMD (see Fig. 3) show that all the GCMs have overestimated the RD for the historical period, except a few instances in the leeward side of the Western Ghats in MTB, where underestimation is observed during June and July months. The mean percentage deviations (%) in RD during the monsoon months (JJAS) for BNU ESM, CanESM2, CNRM CM5, MPI ESM LR, and MPI ESM MR models are −57.4, −33.0, −36.5 and −62.5; −8.8, −3.5, −46.3 and −130.0; 0.4, −12.1, −20.2 and −99.6; −46.1, −25.1, −21.8 and −82.3; and −20.0, −25.1, −29.8 and −99.8 respectively. The mean (and variability range) percentage deviation at annual scale for aforesaid GCM models are −41.5 (−14.7 to −76.0), −42.2 (−11.3 to −85.5), −28.5 (4.1 to −70.3), −36.8 (−15.9 to −65.9) and −36.9 (−17.1 to −67.1) respectively. The RD in September month is poorly simulated by all the GCM models with many fold overestimation. The CNRM CM5 model seems to simulate RDs fairly with the least mean error, probably due to simultaneous over/underestimation at various grids. The overestimation of the RDs and underestimated PRCPTOT, in general, suppress the expected simple daily intensity of the rainfall.

The one-day and five-day maximum rainfall (Rx1D and Rx5D) are significantly important for pluvial flooding and erosion point of view. The mean Rx1D and Rx5D over TRB range from 57.0 to 159.3 mm and 113.0 to 348.8 mm, respectively. The estimated errors in Rx1D show that the GCM simulated one-day maximum rainfall during monsoon months (JJAS) is underestimated by 50% (on average). The percentage deviation (%) range during JJAS for BNU ESM, CanESM2, CNRM CM5, MPI ESM LR and MPI ESM MR models is 45.5–57.2, 48.1–58.6, 39.9–64.1, 41.6–51.6 and 40.5–51.8 respectively, while their respective mean (and variability range) percentage deviations at annual scale are 52.7 (64.1–29.2), 50.0 (64.3 to −23.8), 46.4 (62.4–16.4), 47.8 (62.4–25.5) and 48.6 (62.8–21.2) (see Fig. 4). Similarly, the corresponding results for Rx5D during JJAS months for aforesaid GCM models are 35.0–46.3, 34.6–51.8, 27.1–57.4, 31.2–39.9 and 30.8–39.6 respectively with their annual estimates of mean percentage deviation (variability range) by 44.1

(56.4–23.3), 41.4 (54.5 to −73.6), 41.5 (55.9–7.1), 41.6 (53.7–27.2) and 41.8 (54.3–27.6) respectively (see Fig. 5). The MPI ESM LR can be considered to outperform remaining models for June, July, and August months while CNRM CMS has considerably performed better for September month with minor overestimation of Rx1D and Rx5D for the LTB region. The annual estimates show that MPI ESM LR and CNRM CM5 have shown relatively better estimation of Rx5D and Rx1D across the Tapi basin for the historic period. The underestimation of such extreme events by GCM models might lead to a false representation of reduced chances of pluvial flooding, erosion, and other damages in the study region.

The rainfall amount of more than 95% threshold (R95) plays a crucial role in hydrologic assessments and designs. The mean (spatial variability range) R95 for TRB ranges from 245.0 to 646.9 mm (103.0–458.6 mm). The estimated errors in R95 show that the GCM simulated very wet days during monsoon months (JJAS) are underestimated by 48.1% (on average). The percentage deviation (%) range during JJAS for BNU ESM, CanESM2, CNRM CM5, MPI ESM LR, and MPI ESM MR

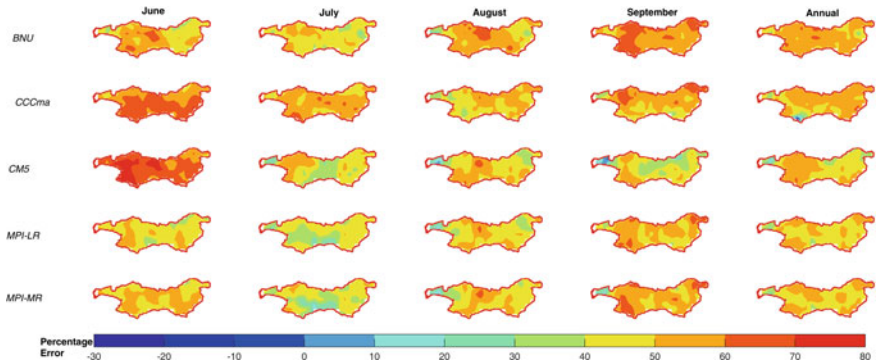

Fig. 4 Percentage error in Rx1D derived from KRSD-Historical period rainfall

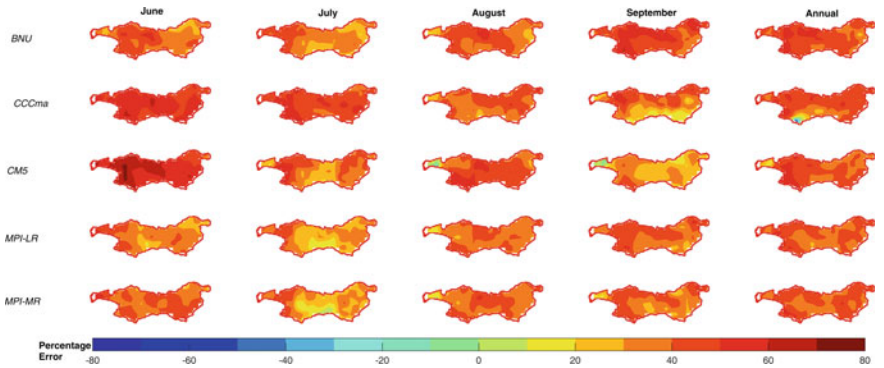

Fig. 5 Percentage error in Rx5D derived from KRSD-Historical period rainfall

models is 37.5–71.6, 34.5–59.1, 29.9–73.6, 34.1–63.0, and 33.4–63.6, respectively, while their respective mean (and spatial variability range) percentage deviations are 48.8 (59.7–33.5), 45.0 (60.8–71.1), 45.2 (61.5–15.7), 45.2 (57.2–32.6), and 46.8 (59.5–26.3) (see Fig. 6). MPI ESM LR, MPI ESM MR, CanESM2, and CNRM CM5 reasonably simulated R95 for June and Annual scale, July, August, and September, respectively, during the historical period.

The consecutive spell of rainy days (CWD) significantly affects predicting hydrological variables in a river basin. The mean (variation) RD for the Tapi basin ranges from 5.0 to 19.7 days (1.0–9.7 days). The large-scale overestimation of the CWD has been seen during the monsoon months with mean overestimation of 75.6% and ranging from 13.8 to 238.3% (see Fig. 7). The percentage overestimation during September month is four to seven-fold larger than June, July, and August months. The MPI ESM LR has been found to reasonably simulate the longest consecutive spells over the Tapi basin.

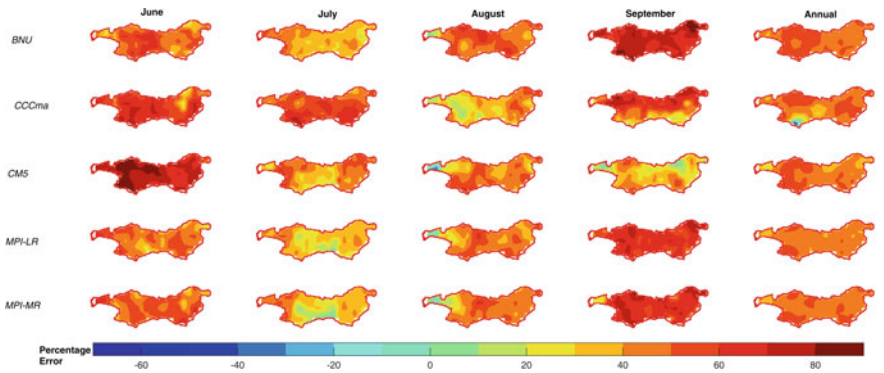

Fig. 6 Percentage error in R95 derived from KRSD-Historical period rainfall

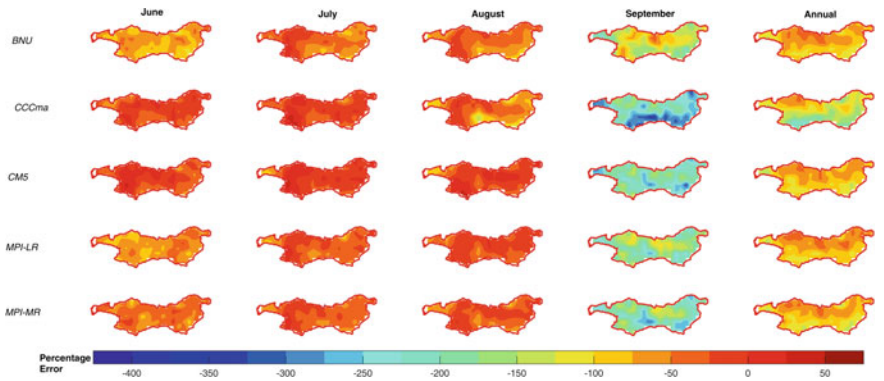

Fig. 7 Percentage error in CWD derived from KRSD-Historical period rainfall

3.2 Sub-Basin Wise Rainfall Distribution

The spatial distribution of rainfall varies significantly due to its geographical setting, i.e., the Western Ghats and the large water mass (the Arabian Sea) is the reason for the highest magnitude of rainfall in LTB. On the other hand, the region on the leeward side of the Western Ghats receives the least rainfall in the basin. The narrow valley of UTB, i.e., Burhanpur sub-catchment between Satpura hills and Gwaligarh hills, also receives rainfall above the average rainfall of TRB. The empirical cumulative distribution functions (eCDF) of observed daily rainfall over three sub-basins of TRB are compared with KRSD rainfall data. The rainfall events are further sub-divided into three categories, i.e., high, medium, and low rainfall depths with their respective exceedance probability ranging above 95%, between 95 and 70%, and below 70%, as shown in Fig. 8. The low rainfall depths are generally overestimated by all the GCM models, particularly for LTB. For UTB and MTB, the low rainfall depths are reasonably overestimated due to mixed behavior. Similar patterns are also evidenced in the simulation of RD in TRB. The large-scale overestimation of RD is mainly due to poor simulation of the low rainfall depth over TRB.

Similarly, the KRSD rainfall underestimates moderate and large rainfall depths, as seen from Fig. 8. However, the deviation in medium rainfall depths is highest in UTB, while the MTB received the least one-day maximum rainfall from KRSD data. Similar evidence can be seen in the spatial variation of the one-day maximum rainfall depth simulation over TRB see Fig. 4. The overall underestimation of the Rx1D rainfall seems to be the primary factor responsible for the general underestimation of mean/total rainfall in TRB. The variation in the simulation of various rainfall depths over TRB, in general, and three sub-basins, in particular, are the indicators that the GCM models and, thus, KRSD models are not able to account for the seasonality of the ISMR, and therefore, the future simulations are required to be interpreted accordingly.

4 Conclusions

The following conclusions are derived from the foregoing study:

- The annual rainfall (PRCPTOT) estimated by the GCM is found to be underestimated by 21.7−28.4% (on average) on annual scale with random over/under estimations. The MPI ESM LR is found to outperform other GCM models in case of PRCPTOT.
- Large-scale overestimations have been observed in the number of rainy days (RD) and maximum spell of consecutive rainy days (CWD) annually, while the overestimation for September months is four-to seven-fold as compared to June, July, and August. The mean overestimation for both the indices ranges from 28.5% to 42.2% and 77.2% to 128.4% wherein CNRM CM5 and MPI ESM LR simulated well these two rainfall indices, respectively.

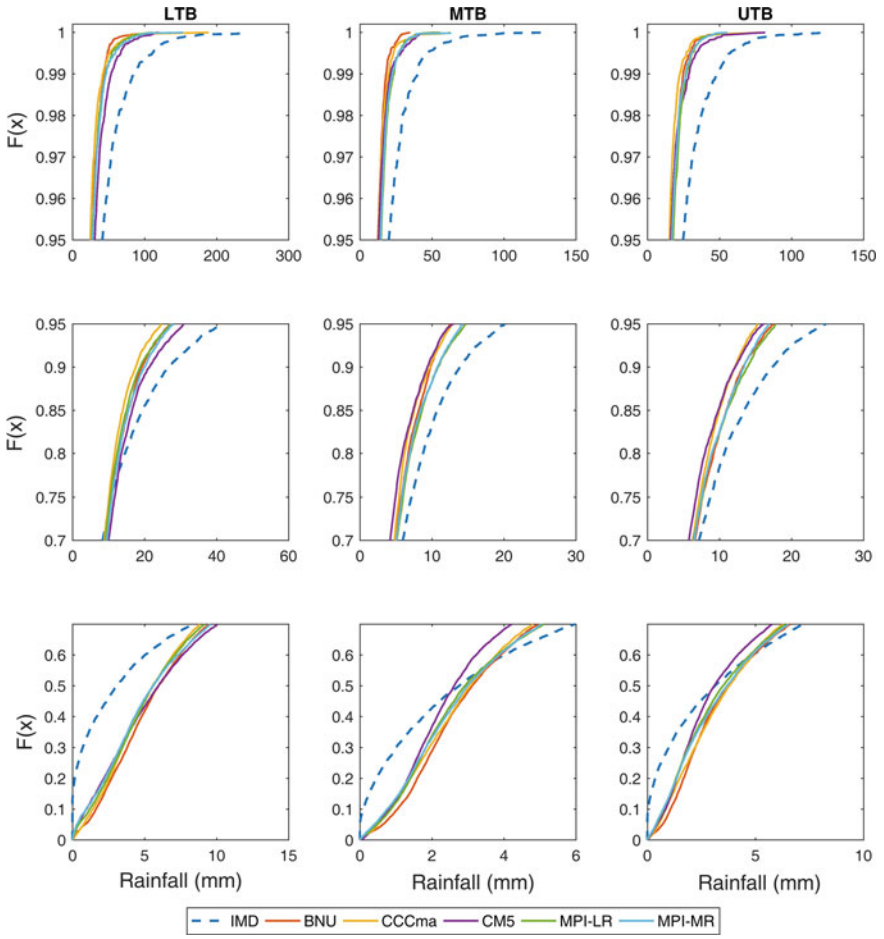

Fig. 8 Empirical cumulative distribution function of daily rainfall for LTB, MTB, and UTB; (a–d–g, b–e–h, and c–f–i show the different segments of eCDF representing extremes, moderate, and low rainfall depths)

- The extreme indices Rx1D, Rx5D, and R95, on annual scale, showed the percentage errors ranging from 46.4% to 52.7%, 41.4% to 44.1% and 45.0% to 48.8%, respectively. MPI ESM LR and CNRM CM5 have been found to fairly simulate Rx5D, R95, and Rx1D during the historical period at annual scale.

Acknowledgements The authors would like to acknowledge the Indian National Committee on Climate Change, Ministry of Jal Shakti, Department of Water Resources, River Development & Ganga Rejuvenation, Government of India (GoI) for providing funding for this research. The statistical downscaling team of INCCC projects is duly acknowledged for making downscaled rainfall data available. The authors are also thankful to Prof. Subimal Ghosh, IIT Bombay for providing healthy discussions related to the data used. The authors would also appreciate the infrastructural

support provided by Centre of Excellence on 'Water Resources and Flood Management', TEQIP-II, Ministry of Education, GoI.

References

1. Vittal H, Karmakar S, Ghosh S (2013) Diametric changes in trends and patterns of extreme rainfall over India from pre-1950 to post-1950. Geophys Res Lett 40(12):3253–3258
2. Kannan S, Ghosh S (2011) Prediction of daily rainfall state in a river basin using statistical downscaling from GCM output. Stoch Env Res Risk Assess 25(4):457–474
3. Singh S, Kannan S, Timbadiya PV (2016) Statistical downscaling of multisite daily precipitation for Tapi basin using kernel regression model. Curr Sci 110(8):1468–1484
4. Salvi K, Ghosh S (2013) High-resolution multisite daily rainfall projections in India with statistical downscaling for climate change impacts assessment. J Geophys Res: Atmospheres 118(9):3557–3578
5. Lee T, Singh VP (2018) Statistical downscaling for hydrological and environmental applications. CRC Press
6. Shashikanth K, Ghosh S, Vittal H, Karmakar S (2018) Future projections of Indian summer monsoon rainfall extremes over India with statistical downscaling and its consistency with observed characteristics. Clim Dyn 51(1–2):1–15
7. Kannan S, Ghosh S (2013) A nonparametric kernel regression model for downscaling multisite daily precipitation in the Mahanadi basin. Water Resour Res 49(3):1360–1385

Analysis of Uncertainty Due to Climate Change Using REA Approach in Different Regions of Western Ghats, South India

Navya Chandu and T. I. Eldho

Abstract The evaluation of climate change impacts on hydrology using Global Climate Models (GCM) and emission scenarios is incomplete, without quantifying the uncertainty associated with it. As the uncertainties play a significant role in such analysis, it is important to quantify them in order to develop productive management and decision-making capabilities. The objective of the present study is to model the GCM and scenario uncertainty in the Western Ghats (WG) region of South India using Reliability Ensemble Average (REA) for the estimation of stream flows. The analysis is carried out grid-wise, for monsoon (JJAS) rainfall in near future (2011–2040). The statistically downscaled (kernel regression) rainfall data at 0.25° resolution for 5 CMIP-5 GCMs CNRM, CCCMA, MPIMR, MPILR, and BNU for RCP 4.5 and 8.5 are used in the present study. The upper-middle and lower regions along with the elevation profile (lowland, midland, and ghats) of WG are chosen as a criterion for quantifying the uncertainty associated with GCM models and emission scenarios. Irrespective of the topography criteria, the uncertainty associated with GCM is found to be more significant than the scenario uncertainty. The GCM model shows a good correlation with the latitude profile in WG. The GCM MPILR and CCCMA have higher weightage in lower and middle regions as compared to the others while the GCM CNRM is less pronounced in the high elevation zones along the basin.

Keywords Climate change · Uncertainty · REA approach

N. Chandu (✉) · T. I. Eldho
Department of Civil Engineering, Indian Institute of Technology Bombay, Mumbai, India
e-mail: nav.nav93@gmail.com

P. V. Timbadiya et al. (eds.), *Climate Change Impact on Water Resources*, Lecture Notes in Civil Engineering 313, https://doi.org/10.1007/978-981-19-8524-9_5

1 Introduction

As the hydrological cycle is severely affected by climate change, the available water resources in a region are dependent on climate change and its impacts. Generally, the climate change projections are carried out based on Global Climate Models (GCM) models. Such models are characterized by lower confidence levels and higher uncertainty levels [2]. Atmosphere–Ocean General Circulation Models (AOGCMs) are capable of showing differences in climate variables under the same forcing scenarios, which thereby results in uncertainty and it is also difficult to identify the most reliable GCMs. Therefore, it is better to create an ensemble product based on the collective information from available GCM simulations.

In the recent past, multi-model averaging techniques have become one of the most common approaches to identify the performance of a model as well as to create a large ensemble of simulations corresponding to climate change [1] and the rainfall-runoff process [3]. The simplest method of taking arithmetic means to a probability-based approach such as Bayesian [6] can be used for the estimation.

With climate change posing the biggest threat to our planet and hydrological cycle, quantitative assessment and possible reduction of the contribution of uncertainty in future climate predictions is very important. In this study, the uncertainty of a few selected GCMs for a hydrological impact study of the Western Ghats region in South India is considered. We consider five CMIP-5 GCMs and introduce the Reliability Ensemble Averaging (REA) method for quantification of uncertainty and reliability associated with climate model projections of JJAS Indian summer monsoon climate. Correlating the uncertainty and performance of GCMs region-wise and understanding their significance is the major scope of this study.

2 Study Area

West flowing rivers from Tadri to Kanyakumari which are classified as West Flowing River Basin -2 (WFRB-2) by Central Water Commission (CWC) is shown in Fig. 1. Basin is geographically located in the south-western corner of peninsular India, and lies between 8° 0’ 00” and 14° 24′ 00′′ N latitudes and 74° 25′ 00”–77° 36′ 00” E longitudes (www.india-wris.nrsc.gov.in). The whole basin consists of 43 small and medium river systems. In the basin terrain, with an average elevation greater than 600 m are Western Ghats hills which act as boundaries for the basin. Figure 1a shows the Tadri to Kanyakumari basin and Fig. 1b represents the different elevation zones in the region. The elevation of the major part of the basin area varies from 10–50 m (www.india-wris.nrsc.gov.in). Most of the area receives an average rainfall of about 2500 mm and the temperature in the basin varies with an average minimum temperature of 17.9 °C to average maximum temperature of 33.04 °C (1979–2015).

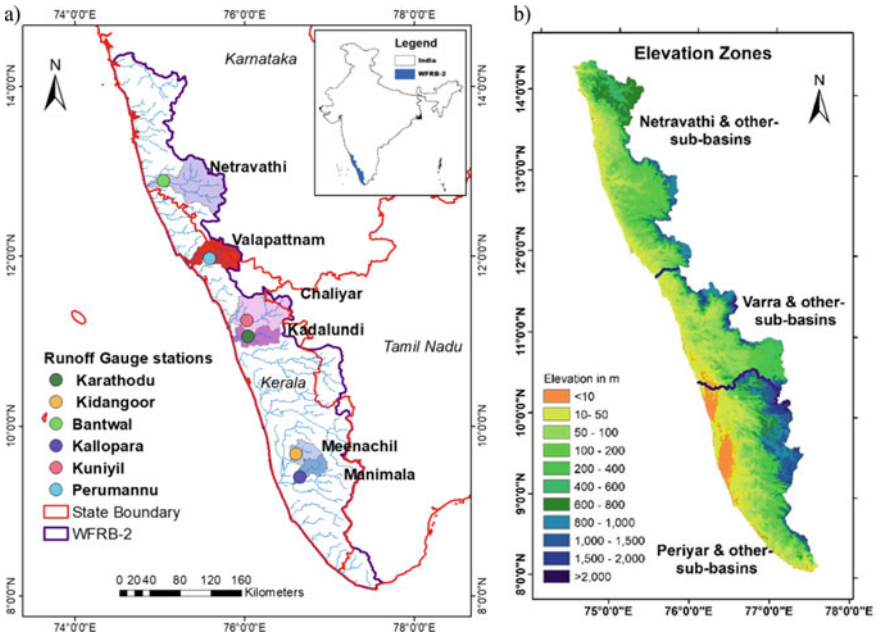

Fig. 1 **a** West flowing river basins from Tadri to Kanyakumari (WFRB-2). *Source* www.india-wris.nrsc.gov.in **b** elevation zones of WFRB-2

3 Material and Methods

In this study, an attempt has been made to estimate the GCM model and scenario uncertainty in projecting the monsoon precipitation for WFRB-2 and correlating the performance of the model in the upper, middle, and lower parts of the basin with varying landform changes. In the present study, only monsoon rainfall (JJAS) for near future (2011–2040) is being used. The performance of GCMs is evaluated based on its ability to capture the monsoon mean precipitation. Six individual river basins are also selected such as Netravathi and Valapattanam from the upper region, Chaliyar and Kadalundi from the middle region, and Meenachil and Maninala from lower part of WFRB-2 to make a comparison of the uncertainty rage (Fig. 1).

GCM Models Used

The future kernel regression-based statistically downscaled [4] precipitation data are procured through INCCC project for five CMIP-5 GCM's (General Circulation Model) in daily time steps for RCP scenarios 4.5 and 8.5. The selection of these five GCMs (CCCMA CanESM2; CNRM CM5; MPI ESM MR; MPI ESM LR and; BNU ESM) is done based on the ability to capture the Indian monsoon rainfall and data available for the region. Descriptions of the GCM models are given in Table 1.

Table 1 GCM models from CMIP-5 experiment

Modelling centre	Model	Institution	Spatial resolution
CCCMA	CanESM2	Canadian Centre for Climate Modelling and Analysis	2.8° × 2.8°
BNU	BNU-ESM (BNU)	"Beijing Climate Centre, China Meteorological Administration"	2.8° × 2.8°
CNRM-CERFACS	CNRM-CM5	"Centre National de Recherches Meteorologiques/Centre Europeen de Recherche et Formation Avancees en Calcul Scientifique"	1.4° × 1.4°
MPI-LR	MPI-ESM-LR	"Max Planck Institute for Meteorology (MPI-M)"	1.8° × 1.8°
MPI-MR	MPI-ESM-MR (MPI-MR)	Max-Planck-Inst. for Meteorology	1.87 × 1.87

REA Methodology

In this study, we focus on Reliability Ensemble Average (REA) technique in detail. REA is an averaging technique, which can be also used for estimating the uncertainty range and reliability range of climate change simulations. REA method helps in assigning weights to different GCM models based on the bias and convergence criterions. Multi-model bias is calculated based on the present climate; model convergence captures the deviation of individual model projections with respect to the central tendency of the ensemble [7]. Therefore, models with less bias are high performance models and whose projections agree are highly converging models, which thereby receives the higher weights. Therefore, $R_{B,i}$ measure the model performance and $R_{D,i}$ measure the model convergence, which are the governing criteria for REA method.

The stepwise procedure for REA, taking JJAS precipitation as the sample parameters is as follows [5]:

Step 1: Estimate precipitation change (~ΔP) using weighted average of the individual GCMs.

$$\sim \Delta P = \sim \mathrm{A}(\Delta P) = \frac{\sum_{i=1}^{N} R_i \Delta P_i}{\sum_{i=1}^{N} R_i} \tag{1}$$

where ~A represents averaging using REA and R_i denotes individual reliability factor for each GCMs.

Step 2: For each 0.25 grid, the overall GCM reliability factor R_i for each model projection i of 5 GCM model can be defined as:

$$R_i = [(R_{B,i})^m \times (R_{D,i})^n]^{[\frac{1}{mn}]} = \left\{ \left[\frac{\varepsilon_p}{\text{abs}(B_{p,i})} \right]^m \times \left[\frac{\varepsilon_p}{\text{abs}(D_{p,i})} \right]^n \right\}^{[\frac{1}{mn}]} \quad (2)$$

where $R_{B,i}$ is a function of model bias $(B_{p,i})$ in simulating historical precipitation (JJAS for recent past (1979–2005). $R_{B,i}$ ranges from 0, for least performing model to 1 for if $B_{p,i}$ is less than natural variance ε_p. For 5 GCM simulations, the Performance factor, B_i is estimated for each grid as:

$$[B_i] = \left[\text{Precip}_i - \text{Precip}_{\text{obs}}\right].$$

where $\text{Precip}_{\text{obs}}$ is the mean annual monsoon (JJAS) precipitation over each grid and Precip_i is the mean annual monsoon precipitation predicted by model i during historic time scale (1976–2005).

Step 3: In the similar way, the convergence coefficient $R_{D,i}$ takes values from 0 for outlier projections to 1, where difference between REA mean and projection is smaller than ε_p. For each GCM, $D_{p,i}$ is calculated for each grid as the difference between the predicted and REA average.

$$D_i = \left[\Delta\text{Precip}_i - \frac{\sum_{i=1}^{N} R_i \Delta\text{Precip}_i}{\sum_{i=1}^{N} R_i} \right]. \quad (3)$$

where ΔPrecip_i is the change in mean precipitation in the 30 years near future of RCP 4.5 and 8.5 compared to the historic 30 years simulation predicted by the GCM i. In the present study we have only considered the near future precipitation (2011–2040). An iterative procedure is developed to find the distance $D_{p,i}$. The first value of $D_{p,i}$ is estimated using the equation $[D_{p,i}]_1 = [\Delta P_i - \sim \Delta P]$. This first value in future is substituted in Eqs. 3 and 4 to obtain $[\sim \Delta P]_1$, first order REA average change. This value is further used in the iteration procedure to calculate $[D_{p,i}]_2 = [\Delta P_i - [\sim \Delta P]_1]$. The distance is only a measure of model convergence criterion given that future conditions are unknown.

Step 4: The parameters m and n used to weigh both the criterions in estimating the weights. It is assumed as one, (equal weightage for both parameters) in the present study. Similarly, $R_{B,i}$ and $R_{D,i}$ are set to 1 when ε_p exceeds B and D. GCM projections

are reliable when both its bias and distance from the ensemble average are within its natural variability, so that $R_i = 1$ in Eq. 3. As the bias /distance grows, the GCM reliability factor reduces.

Step 5: ε_p is a parameter which measures the natural variability in 30 year average JJAS regional precipitation. For this, we compute the time series of observed, gridded precipitation for JJAS series for IMD data for 1901–2005. A 30 year moving average for the de-trended series is calculated and ε_p is estimated as the difference between maximum and minimum values from this 30 year moving average series.

Step 6: Uncertainty range of each GCM can be further estimated using REA technique. The root mean-square difference (rmsd) of the changes $\widetilde{\delta_{\Delta p}}$:

$$\widetilde{\delta_{\Delta p}} = \left[\frac{\sum_{i=1}^{N} R_i \left(\Delta P_i - \widetilde{\Delta \mathrm{P}_{\mathrm{REA}}} \right)^2}{\sum_{i=1}^{N} R_i} \right]^{\left[\frac{1}{2}\right]} \tag{4}$$

4 Results and Discussion

In this study, we consider the model uncertainty by combination of model outputs which provides confidence to decision-makers in formulating policies for climate change impact assessment. The performances of all the 5 GCMs and the proposed REA methodology in terms of reliability measures, namely model bias reliability factor ($R_{B,i}$), model convergence reliability factor ($R_{D,i}$) and collective model reliability factor (Ri), are estimated for precipitations during 2011–2040 under both RCP 4.5 and 8.5, respectively.

4.1 REA Weighted Ensemble and Uncertainty Estimation Grid Wise

Figure 2 shows the grid-wise reliability estimates of monsoon rainfall for the entire Western Ghat region. It is being observed that CCCMA GCM performs better in most of the grids in the lower part of WFRB-2, with a weightage of more than 0.4 in most of the grids. MPIMR also performs better in the lower region. MPIMR is giving better performance in the middle region also compared to other GCMs. CNRM shows weightage less than 0.1 in most part of Kerala region. GCMs BNU and CNRM are performing better in the upper regions of WFRB-2. Overall performance of MPIMR in the Western Ghats region is better given by the REA approach.

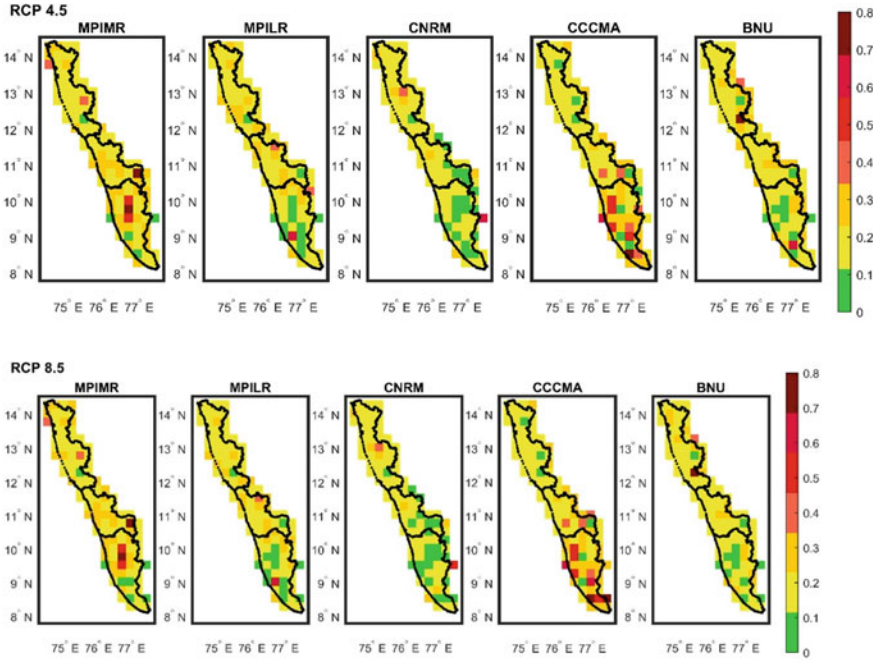

Fig. 2 Grid wise REA weightage factor for all the five GCMs for **a** RCP 4.5 and **b** RCP 8.5

4.2 River Basin Scale REA

River basin wise analysis shows similar results as well. REA weightage of individual GCMs for 6 river basins in WG for both RCP scenarios are given in Table 2. MPIMR is found to be the GCM with highest weightage in Meenachil (0.88), Manimala (0.46), Chaliyar (0.23), and Kadalundi (0.27) river basins. For Netravathi river, GCM CNRM performs better. This analysis helps to choose GCMs for a particular river basin, for climate change impact assessment.

Overall analysis shows, the ability of CMIP-5 GCMs to capture the Western Ghats monsoon rainfall is just average. Also, from the available five GCMs, MPIMR predicts better results in WFRB-2. For all the six river basins, uncertainty range of near future (2011–2040) rainfall is estimated using REA approach and plotted in Fig. 3. Also, the uncertainty ranges of five GCMs, when simple arithmetic mean is considered are also made to compare and validate the REA approach. It is observed that the REA approach brings reduction in uncertainty range to a great extent in all the six river basins. And the impact is more in upper region (Netravathi and Valapattanam) as compared to other regions of WFRB-2.

Table 2 Performance evaluation and ranking of CMIP5 GCM in terms of overall collective model reliability for Near Future Rainfall

Overall collective model reliability (R_i)	BNU	CNRM	CCCMA	MPILR	MPIMR
RCP 8.5					
Meenachil	0.031	0.022	0.036	0.019	**0.88**
Manimala	0.103	0.104	0.237	0.086	**0.46**
Netravathi	0.22	**0.302**	0.143	0.156	0.177
Valapattanam	**0.225**	0.1617	0.196	0.218	0.197
Chaliyar	0.186	**0.23**	0.162	0.189	**0.23**
Kadalundi	0.216	0.149	0.15	0.21	**0.27**
RCP 4.5					
Meenachil	0.031	0.022	0.036	0.018	**0.89**
Manimala	0.103	0.107	0.24	0.083	**0.46**
Netravathi	0.216	**0.302**	0.14	0.16	0.17
Valapattanam	**0.22**	0.17	0.19	0.21	0.18
Chaliyar	0.19	**0.23**	0.15	0.18	**0.23**
Kadalundi	0.22	0.15	0.14	0.2	**0.27**

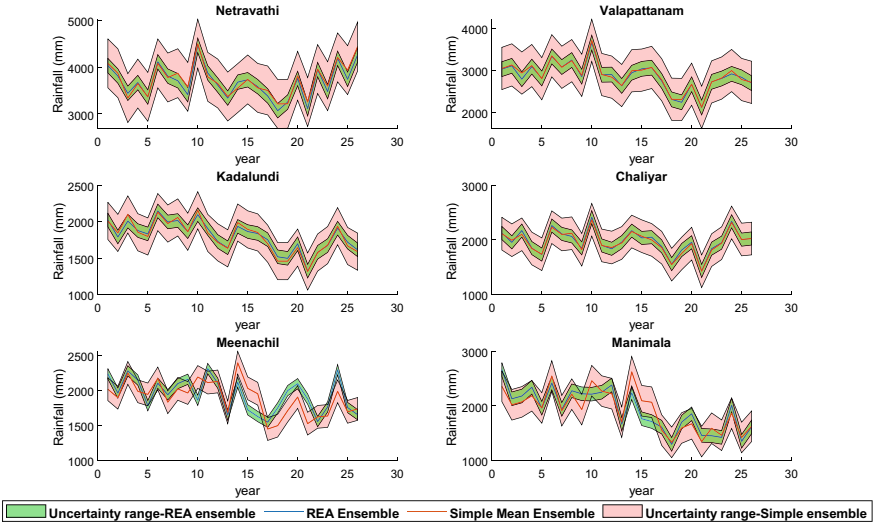

Fig. 3 Comparison of uncertainty range of near future (2012–2040) estimated using REA approach and simple arithmetic mean of GCMs for RCP 8.5

5 Conclusions

In this study, the GCM and scenario uncertainty in Western Ghats (WG) region of South India is attempted for monsoon rainfall using Reliability Ensemble Average (REA) for 5 GCMS and RCP 4.5 and RCP 8.5 scenarios. The following are the conclusions from the present study:

- Reliability Ensemble Approach (REA) is found to be a simple yet powerful technique to estimate the performance and uncertainty associated with multi-model data sets.
- Heterogeneity in the performance of GCMs are observed which coincides with the heterogeneity in WFRB-2 in terms of rainfall patterns, elevation, temperature variation, land use pattern, etc.
- GCM CCMA shows relatively better results in less rainfall region, river basins lying in the lower elevation.
- MPIMR shows better performance in all over WFRB-2, which concludes that it can capture the Indian summer monsoon in Western Ghats.

Acknowledgements We wish to express our deep gratitude to the Central Water Commission and Indian Meteorological Department India for providing hydrological and meteorological data. Authors also acknowledge the sponsorship of the project entitled "Impacts of Climate Change on Water Resources in River Basin from Tadri to Kanyakumari" by INCCC, Ministry of Water Resources, Government of India.

References

1. Bishop CH, Abramowitz G (2013) Climate model dependence and the replicate Earth paradigm. Clim Dyn 41(3–4):885–900
2. Giorgi F, Mearns LO (2002) Calculation of average, uncertainty range, and reliability of regional climate changes from AOGCM simulation via the "Reliability Ensemble Averaging" (REA) method. J Climate 2002(15):1141–1211
3. Huisman JA, Breuer L, Bormann H, Bronstert A, Croke BFW, Frede H-G, Gräff T, Hubrechts L, Jakeman AJ, Kite G, Lanini J, Leavesley G, Lettenmaier DP, Lindström G, Seibert J, Sivapalan M, Viney NR, Willems P (2009) Assessing the impact of land use change on hydrology by ensemble modelling (LUCHEM) III: scenario analysis. Adv Water Resour 32(159–170):2009. https://doi.org/10.1016/j.advwatres.2008.06.009
4. Kannan S, Ghosh S (2013) A nonparametric kernel regression model for downscaling multisite daily precipitation in the Mahanadi basin. Water Resour Res 49(3):1360–1385
5. Sengupta A, Rajeevan M (2013). Uncertainty quantification and reliability analysis of CMIP5 projections for the Indian summer monsoon. Current Sci, 1692–1703
6. Raje D, Krishnan R (2012) Bayesian parameter uncertainty modeling in a macroscale hydrologic model and its impact on Indian river basin hydrology under climate change. Water Resour Res 48(8)
7. Tebaldi C, Mearns LO, Nychka D, Smith RL (2004) Regional probabilities of precipitation change: a Bayesian analysis of multimodel simulations. Geophys Res Lett 31(24)

Assessment of Temperature for Future Time Series Over Lower Godavari Sub-Basin, Maharashtra State, India

Y. J. Barokar and D. G. Regulwar

Abstract Climate change can cause various negative impacts on water resources system, ecosystem, etc. To deal with these effects, it is necessary to study the climate change. There are various ways to study climate change in which one of the way is the study of downscaling. Downscaling is the procedure in which prediction of information is done for local scale area from the available information of a large scale area. In the downscaling of climatic variables, General Circulation Model (GCM) plays an important role. GCM gives larger scale climatic variables. With the help of this downscaling, we can predict different climatic variables such as temperature, precipitation for future time period over the selected area. To perform this downscaling there are different ways, we can classify it as statistical downscaling and dynamical downscaling. In statistical downscaling, we can find relation between predictant and predictors and this statistical relation we use for the future prediction of the selected climatic variable. In dynamical downscaling, we use Regional Climatic Model (RCM), and with the help of this, we carry out downscaling procedure. In this study, statistical downscaling has studied for temperature parameter (Tmax and Tmin) by considering the basic equation given by Wilby in (Inter-research 10:163–178 [1]). The study area selected for this study is lower Godavari Sub-basin, Maharashtra State, India (Latitude: 19° 11′, Longitude: 76° 33′). In this study, in the first step, statistical downscaling has been done with the help of statistical downscaling model (SDSM) software by using HadCM3 GCM with A2a and B2a scenarios for temperature parameter for the future time period up to 2099. In second step, the

Y. J. Barokar (✉)
Department of Civil Engineering, MGM's Jawaharlal Nehru Engineering College, Aurangabad 431003, India
e-mail: yogeshbarokar@gmail.com

D. G. Regulwar
Department of Civil Engineering, Government College of Engineering, Aurangabad 431005, India

P. V. Timbadiya et al. (eds.), *Climate Change Impact on Water Resources*, Lecture Notes in Civil Engineering 313, https://doi.org/10.1007/978-981-19-8524-9_6

statistical downscaling again performed by using basic equation given by Wilby (Inter-research 10:163–178 [1]) in excel which is named as "Excel Model." Temperature values predicted up to 2099. These results are considered with three different series such as 2020s, 2050s, and 2080s. Downscaled results of temperature parameter by "SDSM" model and "Excel Model" were compared for future series. After study of these results, it is concluded that SDSM gives higher value of change in mean monthly daily value of *T*max and *T*min than that of "Excel Model."

Keywords SDSM · Excel model · HadCM3 · A2a · B2a · *T*max · *T*min

1 Introduction

Climate change is [1] the major issue faced by many sectors; there are different causes of changing climate in which one of the major cause is increase in the greenhouse gases. Disturbance in the climate is caused by increase in CO_2 and other greenhouse gases [2]. Global warming causes change in the climatic parameters which affects on the weather patterns [3]. To study these effects, downscaling is the more suitable way in which we can forecast the future climatic variables with the help of General Circulation Models (GCMs) [4]. Downscaling can be carried out with the help of dynamical or statistical methods, but statistical downscaling is preferable than dynamical downscaling [5]. Dynamical downscaling can be carried out with the help of Regional Circulation Model (RCM), whereas statistical downscaling is based on statistical relation between predictor and predictant [5]. Statistical downscaling model is the tool in which we can form statistical relation between predictor and predictant [6]. Such relation we can execute for the future forecasting of the climatic parameters. In the study of the Mahmood and Babel [2], authors have used statistical downscaling model (SDSM) and downscaled the climatic variables with application of bias correction over the trans-boundary region of Jhelum River. In the present study, SDSM has been used for predicting the future values of temperature parameter (*T*max, *T*min) over Lower Godavari Sub-basin, Maharashtra State, India. In addition to this, basic equation of downscaling given by Wilby [1] which is the base for SDSM has been executed in the excel tool, and temperature values for future series have been found out. These results were compared with the SDSM results. For Indian region, various GCMs give better results in which one of the GCM is HadCM3 [7], because of this HadCM3 GCM has been selected for this study with A2a and B2a scenarios.

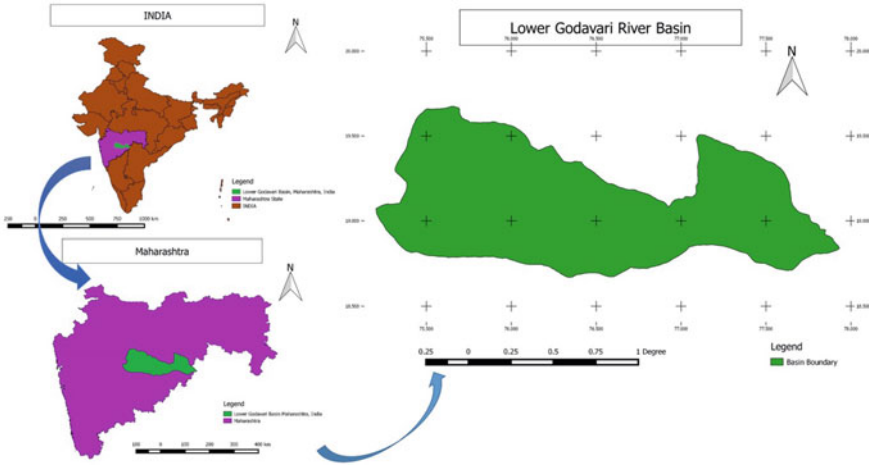

Fig. 1 Map of Lower Godavari Sub-basin

2 Materials and Method

2.1 Downscaling

Downscaling means converting high scale resolution data into finer scale resolution. In this study, statistical downscaling has been used to forecast the future series values of temperature parameter (Tmax, Tmin). In statistical downscaling, statistical relation developed between predictor and predictant. Such statistical relation helps to downscale the climatic variables for future series [2].

2.2 Study Area and Data Source

2.2.1 Lower Godavari Sub-basin, Maharashtra State, India

The study area is Lower Godavari Sub-basin (area≈17,850km^2). Lower basin of Godavari river in Maharashtra lies between 18° 42′ 49″ N to 19° 40′ 27″ N and 75° 12′ 12″ E to 77° 55′ 59″ E. The mean monthly Tmax changes from 29.63 to 38.50 °C over the basin. Map of study area is shown in Fig. 1

2.2.2 Data Collection

For the execution of present study, daily temperature (Tmax and Tmin) values have been obtained from Indian Meteorological Department (IMD), Pune for the period

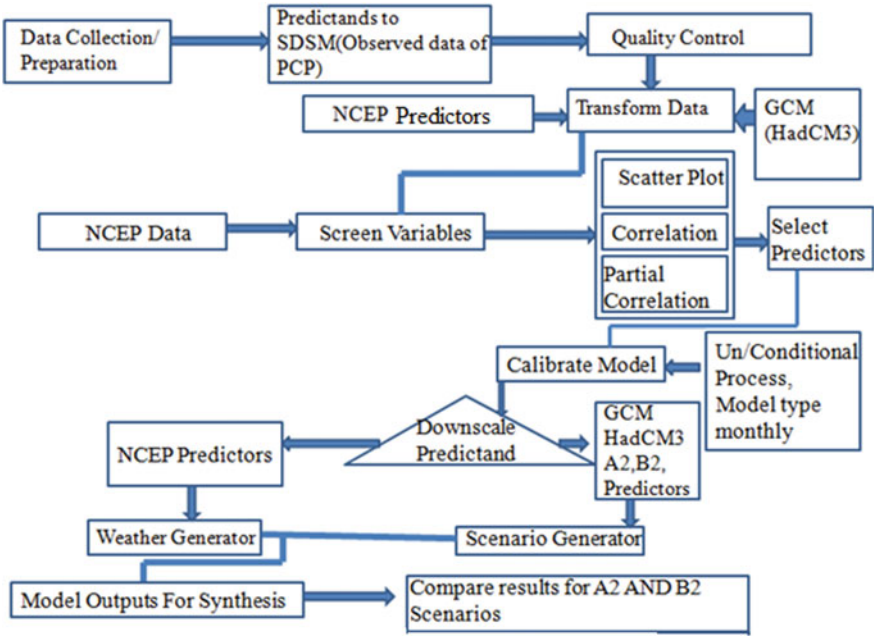

Fig. 2 Flowchart for statistical downscaling method given by Wilby

1961–2000. GCM data of HadCM3 under A2a and B2a scenarios have been obtained from Canadian Climate Impact Scenarios (CCIS) site for the area Lower Godavari Sub-basin, Maharashtra State, India (Latitude: 19° 11′, Longitude: 76° 33′).

Selection of Input Parameters

The flowchart and basic equation for downscaling given by Wilby [5] is as shown in Fig. 2.

Working of statistical downscaling model (SDSM) which is developed by Wilby [5] and Dawson is divided into below steps:

(a) Quality Control, (b) Transforming Predictor data, (c) Screen Variables, (d) Model Calibration, (e) Weather Generator, (f) Finding statistics of the data, and (g) Compare results.

Quality control helps to detect the missing values in our observed data, whereas in Transform data we can apply suitable transformation to the data so that it will be well distributed. Screen variables helps to decide the suitable predictors over the selected region. Model Calibration and Weather Generator helps to develop statistical model and compare it with the observed data. In last step, we can find different statistical values and compare the results.

The basic equation for finding amount of temperature by Wilby [5] is as given below.

Amount of total Temp. (t) downscaled on day "i" is given by

Table 1 List of NCEP predictors

Sr. no	Predictor name	Sr. no	Predictor name
1	p_f-Airfloe strength at surface	14	p8_z-850 hPa vorticity
2	p_u-Zonal velocity at surface	15	p8th-850 hPa wind direction
3	p_v-Meridional velocity at surface	16	p8zh-divergence of 850 hPa
4	p_z-Surface velocity	17	r850-Relative humidity of 850 hPa
5	p_th-Surface wind direction	18	p500-00 hPa geopotential height
6	p_zh-Divergence at surface	19	p5_v-500 hPa meridional velocity
7	rhum-Relative humidity at surface	20	p5_z-500 hPa vorticity
8	p5_f-500 hPa airflow strength	21	p5th-500 hPa wind direction
9	p5_u-500 hPa velocity of zonal	22	p5zh-500 hPa divergence
10	r500-relative humidity of 500 hPa	23	r850-Relative humidity 850 hPa
11	p8_f-850 hPa airflow strength	24	Temp-Mean temperature at a height of 2 m
12	p8_u-Zonal velocity of 850 hPa	25	Shum-Surface-specific humidity
13	p8_v-meridional velocity of 850 hPa	26	mslp Pressure at Mean Sea Level

$$U_i = \gamma_0 + \sum_{i=1}^{n} \gamma_j X_{ij} + e_i \tag{1}$$

where γ_0 = Intercept between predictor and predictant,
X_{ij} = Predictor values for selected predictors.
e_i = Bias correction value.
The list of NCEP predictors used for downscaling purpose is given in Table 1.

3 Results and Discussions

Results for this study are as given below for the downscaling of temperature (Tmax and Tmin) over Lower Godavari Sub-basin for future series.

3.1 Calibration and Validation of the Model

In this study, calibration has been done over a period of 1960 to 1980. Observed monthly mean daily temperature data (Tmax and Tmin) and downscaled monthly mean daily temperature data (Tmax and Tmin) over this selected period have been compared graphically. Graphical comparison for Tmax and Tmin is as given in Figs. 3 and 4.

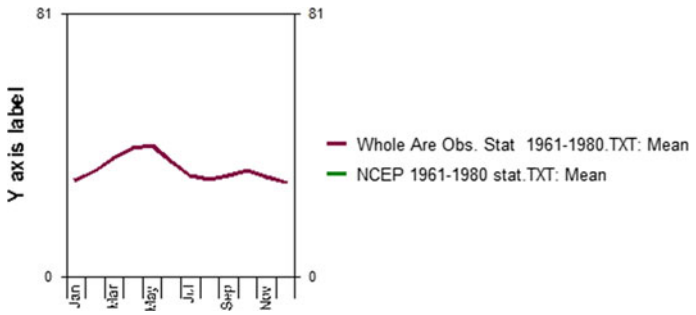

Fig. 3 Graphical representation for calibrated model of *T*max

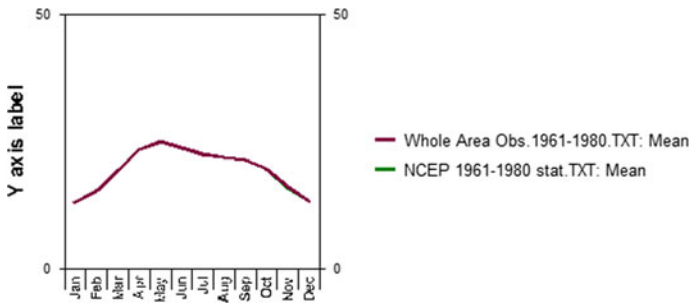

Fig. 4 Graphical representation for calibrated model of *T*min

Graphical results indicate that observed and downscaled values of *T*max and *T*min over a selected period are matching with each other it means our model calibrated successfully.

After successful calibration of the model, we tested this model over next time period. For this, the time period of 1981–2000 have been selected. Observed monthly mean daily temperature data of *T*max and *T*min were compared with downscaled monthly mean daily temperature data of *T*max and *T*min over this period. For this statistical comparison, the coefficient of determination has been used. Results are as shown below (Tables 2).

Table 2 Coefficient of determination between observed and downscaled data over a period of 1981–2000

Model name	GCM	Temperature parameter	R^2 value between observed and downscaled parameter over 1981–2000
SDSM	HadCM3	*T*max	0.99
	HadCM3	*T*min	0.99

The statistical results indicate the downscaled values of monthly mean daily temperature (Tmax and Tmin) are matching with observed monthly mean daily temperature (Tmax and Tmin). So with the help of this selected model, we tried to find out future series values of mean daily temperature (Tmax and Tmin). With the help of this model, temperature values have been downscaled up to 2099 with the help of SDSM under A2a and B2a scenarios. These downscaling results of monthly mean daily temperatures (Tmax and Tmin) have been compared with observed monthly mean daily temperature (Tmax and Tmin) over a base line period of 1961–2000. Statistical comparison has been studied with the help of coefficient of determination as shown (Table 3).

In this statistical comparison, coefficient of determination gives better values over the base line period under both the scenarios.

The same predictors we have selected to perform downscaling with the help of basic equations given by Wilby [5] in Excel. Downscaled temperature values have been compared with the observed temperature values over a base line period (1961–2000) (Table 4).

The above result indicates the good correlation between observed monthly mean daily temperature and downscaled monthly mean daily temperature.

We can find the range of R^2 between observed monthly mean daily temperature and downscaled monthly mean daily temperature (Tmax and Tmin) by using SDSM is in between 0.97 and 0.99 and by using Excel Model it is in between 0.63 and 0.80. Downscaling results with the help of SDSM model and Excel Model are found

Table 3 Coefficient of determination between observed and downscaled data over period 1961–2000

Model name	GCM	Temperature parameter	R^2 value between observed and downscaled parameter over 1961–2000
SDSM	HadCM3 A2a	Tmax	0.97
	HadCM3 A2a	Tmin	0.99
	HadCM3 B2a	Tmax	0.96
	HadCM3 B2a	Tmin	0.99

Table 4 Coefficient of determination between observed and downscaled data over period 1961–2000

Model name	GCM	Temperature parameter	R^2 value between observed and downscaled parameter over 1916–2000
Excel model	HadCM3 A2a	Tmax	0.80
	HadCM3 A2a	Tmin	0.63
	HadCM3 B2a	Tmax	0.78
	HadCM3 B2a	Tmin	0.63

Table 5 Future change in monthly mean daily *T*max and *T*min under different scenarios with respect to base line period 1961–2000

Model	GCM	Series	*T*max (°C)	*T*min (°C)
SDSM	HadCM3 A2a	2020s (2011–2040)	0.92	0.26
		2050s (2041–2070)	1.96	0.82
		2080s (2071–2099)	3.17	1.56
	HadCM3 B2a	2020s (2011–2040)	0.97	0.33
		2050s (2041–2070)	1.6	0.64
		2080s (2071–2099)	2.39	1.07
Excel model	HadCM3 A2a	2020s (2011–2040)	0.16	0.86
		2050s (2041–2070)	0.42	0.86
		2080s (2071–2099)	0.72	0.91
	HadCM3 B2a	2020s (2011–2040)	0.18	0.83
		2050s (2041–2070)	0.33	1.04
		2080s (2071–2099)	0.52	1.07

out for three future series (2020s, 2050s, and 2080s) as given below. The results are shown in terms of future change in monthly mean daily *T*max and *T*min under different scenarios with respect to base line period 1961–2000 (Table 5).

In prediction for these three future series, we identified that SDSM model is giving more change in monthly mean daily temperature values (*T*max and *T*min) in 2080s (2071–2099) under A2a and B2a scenarios. According to the results, there will also be increase in monthly mean daily temperature values (*T*max and *T*min) for the series 2020s (2011–2040) and 2050s (2041–2070), but it will be less in amount compared to 2080s series. The same reflection we identified in the results of Excel model just the change is whatever predicted values are given by Excel model are smaller in amount compared to SDSM results, but the pattern of results with excel is also says that there will be more change in temperature values (*T*max and *T*min) over the series 2080s (2071–2099) compared to the series 2020s (2011–2040) and 2050s (2041–2070).

4 Conclusions

The following conclusions are derived from the foregoing study:

1. In calibration and validation, both the models (SDSM and Excel) give satisfactory results; SDSM is giving more appropriate results compared to excel. It may be because of the bias correction which we apply in SDSM at the start of execution. It means if we change bias correction value in excel, then we may get some more accurate results and also we can predict future climatic values for our region in a better way.

2. SDSM and Excel Model both give increasing trends in the value of *T*max and *T*min in the near future with respect to the baseline period 1961–2000. According to IPCC reports, the amount of greenhouse gases may increase in the future which will lead to an increase in temperature, so these results satisfy the prediction of IPCC.

Acknowledgements The authors are thankful to the India Meteorological Department (IMD) and the organization of Canadian Climate Impact Scenarios (CCIS) for providing the necessary data to conduct the present study.

References

1. Wilby RL (1998) Statistical downscaling of daily precipitation using daily airflow and seasonal teleconnection indices climate research. Inter-Research 10:163–178
2. Mahmood R, Babel MS (2014) Future changes in extreme temperature events using the statistical downscaling model (SDSM) in the trans-boundary region of the Jhelum river basin. Weather Clim Ext, Elsevier. https://doi.org/10.1016/j.wace.2014.09.0012212
3. Saraf VR, Regulwar DG (2018) Impact of climate change on runoff generation in the Upper Godavari River Basin, India. J Hazardous, Toxic Radioact Waste, ASCE,. https://doi.org/10.1061/(ASCE)HZ.2153-5515.0000416
4. Barokar YJ, Saraf VR, Regulwar DG (2019) Simulating maximum temperature for future time series on Lower Godavari Basin, Maharashtra State, India by using SDSM. In: 11th World Congress on Water Resources and Environment (EWRA 2019), Managing Water Resources for a Sustainable Future, Madrid, Spain, 25–29 June
5. Wilby RL, Dawson CW, Barrow EM (2002) SDSM—a decision support tool for the assessment of regional climate change impacts. Environ Model Softw 17:147–159
6. Barokar YJ, Regulwar DG (2019) Climate change effect on maximum temperature on Lower Godavari Basin, Maharashtra State, India by using SDSM. In: National Conference on Environment Pollution Control and Management (EPCM2019), College of Engineering Pune, 1–2 March
7. Komaragiri SR, Kumar DN (2014) Clim Res 60:103–117. https://doi.org/10.3354/cr01222
8. Intergovernmental Panel on Climate Change (IPCC) (2001) Climate change 2001—the scientific basis. In: Contribution of Working Group I to the Third Assessment Report of the Intergovernmental Panel on Climate Change
9. IPCC (2007) General guidelines on the use of scenario data for climate impact and adaptation assessment climate change. In: Fourth Assessment Report of the Intergovernmental Panel on Climate Change

Projection of Daily Rainfall States Over Tapi Basin Using CMIP5 and CMIP6-Based Global Climate Model

Aarti S. Ghate and P. V. Timbadiya

Abstract The daily rainfall projections derived using global climate model (GCMs) plays important role in assessment of the future climate over the study area. The current study represents the future daily rainfall states over Tapi basin using k-means clustering and Classification and Regression Tree (CART) modelling. The Tapi basin spreaded over 65,145 km^2 and represented by 351 grids of 0.25° resolution. The rainfall data collected from India Meteorological Department (IMD) and General Circulation Model (GCM) outputs (i.e., CanESM2, CNRM-CM5, CanESM5, CNRM-CM6) of Coupled Model Intercomparison Project phase 6 CMIP6 (SSP245), and 5 CMIP5 (RCP4.5) and used in the projection of future daily rainfall states over study area. The projected daily rainfall states from CMIP5 and CMIP6 were compared for both aforementioned GCMs. The results based on the CMIP-5 model indicated that the almost dry rainfall state is increasing over the Tapi basin while results based on CMIP-6 model revealed increase in the medium rainfall state. Overall, the almost dry days are decreasing and high and medium state daily rainfall is increasing over the study area under CMIP6.

Keywords Climate change · Daily rainfall states · GCM · CMIP5 · CMIP6

Disclaimer: The presentation of material and details in maps used in this chapter does not imply the expression of any opinion whatsoever on the part of the Publisher or Author concerning the legal status of any country, area or territory or of its authorities, or concerning the delimitation of its borders. The depiction and use of boundaries, geographic names and related data shown on maps and included in lists, tables, documents, and databases in this chapter are not warranted to be error free nor do they necessarily imply official endorsement or acceptance by the Publisher or Author.

A. S. Ghate (✉) · P. V. Timbadiya
Department of Civil Engineering, Sardar Vallabhbhai National Institute of Technology Surat, Surat 395007, India
e-mail: aaryaghate7884@gmail.com

P. V. Timbadiya et al. (eds.), *Climate Change Impact on Water Resources*, Lecture Notes in Civil Engineering 313, https://doi.org/10.1007/978-981-19-8524-9_7

1 Introduction

The intergovernmental panel on climate change (IPCC) in assessment report (AR6) projected the extreme precipitation has increased and will increase in future for South Asia [1]. The world-wide mean temperature may increase up to 4 °C by 2100, and will severely affect the accessibility of water resources and the water requirement around the globe and it will lead to be a task for water management [2]. As per the India Meteorological Department (IMD), the most of the parts of India receives the rainfall of its summer monsoon period from June to September (JJAS) and few regions receives from October to December (OND) as winter monsoon which mainly covers the peninsular Indian region. The boreal summer monsoon season receives around 78% of the annual rainfall and 12% during winter monsoon [3]. The statistical downscaling of daily precipitation under RCP 4.5 and RCP 8.5 for different GCM output for Tapi basin shown the extreme events are decreasing with increase in the medium rainfall events over the basin under CMIP5 [4].

The study using 20 coupled models of CMIP5 for RCP8.5 scenario revealed, projected Indian Monsoon Rainfall (ISMR) magnitude will increase in future climate over core monsoon zone, along with late withdrawal and stretching of the monsoon season [5]. In past there have been studies carried out using CMIP5 model output in simulating the ISMR under various future scenarios [4, 6–10]. Each GCM simulates the ISMR differently, as past studies have shown the performance of different GCM in projecting the ISMR and its ranking in simulating the climate variables [5, 11]. The 3–5 °C warmer and 13–30% wetter climate over South Asia in twenty-first century is projected using 13 GCMs of CMIP6 [12]. Hence, it is important to compare the daily rainfall state over the Tapi Basin using CMIP-5 and CMIP-6-based global climate model to evaluate the water availability in the future.

The present study includes the comparative analysis of CMIP5 and CMIP6 models output under RCP 4.5 and SSP245 scenario for CCCma and CNRM-CERFACS GCM Model for daily rainfall state. Future rainfall states are projected for the duration of 2011–2040, 2041–2070, and 2071–2100 under CMIP5 and 2015–2040, 2041–2070, and 2071–2100 under CMIP6. The comparison between the daily rainfall states over the Tapi basin is also made at the end.

2 Material and Methods

2.1 Study Area

The part of state of Madhya Pradesh, Maharashtra and Gujarat together constitutes the Tapi basin of an area of 65,145 km^2. The basin is bounded between 72°33’ E to 78°17’ E longitudes and 20°9’ N to 21°50’ N latitudes. The basin is located in the Deccan plateau, the spread of Tapi River is vast along with its branches over the lands

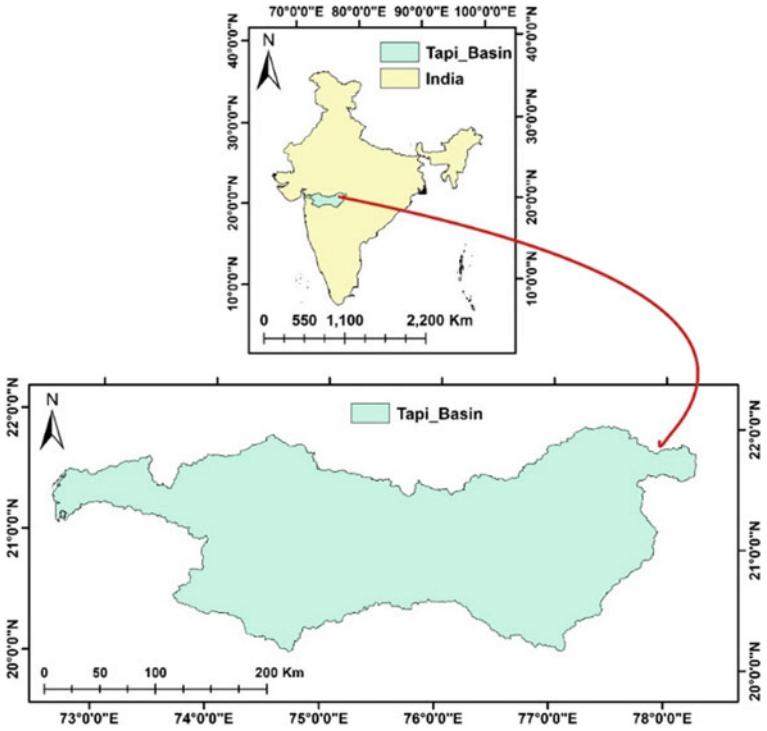

Fig. 1 Index map of Tapi Basin

of Vidharbha, Khandesh, and Gujarat with large part over Maharashtra and minor area over Madhya Pradesh. The index map of the study area is shown in Fig. 1.

The annual rainfall recorded over the basin as the upper basin receives 935.5 mm, middle part receives 631.5 mm, and lower part receives 1042.3 mm [13].

2.2 Data Used

2.2.1 Predictor and Predictand Data

The NCEP/NCAR reanalysis data and GCM data used for RCP4.5 scenario from CMIP5 and SSP245 scenario from CMIP6 used as predictor data and tabulated in Tables 1 and 2 respectively. The daily rainfall data at a grid spacing of $0.25° \times 0.25°$ from IMD is used as predict and variable for present study.

Table 1 Predictor data used from NCEP/NCAR

Heights: surface/250hpa/500hpa/850hpa/1000hpa		
Predictor variables used: air temperature (ta), V-wind (va), U-wind (ua), specific humidity (hus), geopotential height (Zg), mean sea level pressure (mslp)		
Sources	Spatial resolution	Temporal resolution
NCEP/NCAR reanalysis project	2.5° × 2.5°	Daily
GCM output	Varying	Daily

Table 2 Predictor data used from GCM for CMIP5 and CMIP6

Modelling centre	Model	Institution	Spatial resolution	Scenario
CCCma	CanESM2 (CMIP5)	Canadian Centre for Climate Modelling and Analysis	2.8° × 2.8°	[a]RCP 4.5
	CanESM5 (CMIP6)		2.8° × 2.8°	SSP245
CNRM-CERFACS	CNRM-CM5 (CMIP5)	Centre National de Recherches Meteorologiques/Centre Europeen de Recherche et Formation Avancees en Calcul Scientifique	1.4° × 1.4°	RCP 4.5
	CNRM-CM6 (CMIP6)		1.4° × 1.4°	SSP245

[a] RCP—Representative Concentration Pathways
SSP245—update of RCP4.5 based on Shared Socioeconomic Pathways (SSP2)

2.3 Methodology

The methodology adopted to carry out the comparative analysis of projection of future rainfall states using climate models under CMIP5 and CMIP6 project is shown in Fig. 2.

2.3.1 Selection of Spatial Extent

It is observed that the correlation between large scale atmospheric variables and mean rainfall is high for areal domain around the Tapi basin. The predictor variables such as mean sea level pressure, air temperature, zonal and meridional wind, specific humidity and geopotential height at various levels are used for in the current study. In this study the spatial extent from the contour plots is taken as longitude 10° N—35° N and latitude 65° E–95° E. Figure 3 represents the plots of contour by using Pearson correlation coefficient between rainfall and predictor variables at 250 hpa.

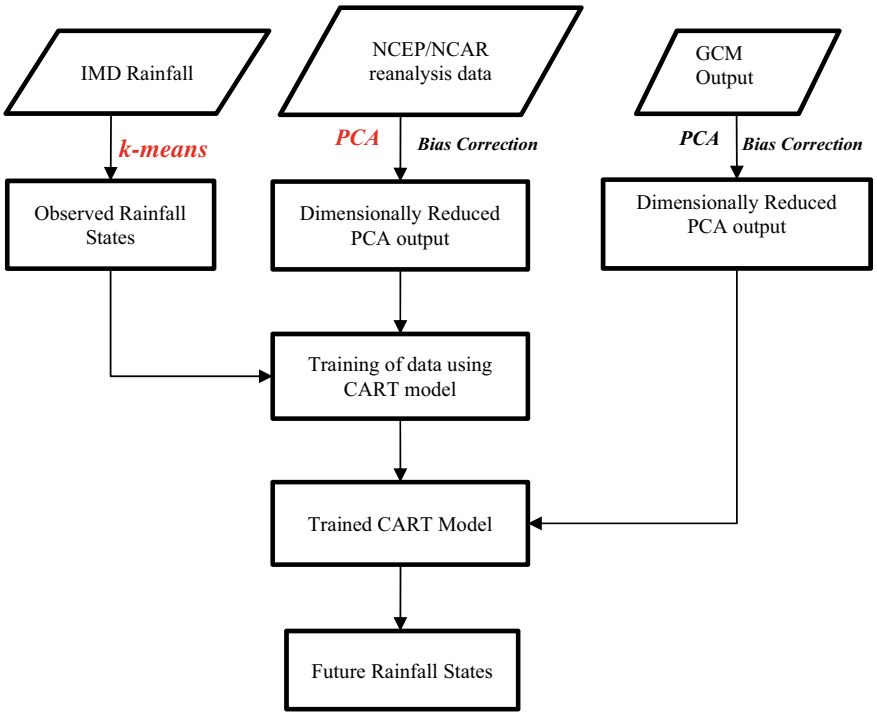

Fig. 2 Methodology adopted in projection of future rainfall states

2.3.2 Principal Component Analysis

The principal component analysis (PCA) is implemented to reduce the multi-dimension and multi-collinearity of the NCEP/NCAR predictor [4]. After PCA the output showed that the original data set comprising of 715 variables can be explained by newly derived 100 dimensions without changing the importance of the data with 98% of the variability. The PCA output on grouped variables as well as combination of variables at different levels for rainfall and predictor data is presented in Table 3.

2.3.3 Identification Rainfall States

The separation of data into groups whose identities are unknown is the process of cluster analysis, and it is categorized under the unsupervised data classification technique. The clustering is helpful in understanding the structure of the data which can be supportive in understanding the pattern of the data. The k-means clustering method is implemented in this study to recognize the rainfall states for the study area. The identification of clusters in data is achieved with k-means clustering [9]. The Dunn's index, The Davies-Bouldin index, and Silhouette index are computed

Fig. 3 Plots of contour by using Pearson correlation coefficient between rainfall and predictor variables (air temperature, specific humidity, geopotential height, V wind, and U wind) at 250 hpa

Table 3 Principal components of predictor variables

Variance Explained (%)	No. of components								
	Grouped surface variables	Grouped 250 hpa variables	Grouped 500 hpa variables	Grouped 850 hpa variables	Grouped 1000 hpa variables	Surface and 250hpa variables	Surface and 500hpa variables	Surface and 850hpa	Surface and 1000 hpa
75	12	**13**	18	14	14	19	20	14	13
90	41	**37**	44	38	42	68	69	48	44
95	74	**61**	70	65	69	123	123	91	83
97	106	**82**	90	86	94	173	171	134	120
98	134	**100**	107	104	115	217	213	175	154

Bold values indicate the selected principal component

to validate clusters. For finding the optimal number of clusters, the total number of clusters is taken in range of 2–10. From the results obtained from cluster validity measures it can be concluded that optimal number of clusters is three for the current study. The three rainfall states are named as 'Almost Dry', 'Medium' and 'High' on the basis of rainfall magnitude present in cluster centroids.

2.3.4 Modelling Rainfall Occurrence with CART

The relationship among the atmospheric variables and rainfall state is modelled by using classification and regression tree (CART). The advantage of the CART modelling is that it chooses the suitable tree structure. For the current study, total three models are selected for training and validation purpose.

$$R(t) = \{m(t), m(t-1), R(t-1)\}, \tag{1}$$

$$R(t) = \{m(t), m(t-1), R(t-1), R(t-2)\}, \tag{2}$$

$$R(t) = \{m(t), m(t-1), R(t-1), R(t-2), R(t-3)\}, \tag{3}$$

where $R\ (t)$, $R\ (t–1)$, $R\ (t–2)$ and $R\ (t–3)$ are the rainfall occurrence on the tth, ($t–1$)th, ($t–2$)th and ($t–3$)th day, respectively. $m(t)$ and $m\ (t–1)$ are the set of atmospheric variables on the tth and ($t–1$)th day, respectively. Equations (1), (2), and (3) are used for training and validation of CART model. Dimensionally reduced and standardized data of NCEP/NCAR and rainfall states derived are used for development of CART model in the current study.

The data from 1981 to 1995 (a period of 15 years) are used as the training set for building of the classification tree, while the remaining data for a period of 10 years (from 1995 to 2005) are used for validation of the CART model under CMIP5 project. The data from 1981 to 2000 (a period of 20 years) are used as the training set for building of the classification tree, while the remaining data for a period of 14 years (from 2001 to 2014) are used for validation of the CART model under CMIP6 project. The consistency of the model for future uses is evaluated by using three skill score measures given by SRMP (success rate of model prediction), HSS (Heidke skill score) and χ^2 goodness-of-fit statistic of the model for future uses. The detail calculations of skill scores can be found in [14]. The results of skill scores indicate that CART model 3 is giving the good results in comparison with Models 1 and 2. For evaluation of future rainfall states over the Tapi basin, Model 3 as mentioned above is selected.

3 Results and Analysis

The projection of future rainfall states under CMIP5 and CMIP6 project is evaluated using NCEP/NCAR reanalysis data. Under CMIP5, for projection of historical states, the training and validation period of rainfall considered were 1981–1995 and 1996–2005, respectively. In CMIP6, this time period is 1981–2000 and 2001–2014 for training and testing respectively. Tables 4, 5, and 6 represents the observed rainfall states under CMIP5 and CMIP6 for k-means clustering and CCCma model, CNRM-CERFACS GCM Model output respectively. Under CMIP5 and CMIP6, observed historical rainfall states are not showing significant changes in results. Table 4 represents the breakup of number of rainy days observed in training and validation period of historical states of rainfall using k-means clustering. Figure 4 indicates the observed rainfall states as 'Almost Dry', 'High', and 'Medium' under CMIP5 and CMIP6.

The breakup of number of rainy days observed in training and validation period of historical states of rainfall for CCCma model under CMIP5 and CMIP6 Project shown in Table 5. Figure 5 illustrates that, under CMIP5, there is increase in 'Almost Dry' state of rainfall while in CMIP6 the model is showing the decrease in the 'Almost Dry' state and increase in the 'Medium' state of rainfall.

The results of CNRM-CERFACS model are shown in Table 6, under CMIP5 the model is showing increase in the 'Almost dry' state and decrease in the 'Medium' state of the rainfall. For the same model under CMIP6, the results are showing the decrease in the 'Almost dry' state and increase in the 'Medium' state. Figure 6 represents the observed rainfall states of CNRM-CM5 and CNRM-CM6 model.

The results of CCCma model are tabulated in Table 7 represents the RCP4.5 and SSP245 scenarios for the CMIP5 and CMIP6 model outputs, respectively. The graphical presentation of projected rainfall states is shown in Fig. 7.

Table 4 Breakup of number of rainy days observed in training and validation period of historical states of Rainfall using k-means clustering for CMIP5 and CMIP6

Rainfall states observations under CMIP5					
Model	Rainfall states	Observations for the period			
		1981–1995		1996–2005	
		Number of days	Percentage	Number of days	Percentage
k-means	Almost dry	1261	68.91	878	71.96
	High	101	5.52	77	6.31
	Medium	468	25.57	265	21.73
Rainfall states observations under CMIP6					
Model	Rainfall states	1981–2000		2001–2014	
		Number of days	Percentage	Number of days	Percentage
k-means	Almost dry	1709	70.04	1188	69.55
	High	126	5.16	113	6.62
	Medium	605	24.80	407	23.83

Table 5 Breakup of number of rainy days observed in training and validation period of historical states of rainfall using CCCma model for CMIP5 and CMIP6

Rainfall states observations under CMIP5					
Model	Rainfall states	Observations for the period			
		1981–1995		1996–2005	
		Number of days	Percentage	Number of days	Percentage
CanESM2	Almost dry	1161	63.44	770	63.12
	High	150	8.20	106	8.68
	Medium	519	28.36	344	28.20
Rainfall states observations under CMIP6					
Model	Rainfall states	1981–2000		2001–2014	
		Number of days	Percentage	Number of days	Percentage
CanESM5	Almost dry	1476	60.49	929	54.40
	High	319	13.08	232	13.58
	Medium	645	26.43	547	32.02

Table 6 Breakup of number of rainy days observed in training and validation period of historical states of rainfall for CNRM-CERFACS model under CMIP5 and CMIP6 project

Rainfall states observations under CMIP5					
Model	Rainfall states	Observations for the period			
		1981–1995		1996–2005	
		Number of days	Percentage	Number of days	Percentage
CNRM-CM5	Almost dry	1148	62.73	798	65.40
	High	147	8.04	101	8.28
	Medium	535	29.23	321	26.32
Rainfall states observations under CMIP6					
Model	Rainfall states	1981–2000		2001–2014	
		Number of days	Percentage	Number of days	Percentage
CNRM-CM6	Almost dry	1278	52.38	760	44.50
	High	334	13.68	267	15.63
	Medium	828	33.94	681	39.87

Under CMIP5, for the period 2011–2040, 2041–2070, and 2071–2100 the Almost Dry state is decreasing slowly and gradual increase in the medium state of rainfall. For the same model under CMIP6, for the period 2015–2040, 2041–2070, and 2071–2100 there is significant decrease in the 'Almost Dry' state and increase in the 'Medium' state of rainfall whereas 'High' state of rainfall is increasingly slightly. Under CMIP5 project, for RCP 4.5 scenarios, CNRM-CERFACS model showing the slight increase in the 'Almost Dry' state and decrease in the 'Medium' state of the rainfall. In CMIP6,

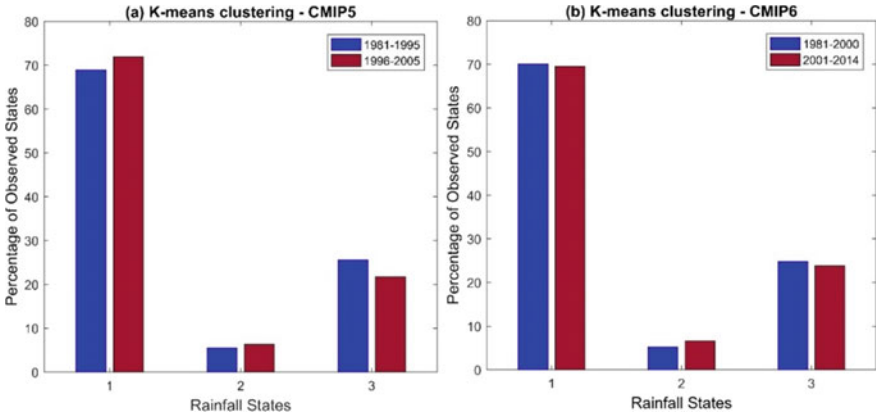

Fig. 4 Observed rainfall states almost dry, high and medium for calibration and validation period

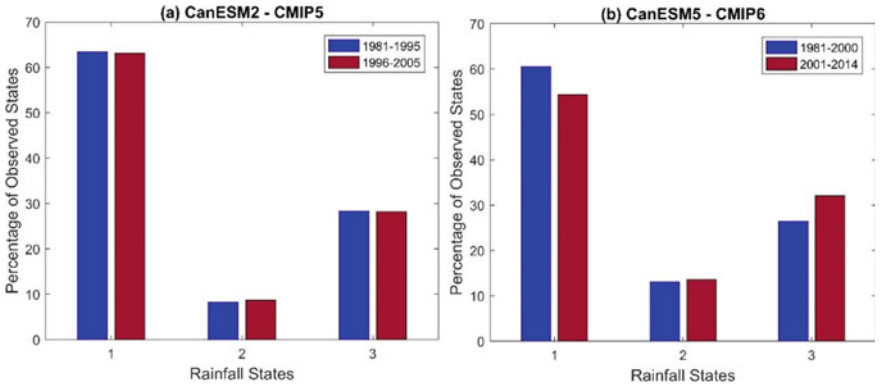

Fig. 5 Observed rainfall states of CanESM2 and CanESM5 model almost dry, high, and medium

the model is showing significant decrease in the 'Almost dry' state and increase in the 'Medium' state of the rainfall while 'High' state is also showing increasing trend.

The results of CNRM-CERFACS model are tabulated in Table 8 represents the RCP4.5/SSP245 scenarios for the CMIP5 and CMIP6 model outputs respectively. The graphical presentation of projected rainfall states is shown in Fig. 8.

4 Conclusions

The daily rainfall states are projected over the Tapi basin using CNRM-CERFACS and CCCma model output for RCP4.5/SSP245 scenario. The results revealed that

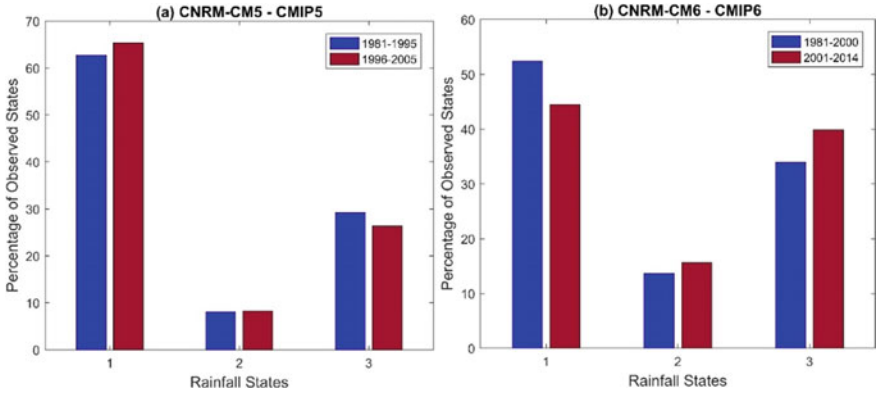

Fig. 6 Observed rainfall states of CNRM-CM5 and CNRM-CM6 model almost dry, high, and medium

Table 7 Breakup of number of rainy days projected for RCP4.5 scenarios for CCCma model under CMIP5 and CMIP6 project

Rainfall states projected using CMIP5 model output							
Model	Rainfall states	Forecast for the period					
		2011–2040		2041–2070		2071–2100	
		Number of days	Percentage	Number of days	Percentage	Number of days	Percentage
CNRM-CM5	Almost Dry	2056	56.17	2083	56.91	2110	57.65
	High	667	18.22	691	18.88	713	19.48
	Medium	937	25.61	886	24.21	837	22.87
Rainfall states projected using CMIP6 model output							
Model	Rainfall states	Forecast for the period					
		2015–2040		2041–2070		2071–2100	
		Number of days	Percentage	Number of days	Percentage		
CNRM-CM6	Almost dry	1283	40.45	1146	31.31	1076	29.40
	High	519	16.36	754	20.60	771	21.06
	Medium	1370	43.19	1760	48.09	1813	49.54

under CMIP5 the model showing almost dry rainfall state was increasing over the study area, the same model was showing the medium and high rainfall states increasing under CMIP6 output. The current study is limited to two GCM models and one future scenario (RCP4.5/SSP245). The inclusion of more GCM models and future scenario for projection of daily rainfall states over the Tapi basin can be treated as future scope of the current study.

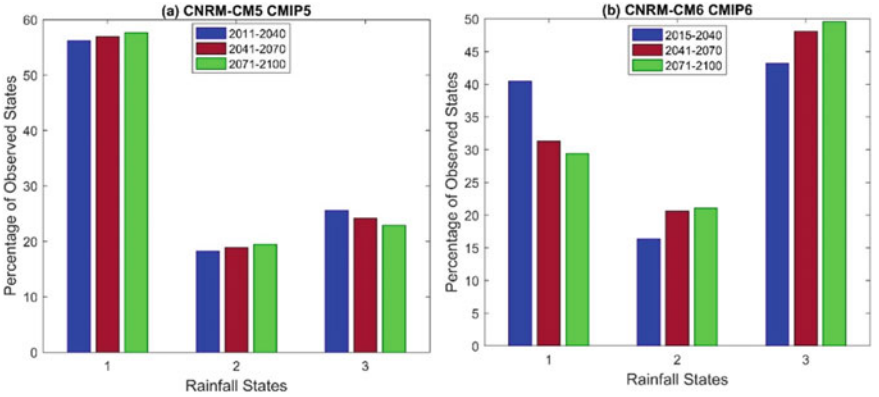

Fig. 7 Projected rainfall states of CNRM-CM5 and CNRM-CM6 model almost dry, high, and medium

Table 8 Breakup of number of rainy days projected for RCP4.5 scenarios for CNRM-CERFACS model under CMIP5 and CMIP6 project

Rainfall states projected using CMIP5 model output							
Model	Rainfall states	Forecast for the period					
		2011–2040		2041–2070		2071–2100	
		Number of days	Percentage	Number of days	Percentage	Number of days	Percentage
CanESM2	Almost dry	2039	55.70	2019	55.17	1930	52.74
	High	682	18.64	671	18.33	715	19.53
	Medium	939	25.66	970	26.50	1015	27.73
Rainfall states projected using CMIP6 model output							
Model	Rainfall states	Forecast for the Period					
		2015–2040		2041–2070		2071–2100	
		Number of days	Percentage	Number of days	Percentage	Number of days	Percentage
CanESM5	Almost dry	1318	41.45	1192	32.57	1030	28.14
	High	560	17.75	770	21.04	774	21.15
	Medium	1294	40.80	1698	46.39	1856	50.71

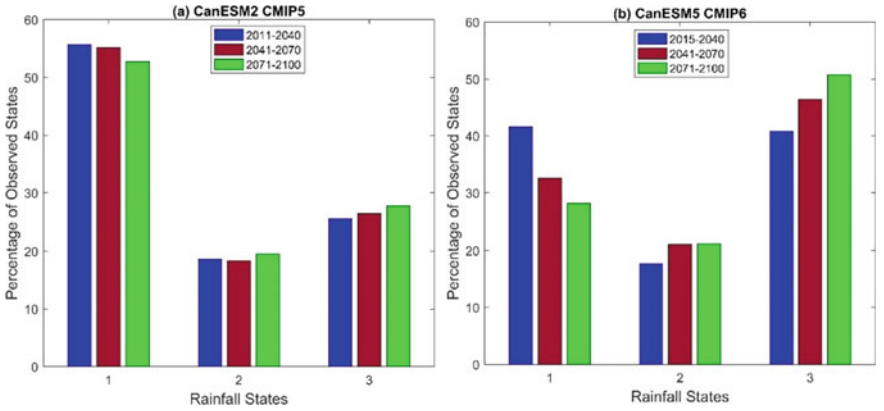

Fig. 8 Projected rainfall states of CanESM2 and CanESM5 model almost dry, high, and medium

Acknowledgements The authors would like to acknowledge the infrastructural support provided by the Centre of Excellence (CoE) on 'Water Resources and Flood Management', TEQIP-II, Ministry of Education (formerly, Human Resources Development (MHRD)), Government of India. The authors express their gratitude towards the India Meteorological Department (IMD), Pune, for the rainfall data used in the present study.

References

1. IPCC, Seneviratne SI, Zhang X, Adnan M, Badi W, Dereczynski C, Di Luca A, Ghosh S, Iskandar I, Kossin J, Lewis S, Otto F, Pinto I, Satoh M, Vicente-Serrano SM, Wehner M, Zhou B (2021) Weather and climate extreme events in a changing climate. In: MassonDelmotte V, Zhai P, Pirani A, Connors SL, Péan C, Berger S, Caud N, Chen Y, Goldfarb L, Gomis MI, Huang M, Leitzell K, Lonnoy E, Matthews JBR, Maycock TK, Waterfield T, Yelekçi O, Yu R, Zhou B (eds) Climate change 2021: the physical science basis. contribution of working group I to the sixth assessment report of the intergovernmental panel on climate change. Cambridge University Press
2. Kumar N, Tischbein B, Kusche J, Laux P, Beg MK, Bogardi JJ (2017) Impact of climate change on water resources of upper Kharun catchment in Chhattisgarh, India. J Hydrol: Regional Stud 13:189–207
3. Jena P, Azad S, Rajeevan MN (2015) CMIP5 projected changes in the annual cycle of Indian monsoon rainfall. Climate 4(1):14
4. Singh S, Kannan S, Timbadiya PV (2016) Statistical downscaling of multisite daily precipitation for Tapi basin using kernel regression model. Curr Sci 110(8):1468
5. Sharmila S, Joseph S, Sahai AK, Abhilash S, Chattopadhyay R (2015) Future projection of Indian summer monsoon variability under climate change scenario: an assessment from CMIP5 climate models. Global Planet Change 124:62–78
6. Ghosh S, Mujumdar PP (2006) projections by statistical downscaling. Curr Sci 90(3):396–404
7. Kannan S, Ghosh S (2013) A nonparametric kernel regression model for downscaling multisite daily precipitation in the Mahanadi basin. Water Resour Res 49(3):1360–1385

8. Menon A, Levermann A, Schewe J, Lehmann J, Frieler K (2013) Consistent increase in Indian monsoon rainfall and its variability across CMIP-5 models. Earth Syst Dynamics 4(2):287–300. https://doi.org/10.5194/esd-4-287-2013
9. Salvi K, Ghosh S (2013) High-resolution multisite daily rainfall projections in India with statistical downscaling for climate change impacts assessment. J Geophys Res: Atmospheres 118(9):3557–3578
10. Shashikanth K, Salvi K, Ghosh S, Rajendran K (2014) Do CMIP5 simulations of Indian summer monsoon rainfall differ from those of CMIP3? Atmosph Sci Lett 15(2):79–85
11. Raju KS, Sonali P, Kumar DN (2017) Ranking of CMIP5-based global climate models for India using compromise programming. Theoret Appl Climatol 128(3–4):563–574
12. Mishra V, Bhatia U, Tiwari AD (2020). Bias-corrected climate projections from coupled model inter comparison project-6 (CMIP6) for South Asia. arXiv preprint arXiv:2006.12976
13. SMC (2021) https://www.suratmunicipal.gov.in/TheCity/Weather (visited on 10-November 2021)
14. Kannan S, Ghosh S (2011) Prediction of daily rainfall state in a river basin using statistical downscaling from GCM output. Stoch Env Res Risk Assess 25(4):457–474

Assessment of Precipitation Extremes in Northeast India Under CMIP5 Models

Jayshree Hazarika and Deepjyoti Phukan

Abstract The northeastern region of India receives very high rainfall during the pre-monsoon and summer monsoon season, causing flood events, landslides, damage of crops, etc. The magnitude of these extreme events is increasing day by day. Therefore, the study of extreme precipitation has become very critical in predicting its consequences. Impacts of the changes in extreme events in the near as well as far future may be assessed by utilizing Intergovernmental Panel on Climate Change's (IPCC) global climate models (GCMs). However, the applicability of these models varies from region to region and is highly dependent on the characteristics of the region. Hence, correlation amongst the datasets should be studied before utilizing these climate models in planning and management-related works. In the present work, an attempt is made to assess the suitability of three global climate model (GCM) data from the coupled model intercomparison project phase 5 (CMIP5) under the extreme carbon concentration scenario (RCP8.5) in capturing the extreme precipitations occurring in the northeastern region of India. For this purpose, 30-year observed precipitation data (1971–2000) of 2 different stations have been used. For assessing the extremes, 2 extreme precipitation indices (EPIs) have been utilized, viz. mean precipitation (MP), cumulative wet days (CWD), cumulative dry days (CDD), annual maximum 1-day precipitation (AMP1), annual maximum 5-day precipitation (AMP5), precipitation less than 1 mm (P1), precipitation less than 3 mm (P3), and precipitation more than 40 mm (P40). The results indicate fair correlations between the observed and climate model datasets. However, coming to a definite conclusion still needs further

J. Hazarika · D. Phukan (✉)
Department of Civil Engineering, Assam Engineering College, Jalukbari, Guwahati, Kamrup-Metro 781013, Assam, India
e-mail: deepjyotiphukan814@gmail.com

J. Hazarika
e-mail: jayshree@iitg.ac.in

P. V. Timbadiya et al. (eds.), *Climate Change Impact on Water Resources*, Lecture Notes in Civil Engineering 313, https://doi.org/10.1007/978-981-19-8524-9_8

research by including more GCMs, which may give better results. Studies on annual rainfall over the region have shown no significant trends.

Keywords CMIP5 · GCM · RCP · ESM · Extreme precipitation indices (EPIs)

1 Introduction

Global warming is now becoming the most threatening issue for the today's world. Because of this, it affects on the climate. As a result, rainfall pattern is now changed globally. The effect of this change in the rainfall pattern is greatly seen in [1, 2] India and the northeastern region of India [3, 4]. Since this region mostly depends on the agriculture and flood, droughts occur very severely here, therefore, the trend analysis of the rainfall pattern is very important.

In this study, assessment of extreme precipitation events is done to study the rainfall trend for the period of 30 years from 1971 to 2000. Two stations of northeastern Region are selected, viz. (1) Guwahati and (2) North Lakhimpur for this study, and GCM models, viz. ESM2G, ESM2M, and CM3 are used for analysis the trends.

2 Study Area and Data Collection

2.1 Study Area

The topography and geographical position of the northeastern region is different from the rest of the states of India. This region consists of 8 states, namely Assam, Meghalaya, Manipur, Nagaland, Arunachal Pradesh, Mizoram, Tripura, and Sikkim. The 2nd longest river of India, the Brahmaputra, flows through this region (mainly Assam and Arunachal Pradesh) which predominantly affects the rainfall pattern of NER. Also large number of forest covers including the hills surrounding the region greatly affects the ecosystem of this region.

2.2 Data Collection

Observed daily precipitation data for the two stations were collected from Indian Meteorological Department (IMD), and the GCM data were downloaded from Intergovernmental Panel on Climate Change (IPCC).

The present study considers total rainfall (in 0.1 mm) in 24 h for a period of 30 years from 1971 to 2000. The EPIs considered are mean precipitation in mm,

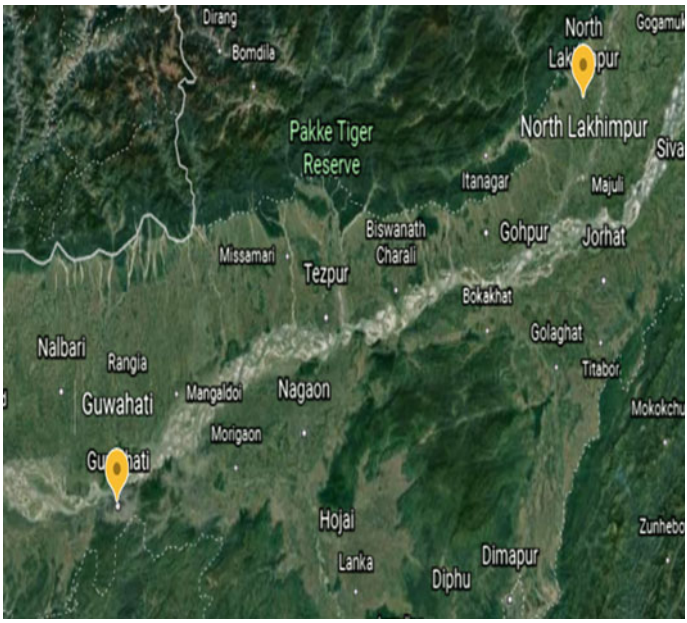

Fig. 1 Location of IMD stations

CWD, CDD, annual maximum 1-day precipitation, annual maximum 5-days precipitation, precipitation < 1 mm, precipitation < 3 mm, and precipitation > 40 mm. The location of the two IMD stations is shown in Fig. 1.

2.3 Calculated Values of EPIs

See Tables 1, 2, and 3.

Table 1 EPIs calculated from observed data of IMD for Guwahati and North Lakhimpur stations

Station	Mean ppt (in mm)	CWD	CDD	ppt < 1 mm (in days)	ppt < 3 mm (in days)	ppt > 40 mm (in days)	Annual max 1-day ppt (in mm)	Annual max 5-day ppt (in mm)
Guwahati	1723.86	136	229	255	279	9	101.21	199.28
North Lakhimpur	3189.047	170	195	219	243	24	101.21	312.15

Table 2 EPIs calculated from historical data of ESM2M model for Guwahati and North Lakhimpur stations

Station	Mean ppt (in mm)	CWD	CDD	ppt < 1 mm (in days)	ppt < 3 mm (in days)	ppt > 40 mm (in days)	Annual max 1-day ppt (in mm)	Annual max 5-day ppt (in mm)
Guwahati	1723.7833	211	154	203	233	4	81.142	200.07
North Lakhimpur	3192.418	303	63	131	171	11	129.078	346.15

Table 3 EPIs calculated from historical data of CM3 model for Guwahati and North Lakhimpur stations

Station	Mean ppt (in mm)	CWD	CDD	ppt < 1 mm (in days)	ppt < 3 mm (in days)	ppt > 40 mm (in days)	Annual max 1-day ppt (in mm)	Annual max 5-day ppt (in mm)
Guwahati	1723.85	333	33	158	202	1	61.053	141.678
North Lakhimpur	3192.414	335	30	126	169	8	89.054	246.67

3 Results and Discussion

Yearly variation of EPIs calculated from observed data and simulated climate model data over 30 years (1971–2000) for Guwahati and North Lakhimpur Stations are depicted in the following charts (Figs. 2, 3, 4, 5, 6, 7, 8, and 9).

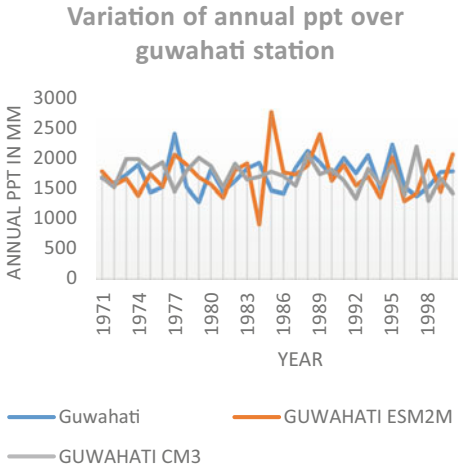

Fig. 2 Annual ppt graph between observed and GCM data for Guwahati station

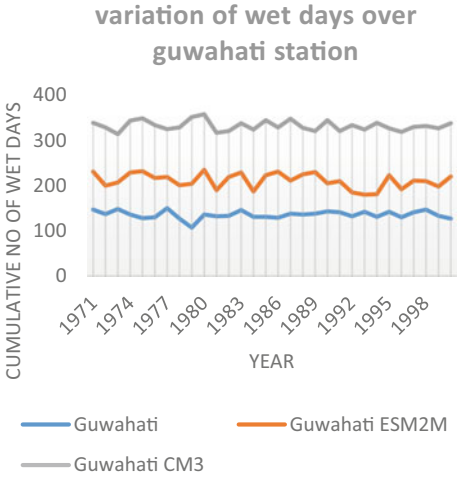

Fig. 3 No. of wet days graph between observed and GCM data for Guwahati station

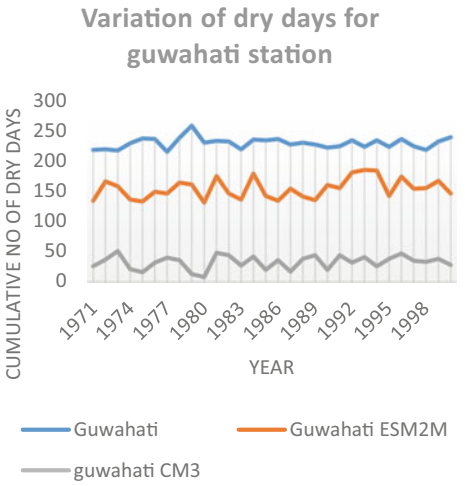

Fig. 4 No. of dry days graph between observed and GCM data for Guwahati station

4 Assessment of Simulated Historical Data

4.1 For the Station Guwahati

From the model ESM2M

Mean precipitation (PR) of Guwahati Station from the period 1971 to 2000 calculated from simulated historical data is similar to observed data collected from IMD. The value of CWD calculated is slightly large as compared to observed data, whereas

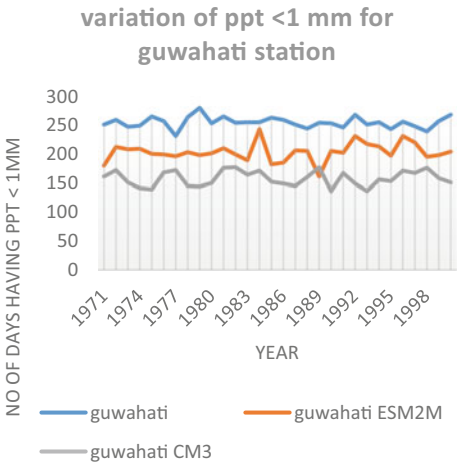

Fig. 5 No. of days having ppt < 1 mm graph between observed and GCM data for Guwahati station

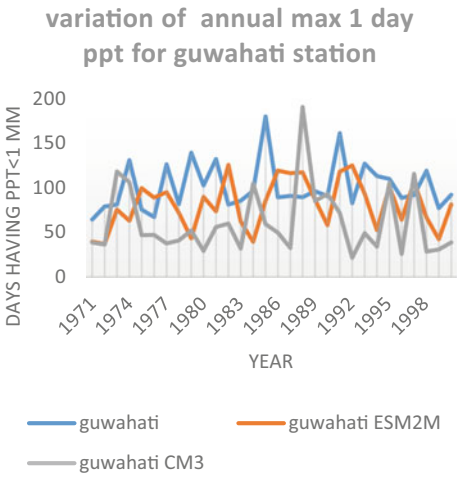

Fig. 6 Annual max 1-day ppt graph between observed and GCM data for Guwahati station

CDD value is less. Moreover, 1-day max precipitation value is more for observed data.

From the model CM3

Mean precipitation (PR) of Guwahati Station calculated from simulated historical data is similar to observed data collected from IMD. The value of CWD calculated is very large as compared to observed data, whereas CDD value stands at very low value. Moreover, no. of days having ppt value is only 1 obtained from CM3 against 9 from observed value.

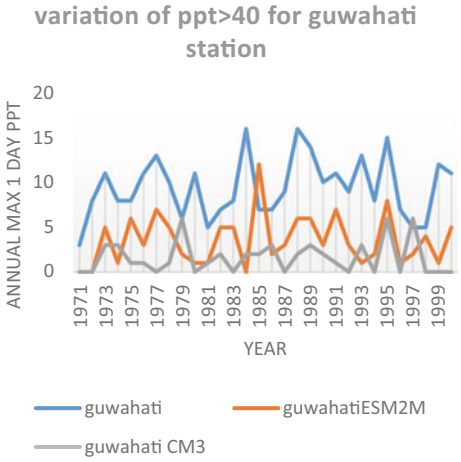

Fig. 7 No. of days having ppt > 40 graph between observed and GCM data for Guwahati station

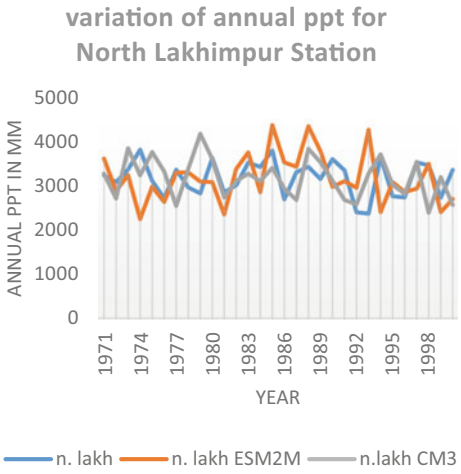

Fig. 8 Annual ppt graph between observed & GCM data for North Lakhimpur station

4.2 For the Station North Lakhimpur

From the model ESM2M

Mean precipitation (PR) of North Lakhimpur Station from the period 1971 to 2000 calculated from simulated historical data is similar to observed data collected from IMD. The value of CWD calculated is slightly large as compared to observed data, whereas CDD value is less. Moreover, 1-day max precipitation value is more for observed data.

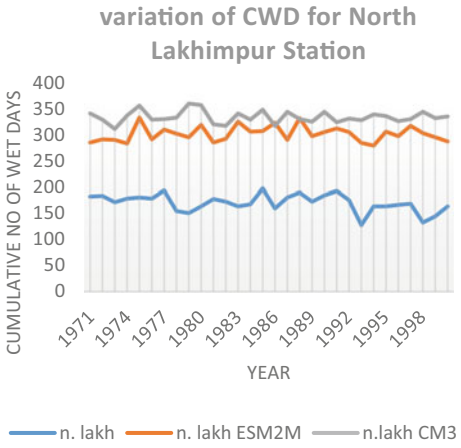

Fig. 9 No. of wet days graph between observed and GCM data for North Lakhimpur station

From the model CM3

Mean precipitation (PR) of North Lakhimpur Station calculated from simulated historical data is similar to observed data collected from IMD. The value of CWD calculated is very large as compared to observed data, whereas CDD value stands at very low value. Moreover, no. of days having ppt value is only 8 obtained from CM3 against 24 from observed value.

Similar kind of trend has been observed for the model ESM2G for both the stations.

5 Comparison with the Previous Studies

A similar study was carried out by Jain et al. [5] to analyze the annual rainfall trends for the northeastern region. From the year 1871 to 2008, they divided the timescale into smaller scales to detect local trends for rainfall, i.e. 1871–1950 and 1951–2008. In their study, they found no clear cut trend for the rainfall data series from 1871 to 2008 for the North Eastern Region, and hence, they also could not reach at the finding final trend of the rainfall pattern for the NER.

6 Conclusions

From the results, it is seen that mean precipitation value obtained from the models ESM2M and CM3 for the Stations Guwahati and North Lakhimpur is same with the observed value obtained from IMD. The value of other indices, viz. CDD, CWD, ppt < 1 mm, ppt > 40 mm obtained from the models varies greatly with the observed values.

The analysis of the rainfall data for the stations revealed that there is no significant trend of the precipitation indices except mean precipitation value which has almost similar value for both observed and historical data.

Also, the rainfall data are varied from model to model. Datasets, we have obtained from ESM2M and ESM2G models, have almost similar values but it varies for CM3 model which showed relatively greater values than these two. Therefore, from the analysis, we can conclude that historical values highly differed from the observed values of IMD. In predicting future scenarios, to obtain better results, we need to enhance these models by further research and including more GCMs.

Acknowledgements The authors will be always thankful to Indian Meteorological Department (IMD) for providing us the necessary data which has helped us to fulfil the present study.

References

1. Gupta V, Singh V, Jain MK (2020) Assessment of precipitation extremes in India during the 21st century under SSP1–1.9 mitigation scenarios of CMIP6 GCMs. J Hydrol 590:125422
2. Dunne JP et al (2012) GFDL's ESM2 global coupled climate–carbon earth system models. Part I: physical formulation and baseline simulation characteristics. J Clim 25(19):6646- 6665
3. Dash SK et al (2012) Temperature and precipitation changes in the north-east India and their future projections. Global Planet Change 98:31–44
4. Mukherjee S et al (2018) Increase in extreme precipitation events under anthropogenic warming in India. Weather Clim Ext 20:45–53
5. Jain SK, Kumar V, Saharia M (2013) Analysis of rainfall and temperature trends in northeast India. Int J Climat 33(4):968–978

Impact of Climate Change on Precipitation Extremes in Northeast India Under CMIP5 Models

Jayshree Hazarika and Mridusmita Boro

Abstract The increase in greenhouse gases has triggered substantial changes in the precipitation patterns and extremes both at local as well as global scale. Hence, a great interest has emerged in society for assessing the impacts of climate change under various plausible future scenarios. The north-eastern region of India receives a high amount of rainfall during the monsoon season which brings heavy floods to the region every year. The devastation caused by these annual flood events is of very high magnitude. Therefore, assessment of occurrences of these events in the coming years has become very crucial for proper water resources planning and management. In this study, an attempt is made for assessing the impact of climate change on precipitation extremes in the north-eastern region of India in future from 2006 to 2100. For this purpose, 30-year observed precipitation data (1971–2000) and three Global Climate Models (GCMs)–GFDL-CM3, GFDL-ESM2G and GFDL-ESM2M data from the Coupled Model Intercomparison Project Phase 5 (CMIP5) under the extreme carbon concentration scenario (RCP8.5) has been used. For assessing the extremes, 8 extreme precipitation indices (EPIs) have been utilized, viz. mean precipitation (MP), cumulative wet days (CWD), cumulative dry days (CDD), annual maximum 1-day precipitation (AMP1), annual maximum 5-day precipitation (AMP5), precipitation less than 1 mm (P1), precipitation less than 3 mm (P3) and precipitation more than 40 mm (P40). The results have shown significant increase in the case of indices like MP, CWD and AMP1. These changes indicate the possibility of increase in extreme flood events and subsequently points towards future risks associated with them.

J. Hazarika · M. Boro (✉)
Department of Civil Engineering, Assam Engineering College, Jalukbari, Guwahati, Kamrup-Metro, Assam 781013, India
e-mail: mridusmita2boro72@gmail.com

J. Hazarika
e-mail: jayshree@iitg.ac.in

P. V. Timbadiya et al. (eds.), *Climate Change Impact on Water Resources*, Lecture Notes in Civil Engineering 313, https://doi.org/10.1007/978-981-19-8524-9_9

Keywords GCM · CMIP5 · ESM · RCP · Extreme precipitation indices (EPIs)

1 Introduction

The present population of the world is 7.9 billion; by 2050 it will be 9 billion and by 2100 there will be 12 billion people in the world. So, increase in CO_2 is inevitable in future; since more population indicates more consumption of energy. However, the percentage increase in CO_2 can be controlled by adding wind and solar energy projects. Increase in CO_2 content is a major factor of climate change. There is a great curiosity amongst climatologists and environmentalists for assessing the impacts of projected climate change in extreme events that could accompany global climate change predictions. North-East India exhibits the character of tropical climate, especially in the valleys. Very heavy rainfall occurs in this region confined within four months of summer from June to September. Therefore, assessment of impact of climate change on precipitation extremes is of utmost importance in the present day scenario for proper water resources planning and management. Studies on temporal and spatial variability of rainfall over India, highlighting the need for water resources planning and management has shown decreasing trend in monsoon rainfall and liability of flash flood [1–10].

In this study, assessment of impact of climate change on rainfall extremes is done for 8 IMD stations–Guwahati, Cherrapunji, Imphal, Mohanbari, North Lakhimpur, Passighat, Shillong and Tezpur located in North-Eastern region (NER) of India. For this purpose, 30-year observed precipitation data (1971–2000) and three Global Climate Models (GCMs)–GFDL-CM3, GFDL-ESM2G and GFDL-ESM2M data from the Coupled Model Intercomparison Project Phase 5 (CMIP5) under the extreme carbon concentration scenario (RCP8.5) is used. The GCM data is first bias-corrected using CMhyd tool, as GCM data are only available at grid points. The bias-corrected simulated historical and future data is then utilized for the calculation of Extreme Precipitation Indices (EPIs).

2 Study Area and Data Source

2.1 North-Eastern Region (NER)

The climate of north-eastern region of India is influenced by its topography and the southwest and northeast monsoons (Fig. 1). NER has a tropical climate with heavy rainfall in summer. The Himalayas to the north, the Meghalaya plateau to the south and the hills of Nagaland, Mizoram and Manipur to the east influences the climate. Monsoon winds originating from the Bay of Bengal move towards northeast. After hitting the mountains, the moist winds move upwards, causing them to cool

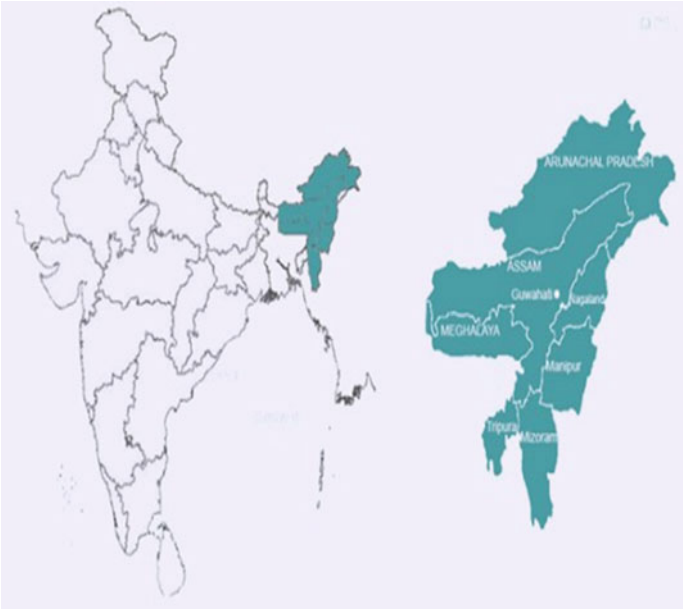

Fig. 1 Map of India showing NER

adiabatically and condense into clouds, resulting in orographic precipitation on these slopes. The locations of 8 IMD stations chosen in NER for this study are shown in Fig. 2 [11, 12].

2.2 Data Used

Observed daily precipitation data of each station were collected from Indian Meteorological Department (IMD) and Global Climate Models (GCM) data were downloaded from Intergovernmental Panel on Climate Change (IPCC) (Table 1).

3 Results and Discussion

See Tables 2, 3, and 4.

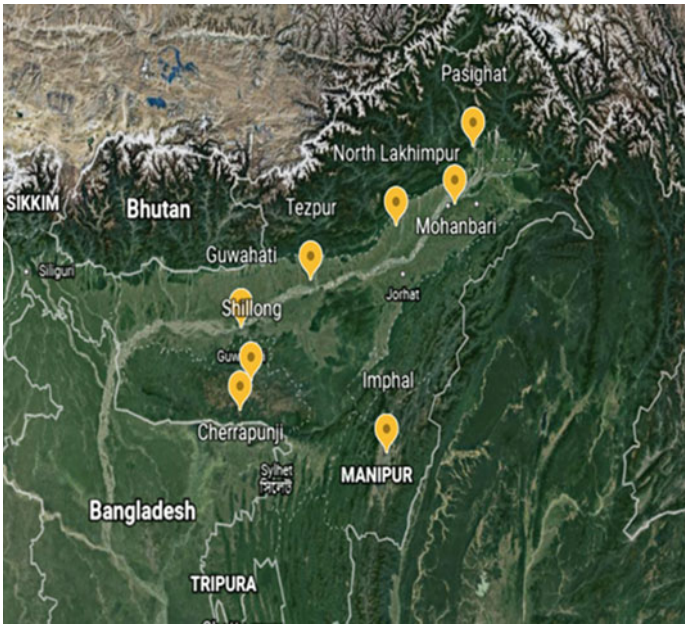

Fig. 2 Location of IMD station

Table 1 Definition and units of EPIs considered

Index	Indicator name	Definition	Unit
MP	Mean precipitation	Total Precipitation amount in a year	mm
CWD	Cumulative wet days	Total Number of days Precipitation is > 0 mm	Days
CDD	Cumulative dry days	Total number of days precipitation is 0 mm	Days
AMP1	Maximum 1-day Precipitation	Highest precipitation in a year in a single day	mm
AMP5	Maximum 5-days precipitation	Highest cumulative 5-days precipitation in a year	mm
P1	Precipitation < 1 mm	Total number of days precipitation is < 1 mm	Days
P3	Precipitation < 3 mm	Total number of days precipitation is < 3 mm	Days
P40	Precipitation > 40 mm	Total number of days precipitation is > 40 mm	Days

Table 2 EPIs calculated from observed, simulated historical and simulated future data of CM3 model

Sl. no	Indices	Station	Observed	Historical	Future		
			1971–2000	1971–2000	2006–2040	2041–2070	2071–2100
1	MP	Cherrapunji	11,514	11,513	12,028	12,817	12,786
		Guwahati	1724	1724	1850	1942	2113
		Imphal	1386	1248	1261	1311	1191
		Mohanbari	2607	2607	2454	2544	2635
		N. Lakhimpur	3189	3192	3174	3246	3321
		Passighat	4598	4598	4426	4949	5284
		Shillong	2160	2160	2438	2498	2405
		Tezpur	1821	1831	1810	1865	1930
2	CWD	Cherrapunji	172	256	251	253	246
		Guwahati	136	333	282	291	289
		Imphal	148	267	236	234	222
		Mohanbari	174	328	293	286	277
		N. Lakhimpur	170	335	317	317	312
		Passighat	196	358	344	348	343
		Shillong	172	272	241	243	237
		Tezpur	133	331	304	304	299
3	CDD	Cherrapunji	193	109	114	112	119
		Guwahati	229	33	83	74	76
		Imphal	218	98	129	131	143
		Mohanbari	191	37	72	79	88
		N. Lakhimpur	195	30	48	48	53
		Passighat	169	7	21	17	22
		Shillong	193	94	124	122	128
		Tezpur	232	35	61	61	66
4	AMP1	Cherrapunji	605	369	386	395	374
		Guwahati	101	61	67	77	75
		Imphal	91	57	72	48	47
		Mohanbari	135	74	65	66	76
		N. Lakhimpur	156	89	88	97	96
		Passighat	250	132	132	162	165
		Shillong	145	101	123	105	96

(continued)

Table 2 (continued)

Sl. no	Indices	Station	Observed	Historical	Future		
			1971–2000	1971–2000	2006–2040	2041–2070	2071–2100
		Tezpur	104	49	53	55	58
5	AMP5	Cherrapunji	1558	933	1009	1088	1007
		Guwahati	199	142	168	185	198
		Imphal	160	118	129	121	101
		Mohanbari	457	218	180	184	215
		N. Lakhimpur	312	247	239	257	273
		Passighat	633	406	396	477	490
		Shillong	493	208	275	251	221
		Tezpur	191	135	140	148	167
6	P1	Cherrapunji	200	180	146	141	145
		Guwahati	255	158	163	155	153
		Imphal	246	172	174	177	188
		Mohanbari	217	133	139	141	147
		N. Lakhimpur	219	126	120	120	125
		Passighat	211	54	79	76	80
		Shillong	224	161	165	162	164
		Tezpur	250	134	146	145	148
7	P3	Cherrapunji	216	194	163	158	159
		Guwahati	279	202	201	197	192
		Imphal	275	222	225	224	235
		Mohanbari	237	179	188	186	187
		N. Lakhimpur	243	169	175	170	170
		Passighat	238	148	144	140	137
		Shillong	259	196	193	194	196
		Tezpur	273	196	202	202	196
8	P40	Cherrapunji	72	95	118	116	115
		Guwahati	9	1	2	3	4
		Imphal	4	1	1	1	1
		Mohanbari	16	5	3	4	5
		N. Lakhimpur	24	8	8	8	11

(continued)

Table 2 (continued)

Sl. no	Indices	Station	Observed	Historical	Future		
			1971–2000	1971–2000	2006–2040	2041–2070	2071–2100
		Passighat	36	27	25	29	35
		Shillong	12	3	3	4	3
		Tezpur	11	1	1	2	3

Table 3 EPIs calculated from observed, simulated historical and simulated future data of ESM2G model

Sl. no.	Indices	Station	Observed	Historical	Future		
			1971–2000	1971–2000	2006–2040	2041–2070	2071–2100
1	MP	Cherrapunji	11,514	11,513	13,810	13,756	14,413
		Guwahati	1724	1723	2092	2032	2154
		Imphal	1386	1247	1470	1459	1525
		Mohanbari	2607	2606	2824	3060	3146
		N. Lakhimpur	3189	3192	3684	3894	4110
		Passighat	4598	4583	5232	5389	5473
		Shillong	2160	2159	2862	2678	2717
		Tezpur	1821	1830	2106	2222	2346
2	CWD	Cherrapunji	172	198	209	204	211
		Guwahati	136	185	191	186	193
		Imphal	148	195	196	190	196
		Mohanbari	174	275	281	272	281
		N. Lakhimpur	170	271	277	273	285
		Passighat	196	281	287	277	288
		Shillong	172	186	193	188	195
		Tezpur	133	265	269	266	278
3	CDD	Cherrapunji	193	167	156	161	154
		Guwahati	229	180	174	179	172
		Imphal	218	171	169	175	169
		Mohanbari	191	90	84	93	84
		N. Lakhimpur	195	95	88	92	80
		Passighat	169	84	78	88	77

(continued)

Table 3 (continued)

Sl. no.	Indices	Station	Observed	Historical	Future		
			1971–2000	1971–2000	2006–2040	2041–2070	2071–2100
		Shillong	193	179	172	177	170
		Tezpur	232	100	96	99	87
4	AMP1	Cherrapunji	605	526	773	1009	1161
		Guwahati	101	82	138	154	164
		Imphal	91	71	83	105	120
		Mohanbari	135	82	107	127	152
		N. Lakhimpur	156	128	159	198	230
		Passighat	250	157	214	240	299
		Shillong	145	115	223	226	219
		Tezpur	104	69	87	107	122
5	AMP5	Cherrapunji	1558	1349	1956	2435	2439
		Guwahati	199	200	328	335	359
		Imphal	160	151	192	227	246
		Mohanbari	457	220	276	324	369
		N. Lakhimpur	312	356	430	550	577
		Passighat	633	430	547	622	704
		Shillong	493	273	532	490	485
		Tezpur	191	192	236	300	311
6	P1	Cherrapunji	200	187	184	188	181
		Guwahati	255	211	206	211	206
		Imphal	246	207	205	212	208
		Mohanbari	217	137	138	140	132
		N. Lakhimpur	219	134	133	133	125
		Passighat	211	124	121	126	118
		Shillong	224	207	200	206	201
		Tezpur	250	151	151	150	143
7	P3	Cherrapunji	216	202	197	202	196
		Guwahati	279	236	232	238	234
		Imphal	275	243	239	247	244
		Mohanbari	237	176	177	180	176

(continued)

Table 3 (continued)

Sl. no.	Indices	Station	Observed	Historical	Future		
			1971–2000	1971–2000	2006–2040	2041–2070	2071–2100
		N. Lakhimpur	243	173	171	173	165
		Passighat	238	158	159	160	154
		Shillong	259	231	224	230	228
		Tezpur	273	198	194	197	192
8	P40	Cherrapunji	72	98	100	93	97
		Guwahati	9	3	5	7	7
		Imphal	4	1	3	4	4
		Mohanbari	16	5	8	10	11
		N. Lakhimpur	24	10	13	15	18
		Passighat	36	24	32	33	34
		Shillong	12	6	10	11	11
		Tezpur	11	3	5	7	8

Table 4 EPIs calculated from observed, simulated historical and simulated future data of ESM2M model

Sl. no.	Indices	Station	Observed	Historical	Future		
			1971–2000	1971–2000	2006–2040	2041–2070	2071–2100
1	MP	Cherrapunji	11,514	11,514	12,689	13,938	14,329
		Guwahati	1724	1724	1876	2010	2041
		Imphal	1386	1248	1447	1397	1370
		Mohanbari	2607	2607	2843	2956	2857
		N. Lakhimpur	3189	3192	3533	3859	3771
		Passighat	4598	4598	5017	5212	4988
		Shillong	2160	2160	2551	2633	2629
		Tezpur	1821	1830	2016	2180	2142
2	CWD	Cherrapunji	172	205	202	201	196
		Guwahati	136	211	191	189	184
		Imphal	148	222	197	197	189
		Mohanbari	174	306	283	281	273

(continued)

Table 4 (continued)

Sl. no.	Indices	Station	Observed	Historical	Future		
			1971–2000	1971–2000	2006–2040	2041–2070	2071–2100
		N. Lakhimpur	170	303	280	278	274
		Passighat	196	313	290	287	280
		Shillong	172	211	194	192	186
		Tezpur	133	297	272	271	266
3	CDD	Cherrapunji	193	160	163	164	169
		Guwahati	229	154	174	176	181
		Imphal	218	143	168	168	176
		Mohanbari	191	59	82	84	92
		N. Lakhimpur	195	63	85	87	91
		Passighat	169	53	75	78	85
		Shillong	193	154	171	173	179
		Tezpur	232	68	93	94	99
4	AMP1	Cherrapunji	605	548	837	1050	1383
		Guwahati	101	81	118	138	187
		Imphal	91	62	92	99	112
		Mohanbari	135	93	123	145	154
		N. Lakhimpur	156	129	168	213	221
		Passighat	250	112	244	280	306
		Shillong	145	116	176	185	262
		Tezpur	104	112	90	112	120
5	AMP5	Cherrapunji	1558	2179	1935	2410	3432
		Guwahati	199	200	270	318	457
		Imphal	160	138	219	205	245
		Mohanbari	457	234	315	373	367
		N. Lakhimpur	312	346	419	574	594
		Passighat	633	430	621	725	727
		Shillong	493	271	405	418	640
		Tezpur	191	187	226	304	313
6	P1	Cherrapunji	200	180	182	185	189
		Guwahati	255	203	206	210	214

(continued)

Table 4 (continued)

Sl. no.	Indices	Station	Observed	Historical	Future		
			1971–2000	1971–2000	2006–2040	2041–2070	2071–2100
		Imphal	246	201	205	210	220
		Mohanbari	217	130	138	139	144
		N. Lakhimpur	219	131	136	132	137
		Passighat	211	111	120	121	128
		Shillong	224	199	200	204	210
		Tezpur	250	147	155	151	143
7	P3	Cherrapunji	216	194	197	200	204
		Guwahati	279	233	236	240	244
		Imphal	275	242	243	250	257
		Mohanbari	237	173	183	184	187
		N. Lakhimpur	243	171	180	176	178
		Passighat	238	149	162	162	165
		Shillong	259	226	227	231	236
		Tezpur	273	199	202	202	205
8	P40	Cherrapunji	72	95	95	93	87
		Guwahati	9	4	5	6	6
		Imphal	4	2	4	3	5
		Mohanbari	16	7	8	10	10
		N. Lakhimpur	24	11	14	17	15
		Passighat	36	24	28	29	27
		Shillong	12	6	10	10	9
		Tezpur	11	4	5	8	8

3.1 Assessment of Simulated Historical Data

The Mean Precipitation (MP) calculated from simulated historical data of all the three models is similar to MP calculated from observed data collected from IMD (Fig. 3a). The values of CWD estimated by the climate models are seen to be very large as compared to observed data, whereas CDD values are comparatively very less (Fig. 3b, c). For CM3 model data, AMP1 and AMP5 values are very low; almost half the observed values whereas for the other two models ESM2G and ESM2M the values are almost similar with observed values. P1 and P3 values are underestimated as per these three models (Fig. 3f, g). Whereas P40 values are overestimated by the models (Fig. 3h).

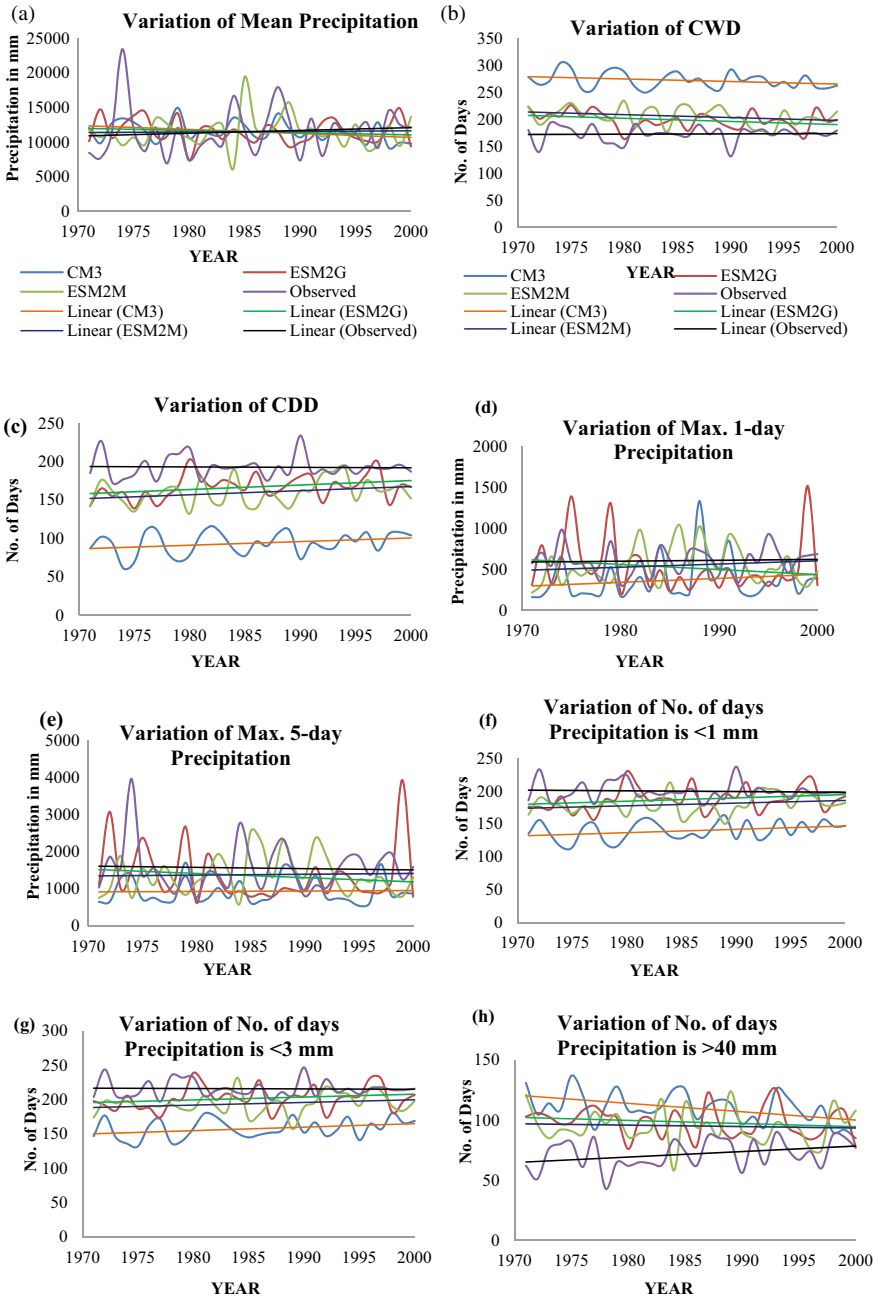

Fig. 3 Variation of EPIs calculated from observed data and simulated historical data over 30 years at Cherrapunji station for all the three climate models

The yearly variation of EPIs calculated from observed data and simulated historical climate model data over 30 years (1971–2000) for Cherrapunji station are depicted in the following charts (Fig. 3a–h).

3.2 Assessment of Simulated Future Data

From the study it is seen that there will be an increase of 10–20% in MP value by 2100. The simulated future data for all the three models are almost in the same range (Fig. 4a). The CWD estimated for future is showing large variation, CM3 model has overestimated the value largely (Fig. 4b). The CDD value predicted by the models is seen to be underestimated. ESM2G and ESM2M have predicted large values for AMP1, whereas CM3 on the other hand underestimated it (Fig. 4c). Similarly for AMP5, according to ESM2M and ESM2G the value will increase by 2100 but according to CM3's estimation it will decrease (Fig. 4e). For P1 and P3, the variation is similar; it will have less value in future as compared to present day (Fig. 4f, g). P40 will have higher values compared to present observed data (Fig. 4h).

The yearly variation of EPIs over 95 years (2006–2100) calculated from simulated future data for all the three models at Cherrapunji station is shown in the following charts (Fig. 4a–h).

4 Conclusions

The variation of monthly precipitation extracted from the simulated historical data of the models is similar with observed monthly precipitation data. The mean precipitation value is almost alike with the mean precipitation calculated from observed data. The other EPIs calculated from simulated historical data for all the three models shows large variation with the ones calculated from observed values.

Mean Precipitation (MP) is likely to increase in future considering RCP8.5 scenario; all the models have yielded the same result although with varying increase in percentage for different stations. The peak increase is seen in the last half, i.e. 2071–2100.CWD is also seen to increase with peak increase in 2nd half, i.e. 2041–2070. CDD will get decreased by 2100. AMP1 and AMP5 are seen to increase for all stations except Mohanbari, according to ESM2G and ESM2M simulated data. Whereas according to CM3 model, these two parameters will get decreased in future in all the stations. P1 & P3 will decrease in NER in future according to the models used. P40 is also seen to decrease; except at Cherrapunji station. The ultimate decrease in P40 value will be seen by the last half 2071–2100. Hence it can be concluded that climate change will have a great impact in rainfall patterns and subsequently on rainfall indices in the near future. Considering the increase in mean precipitation, the design of hydraulic structures for future should be such that it can accommodate sufficient flood water.

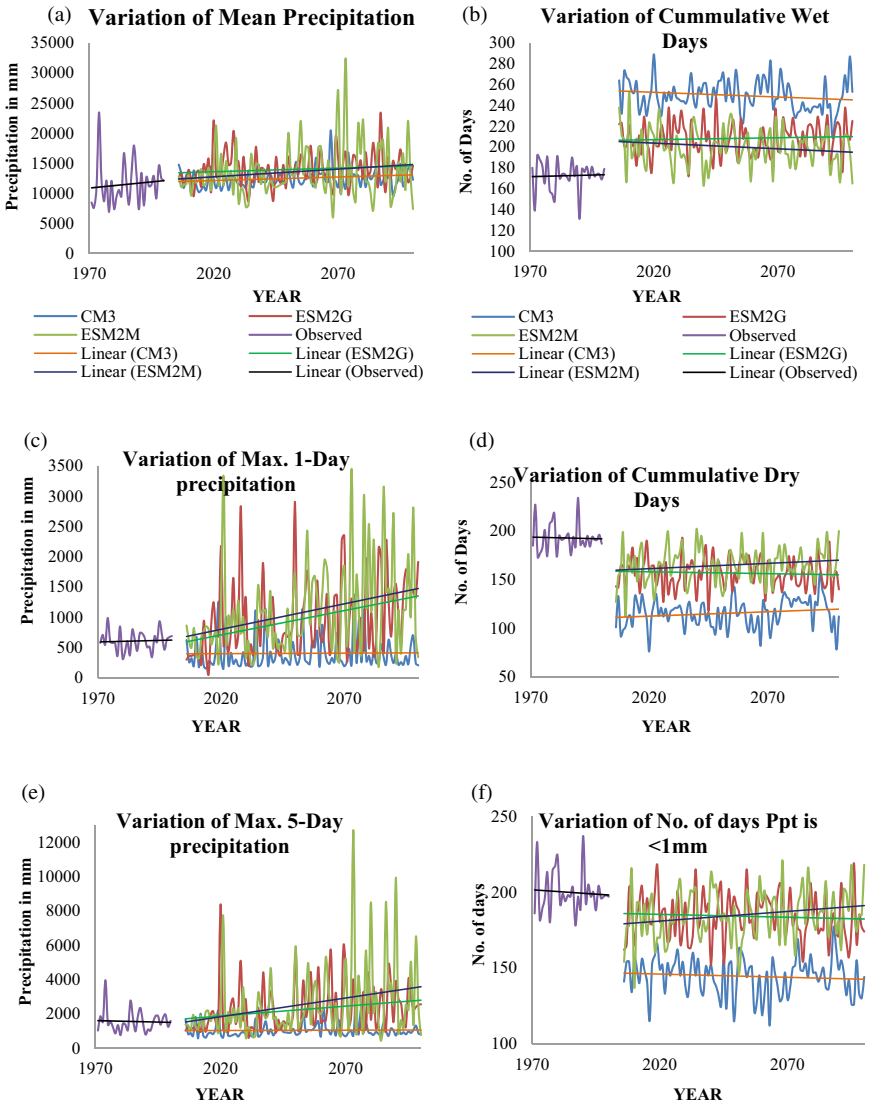

Fig. 4 Variation of EPIs calculated from observed data over 30 years (1971–2000) and simulated future data over 95 years (2006–2100) at Cherrapunji station for all the three climate models

The results varied from model to model. Although ESM2G and ESM2M generated data was seen to yield similar results, CM3 generated data showed completely different results. Some unusual behaviour was also observed in the results, which might have resulted from worst case scenario considered, i.e. RCP8.5 or due to unusual distance between gauges (IMD stations) and the nearest climate model grid cell or non-overlapping time periods between observed and simulated climate data.

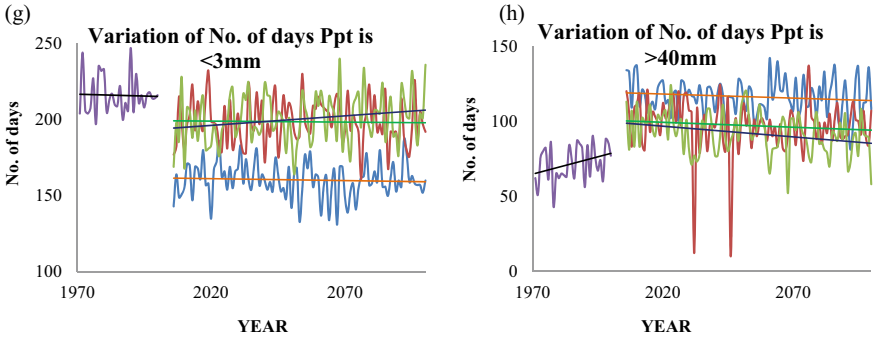

Fig. 4 (continued)

Since GCM data is available only at grid points, so these data after being extracted are again downscaled to the gauge stations and then it is used for further analysis. So depending on Bias-correction method used, the results might show such unusual behaviour.

Further studies can be done in this field using different climate models of CMIP5 as well as CMIP6 and considering more IMD stations. The study area can also be expanded to other parts of India. Another study can be made on climate models; as to why different climate models yield different results for the same IMD station irrespective of the same observed precipitation data being used for analysis.

Acknowledgements The authors are thankful to India Meteorological Department (IMD) for providing necessary data to carry out the present study.

References

1. Ghosh S et al (2016) Indian summer monsoon rainfall: implications of contrasting trends in the spatial variability of means and extremes. PloS one 11(7):e0158670
2. Guhathakurta P et al (2015) Observed changes in southwest monsoon rainfall over India during 1901–2011. Int J Climatol 35(8):1881–1898
3. Khan M, et al (2019) Spatial heterogeneity of temporal shifts in extreme precipitation across India. J Clim Change 5(1):19–31
4. Mishra AK et al (2019) Evidence of links between regional climate change and precipitation extremes over India. Weather 74(6):218–221
5. Dunne JP et al (2012) GFDL's ESM2 global coupled climate–carbon earth system models. Part I: physical formulation and baseline simulation characteristics. J Clim 25(19):6646–6665
6. Gupta V, Singh V, Jain MK (2020) Assessment of precipitation extremes in India during the 21st century under SSP1–1.9 mitigation scenarios of CMIP6 GCMs. J Hydrol 590:125422
7. Mehrotra D, Mehrotra R (1995) Climate change and hydrology with emphasis on the Indian subcontinent. Hydrol Sci J 40(2):231–242
8. Mukherjee S et al (2018) Increase in extreme precipitation events under anthropogenic warming in India. Weather Clim Ext 20:45–53

9. Myhre G, et al (2019) Frequency of extreme precipitation increases extensively with event rareness under global warming. Scient Reports 9(1):1–10
10. Sharma RH, Shakya NM (2006) Hydrological changes and its impact on water resources of Bagmati watershed, Nepal. J Hydrol 327(3–4):315–322
11. Dash SK et al (2012) Temperature and precipitation changes in the north-east India and their future projections. Global Planet Change 98:31–44
12. Jain SK, Kumar V, Saharia M (2013) Analysis of rainfall and temperature trends in northeast India. Int J Climat 33(4):968–978

Climate Change Impact Assessment on Water Resources–A Review

Prajakta Prabhakar Surkar and M. K. Choudhary

Abstract Water been a spatio-temporal variable resource have various uncertainties affecting the hydrological cycle that should be properly understood for management of water resources. Hydro-meteorological events like floods, droughts, cyclones, glacier melting, etc. are occurring frequently nowadays and are of great concern to hydrologist and climate scientists. These events are ignited due to combined effect of climate change, land use and land cover (LULC) changes and anthropogenic activities in the watershed. Various researchers, scientists and organizations are now working on climate change impact along with its mitigation and adaptation strategies to be adopted in regional and global level. This review paper aims in providing basic, essential and integrated information for hydrologist and beginners working in the field of climate change impact assessment on water resources. The terms such as emission scenarios, representative concentration pathways (RCPs), general circulation model (GCM), regional climate model (RCM), data downscaling, bias correction and uncertainties in climate modelling are discussed. The paper summarizes past literature and concludes with appropriate and most frequently used models and methods adopted in each step of climate change impact assessment. This will help researchers to perform acceptable assessment and give rational results that can help policy makers to take appropriate decisions regarding adaptation and mitigation strategies.

Keywords Downscaling · Bias correction · GCM · RCM · RCP

P. P. Surkar (✉) · M. K. Choudhary
Department of Civil Engineering, Maulana Azad National Institute of Technology Bhopal, Bhopal, Madhya Pradesh 462003, India
e-mail: prajaktasurkar35@gmail.com

P. V. Timbadiya et al. (eds.), *Climate Change Impact on Water Resources*, Lecture Notes in Civil Engineering 313, https://doi.org/10.1007/978-981-19-8524-9_10

1 Introduction

Climate and weather are two terms that are often mistaken and misunderstood. Weather is a short-term phenomenon where one can observe changes in the temperature, cloud cover, precipitation, humidity and wind in a region within hours or days or months. Whereas, climate is a long-term phenomenon, that is, the average weather of a region over many years. These long-term changes in the average weather pattern at a local, regional and global level is called climate change. The increase in urbanization and industrialization leads to an increase in greenhouse gases emissions causing global warming (rising in the earth's average temperature) and climate change. This climate change affects the water budget of hydrology and is an increasing concern for climate scientists, hydrologists, environmentalists and policymakers. The increase in hydro- meteorological events such as floods, drought, cyclones, glacier melting, heatwaves, sea-level rise, etc., are more frequently seen nowadays and are an alarming sign of degrading climate.

The Intergovernmental Panel on Climate Change (IPCC is the UN organization that works to obtain the science associated with climate change. This body releases reports after certain years that give consolidated and integrated facts, statistics and guidelines. The recently released report by working group I for AR6 (AR6 Climate Change 2021: The Physical Science Basis) [25] clarifies that anthropogenic activities are causing climate change and this ultimately affects the atmosphere, ocean, cryosphere and biosphere, leading to an impact on the hydrological cycle and water resources locally, regionally and globally. In the same report of AR6, it is also stated that the damage caused to the climate is already irreversible and will lead to an increase in extreme events along with chances of compound extreme events in the future, at least till the end of the twenty-first century, even under lowest scenario consideration [25]. This leads to the seriousness of studying the impact of climate change on water resources, so that proper adaptation and mitigation strategies can be made.

2 Climate Change Impact on Water Resources

Hydrological cycle theoretically plays a vital role in studying climate change impact on water resources. Hydrological cycle is classified as natural hydrological cycle and binary hydrological cycle depending on the driving factors (natural factors or both natural and anthropogenic factors respectively). Due to the interference of human activities and climate change, the original natural hydrological cycle system is imbalanced and is now converted to the binary hydrological cycle [49]. Long-term variation studies or trend analysis of precipitation, temperature and evapotranspiration has been extensively given importance for studying the impact of climate change on hydrological cycle and ultimately on water resources [21]. The hydrological responses to these variables (that are substantially studied to address water issues) are runoff and

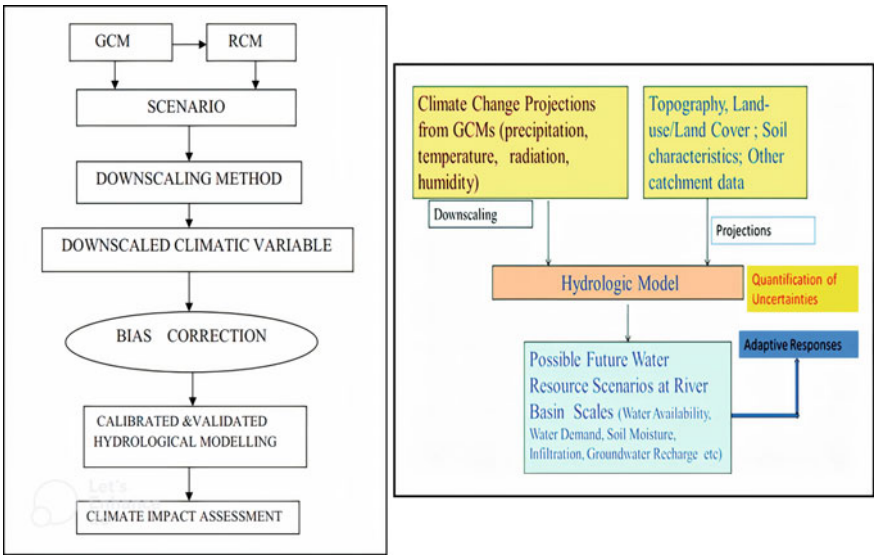

Fig. 1 Methodology for climate change impact assessment on water resources. *Source* [6, 8]

river discharge, water availability, glacier melting, sea-level rise, mean and extreme precipitation variation, drought and flood analysis, evapotranspiration analysis, soil moisture analysis, groundwater analysis and water quality analysis.

The climate change impact assessment of water resources is carried out with a proper methodology that has been addressed in several studies such as [7, 29, 46]. The basic and simple flow chart given by [6, 8] is shown in Fig. 1. This explains that the climate data or climate projections from GCMs or RCMs (historical data or future scenario data) are downscaled to the required scale and further bias correction is applied. This processed climate data along with other data (such as topographical data, land use land cover (LULC) data, soil data, catchment data.) is applied to the calibrated and validated hydrological model selected for the study. The hydrological model is chosen depending on the requirement of output or hydrological response to be studied. Further, analysis of the output obtained from the hydrological model is done to take appropriate adaptation and mitigation strategies.

2.1 Climate Change Scenarios

The future is always uncertain and it is highly difficult and challenging to exactly state the future conditions and happenings. So, to study the earth's climate change and impact on various sectors, different scenarios are developed. These scenarios are alternate images of the future, with certain assumptions, answering how the future might be. In short, these are essential scientific tools or methods for exploring

possible future in context of climate change and its impact. The development of scenarios started in 1990s with the IS92 scenarios (first developed set of long-term scenarios) [23] and most widely used the IPCC Special Report on Emission Scenarios (SRES) in 2000 [30]. The Four storylines A1, A2, B1 and B2 were developed and for each storyline separate scenarios were developed leading to a total of 40 scenarios, of which six were selected as demonstrative scenarios that can be widely used (one for each of the storylines in addition with high and low emissions variants of A1 storyline) [9, 14].

With the emerging challenges and addressing uncertainties, the need for scenarios that are more detailed and used for comparing future changes with different climate policies instead of no climate policy (as SRES) was needed. To address this need, scientific communities working with earth/climate models (CM), Integrated assessment models (IAM) and impact, adaptation and vulnerability (IAV) developed a new set of scenarios in three phases [14, 45]. Firstly, development of Representative Concentration Pathways (RCPs). Secondly, development of Shared Socioeconomic Pathways (SSPs). And lastly, a final integrated and disseminated scenario development to be used by climate change science community. The road map of this three-phase design is properly explained by [28]. Further, the use of RCPs along with SSPs for combining future socioeconomic conditions with possible mitigation and adaptation policies, a conceptual framework approach or scenario matrix approach is being adopted. This is explained by [3, 14, 31, 44]. These scenarios and the framework or matrix approach are used depending upon the availability of data from GCM/RCM and the requirement of one's study.

The four Representative Concentration Pathways (RCP2.6, 4.5, 6.0 and 8.5), as its name explains, are trajectories of GHG concentrations with radiative forcing (in W/m^2) along with mitigation actions in their formulation to stabilize the radiative forcing at the end of twenty-first century. RCP2.6 is considered as the best-case scenario whereas RCP8.5 is considered as worst-case scenario. The RCPs and its development are further elaborated by [45]. The five Shared Socioeconomic Pathways (SSP1, SSP2, SSP3, SSP4, SSP5) are development scenarios, each with different qualitative and quantitative characteristics that describes how the societal future might appear in terms of population growth, administrative effectiveness, inequality, socioeconomic developments, institutional elements, technological evolution and environmental conditions [3]. The characteristics of SSPs explained by [32] and extracted in short table format by [3] is shown in Table 1.

2.2 Climate Models and Its Approach in Impact Assessment

Climate models are basically quantitative methods or models that are used to stimulate the interaction of climate drivers (atmosphere, ocean, land surface and ice) to study the dynamics of future projection [10]. In climate change impact assessment for water resources, General Circulation Models also called as global climate models (GCMs) are the climate models that helps to simulate the climate response

Table 1 Shared Socioeconomic Pathways (in context to mitigation and adaptation challenges level)

SSP	Path	Challenges to mitigation and adaptation
SSP1	Sustainability	Low challenges to mitigation or adaptation
SSP2	Middle of the road	Intermediate challenges
SSP3	Fragmentation	High challenges to both mitigation and adaptation
SSP4	Inequality	Low challenges to mitigation, but high adaptation challenges
SSP5	Conventional development	Low challenges to adaptation, but high challenges to mitigation

Source [3, 32]

for different scenarios. The scenarios are inputs for the GCMs and the "RUN" of GCMs are the outputs that are used for impact studies. The GCMs have evolved from Atmospheric GCMs (AGCM) to coupled Atmosphere–ocean GCMs (AOGCM) and further addition of various other components such as aerosols, carbon cycle, dynamic vegetation, atmospheric chemistry and land use leading to an integrated model called as Earth system models or GCMs [17]. Figure 2. shows this evolution of GCMs with time and IPCC reports [2].

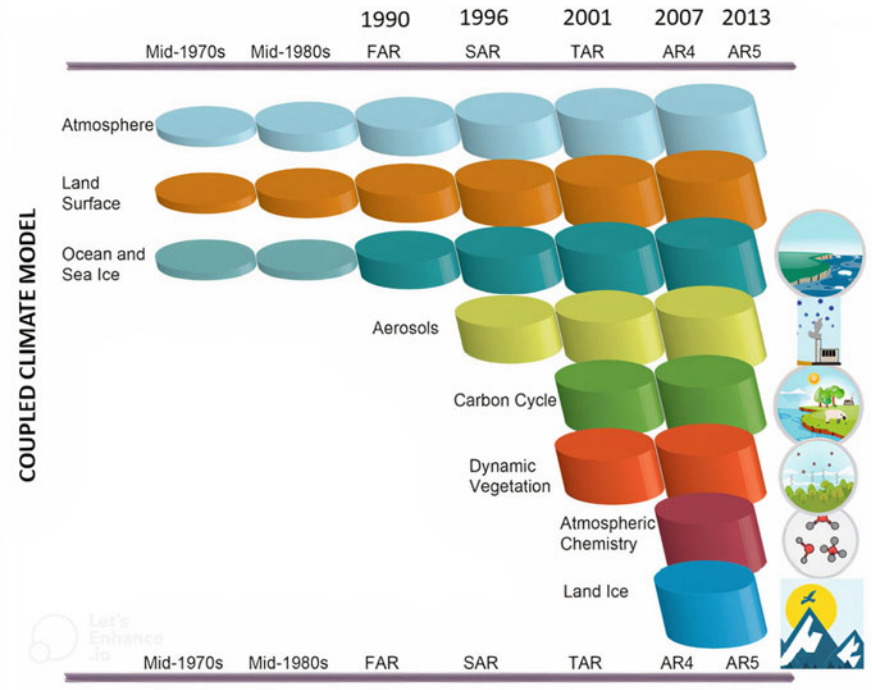

Fig. 2 Evolution of GCMs used in IPCC assessment report with respect to time. *Source* [2]

The most widely used GCMs are models under Coupled Model Intercomparison Project (CMIP) coordinated by the World Climate Research Programme (WCRP). These CMIP models are evolved into five phases and are used in IPCC assessment reports from time to time. The CMIP3 models run with SRES scenarios whereas CMIP5 run with RCP scenarios. The current and new CMIP6 models are in wide used and are appreciated for its improved climate sensitivity compared to previous CMIP models. These CMIP6 models runs with SSP-RCP framework leading to combined socioeconomic and radiative forcing scenario inputs. Figure 3 shows the progressive evolution of CMIP models [15].

These GCMs work at a courser level of resolution (typically 100–500 km) and therefore cannot be used for local or regional level of impact assessment studies. Due to this, a concept of Regional Climate Models (RCMs) was brought that works at high resolution (typically 10–50 km). These RCMs basically work with the principal of dynamic downscaling and with the primary assumption of working with set of boundary conditions provided by their host GCM. Various projects and groups have come up to work for RCM modelling like PRUDENCE (Europe), ENSEMBLES (Europe and Africa), NARCCAP (North America), CLARIS (Europe and South America) [2, 35]. To stabilize and have a single platform, the COordinated Regional climate Downscaling EXperiment (CORDEX) under the WCRP was formed. At present, CORDEX runs for total 14 domains (region for which downscaling is taking place) [11]. Further, more details regarding RCM models are properly put together by [2, 35, 40].

The climate model output data can be obtained from ESGF website (https://esgf-data.dkrz.de/projects/esgf-dkrz/) and IPCC Data Distribution Centre (DCC) (https://www.ipcc-data.org/). These files are in NetCDF format and require other data extraction tools to work with these data files. While using these climate models or their outputs in impact assessment studies, we can observe two types of approach as single model approach and multi-model ensemble (MME) approach [17]. These approaches as the name explains work with a single GCM/RCM output and a group of GCM/RCM outputs, respectively. With the improvement in impact studies, it is

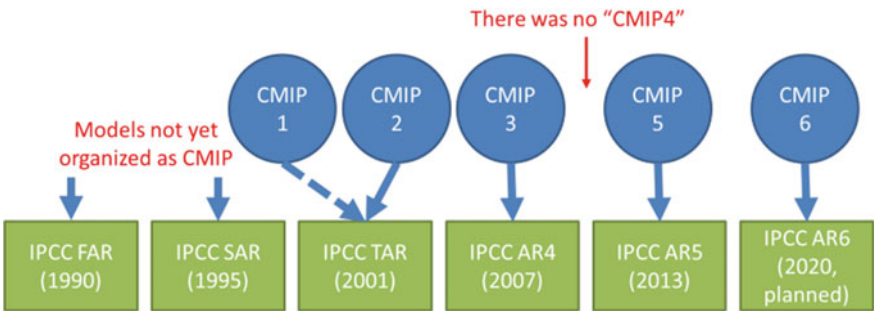

Fig. 3 CMIP models evolution with time and IPCC reports. *Source* [15]

highly recommended to use multi-model ensemble approach as it helps in quantifying the uncertainty associated with climate model [33, 40]. There is always a clash in opinion of researchers whether GCM or RCM is better for regional climate modelling [8, 22, 26, 47]. One always needs to evaluate the model performance in a region along with addressing the uncertainty associated with it.

2.3 *Downscaling and Bias Correction*

While studying the impact of climate change on water resources and hydrology, one serious limitation that need to be address is the scale mismatch due to gap between the scale of climate model output and the scale requirement of hydrological model. This gap and mismatching can be overcome by downscaling the GCM data or coarser resolution data. Downscaling is commonly divided into two types as dynamic and statistical downscaling. These methods are more elaborated by [1, 5, 18, 48]. Dynamic downscaling is basically use of RCM models by applying large scale and lateral boundary conditions and in addition parameterizing physical atmospheric processes. On the other hand, statistical downscaling is based on the hypothesis used to determine the relationship between coarse GCM data and fine scale observational data. Few methods under each of these two types, that are commonly used and known, are mentioned in Fig. 4.

Due to lack of scientific knowledge or observational data, GCM obtain is said to have systematic and random model errors called as bias. So, after downscaling, RCM also tend to possess some bias in its output values. This bias should be properly handled (at least reduce if not completely eliminated). There are various methods of bias correction proposed and few of them are listed in Fig. 4. They aim to correct the mean, variance and quantile of the time series variable. Among all these methods,

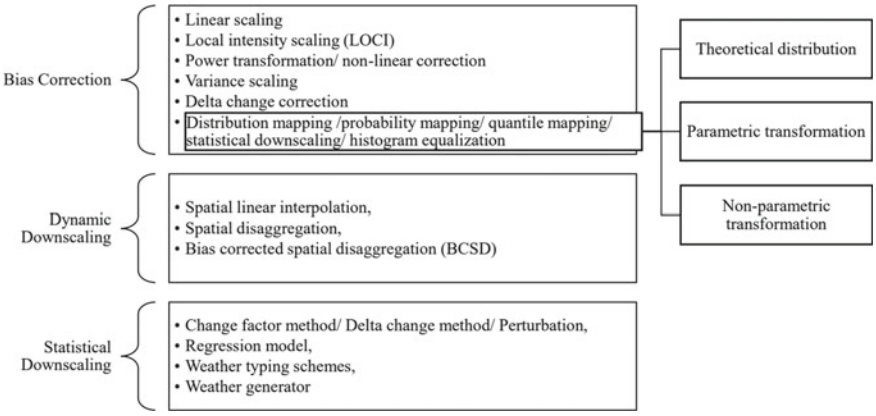

Fig. 4 Methods of downscaling and bias correction

commonly adopted methods are linear scaling and delta change correction method. Whereas the one with comparatively better performance is distribution mapping or quantile mapping method [36, 41, 42]. For hydrological impact studies (precipitation and temperature data to be bias corrected), one must note that there are certain methods that could be applicable only to precipitation (LOCI method) or temperature (power transformation and variance scaling method) while some could be applied to both [16, 38].

2.4 Hydrological Modelling

Discussing about hydrological models in climate change impact studies, they are computer-based model that represents the real-world catchment and hydrological processes. These hydrological models are primarily classified as deterministic and stochastic models and process-based models [13]. The deterministic models do not consider randomness and hence gives a single output with the particular set of input parameters. Whereas the stochastic models consider randomness and produces output depending upon uncertainties of input variables, boundary conditions and model parameter [20]. The deterministic models are further categorized as lumped models, semi-distributed models (like SWAT, HEC-HMS) and distributed models (like MIKE SHE). The lumped models usually consider entire catchment as a single unit with same hydrological characteristic unlike distributed model that divide catchment into uniform grid with varying catchment characteristics. Whereas the semi-distributed models divide the catchment into hydrological response units (HRUs) having same properties in each subunit/ HRU [20]. The process-based hydrological models are categorized into empirical, conceptual and physical hydrological models. Empirical models such as artificial neural networks (ANNs), fuzzy logic, genetic algorithm (GA) does not contain any physical process-based function and relationship. They are completely based on statistical hydro-meteorological data. The conceptual models work with the empirical equations that are based on certain physical and observational processes. Unlike the other two types, the physical models describe and considers the complete catchment characteristics with its spatial variability as well as climate parameters [13].

Figure 5 shows the types of hydrological models in the form of tree diagram. There are also global hydrological models (GHM) in use which try to stimulate global hydrology and its connected processes [39]. Table 2 shows review of few papers in tabular form that can give an outline for various types of methods and models used in different studies.

In climate change impact assessment studies, uncertainties associated with the hydrological models or due to climate models or the methods of downscaling and bias correction used plays a vital role. One must understand that the uncertainties can never be completely eliminated in climate change studies but can be reduced. Uncertainties itself being a vast and separate topic is studied by several researchers and few of such work and related paper are [6, 7, 12, 29].

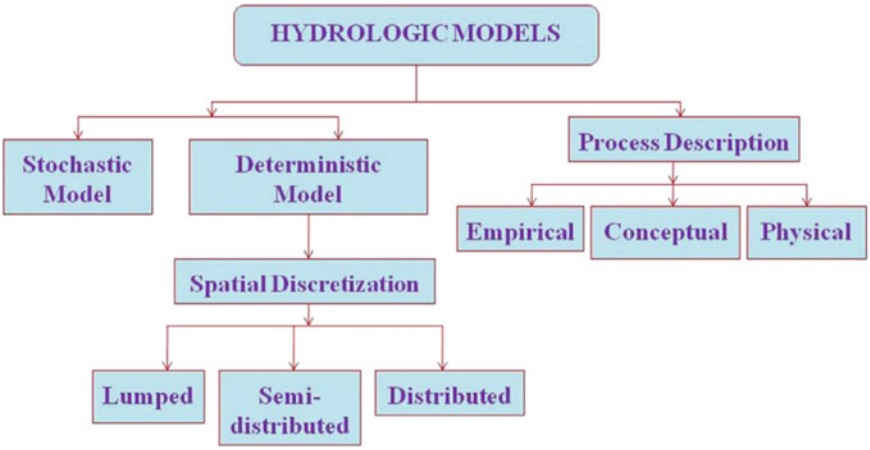

Fig. 5 Types of hydrological models. *Source* [13]

3 Summary

The aim of this paper is to provide basic essential and integrated information for beginners in an abounding field of climate change impact assessment of water resources and hydrology. The basic outline of assessment methodology starting with climate change scenarios followed by climate models, modelling approach, downscaling methods, bias correction methods to hydrological models used in impact assessment are reviewed. It is concluded that the climate scenarios, climate models and modelling approach (single model or multi-model ensemble), downscaling methods and hydrological models should be chosen taking into consideration the model prediction capacity along with level of accuracy and certainty required in a study, limitations and uncertainties associated with it. Performance evaluation of models should also be given importance. It is recommended to use multi-model ensemble approach and using GCM along with proper downscaling and also apply bias correction or RCM along with bias correction to address the uncertainties. It is also recommended using distributed deterministic and integrated hydrological models, whereas using a semi-distributed deterministic models like SWAT is also used broadly and can be taken into consideration.

Table 2 Tabular review of climate change impact assessment studies

References	Scenario used	Climate models used	Downscaling method used	Bias correction method used	Hydrological model used
[19]	GHG scenarios	**RCM**: HadRM2	–	–	SWAT
[29]	(SRES scenario) A2, B2	**3 GCM**: CCSR/NIES, HadCM3, CGCM2	Statistical downscaling models	–	–
[3]	4RCPs-5SSPs	**19 GCM^{E}**: 19 CMIP5 models	–	–	Global hydrological model MacPDM.09
[27]	RCP4.5, RCP8.5	**6 GCM^{E}**: NorESM, MPI, CanESM, CNRM, IPSL, MIROC	–	Quantile mapping	SWAT
[24]	RCP2.6, RCP4.5, RCP8.5	**GCM^{E}**: CMIP5	Delta change, Advanced quantile Perturbation	–	MIKE-SHE, SWAT
[43]	RCP4.5	**6 GCM**: ACCESS1-0, CANESM2, GFDL-ESM2M, GISS-E2-R, IPSL-CM5A-MR, MIROC-ESM	Statistical downscaling change factor method	–	VIC
[36]	Historical data	**3 RCM**: ACCESS1.0, CNRM-CM5, MPI-ESM-LR	–	Linear scaling, quantile mapping	SWAT
[12]	RCP4.5, RCP8.5	**6 GCM^{E}**: ACCESS1.0, CNRM-CM5, CCSM4, GFDL-CM3, MPI-ESM-LR, NorESM1-M	Dynamically downscaled using RCM (CORDEX)	Non-parametric quantile mapping	VIC
[22]	RCP8.5	**1 GCM**: HadGEM **2 RCM**: RegCM, WRF	Dynamic downscaling using RCM	Quantile mapping	SWAT
[33]	RCP4.5, RCP8.5	**2 GCM^{E}**: CNRM-CM5.0, GFDL-CM3.0	Statistical downscaling model (SDSM)	Non-parametric quantile mapping	SWAT
[4]	RCP4.5, RCP8.5	**4RCM**: REMO, RCA4, MPI_CCAM, CNRM_CCAM	Dynamic downscaling using RCM	Distribution mapping	HBV-light, HEC-HMS, SRM

(continued)

Table 2 (continued)

References	Scenario used	Climate models used	Downscaling method used	Bias correction method used	Hydrological model used
[37]	RCP4.5, RCP8.5	**1 RCM**: RegCM4 CSIRO-Mk3.6.0	Dynamic downscaling using RCM	Delta change	SWAT
[34]	RCP4.5, RCP8.5	**1 RCM**: RegCM4	–	–	MIKE-SHE
[50]	RCP4.5, RCP8.5	**1 GCM**: BNU-ESM	Statistical downscaling	Quantile mapping	MIKE-SHE

X^E means multi-model ensemble (MME) approach

References

1. Ahmad B, Rasul G (2018) Statistically downscaled projections of CORDEX South Asia using quantile mapping approach over Pakistan region. Int J Global Warm 16:435–460
2. Ambrizzi T, Reboita MS, Rocha RP, Llopart M (2018) The state-of-the-art and fundamental aspects of regional climate modeling in South America. Annal New York Acad Sci: Climate Sci, 1–23. https://doi.org/10.1111/nyas.13932
3. Arnell NW, Lloyd-Hughes B (2014) The global-scale impacts of climate change on water resources and flooding under new climate and socio-economic scenarios. Springer: Clim Change 122:127–140. https://doi.org/10.1007/s10584-013-0948-4
4. Azmat M, Wahab A, Huggel C, Qamar MU, Hussain E, Ahmed S, Waheed A (2019) Climatic and hydrological projections to changing climate under CORDEX-South Asia experiments over the Karakoram-Hindukush-Himalayan water tower. Science of the Total Environment
5. Bhuvandas N, Timbadiya PV, Patel PL, Porey PD (2014) Review of downscaling methods in climate change and their role in hydrological studies. Int J Environ Ecol Geol Mining Eng 8(10)
6. Chandra Rupa R, Mujumdar PP (2018) Hydrologic impacts of climate change: quantification of uncertainties. Indian Nat Sci Academy 85:77–94
7. Chawla I, Mujumdar PP (2017) Partitioning uncertainty in streamflow projections under nonstationary model conditions. Adv Water Res
8. Chokkavarapu N, Mandla VR (2019) Comparative study of GCMs, RCMs, downscaling and hydrological models: a review toward future climate change impact estimation. Springer Nature Switzerland Applied Science. https://doi.org/10.1007/s42452-019-1764-x
9. Climate Change 2007: synthesis report. Contribution of Working Groups I, II and III to the Fourth Assessment Report of the Intergovernmental Panel on Climate Change. Geneva, Switzerland: IPCC
10. Climate Models (2021). Retrieved from Wikipedia: https://en.wikipedia.org/wiki/Climate_model
11. CORDEX Domains (2021). Retrieved from WCRP CORDEX: https://cordex.org/domains/
12. Das J, Treesa A, Umamahesh NV (2018) Modelling Impact of climate change on a River Basin: analysis of uncertainty using REA & possibilistic approach. Water Resour. Manage
13. Dwarakish GS, Ganasri BP (2015) Impact of land use change on hydrological systems: a review of current modeling approaches. Cogent Geosci, 1–18
14. Ebi KL, Hallegatte S, Kram T, Arnell NW, Carter TR, Edmonds J, Zwickel T, et al (2014) A new scenario framework for climate change research: background, process, and future directions. Springer: Climat Chang 122:363–372
15. Emori S, Taylor K, Hewitson B, Zermoglio F, Juckes M, Lautenschlager M, Stockhause M (2016) IPCC data distribution centre. Fact sheet of the task group on data and scenario support

for impact and climate analysis (TGICA) of the Intergovernmental Panel on Climate Change (IPCC)
16. Fang GH, Yang J, Chen YN, Zammit C (2015) Comparing bias correction methods in downscaling meteorological variables for a hydrologic impact study in an arid area in China. Hydrol Earth Syst Sci 19:2547–2559. https://doi.org/10.5194/hess-19-2547-2015
17. Flato G, Marotzke J, Braconnot P, Chou SC, Collins W, Cox P, Rummukainen M, et al (2013) Evaluation of climate models. In: Climate Change 2013: the Physical Science Basis. Contribution of Working Group I to the Fifth Assessment Report of the Intergovernmental Panel on Climate Change. Cambridge University Press, Cambridge, UK
18. Fowler HJ, Blenkinsop S, Tebaldi C (2007) Review Linking climate change modelling to impacts studies: recent advances in downscaling techniques for hydrological modelling. Int J Climatol 27:1547–1578. https://doi.org/10.1002/joc.1556
19. Gosain AK, Rao S, Basuray D (2006) Climate change impact assessment on hydrology of Indian river basins. Curr Sci 90:346–353
20. Gosling SN, Taylor RG, Arnell NW, Todd MC (2011) A comparative analysis of projected impacts of climate change on river runoff from global and catchment-scale hydrological models. Hydrol Earth Syst Sci 15:279–294
21. Kusangaya S, Warburton ML, Garderen EA, Jewitt GP (2013) Impacts of climate change on water resources in Southern Africa: a review. Elsevier Physics and Chemistry of the Earth, 1–8
22. Lee MH, Im ES, Bae DH (2019) Impact of the spatial variability of daily precipitation on hydrological projection: a comparison of GCM- and RCM-driven cases in the Han River basin, Korea. Hydrol Proces 33:2240–2257
23. Leggett J, Pepper WJ, Swart RJ (1992) Emissions scenarios for IPCC. an update. In: Climate Change 1992. The supplementary report to the IPCC Scientific Assessment. Cambridge University Press, Cambridge, UK
24. Luo M, Meng F, Liu T, Duan Y, Frankl A, Kurban A, Maeyer PD (2017) Multi-model ensemble approaches to assessment of effects of local climate change on water resources of the Hotan River Basin in Xinjiang, China. MDPI: Water 9:584. https://doi.org/10.3390/w9080584
25. Masson-Delmotte VP (2021) IPCC, 2021: summary for policymakers. In: Climate Change 2021: The Physical Science Basis. Contribution of Working Group I to the Sixth Assessment Report of the Intergovernmental Panel on Climate Change. Cambridge University Press
26. Mishra V, Kumar D, Ganguly AR, Sanjay J, Mujumdar M, Krishnan R, Shah RD (2014) Reliability of regional and global climate models to simulate precipitation extremes over India. J Geophys Res: Atmos 119:9301–9323
27. Mohd MF, Mispan MR, Juneng L, Tangang FT, Rahman NA, Khalid K, Haron SH (2015) Assessment of impact of cliamte change on streamflow trend in Upper Kuantan Watershed. J Eng Appl Sci 10:6634–6642
28. Moss RH, Edmonds JA, Hibbard KA, Manning MR, Rose SK, Van Vuuren DP, Wilbanks TW (2010) The next generation of scenarios for climate change research and assessment. Nature 463:747–756
29. Mujumdar PP, Ghosh S (2008) Modeling GCM and scenario uncertainty using a possibilistic approach: application to the Mahanadi River, India. Water Resour Res 44:1–15
30. Nakicenovic N, Alcamo J (2000) Special report on emissions scenarios. Working Group III of the intergovernmental panel on climate change, IPCC. Cambridge University Press, Cambridge
31. Nakicenovic N, Lempert RJ, Janetos AC (2014) A framework for the development of new socio-economic scenarios for climate change research: introductory essay. Springer: Climatic Chang. 122**:**351–361. https://doi.org/10.1007/s10584-013-0982-2
32. O'Neill BC, Kriegler E, Riahi K, Ebi KL, Hallegatte S, Carter TR, Van Vuuren DP (2014) A new scenario framework for climate change research: the concept of shared socioeconomic pathways. Springer: Climatic Chang. 122:387–400
33. Padhiary J, Patra KC, Dash SS, Kumar AU (2019) Climate change impact assessment on hydrological fluxes based on ensemble GCM outputs: a case study in Eastern Indian River Basin. J Water Clim Chang, 1–19

34. Ramteke G, Singh R, Chatterjee C (2020) Assessing impacts of conservation measures on watershed hydrology using MIKE SHE model in the face of climate change. Springer, Water Resources Management
35. Rummukainen M (2010) State of the art with regional climate models. WIREs Clim Chang 1:82–96
36. Shrestha M, Acharya SC, Shrestha PK (2017) Bias correction of climate models for hydrological modelling—are simple methods still useful? Meteorol Appl 24:531–539. https://doi.org/10.1002/met.1655
37. Singh L, Saravanan S (2020) Impact of climate change on hydrology components using CORDEX South Asia climate model in Wunna, Bharathpuzha, and Mahanadi, India. Springer Nature Switzerland 678:1–21
38. Smitha PS, Narasimhan B, Sudheer KP, Annamalai H (2018) An improved bias correction method of daily rainfall data using a sliding window technique for climate change impact assessment. J Hydrol 556:100–118
39. Sood A, Smakhtin V (2015) Global hydrological models: a review. Hydrol Sci J [Journal des Sciences Hydrologiques] 60(4):549–565
40. Teutschbein C, Seibert J (2010) Regional climate models for hydrological impact studies at the catchment scale: a review of recent modeling strategies. Geography. Compass, 834–869
41. Teutschbein C, Seibert J (2012) Bias correction of regional climate model simulation for hydrological climate-change impact studies: review and evaluation of different methods. J Hydrol, 12–29
42. Thrasher B, Maurer EP, McKellar C, Duffy PB (2012) Technical note: bias correcting climate model simulated daily temperature extremes with quantile mapping. Hydrol Earth Sys Sci 16:3309–3314. https://doi.org/10.5194/hess-16-3309-2012
43. Treesa A, Das J, Umamahesh NV (2017) Assessment of impact of climate change on streamflows using VIC model. European Wat 59:61–68
44. van Vuuren DP, Kriegler E, O'Neill BC, Ebi KL, Riahi K, Carter TR, Winkler H et al (2014) A new scenario framework for climate change research: scenario matrix architecture. Springer Science: Clim Chang 122:373–386. https://doi.org/10.1007/s10584-013-0906-1
45. Van Vuuren DP, Edmonds J, Kainuma M, Riahi K, Thomson A, Hibbard K, Rose SK et al (2011) The representative concentration pathways: an overview. Springer Clim Chang 109:5–31
46. Vicuna S, Dracup JA (2007) The evolution of climate change impact studies on hydrology and water resources in California. Springer Science Clim Chang 82:327–350
47. Vishwakarma A, Choudhary MK, Chauhan M.S (2020) Assessment of the performance of CMIP5 and CORDEX-SA models over the drought-prone Bundelkhand region, India. J Water Clim Chang, 133–144
48. Wood AW, Leung LR, Sridhar V, Lettenmaier DP (2004) Hydrological implications of dynamical and statistical approaches to downscaling climate model outputs. Clim Chang, 189–216
49. Yang N, Men B, Lin C (2011) Impact analysis of climate change on water resources. Proced Eng SciVerse ScienceDirect 24:643–648
50. Zhang J, Zhang M, Song Y, Lai Y (2021) Hydrological simulation of the Jialing River Basin using the MIKE SHE model in changing climate. J Water Clim Change, 1–20. https://doi.org/10.2166/wcc.2021.253

Trends in Extreme Streamflow Indices in the Godavari River Basin

Aajaz Ahmad Padder and Priyank J. Sharma

Abstract This study assesses the spatio-temporal changes in trends in extreme streamflow indices for nineteen stream gauging stations in the Godavari River basin (area $\approx$ 312,812 km^2), India. The daily streamflow data were quality checked and thereafter adopted to derive the magnitude (total annual runoff, annual maximum 1-day and 5-day streamflows) and threshold (total streamflow exceeding the threshold corresponding to 95th and 99th percentile discharge and mean annual flood discharge) based extreme streamflow indices for each station. The non-parametric Pettit's test is adopted for change point detection, while the Spearman's Rho and Modified Mann–Kendall tests are executed to detect the significance of trends in the extreme streamflow indices. Further, the changes in the distributional characteristics of mean and extreme flows are analyzed using a non-parametric kernel density estimate and Mann–Whitney test by dividing the entire duration into three sub-periods (i.e., before 1980, during 1981–1995, and after 1995). The results indicated declining trends in total annual runoff and extreme streamflows at most stations across the basin. The significant changes in the distributional characteristics of streamflows are observed in the sub-period after 1995 compared to the other sub-periods. The reported decrease in total runoff would put additional stress on the freshwater ecosystem services, which are already stressed due to human interventions.

A. A. Padder (✉)
Department of Civil Engineering, Punjab Engineering College (Deemed to be University), Chandigarh 160036, India
e-mail: aajazahmadpadder.mtwtr20@pec.edu.in

P. J. Sharma
Department of Civil Engineering, Indian Institute of Technology Indore, Indore, Madhya Pradesh 453552, India
e-mail: priyanksharma@iiti.ac.in

P. V. Timbadiya et al. (eds.), *Climate Change Impact on Water Resources*, Lecture Notes in Civil Engineering 313, https://doi.org/10.1007/978-981-19-8524-9_11

Keywords Non-parametric tests · Trend analysis · Extreme streamflow indices · Distributional changes · Godavari River basin

1 Introduction

Trend analysis of streamflow at the river basin scale provides valuable information for effective planning, designing, and management of freshwater resources. Assessing historical and future streamflow changes helps the water resources planners develop adaptive management plans while dealing with the likely adverse changes. A substantial spatial and temporal heterogeneity was reported as one of the significant obstacles to trend attribution in the river flow regime in the United Kingdom [1]. Salarijazi et al. [2] analyzed the streamflow series of the annual maximum, minimum and mean values at the Ahvaz hydrometric station of the Karun watershed and reported an increasing trend in streamflows. Zhang et al. [3] analyzed the streamflow variations in the Heihe River Basin, northwest China and reported a slightly upward (downward) trend for the gauging stations located upgradient (downgradient) to the irrigation area. Abeysingha et al. [4] studied the relationship between trends in streamflow and rainfall of the Gomati River basin through correlation analysis, wherein a gradually decreasing trend in the streamflow was associated with increased water withdrawal, increase in air temperature, population escalation, and significant declining trend of post-monsoon rainfall. Drissia et al. [5] reported a significant decreasing trend in daily streamflow at 53% of stations on west flowing rivers of Kerala, while a significant increasing trend and no significant trend were found at 28% and 19% stations, respectively. Sharma et al. [6] reported that the anthropogenic changes were prominently responsible for the decline in streamflows in the Tapi basin compared to the rainfall variability. Kuriqui et al. [7] reported a significant decreasing trend in summer and autumn seasonal streamflows and annual peak flows at all stations analyzed in the Godavari basin. Das et al. [8] documented a significant decline in the water and sediment discharges in the Godavari River basin, particularly after 1990, which was attributed to extensive watershed development. The decrease in sediment discharge of the river would accelerate the coastal erosion process in the future owing to the sea level rise. However, the earlier studies on the Godavari basin did not focus on evaluating the changes in the extreme streamflow characteristics (viz., magnitude, frequency, and distribution) and their implications on water resources management. The present study is aimed to assess the changes in (gradual and abrupt) trends and distributional characteristics of extreme streamflow indices in the Godavari River basin.

2 Study Area and Data Source

The Godavari River is the largest river in peninsular India and the third-largest in India, draining nearly 10% of the total geographical area of India. The Godavari basin is spread across an area of 3,12,812 sq. km while covering the states of Maharashtra (48.8%), Andhra Pradesh (3.7%), Telangana (20%), Madhya Pradesh (7.9%), Chhattisgarh (12.4%), Orissa (5.7%), and Karnataka (1.5%) [9]. The basin is situated between North latitudes 16° 16′–22° 36′ and East longitudes 73° 26′–83° 07′ (Fig. 1). The Godavari River originates in the Western Ghats near Triambak Hills in Maharashtra's Nasik district at an elevation of about 1067 m above mean sea level [8]. It flows for around 1465 km in the southeast direction before entering the Bay of Bengal. Right bank tributaries such as the Pravara, Manjira, and Maner Rivers cover about 16.14% of the total basin area, while left bank tributaries such as the Purna, Pranhita, Indravathi, and Sabari Rivers cover nearly 59.7% of the total basin area.

The Godavari basin receives around 84% of its annual rainfall during the southwest monsoon, which sets in mid-June and withdraws by mid-October. The long-term annual average rainfall in the Godavari catchment is about 1100 mm, wherein the spatial variation in the average basin rainfall is observed in the range of 755–1531 mm [9]. A noticeable eastward declining rainfall gradient is noticed in the basin, wherein the regions closer to the Western Ghats receive rainfall in the range of 1000–3000 mm. In addition, the regions near the East coast receive around 900 mm of rainfall, and the leeward side of the Western Ghats receives scanty rainfall of about 600 mm. The mean annual temperature across the basin varies from 31 to 33.5 °C. The agricultural

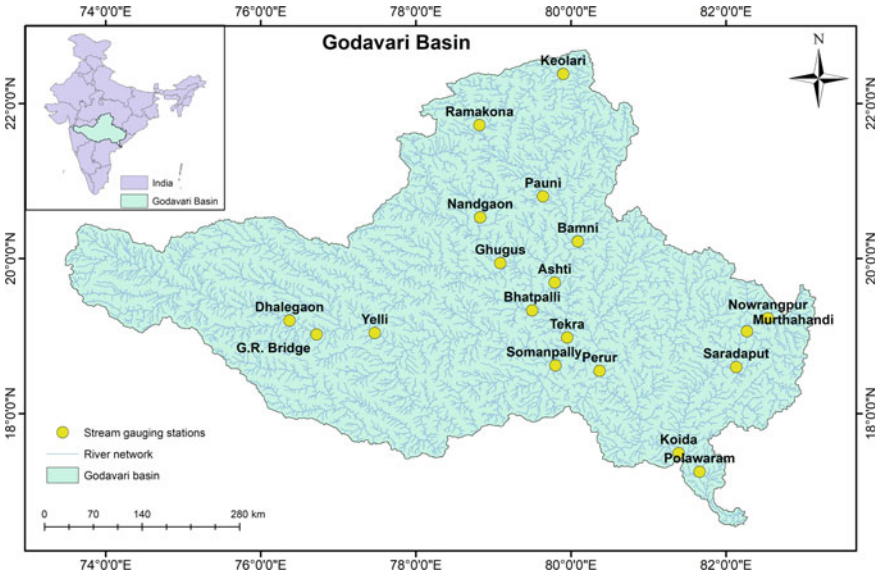

Fig. 1 Index map of Godavari basin showing the location of stream gauging stations

lands are spread across the majority of the Godavari basin (i.e., 59.57% of the total basin area), followed by the forest area and water bodies which occupy about 29.78% and 2.06% of the total basin area, respectively [9].

The daily observed streamflow data of the stream gauging stations in the Godavari basin, marked in Fig. 1, is collected from the India Water Resources Information System (WRIS) web portal (https://indiawris.gov.in/wris/) of the Central Water Commission (CWC), India. The data of sixty-nine stations was collected, and quality checked, wherein the stations having continuous data length lesser than 25 years were not included in the analysis. The description of nineteen stream gauging stations analyzed in the current study is included in Table 1. The streamflow data has been checked for consistency and homogeneity prior to its analysis.

Table1 Details of stream gauging stations adopted in this study

Stream gauging station	River	Latitude (North)	Longitude (East)	Catchment area (km^2)	Normal rainfall (mm)	Data length (years)
Ashti	Wainganga	19.69	79.79	50,990	896.7	54
Bamni	Kathani Nadi	20.22	80.09	46,020	1251.5	53
Bhatpalli	Pedda Vagu	19.33	79.50	3100	1101.8	31
Dhalegaon	Godavari	19.20	76.37	30,840	744.1	49
G.R. Bridge	Godavari	19.02	76.72	33,934	892.0	38
Ghugus	Wardha	19.94	79.09	21,429	1172.3	38
Keolari	Wainganga	22.38	79.90	2970	1204.5	32
Koida	Godavari	17.49	81.39	305,460	1415.5	29
Murtahandi	Jouranala	19.06	82.27	N.A	1545.3	25
Nandgaon	Vena	20.53	78.83	4580	594.5	32
Nowrangpur	Indravati	19.23	82.54	3545	1497.4	48
Pauni	Wainganga	20.80	79.64	35,520	1345.3	42
Perur	Godavari	18.55	80.37	268,200	1522.0	42
Polawaram	Godavari	17.25	81.66	307,800	1178.8	48
Ramakona	Kanhan	21.72	78.82	2500	1024.5	31
Saradaput	Kolab	18.60	82.13	3047	1500.7	44
Somanpally	Maner	18.62	79.80	12,691	N.A	39
Tekra	Pranhitha	18.98	79.95	108,780	1377.7	50
Yelli	Godavari	19.04	77.47	53,630	977.1	31

N.A. indicates data is not available

3 Methodology

The step-by-step procedure adopted to detect the change point and analyze trends and distributional changes in the extreme streamflow indices for the Godavari River basin is shown in Fig. 2.

3.1 Streamflow Indices

The streamflow indices, listed in Table 2, are derived from daily observed data on a water year basis (i.e., June–May) for each station. The total annual runoff (QTOT) is expressed as the cumulative volume of water collected at the catchment outlet (represented by a stream gauging station) each year. The maximum flow observed for

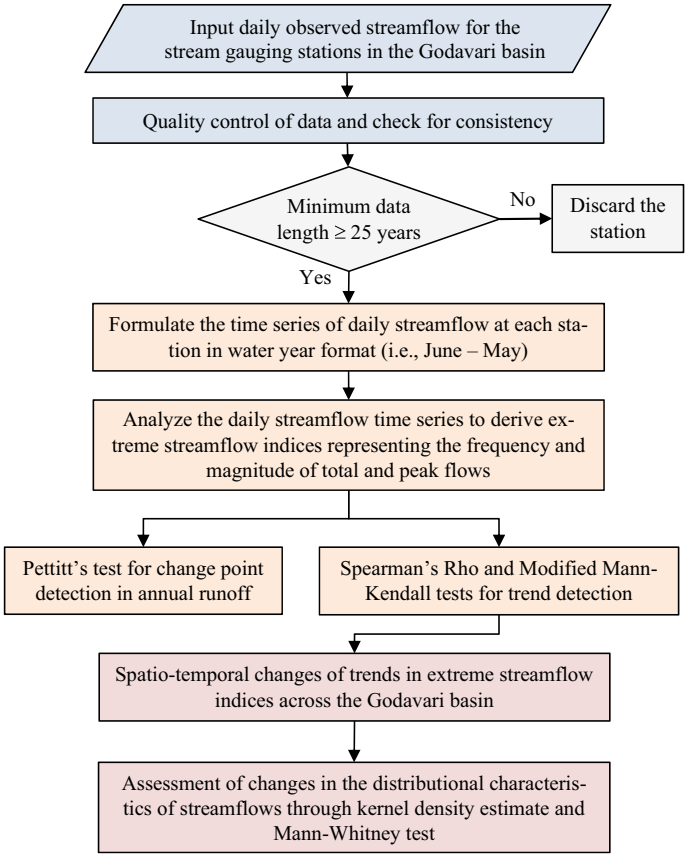

Fig. 2 Methodology adopted in the present study

Table 2 Description of the streamflow indices adopted in the study

Streamflow index	Notation	Unit
Total annual runoff	QTOT	Mm^3
Annual maximum 1-day discharge	Qx1day	m^3/s
Annual maximum 5-day discharge	Qx5day	m^3/s
Total streamflow exceeding the 95th percentile discharge	Q95p	m^3/s
Total streamflow exceeding the 99th percentile discharge	Q99p	m^3/s
Total streamflow exceeding the mean annual flood discharge	QTMEAN	m^3/s
Number of times the streamflow exceeds mean annual flood discharge	QCMEAN	m^3/s

1-day (Qx1day) and 5-day (Qx5day) duration represents the characteristics of short- and long-duration floods at a station each year. An Empirical Cumulative Distribution Function (ECDF) is fitted to the daily streamflow time series (i.e., considering entire data) at each station to estimate the thresholds corresponding to 95th and 99th percentile streamflows, and the total streamflow exceeding these thresholds are computed for each water year and denoted as Q95p and Q99p, respectively [6]. The mean annual flood discharge is computed by fitting Gumbel's distribution to the Qx1day series at a station and estimating the value corresponding to a return period of 2.33 years [10]. Further, the time series of total streamflow exceeding the mean annual flood discharge is denoted as QTMEAN, whereas the number of instances of streamflow exceeding the mean annual flood discharge is denoted as QCMEAN for each year.

3.2 Non-parametric Statistical Techniques

Pettit's test [11] is adopted to detect a change point wherein the null hypothesis, that there is no change in the mean value of the divided segments of a time series, which is tested against the alternate hypothesis that there is a significant change in the mean value at a given significance level (α).

$$D_{ij} = \begin{cases} -1\left(X_i - X_j\right) < 0 \\ 0\left(X_i - X_j\right) = 0 \\ +1\left(X_i - X_j\right) > 0 \end{cases} \tag{1}$$

where X_i and X_j are the random variables, where X_i following X_j in time. The test statistic $U_{t,T}$ depend on D_{ij} is defined in Eq. (2). $U_{t,T}$ is assessed for all random variables from 1 to T; then, the most significant change point is selected where the value of $|U_{t,T}|$ is the largest.

$$U_{t,T} = \sum_{i=1}^{t} \sum_{j=t+1}^{T} D_{ij} \tag{2}$$

$$K_T = \max_{1 \le t < T} |U_{t,T}| \tag{3}$$

A change point occurs at time t when the K_T is significantly different from zero at a given α.

A modified Mann–Kendall (MMK) test is adopted for trend detection. It overcomes the drawback of the Mann–Kendall test in detecting trends within the time series that are serially correlated. The null hypothesis of the MMK test is that the data is independent and randomly ordered. The MMK test statistic Z is defined as [12]:

$$z = \begin{cases} \frac{s-1}{\sqrt{\mathrm{Var}(S)}} & \text{if } S > 0 \\ 0 & \text{if } S = 0 \\ \frac{s+1}{\sqrt{\mathrm{Var}(S)}} & \text{if } S < 0 \end{cases} \tag{4}$$

A positive (negative) value of Z indicates the presence of an increasing (decreasing) trend in the time series, wherein the test statistic is assessed at a 5% significance level (α). Further details about the MMK test can be found in Hamed and Rao [12].

Spearman's Rho test, a rank-based test that assumes the time series as independent and identically distributed, is also used for trend detection. The null hypothesis in this test is that the association between the two ordered values is zero (i.e., no trend). The test statistic (ρ) is defined as:

$$\rho = 1 - \frac{6\Sigma di^2}{n\left(n^2 - 1\right)} \tag{5}$$

where d_i represents the difference in ranking for the observation i and n is the number of observations.

Kernel density estimate [13] is adopted to evaluate and compare the probability densities of streamflow indices for different sub-periods (i.e., before 1980, during 1981–1995, and after 1995). The statistically significant difference between the probability densities for various sub-periods is estimated using the Mann–Whitney test at a 5% significance level [13].

4 Results and Discussion

The statistical assessment of abrupt, gradual, and distributional changes in the mean and extreme streamflow characteristics and their spatial variation across the Godavari basin is presented using several non-parametric techniques.

4.1 Change Point and Trends in Extreme Streamflow Indices

The non-parametric Pettit's test has been used for change point detection in QTOT series at each station. The results indicate insignificant change (at a 5% level of significance) in the total annual runoff at most gauging stations. However, three stations, viz., Dhalegaon (on Godavari River), Murtahandi (on Jouranala River), and Nowrangpur (on Indravati River) had shown significant change points resulting in an abrupt decrease in the runoff at these stations after the change point. The change point year for Dhalegaon, Murtahandi, and Nowrangpur stations are reported to be 1984, 1995, and 1996, respectively. The assessment of changes in extreme streamflows in the Godavari basin is carried out by applying several non-parametric trend detection tests, viz., Spearman Rho (SR) and Modified Mann–Kendall (MMK) tests. The SR and MMK tests are carried out to determine the trend in streamflow indices (listed in Table 2) at nineteen gauging stations in the Godavari River basin, and their results are shown in Table 3. Further, the spatial variability of nature of trend (i.e., increasing, decreasing or no trend), derived from the MMK test, for all the streamflow indices are shown on the basin map with the help of a spatial analyst tool in a geographical interface system (GIS) interface.

The results indicate a declining trend in the total annual runoff (QTOT) is observed at sixteen stream gauging stations in the Godavari basin, while an increase in QTOT is noticed at three stations (see Fig. 3a). A significant decrease in QTOT is detected at Dhalegaon, Ghugus, Murtahandi, and Nowrangpur stations at a 5% significance level. The reduction in total annual runoff is plausibly linked with the decline in total precipitation across the Godavari [8, 14]. Such a decrease in runoff would put additional stress on the freshwater ecosystem services, such as water for drinking, municipal, industrial, and irrigation use; water for navigation, power generation, recreation, and spiritual needs of the residents in the basin. The decrease in freshwater availability and increase in water needs due to rapid population growth could exacerbate the water stress conditions in the basin.

Table 3 Results of trend detection in extreme streamflow indices

Stream gauging station	QTOT		Qx1day		Qx5day		Q95p		Q99p		QTMEAN		QCMEAN	
	MMK *Z*	SR ρ	MMK *Z*	SR ρ	MMK *Z*	SR ρ	MMK *Z*	SR ρ	MMK *Z*	SR ρ	MMK *Z*	SR ρ	MMK *Z*	SR ρ
Ashti	− 0.76	− 0.09	0.03	0.00	− 0.45	− 0.05	− 0.87	− 0.11	− 1.06	− 0.14	0.08	0.02	0.02	0.01
Bamni	− 1.48	− 0.21	− 1.32	− 0.21	− 1.59	− 0.25	− 1.24	− 0.21	− 0.70	− 0.14	− 0.65	− 0.15	− 0.59	− 0.14
Bhatpalli	− 1.53	− 0.27	− 1.19	− 0.21	− 1.19	− 0.21	− 1.46	− 0.25	− 1.26	− 0.25	− 0.84	− 0.26	− 0.71	− 0.26
Dhalegaon	**− 4.51**	**− 0.62**	**− 2.57**	**− 0.39**	**− 3.71**	**− 0.41**	**− 4.11**	**− 0.57**	**− 2.63**	**− 0.39**	**− 2.17**	**− 0.35**	− 1.71	**− 0.36**
G.R. Bridge	− 1.60	− 0.24	− 1.29	− 0.28	− 1.57	− 0.28	− 1.43	− 0.26	− 1.16	− 0.21	− 1.08	− 0.25	− 0.94	− 0.25
Ghugus	**− 2.11**	**− 0.42**	− 1.63	− 0.22	− 1.84	− 0.29	**− 2.33**	**− 0.38**	− 1.32	− 0.27	− 0.22	− 0.10	− 0.23	− 0.11
Keolari	− 0.21	− 0.03	− 0.02	− 0.03	− 0.34	− 0.08	− 0.79	− 0.13	0.18	0.00	− 0.01	− 0.02	− 0.07	− 0.03
Koida	− 1.03	− 0.17	− 0.69	− 0.14	− 1.46	− 0.21	− 0.96	− 0.19	− 0.88	− 0.20	− 0.58	− 0.21	− 0.60	− 0.21
Murtahandi	**− 2.41**	**− 0.50**	− 0.44	− 0.10	− 1.14	− 0.27	− 1.75	− 0.36	− 0.56	− 0.17	− 0.82	− 0.23	− 0.64	− 0.24
Nandgaon	0.15	0.03	0.24	0.05	0.08	0.02	− 0.05	0.00	0.24	0.05	− 0.09	− 0.04	0.03	0.02
Nowrangpur	**− 5.21**	**− 0.62**	**-4.52**	**-0.58**	**-4.06**	**-0.59**	**-3.58**	**-0.53**	**-3.67**	**-0.51**	**-2.55**	**-0.49**	**-2.39**	**-0.47**
Pauni	− 1.32	− 0.19	− 0.87	− 0.15	− 1.08	− 0.17	**− 2.03**	− 0.28	− 1.34	− 0.23	− 0.74	− 0.20	− 1.05	− 0.21
Perur	− 0.72	− 0.13	− 0.35	− 0.07	− 0.93	− 0.17	− 1.19	− 0.18	− 0.89	− 0.21	− 0.22	− 0.06	− 0.33	− 0.07
Polawaram	− 0.29	− 0.05	− 0.26	− 0.04	− 0.34	− 0.06	− 0.46	− 0.09	− 0.10	− 0.02	− 0.03	− 0.01	− 0.04	− 0.01
Ramakona	0.17	0.04	− 0.07	− 0.04	0.34	0.04	− 0.24	− 0.05	− 0.99	− 0.13	0.64	0.22	0.65	0.23
Saradaput	0.39	0.07	− 0.70	− 0.13	− 1.35	− 0.23	− 0.19	− 0.04	− 1.44	− 0.25	− 0.30	− 0.09	− 0.18	− 0.06
Somanpally	− 0.22	− 0.05	− 0.80	− 0.11	− 1.05	− 0.10	− 0.52	− 0.09	− 0.28	− 0.04	− 0.10	− 0.04	− 0.08	− 0.03
Tekra	− 0.55	− 0.10	− 1.01	− 0.14	− 1.24	− 0.14	− 0.79	− 0.16	− 0.63	− 0.13	− 0.49	− 0.17	− 0.67	− 0.18
Yelli	− 1.59	− 0.15	0.88	0.16	1.02	0.17	− 0.11	0.02	0.29	0.07	− 0.01	− 0.01	− 0.05	− 0.01

Note **Bold** values indicate statistically significant trends at a 5% significance level. MMK *Z* and SR ρ denote test statistics of Modified Mann–Kendall (Eq. (4)) Spearman's Rho (Eq. (5)) tests, respectively

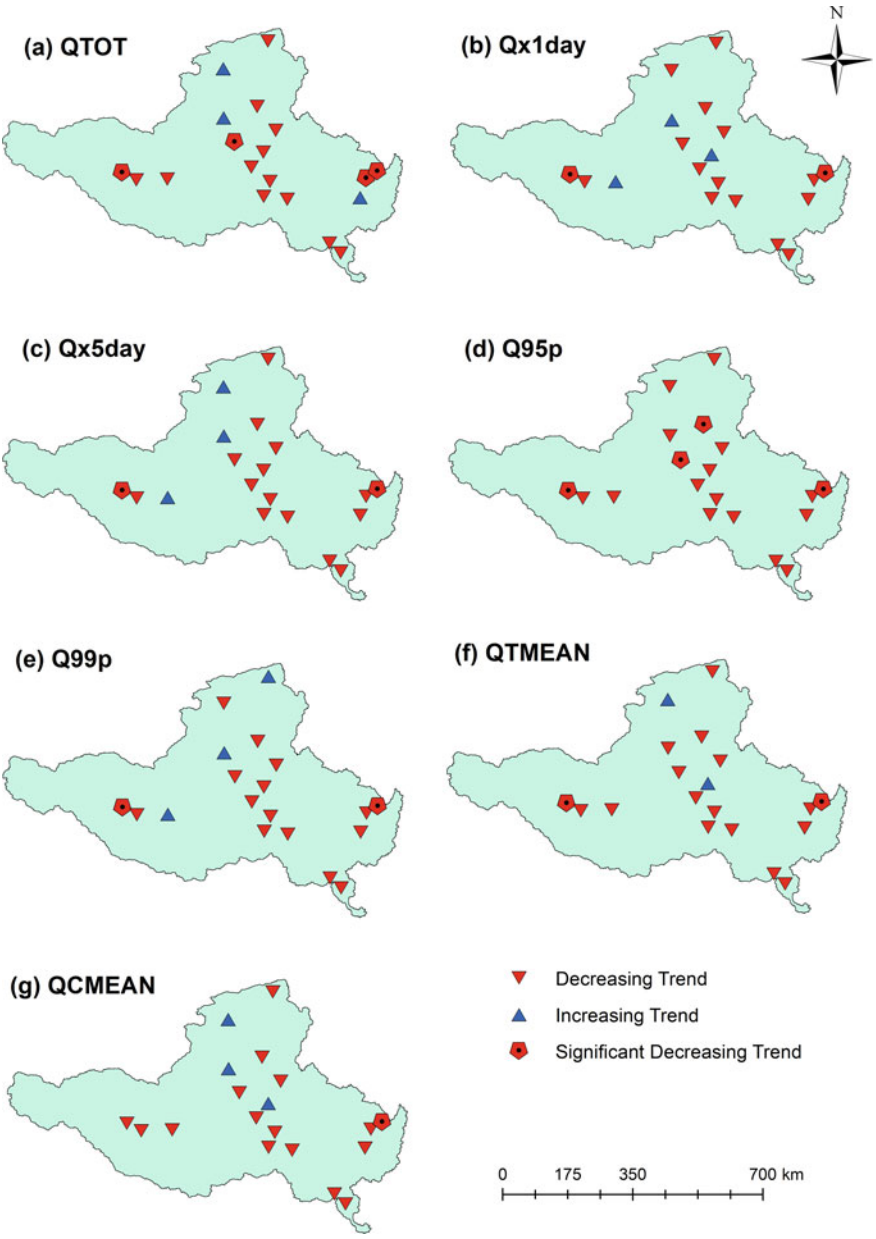

Fig. 3 Spatial variability of trends in streamflow indices across the Godavari River basin

4.2 *Changes in the Distributional Characteristics of Streamflows*

The changes in the distributional characteristics of mean and extreme flows are analyzed using a non-parametric kernel density estimate and Mann–Whitney test. The entire streamflow period is divided into three sub-periods, viz., before 1980, during 1981–1995 and after 1995 and analyzed further. The kernel density estimation is used to derive the distributional characteristics of the streamflows, and statistically significant changes in the distributions between the sub-periods mentioned above are evaluated using the Mann–Whitney test at a 5% significance level. From Fig. 4, a distinct shift in the location parameter for QTOT toward the origin (i.e., decrease in QTOT) is noticed for the stations G. R. Bridge and Nowrangpur in the sub-period after 1995 vis-à-vis the sub-period during 1981–1995. On the other hand, the shift in QTOT for Dhalegaon station is noticed during the sub-period 1981–1995 vis-à-vis the sub-period before 1980. These shifts in the distributional characteristics are found to be statistically significant at a 5% significance level.

Further, significant changes in the distributional characteristics of Qx1day (see Fig. 5), Qx5day (see Fig. 6), Q99p, and Q95p indices are observed for Dhalegaon, G. R. Bridge, and Nowrangpur stations like that of QTOT. However, the significant changes in characteristics of QTMEAN and QCMEAN are noted at G. R. Bridge and

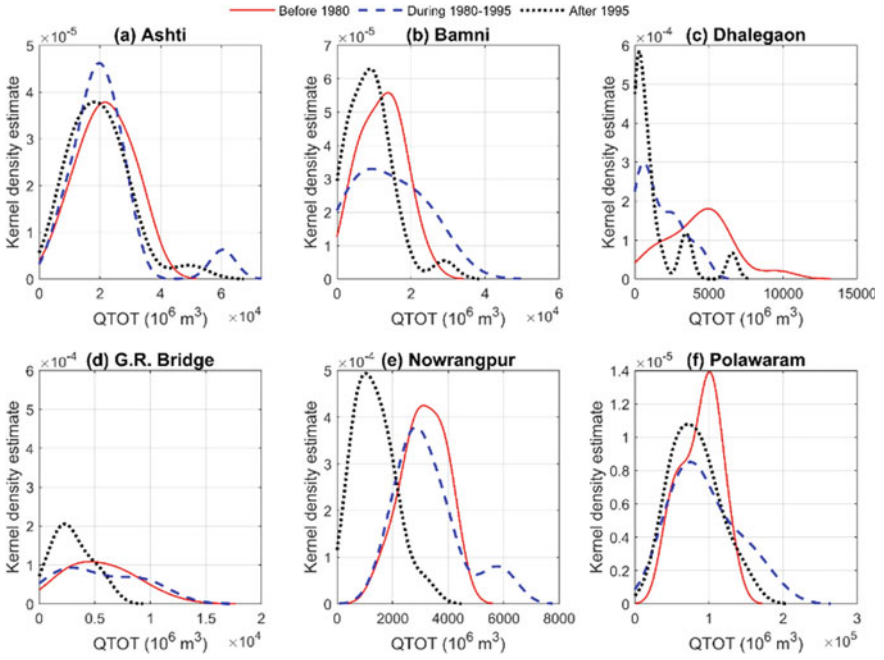

Fig. 4 Changes in distributional characteristics of total annual runoff (QTOT)

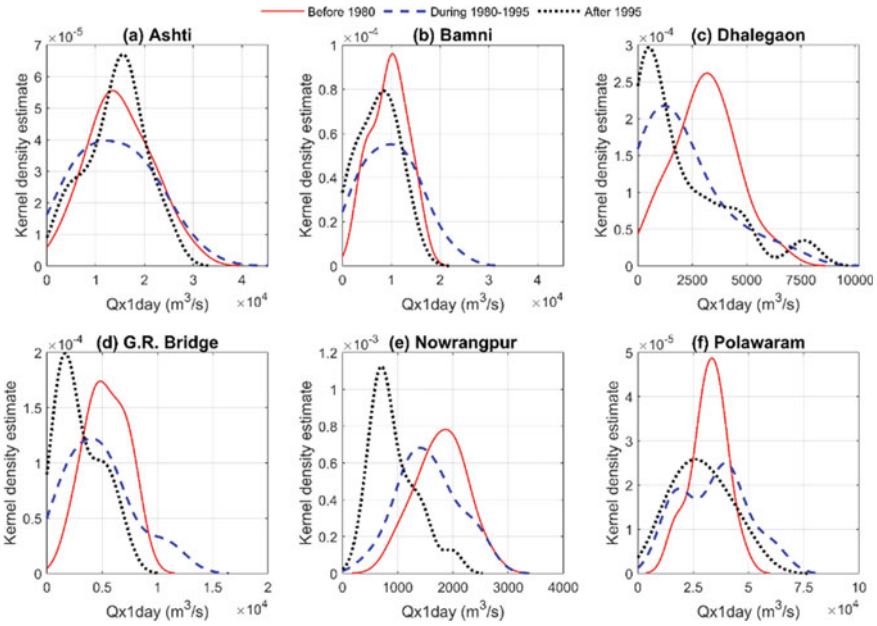

Fig. 5 Changes in distributional characteristics of annual maximum 1-day streamflow (Qx1day)

Nowrangpur stations for the sub-period after 1995 vis-à-vis the sub-period during 1981–1995. The analyses show that most changes are observed in the sub-period after 1995 compared to the other sub-periods. It is interesting to note that the Dhalegaon and G. R. Bridge stations located on the upper reaches of the Godavari River have shown significant shifts in the streamflow characteristics. In contrast, the Koida, Perur, and Polawaram stations situated in the lowermost reaches of the Godavari River do not exhibit substantial changes in the streamflow distributions. The Nowrangpur station on the Indravati River has consistently shown significant changes in streamflow characteristics across all sub-periods. The attributional analysis of such spatio-temporal changes in the streamflow characteristics would provide deep insights about the hydroclimatological changes in the Godavari basin.

5 Conclusions

The present study analyzes the abrupt, gradual, and distributional changes in the streamflow indices representing mean, peak, and exceedance of mean annual flow conditions across the Godavari River basin. The conclusions drawn from the foregoing study are as follows:

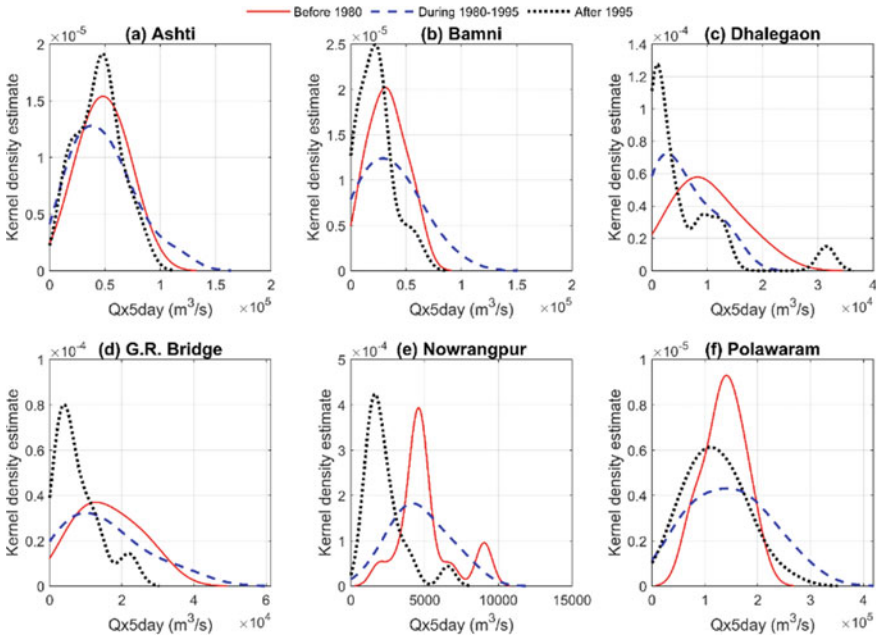

Fig. 6 Changes in distributional characteristics of annual maximum 5-day streamflow (Qx5day)

- A decrease in total annual streamflow is observed across the entire basin, indicating a reduction in freshwater availability and a likely increase in the water stress condition.
- The streamflow indices representing the peak flow (Qx1day, Qx5day, Q95th, Q99th, QCMEAN, QTMEAN) have also shown a decreasing trend across the basin, indicating the reduction of magnitude as well as the occurrence of floods in the entire basin.
- The decrease in water availability is observed in the recent period (i.e., after 1995) as compared to the earlier periods, which would likely have severe implications on the freshwater ecosystem services and the morphodynamics of the Godavari River and its tributaries.
- The attribution analysis of such streamflow decline to climate and/or human interventions would provide a better understanding of the dynamics of such change and help us make policy decisions in restoring the freshwater ecosystem services. Basin-level water management and conservation plans need to be formulated to avert a water scarcity crisis in the near future in the advent of changing climate.

Acknowledgements The authors would like to acknowledge the India Water Resource Information system (WRIS) and the Central Water Commission Government of India for providing the necessary data to conduct this research. The authors would like to acknowledge the resourceful support offered by the Punjab Engineering College during the study.

References

1. Hannaford J, Buys G (2012) Trends in seasonal river flow regimes in the UK. J Hydrol 475:158–174
2. Salarijazi M, Akhond-Ali A, Adib A, Daneshkhah A (2012) Trend and change-point detection for the annual streamflow series of the Karun River at the Ahvaz hydrometric station. Afr J Agric Res 7(32):4540–4552
3. Zhang A, Zheng C, Wang S, Yao Y (2015) Analysis of streamflow variations in the Heihe River Basin, northwest China: trends, abrupt changes, driving factors and ecological influences. J Hydrol Regional Stud 3:106–124
4. Abeysingha N, Singh M, Sehgal V, Khanna M, Pathak H (2016) Analysis of trends in streamflow and its linkages with rainfall and anthropogenic factors in Gomti River basin of North India. Theoret Appl Climatol 23(3):785–799
5. Drissia T, Jothiprakash V, Anitha A (2018) Statistical classification of streamflow based on flow variability in west flowing rivers of Kerala, India. Theor Appl Climatol 137(3):1643–1658
6. Sharma P, Patel P, Jothiprakash V (2019) Impact of rainfall variability and anthropogenic activities on streamflow changes and water stress conditions across Tapi Basin in India. Sci Total Environ 687:855–897
7. Kuriqi A, Ali R, Pham Q, Gambini J, Gupta V (2020) Seasonality shift and streamflow flow variability trends in central India. Acta Geophys 68(5):1461–1475
8. Das S, Sangode S, Kandekar A (2021) Recent decline in streamflow and sediment discharge in the Godavari basin, India (1965–2015). CATENA 206:105537
9. CWC (2014) Basin report—Godavari Basin. Central Water Commission, New Delhi
10. Chow VT, Maidment D, Mays L (1988) Applied hydrology, International Edition. MacGraw-Hill, New York
11. Pettitt A (1979) A non-parametric approach to the change-point problem. J Stat Soc Ser C (Appl Stat) 28(2):126–135
12. Hamed K, Rao A (1998) A modified Mann-Kendall trend test for autocorrelated data. J Hydrol 204(1–4):182–196
13. Teegavarapua R, Goly A, Obeysekera J (2013) Influences of atlantic multidecadal oscillation phases on spatial and temporal variability of regional precipitation extremes. J Hydrol 495:74–93
14. Jain S, Kumar V (2012) Trend analysis of rainfall and temperature data for India. Curr Sci 102(1):37–49

Spatio-Temporal Changes in the Streamflow Regimes Across Mahanadi River Basin

Ashutosh Sharma and Priyank J. Sharma

Abstract The current study analyses the changes in streamflow regimes using daily observed streamflow data at sixteen stream gauging stations in the Mahanadi River basin. In this study, non-parametric Pettit's test is used for detection of abrupt change, while Spearman's Rho and modified Mann–Kendall tests are used for trend assessment in annual total (QTOT) and maximum (Qx1day) streamflow series at a 5% significance level. Further, flow duration curves (FDCs) are derived at decadal time scales from daily streamflow data at each station to analyze the changes in streamflow regimes. The percentage change in the FDC quantiles representing low, moderate, high and peak flow conditions for the current period with respect to the baseline period are evaluated. The results indicate the presence of a significant change point in QTOT and Qx1day for the Bamnidhi and Kesinga stations. A contrasting pattern in the streamflow trends is evident between the northern (decreasing trend) and southern (increasing trend) parts of the Mahanadi basin, particularly upstream of the Hirakud reservoir. The changes in the decadal FDCs are classified into two broad categories based on the changes in magnitude and timing of streamflows; wherein seven stations have shown a notable transition from perennial to intermittent behavior. In contrast, no changes in the perennial nature of the stream were noticed at eight stations. The changes in the streamflow quantiles indicate an increase (decrease) in peak and high flow (dry and low flow) conditions in the region upstream of the

A. Sharma (✉)
Department of Civil Engineering, Punjab Engineering College (Deemed to be University), Chandigarh 160036, India
e-mail: ashutoshpec20@gmail.com

P. J. Sharma
Department of Civil Engineering, Indian Institute of Technology Indore, Indore, Madhya Pradesh 453552, India
e-mail: priyanksharma@iiti.ac.in

P. V. Timbadiya et al. (eds.), *Climate Change Impact on Water Resources*, Lecture Notes in Civil Engineering 313, https://doi.org/10.1007/978-981-19-8524-9_12

Hirakud dam. Such contrasting changes in the streamflow characteristics would need careful consideration by the local authorities to resolve water management issues in the basin.

Keywords Change point · Trend analysis · Streamflow regimes · Flow duration curves · Mahanadi river basin

1 Introduction

Managing hydro climatological extremes, viz., floods and droughts, has been a major concern since the beginning of human civilization. The freshwater scarcity is engulfing new geographical domains due to the rapid pace of population expansion and development. On the one hand, water scarcity makes human settlements and ecosystems vulnerable to droughts, while the flood losses also continue to grow [1]. Thus, assessing changes in the magnitude and probability of occurrence of streamflow regimes is vital for the design of structural measures for flood protection, risk and vulnerability of water resources systems, operation of reservoirs, and development of early warning systems [2]. The climate change impact assessment should consider the timing and magnitude of streamflows since these characteristics are essential for making operational decisions for water resources infrastructure [3].

Several studies (Silvestro et al. [2], Sharif and Burn [3], Jain et al. [4], and Gudmundsson et al. [5]) have analyzed the changes in extreme streamflow indices at regional and global scales. At the river basin scale, Panda et al. [6] assessed the trends in seasonal streamflow and rainfall, and showed considerable differences in the basin's sub-seasonal streamflow and rainfall patterns. The coastal proximity of the basin and its complex physiographic settings were attributed to the contrasting pattern observed in the sub-seasonal streamflow and rainfall. Jena et al. [7] analyzed the trends in rainfall and streamflow indices across the Mahanadi River basin. The study revealed an increasing (discharge) trend in peak discharge at Naraj station (near Hirakud dam), thereby indicating an increase in the contribution from the middle reaches of Mahanadi River due to the rise in the incidences of extreme rainfall. Hu et al. [8] analyzed the changes in extreme streamflow indices, representing flood and drought conditions, across the Kamo River basin, Japan, from 1951 to 2012. The flood indices, viz., daily peak flow and 5-day maximum flow, reported a decrease in 100-year flood during the period 1982–2012 vis-à-vis 1951–1981, while an increase in the 100-year drought index (i.e., the maximum number of consecutive low flow days) is also noticed across the basin. Goyal and Surampalli [9] reported a decrease in the drought severity in the lower Mahanadi basin, whereas an increase in the drought severity was noted in the upper Mahanadi basin. Sharma et al. [10] reported a decrease in the freshwater availability in the Tapi basin primarily driven by anthropogenic changes such as land use land cover change, streamflow regulation, and population growth. On the other hand, the peak flows were observed to decline across the Tapi basin (except in the upper reaches of the Tapi River), while a

significant increase in the low flow days was noted by Sharma et al. [11]. Thus, the studies point out different spatial and temporal variability in the streamflow characteristics, which are driven by the rainfall variability, physiographic conditions, and demographic changes in the basin.

The Mahanadi River basin, located in the proximity of the Bay of Bengal, receives frequent spells of extreme rainfall due to the landfall of tropical cyclones. Gudmundsson et al. [12] predicted that climate change would intensify the floods in the Mahanadi River basin in the near future, whereas Ghosh et al. [13] suggested a declining trend in the observed flow in the Mahanadi River at Hirakud dam in the near future. Such contrasting future streamflow behavior would result in complexities for water resources management in the basin. The present study aims to assess the changes in streamflow regimes through flow duration curves across the Mahanadi River basin.

2 Materials and Methods

2.1 Study Area and Data Source

The Mahanadi River is one of the major east-flowing rivers in peninsular India. During its traverse, it drains an area of 141,600 km^2, comprising fairly large areas of Chhattisgarh and Odisha and relatively smaller areas in Jharkhand, Maharashtra and Madhya Pradesh. The basin encompasses the area within geographical co-ordinates of 80° 28′ and 86° 43′ East longitudes and 19° 08′ and 23° 32′ North latitudes [14]. The Mahanadi River traverses a distance of 851 km before draining into the Bay of Bengal. During its traverse, six major tributaries join it upstream of the Hirakud reservoir, while two tributaries join it downstream of the Hirakud reservoir. The catchment area upstream and downstream of the Hirakud reservoir are 83,400 km^2 and 58,200 km^2, respectively. The major tributaries in the upstream reach are Seonath, Ib, Pairi, Jonk, Hasdeo, and Mand, while Tel and Ong are the major tributaries in the downstream reach. Though the catchment area of the downstream portion is less than that of the catchment upstream of Hirakud reservoir, the contribution of the downstream area to the total flood in the Mahanadi River is equally significant [15]. The southwest monsoon (June–October) is the principal rainy season, wherein more than 90% of the total annual rainfall occurs. The average annual rainfall in the Mahanadi basin is around 1400 mm [14]. The Mahanadi basin exhibits wide spatial variation in hydro-meteorological characteristics due to its vast geographical extent. The mean daily temperature during the winter and summer seasons vary in the range of 13 °C–20 °C and 30 °C–37 °C, respectively. The Hirakud Dam is a prominent water storage structure in the basin, located at the outlet of the middle Mahanadi basin, having a gross storage capacity of 8136 Mm^3.

The daily observed streamflow data used for this study is downloaded from the India Water Resources Information System (WRIS) web portal of Central Water

Table 1 Details of stream gauging stations located in Mahanadi Basin analyzed in this study

S. No.	Stream gauging station	River	Latitude (North)	Longitude (East)	Zero gauge (m)	Data length (years)
1	Andhiyar Khore	Hanp	21.83	81.60	252	43
2	Bamnidhi	Hasdeo	21.91	82.71	223	50
3	Basantpur	Mahanadi	21.74	82.79	206	49
4	Ghatora	Arpa	22.05	82.22	246	41
5	Jondhra	Seonath	21.71	82.33	219	41
6	Kantamal	Tel	20.66	83.73	118	49
7	Kesinga	Tel	20.29	83.22	166	42
8	Kotni	Seonath	21.24	81.25	268	42
9	Kurubhata	Mand	21.98	83.21	215	43
10	Manendragarh	Hasdeo	23.21	82.22	411	31
11	Pathardihi	Kharun	21.34	81.59	271	32
12	Rampur	Matwali	21.73	84.02	219	50
13	Salebhata	Ong	20.98	83.54	130	49
14	Seorinarayan	Mahanadi	21.72	82.60	209.5	35
15	Simga	Seonath	21.63	81.68	244	49
16	Sundergarh	Ib	22.11	84.03	214	45

Commission (CWC) India, which can be accessed through website [16]. The details of stream gauging stations in the Mahanadi basin, analyzed in the present study, are included in Table 1. The Mahanadi basin's digital elevation model (DEM) is derived from the USGS Earth Explorer [17] at 30 m resolution. The index map of the Mahanadi basin with locations of stream gauging stations, river network and DEM is shown in Fig. 1. The land use land cover LULC maps are derived from the Bhuvan portal [18] at the scale of 1:50,000 (see Fig. 2a), while the extent of soil erosion, slope classification and soil type in the basin are extracted from India WRIS portal (see Fig. 2b–d). The majority of the basin is covered with agricultural land, accounting for 54.27% of the total basin area, followed by forest land (i.e., 32.74%) [14].

2.2 Methodology

The daily streamflow data is checked for homogeneity and continuity before analysis. The streamflow data is checked for outliers or missing data and converted to water year format after that. The data sufficiency ensures a minimum of 25–30 years of continuous data availability at a given station for further analysis. The statistical analysis of the data is carried out. The non-parametric change point and trend detection tests are applied on the total annual runoff (QTOT) time series and annual maximum

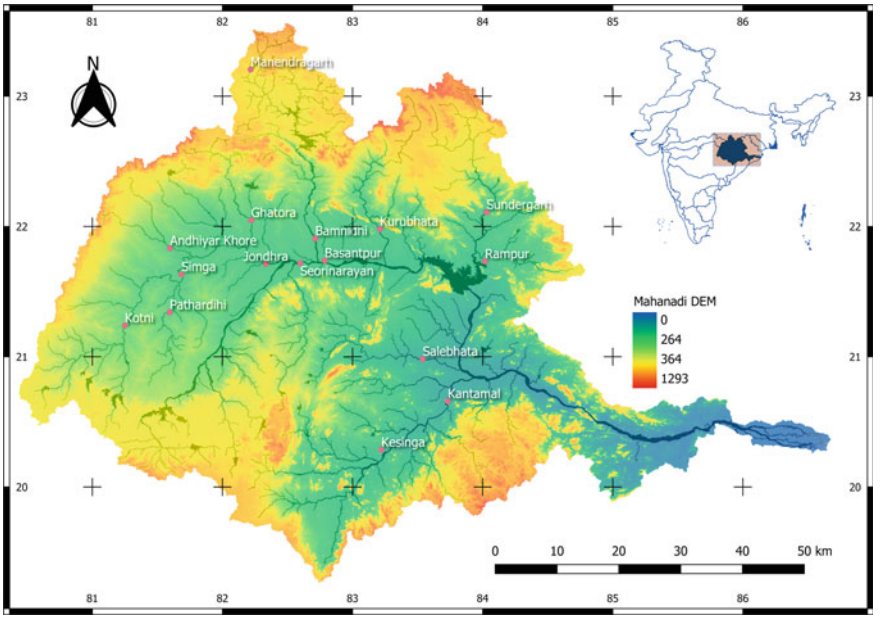

Fig. 1 Index map of Mahanadi River basin with locations of stream gauging stations, river network and digital elevation model

1-day streamflow (Qx1day) for each station. The trend analysis results derived from SR and MMK tests for QTOT and Qx1day are visualized on the basin map using QGIS. The FDCs are plotted on the decadal time scale and compared. Further, the percentage change in FDC flow quantiles (viz., $Q_{0.01}$, $Q_{0.25}$, $Q_{0.50}$, and $Q_{0.90}$) are estimated for the current decade (i.e., 2010s) with respect to the baseline period (i.e., 1970s or 1980s) and visualized on the basin map. The flowchart of the methodology adopted in the present study is shown in Fig. 3.

Pettit's Test

Pettitt's test [19] is a commonly applied non-parametric test to detect a change point in a continuous hydroclimatic time series $X = \{x_1, x_2, ..., x_n\}$. . It tests the null hypothesis (H_0) that both the time series have the same location parameter (i.e., no change) against the alternative hypothesis (H_1) that a change point exists. The test statistic is defined as:

$$K_T = \max\left(\left|U_{t,T}\right|\right) \tag{1}$$

where

$$U_{t,T} = \sum_{i=1}^{t} \sum_{j=t+1}^{T} \operatorname{sgn}\left(X_i - X_j\right) \tag{2}$$

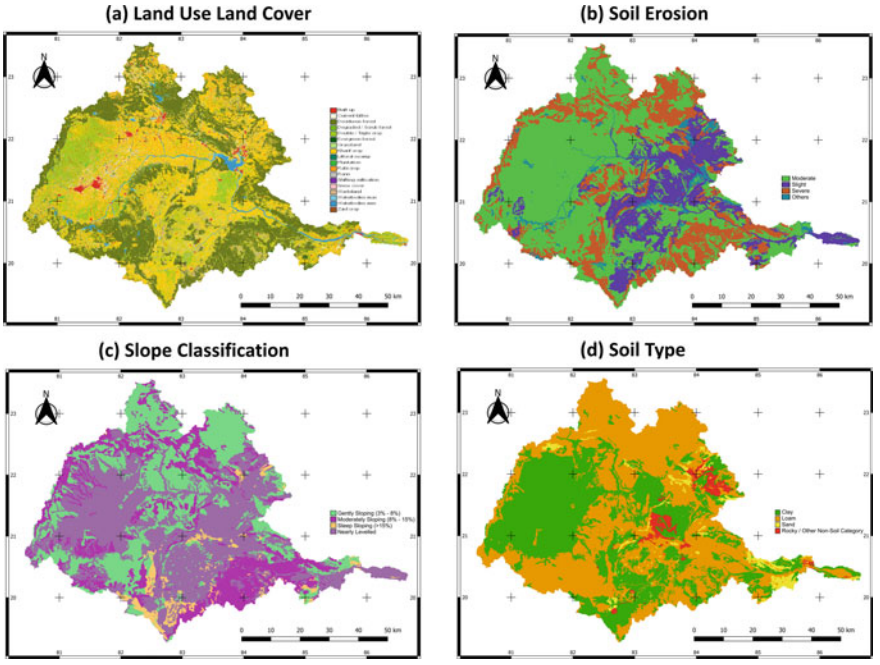

Fig. 2 **a** Land use land cover, **b** extent of soil erosion, **c** slope classification, and **d** soil type in the Mahanadi basin

The change point of the series is located at K_T provided that the statistic is significant. The probability of K_T is approximated as:

$$p \approx 2\exp\left(-6K_T^2/\left(T^3 + T^2\right)\right) \tag{3}$$

Spearman's Rho Test

Consider two datasets $X = \{x_1, x_2, ..., x_n\}$ and $Y = \{y_1, y_2, ..., y_n\}$, , to estimate the Spearman's Rho (SR) test statistic as the sum of squares of the differences between the corresponding ranks of X and Y. The SR test statistic (r) [20] is given as:

$$r = 1 - \frac{6\sum_{i=1}^{n}[R(x_i) - R(y_i)]^2}{n^3 - n} \tag{4}$$

where $R(x_i)$ and $R(y_i)$ denote the ranks of samples in the dataset X and Y, respectively, while n denotes the sample size. A positive (negative) value of r indicates an increasing (decreasing) trend whose significance is determined at a 5% significance level.

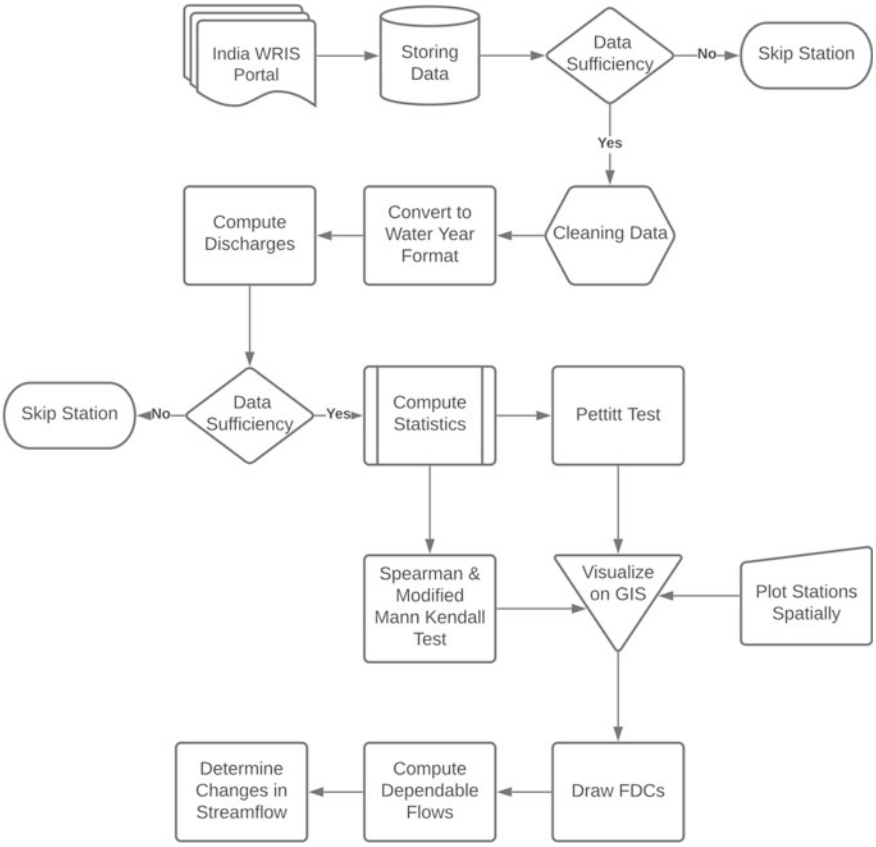

Fig. 3 Flowchart of the methodology adopted in the present study

Modified Mann–Kendall Test

The modified Mann–Kendall (MMK) test was proposed by Hamed and Rao [21] to address serial autocorrelation issues in trend estimation. They suggested a variance correction approach to improve trend analysis which was used to compute the test. The details of this test can be found in [21].

2.3 Flow Duration Curve

The flow duration curve (FDC) is a graphical representation of the percentage of time that flow in a stream is likely to equal or exceed some specified value. The FDC describes the ability of the basin to provide flows of various magnitudes. The shape of the flow duration curve evaluates the basin and stream characteristics in its

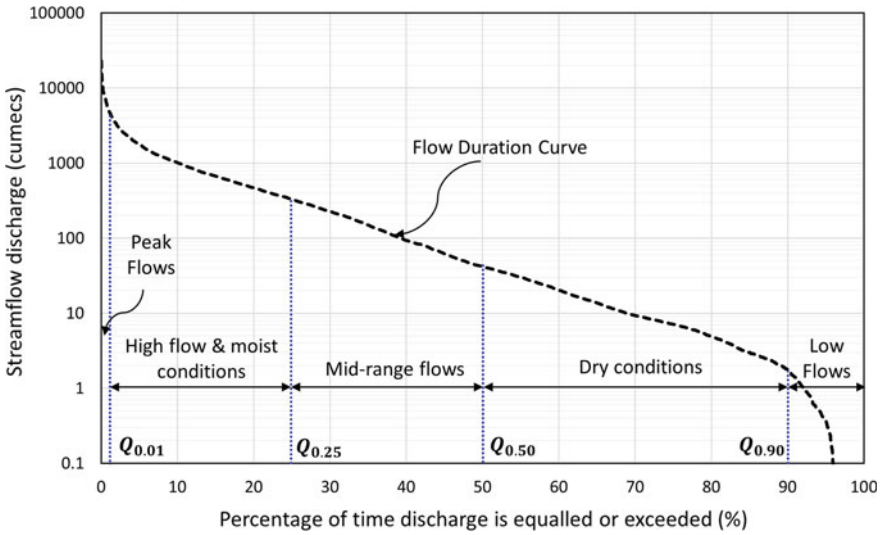

Fig. 4 Visualization of streamflow regimes through a flow duration curve

upper and lower regions. The shape of the curve in the high discharge region shows the type of flood regime, whereas the shape of the low-discharge region shows the ability of the basin to sustain low flows during dry seasons. A steep curve would be expected for floods caused by rain, whereas a flatter curve near the upper limit will result from snowmelt floods or regulation of floods with dam storage. In the low-discharges region, intermittent streams would exhibit periods of no flow. In contrast, a flat curve indicates that moderate flows are sustained throughout the year, which may be due to natural or artificial streamflow regulation.

The current study aggregates the daily streamflow values for a decade at a stream gauging station to derive FDC. Similarly, FDCs for other decades are derived and plotted on a single graph to analyze the changes in streamflow regimes at a stream gauging station. The FDC is used to analyze the temporal changes in the streamflow quantiles (viz., $Q_{0.01}$, $Q_{0.25}$, $Q_{0.50}$, and $Q_{0.90}$) on a decadal time scale. The streamflow regimes can be visualized as: peak flows for $Q \leq Q_{0.01}$, high flow and moist conditions for $Q_{0.01} < Q \leq Q_{0.25}$, mid-range flows for $Q_{0.25} < Q \leq Q_{0.50}$, dry conditions for $Q_{0.50} < Q \leq Q_{0.90}$, and low flows for $Q > Q_{0.90}$ (see Fig. 4).

3 Results and Discussion

The daily streamflow data is analyzed to derive each station's total annual streamflow (QTOT) and annual maximum 1-day streamflow (Qx1day) time series. The change point in QTOT and Qx1day series are assessed using non-parametric Pettit's test,

while their trend analysis is carried out using Spearman's rho and Modified Mann–Kendall tests. The changes in streamflow quantiles, derived from FDC, are estimated for the present decade (2010s) as compared to the baseline period (1970s or 1980s, whichever is available).

3.1 Change Point Detection

The analysis of the change point in annual total runoff (QTOT) and annual maximum 1-day streamflow (Qx1day) indicated the presence of a significant change point (at $\alpha = 0.05$) only for two stations (see Table 2). The change point year for QTOT and Qx1day at Bamnidhi station was estimated to be 2007 and 1989, respectively, whereas the corresponding change point years at Kesinga station were 2001 and 2006. The remaining stations did not exhibit any significant change point. For Bamnidhi and Kesinga stations, a decrease in mean flow was observed after the change point. However, this assessment cannot infer the changes in other streamflow characteristics.

Table 2 Change point assessment in annual total and maximum 1-day streamflows

Stream gauging station	QTOT		Qx1day	
	Change point year	Pettitt's *U* statistic	Change point year	Pettitt's *U* statistic
Andhiyar Khore	2006	165	2000	119
Bamnidhi	**2007**	340	**1989**	324
Basantpur	2016	138	1987	128
Ghatora	2000	179	2001	130
Jondhra	2015	112	1990	116
Kantamal	1990	211	2005	88
Kesinga	**2001**	234	**2006**	219
Kotni	1990	80	1986	162
Kurubhata	2005	163	2004	115
Manendragarh	2006	125	1982	174
Pathardihi	1991	54	1991	56
Rampur	1996	120	2010	146
Salebhata	1980	121	2001	122
Seorinarayan	2015	84	1990	111
Simga	1987	92	2015	118
Sundergarh	2001	161	2002	102

Note Bold values indicate that the change point is statistically significant at a 5% significance level

3.2 Trend Detection

The trend analysis of QTOT and Qx1day is performed using MMK and SR tests for each station. The results from both these tests are found to agree with each other. From Table 3, decreasing and increasing trends in QTOT (Qx1day) are reported for ten (eight) and six (eight) stations, respectively. However, a significant decreasing trend in QTOT is noted for Bamnidhi and Manendragarh stations located on the Hasdeo tributary, whereas a significant increasing trend in QTOT is observed at Kesinga station located on the Tel tributary. The spatial distribution of trend characteristics of QTOT and Qx1day are shown in Fig. 5. From Fig. 5, an increase in total and peak flows are noticeable in the region downstream of the Hirakud reservoir. A clear contrasting pattern in the streamflow trends is evident between the northern (decreasing trend) and southern (increasing trend) part of the Mahanadi basin, particularly upstream of Hirakud reservoir, see Fig. 5.

Table 3 Results of trend detection in annual total and maximum 1-day streamflows

Stream gauging station	QTOT		Qx1day	
	SR r statistic	MMK Z statistic	SR r statistic	MMK Z statistic
Andhiyar Khore	– 0.15	– 0.93	– 0.03	– 1.37
Bamnidhi	– **0.44**	– **3.41**	– **0.44**	– **3.39**
Basantpur	– 0.14	– 1.42	– 0.22	– 1.04
Ghatora	– 0.23	– 1.66	0.05	– 0.11
Jondhra	– 0.07	– 0.27	0.08	– 1.43
Kantamal	0.25	1.54	0.05	0.68
Kesinga	**0.40**	**2.92**	– 0.22	0.43
Kotni	0.10	0.48	0.16	0.17
Kurubhata	– 0.11	– 0.43	– 0.28	0.95
Manendragarh	– **0.38**	– **4.14**	– 0.15	– 1.57
Pathardihi	0.03	0.14	0.05	0.17
Rampur	– 0.12	– 0.95	– 0.12	– 0.73
Salebhata	0.07	0.47	0.08	0.58
Seorinarayan	0.03	0.12	0.18	0.89
Simga	– 0.02	– 0.06	– 0.09	– 1.08
Sundergarh	– 0.15	– 0.89	– 0.01	0.04

Note Bold values indicate that the trend is statistically significant at a 5% significance level

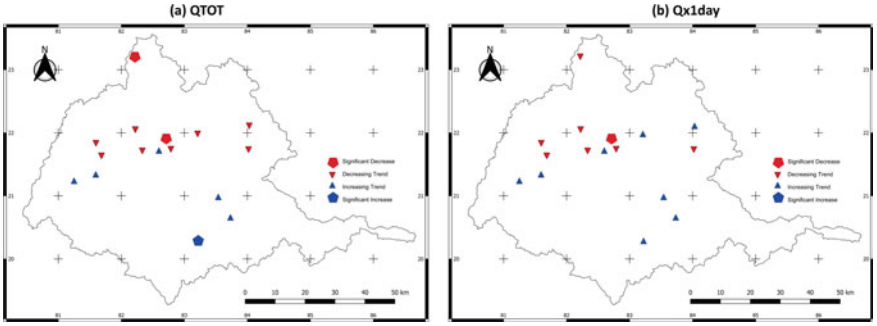

Fig. 5 Spatial variability of trends in **a** QTOT and **b** Qx1day across Mahanadi basin

3.3 Changes in Streamflow Characteristics Through Flow Duration Curve

The decadal FDCs are derived for each station and compared to visualize the changes in streamflow characteristics at each station, as shown in Fig. 6. The FDCs of only eight stations are shown in Fig. 6 due to the paucity of space. On investigation of changes in the decadal FDCs, the stations can be classified into two broad categories, viz., (i) unchanged streamflow characteristics (i.e., a perennial stream remains perennial with nominal changes in streamflow magnitude and timing), (ii) considerable changes in streamflow characteristics (i.e., a perennial stream exhibits intermittent nature with significant changes in the streamflow magnitude and timing). The Basantpur (see Fig. 6e) and Seorinarayan (see Fig. 6g) stations on the Mahanadi River; Kantamal and Kesinga (see Fig. 6b) stations on the Tel River; while Bamnidhi (see Fig. 6a), Kurubhata, Salebhata, and Sundergarh (see Fig. 6h) stations on the Hasdeo, Mand, Ong, and Ib Rivers, respectively, have shown perennial characteristics throughout the decades the 1970s–2010s.

On the other hand, the Jondhra and Simga stations on the Seonath River; the Andhiyar Khore (see Fig. 6d), Ghatora, Manendragarh (see Fig. 6c), Pathardihi, and Rampur stations on the Hanp, Arpa, Hasdeo, Kharun, and Matwali Rivers have undergone a transformation from perennial to intermittent nature with significant changes in the streamflow characteristics. The Kotni (see Fig. 6f) station on the Seonath River has shown ephemeral nature wherein the streamflow was recorded lesser than 20% of the time in the decade 2010s. The changes in the streamflow characteristics from perennial to intermittent could plausibly be due to changes in climatic and/or anthropogenic conditions, which needs further investigation.

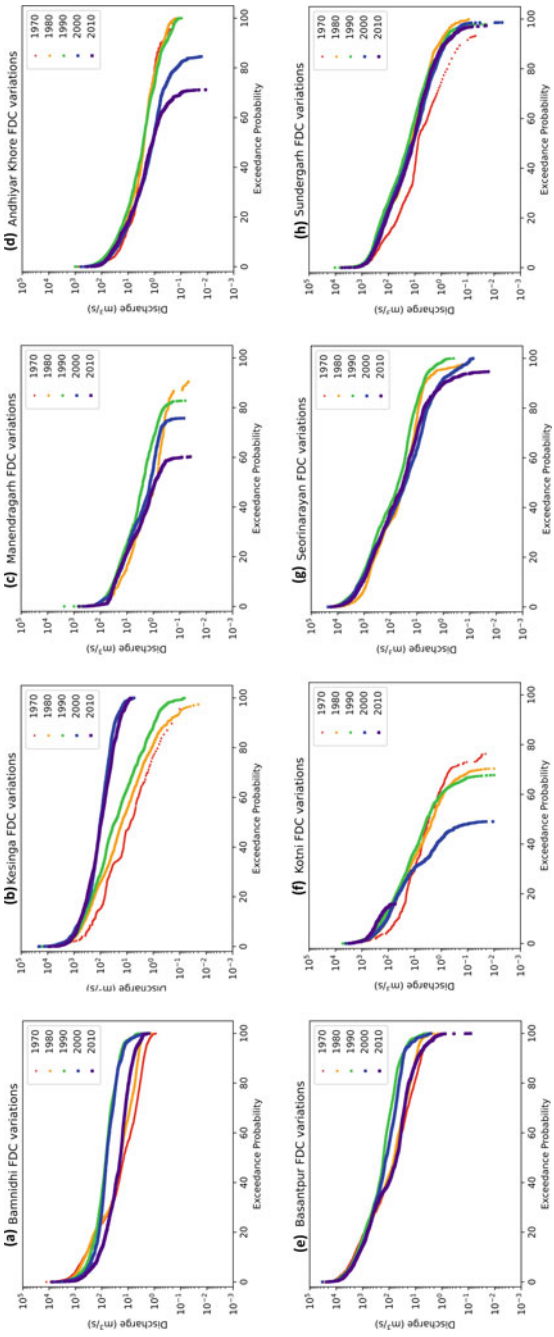

Fig. 6 Decadal variations in FDCs across stream gauging stations in Mahanadi River basin

3.4 Changes in Streamflow Quantiles

The percentage change in the streamflow quantiles are computed for the current period (2010s) with respect to the baseline period (1970s or 1980s). The spatial variability of percentage changes in the streamflow quantiles is shown in Fig. 7. An increase (decrease) in the peak flow quantile, i.e., $Q_{0.01}$, is observed at seven (nine) stations, wherein a considerable increase in the same is noticed at the Ghatora, Jondhra, Kurubhata, and Pathardihi stations (see Fig. 7a). The streamflow quantile representing high flows and moist conditions (i.e., $Q_{0.25}$) is found to increase at thirteen out of sixteen sites in the Mahanadi basin. However, this increase in moist flow conditions could augment the storage in the Hirakud dam, which will benefit irrigation and hydropower generation. The moist flow conditions are also increasing in the region downstream of the Hirakud dam also (see Fig. 7b). On the other hand, the moderate, dry, and low flow conditions are found to decrease across most parts of the basin, particularly upstream of the Hirakud dam (see Fig. 7c, d). Such a decrease in the low flow conditions upstream of the Hirakud dam is attributed to extensive watershed development in terms of the construction of several minor and medium storage structures.

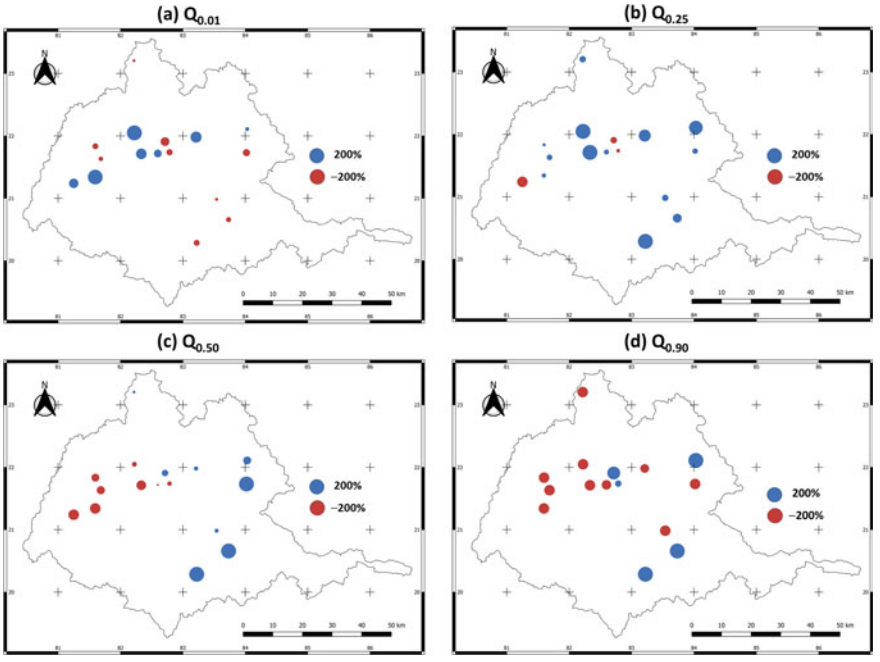

Fig. 7 Percentage change in the FDC characteristics of streamflow quantiles **a** $Q_{0.01}$, **b** $Q_{0.25}$, **c** $Q_{0.50}$, and **d** $Q_{0.90}$, for the present decade (2010s) with respect to the baseline decade (1970s or 1980s)

Thus, the assessment of changes in streamflow quantiles provides a comprehensive assessment of the fluctuations in the streamflow characteristics. However, a detailed attribution of climatic and anthropogenic conditions for the detected streamflow changes needs to be undertaken for a better understanding of the catchment dynamics. The water resources planners and managers can utilize this information to formulate policies for flood and drought mitigation in the Mahanadi basin.

4 Conclusions

The current study examined the spatio-temporal changes in the streamflow characteristics through non-parametric statistical tests and flow duration curves for the Mahanadi River basin. The following key conclusions are derived from the foregoing study:

- A statistically significant change point is noted across two stations in the basin, while the rest of the stations do not exhibit significant changes in the mean streamflows. The trend analysis results highlight an increase in total and peak flows in the region downstream of the Hirakud reservoir. Thus, a clear contrasting pattern in the streamflow trends is evidently noticed between the northern (decreasing trend) and southern (increasing trend) part of the Mahanadi basin, particularly upstream of Hirakud reservoir.
- The decadal flow duration curves indicate that the stations located across the Mahanadi, Tel, Hasdeo, Mand, Ong, and Ib Rivers do not exhibit significant changes in their characteristics and show perennial nature from the period 1970-2010. On the other hand, the stations located across the Seonath, Hanp, Arpa, Hasdeo, Kharun, and Matwali Rivers exhibit a gradual transformation from perennial to intermittent streamflow behavior, wherein the streamflows are recorded around 40–65% of the times in the river in the current period (2010s) as compared to the baseline period (1970s).
- The spatial variation of changes in the streamflow quantiles indicates an increase (decrease) in peak and high flow (dry and low flow) conditions in the region upstream of the Hirakud dam. Such contrasting changes in the streamflow characteristics could lead to water management issues in the basin and need careful consideration of the local authorities for their resolution.

Acknowledgements The researchers are thankful to the India Water Resource Information System (WRIS) and Central Water Commission (CWC) for providing the necessary data to conduct this research. The authors would like to acknowledge the resourceful support offered by the Punjab Engineering College during the study.

References

1. Kundzewicz ZW, Kaczmarek Z (2000) Coping with hydrological extremes. Water Int 25(1):66–75
2. Silvestro F, Parodi A, Campo L, Ferraris L (2018) Analysis of the streamflow extremes and long-term water balance in the Liguria region of Italy using a cloud-permitting grid spacing reanalysis dataset. Hydrol Earth Syst Sci 22(10):5403–5426
3. Sharif M, Burn D (2009) Detection of linkages between extreme flow measures and climate indices. Int J Civ Environ Struct Constr Archit Eng 3(12):495–500
4. Jain S, Nayak P, Singh Y, Chandniha S (2017) Trends in rainfall and peak flows for some river basins in India. Curr Sci 112(8):1712–1726
5. Gudmundsson L, Boulange J, Do HX, Gosling SN, Grillakis MG, Koutroulis AG, Zhao F (2021) Globally observed trends in mean and extreme river flow attributed to climate change. Science 371(6534):1159–1162
6. Panda DK, Kumar A, Ghosh S, Mohanty RK (2013) Streamflow trends in the Mahanadi River basin (India): linkages to tropical climate variability. J Hydrol 495:135–149
7. Jena PP, Chatterjee C, Pradhan G, Mishra A (2014) Are recent frequent high floods in Mahanadi basin in eastern India due to increase in extreme rainfalls? J Hydrol 517:847–862
8. Hu M, Sayama T, Duan W, Takara K, He B, Luo P (2017) Assessment of hydrological extremes in the Kamo River Basin, Japan. Hydrol Sci J 62(8):1255–1265
9. Goyal MK, Surampalli RY (2018) Impact of climate change on water resources in India. J Environ Eng 144(7):04018054
10. Sharma PJ, Patel PL, Jothiprakash V (2019) Impact of rainfall variability and anthropogenic activities on streamflow changes and water stress conditions across Tapi Basin in India. Sci Total Environ 687:885–897
11. Sharma PJ, Patel PL, Jothiprakash V (2020) Hydroclimatic teleconnections of large-scale oceanic-atmospheric circulations on hydro-meteorological extremes of Tapi Basin, India. Atmosph Res 235:104791
12. Gosain AK, Rao S, Basuray D (2006) Climate change impact assessment on hydrology of Indian river basins. Curr Sci 346–353
13. Ghosh S, Raje D, Mujumdar PP (2010) Mahanadi streamflow: climate change impact assessment and adaptive strategies. Curr Sci:1084–1091
14. CWC (2014) Mahanadi Basin watershed atlas. Central Water Commission, New Delhi
15. CWC (2018) Water year book (2017–2018): Mahanadi Basin. Central Water Commission, Bhubaneshwar
16. www.indiawris.gov.in/wris/. Accessed on 25 June 2021
17. www.earthexplorer.usgs.gov/. Accessed on 25 June 2021
18. www.bhuvan-app1.nrsc.gov.in/. Accessed on 25 June 2021
19. Pettitt AN (1979) A non-parametric approach to the change-point problem. J Roy Stat Soc: Ser C (Appl Stat) 28(2):126–135
20. Lehmann EL (1975) Non parametrics: statistical methods based on ranks. Holden-Day, San Francisco
21. Hamed KH, Rao AR (1998) A modified Mann–Kendall trend test for autocorrelated data. J Hydrol 204(1–4):182–196

Assessment of Temporal Changes in Streamflow Characteristics Across Cauvery River Basin

Nidhi Kaundal and Priyank J. Sharma

Abstract Changes in freshwater water availability have been noticed across several river basins over the years due to climatic and anthropogenic influences. The current study investigates the changes in streamflow characteristics over a semi-arid river basin in South India, viz., Cauvery River basin (area $\approx$ 81,155 km^2), using daily streamflow data. The data has been thoroughly checked for consistency and completeness. Several streamflow indices representing the magnitude, frequency, and duration of peak and low flow conditions are derived from the daily data at fourteen stream gauging stations in the Cauvery basin. The change point and trend in the streamflow indices are analyzed by non-parametric Pettitt's and Modified Mann–Kendall and Spearman's rho tests, respectively. A significant change point in total annual runoff was reported for three stations, while the extreme flows did not exhibit any change point. The results indicated a decrease in the water availability, peak as well as low flows in the basin across most stations. Such a decrease in water availability and low flows would aggravate the water stress conditions in the basin and have adverse impacts on the stream ecology.

Keywords Change point · Trend analysis · Non-parametric test · Extreme streamflow indices · Cauvery River basin

N. Kaundal (✉)
Department of Civil Engineering, Punjab Engineering College (Deemed to be University), Chandigarh 160036, India
e-mail: kaundal.nidhi279@gmail.com

P. J. Sharma
Department of Civil Engineering, Indian Institute of Technology Indore, Madhya Pradesh, Indore 453552, India
e-mail: priyanksharma@iiti.ac.in

P. V. Timbadiya et al. (eds.), *Climate Change Impact on Water Resources*, Lecture Notes in Civil Engineering 313, https://doi.org/10.1007/978-981-19-8524-9_13

1 Introduction

India's current population (1.39 billion) is around 17.7% of the world's total population, which is expected to reach 1.6 billion by 2050 [1]. The timely and adequate availability of necessities such as food and water are vital for sustainable living, especially in developing and highly populated countries. The freshwater resources are non-uniformly distributed throughout India, wherein water availability and water use patterns show wide variability across different river basins. Hence, it is important to assess the spatio-temporal changes in streamflow characteristics at the river basin scale for sustainable water resources management. Gosain et al. [2] assessed the impact of climate change on the hydrological cycle of various Indian river basins using a semi-distributed hydrologic model. The results highlighted the susceptibility of droughts and flash floods in regions across twelve Indian river basins, specifically the Krishna and Mahanadi basins, which would experience severe drought and flood conditions, respectively. Pathak et al. [3] evaluated the impacts of the availability of water and climate change on Indian agriculture. The study reported a projected increase in the water requirement of around 3.5–5% and 6–8% by the years 2025 and 2075, respectively, particularly for irrigation purposes. Several adaptation measures were suggested to cope with such demand increase, viz., building micro-storage facilities in watersheds, implementing rainwater harvesting techniques, and recharging groundwater aquifers. Various strategies were also proposed to mitigate water stress due to climate change by increasing the availability of usable water, improving water efficiency, altering agronomic crops and interlinking rivers, and practicing integrated water resources management.

As compared to regional or continental-scale studies, the basin-scale studies provide specific insights into the hydroclimatological changes due to the influence of local factors for deriving efficient water resources management policies. Abeysingha et al. [4] investigated trends in hydro-climatic parameters such as temperature, rainfall, and streamflow of four stations in the Gomti River basin from 1982 to 2012, using Sen's slope and Mann–Kendall trend detection tests. The results indicated a gradual decrease in trends of annual, winter, and monsoon streamflows in the midstream to downstream reaches of the Gomti River. Jain et al. [5] examined the peak flows and rainfall trends in seven major river basins of India. A decrease (increase) in the extreme rainfall was reported in the upstream (plain) areas of major river basins. The east-flowing rivers exhibit a higher number of rainy days than the west-flowing rivers. A decreasing trend in the smaller magnitude floods is evident across most river basins (viz., Cauvery, Godavari, Krishna, Narmada), plausibly due to higher upstream water utilization and watershed development. In contrast, the high magnitude floods do not exhibit appreciable changes across all major river basins. Sharma et al. [6] analyzed the changes in extreme rainfall and streamflow indices across the Tapi River basin in western India. The drier (wetter) conditions were observed in the Tapi basin's upper and eastern middle (western middle and lower) parts. The total and extreme streamflows were found to decrease (except in the upper reaches of Tapi River), while a significant increase in the low flow days was reported.

The studies are scarce in the literature, which has reported extensive analysis of the temporal changes in streamflow regimes at the river basin scale, particularly for the Cauvery River basin. Sreelash et al. [7] analyzed the hydrologic behavior of rivers flowing through the southern Western Ghats due to rainfall variability using Sen's slope estimator and Mann–Kendall tests. Decreasing (increasing) trend in rainfall in the southwest (northeast) monsoon is noticed. A significant decrease in annual discharge noted in the east-flowing rivers is attributable to a reduction of southwest monsoon rainfall, while an increasing trend is detected in the Cauvery River. Sreelash et al. [8] evaluated streamflow trends at twenty stream gauging stations in the Cauvery basin and linked them to the changes in hydrological parameters. A decline in the annual and seasonal streamflows observed in the basin was linked to a decrease in total rainfall and rainy days while an increase in evapotranspiration (ET) in the region. Further, a significant negative association was observed between ET and groundwater levels.

The Cauvery River basin (area $\approx$ 81,155 km^2) shows wide spatial and temporal heterogeneity in the physiography and rainfall occurrence. It receives rainfall during both southwest and northeast monsoon seasons, whereas higher rainfall is recorded in the middle and lower regions of the basin, which are closer to the Western Ghats [8]. Moreover, the Cauvery basin exhibits a semi-arid tropical climate and is considered a water-scarce region. Thus analyzing the changes in freshwater availability across the basin is of prime importance for sustainable living and the environment. The present study aims to assess the temporal changes in streamflow indices representing the magnitude, frequency, and duration of peak and low flow conditions across the Cauvery River basin.

2 Materials and Methods

2.1 Study Area: Cauvery Basin

The Cauvery River originates from Talakaveri in the Brahmagiri Range of the Western Ghats in Kodagu district, Karnataka (India) [5]. It is the fourth largest peninsular river and flows eastwards, passing through three Indian states, viz., Tamil Nadu, Karnataka, Kerala, and one Union Territory (i.e., Puducherry). The Cauvery River drains a total area of 81,155 km^2, which comprises 2.7% of the total geographical area of India [9]. It covers about 800 km before draining into the Bay of Bengal in Tamil Nadu. The Cauvery River basin lies between 75° 27′ and 79° 54′ east longitudes and 10° 09′–13° 30′ north latitudes (Fig. 1). The locations of the stream gauging stations analyzed in the present study are marked in Fig. 1, along with the stream network. The major tributaries of the Cauvery River are the Hemavati, Harangi, Arkavathy, Shimsha, Kabini, Lakshmana Tirtha, Bhavani, Amravati, Moyar, and Noyyal.

The Cauvery basin is bounded by the Western Ghats to its west while the Bay of Bengal to its east. The Cauvery basin receives about 50% (33%) of rainfall during

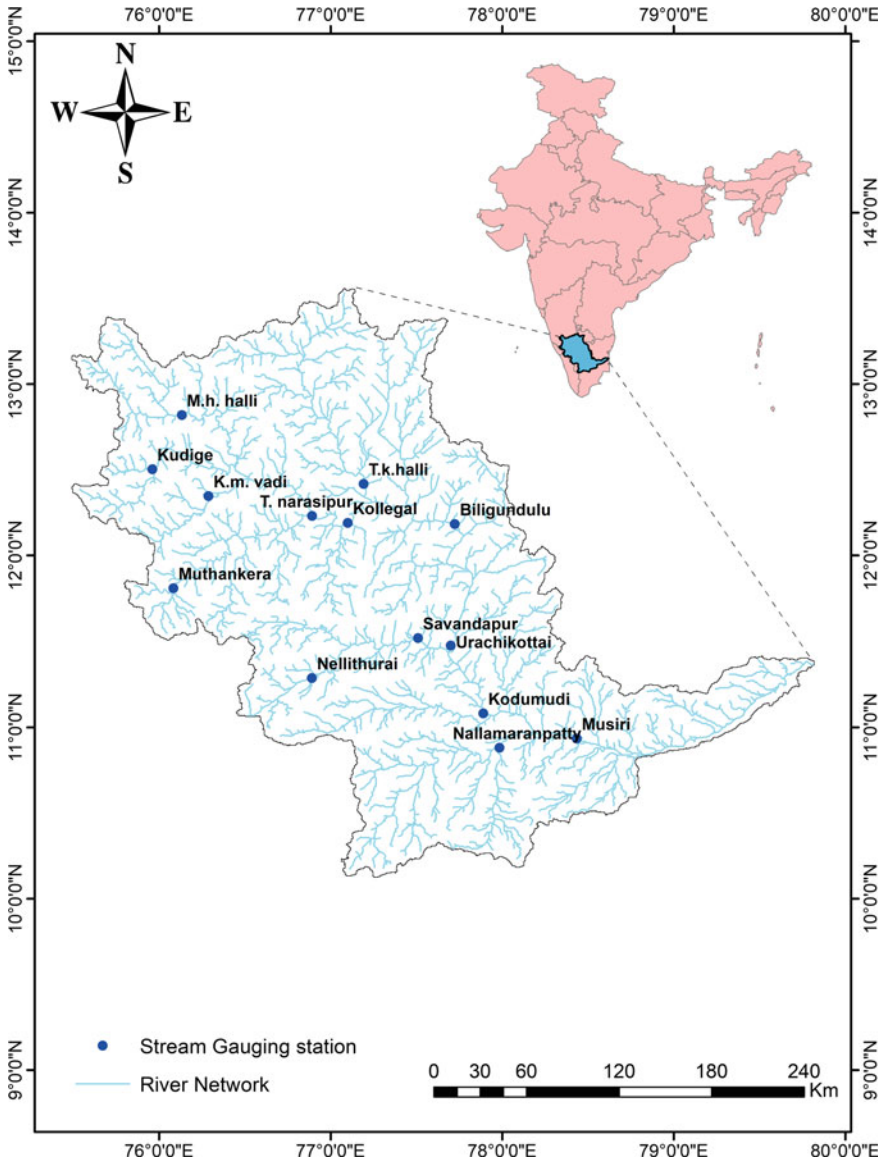

Fig. 1 Index map of Cauvery River basin

the southwest (northeast) monsoon season, while the remaining rainfall is received during winter and pre-monsoon seasons [8]. The annual rainfall in the basin varies from 630 to 2430 mm, while the number of rainy days varies from 40 to 115. The mean annual rainfall in the Cauvery basin is about 1075.2 mm [9]. Due to thick forest cover and higher rainfall in the Western Ghats region, the evapotranspiration losses

are higher in many parts of the basin than rainfall, thus characterizing the climate of the Cauvery basin as semi-arid. The mean maximum and minimum temperatures in the basin are 34.3 °C and 17.1 °C, respectively [9].

2.2 Methodology

The stepwise procedure adopted to ascertain the changes and trends in streamflow indices across the Cauvery River basin is shown in Fig. 2. In the present study, the daily streamflow data measured by the Central Water Commission (CWC), India, has been downloaded from the India WRIS web portal (https://indiawris.gov.in/wris). The data has been collected for 47 stream gauging stations in the basin that have been quality checked and the stations with a continuous data length of 30 years have been selected. After a quality check, 14 stream gauging stations (shown in Table 1) are selected for further analysis. The missing data, wherever applicable, have been filled using the moving average method. The data is converted into water year (June–May) format for further analyses. In this study, eight streamflow indices are derived using each station's daily streamflow time series and analyzed (shown in Table 2). In Table 2, QTOT represents the total volume collected at a stream gauging station in a water year. The indices representing extreme (or peak) flow variability are classified as absolute (Qx1day and Qx5day) and percentile-based (Q95p and Q99p). The percentile-based indices are derived by fitting an Empirical Cumulative Distribution Function (ECDF) to the entire data at a given stream gauging station, and thresholds corresponding to 95th and 99th percentile streamflow are estimated from ECDF [6]. The streamflow total exceeding or equalling these thresholds is estimated for deriving their respective time series of Q959 and Q99p. The indices Q7min, Q30min, and LFD, represent the changes in frequency and magnitude of low flows. Q7min and Q30min refer to the average flow over a 7-day (weekly) and 30-day (monthly) moving average window for each water year, while LFD is estimated by computing the maximum number of consecutive days with flows less than or equal to 10th percentile streamflow at a given station.

The streamflow indices (listed in Table 2) are estimated for each stream gauging station. The non-parametric Pettit's test is applied to the time series of total annual runoff (QTOT) and annual maximum 1-day streamflow (Qx1day) to determine the presence of a statistically significant change point. Further non-parametric tests, viz., Spearman's rho (SR) and Modified Mann–Kendall (MMK) tests, are adopted for trend detection in all streamflow indices. Meanwhile, preliminary analysis of streamflow data, viz., data filtering and cleaning, is performed using a spreadsheet application, while Spyder (Python 3.8) and MATLAB software are used to implement code for Pettitt's, SR, and MMK tests. The spatial variation of trends is thereafter represented in a geographic information system environment.

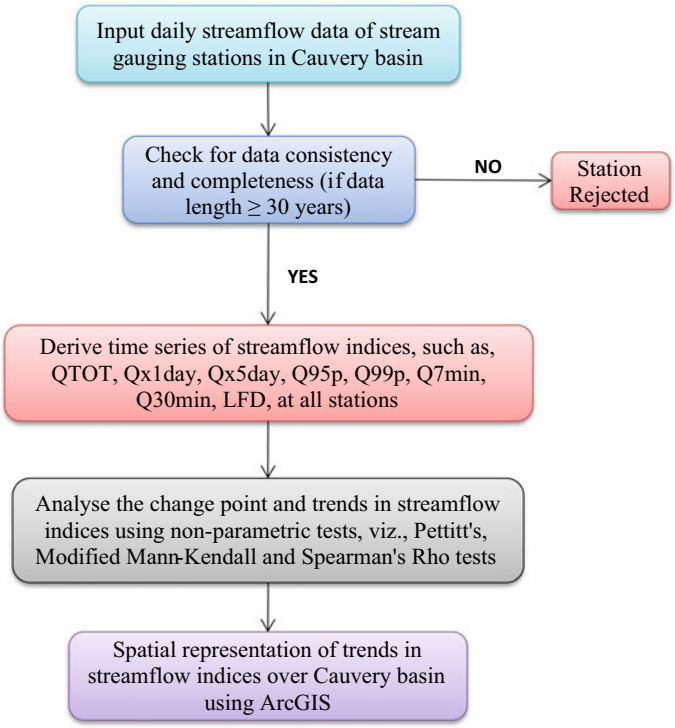

Fig. 2 Methodology adopted in the present study

3 Results and Discussion

3.1 Change Point Detection

The non-parametric Pettitt's test has been applied to QTOT and Qx1day series at each station. The Pettitt's test is interpreted with the null hypothesis that there is no change point in the time series against the alternative hypothesis that there is a statistically significant change point in the time series at 5% significance level. The results indicate that only three out of fourteen stations, i.e., M. K. Halli, Biligundulu, and Kodumudi, have shown significant change points in QTOT in the years 1994, 1984, and 1981, respectively (Fig. 3). On the other hand, no significant change point is detected for Qx1day at all the stations.

Table 1 Details of stream gauging stations adopted in the present study

Stream gauging station	Latitude (N)	Longitude (E)	Sub-basin	Data availability	
				Start date	End date
Biligundulu	12.18	77.72	Cauvery middle	Aug-71	Mar-19
K. M. Vadi	12.35	76.29	Cauvery upper	Jun-79	Jan-19
Kodumudi	11.08	77.89	Cauvery middle	Jun-71	Mar-19
Kollegal	12.19	77.10	Cauvery middle	Feb-71	Dec-18
Kudige	12.50	75.96	Cauvery upper	Nov-73	Jan-19
M. H. Halli	12.82	76.13	Cauvery upper	Oct-78	Jan-19
Musiri	10.94	78.44	Cauvery lower	Jun-72	Mar-19
Muthankera	11.81	76.08	Cauvery middle	Jun-73	Jan-19
Nallamaranpatty	10.88	77.98	Cauvery middle	Dec-77	Dec-17
Nellithurai	11.29	76.89	Cauvery middle	Jun-79	Jul-17
Savandapur	11.52	77.51	Cauvery middle	Jun-78	Feb-19
T. Narasipur	12.23	76.89	Cauvery middle	Mar-71	Jan-19
T. K. Halli	12.42	77.19	Cauvery middle	Jun-78	Dec-17
Urachikottai	11.48	77.70	Cauvery middle	Jun-79	Jan-19

Table 2 Description of streamflow indices adopted in the present study

Streamflow index description	Abbreviation	Unit
Total annual runoff	QTOT	MCM
Annual maximum 1-day streamflow	Qx1day	m^3/s
Annual maximum 5-day streamflow	Qx5day	m^3/s
95th percentile streamflow total	Q95p	m^3/s
99th percentile streamflow total	Q99p	m^3/s
Mean weekly minimum streamflow	Q7min	m^3/s
Mean monthly minimum streamflow	Q30min	m^3/s
Maximum consecutive low flow days (days with flows less than or equal to 10th percentile streamflow)	LFD	days

Note MCM denotes million cubic meter (10^6 m^3)

3.2 Trends in Streamflow Indices

The trends in streamflow indices (listed in Table 2) are evaluated using non-parametric statistical tests. The MMK test evaluates the null hypothesis that there is no trend in the time series against the alternate hypothesis of the presence of an increasing or decreasing trend in the time series at a 5% significance level. The Spearman's rho test establishes the statistical significance of the degree of association of hydrologic variables with time. The results of trend detection in streamflow

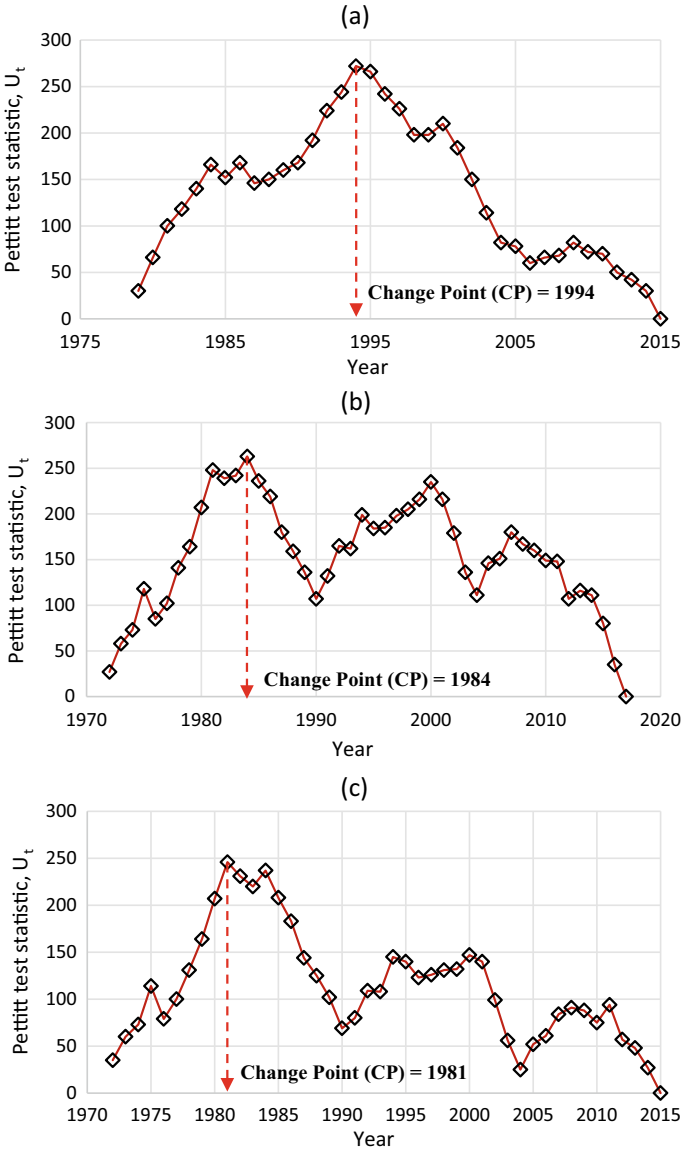

Fig. 3 Change point detection in total annual runoff for **a** M. H. Halli, **b** Biligundulu, and **c** Kodumudi stations

indices using both the non-parametric tests are shown in Table 3. The spatial variability of nature of trend (i.e., increasing, decreasing or no trend), derived from the MMK test, for all the streamflow indices are shown on the basin map with the help of the spatial analyst tool in ArcGIS and shown in Fig. 4. For the spatial analysis, the shapefile of the Cauvery basin was downloaded from *HydroSHEDS* (https://www.hydrosheds.org/).

From Fig. 4 and Table 3, twelve out of fourteen stations have shown decreasing trend in QTOT, while increasing trends are noticed at the remaining two stations (i.e., K. M. Vadi and T. K. Halli). Also, four stations have shown significant decreasing trends: Biligundulu, Kodumudi, M. H. Halli, and Savandapur. Thus, a decrease in freshwater availability in the basin is reported, which could further exacerbate the water-scarce conditions. The extreme streamflows represented by Qx1day, Qx5day, Q95p, and Q99p have also shown decreasing trend across most stations, while an increasing trend is noted only at a couple of stations (i.e., Nellithurai and T. K. Halli (except Qx1day and Q99p)) (see Table 3; Fig. 4). Significant decreasing trends in peak flows are observed at Biligundulu and Savandapur (Qx1day, Qx5day, and Q95p). Thus, the peak or extreme flows in the basin are found to decrease over time which indicates reduction in the magnitude and occurrence of floods in the basin.

The magnitude of short-term and medium-term low flows, represented by Q7min and Q30min, have shown decreasing trend at eleven out of fourteen stations, while two (Musiri and Nellithurai) and three (Kodumudi, Musiri, and Nellithurai) stations have shown an increasing trend for Q7min and Q30min, respectively (see Fig. 4; Table 3). The low flow days have shown increasing trends at twelve stations, out of which six stations, namely, Biligundulu, M. H. Halli, Nallamaranpatty, T. Narasipur, T. K. Halli, and Urachikottai, have exhibited significant increasing trends. The Nellithurai station has shown a decreasing trend in LFD. Hence, it is evident that a considerable decrease in the low flows is noticed in the Cauvery basin. Overall, the water availability as well as the peak and low flows have shown a consistent decrease in the Cauvery River basin except for one or two stations. Thus, the reduction in water availability would imply aggravating water-scarce conditions, while the decline in low flows would make the river dry and reduce the groundwater contribution as well as could create an ecological imbalance. Therefore, strategies and mitigation measures need to be formulated to avert severe water scarcity conditions in the basin.

4 Conclusions

The present study analyzed the abrupt and gradual changes in the streamflow indices representing mean, peak, and low flow conditions across the Cauvery basin. The conclusions drawn from the foregoing study are as follows:

- A decrease in the total annual runoff is observed coherently across the entire basin, implying a reduction in freshwater availability and likely aggravating the water stress conditions.

Table 3 Results of trend detection in streamflow indices using non-parametric tests

Stream gauging station	QTOT		Qx1day		Qx5day		Q95p		Q99p		Q7min		Q30min		LFD	
	MMK-Z	SR-r	MMK-Z	SR-r	MMK-Z	SR-r	MMK-Z	SR-r	MMK-Z	SR-r	MMK-Z	SR-r	MMK-Z	SR-r	MMK-Z	SR-r
Biligundulu	**– 3.87**	**– 0.44**	**– 2.35**	**– 0.35**	**– 2.71**	**– 0.37**	**– 3.04**	**– 0.45**	– 1.66	**– 0.34**	**– 2.79**	**– 0.42**	– 1.82	– 0.28	**2.47**	**0.39**
K. M. Vadi	0.26	0.03	– 0.10	0.02	– 0.20	– 0.02	– 0.12	– 0.02	– 0.07	0.03	– 0.05	– 0.09	– 0.05	– 0.09	0.04	0.02
Kodumudi	**– 2.22**	**– 0.35**	– 1.18	– 0.20	– 1.61	– 0.26	– 1.66	**– 0.38**	– 0.71	– 0.26	– 0.04	– 0.02	0.29	0.04	0.18	0.06
Kollegal	– 1.85	**– 0.31**	– 0.05	– 0.02	– 0.64	– 0.09	**– 2.02**	**– 0.30**	– 0.32	– 0.06	**– 2.05**	– 0.21	– 1.55	– 0.20	1.11	0.17
Kudige	– 1.06	– 0.16	**– 2.23**	**– 0.35**	– 1.95	**– 0.30**	– 1.75	– 0.27	– 1.80	– 0.25	– 0.70	– 0.12	– 1.36	– 0.24	1.76	0.23
M. H. Halli	**– 2.46**	**– 0.59**	– 0.96	– 0.20	– 1.22	– 0.22	– 1.54	**– 0.33**	– 1.14	– 0.30	**– 3.77**	**– 0.53**	**– 4.45**	**– 0.70**	**2.60**	**0.48**
Musiri	– 0.85	– 0.13	– 0.45	– 0.08	– 0.42	– 0.06	– 1.09	– 0.23	– 0.50	– 0.19	0.15	0.03	0.51	0.03	0.00	0.02
Muthankera	– 1.57	– 0.24	– 1.93	**– 0.29**	– 1.73	– 0.27	**– 3.99**	– 0.28	– 1.45	– 0.23	– 1.22	– 0.18	– 0.55	– 0.09	0.90	0.16
Nallamaranpatty	– 0.75	– 0.11	– 0.19	– 0.04	– 0.05	– 0.01	– 0.41	– 0.08	0.16	0.03	0.00	0.00	– 0.16	– 0.26	**2.28**	**0.35**
Nellithurai	– 0.25	– 0.02	0.17	0.03	0.59	0.11	**2.56**	**0.41**	0.24	0.04	**2.68**	**0.39**	1.31	0.22	– 1.79	– 0.23
Savandapur	**– 2.67**	**– 0.42**	– 1.06	**– 0.31**	**– 2.06**	**– 0.38**	**– 2.33**	**– 0.46**	– 1.42	**– 0.35**	– 0.27	– 0.05	– 0.29	– 0.06	0.65	0.14
T. Narasipur	– 0.67	– 0.16	– 1.56	– 0.26	– 1.18	– 0.20	– 1.03	– 0.19	– 1.01	– 0.23	– 1.99	**– 0.48**	– 1.91	**– 0.51**	**3.73**	**0.59**
T. K. Halli	1.75	0.33	– 0.67	– 0.08	0.45	0.09	0.79	0.17	– 0.09	– 0.02	– 1.16	– 0.28	**– 2.02**	**– 0.43**	**2.85**	**0.53**
Urachikottai	– 1.58	– 0.25	– 0.71	– 0.16	– 0.55	– 0.12	– 1.02	– 0.24	– 0.54	– 0.20	**– 2.75**	**– 0.68**	**– 4.88**	**– 0.79**	**4.32**	**0.75**

Note MMK-Z and SR-r denote the test statistic values of Modified Mann–Kendall and Spearman's rho tests. **Bold values** indicate a statistically significant trend at a 5% significance level for both MMK and SR tests

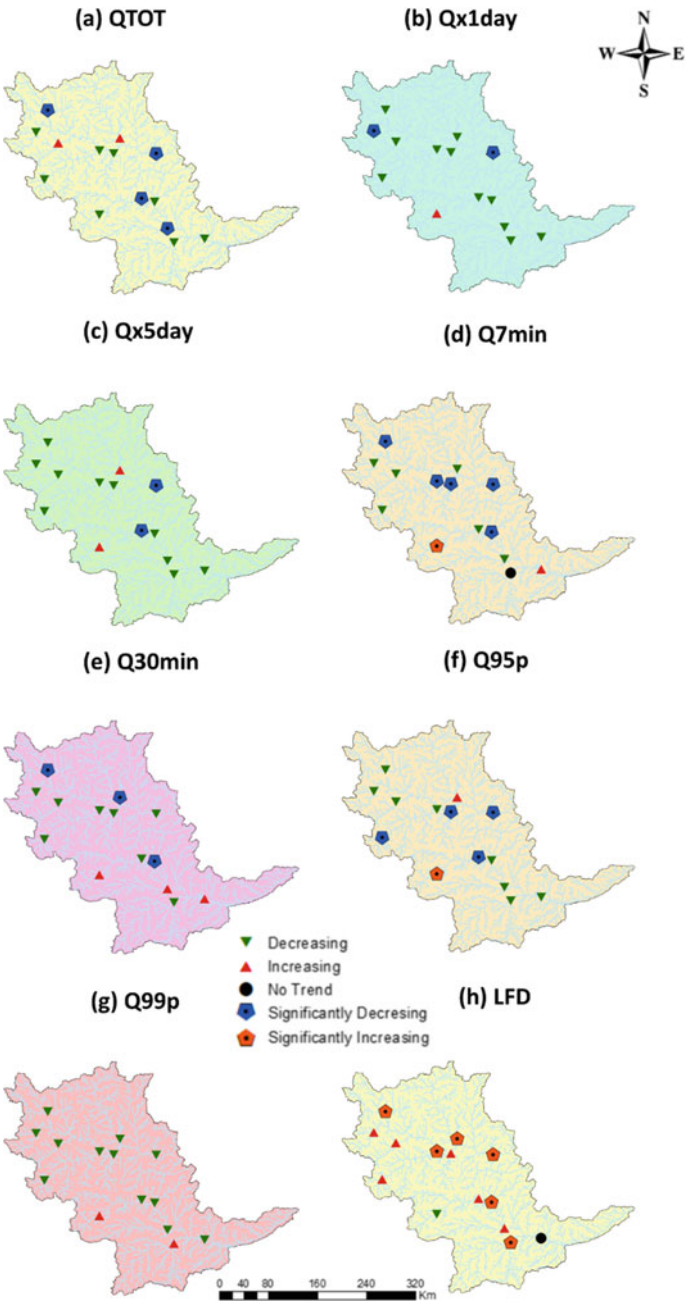

Fig. 4 Spatio-temporal variability of trends in streamflow indices

- The streamflow indices representing the peak flow (viz., Qx1day, Qx5day, Q95p, and Q99p) have shown a declining trend across the basin, indicative of infrequent flood occurrences and a reduction in their magnitude as well.
- The magnitude and frequency of low flows in the Cauvery River and its tributaries have also shown a persistent decrease across the basin. Such a decrease in low flows would impact the navigability of the river and stream ecology and reduce the streamflow contribution to the local groundwater table.
- Thus, the water managers and concerned authorities should reinforce efforts to undertake effective water conservation and management practices to avert drought and water-scarce conditions in the basin in the near future.

Acknowledgements The researchers are thankful to the India Water Resource Information System (WRIS) and Central Water Commission (CWC) for providing the necessary data to conduct this research. The authors would like to acknowledge the resourceful support offered by the Punjab Engineering College during the study.

References

1. https://www.worldometers.info/world-population/india-population/. Accessed on 20 Sept 2021
2. Gosain AK, Rao S, Basuray D (2006) Climate change impact assessment on hydrology of Indian river basins. Curr Sci:346–353
3. Pathak H, Pramanik P, Khanna M, Kumar A (2014) Climate change and water availability in Indian agriculture: impacts and adaptation. Ind J Agric Sci 84:671–679
4. Abeysingha NS, Singh M, Sehgal VK, Khanna M, Pathak H (2016) Analysis of trends in streamflow and its linkages with rainfall and anthropogenic factors in Gomti River basin of North India. Theoret Appl Climatol 123(3–4):785–799
5. Jain SK, Nayak PC, Singh Y, Chandniha SK (2017) Trends in rainfall and peak flows for some river basins in India. Curr Sci:1712–1726
6. Sharma PJ, Patel PL, Jothiprakash V (2020) Hydroclimatic teleconnections of large-scale oceanic-atmospheric circulations on hydrometeorological extremes of Tapi Basin, India. Atmosph Res 235:104791
7. Sreelash K, Sharma RK, Gayathri JA, Upendra B, Maya K, Padmalal D (2018) Impact of rainfall variability on river hydrology: a case study of southern western ghats, India. J Geol Soc India 92(5):548–554
8. Sreelash K, Mathew MM, Nisha N, Arulbalaji P, Bindu AG, Sharma RK (2020) Changes in the hydrological characteristics of Cauvery River draining the eastern side of southern Western Ghats, India. Int Jo River Basin Manage 18(2):153–166
9. CWC (2014). Cauvery Basin watershed atlas. Central Water Commission, New Delhi
10. https://indiawris.gov.in/wris. Accessed on 16 Apr 2021
11. https://www.hydrosheds.org/. Accessed on 2 Sept 2021
12. Goyal MK, Surampalli RY (2018) Impact of climate change on water resources in India. J Environ Eng 144(7):04018054

Comparison of Three Trend Detection Methods for Hydrological Parameters of Wainganga Basin, India

Madhura Aher and S. M. Yadav

Abstract Based on daily streamflow and suspended sediment load data from five gauging stations located on Wainganga basin, spatial and temporal variations in seasonal streamflow and suspended sediment load from 1969 to 2018 are investigated. The Mann–Kendall (MK) test, Spearman's rank correlation and Innovative trend technique (ITA) are applied to detect the trend in seasonal streamflow and suspended sediment load. The Sen's slope test is used to find the trend magnitude. MK test indicates increasing trend in streamflow at Kumhari and Rajegaon stations, whereas Spearman's rank correlation test and Innovative trend techniques report decreasing trend for both the stations. Similarly, MK test reported increasing trend in suspended sediment load at Rajegaon and Satrapur stations. But, Spearman's rank correlation test and Innovative trend techniques report decreasing trend for both the stations. Compared to MK trend test, ITA technique showed good agreement with Spearman's rank correlation.

Keywords Streamflow · Suspended sediment load · Wainganga basin · Mann–Kendall test · Spearman's rank correlation · Innovative trend technique

M. Aher · S. M. Yadav (✉)
Department of Civil Engineering, Sardar Vallabhai National Institute of Technology, Surat, Gujarat 395007, India
e-mail: shivam27@gmail.com

M. Aher
e-mail: madhura.aher@gmail.com

P. V. Timbadiya et al. (eds.), *Climate Change Impact on Water Resources*, Lecture Notes in Civil Engineering 313, https://doi.org/10.1007/978-981-19-8524-9_14

1 Introduction

River systems are very important and serve as a life line to many sectors such as agriculture, domestic and industrial. The likelihood of the majority of the people are predominantly depended on the income from the agriculture sectors, especially for the developing countries like India. Rivers carry water as well as large quantity of sediment load along with it. The transportation of sediments from the land to the ocean is also a vital feature of global biological, geological and chemical cycle [8]. Several factors such as climate change and anthropogenic actions have direct impact on hydrological cycles which can be seen in the form of rainfall intensity and duration in the form of extreme rainfall which occurred within short duration of time. The effect of changing climate with intensified human activities is also visible on the streamflow and sediment transport [3, 10]. Scientists are trying to recognize the river system behavior toward the changing climatic and increasing human activities [9]. Many researchers have accessed the trends and patterns in streamflow and sediment yield [2, 5]. The discharge and sediment load of tributaries of Yangtze River, China, was analyzed and testified significant change in the hydrological parameters [13]. Also, significant decline in sediment load is noticed for rivers in Central Japan for the past decades, though streamflow did not show significant trend [21]. The tributaries of Ganga River also deliberate the temporal variation in sediment load and huge variation in suspended sediment load which is observed during the monsoon and non-monsoon seasons [4].

The hydroclimatic parameters' trend analysis gives an understanding about the stationarity of hydrological cycle in a specific river basin. The gradual or abrupt (shift) change may affect the statistical parameters such as mean, median, variance [1, 12]. Many researchers have examined trend in climatic parameters (precipitation, temperature, evaporation), hydrological parameters (streamflow, suspended sediment load), environmental field (water quality) of the river basin using parametric and non-parametric tests [11, 15–17]. The difference between these two tests lies in the distribution of the dataset. The parametric tests assume the normal distribution of the data, and non-parametric tests are applicable for data which is distribution free. The Mann–Kendall [7, 14] test and Spearman's rho test are most frequently used trend tests. The Mann–Kendall test does not require normality assumption, but the time series should be free from serial correlation. The presence of positive autocorrelation rises the possibility that test identifies certain trend when essentially there is absence of trend in time series [23]. The Innovative trend analysis (ITA) technique presented by Sen [19, 20] is used to check the monotonic and non-monotonic trends in environmental, meteorological and hydrological variables, regardless of any prior conditions regarding distributions and serial correlation, seasonal period and time series size [19, 22].

In the current research, streamflow and sediment load for the period of 1969–2019 for the Wainganga River Basin is considered. The Wainganga River Basin is an important sub-basin of Godavari Basin, India. The temporal and spatial variation is

observed in streamflow and sediment load across the main stream as well as in the sub-basins. In past studies, several applications of parametric and non-parametric tests are available on the Godavari as whole. But, no references are available on comparison of trend analysis technique of streamflow and sediment load using statistical method and graphical method. The aim of study is (1) to determine trend in annual streamflow and sediment load using three different methods and (2) comparison of ITA technique with MK and Spearman's correlation method.

2 Study Area and Data Used

2.1 Study Area

Wainganga basin is a largest sub-basin of Godavari basin located at the Northern part. The Wainganga basin lies in longitude 77° E to 82° 53′ E and Latitude 20° 48′ to 22° 30′ N (Fig. 1). The catchment area of the basin is 51,421 km^2 which covers main parts of the Maharashtra (27,350 km^2), Madhya Pradesh (23,109 km^2) and fewer portions of Chhattisgarh states (962 km^2). The Wainganga has three principal tributaries, viz., Penganga, Wainganga and Wardha. On the right bank, five tributaries, viz., Bawanthari, Peddavagu, Andhari, Kanhan, and Wardha connect to the Wainganga. And, on the left bank, five tributaries, viz., Kathani, Chulband, Garhvi, Kobragarhi and Bagh drain in the main channel. The maximum rainfall is received during the June–October, i.e., Southwest monsoon. The maximum temperature varies from 39 to 47 °C, and in winter, the minimum temperature ranges from 7 to 13 °C. May and December are the hottest and coldest months, respectively.

2.2 Data Used

Five gauging stations, namely, Kumhari, Rajegaon, Satrapur, Pauni and Ashti are located on the whole Wainganga basin as shown in Fig. 1. The daily data of streamflow and suspended sediment concentration are collected from the water and sediment year book published by Central Water Commission (CWC) of India. For different stations, data period is varied in between 1969 and 2018 (49 years), according to availability of records (Table 1). The suspended sediment load at a specific station is calculated by multiplying the water discharge (m^3/s) by the sediment concentration of the identical day.

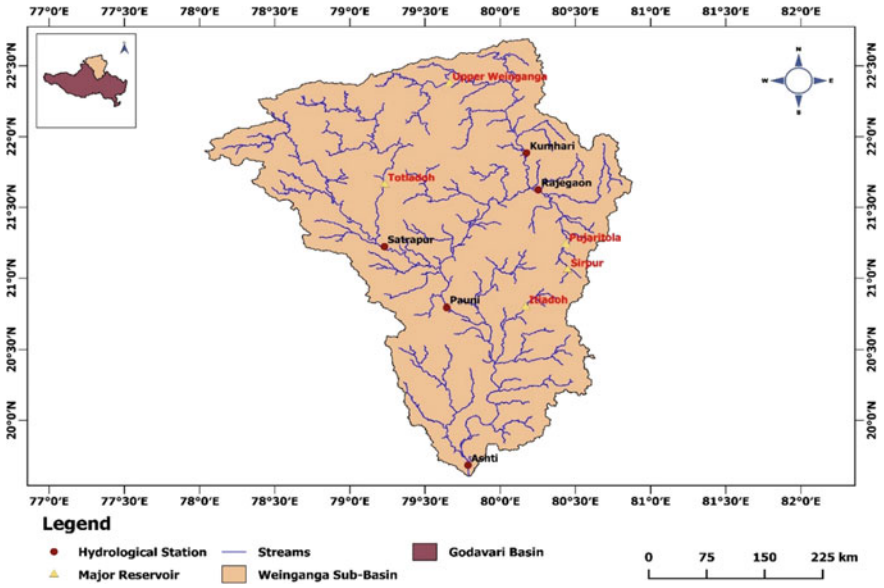

Fig. 1 Index map of Wainganga basin

Table 1 Description of hydrological stations in the study area

S. No.	Hydrological station	Longitude	Latitude	Drainage area (km^2)	Time series	No. of years
1	Kumhari	80° 10′ 36″	21° 53′ 03″	8070	1988–2018	30
2	Rajegaon	80° 15′ 14″	21° 37′ 32″	5380	1990–2018	28
3	Satrapur	79° 13′ 59″	21° 13′ 00″	11,100	1988–2018	30
4	Pauni	79° 38′ 40″	20° 47′ 45″	35,520	1969–2005	36
5	Ashti	79° 47′ 13″	19° 41′ 12″	50,990	1969–2015	46

3 Methodology

Annual time series is prepared for each station from the daily observations of streamflow and sediment load. Following steps were used to carry out trend analysis.

(1) The presence of serial correlation or autocorrelation was checked using method suggested by Salas [18], Gucic and Trajkovik [6].
(2) Pre-whitening of the time series is done by method suggested by Von Storch [23].
(3) Mann–Kendall test and Spearman's rank correlation test were used to check the trend in annual streamflow and sediment load.
(4) Theil and Sen's slope estimator test was used to find the magnitude of trend.
(5) The percentage change in magnitude was calculated over a period of 49 years.

(6) The Innovative tend analysis technique is applied to detect the trend in annual time series.
(7) Comparison of nature of trend obtained from statistical method and graphical method is carried out.

3.1 Mann–Kendall Test

The Mann–Kendall was used to check the gradual trend in the annual time series. Mann was the first used test; later, the statistical distribution is determined by Kendall [7, 14]. Owing to simple technique, it is strong against outliers, can consider missing values and does not need to assume normality. For a given time series X (x_1, x_2 …, x_n), the null hypothesis (H_o) shows absence of trend and alternative hypothesis (H_a) signifies the either gradual increasing or decreasing trend.

The Mann–Kendall trend analysis method is given below.

The standardized test statistics, i.e., Z is calculated as

$$Z = \begin{cases} S - 1/\sqrt{\text{Var}\, S} & S > 0 \\ 0 & S = 0 \\ S + 1/\sqrt{\text{Var}\, S} & S < 0 \end{cases} \tag{1}$$

The positive and negative Z values specify an upward and downward trends, respectively. The test is carried out at 5% significance level,

where

$$S = \sum_{j=1}^{n-1} \sum_{j=i+1}^{n} \text{sgn}(xj - xi), \tag{2}$$

$$\sin(xj - xi) = \begin{cases} +1 & xj > xi \\ 0 \quad \text{if} & xj = xi \\ -1 & xj < xi \end{cases}, \tag{3}$$

$$\text{Var}(S) = \left\{ n\,(n-1)\,(2n+5) - \sum_{i=1}^{n} ti(i-1)(2i+5) \right\} / 18. \tag{4}$$

3.2 Sen's Slope Estimator

This is the non-parametric test used to check the trend in the hydrologic time series and is proposed by Hirsch et al.

The equation is given as

$$\beta = \text{Median}\left(\frac{xj - xi}{j - i}\right) \quad \text{for} \quad j > i, \tag{5}$$

where β = slope in data points x_i and x_j, x_i = values at time i, x_j = values at time j. A positive value of β agrees an 'increasing trend in the time series', and the negative value agrees a 'decreasing trend in the time series'.

3.3 Innovative Trend Analysis

A new method for finding the trend in the time series is proposed by Sen. It consists of 1:1 (45°) as the straight line on the Cartesian coordinate system. And, the hydrological time series is divided into two equal sub-series, and then, both the sub-series are organized according to ascending order. Then, the first sub-series series is plotted as abscissa against the second sub-series as ordinate based on the Cartesian coordinate system. If the plotted points are appearing on the 1:1 (45°) line, this specifies no trend in the time series. And, if the data points are collected in the lower triangular part of 1:1 line, it signifies a negative trend, whereas if the data points are collected in the upper triangular part of 1:1 line, it signifies the positive trend. This method also permits finding the trends in low, medium and high hydrologic regimes.

4 Results

4.1 Preliminary Analysis

The preliminary investigation of streamflow shows that daily mean streamflow varies from 161 m^3/s at Satrapur station to 1802 m^3/s at Ashti station, and the standard deviation varies from 457 m^3/s to 2917 m^3/s at Satrapur and Ashti stations, respectively (Table 2) The minimum values of streamflow are observed 0 m^3/s at Kumhari, Rajegaon and Ashti, whereas at Satrapur and Pauni stations, the minimum values of streamflow are 0.137 m^3/s and 0.115 m^3/s, respectively. And, the maximum values of streamflow vary from 9682 to 28,200 m^3/s. The primary analysis of sediment load shows that daily mean sediment load varies from 12,037 to 104,407 t/d (Table 3). And, the standard deviation varies from 58,624 to 370,398 t/d. At all five gauging stations, the minimum value of daily sediment load is zero, whereas maximum value of sediment load varies from 1,326,865 t/d at Kumhari station to 12,034,915 t/d at Ashti station. Preliminary analysis concluded that large variation is observed in streamflow and sediment load of Wainganga basin.

Table 2 Statistics of streamflow

Station	No. of observations	Minimum (m^3/s)	Maximum (m^3/s)	Mean (m^3/s)	St. deviation (m^3/s)
Kumhari	3782	0	16,747	270	638
Rajegaon	3533	0	9682	247	590
Satrapur	3783	0.137	14,161	161	457
Pauni	4514	0.115	27,124	1012	1792
Ashti	5978	0	28,200	1802	2917

Table 3 Statistics of sediment load

Station	No. of observations	Minimum (t/d)	Maximum (t/d)	Mean (t/d)	St. deviation (t/d)
Kumhari	3782	0	1,326,865	12,037	58,624
Rajegaon	3533	0	2,686,963	18,757	106,401
Satrapur	3783	0	2,265,861	14,944	80,722
Pauni	4514	0	8,564,227	104,407	370,398
Ashti	5978	0	12,034,915	102,312	363,495

4.2 Trend Analysis Using Statistical Methods

The trend analysis of annual mean streamflow and sediment load is carried out by using Mann–Kendall test and Spearman's rank correlation test. And, the magnitude of the trend is estimated by using Sen's slope method. The MK test is carried out at 5% significance level. Prior to the use of MK test, the time series is checked for autocorrelation by using method stated in methodology. The effect of positive correlation is removed by pre-whitening of the time series. The MK test statistics of annual streamflow are summarized in Table 4. The Kumhari, Satrapur, Pauni and Ashti stations show significant decreasing trend in the streamflow with Z_{mk} values as − 3.91, − 5.84, − 2.86 and − -0.97, respectively, whereas the Rajegaon station detects increasing trend in annual streamflow with Z_{mk} value 0.45. The Sen's slope results are in agreement with the MK trend test.

Table 4 Mann–Kendall test results of streamflow

Station	Kendall's tau	*S*	Var (*S*)	*P*-value (two-tailed)	Z_{mk}	Sen's slope (m^3/s)
Kumhari	− 0.050	− 359,311	8,438,792,865	< 0.0001	− 3.91	− 0.004
Rajegaon	0.008	51,338	12,861,636,767	0.651	0.45	0.000
Satrapur	− 0.066	− 468,328	6,439,322,839	< 0.0001	− 5.84	− 0.005
Pauni	− 0.062	− 632,110	48,772,733,358	0.004	− 2.86	− 0.031
Ashti	− 0.008	− 134,641	19,098,736,522	0.330	− 0.97	− 0.001

The variation of annual streamflow at five gauging stations is shown in Fig. 2. The linear trend line is plotted to show the decreasing or increasing trend. Ashti, Kumhari, Rajegaon, Satrapur and Pauni stations show decreasing trend in annual steam flow.

The MK test statistics of annual sediment load are summarized in Table 5. The Kumhari, Satrapur, Pauni and Ashti stations show decreasing trend in the sediment load with Z_{mk} values as − 3.76, − 7.69, − 2.79 and − 2.38, respectively, whereas the Rajegaon station detects increasing trend in annual sediment load with Z_{mk} value 3.80. The Sen's slope results are in agreement with the MK trend test.

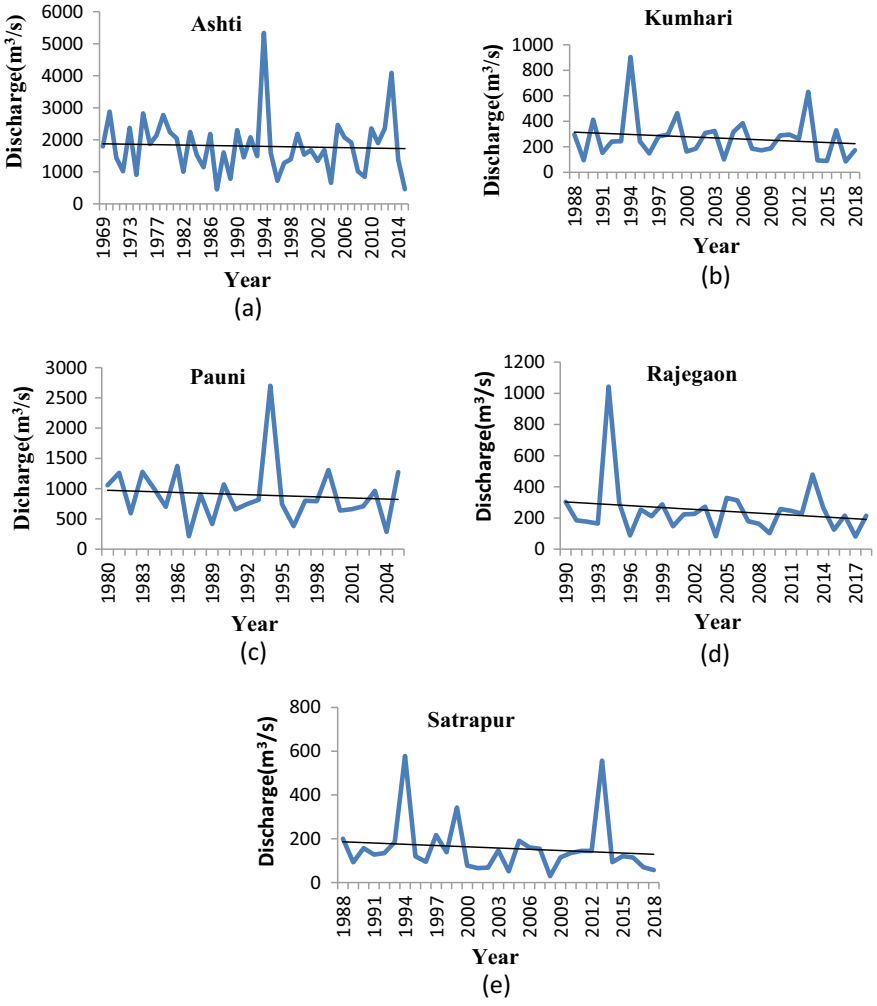

Fig. 2 Variation in annual discharge at **a** Ashti, **b** Kumhari, **c** Pauni, **d** Rajegaon, **e** Satrapur gauging stations

Table 5 Mann–Kendall test results of sediment load

Station	Kendall's tau	S	Var (S)	P-value (two-tailed)	Z_{mk}	Sen's slope (t/year)
Kumhari	− 0.052	− 372,644	9,808,661,923	0.000	− 3.76	− 0.015
Rajegaon	0.033	203,181	2,860,469,901	0.000	3.80	0.004
Satrapur	− 0.082	− 587,281	5,831,992,739	< 0.0001	− 7.69	− 0.061
Pauni	− 0.082	− 838,538	90,289,985,375	0.005	− 2.79	− 0.640
Ashti	− 0.081	− 1,454,729	372,497,145,443	0.017	− 2.38	− 0.487

The variation of annual streamflow at five gauging stations is shown in Fig. 3. The linear trend line is plotted to show the decreasing or increasing trend. Ashti, Kumhari, Rajegaon, Satrapur and Pauni stations show decreasing trend in annual steam flow.

Spearman's rank correlation test was also performed to find the trend in annual streamflow and sediment load at all five gauging stations located on Wainganga River Basin. The Spearman's test statistics are summarized in Tables 6 and 7. The test was carried out at 5% significance level. Decreasing trend in streamflow is observed at Kumhari, Rajegaon, Satrapur, Pauni and Ashti gauging stations. The coefficient of correlation is obtained as − 0.14, − 0.12, − 0.29, − 0.16 and − 0.12, respectively, at Kumhari, Rajegaon, Satrapur, Pauni and Ashti gauging stations.

Similarly, for the annual sediment load, the Spearman's rank correlation results show decreasing trend at all five gauging stations (Table 7), whereas significant decreasing trend is observed at Satrapur ($p = 0.00003$) and Ashti ($p = 0.00021$) stations. The coefficient of correlation values is obtained as − 0.19, − 0.09, − 0.17, − 0.36 and − 0.52 at Kumhari, Rajegaon, Satrapur, Pauni and Ashti stations, respectively.

4.3 Trend Analysis Using ITA Technique

The Innovative trend analysis technique was applied on annual streamflow and sediment load of Wainganga basin. In ITA analysis, the time series was separated into equivalent portions as shown in Figs. 4 and 5.

The Innovative trend analysis technique was effective and potential in trend detection without considering some assumptions of length of data, serial correlation and distribution free. The data points were randomly appeared parallel to trend line. In the ITA technique, whole area of plot is categorized as low, medium and high zones, in which the data points may be scattered. All the plots from 'a' to 'e' (Fig. 4) represent non-monotonic trend in annual streamflow. Plots 'a' and 'c' showed increasing trend in the high magnitude region. And, plots 'b', 'd' and 'e' are displayed decreasing trend in the high magnitude region.

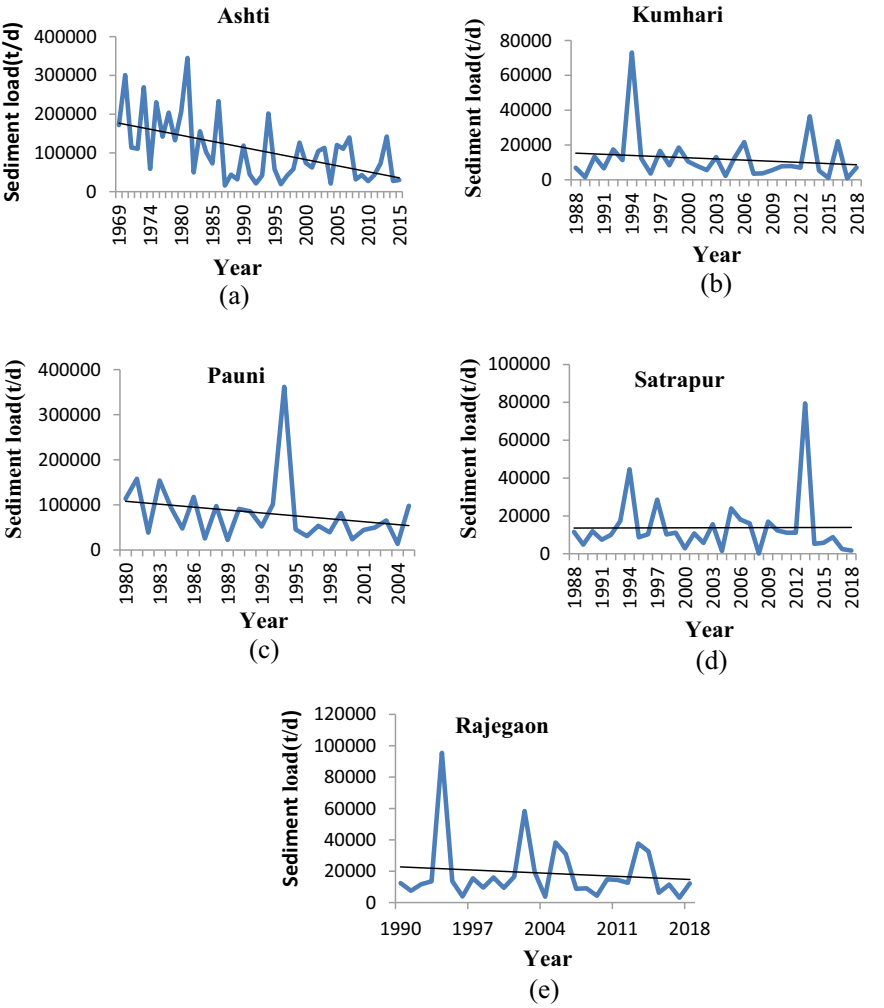

Fig. 3 Variation in annual sediment load at **a** Ashti, **b** Kumhari, **c** Pauni, **d** Satrapur, **e** Rajegaon gauging stations

Table 6 Spearman's rank correlation test results of water discharge

Station	Coefficient (r_s)	N	T statistics	DF	P-value
Kumhari	− 0.14	31	0.76	30.24	0.45
Rajegaon	− 0.12	29	0.63	28.37	0.54
Satrapur	− 0.29	31	1.61	29.39	0.12
Pauni	− 0.16	26	0.79	25.21	0.44
Ashti	− 0.12	46	0.77	45.23	0.44

Table 7 Spearman's rank correlation test results of sediment load

Station	Coefficient (r_s)	N	T statistics	DF	P-value
Kumhari	− 0.19	31	1.037	29.96	0.308
Rajegaon	− 0.09	29	0.444	28.55	0.660
Satrapur	− 0.17	31	5.146	25.85	0.00003
Pauni	− 0.36	26	1.907	24.09	0.069
Ashti	− 0.52	46	4.066	42	0.00021

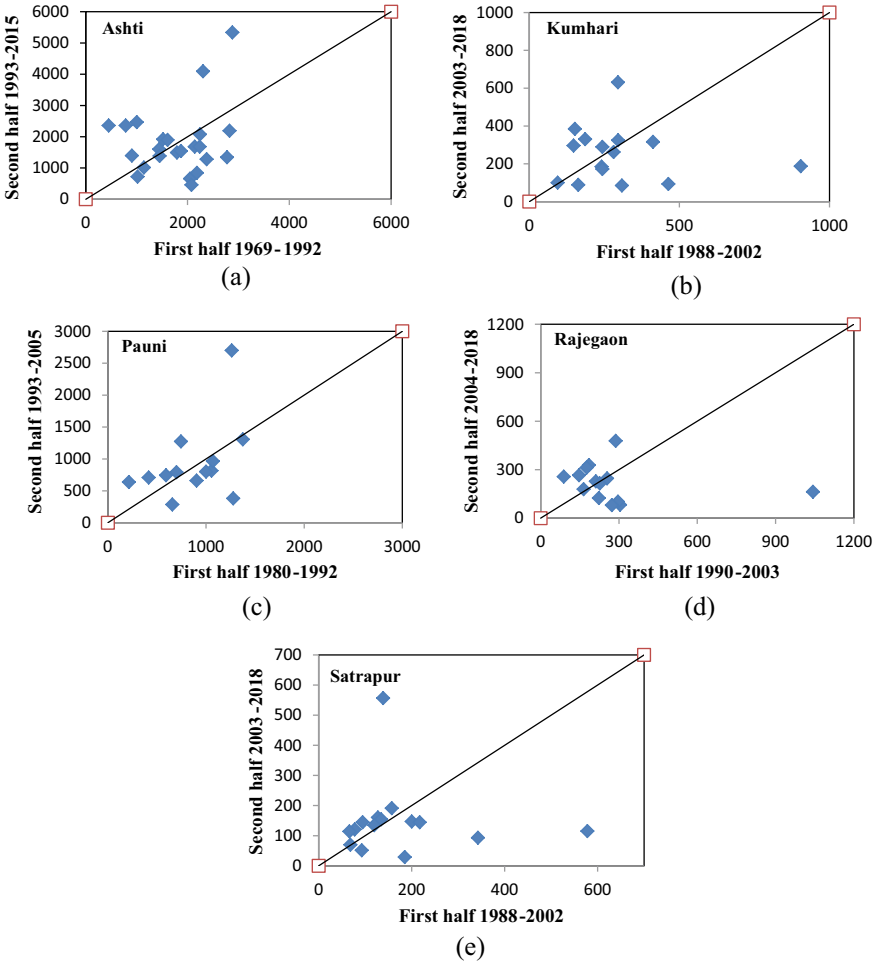

Fig. 4 Innovative trend analysis plots of annual streamflow time series at **a** Ashti, **b** Kumhari, **c** Pauni, **d** Rajegaon, **e** Satrapur gauging stations

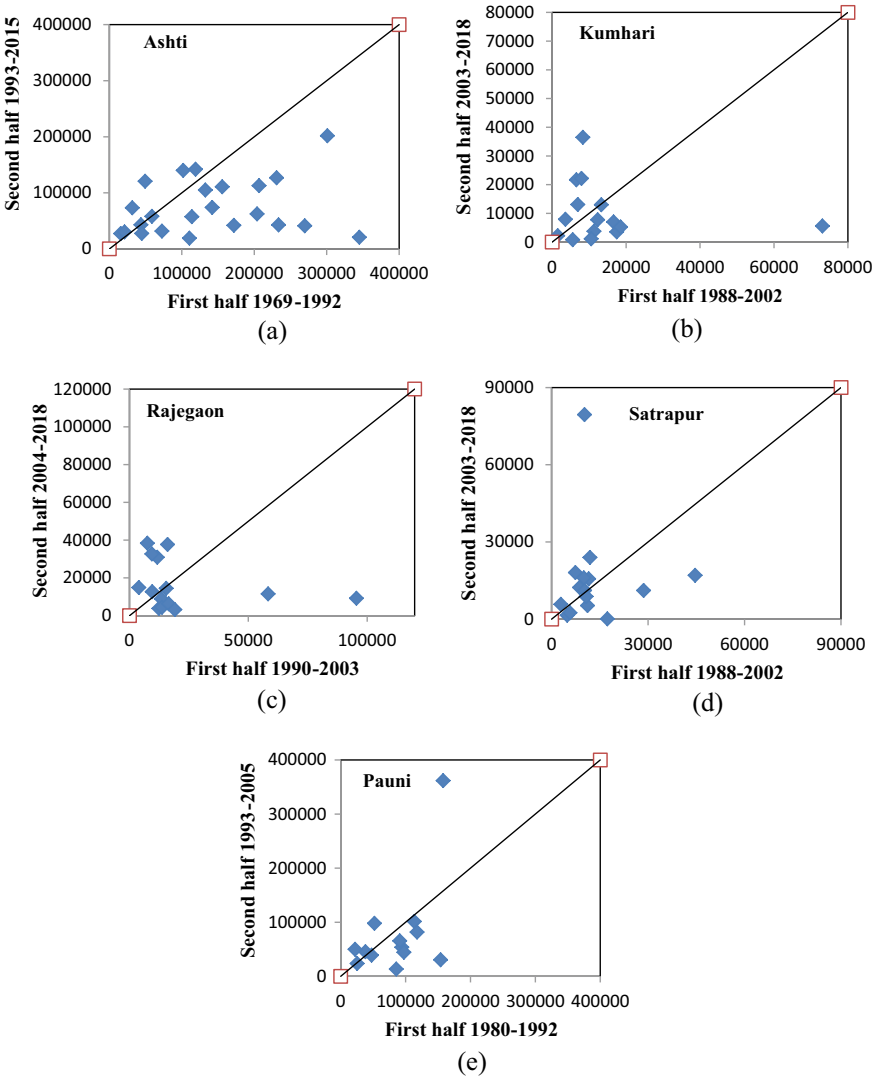

Fig. 5 Innovative trend analysis plots of suspended sediment load at **a** Ashti, **b** Kumhari, **c** Rajegaon, **d** Satrapur, **e** Pauni gauging stations

Similarly, ITA plots for annual sediment load at five gauging stations are displayed in Fig. 5a–e. Data points were randomly appeared parallel to trend line. The ITA plots for stations Ashti, Kumhari, Rajegaon, Pauni and Satrapur represent non-monotonic trend in annual sediment load. Monotonic trend is observed in the magnitude of low region for all the plots. All the plots from 'a' to 'd' are displayed decreasing trend in the high magnitude region. For the plot 'e' (Pauni station), the increasing trend is detected in the high region. Since graphical representation displays hidden sub-trends

in time series that overcomes the assumptions of length of dataset, dependence of dataset and normality distribution the Innovative trend analysis technique demonstrated good tendency in detecting trend as compared with non-parametric trend tests. An agreement and disagreement between the applied trend detection methods have been observed in the current study. On the basis of discrepancy among different methods, it is essential to adopt more than one technique to check the trend. In the current study, Mann–Kendall and Spearman's rank correlation tests exhibited equal capability in trend detection in case of streamflow and sediment load at Satrapur, Kumhari, Pauni and Ashti stations.

5 Conclusion

Five stations located at different parts of Wainganga River Basin were considered to detect the annual streamflow and sediment load trend. Statistical methods, i.e., Mann–Kendall trend test, Spearman's rank correlation tests and graphical method, i.e., Innovative trend analysis technique were used for trend detection. Sen's slope estimator method is applied to measure magnitude of trend. The following conclusions were made from the study:

(i) Mann–Kendall trend test reported significant decreasing trend in streamflow at three out of five stations, namely, Kumhari, Satrapur and Pauni stations. Non-significant increasing trend is observed at Rajegaon station, while all the five stations reported significant decreasing trend in sediment load.

(ii) Spearman's rank correlation test reported non-significant decreasing trend in streamflow for all the five stations. Satrapur and Ashti stations reported significant decreasing trend in sediment load. And, non-significant decreasing trend is observed at Kumhari, Rajegaon and Pauni stations.

(iii) Innovative trend analysis technique reported non-monotonic trend for streamflow and sediment load at all the five stations. Out of five stations, three stations, namely, Kumhari, Rajegaon and Satrapur stations indicate decreasing trend in the streamflow and increasing trend at Ashti and Pauni stations, whereas ITA results indicates decreasing trend in sediment load at four stations (Ashti, Rajegaon, Satrapur and Kumhari) and increasing trend is observed at Pauni station.

(iv) Both the agreement and disagreement were observed in between statistical and graphical trend tests. It is also observed that Mann–Kendall trend test and Spearman's rank correlation test exhibited a good agreement as compared to Innovative trend analysis technique. It is suggested to apply more than one detection methods to handle the irregularity of assumption in trend analysis.

References

1. Beaulieu C, Chen J, Sarmiento JL (2012) Change-point analysis as a tool to detect abrupt climate variations. Physiol Trans R Soc A 370(1962):1228–1249. https://doi.org/10.1098/rsta.2011.0383
2. Benzater B, Elouissi A, Benaricha B, Habi M (2019) Spatio-temporal trends in daily maximum rainfall in northwestern Algeria (Macta watershed case, Algeria). Arab J Geosci 12(11):370
3. Cantón Y, Solé-Benet A, De Vente J, Boix-Fayos C, Calvo-Cases A, Asensio C, Puigdefábregas J (2011) A review of runoff generation and soil erosion across scales in semiarid south-eastern Spain. J Arid Environ 75(12):1254–1261
4. Chakrapani GJ, Saini RK (2009) Temporal and spatial variations in water discharge and sediment load in the Alaknanda and Bhagirathi Rivers in Himalaya, India. J Asian Earth Sci 35(6):545–553
5. Elouissi A, Habi M, Benaricha B, Boualem SA (2017) Climate change impact on rainfall spatio-temporal variability (Macta watershed case, Algeria). Arab J Geosci 10(22):496
6. Gucic M, Trajkovik S (2013) Analysis of changes in meteorological variables using Mann-Kendall and Sen's slope estimator statistical tests in Serbia. Global Planetary Change 100:172–182. https://doi.org/10.1016/j.gloplacha.2012.10.014
7. Kendall MG (1975) Rank correlation methods. Griffin, London, UK
8. Khattab MF, Merkel BJ (2014) Application of Landsat 5 and Landsat 7 images data for water quality mapping in Mosul Dam Lake, Northern Iraq. Arab J Geosci 7(9):3557–3573
9. Khazaei S, Barati R, Ghandehary A, Sadeghifard MR (2019) Rainfall trend analysis using innovative-Şen method and comparison with traditional methods (case study: Khorasan Razavi province). J Water Sustain Dev 6(1):41–50
10. Kheirfam H, Vafakhah M (2015) Assessment of some homogeneous methods for the regional analysis of suspended sediment yield in the south and southeast of the Caspian Sea. J Earth Syst Sci 124(6):1247–1263
11. Kumar KS, Rathnam EV (2019) Analysis and prediction of groundwater level trends using four variations of Mann Kendall tests and ARIMA modelling. J Geol Soc India 94:281–289. https://doi.org/10.1007/s12594-019-1308-4
12. Kundzewicz ZW, Robson AJ (2004) Change detection in hydrological records-a review of the methodology. Hydrol Sci J 49(1):7–19. https://doi.org/10.1623/hysj.49.1.7.53993
13. Lu XX, Ashmore P, Wang JF (2003) Seasonal water discharge and sediment load changes in the Upper Yangtze, China. Mountain Res Dev 23(1):56–64
14. Mann HB (1945) Nonparametric test against trend. Econometrica 13:245–259
15. Pal L, Ojha CSP, Chandniha SK, Kumar A (2019) Regional scale analysis of trends in rainfall using nonparametric methods and wavelet transforms over a semi-arid region in India. Int J Climatol 39(5):2737–2764. https://doi.org/10.1002/joc.5985
16. Patel GT, Singh DK, Sarangi A, Rai A, Khanna M, Sahoo RN (2013) Temporal variability of climatic parameters and potential evapotranspiration. Ind J Agric Sci 83(4):518–524
17. Ramazanipour M, Roshani M (2011) Seasonal trend analysis of precipitation and discharge parameters in Guilan, north of the Iran. In: International conference on humanities geographical economics (ICHGE'2011) Pattaya, pp 290–293
18. Salas JD, Delleur JW, Yevjevich V, Lane WL (1980) Applied modelling of hydrologic time series. Water Resources Publication, Littleton, Colorado, USA
19. Şen Z (2012) Innovative trend analysis methodology. J Hydrol Eng 17(9):1042–1046
20. Sen Z (2014) Trend identification simulation and application. J Hydrol Eng 19:635–642. https://doi.org/10.1061/(ASCE)HE.1943-5584.0000811
21. Siakeu J, Oguchi T, Aoki T, Esaki Y, Jarvie HP (2004) Change in riverine suspended sediment concentration in central Japan in response to late 20th century human activities. CATENA 55(2):231–254

22. Timbadiya PV, Mirajkar AB, Patel PL, Porey PD (2013) Identification of trend and probability distribution for time series of annual peak flow in Tapi Basin, India. ISH J Hydraul Eng 19(1):11–20. https://doi.org/10.1080/09715010.2012.739354
23. von Storch H (1995) Misuses of statistical analysis in climate research, in analysis of climate variability: applications of statistical techniques. Springer-Verlag, New York, pp 11–26

Trend Analysis of Groundwater Levels in Visakhapatnam Coastal Aquifer

V. M. Priyanka, M. Ramesh, and Y. Srinivas

Abstract Groundwater exploitation has been increasing day by day due to the population increase, and overexploitation advances to severe groundwater depletion. This paper examines the trend analysis and spatiotemporal disparity for groundwater levels (GWL) in three Mandals, i.e., Bheemunipatnam, Visakhapatnam rural, and Visakhapatnam urban areas in Visakhapatnam district for the period from 2008 to 2020. The data of GWL in piezometric wells and open wells are used to predict the GWL trend present in the study area. For spatial analysis, the interpolation technique of inverse distance weighted is applied to develop the GWL maps. Mann–Kendall test and Sen's slope estimator were considered to predict the trend present in the GWL. From the exploration of the analysis, it is reflected that there is an increasing trend in GWL in some locations in the study area. Bheemunipatnam, Venkatapuram, Sivajipalem, Madhuravada, Chukkavanipalem, and YSR park are the significant places where groundwater is declining. Increasing depth trends to GWL, especially near the coast, can cause a decline in water quality and may lead to seawater intrusion.

Keywords Groundwater levels · Spatio-temporal variability · Trend analysis · Mann–Kendall test

Disclaimer: The presentation of material and details in maps used in this chapter does not imply the expression of any opinion whatsoever on the part of the Publisher or Author concerning the legal status of any country, area or territory or of its authorities, or concerning the delimitation of its borders. The depiction and use of boundaries, geographic names and related data shown on maps and included in lists, tables, documents, and databases in this chapter are not warranted to be error free nor do they necessarily imply official endorsement or acceptance by the Publisher or Author.

V. M. Priyanka (✉) · M. Ramesh
Department of Civil Engineering, GST, GITAM Deemed to be University,
Visakhapatnam 530045, India
e-mail: gvspriyanka@gmail.com

M. Ramesh
e-mail: rmaddams@gitam.edu

Y. Srinivas
Department of Computer Science and Engineering, GST, GITAM Deemed to be University,
Visakhapatnam 530045, India
e-mail: syarrama@gitam.edu

P. V. Timbadiya et al. (eds.), *Climate Change Impact on Water Resources*, Lecture Notes in Civil Engineering 313, https://doi.org/10.1007/978-981-19-8524-9_15

1 Introduction

Groundwater plays an important role in freshwater resources to meet domestic, agricultural, and industrial water needs. For sustainable management of natural resources, it is essential to a statistical assessment of GWL, especially in coastal regions where groundwater dependence is increasing. A study on GWL trend analysis is an important element of groundwater management. Trend analysis gives major knowledge about the characteristics of the groundwater direction, trend, and causes of decline in groundwater [1–3].

Mann–Kendall (MK) test is the most predominant technique for action information to analyze the different types of temporal datasets. In trend analysis, the MK test is a test without distribution based on statistics [4, 5]. Many researchers have been applied to groundwater-related applications [6, 7]. Different authors have used the MK test analysis to explore the various seasonal data for different scenarios. [8].

This study endeavors to provide the trend analysis and behavior of the seasonal GWL in the Visakhapatnam coastal aquifer over the past ten years. This study is significant in increasing the climate change impacts and overexploitation of the groundwater for efficient management of the resources.

2 Approach

2.1 Study Area

The study area is Visakhapatnam, which is positioned along the east coast of Andhra Pradesh in India at latitude 17° 45^{1} North and longitude 83° 16^{1} Eashe. Figure 1 shows the study area and locations of the groundwater wells. The rapid growth of population, industry, and agricultural practice has increased the significant diversion of surface water. To meet the requirements, dependence on groundwater is increasing. Overexploitation of groundwater leads to scarcity, resulting in the deterioration of water quality. Total eight groundwater wells data in three Mandals, i.e., Bheemunipatnam, Visakhapatnam rural, and Visakhapatnam urban areas in Visakhapatnam district, are considered for this study.

3 Data Collection

From the State Groundwater Department and Central Groundwater Department, the monthly GWL data of piezometric wells and observation wells were gathered. The data used in this study include the depth (d) of groundwater each month, which is "d" in meter below the ground level from 2008 to 2020 in these three Mandals and locations of the wells. In this study, total of eight wells are randomly picked to cover

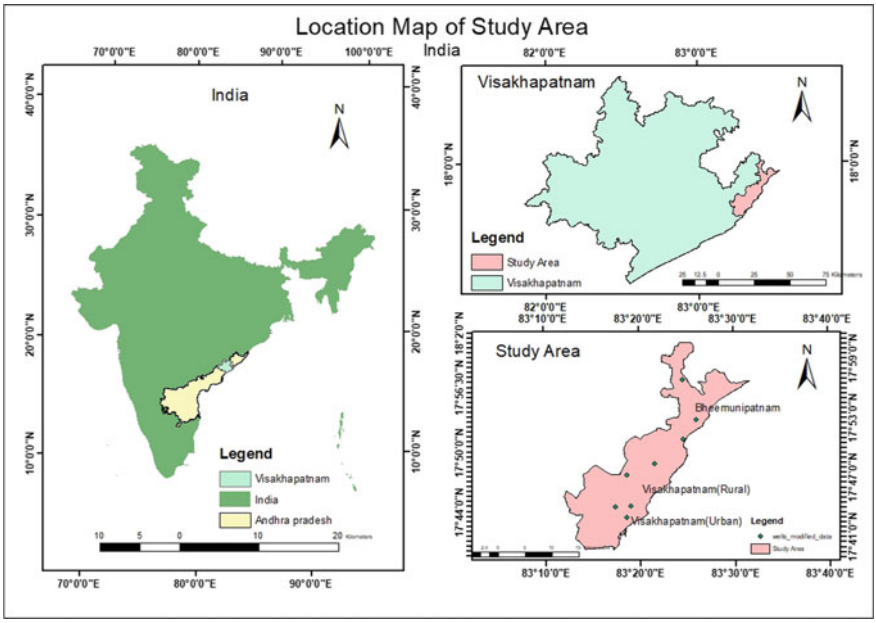

Fig. 1 Study area location map

the whole study area. The 12 years dataset of eight wells was considered to assess the spatial and temporal trend analysis. The GWL data are organized to signify the pre-monsoon (PRMS) and post-monsoon (POMS) seasons.

3.1 Spatial Variation of Groundwater Level

In the present study, the spatial analysis is aimed to understand the changes in the groundwater level over space. For reasonable management of natural water resources, spatial analysis is one of the vital techniques. The present work is to study the spatial analysis of GWL, and total of 12 years, i.e., from 2008 to 2020, were considered. Geographical information system has been used for spatial analysis [9]. The inverse distance weighted (IDW) method [10, 11] is applied to develop the seasonal depth to groundwater level variations maps from eight wells monthly GWL data, i.e., for PRMS and POMS seasons.

3.2 *Mann-Kendall (MK) Test*

In this study, MK test is employed for trend analysis of the GWL in the study area. Many researchers widely used this MK test to analyze different time-series data like temperature, rainfall, and groundwater level [12, 13]. The null hypothesis H_0 describes the n-quantity of data points, and x_j signifies the data points at time j and investigates depersonalized data, i.e., $x_1, x_2, \ldots x_n$. Thus, MK statistic (S) specified [4] as follows:

$$S = \sum_{k=1}^{n-1} \sum_{j=k+1}^{n} \operatorname{sgn}(x_j - x_k) \tag{1}$$

where "n" is the dataset length, x_j and x_k are the consecutive series of data.

$$\operatorname{sgn}(x_j - x_k) = \begin{Bmatrix} +1 & if & x_j - x_k > 0 \\ +0 & if & x_j - x_k = 0 \\ -1 & if & x_j - x_k < 0 \end{Bmatrix} \tag{2}$$

$$\operatorname{Var}(S) = \frac{\left[n(n-1)(2n+5) - \sum_t t(t-1)(2t+5)\right]}{18} \tag{3}$$

where "t" is the array of any expected tie of sample points. $\sum_t$ implies the summation of all the ties. Here, the trial size is $n > 10$, and the regular standard input "Z" value can be assessed by Eq. 4.

$$z = \begin{cases} \frac{s-1}{\sqrt{\operatorname{Var}(S)}} & \text{if } S > 0 \\ 0 & \text{if } S = 0 \\ \frac{s+1}{\sqrt{\operatorname{Var}(S)}} & \text{if } S < 0 \end{cases} \tag{4}$$

Here, the positive values of the normal standard input "Z" show an ascendant or rising trend, while the negative value of the normal standard input "Z" indicates a descendant or declining trend.

4 Sen's Slope Test

This Sen's slope test is used to deal with a balanced trend estimator, wherever the data are very biased [14]. In this paper, GWL fluctuations are uneven over a period of 12 years. When the GWL trends are linear, the calculated variation of the measurement slope over time was calculated by a modest non-parametric technique [15]. Equation (5) depicts the equation for Sen's slope.

$$Q = \frac{x_j - x_k}{j - k} \tag{5}$$

where "Q" denotes the Sen's slope of the data points between x_j and x_k. While xj denotes the dimension of the data in a certain time period of j, and x_k indicates the volume of data in the time period of k.

5 Summarizations

5.1 Spatial Analysis of GWL

The IDW method was applied to create depth to groundwater level spatial maps for two seasons. The water levels of PRMS in 2008 and 2020 vary from 1.08 to 7.39 m and 1.89 to 16.01 m, respectively. Similarly, the water levels of POMS in 2008 and 2020 range from 0.12 to 4.56 m and 1.06 to 12.69 m, respectively.

From the Fig. 2, it is observed that GWL is declining from 2008 to 2020. For PRMS, the maximum groundwater level depth from 2008 to 2020 is increased from 8 m to 18, similarly for POMS 6–14 m.

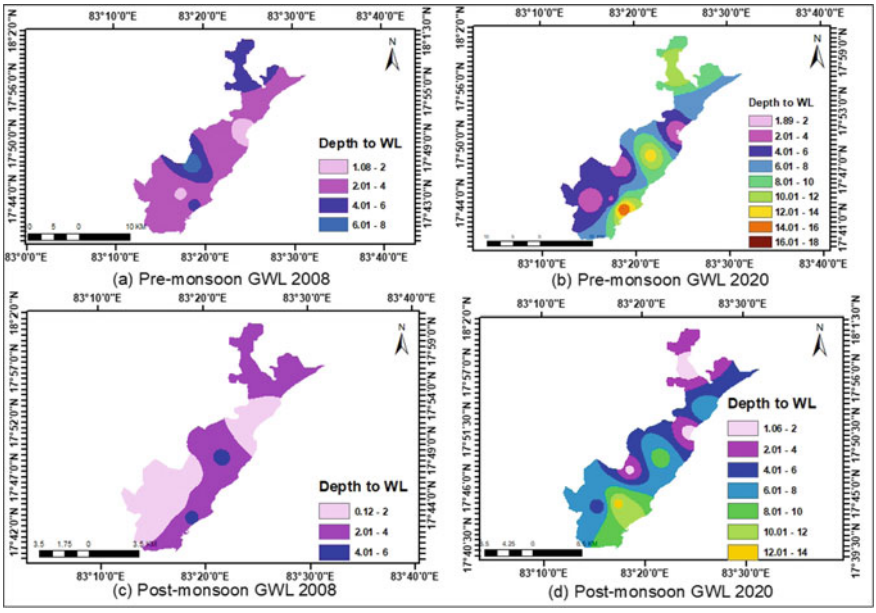

Fig. 2 Spatial variation of groundwater levels

Table 1 Results of MK "*Z*" statistics and Sen's slope "*Q*"

S. No.	Location of well	PRMS			POMS		
		Z	Sen's slope *Q*	Trend	*Z*	Sen's slope *Q*	Trend
1	Bheemunipatnam	3.11	0.711	↑	2.01	0.499	↑
2	Rajapulova	− 2.75	− 0.608	↓	− 2.50	− 0.298	↓
3	Venkatapuram	2.26	0.087	↑	1.90	0.072	↑
4	Sivajipalem	1.61	0.300	↑	0.23	0.100	↑
5	Madhuravada	1.79	0.348	↑	–	–	→
6	Paradesipalem	− 0.54	− 0.078	↓	–	–	→
7	Chukkavanipalem	1.47	0.048	↑	0.43	0.003	↑
8	YSR park	2.75	0.688	↑	2.26	0.623	↑

5.2 Mann–Kendall (MK) Test of Groundwater Level

In the field of study, trends have been identified through MK test, and the results are presented in Table 1. The trend was detected using a 99% significance of level. To find the trend line slope for PRMS and POMS seasons, Sen's slope method was used; PRMS values vary from − 0.608 to 0.711, and POMS varies from − 0.298 to 0.623.

The above results showed an increasing trend observed for PRMS in well 1, 3, 4, 5, 7, and 8; a decrease was observed in wells 2 and 6. An increase in trend means that the depth to water levels is increasing, i.e., water is declining in 75% of wells and rising in 25% of the wells in PRMS. Similarly, for POMS, there was an increasing trend in well 1, 3, 4, 7, and 8, a decreasing trend in well 2, and there is no trend observed in well 5 and 6. Water is declining in 62.5% of wells, increasing in 12.5% of the wells, and no trend was identified in 37.5% of wells in POMS.

6 Conclusions

The groundwater trend analysis is evaluated using MK test statistics in three Mandals, i.e., Bheemunipatnam, Visakhapatnam rural, and Visakhapatnam urban areas in Visakhapatnam district for the period of 12 years, from 2008 to 2020. The groundwater level of eight wells was employed in the study area to analyze and understand groundwater level fluctuations over time and space. According to the spatial interpolation, it is observed that there has been a decline in groundwater depths from 2008 to 2020.

From the MK trend analysis, an increase in trend means that the depth to water levels is increasing, i.e., water is declining in 75% of wells and rising in 25% of the wells in PRMS. Bheemunipatnam, Venkatapuram, Sivajipalem, Madhuravada,

Chukkavanipalem, and YSR park are the significant places where groundwater is declining. GWL is reducing in 62.5% of wells, increasing in 12.5% of the wells, and no trend was identified in 37.5% of wells in POMS. Decreasing trends of GWL, especially near the coast, can cause a decline in water quality and lead to seawater intrusion. It is mandatory to take measures to improve the GWL.

Acknowledgements The authors would like to acknowledge the Ground Water and Water Audit Department, Visakhapatnam, Govt of Andhra Pradesh, for providing the data of groundwater levels.

References

1. Abdullahi MG, Toriman ME, Gasim MB, Garba (2019). Trends analysis of groundwater: using non-parametric methods in Terengganu Malaysia. J Earth Sci Climatic Change 6:251–253
2. Das J, Sakiur Rahman ATM, Mandal T, Saha P (2020) Exploring driving forces of large-scale unsustainable groundwater development for irrigation in lower Ganga River basin in India. Environ Dev Sustain
3. Luong VV, Bui DH (2019) The impact of the decline in area of the storage areas on water level at downstream of the Sai Gon—Dong Nai river system. Int J River Basin Manage
4. Mann HB (1945) Non-parametric tests against trend. Econometrica 13:245–259. https://doi.org/10.2307/1907187
5. Kendall MG (1975) Rank correlation methods. Griffin, London
6. Ribeiro L, Kretschmer N, Nascimento J, Buxo A, Rötting T, Soto G, Señoret M, Oyarzún J, Maturana H, Oyarzún R (2015) Evaluating piezometric trends using the Mann Kendall test on the alluvial aquifers of the Elqui River Basin, Chile. J Data Sci Hydrol 60(10):1840–1852
7. Anand B, Karunanidhi D, Subramani T, Srinivasmoorthy K, Suresh M (2018) Long-term trend detection and spatiotemporal analysis of groundwater levels using GIS techniques in Lower Bhavani River basin, Tamil Nadu, India. J Environ Dev Sustain 22:2779–2800
8. Vousoughi FD, Dinpashoh Y, Aalami MT, Jhajharia D (2013) J Stoch Environ Res Risk Assess 27:547–559
9. Alipour A, Hashemi S, Shokri SBS, Moravej M (2018) Spatio-temporal analysis of groundwater level in an arid area. Int J Water
10. Kumar P, Chandniha SK, Lohani AK, Krishnan G, Nema AK (2018) Trend analysis of groundwater level using non-parametric tests in alluvial aquifers of Uttar Pradesh, India. Curr World Environ 13(1):44–54
11. Goyal SK, Chaudhary BS, Singh O, Sethi GK, Thakur PK (2010) Variability analysis of groundwater levels—a GIS based case study. J Indian Soc Remote Sens 38(2):355–364
12. Agarwal E, Garg RD, Srivastav SK (2017) Spatio-temporal trend analysis of groundwater level in Unnao District, Uttar Pradesh, India. Int J Creative Res Thoughts 5:1618–1628
13. Singh A, Sharma CS, Jeyaseelan AT, Chowdary VM (2015) Spatio-temporal analysis of groundwater resources in Jalandhar district of Punjab state, India. Sustain Water Resour Manage
14. Sarma R, Singh SK (2021) Temporal variation of groundwater levels by time series analysis for NCT of Delhi, India. Springer Science and Business Media LLC
15. Sen PK (1968) Estimates of the regression coefcient based on Kendall's tau. J Am Stat Assoc 63(324):1379–1389

Spatiotemporal Analysis of Rainfall and Temperature Over Pennar River Basin, India

G. Roshan Chand Naik and Ashwini B. Mirajkar

Abstract The purpose of the current study is to identify the temporal trends in rainfall and temperature trends in Peninsular India's Pennar Basin. Rainfall data were taken for a period of 1971–2020 (50 years) at 0.25° × 0.25° and temperature data were taken for a period of 1996–2020 (25 years) at 1° × 1° resolution, respectively, from IMD, Pune, and are analyzed at annual, monsoon seasonal and daily peak time scales. Trends in the rainfall and temperature are detected by non-parametric modified Mann–Kendall (MMK) and Spearman's correlation ratio (SCR) tests, and their change in magnitude with time is reported using Sen's slope estimator. A graphical method 'Innovative Trend analysis' is also used to obtain the nature of the pattern for the respective time series data at different time scales. The annual rainfall data have shown a significantly positive trend across most of the grids. The monsoon seasonal rainfall data have shown a mix of both positive and negative trends, while the daily peak rainfall data have shown more of a negative trend. The maximum and minimum temperature data in all the time scales show either negative trend or no trend. These trends have been confirmed by non-parametric tests and a graphical method used in the study.

Keywords Non-parametric tests · Pennar Basin · Modified Mann–Kendall · Sen's slope estimator test · Innovative trend analysis

G. Roshan Chand Naik (✉) · A. B. Mirajkar
Department of Civil Engineering, Visvesvaraya National Institute of Technology Nagpur, Nagpur, Maharashtra 440010, India
e-mail: gugulothroshan@gmail.com

A. B. Mirajkar
e-mail: abmirajkar@civ.vnit.ac.in

P. V. Timbadiya et al. (eds.), *Climate Change Impact on Water Resources*, Lecture Notes in Civil Engineering 313, https://doi.org/10.1007/978-981-19-8524-9_16

1 Introduction

One of the elements of the hydrological cycle, precipitation typically changes in both time and space as a result of anthropogenic influences and global warming. This in turn would modify the frequency of droughts and floods as well as the distribution of runoff, soil moisture and groundwater reserves. According to the Intergovernmental Panel on Climate Change report, the Earth's average temperature climbed by 0.6 °C in the twentieth century, while other climate prediction models estimate that temperature changes will range from 1.4 to 5.4 °C [1, 2]. Thus, to effectively implement any water resources management plan and know its spatiotemporal trends, it is a must to study the influence of climatic variables on rainfall and temperature patterns. The objectives of this study include trend detection using MMK test: to know the magnitude of change in slope using Sen's slope test, to know the change in trend of both rainfall and temperature using ITA method, to also know maximum rainfall and temperature values over the time period for Pennar basin. Time series analysis, which employs a variety of non-parametric techniques such as the modified Mann–Kendall test, Spearman's correlation test and Sen's slope estimator, is a technique for comprehending systematic fluctuations [3]. Under a variety of climatic situations, time series analysis has proven to be the most effective at identifying hydrological and meteorological trends. Innovative trend analysis, a graphical method developed by Şen, has also been used for trend detection studies.

2 Study Area and Data Source

2.1 Pennar River Basin

The Pennar basin, which is in Peninsular India, spans the states of Andhra Pradesh and Karnataka and has a maximum length and width of 433 km and 266 km, respectively. Only 4.97% of the fan-shaped basin is covered by water bodies, with agricultural covering the majority of its 58.64% total area. The basin is regularly affected by famine because it is located in an area with little rainfall. The basin's boundaries are 13° 18′–15° 49′ N latitude and 77° 1′–80° 10′ E longitude. The river is 597 km long and has a catchment area of 55,213 km^2 (Fig. 1).

2.2 Data Used

High-resolution daily gridded rainfall dataset obtained from IMD, Pune, at 0.25° × 0.25° frequency for period of 50 years (1971–2020) and daily gridded temperature data at 1° × 1° frequency for period of 25 years (1996–2020) have been analyzed at annual, daily and monsoon seasonal scale. The data series downloaded was complete

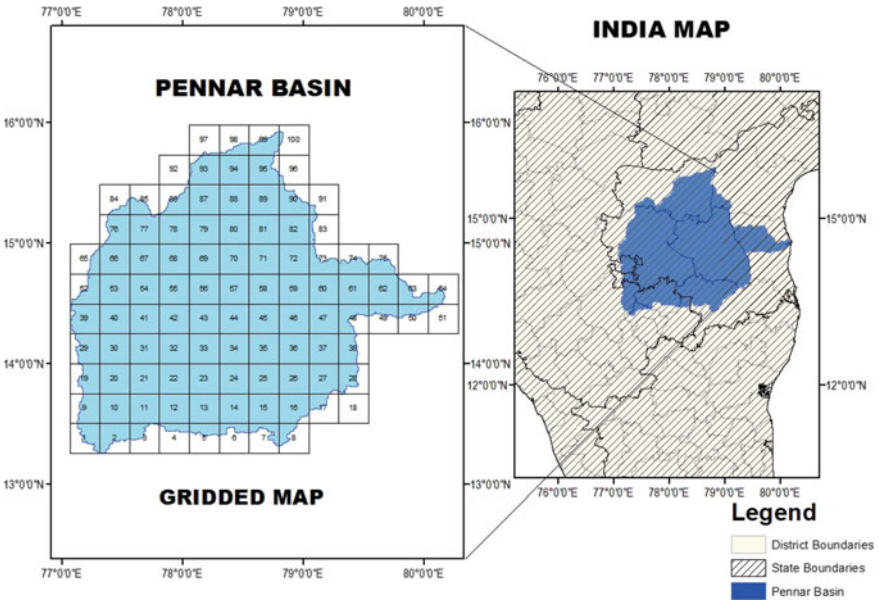

Fig. 1 Gridded map showing Pennar River Basin

and homogenous; hence, no missing data estimation was required for the study area, i.e., Pennar River basin.

2.3 Methodology Adopted

2.3.1 Modified Mann–Kendall Test

Long-term data were subjected to the rank-based non-parametric Mann–Kendall test in order to identify statistically significant patterns. The mathematical equations for calculating Mann–Kendall Statistics are as follows:

$$\mathrm{Sp} = \sum_{i=1}^{n-1} \sum_{j=i+1}^{n} j\mathrm{sgn}(Xj - Xi)$$

$$\mathrm{Sgn}(Xjj - Xi) = \left\{ \begin{cases} +1, & \text{if } (Xj - Xi) > 0 \\ 0, & \text{if } (Xjp - Xi) = 0 \\ -1 & \text{if } (Xj4 - Xi) < 0 \end{cases} \right\}. \quad (1)$$

The mean of S is $E[S] = 0$, and the variance σ_2 is given by

$$\sigma^2 = \frac{\{n(n-1)(2n+5) - \sum tp(tp-1)(2tp+5), (p=1 \text{ to } q)}{18}, \tag{2}$$

$$Z = \begin{cases} \frac{S-1}{\sqrt{\sigma 2}}, & \text{If } S > 0 \\ 0, & \text{If } S = 0 \\ \frac{S+1}{\sqrt{\sigma 2}}, & \text{If } S < 0 \end{cases} \tag{3}$$

where *Xj* and *Xi* are the annual values in years' j and $i, j > I$, respectively, and n is the number of data points ink Eq. (2). q is the numberpof tied (zero difference between compared values) groups, and t_p is the number of data values in the pth group.

2.3.2 Sen's Slope Estimator

Sen's slope technique is a non-parametric approach that uses slope calculation to anticipate trend at 95% significance level. The details of the calculation of Sen's slope are given by:

$$S = \frac{xj - xk}{j - k} \quad \text{for} \quad i = l \quad 1, 2, 3, \ldots n, \tag{4}$$

where x_j and x_k are the values at respective times of j and k.

If there isponly a single data point forlthe given time period, then $N = n \times (n - 1)/2$, p and for multiple data points, $pNj < n \times (n - 1)\, 2$, where n is the total number of observations. A positive value of Sen's estimator (Q) indicates increase in trend, while the negative value of Q represents a downward trend of data series.

2.3.3 Spearman's Correlation Test

Spearman's correlation test is a rank-based non-parametric test used for trend analysis. The alternative hypothesis (H_a) suggests that a trend exists and that the data rise or decrease with I, whereas the null hypothesis (H_o) shows that there is no trend over time. The test statistics r_{src} and standardized statistics t_{src} are defined as follows:

$$r_{SRC} = 1 - \left\{ \frac{6 \sum_{i=1}^{n} [d_i]^2}{n\left(n^2 - 1\right)} \right\}, \tag{5}$$

$$t_{SRC} = r_{sRC} \sqrt{\frac{(n-2)}{1 - r^2 \text{sRC}}}. \tag{6}$$

In these equations, d_i is the rank of ith observation, i is the order number, n is the total length of timekseries data and t_{SRC} is the Student's t-distribution with $(n - 2)$ degree of freedom. The positive value of t_{SRC} represents an upward trend across the

time series data; negative value represents the downward trends at 5% significance level of t's distribution table.

2.3.4 Innovative Trend Analysis

This method divides the hydrometeorological time series into two equal sections and then calculates the arithmetic averages of each segment ($y1$ and $y2$), independently. The trend slope (s) is calculated as shown below:

$$E(s) = \frac{2}{n}\left[E\left(\overline{y}_2\right) - E\left(\overline{y}_1\right)\right], \tag{7}$$

$$\sigma_s^2 = \frac{8}{n^2}\left[E\left(\overline{y}_2^2\right) - E\left(\overline{y}_2\overline{y}_1\right)\right], \tag{8}$$

$$\rho_{\overline{y}_2\overline{y}_1} = \frac{E\left(\overline{y}_2\overline{y}_1\right) - E\left(\overline{y}_2\right) - E\left(\overline{y}_1\right)}{\sigma_{\overline{y}_2}\sigma_{\overline{y}_1}}, \tag{9}$$

$$\sigma_S^2 = \frac{8}{n^2}\frac{\sigma^2}{n}\left(1 - \rho_{\overline{y}_2\overline{y}_1}\right), \tag{10}$$

$$\sigma_S^2 = \frac{2\sqrt{2}}{n\sqrt{n}}\sqrt{(1 - \rho_{\overline{y}_2\overline{y}_1}}\Bigg). \tag{11}$$

The first-order moment of the slope, n, the length of the data, the cross-correlation coefficient between two portions, $s2$, the variance of the trend slope and s, the standard deviation of the trend slope are all included in these equations.

3 Results and Discussions

3.1 Preliminary Statistical Analysis

The annual mean value and standard deviation value of annual rainfall for Pennar basin area are 961 mm and 191.186, respectively, and the obtained maximum and minimal rainfall values are 1453 and 577 mm. For monsoon season, the mean annual rainfall is 455 mm, its standard deviation is 121.799, and the highest and minimal rainfall values are 769 and 289 mm. For daily peak rainfall, mean is 58 mm, standard deviation is 23.63, and its largest and smallest daily rainfall values are 118 and 23 mm. The average temperature varies from 24 ˚C to 34 ºC every year, while the highest and smallest temperatures recorded are from May and January months with 40 ºC and 19 ºC, respectively. In monsoon season, the temperature ranges from 27

to 35 ºC, whereas the daily temperature ranges from 15 to 41 ºC over the period of 25 years (1996–2020).

The non-parametric tests such as MMK, Spearman's correlation test and Sen's slope estimator tests have been applied on annual rainfall and temperature, monsoon season rainfall and temperature, daily peak rainfall and daily peak temperature for a period of 50 years (1971–2020) along with Innovative trend analysis, which is a graphical method.

3.2 Trends in Annual Rainfall and Temperature Time Series

The MK statistics (*p*-value) for annual rainfall is 0.707 at 5% significance, which indicates significant upward (positive) trend as the value is above 0.5 in the trend detection of null hypothesis. The *p*-value for annual maximum temperature is 0.164, which indicates significant downward (negative) trend, and for annual minimum temperature is 0.409, which indicates significant downward trend as the *p*-values lies below 0.5 in the trend detection of null hypothesis, see Table 1. The Sen's slope value is 0.75 at 95% significance which shows an increasing trend in the annual rainfall pattern for a period of 50 years, while the Sen's slope value for both maximum and minimum annual temperatures is 0 indicating no trend in the time series data, see Table 1. The Spearman's correlation test gives the correlation value as 0.037, indicating no trend (correlation) across the annual rainfall time scale, while annual maximum and minimum temperatures have shown a mild correlation with values 0.291 and 0.206, respectively, see Table 1. The Innovative trend analysis, a graphical method, tells that 11 observations of annual rainfall show an increasing trend and five observations show a decreasing trend, while the rest eight observations show no trend. In case of annual maximum and annual minimum temperatures, 95% of the temperature values show absolutely no trend, see Figs. 2, 3 and 4. Also, the results indicated an upward trend in 44% (44 grids), while 40% (40 grids) showed downward trend and the remaining 16% (16 grids) out of all 100 grids showed no trend. The minimum and maximum average temperatures are found to be 22 ºC at grids 1, 2, 3 and 35 ºC at grids 11 and 12, respectively.

3.3 Trends in Rainfall and Temperature for Monsoon Season Time Series

The MK statistics (*p*-value) for monsoon season rainfall series is 0.169 at 5% significance level, which indicates significant downward (negative trend) trend as the value lies below 0.5. The *p*-values in monsoon season for maximum and minimum temperatures are 0.928 and 0.755, respectively, where both indicate a significant upward trend in the trend detection, see Table 1. The Sen's slope value for monsoon season

Table 1 Test results of annual and monsoon time-scale series

	Annual rainfall	Annual maximum temperature	Annual minimum temperature	Monsoon rainfall	Monsoon season max temperature	Monsoon season min temperature
MK (*p*-value)	0.707	0.164	0.409	0.169	0.928	0.755
Trend	Positive	Negative	No trend	Negative	Positive	Positive
Sen's slope value	0.75	0.0	0.0	1.313	0.0	0.0
Trend	Positive	No trend	No trend	Positive	No trend	No trend
Spearman's correlation	0.037	0.291	0.206	0.150	0.027	0.082
Trend	No correlation observed	Mild positive correlation observed	Mild positive correlation observed	No correlation observed	No correlation observed	No correlation observed

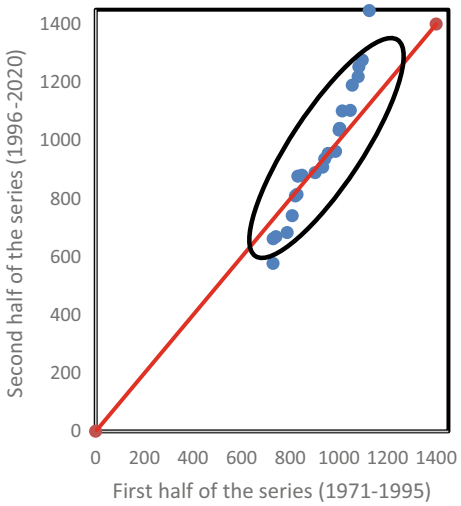

Fig. 2 ITA graph of annual rainfall series for a period of 50 years (1971–2020) at Pennar River Basin

rainfall series is 1.313 at 95% significance level which indicates an increasing trend, whereas Sen's slope value for both maximum and minimum temperatures in monsoon season is 0, indicating no trend in the time series data, see Table 1. The Spearman's correlation test gives the correlation value as 0.150 at 5% significance level, indicating that no trend is observed for the monsoon seasonal rainfall time series; also, maximum and minimum temperature values in monsoon period exhibit no correlation in the trend, see Table 1. The Innovative trend analysis tells that all observations of monsoon rainfall show an increasing trend except for the five observations which

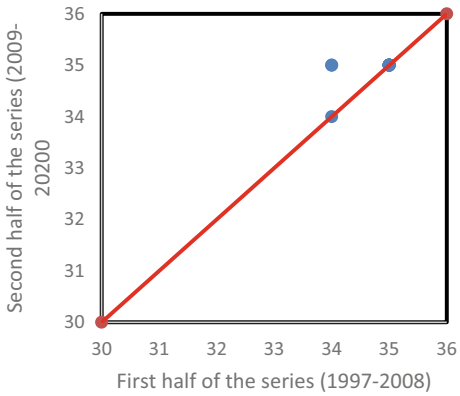

Fig. 3 ITA graph of annual maximum temperature series for a period of 24 years (1997–2020) at Pennar River Basin

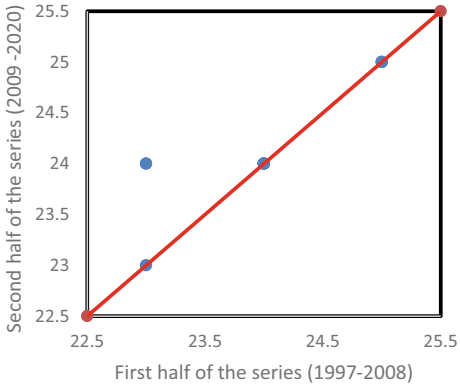

Fig. 4 ITA graph of annual minimum temperature series for a period of 24 years (1997–2020) at Pennar River Basin

show no trend. In case of monsoon seasonal maximum and minimum temperatures, all the temperature values show absolutely no trend, see Figs. 5, 6 and 7.

3.4 Trends in Daily Peak Rainfall and Daily Peak Temperature Time Series

The MK statistics (p-value) for daily peak rainfall time series is 0.642 at 5% significance level, which shows significant upward trend in the trend detection. The p-values in daily peak of maximum temperature and daily peak of minimum temperature time series are 0.158 and 0.941, which show downward and upward trends, respectively, see Table 2. The Sen's slope value for daily peak rainfall time series is − 0.114 at 95% significance level, which shows a significantly decreasing trend, while in both daily peak of maximum temperature and daily peak of minimum temperature time series, there is no trend observed, see Table 2. In Spearman's correlation test

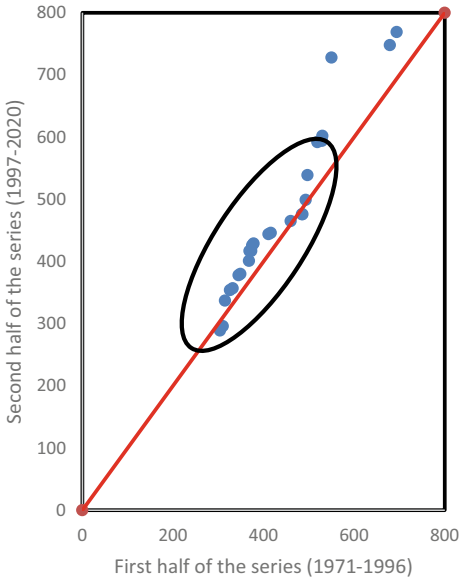

Fig. 5 ITA graph of monsoon rainfall series for a period of 50 years (1971–2020) at Pennar River Basin

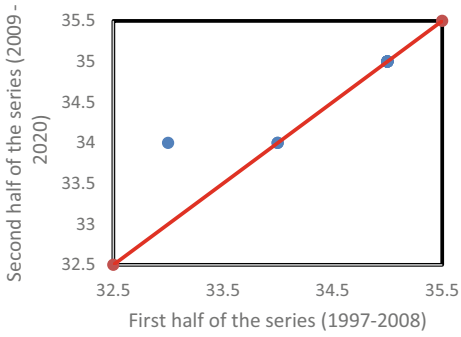

Fig. 6 Trend analysis of monsoon seasonal maximum temperature series for a period of 24 years (1997–2020) at Pennar River Basin

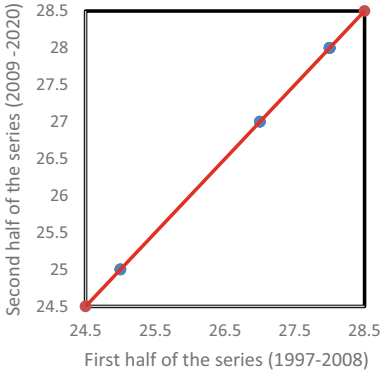

Fig. 7 ITA graph of monsoon seasonal minimum temperature series for a period of 24 years (1997–2020) at Pennar River Basin

Table 2 Test results of daily peak time scale series

	Daily peak rainfall	Daily peak of maximum temperature	Daily peak of minimum temperature
MK (*p*-value)	0.642	0.158	0.941
Trend	Positive	Negative	Positive
Sen's slope value	− 0.114	0.0	0.0
Trend	Negative	No trend	No trend
Spearman's	− 0.071	− 0.267	− 0.035
Trend	Negative correlation observed	Negative correlation observed	Negative correlation observed

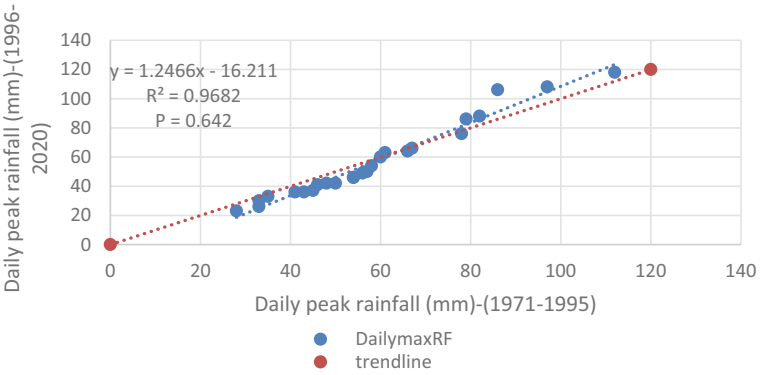

Fig. 8 Trend analysis of daily peak rainfall series for a period of 50 years (1971–2020) at Pennar River Basin

for daily peak rainfall, daily peak maximum temperature and daily peak minimum temperature, the correlation observed is negative, i.e., decreasing trend is obtained, see Table 2. The Innovative trend analysis tells that 13 observations of daily peak rainfall show a decreasing trend. Other five observations show an increasing trend, while the rest six observations show no trend. In case of daily peak maximum and minimum temperatures, all the temperature values mostly show a decreasing (negative) trend, see Figs. 8, 9 and 10. From the return period calculations, we infer that the lowest annual rainfall 577 mm is occurring every year.

3.5 Conclusions

Spatiotemporal analysis of rainfall and temperature data for a period of 50 years (1971–2020) and 25 years (1996–2020) in the annual, monsoon seasonal and daily peak time scales, respectively, revealed the following related to Pennar river basin:

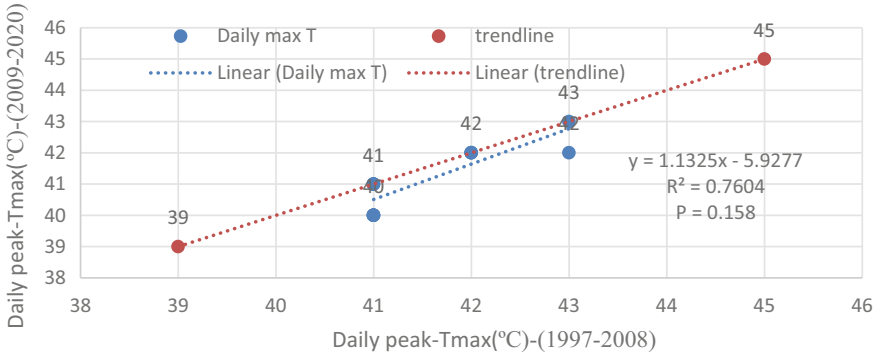

Fig. 9 Trend analysis of daily peak maximum temperature series for a period of 24 years (1997–2020) at Pennar River Basin

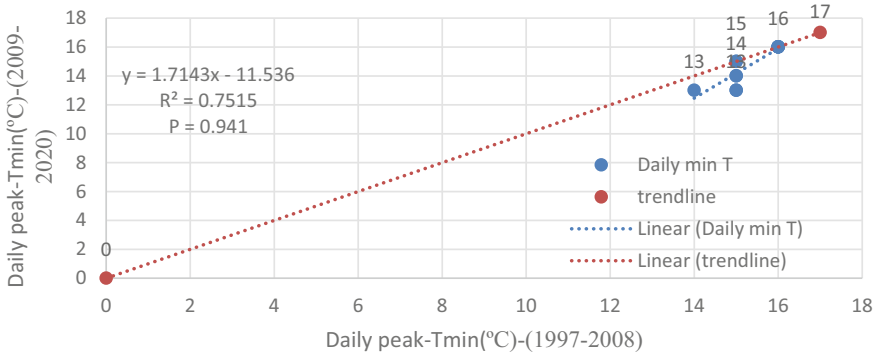

Fig. 10 Trend analysis of daily peak minimum temperature series for a period of 24 years (1997–2020) at Pennar River Basin

- In annual time scale, the annual rainfall series data have shown a significantly positive trend.
- For annual maximum and annual minimum temperature series data, a mix of negative trends and no trends is observed.
- In monsoon seasonal time scale, the monsoon rainfall series data have shown a mix a negative and positive trend.
- For monsoon season—maximum and minimum temperature series data, a mix of positive trends and no is are observed.
- In daily peak time scale, the daily peak rainfall data series shows a persistent negative trend with a mix of positive trend as well.
- For daily peak maximum and minimum temperature series data, a mix of positive trend and no trends is observed.

- Annual average rainfall for a period of 50 years is 962 mm, and annual average of maximum temperature and annual average of minimum temperature for a period of 25 years are 35 and 25 ºC.
- Monsoon seasonal average rainfall for a period of 50 years is 456 mm, and seasonal average of maximum temperature and minimum temperature for a period of 25 years is 35 and 27 ºC.
- According to grid-wise data series, peak rainfall obtained is 1963 mm at grids 8, 9, 10 and 11 and peak average rainfall obtained is 1083 mm at grids 9, 10, 11 and 12.
- The peak maximum and peak minimum temperatures are 35 ºC at grids 3, 4 and 5 and 22 ºC at grids 1, 2 and 3, respectively.

Acknowledgements The authors wish to express their sincere gratitude to the India Meteorological Department (IMD), Pune, for providing daily gridded rainfall data.

References

1. Malik A, Kumar A (2020) Spatio-temporal trend analysis of rainfall using parametric and non-parametric tests: case study in Uttarakhand, India. Theor Appl Climatol 140(1–2):183–207. https://doi.org/10.1007/s00704-019-03080-8
2. Griggs DJ (n.d.) SECTEUR: sector engagement for copernicus climate services view project climate change: public health evidence view project. https://www.researchgate.net/publication/216811760
3. Gajbhiye S, Meshram C, Mirabbasi R, Sharma SK (2016) Trend analysis of rainfall time series for Sindh River basin in India. Theoret Appl Climatol 125(3–4):593–608. https://doi.org/10.1007/s00704-015-1529-4
4. Mahyavanshi P, Loliyana VD, Sharma PJ (2018) Variability of rainfall, temperature and potential evapotranspiration at annual time scale over Tapi to Tadri River Basin, India. https://www.researchgate.net/publication/336148503
5. Singh RN, Sah S, Das B, Vishnoi L, Pathak H (2020) Spatio-temporal trends and variability of rainfall in Maharashtra, India: Analysis of 118 years. https://doi.org/10.1007/s00704-020-03452-5/Published
6. Chhetri R (2020) Analysis of rainfall and return periods to assess flood risks in hilly areas of Nepal Inflating the life Rifts of NCLB-Frederic M. Hess View project TVET in Bhutan: An Explorative Study of Issues and Challenges in TVET View project. Int Res J Environ Sci
7. https://www.researchgate.net/publication/344310702
8. Rahman A, Dawood M (2017) Spatio-statistical analysis of temperature fluctuation using Mann–Kendall and Sen's slope approach. Climate Dyn 48(3–4):783–797.https://doi.org/10.1007/s00382-016-3110-y
9. Gupta PK, Chauhan S, Oza MP (2016) Modelling surface run-off and trends analysis over India. J Earth Syst Sci 125(6):1089–1102
10. https://doi.org/10.1007/s12040-016-0720-z
11. Abeysingha NS, Singh M, Sehgal VK, Khanna M, Pathak H (2016) Analysis of trends in streamflow and its linkages with rainfall and anthropogenic factors in Gomti River basin of North India. Theoret Appl Climatol 123(3–4):785–799. https://doi.org/10.1007/s00704-015-1390-5
12. Dash SK, Nair AA, Kulkarni MA, Mohanty UC (2011) Characteristic changes in the long and short spells of different rain intensities in India. Theoret Appl Climatol 105(3):563–570

13. https://doi.org/10.1007/s00704-011-0416-x
14. Ahmad I, Tang D, Wang T, Wang M, Wagan B (2015) Precipitation trends over time using Mann-Kendall and spearman's Rho tests in swat river basin, Pakistan. Adv Meteorol.https://doi.org/10.1155/2015/431860

Trend Analysis of Rainfall and Temperature in the Damoh District, Central India

Amit Jain, V. L. Manekar, and J. N. Patel

Abstract Trend detection of hydroclimatic variables has a significant impact in the context of climate change. Rainfall and temperature are the major factors that affect the entire hydrological cycle. This study has been carried out to find the trend of rainfall and temperature in the Damoh District of Madhya Pradesh. Trend analysis is carried out in this study from 1984 to 2012 for monthly, seasonal, and yearly time series. Mann–Kendall and Sen's slope tests were carried out to find the trend of both rainfall and temperature over the study area. There is falling trend in Pre-Monsoon rainfall ($Z = -0.26$ and $S = -0.104$) and Monsoon rainfall ($Z = -0.61$ and $S = -5.404$) and slightly rising trend in Post-Monsoon rainfall ($Z = 0.04$ and $S = 0.000$). There is a significant falling trend in the annual rainfall ($Z = -1.36$ and $S = -12.124$). There is a steep fall in the trend of annual rainfall after 1994. All three seasons show the falling trend for seasonal temperature: Pre-Monsoon temperature ($Z = -0.18$ and $S = -0.007$), Monsoon temperature ($Z = -1.44$ and $S = -0.028$), and Post-Monsoon temperature ($Z = -0.81$ and $S = -0.018$). The results of this study indicate that there is a significant impact of temperature on rainfall.

Keywords Trend analysis · Rainfall · Temperature · Mann–Kendall test · Sen's slope

A. Jain (✉) · V. L. Manekar · J. N. Patel
Department of Civil Engineering, Sardar Vallabhbhai National Institute of Technology Surat, Surat 395007, India
e-mail: ds20ce011@ced.svnit.ac.in

V. L. Manekar
e-mail: vlm@ced.svnit.ac.in

J. N. Patel
e-mail: jnp@ced.svnit.ac.in

P. V. Timbadiya et al. (eds.), *Climate Change Impact on Water Resources*, Lecture Notes in Civil Engineering 313, https://doi.org/10.1007/978-981-19-8524-9_17

1 Introduction

Any future planning and development have the effect of its water resources on it including drainage system, watershed management, and flood mitigation [9]. The precipitation in any area is a vital factor for ascertaining the accessibility of water to satisfy the different requirements mainly domestic, agriculture, and industrial. The convenient accessibility of water impacts the irrigation system and hydropower generation. This study is an attempt toward gaining knowledge and building a deep understanding of the variation and trend in rainfall and temperature in the study area on a monthly, seasonal, and yearly basis. All the activities in the hydrological cycle are affected by temperature. Any temperature variation will result in changes in the hydrological cycle.

Numerous methods are available for identifying hydrometeorological time series. After analyzing various studies, it can be concluded that the non-parametric methods are normally used in trend analysis of hydrometeorological variables [6]. Non-parametric tests do not assume about the parameters of the population and hence do not use the parameters of the distribution [3]. One major advantage of using non-parametric methods is that they did not assume that the data are following any particular distribution.

The main object of this work is to get familiar with the recent trend of different metrological factors and to get familiar with different methods to analyze these trends. With the help of this study, the trend of runoff for the study can also be found out and change in the metrological parameters of the study area and their impact on the hydrological cycle can be find out.

2 Study Area and Data Source

2.1 Damoh District

Damoh is a district of the state of Madhya Pradesh situated in Central India. The city of Damoh is a district headquarter. The district is the part of Sagar Division. Damoh is located at 23.080° N–24.280° N and 79° E–79.52° E, with an average elevation of 595 m (1952 ft). The total population of Damoh District is 1,264,219; out of this, rural population is 1,013,668 and urban population is 250,551. The district of Damoh has an area of 7306 km^2. The Tropic of Cancer passes through the southern part of the study area. The topography of Damoh District is of very undulating type with low-rising hills scattered all around. Damoh District is located in the southeastern part of the huge Vindhya plateau. This plateau is irregularly spread in the district and divided between sonar valley and forms northeastern chain of mountain. Average rainfall in this area is 117 cm. Due to hilly terrain, major part of rainfall is converted into runoff and drains off into the streams. There is no perineal river or any major surface water reservoir in this area (Fig. 1).

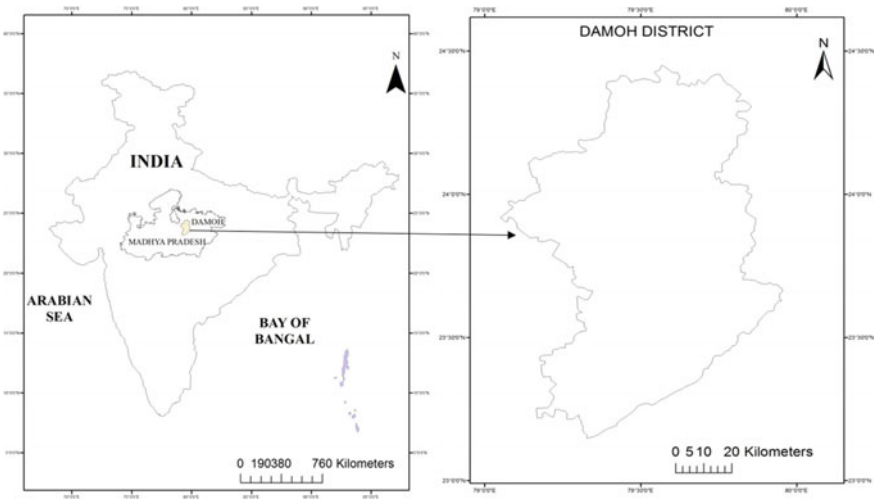

Fig. 1 Index map of the study area

2.2 Data Used

Rainfall data of rain gauge stations for monthly rainfall were collected from the land record section of the Collectorate Office of Damoh District for the duration of 1984–2012. The data for temperature are downloaded from the website https://power.larc.nasa.gov/data-access-viewer for the duration of 1984–2012. All the data were checked for consistency in data, and pre-whitening of data was performed wherever it is necessary.

3 Methodology

All the data used in this study are checked for autocorrelation first, and pre-whitening of data is performed. For trend analysis of rainfall and temperature, Mann–Kendall and Sen's slope methods are being used in this study.

3.1 Mann–Kendall (MK) Test

For analyzing patterns, the non-parametric Mann–Kendall test is used [2, 7]. The Mann–Kendall test is used to identify statistically significant trends in variables such as streamflow, temperature, and precipitation [11, 10]. Recognizing monotonic (linear/nonlinear) trends in hydroclimatological time series has generally been

done using the non-parametric position-based Mann–Kendall technique. This test compares an elective hypothesis with a significant increasing or decreasing trend versus an invalid theory with no pattern. The evaluating parameter (S) is

$$S = \sum_{i=1}^{n-1} \sum_{j=i+1}^{n} \operatorname{sgn}\left(x_j - x_i\right).$$

Here, *xi* and *xj* are the sequent data values, n is the number of the data set, and

$$\operatorname{sgn}(t) = \begin{cases} 1, & \text{for } t > 0 \\ 0, & \text{for } t = 0 \\ -1, & \text{for } t < 0 \end{cases},$$

S denotes the trend's direction in this instance. A positive sign indicates a positive trend, whereas a negative sign indicates a negative trend. According to Mann–Kendall's recommendations, the test statistic S is approximately normally distributed with the following mean and variance when $n \geq 8 E(S) = 0$,

$$\operatorname{Var}(S) = \frac{n(n-1)(2n+5) - \sum_{i=1}^{m} t_i (t_i - 1)(2t_i + 5)}{18}.$$

The standardized test statistics Z is calculated as follows:

$$Z_{MK} = \begin{cases} \frac{S-1}{\sqrt{\operatorname{Var}(S)}}, & \text{for } S > 0 \\ 0, & \text{for } S = 0 \\ \frac{S+1}{\sqrt{\operatorname{Var}(S)}}, & \text{for } S < 0 \end{cases}$$

where *ti* is the size of the *i*th couple group and m is the total number of couple groups. Similar to how ZMK follows the normal distribution, a positive ZMK shows an upward trend during the time, and a negative ZMK shows a downward trend. At the ZMK $Z/2$ level of significance, the data are deemed to have a significant trend. The Mann–Kendall test compares an alternate hypothesis with a trend in the data against the null hypothesis, which has no trend, in the data. When there are more than ten observations, the aforementioned formula can be applied.

3.2 Sen's Slope Test

Q_{Sen} from the non-parametric Sen's slope (SS) approach stated both the direction and magnitude of trend in the time series, just like the parametric linear regression technique. The following equation can be used to determine the slope's magnitude:

$$Q_{\text{sen}} = \text{Median}\left[\frac{Y_i - Y_j}{(i-j)}\right] \quad \text{for all} \quad j < i,$$

where the values at time points *I* and *j*, respectively, are *Yi* and *Yj*. The total number of slope estimates will be $(n(n-1))/2$ if there are n total data points in the series. The average of all the slope estimates is the test statistic Q_{Sen}. The test result's positive indication denotes an upward trend, and vice versa.

4 Result and Analysis

For sessional analysis, year is divided into three sessions as follows:

(I) Pre-Monsoon (February–May),
(II) Monsoon (June–Sep),
(III) Post-Monsoon (October–January).

4.1 Trend Analysis of Rainfall

Preliminary data examination has been performed to find out the mean and standard deviation of rainfall for the time period of 1984–2012. Yearly rainfall in the study area ranges between 1146.19 mm (2007) and 2589.07 mm (1994). The test results of Mann–Kendall and Sen's slope are shown in Table 1.

The results shown in Table 1 indicated a rising trend in the month of April, May, September, and November with a maximum $Z = +1.24$ in the month of September, while there is a falling trend in the remaining months with a maximum $Z = -2.27$ in the month of August. There is a falling trend in annual rainfall with $Z = -1.36$. In the seasonal analysis, there is a falling trend in Pre-Monsoon ($Z = -0.26$) and Monsoon ($Z = -0.61$), while a rising trend in Post-Monsoon ($Z = +0.04$) (Figs. 2, 3, 4 and 5).

4.2 Trend Analysis of Temperature

Preliminary data examination has been performed to find out the mean and standard deviation of temperature for the time period of 1984–2012. The average monthly temperature in the study area ranges between 21.22 ˚C (1997) and 45.06 ˚C (1988). The test results of Mann–Kendall and Sen's slope are shown in Table 2.

The results shown in Table 2 indicated a rising trend in the month of February and October with a maximum $Z = +0.005$ in the month of October, while there is a falling trend in the remaining months with a maximum $Z = -0.048$ in the month of June. There is a falling trend in average annual temperature with $Z = -0.014$. In the

Table 1 Results of trend analysis of rainfall using MK test and Sen's slope

Time series	Kendall's tau	*p*-value	*Z*	Sen's slope
January	− 0.026	0.860	− 0.15	0.000
February	− 0.178	0.210	− 1.23	0.000
March	− 0.060	0.685	− 0.38	0.000
April	0.026	0.857	0.16	0.000
May	0.006	0.967	0.02	0.000
June	− 0.058	0.664	− 0.41	− 1.148
July	− 0.053	0.693	− 0.38	− 1.844
August	− 0.307	0.022	− 2.27	− 8.902
September	0.169	0.206	1.24	3.240
October	− 0.116	0.415	− 0.79	0.000
November	0.132	0.396	0.82	0.000
December	− 0.097	0.518	− 0.62	0.000
Annual rainfall	− 0.185	0.167	− 1.36	− 12.124
Pre-monsoon	− 0.037	0.782	− 0.26	− 0.104
Monsoon	− 0.085	0.527	− 0.61	− 5.404
Post-monsoon	0.008	0.953	0.04	0.000

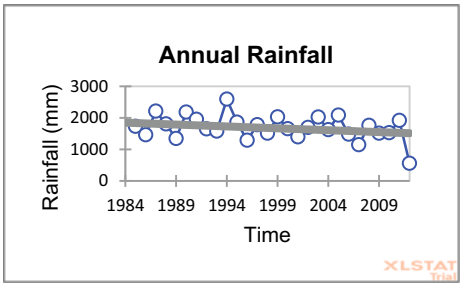

Fig. 2 Variation in annual rainfall

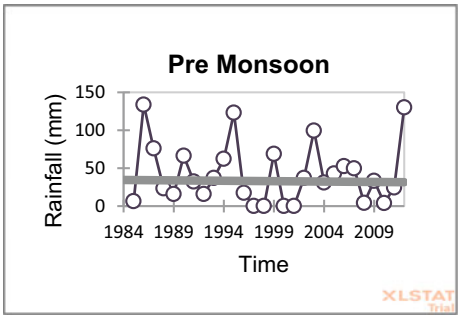

Fig. 3 Variation in rainfall for pre-monsoon season

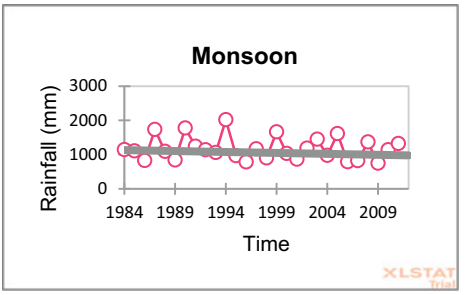

Fig. 4 Variation in rainfall for monsoon season

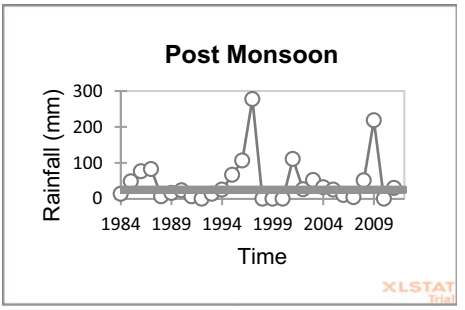

Fig. 5 Variation in rainfall for post-monsoon season

Table 2 Results of trend analysis of temperature using MK test and Sen's slope

Time series	Kendall's tau	*p*-value	*Z*	Sen's slope
January	− 0.074	0.574	− 0.54	− 0.020
February	0.025	0.851	0.17	0.003
March	− 0.005	0.970	− 0.02	− 0.001
April	− 0.138	0.294	− 1.03	− 0.019
May	− 0.197	0.133	− 1.48	− 0.041
June	− 0.153	0.245	− 1.14	− 0.048
July	− 0.187	0.154	− 1.41	− 0.045
August	− 0.015	0.910	− 0.09	− 0.002
September	− 0.069	0.599	− 0.51	− 0.007
October	0.025	0.851	0.17	0.005
November	− 0.074	0.574	− 0.54	− 0.019
December	− 0.054	0.680	− 0.39	− 0.011
Annual temperature	− 0.163	0.216	− 1.22	− 0.014
Pre-monsoon temperature	− 0.026	0.843	− 0.18	− 0.007
Monsoon temperature	− 0.192	0.143	− 1.44	− 0.028
Post-monsoon temperature	− 0.111	0.407	− 0.81	− 0.018

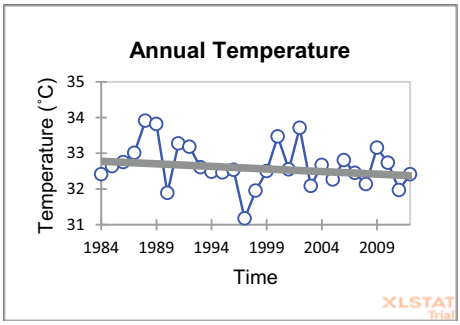

Fig. 6 Variation in annual temperature

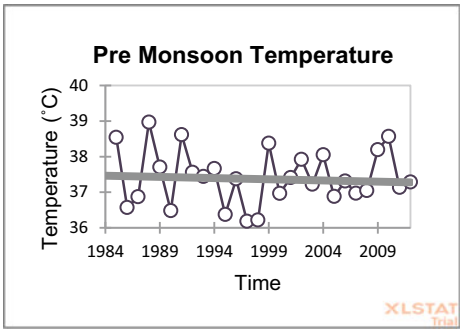

Fig. 7 Variation in temperature for pre-monsoon season

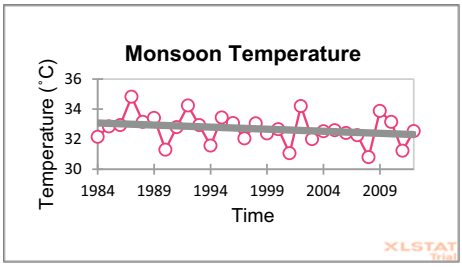

Fig. 8 Variation in temperature for monsoon season

seasonal analysis, there is falling trend in Pre-Monsoon ($Z = -0.007$), Monsoon ($Z = -0.028$), and Post-Monsoon ($Z = -0.018$) (Figs. 6, 7, 8 and 9).

5 Discussion

The study area is unique in nature with an average elevation of 595 m and is of very undulating type with low-rising hills scattered all around. The study area is located in the southeastern part of the huge Vindhya plateau. The Tropic of Cancer

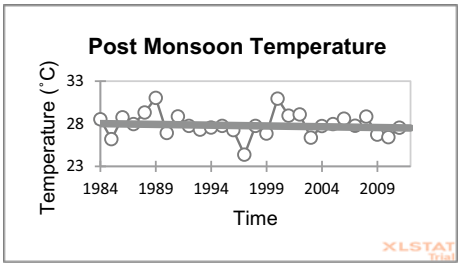

Fig. 9 Variation in temperature for post-monsoon season

passes through the southern part of the study area. The top surface of the study area mainly consists of sandstone, gravel, and yellow soil. There is significant variation in the data of each month of each year for both rainfall and temperature. The average monthly temperature varies from 21.22 ˚C (December 1997) to 45 ˚C (May 1988). The average annual rainfall for the time period of 1984–2012 is 1688.74 mm.

There is a significant falling trend in annual rainfall by the Mann–Kendall test ($Z = -1.36$) and Sen's slope test ($S = -12.124$). Annual rainfall varies from 553.82 mm (2012) to 2579.01 mm (1994) with a mean of 1688.74 mm. There is a steep fall in the trend of annual rainfall after 1994. The mean annual rainfall from 1984 to 1994 is 1847.55 mm (> 1688.74 mm), while the mean annual rainfall for the time duration of 1994–2012 is 1652.54 mm (< 1688.74 mm).

There is also a falling trend in Pre-Monsoon and Monsoon rainfalls, while a very slightly rising trend in Post-Monsoon rainfall. For Pre-Monsoon season, Mann–Kendall (Z) = − 0.26 and Sen's slope (S) = − 0.104. For Monsoon season, Mann–Kendall (Z) = − -0.61 and Sen's slope (S) = − 5.404. For Post-Monsoon season, Mann–Kendall (Z) = 0.04 and Sen's slope (S) = 0.000. Pre-Monsoon rainfall varies from 0 mm in 1997, 1998, 2000, and 2001 to 133 mm in 1985. Monsoon rainfall varies from 745.20 mm in 2009 to 2016.40 mm in 1994. Post-Monsoon rainfall varies from 0 mm in 1992, 1999, 2000, and 2010 to 277.20 mm in 1997. There is also a steeper change in the seasonal rainfall trend after 1994. Pre-Monsoon and Monsoon rainfalls show more steeper falling trend from 1994 to 2012 than 1984 to 1994, while there is a steeper rising trend in Post-Monsoon rainfall from 1994 to 2012 than 1984 to 1994.

Monthly rainfall trend for monsoon season is negative for June ($Z = -0.41$ and $S = -1.148$), July ($Z = -0.38$ and $S = -1.844$,) and August ($Z = -2.27$ and $S = -8.902$), while positive trend for month of September ($Z = 1.24$ and $S = 3.240$). Also, there is positive trend for Post-Monsoon rainfall.

There is a falling trend in annual temperature by the Mann–Kendall test ($Z = -1.22$) and Sen's slope test ($S = -0.014$). Annual temperature varies from 31.17 ˚C (1997) to 33.91 ˚C (1988) with a mean of 32.65 ˚C.

There is also a falling trend in seasonal temperature for all three seasons (Pre-Monsoon, Monsoon, and Post-Monsoon). For Pre-Monsoon season, temperature varies from 36.18 ˚C (1997) to 38.97 ˚C (1988) with Mann–Kendall (Z) = − 0.18

and Sen's slope (S) = − 0.007. For Monsoon season, temperature varies from 30.8 °C (2008) to 34.82 °C (1987) with Mann–Kendall (Z) = − 1.44 and Sen's slope (S) = − 0.028. For Post-Monsoon season, temperature varies from 21.19 °C (2012) to 31.03 °C (1989) with Mann–Kendall (Z) = − 0.81 and Sen's slope (S) = − 0.018.

There is also falling trend for average monthly temperature of all months except February ($Z = 0.17$ and $S = 0.007$) and October ($Z = 0.17$ and $S = 0.005$). Average monthly temperature varies from 21.19 °C in December 2012 to 45.06 °C in May 1988 with a mean monthly temperature of 32.65 °C for the duration of 1984–2012.

From this study, we can conclude that there is a falling trend in rainfall and temperature. This falling trend is increasing more rapidly for rainfall, especially after 1994. Rainfall is increasing in the last month of the Monsoon season (September) and Post-Monsoon season.

6 Conclusions

The following conclusions are derived from the foregoing study:

I. Both the test results show that overall, there is a falling trend in rainfall and temperature on monthly, seasonal, and yearly time series.
II. In the case of rainfall, this falling trend is increasing more rapidly, especially after 1994.
III. Rainfall is increasing in the last month of the Monsoon season (September) and Post-Monsoon season.

References

1. Guzman LA, Moncada CA, Gómez S (2018) Fare discrimination and daily demand distribution in the BRT system in Bogotá. Publ Transp 10:191–216
2. Kendall MG (1975) Rank correlation methods. Charless Griffin, London
3. Kothari CR, Garg G (2019) Research methodology—methods and techniques, 4th edn. New Age International (P) Limited Publishers
4. Kumar V, Jain SK, Singh Y (2010) Analysis of long-term rainfall trends in India. Hydrol Sci J 49:484–496
5. Kundzewicz ZW, Robson AJ (2011) Change detection in hydrological records—a review of the methodology. Hydrol Sci J 49:7–19
6. Machiwal D, Jha MK (2012) Hydrologic time series analysis : theory and practice. Capital Publishing Company
7. Mann HB (1945) Nonparametric tests against trend. Econometrica 13:245– 259
8. Mondal A, Kundu S, Mukhopadhyay A (2012) Rainfall trend analysis by Mann-Kendall test: a case study of north-eastern part of Cuttack district, Orissa. Int J Geol Earth Environ Sci 2:70–78
9. Pal AB, Deepak Khare PK, Mishra LS (2017) Trend analysis of rainfall, temperature and runoff data: a case study of Rangoon watershed in Nepal. Int J Stud Res Technol Manage 5(3):21–38

10. Sonali P, Nagesh Kumar D (2013) Review of trend detection methods and their application to detect temperature changes in India. J Hydrol 476:212–227
11. Sonali P, Nagesh Kumar D (2016) Spatio-temporal variability of temperature and potential evapotranspiration over India. J Water Climate Change 7:810–822

A Trend Analysis of Rainfall and Temperature Pattern Using Non-parametric Tests of a Bharuch District, Gujarat, India

K. A. Jariwala and P. Agnihotri

Abstract Rapid urbanization is a factor in climate change, which has negative effects on the environment. Change must occur as much as feasible in order to lessen the effects. Understanding the climatic conditions over years, if not decades, is necessary to analyze the shift. The temperature and rainfall patterns for a certain site are the most frequently researched climate change factors; however, it differs from place to place. As a result, it is essential to understand the spatiotemporal dynamics of meteorological variables in the context of a changing climate in order to identify effective adaptation strategies, particularly in nations where agriculture dominates the economy. As a result, this study looks at both long-term trends and short-term fluctuations in rainfall and temperature in the Gujarat city of Bharuch. Researchers examined data on precipitation and temperature from 1981 to 2020. The difficulties were looked at and analyzed using statistical trend analysis techniques like the Mann–Kendall test and Sen's slope estimator. The annual maximum and minimum temperatures have showed a growing trend, whereas the monsoon's maximum temperature has shown a falling trend, according to a thorough analysis of the statistics over the past 39 years. Throughout the monsoon season, rainfall is gradually increasing (Sen's slope = 0.76). The lowest temperature trend was modestly warming or growing over the study period, while the maximum temperature trend was declining (Sen's slope = − 0.13). The lowest temperature trend analysis result, however, is statistically significant at the 95 percent level of confidence, but the highest temperature trend analysis result is not.

K. A. Jariwala (✉) · P. Agnihotri
Department of Civil Engineering, Sardar Vallabhbhai National Institute of Technology Surat, Surat 395007, India
e-mail: khushboojariwala247@gmail.com

P. Agnihotri
e-mail: pga@ced.svnit.ac.in

P. V. Timbadiya et al. (eds.), *Climate Change Impact on Water Resources*, Lecture Notes in Civil Engineering 313, https://doi.org/10.1007/978-981-19-8524-9_18

Keywords Climate variability · Mann–Kendall's test · Sen's slope estimator · Trend analysis

1 Introduction

The climate is a crucial component of the Earth's system. Temperature, precipitation, air pressure, and humidity are only a few of the factors that affect the weather and climate. The term "climate" is frequently used to describe the weather on a specific day. It is, broadly speaking, the statistical evaluation of relevant features in terms of their mean and variability over time scales ranging from months to hundreds of millions of years [1]. Analyzing long-term changes in climatic variables is a fundamental challenge in the research of climate change detection. Several dataset extensions and improvements, as well as more difficult data analyses, have allowed for a greater understanding of past and present climate change throughout the world [2]. Global climate change may cause long-term rainfall patterns to change, depleting water supplies and increasing the danger of droughts and floods [2]. Rainfall and temperature are the two main physical aspects of a region's climate that determine its environmental state, which has an impact on agricultural productivity [3, 4]. The timely availability of sufficient water supplies and a favorable environment in any location are requirements for the security of food, energy, and related industries. The amount of rainfall that an area receives impacts how much water is available to support a variety of needs, including those for agriculture, industry, home water supply, and hydroelectric power generation. Rainfall patterns and levels are among the most significant factors that affect agricultural production because agriculture is crucial to India's economy and people's livelihood [5]. Millions of India's numerous citizens still rely on agricultural products for their livelihood despite recent technological improvements. For millions of people, agriculture provides their primary source of income, and the majority of their crops depend on seasonal rainfall.

The temperature and rainfall, two essential climate study variables, are examined in depth in this article. Temperature and temperature variations have an effect on a number of hydrological processes, including rainfall [6]. These processes then influence temperature. Trend study of temperature, rainfall, and other climatic variables on various geographical scales can aid in the creation of future climate scenarios [2]. As a result, this study's objective is to examine how frequently it rains and how hot it gets in Bharuch, one of Gujarat's poorest districts. The seasonal trends of both parameters were looked at on an annual basis, and the monthly swings were generally predicted with the monsoon season (June–September) in mind. This requires an understanding of the local climate and rainfall patterns. Understanding the uncertainties associated with rainfall and temperature patterns would help the targeted region manage agricultural, irrigation, and other water-related activities more effectively.

2 Study Area and Data Source

2.1 Bharuch District

Bharuch is situated at 21.7° N 72.97 °E and is typically 15 m above sea level. Vadodara is located in the north, Narmada Vadodara is in the east, and Surat Vadodara is in the south. Its western border is formed by the Gulf of Khambhat.

In Bharuch, which has a tropical savanna environment, the Arabian Sea has a significant role in controlling the weather. Early March through the end of June marks the start of the summer season. With maximum average temperatures of roughly 40 °C, April and May are the warmest months.

With an average rainfall of 800 mm, the monsoon season starts in late June and lasts until September (31 in.). During these months, the highest temperature is typically around 32 °C (90 °F). Up until late November, when winter officially starts, the temperature starts to rise again in October. December to late February is considered to be winter, when temperatures often hover around 23 °C (73 °F).

2.2 Data Collection

From 1980 to 2017, the India Meteorological Department in Pune provides monthly average observed station data for rainfall, maximum and lowest temperatures for the district of Bharuch (37 years). The missing values were imputed using the "Imputation (most frequent)" approach, a statistical technique for replacing missing data with the most frequent values within each column.

Trend is defined as a series' overall movement over a lengthy period of time or a long-term change in the dependent variable [7]. The temporal resolution of rainfall and how it relates to temperature have an impact on trend. To evaluate the importance of temperature and rainfall patterns, statistical techniques like regression analysis and the coefficient of determination R2 are applied. The Mann–Kendall (M–K) trend test was used to identify and assess the trend, and the least squares approach was used to determine the slope of the regression line. To analyze the link, the average, standard deviation, and coefficient of variation (CV) of rainfall and temperatures were calculated (Fig. 1).

2.3 Mann–Kendall's Test

A non-parametric statistical test called the M–K test is used to analyze trends in time series data from climatology and hydrology. Since Mann first established the test in 1945, environmental time series have routinely employed it. The decision to take this test has two benefits. The data do not have to be evenly distributed because it is

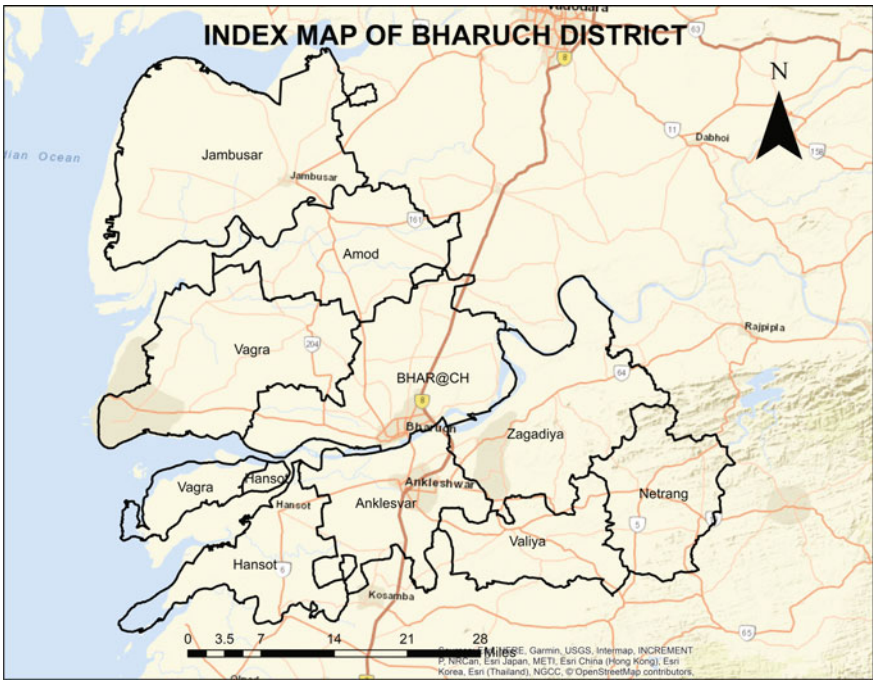

Fig. 1 Bharuch district index map

a non-parametric test. Due to inhomogeneous time series, the test is less sensitive to unexpected breakdowns. The null hypothesis H0 states that there is no trend in this test (the data are independent and randomly ordered). Comparing this to alternative hypothesis H1, which asserts that a trend exists, the M–K statistic is calculated using the formula shown below:

$$\mathbf{S} = \sum_{k=1}^{n-1} \sum_{j=k+1}^{n} \operatorname{sgn}(xj - xk).$$

The trend test is performed on a time series *Xk*, which is ranked from $k = 1, 2, 3, \ldots, n1$ and $j = I + 1, i + 2, i + 3 \ldots n$. As a reference point, each of the data points *xj* is used.

$$\begin{aligned} \operatorname{sgn}(xj - xk) &= 1 \text{ if } xj - xk > 0 \\ &= 0 \text{ if } xj - xk = 0 \\ &= -1 \text{ if } xj - xk < 0. \end{aligned}$$

This particular test was computed using the XLSTAT 2017 application. Indicating an upward tendency is a very high positive *S* number, while a very low negative value

suggests a downward trend. In order to establish if a trend is statistically significant, the Z value is utilized.

2.4 Sen's Slope Estimator Test

A non-parametric technique for determining the size of a time series trend is Sen's estimate. Sen's non-parametric method was used in the test to establish the true slope of an existing trend, such as the rate of change over time, using the XLSTAT 2017 program. A positive Sen's slope value denotes an upward or developing trend in the time series, whereas a negative value denotes a downward or declining trend.

3 Results and Discussions

3.1 Results

According to a trend analysis of numerous studies, non-parametric [1] approaches are widely employed, with the M–K test [8] being one of the best among them and favored by many researchers [3]. Table 1 discusses the descriptive statistics for rainfall, such as mean, SD, coefficient of variation, kurtosis, and skewness. The gathered data show that the coefficient of variation (CV) of the monthly average rainfall ranges from 55 to 358%. February was the month with the highest kurtosis coefficient at 29.47 and the highest skewness at 5.45. The research area has the maximum rain during the monsoon season, which lasts from June to September, as seen by the monthly rainfall pattern shown in Figs. 2 and 3.

Tables 2 and 3 contain the recorded temperature data as well as descriptive statistics for the highest and lowest temperatures, including mean, standard deviation, and coefficient of variation, skewness, and kurtosis, respectively. Even while the CV for the highest and lowest temperatures is less than that for rainfall, the skewness and kurtosis values show more extreme variation. The findings from the analysis of the observed data for the years 1981–2020 are displayed in Figs. 4 and 5. Both of these numbers unequivocally demonstrate that the highest and lowest temperatures are greater in the months preceding monsoons and lower during monsoon seasons. The maximum and lowest temperature data from 1981 to 2020 were analyzed for seasonal changes, although these trends are not very important in terms of temperature. The examination of the highest and lowest temperature trends is shown in Figs. 6 and 7, respectively.

The M–K test is also used in trend analysis. The M–K test is a non-parametric technique for determining if a variable displays a monotonic upward or decreasing trend over time. The statistics (Table 1) show that there is no trend in any of the research areas' seasonal rainfall patterns. Over the period 1981–2019, rainfall patterns are not

Table 1 Descriptive statistics for monthly rainfall data

Statistic	January	February	March	April	May	June	July	August	September	October	November	December
Number of observations	39.00	39.00	39.00	39.00	39.00	39.00	39.00	39.00	39.00	39.00	39.00	39.00
Minimum	0.00	0.00	0.00	0.00	0.00	6.77	18.45	5.46	1.58	0.13	0.00	0.00
Maximum	13.76	37.59	23.26	12.10	63.38	962.19	1007.06	793.96	491.63	172.81	69.72	32.27
First quartile	0.01	0.01	0.01	0.08	0.22	81.31	253.75	169.39	74.61	14.54	0.08	0.01
Median	0.07	0.08	0.07	0.62	1.50	157.96	476.77	265.18	176.39	24.21	0.71	0.04
Third quartile	1.02	0.93	0.64	1.94	5.37	355.69	651.18	384.50	295.46	66.27	4.13	0.67
Mean	1.34	1.70	1.39	1.53	7.67	240.91	455.32	296.65	189.63	42.64	7.74	1.68
Variance ($n-1$)	8.99	37.17	15.96	6.37	216.79	45,682.55	63,848.68	34,537.99	19,385.95	1999.07	278.68	28.62
Standard deviation ($n-1$)	3.00	6.10	4.00	2.52	14.72	213.73	252.68	185.84	139.23	44.71	16.69	5.35
Skewness (Pearson)	2.97	5.45	4.55	2.76	2.47	1.40	0.09	0.89	0.35	1.52	2.78	5.03
Kurtosis (Pearson)	8.24	29.47	21.58	7.96	5.29	1.92	− 0.78	0.55	− 0.95	1.82	7.09	25.95

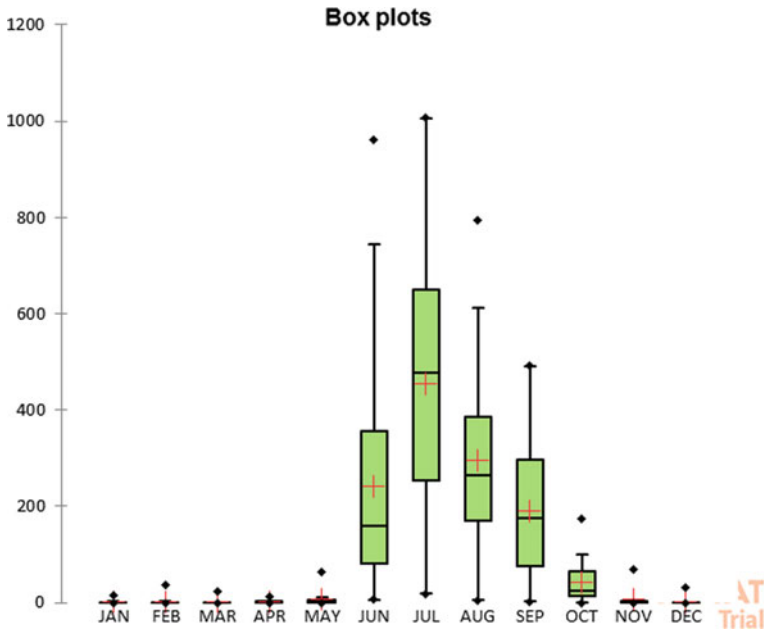

Fig. 2 Box and whisker plot of monthly rainfall data (mm)

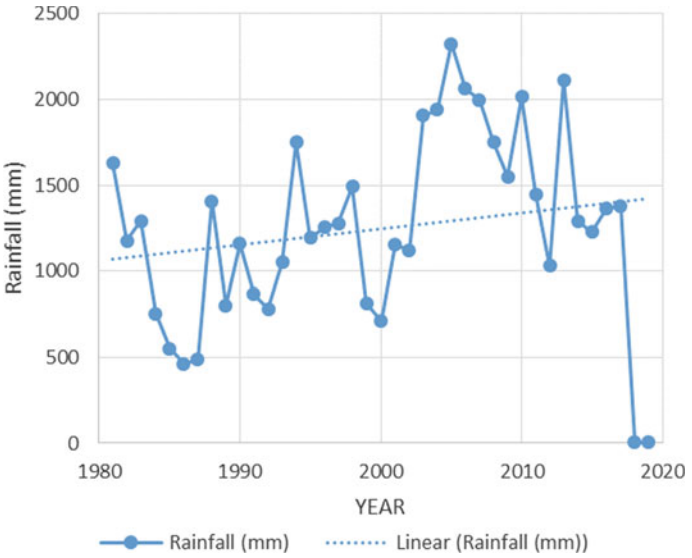

Fig. 3 Trend analysis of rainfall data

Table 2 Descriptive analysis of maximum temperature

Statistic	Number of observations	Minimum	Maximum	First quartile	Median	Third quartile	Mean	Variance (*n*)	Standard deviation (*n*)	Variation coefficient (*n*)	Skewness (Pearson)	Kurtosis (Pearson)
January	40.0	26.2	29.7	27.3	27.7	28.2	27.8	0.6	0.8	0.0	0.4	0.4
February	40.0	27.2	31.3	28.2	28.8	29.2	28.8	0.7	0.8	0.0	0.4	0.4
March	40.0	30.0	33.4	31.0	31.4	32.1	31.5	0.6	0.8	0.0	0.3	– 0.4
April	40.0	31.7	35.3	33.1	33.4	33.8	33.4	0.5	0.7	0.0	-0.3	1.1
May	40.0	32.0	35.0	33.3	33.6	34.0	33.6	0.4	0.6	0.0	– 0.2	0.6
June	40.0	30.0	33.0	31.2	31.7	32.1	31.6	0.5	0.7	0.0	– 0.3	– 0.3
July	40.0	27.9	30.6	28.7	29.1	29.4	29.1	0.3	0.5	0.0	0.3	0.7
August	40.0	27.3	29.8	27.9	28.3	28.6	28.3	0.2	0.5	0.0	0.5	0.8
September	40.0	28.1	30.9	28.7	29.0	29.4	29.1	0.3	0.6	0.0	0.8	0.8
October	40.0	29.1	33.7	30.1	30.9	31.6	31.0	1.3	1.2	0.0	0.6	– 0.4
November	40.0	28.6	32.8	29.9	30.7	31.7	30.7	1.2	1.1	0.0	0.0	– 0.8
December	40.0	26.6	30.5	28.6	29.1	29.5	29.0	0.7	0.8	0.0	– 0.7	0.3
Winter	40.0	27.4	29.4	27.9	28.4	28.7	28.4	0.3	0.6	0.0	0.1	– 0.8
Spring	40.0	28.7	31.3	29.6	30.2	30.6	30.2	0.4	0.6	0.0	-0.1	– 0.7
Summer	40.0	31.8	33.9	32.4	32.9	33.2	32.9	0.2	0.5	0.0	– 0.1	– 0.5
Monsoon	40.0	27.8	30.2	28.4	28.6	28.9	28.7	0.2	0.5	0.0	0.6	1.5
Autumn	40.0	28.9	32.4	29.6	30.2	30.8	30.3	0.7	0.8	0.0	0.6	– 0.1

Table 3 Descriptive statistics of minimum temperature

Statistic	Number of observations	Minimum	Maximum	First quartile	Median	Third quartile	Mean	Variance (*n*)	Standard deviation (*n*)	Variation coefficient (*n*)	Skewness (Pearson)	Kurtosis (Pearson)
January	39.0	16.9	20.7	18.4	18.9	19.5	18.9	0.7	0.8	0.0	− 0.1	− 0.2
February	39.0	17.4	21.6	19.5	19.8	20.5	19.9	0.9	0.9	0.0	− 0.4	0.3
March	39.0	21.1	23.7	22.2	22.6	23.0	22.6	0.4	0.6	0.0	− 0.1	− 0.4
April	39.0	23.7	26.5	25.0	25.3	25.6	25.3	0.3	0.6	0.0	− 0.3	0.4
May	39.0	26.5	28.6	27.0	27.4	27.7	27.4	0.2	0.5	0.0	0.3	− 0.3
June	39.0	27.2	28.6	27.8	28.0	28.3	28.0	0.1	0.3	0.0	− 0.2	− 0.9
July	39.0	26.2	27.6	26.6	26.9	27.2	26.9	0.1	0.4	0.0	0.0	− 1.0
August	39.0	25.2	27.2	25.8	26.0	26.2	26.0	0.2	0.4	0.0	0.3	0.4
September	39.0	24.7	26.8	25.6	25.9	26.2	25.9	0.2	0.5	0.0	− 0.5	0.0
October	39.0	23.5	26.4	24.5	25.0	25.4	25.0	0.4	0.7	0.0	0.0	− 0.6
November	39.0	19.9	24.7	21.9	22.8	23.6	22.6	1.3	1.1	0.1	− 0.3	− 0.5
December	39.0	18.6	21.8	19.6	20.4	20.9	20.3	0.6	0.8	0.0	− 0.2	− 0.9
Winter	39.0	18.4	20.8	19.2	19.6	19.9	19.6	0.3	0.5	0.0	0.0	− 0.3
Spring	39.0	19.7	22.5	21.0	21.2	21.8	21.2	0.4	0.7	0.0	− 0.4	− 0.1
Summer	39.0	26.1	27.9	26.7	26.8	27.2	26.9	0.1	0.4	0.0	0.2	− 0.1
Monsoon	39.0	25.8	27.4	26.2	26.4	26.7	26.4	0.1	0.4	0.0	0.2	− 0.5
Autumn	39.0	23.4	25.7	24.2	24.4	24.9	24.5	0.3	0.5	0.0	0.1	− 0.6

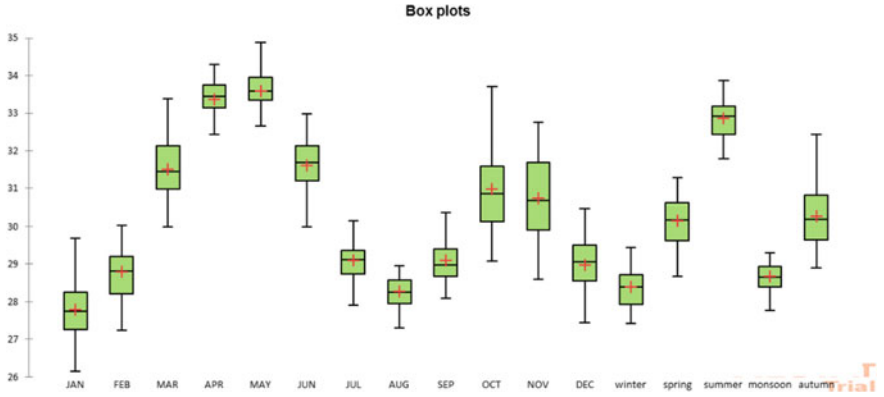

Fig. 4 Box and whisker plot of monthly maximum temperature (°C)

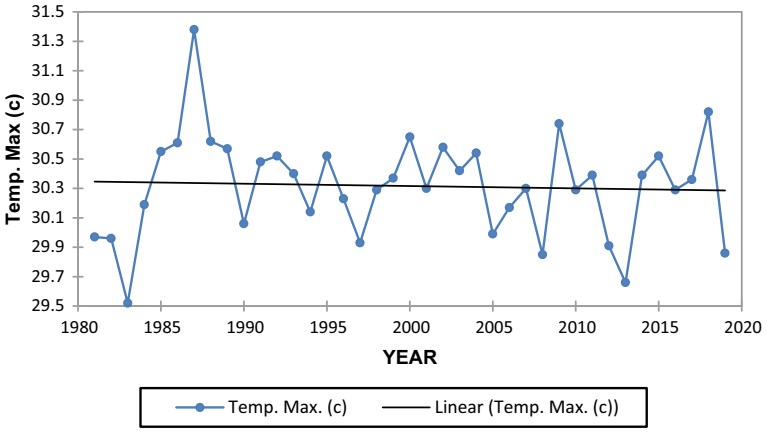

Fig. 5 Trend analysis of monthly maximum temperature (°C)

statistically significant, and the finding is not significant at the 95% confidence level. Averaged over all of the recorded periods, the greatest temperature trend demonstrated a slight warming or increasing tendency (Sen's slope $= -1.621$), while the lowest temperature trend showed a cooling tendency (Sen's slope $= 0.1498$). However, the lowest temperature trend analysis result, as opposed to the highest temperature trend analysis result, is not statistically significant at the 95% level of confidence.

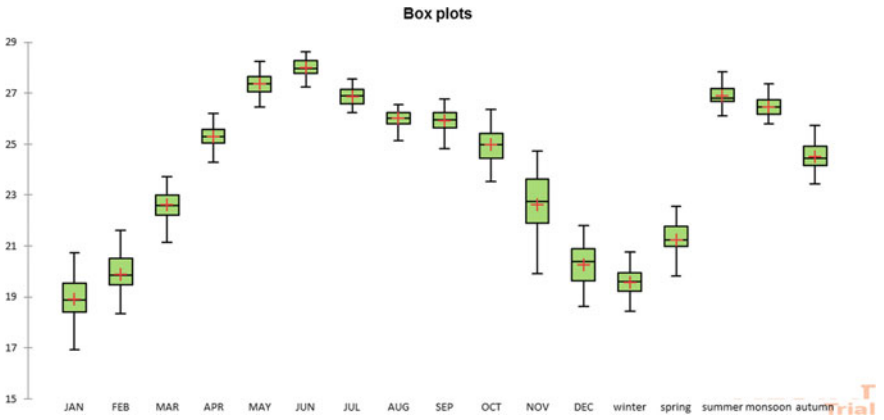

Fig. 6 Box and whisker plot of monthly minimum temperature (°C)

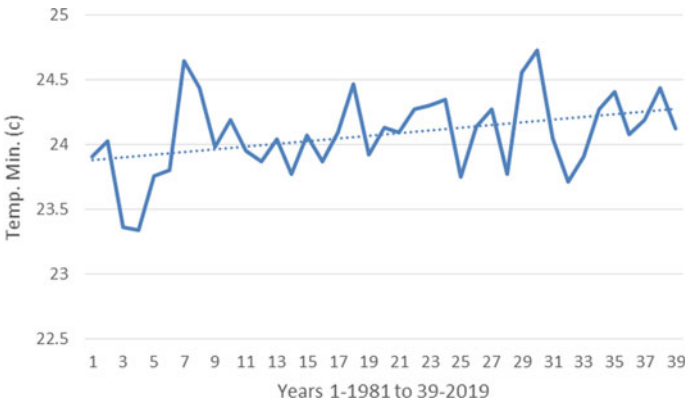

Fig. 7 Trend analysis of monthly minimum temperature (°C)

3.2 Discussion

Researchers and policymakers must take into account the erratic nature of meteorological conditions when making decisions because rainfall has such a significant impact on how water is used in various locations. The earliest method for displaying changes in monthly rainfall was box and whisker graphs. Contrary to more exhaustive representations like the histogram, box and whisker plots [9] feature a compact structure that enables side-by-side comparisons of different datasets [6]. These graphs provide an easily understandable visual representation of the statistical distribution. A horizontal line represents the box and whisker figure's median, and top and bottom horizontal lines represent the interquartile range (shown by the box). The 25th and 75th percentiles are shown by the horizontal lines at the bottom and top of the boxes, respectively. Vertical lines display outside ranges [7]. The distribution may

be skewed if the median line is greatly deviated from the center. The length of each whisker, which reflects the dataset's outer range (10th–25th percentiles and 75th–90th percentiles), displays the interquartile range (box), which denotes the dataset's middle 50% relative dispersion. It is clear that the dataset is not normally distributed because the vast majority of the values is in the top whisker, or fourth quartile.

Low (CV < 20%), moderate (20% < CV < 30%), high (CV > 30%), extremely high (CV > 40%), and CV > 70% are the categories used to categorize the degree of variability. CV > 70% indicates exceptionally high interannual variability of rainfall. According to the data, it was discovered that every month had a CV of at least 30%, emphasizing the region's substantial precipitation variability. According to the statistics, the amount of rainfall in the area varies greatly.

Since the kurtosis values and the skewness value are lower in the monsoon months, it is evident from the kurtosis values' analysis that the dataset is light tailed and exhibits a symmetric pattern (July, August, and September). In other words, the area under investigation experiences symmetrical patterns of rainfall throughout the monsoon season. The post- and pre-monsoon months, however, exhibit a high kurtosis value in the dataset, showing that rainfall during these months is strongly tailed, reflecting the occurrence of outliers or extreme values. The studied area's rainfall is fundamentally uneven before and after the monsoon season. Understanding the behavior of surface air temperature, which can change geographically and temporally on local, regional, and global scales, is essential for understanding climatic variability. One of the most crucial variables in forecasting weather and climate is surface air temperature [10]. Despite the plethora of evidence for rising global temperatures, precise temporal trend forecasting remains difficult [8]. Similar to how air temperature impacts the water cycle in the research area, a thorough investigation of the nature of its occurrence is necessary. The monthly maximum and lowest temperatures show a falling tendency even though the study region experiences its highest rainfall in July, August, and September. Additionally, the temperature rises both before and after the monsoon season. Figure 6 displays the seasonal mean maximum temperature and its trend over the time period under consideration.

4 Conclusions

Gujarat has a long history of climatic change and unpredictability, and the Bharuch region is no exception. In the study locations, there are frequent climatic variations or shifts. Climate change exacerbates already existing social and economic problems in this region since communities there rely mostly on resources that are climate-sensitive, particularly, wet agriculture. Reduced societal, economic, and personal losses may result from improved ability to adjust to severe future climatic unpredictability. Since more than 80% of agriculture depends on rain, rainfall and temperature are the two primary climatic variables in the area. The current study looked at weather data for the Gujarati city of Bharuch. The time series was examined using Sen's slope estimator and the non-parametric M–K test, two well-known methods

for trend analysis. The variability analysis, monthly rainfall, maximum temperature, and minimum temperature are all represented using box and whisker graphs.

The plots show that the monsoonal months, from June through September, receive the most rainfall, despite the fact that the variation in maximum and minimum temperatures is roughly the same for all months. To suggest that because rainfall is the main factor driving agricultural growth in the studied region, its extreme occurrence during monsoon, as well as post- and pre-monsoon months, is crucial to growth. An underdeveloped region, such as Bharuch district, is particularly vulnerable to significant influences of climate variability, particularly rainfall variability.

The inquiry has shown that the maximum and lowest temperatures in the research region do not vary much over the course of the year, and as a result, temperature variations are not anticipated to have an impact on agricultural output. The parties involved should consider rainfall variability and general temperature variance in order to plan for climate change.

Acknowledgements The India Meteorological Department in Pune provided the information we needed for our study, and we appreciate their quick response. The tutorials and user-friendliness of programs like ArcGIS 10.2, R, and XLSTAT, which were used to make the graphs in this piece, deserve praise. The resources and responsiveness of the library and computer center of the Sardar Vallabhbhai National Institute of Technology, Surat, would definitely be lauded.

References

1. Parajka J, Merz R, Blöschl G (2005) A comparison of regionalisation methods for catchment model parameters. Hydrol Earth Syst Sci 9:157–171
2. Oni SK, Futter MN, Ledesma JLJ, Teutschbein C, Buttle J, Laudon H. Using hydroclimatic extremes to guide future 1 hydrologic predictions. Hydrol Earth Syst Sci Discuss. https://doi.org/10.5194/hess-2016-7
3. Kim J-B, Bae D-H. Intensification characteristics of hydroclimatic extremes in the Asia monsoon region under 1.5 and 2.0 °C of global warming. Hydrol Earth Syst Sci
4. Pechlivanidis IG, Arheimer B, Donnelly C, Hundecha Y, Huang S, Aich V, Samaniego L, Eisner S, Shi P (2017) Analysis of hydrological extremes at different hydro-climatic regimes under present and future conditions. Climatic Change 141:467–481. https://doi.org/10.1007/s10584-016-1723-0.
5. Corzo Perez GA, Diaz V, Laverde M (2018) Spatiotemporal hydrological analysis. Int J Hydrol 2(1)
6. Fang J, Kong F, Fang J, Zhao L. Observed changes in hydrological extremes and flood disaster in Yangtze River Basin: spatial–temporal variability and climate change impacts. Springer
7. Romanowicz RJ et al. Climate change impact on hydrological extremes: preliminary results from the Polish-Norwegian project. Institute of Geophysics, Polish Academy of Sciences
8. Hartmann A, Mudarra M, Andreo B, Martin A, Wagener T, Lange J (2014) Modeling spatiotemporal impacts of hydroclimatic extremes on groundwater recharge at a Mediterranean karst aquifer. American Geophysical Union
9. Hao Z, Singh VP, Hao F (2018) Compound extremes in hydroclimatology: a review. Water 10:718
10. Pathak S, Ojha CSP, Garg RD, Liu M, Jato-Espino D, Singh RP (2020) Spatiotemporal analysis of water resources in the Haridwar Region of Uttarakhand, India. Sustainability 12:8449

Evaluation of Impacts of Climate Change on Temperature Variation: The Case Study of Amaravati City, India

Lakshmi Raghu Nagendra Prasad Rentachintala, Muni Reddy Mutukuru Gangireddy, and Pranab Kumar Mohapatra

Abstract Study on extremes of climate is necessary as they impact distressingly on life and economy. A necessity exists to know effect of change in climate on temperature for a proposed city. Thus, in the present study, the climate change impacts on temperature are assessed for the proposed Amaravati city, Andhra Pradesh state, India. Trends of temperature variations during the time period, 1981–2021, are found by considering temperature time series as daily data from POWER LaRC NASA portal. Mann–Kendall [M–K] test and Sen's slope estimator are applied to perform trend analysis of temperature because of climate change. Various revised versions of Mann–Kendall (M–K) test and R are applied to analyze trend as the temperature time series is significantly autocorrelated. The trend analysis shows that the result of climate change on minimum temperature in the considered study area is about 1.12e − 02 °C/year with increasing trend and is about 8.38e − 03 °C/year with increasing trend for maximum temperature. The findings from the present study may aid to find temperature impacts because of climate change for any existing and/or proposed city for transforming as a smart city.

L. R. N. P. Rentachintala (✉)
Department of Civil Engineering, Bapatla Engineering College, GBC Road, Mahatmajipuram, Bapatla 522102, Andhra Pradesh, India
e-mail: lrnagendraprasad.rentachintala@becbapatla.ac.in

M. R. M. Gangireddy
Department of Civil Engineering, A.U. College of Engineering (A), Andhra University, Visakhapatnam 530003, Andhra Pradesh, India
e-mail: dr.mgmreddy@andhrauniversity.edu.in

P. K. Mohapatra
Department of Civil Engineering, Indian Institute of Technology Gandhinagar, Palaj, Gandhinagar 382355, Gujarat, India
e-mail: pranabm@iitgn.ac.in

P. V. Timbadiya et al. (eds.), *Climate Change Impact on Water Resources*, Lecture Notes in Civil Engineering 313, https://doi.org/10.1007/978-981-19-8524-9_19

Keywords Climate change · Temperature · Mann–Kendall test · Sen's slope · R programming

1 Introduction

There is a continuously increasing insight on the consequences of climate change on diverse parameters which can affect hydrologic cycle. Also, there is a need to determine the impacts of different parameters caused by climate change. Extreme climatic conditions such as heat waves and rise of global mean surface temperature are owing to climate change effect on well-being of community [12]. A requirement exists to know impact from climate change occurring to temperature variation, especially on urban areas with more population.

Thus, the current study is intended to study outcomes of climate change affecting temperature for the study area, proposed Amaravati city, India.

2 Climate Change Effect Evaluation Studies

The climate change effects on spread of Himalayan pheasants were investigated [5]. It was observed that Himalayan pheasants shifting would occur under climate scenarios in the future [5]. The climate change impacts which are significant in urban regions and strategies of adaptation were reviewed for climate change to build further robust urban environments [19]. Aparicio et al. [2] assessed that the annual average temperatures projected showed a projected rise of 1.5–3.3 °C as climate change impact. Dhar and Mazumdar [7] found that parameters considered illustrate an increasing trend over time period under various climate change scenarios. Wang et al. [22] studied on hydrologic behavior of a river basin in various climate change and land-use scenarios and determined that the runoff reduces with increase of mean temperature. Fontaine et al. [8] observed that increase of CO_2 in atmosphere dampens loss of water yield because of rise in temperature. Larbi et al. [12] found that various indices of temperature indicate an increasing trend. Mohammad and Goswami [15] assessed that temperature trend was in a decreasing trend for northwestern part cities and with rising trend for southeastern part cities in India.

Yue and Pilon [25] used Monte Carlo simulation to weigh against various statistical tests' power, i.e., the parametric *t*-test, the Mann–Kendall (M–K), bootstrap-based slope (BS-slope), and bootstrap-based M–K (BS-M–K) tests.

3 Objectives of the Present Study

The current study is determined to find climate change effects acting on temperature for the study area. Also, the considered study is set an objective to determine effect of climate change on maximum and minimum temperatures for the considered study area.

4 Study Area

Amaravati city is situated on the Krishna River bank, district Guntur. Proposed Amaravati city is of 217.50 km^2 area and it is positioned at 16.51°N latitude and 80.52°E longitude (Figs. 1 and 2).

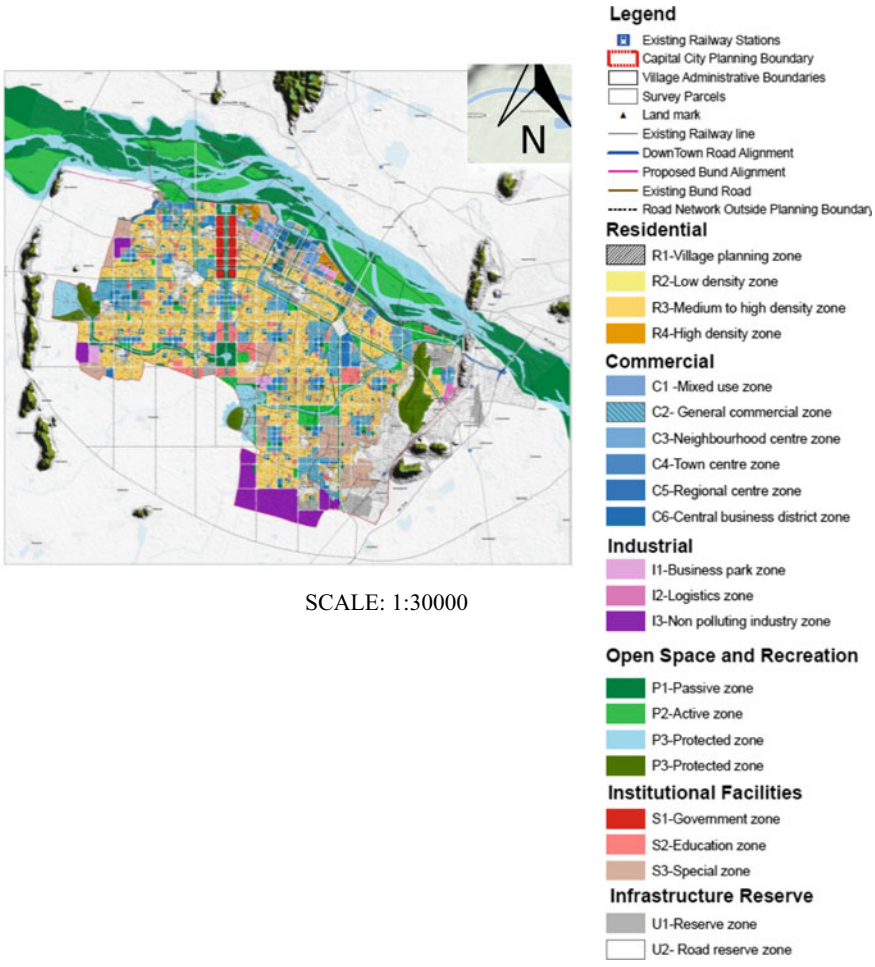

Fig. 1 Amaravati city in detail master plan (*source* AP CRDA/AMRDA)

Fig. 2 Index map

5 Methodology

Mann–Kendall test [10, 14] and Sen's slope estimator [20] are being commonly applied for analysis of trend of a parameter due to change in climate.

5.1 Mann–Kendall Test

This test is for testing S statistic which is defined by

$$S = \sum_{i=1}^{n-1} \sum_{j=i+1}^{n} \operatorname{sgn}(x_j - x_i), \tag{1}$$

where

$x_1, x_2 \ldots x_n$ are n dataset,

x_i and x_j are data values at time, i and j, respectively.

$$\operatorname{sgn}(x_j - x_i) = \begin{cases} -1 \text{ if } (x_j - x_i) < 0 \\ 0 \quad \text{if } (x_j - x_i) = 0 \\ 1 \quad \text{if } (x_j - x_i) > 0 \end{cases}, \tag{2}$$

$$\operatorname{Var}(S) = \frac{n(n-1)(2n+5) - \sum_{i=1}^{m} t_i(t_i-1)(2t_i+5)}{18}, \tag{3}$$

where, n is data points number, m is the groups tied number, and t_i indicates ties number of extent i.

M–K statistic standard Z is defined below:

$$Z = \begin{cases} \frac{S-1}{\sqrt{\operatorname{Var}(S)}} \text{ if } S > 0 \\ 0 \quad \text{if } S = 0 \\ \frac{S+1}{\sqrt{\operatorname{Var}(S)}} \text{ if } S < 0 \end{cases}. \tag{4}$$

If Z is positive, then trend is an upward trend, and if Z is negative, then it signifies a downward trend.

$$\text{Significance Level, } p = 0.5 - \varphi|Z| \tag{5}$$

where, $\phi()$ specifies CDF, the cumulative distribution function of a standard normal variate. At 0.1 value significance level, if $p \leq 0.1$, the trend is viewed as statistically significant [6].

5.2 Sen's Slope Estimator [20]

Method of Sen's slope estimate is a non-parametric method to find the magnitude of trend as trend slope. In a time series given, $x_i = x_1, x_2 \ldots x_n$, with N pairs data, the slope is found as

$$\beta_j = \frac{x_j - x_k}{j - k}, \forall k \leq j, i = 1, 2 \ldots N \tag{6}$$

Median of values N of β_i gives Sen's slope estimator, β.

$$\beta = \begin{cases} \beta_{\frac{N+1}{2}} & \text{if } N \text{ is odd} \\ \frac{1}{2}\left[\beta_{\frac{N}{2}} + \beta_{\frac{N+2}{2}}\right] & \text{if } N \text{ is even} \end{cases} \tag{7}$$

5.3 Autocorrelation

When a time series is serially correlated or significantly autocorrelated, modified [revised] version(s) of Mann–Kendall test for trend need to be used.

In a time series $x_i = x_1, x_2 \ldots x_n$, lag-1 autocorrelation or serial correlation coefficient (r_1) is found as [11, 18]

$$r1 = \frac{\frac{1}{n-1}\sum_{i=1}^{n-1}(x_i - E(x_i)).(x_{i+1} - E(x_i))}{\frac{1}{n}\sum_{i=1}^{n}(x_i - E(x_i))^2}, \tag{8}$$

where, $E(x_i)$ is sample average and n is sample size.

$$E(x_i) = \frac{1}{n}\sum_{i=1}^{n} x_i. \tag{9}$$

The probability limits of r_1 on the correlogram of a series independent are [1]

$$r_1 = \left\{ \begin{array}{ll} \frac{-1 \pm 1.645\sqrt{n-2}}{n-1} & \text{for the one - tailed test} \\ \frac{-1 \pm 1.96\sqrt{n-2}}{n-1} & \text{for the two - tailed test.} \end{array} \right\} \tag{10}$$

6 R Programming

RStudio has built up as Integrated Development Environment [IDE] of R, a programming tool to carry statistical analysis [16, 17, 23].

7 Considered Data

Temperature time series based on satellite observations [½ × ½ degree datasets] is considered from POWER LaRC NASA portal for trend analysis [4, 12]. Temperature daily data from POWR LaRC NASA portal are obtained for the period from January 3, 1981, to June 30, 2021, for the considered study area for trend analysis.

8 Results and Discussion

As time series of temperature for each time period related to the considered study area is significantly autocorrelated, hence, revised Mann–Kendall test is to be adapted

for analysis of trend of this change in climate study. Different versions available are applied for Mann–Kendall test amended version (Table 1).

Few of the trend results are insignificant and few are significant at 95% confidence level for temperature, minimum temperature, and maximum temperature time series (Tables 2, 3 and 4).

Average Sen's slope for temperature trend = 6.31e − 06 °C per year with increasing trend. Sen's slope value remains same from both the trend tests, i.e., amended Mann–Kendall test with the use of the Rao and Hamed [9] and Wang and Yue [24] variance correction approaches. Test static, Z, and correlation coefficient remain same for minimum and maximum temperatures.

Average Sen's slope for minimum temperature = 1.12e − 02 °C per year with increasing trend.

Sen's slope obtained for the period 1981–1990 remains same as − 3.20e − 05 °C/year for all trend tests for minimum temperature (Table 3). Sen's slope value remains same for all tests of trend except bootstrapped M–K test of trend with bias-corrected pre-whitening (optional) for simulation periods, 1991–2000, 2001–2010, 2011–2020, and 2020–2021. Sen's slope varies from 1.93e − 06 °C/year to − 6.33e − 06 °C/year for minimum temperature (Table 3). Spearman's test static varies from − 0.64 to 11.54 for minimum temperature (Table 3).

Average Sen's slope for maximum temperature = 8.38e − 03 °C per year with increasing trend.

Sen's slope value remains same for all trend tests except for bootstrapped M–K test of trend with bias-corrected pre-whitening (optional) for each simulation period for maximum temperature (Table 4). Sen's slope value varies from − 2.66e − 05 °C/year for the period 2001–2010 to 5.71e − 02 °C/year for the period 2020–2021 (Table 4). Test static of Spearman's rank correlation test varies from − 7.53 to 7.08 for maximum temperature (Table 4).

Figure 3 shows variations of temperature, minimum temperature, and maximum temperature with time as time series plots for the considered time period January 3, 1981, to June 20, 2021, within the study area. Maximum temperature varies from 48.25 to 21.92 °C, while minimum temperature varies from 33.83 to 10.22 °C during 1981–2021 period (Fig. 3). Temperature varies from 39.89 to 17.56 °C during 1981–2021 period (Fig. 3). Figures 4 and 5 present Sen's slope profile within various time periods starting from 1981–1990 to 2011–2020 of extreme temperatures from

Table 1 Significant autocorrelation check

Temperature type	Higher limit	Lag-1 autocorrelation coefficient	Lesser limit	Occurrence of significant autocorrelation
Temperature	0.06	0.98	− 0.06	True
Minimum temperature	0.06	0.97	− 0.06	True
Maximum temperature	0.06	0.95	− 0.06	True

Table 2 Temperature-wise trend results

Type of temperature	Time period	Trend test	*Z*	Sen's slope	Correlation coefficient
Temperature	1981–2021	Revised M–K test applying the Rao and Hamed [9] correction approach of variance	5.36e − 01	6.31e − 06	
		Revised M–K test applying the Wang and Yue [24] correction approach of variance	8.63e − 01	6.31e − 06	
		Spearman's test [of rank correlation] [Spearman [21], Lehman [13]]	1.09		0.009
Minimum temperature	1981–2021	Spearman's test	− 1.19		− 0.01
Maximum temperature	1981–2021	Spearman's test	− 1.19		− 0.01

trend analysis applying numerous modified versions of Mann–Kendall test of trend to find change in climate effects on temperature to the proposed city. Sen's slope of temperature maximum trends varies from − 5.14e − 04 to − 2.66e − 05 of 2001–2010 time period (Fig. 4). Sen's slope for minimum temperature trends varies from 1.93e − 06 of time period 2011–2020 to − 6.33e − 06 of time period 2001–2010 (Fig. 5). The obtained trend result for minimum temperature as 1.12e − 02 °C per year increasing trend is in excellent agreement with earlier studies on a regional basis for Southern India as 1.06e − 02 °C per year rising trend for temperature [3].

9 Conclusions

In the current study, the climate change impacts on temperature for the study area are assessed for the time period 1981–2021. The trend analysis results indicate that the temperature is assessed as having a trend at 6.31e − 06 °C per year with increasing trend. Also, the minimum temperature is determined to have a trend of 1.12e − 02 °C per year with increasing trend. Further, the maximum temperature is determined to have a trend of 8.38e − 03 °C per year with increasing trend. The findings from the present study can assist for assessment of climate change impacts on temperature for any existing and/or proposed city for longer duration.

Table 3 Minimum temperature trend results

Time period	Test for trend	*Z*	Sen's slope
1981–1990	Mann–Kendall [M–K] test of trend without modifications	− 6.13e − 01	− 3.20e − 05
	Bootstrapped M–K test of trend with bias-corrected pre-whitening (optional)	− 6.13e − 01	− 3.20e − 05
	Revised M–K test applying the Rao and Hamed [9] correction approach of variance	− 2.69e − 01	− 3.20e − 05
	Amended M–K test with the use of the Wang and Yue [24] correction approach of variance	− 4.80e − 01	− 3.20e − 05
	Spearman's test [of rank correlation]	− 0.003	
1991–2000	M–K test of trend without modifications	4.88e − 01	2.67e − 05
	Bootstrapped M–K test of trend test with bias-corrected pre-whitening (optional)	4.11e − 01	5.39e − 06
	Modified M–K test applying the Rao and Hamed [9] correction approach of variance	1.93e − 01	2.67e − 05
	Amended M–K test with the use of the Wang and Yue [24] correction approach of variance	3.37e − 01	2.67e − 05
	Spearman's test	0.95	
2001–2010	M–K test of trend without modifications	− 1.02	− 5.49e − 05
	Bootstrapped M–K test of trend with bias-corrected pre-whitening (optional)	− 4.80e − 01	− 6.33e − 06
	Amended M–K test applying the Rao and Hamed [9] correction approach of variance	− 4.09e − 01	− 5.49e − 05
	Modified M–K test with the use of the Wang and Yue [24] correction approach of variance	− 6.87e − 01	− 5.49e − 05
	Spearman's test	− 0.64	
2011–2020	M–K test of trend without modifications	1.74e + 00	9.07e − 05
	Bootstrapped M–K trend test with bias-corrected pre-whitening (optional)	1.45e − 01	1.93e − 06
	Revised M–K test applying the Rao and Hamed [9] correction approach of variance	7.65e − 01	9.07e − 05
	Modified M–K test with the use of the Wang and Yue [24] correction approach of variance	1.35e + 00	9.07e − 05
	Spearman's test	2.23	
2020–2021	M–K test of trend without modifications	1.38e + 01	7.25e − 02
	Bootstrapped M–K trend test with bias-corrected pre-whitening (optional)	5.11e + 00	7.26e − 03
	Modified M–K test applying the Rao and Hamed [9] correction approach of variance	5.34e + 00	7.25e − 02
	Amended M–K test with the use of the Wang and Yue [24] correction approach of variance	9.11e + 00	7.25e − 02
	Spearman's test	11.54	

Table 4 Maximum temperature trend results

Time period	Test for trend	Z	Sen's slope
1981–1990	Mann–Kendall test of trend without modifications	− 1.66e + 00	− 1.09e − 04
	Bootstrapped M–K test of trend with bias-corrected pre-whitening (optional)	− 8.66e − 01	− 1.75e − 05
	Revised M–K test applying the Rao and Hamed [9] correction approach of variance	− 5.45e − 01	− 1.09e − 04
	Amended M–K test with the use of the Wang and Yue [24] correction approach of variance	− 9.86e − 01	− 1.09e − 04
	Spearman's test [of rank correlation]	− 1.88	
1991–2000	M–K trend test without modifications	− 2.46e + 00	− 1.77e − 04
	Bootstrapped M–K test of trend with bias-corrected pre-whitening (optional)	− 9.66e − 01	− 1.68e − 05
	Revised M–K test with the use of the Rao and Hamed [9] correction approach of variance	− 8.02e − 01	− 1.77e − 04
	Amended M–K test applying the Wang and Yue [24] correction approach of variance	− 1.49e + 00	− 1.77e − 04
	Spearman's test	− 2.29	
2001–2010	M–K Test of Trend without modifications	− 7.53e + 00	− 5.14e − 04
	Bootstrapped M–K trend test with bias corrected pre-whitening (optional)	− 1.40e + 00	− 2.66e − 05
	Amended M–K test applying the Rao and Hamed [9] correction approach of variance	− 2.39e + 00	− 5.14e − 04
	Modified M–K test applying the Wang and Yue [24] correction approach of variance	− 4.26e + 00	− 5.14e − 04
	Spearman's test	− 7.53	
2011–2020	M–K test of trend without modifications	− 6.08e + 00	− 3.93e − 04
	Bootstrapped M–K trend test with bias-corrected pre-whitening (optional)	− 1.40e + 00	− 2.56e − 05
	Revised M–K test applying the Rao and Hamed [9] correction approach of variance	− 1.56e + 00	− 3.93e − 04
	Modified M–K test with the use of the Wang and Yue [24] correction approach of variance	− 2.87e + 00	− 3.93e − 04
	Spearman's test	− 5.93	
2020–2021	M–K test of trend without modifications	7.92e + 00	5.71e − 02
	Bootstrapped M–K trend test with bias-corrected pre-whitening (optional)	− 1.11e − 01	− 1.15e − 04
	Modified M–K test applying the Rao and Hamed [9] correction approach of variance	1.88e + 00	5.71e − 02
	Amended Mann–Kendall test applying the Wang and Yue [24] correction approach of variance	3.05e + 00	5.71e − 02
	Spearman's test	7.08	

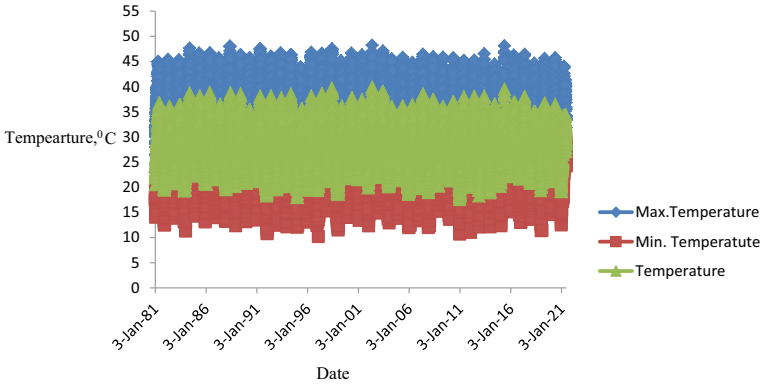

Fig. 3 Extreme temperature and temperature time series plots

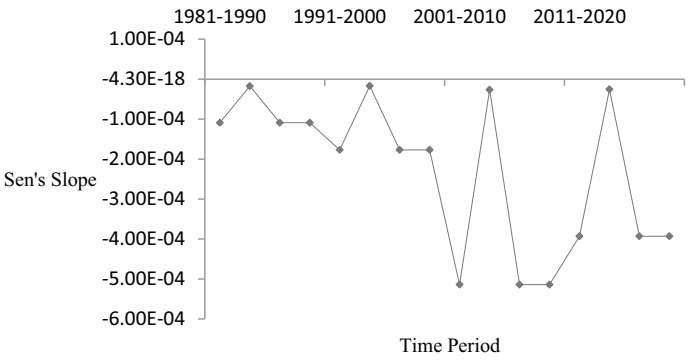

Fig. 4 Sen's slope for maximum temperature

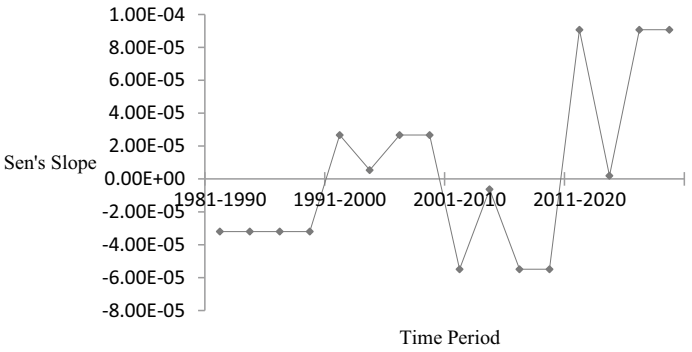

Fig. 5 Sen's slope for minimum temperature

References

1. Anderson RL (1942) Distribution of the serial correlation coefficient. Ann Math Stat 13:1–13
2. Aparicio JS et al (2017) Using SWAT and fuzzy TOPSIS to assess the impact of climate change in the headwaters of the Segura River Basin (SE Spain). Water 9:149. https://doi.org/10.3390/w9020149
3. Arora M, Goel NK, Singh P (2005) Evaluation of temperature trends over India. Hydrol Sci J 50(1):81–93. https://doi.org/10.1623/hysj.50.1.81.56330
4. Bodian A et al (2020) Trend and sensitivity analysis of reference evapotranspiration in the Senegal River basin using NASA Meteorological Data. Water 12(1957). https://doi.org/10.3390/w12071957
5. Chhetri B et al (2021) Modelling climate change impacts on distribution of Himalayan pheasants. Ecol Ind 123:107368
6. Coulibaly P, Shi X (2005) Identification of the effect of climate change on future design standards of drainage infrastructure in Ontario. Final Report McMaster University, Department of Civil Engineering, Ontario
7. Dhar S, Mazumdar A (2009) Hydrological modelling of the Kangsabati river under changed climate scenario: case study in India. Hydrol Process 23:2394–2406
8. Fontaine TA et al (2001) Hydrological response to climate change in the Black Hills of South Dakota, USA. Hydrol Sci J 46(1):27–40. https://doi.org/10.1080/02626660109492798
9. Hamed KH, Ramachandra Rao A (1998) A modified Mann-Kendall trend test for autocorrelated data. J Hydrol 204:182–196
10. Kendall MG (1955) Rank correlation methods. Charles Griffin & Company Limited, London, UK
11. Kendall MG, Stuart A (1968) The advanced theory of statistics: design and analysis, and time-series, 3rd edn. Charles Griffin & Company Limited, London, UK
12. Larbi I et al (2018) Spatio-temporal trend analysis of rainfall and temperature extremes in the Vea Catchment, Ghana. Climate 6(87). https://doi.org/10.3390/cli6040087
13. Lehman EL (1975) Nonparametric statistical methods based on ranks. Holden-Day Press, San Francisco, CA, USA
14. Mann HB (1945) Nonparametric tests against trend. Econometrica 13:245–259
15. Mohammad P, Goswami A (2019) Temperature and precipitation trend over 139 major Indian cities: an assessment over a century. Model Earth Syst Environ 5:1481–1493
16. Patakamuri SK, O'Brien N (2020) modifiedmk: modified versions of Mann Kendall and Spearman's Rho trend tests R package version 1.5.0. https://CRAN.R-project.org/package=modifiedmk
17. R Core Team (2020) R: a language and environment for statistical computing R foundation for statistical computing, Vienna, Austria. https://www.R-project.org/
18. Salas JD, Delleur JW, Yevjevich VM, Lane WL (1980) Applied modeling of hydrologic time series. Water Resources Publications, Littleton, Colorado, USA
19. Salimi M, Al-Ghamdi SG (2020) Climate change impacts on critical urban infrastructure and urban resiliency strategies for the Middle East. Sustain Cities Soc 54:101948
20. Sen PK (1968) Estimates of the regression coefficient based on Kendall's Tau. J Am Stat Assoc 63(324):1379–1389
21. Spearman C (1904) The proof and measurement of association between two things. Am J Psychol 15:72–101
22. Wang S et al (2008) Modelling hydrological response to different land use and climate change scenarios in the Zamu River basin of northwest China. Hydrol Process 22:2502–2510
23. Wickham H, Bryan J (2019) readxl: read excel files R package version 1.3.1. https://CRAN.R-project.org/package=readxl
24. Yue S, Wang CY (2004) The Mann-Kendall test modified by effective sample size to detect trend in serially correlated hydrological series. Water Resour Manage 18:201–218
25. Yue S, Pilon P (2004) A comparison of the power of the t test, Mann-Kendall and bootstrap tests for trend detection. Hydrol Sci J 49(1):21–37

Analysis of Rainfall Variability and Drought Over Bardoli Region

Priyank Patel, Darshan Mehta, Sahita Waikhom, and Kinjal Patel

Abstract Both climatology and hydrology are involved in trend analysis to investigate climate change scenarios and improve the efficiency of climate impact studies. The long-term variation in precipitation, temperature, humidity, evaporation, wind speed, and other meteorological factors is referred to as climatic variability for an area. The purpose of this study was to investigate and estimate the relevance of the possible trend of variables such as rainfall in the Mindhola River Basin in the Bardoli Taluka of Gujarat's Surat District. The study's objective is to look at rainfall variability in the Mindhola River Basin for the next 30 years, from 1990 to 2020. Innovative trend analysis (ITA) for rainfall variability in the Mindhola River Basin was used to conduct a rainfall trend analysis on a monthly, seasonal, and annual basis in this study. The ITA approach could discover some trends that the MK test would miss. This test was used to determine the magnitude and direction of a current trend over time. This will give an understanding about rainfall trends or changes. This study also includes the drought analysis of rainfall using the Standardized Precipitation Index (SPI). In this study, SPI values and SPI plots are prepared in the RStudio software. The monthly, seasonal, and annual trends of precipitation for Bardoli region are in monotonic increasing trends or it is best fitted for the region. The drought study on the basis of rainfall suggests that at present, Bardoli region may not affected by the severe drought because it lies in near normal condition or moderately wet condition. This study helps policymakers, managers, and local authorities in taking protective measures for drought.

P. Patel (✉) · D. Mehta (✉) · S. Waikhom · K. Patel
Department of Civil Engineering, Dr. S. & S. S. Ghandhy Government Engineering College, Surat, India
e-mail: priyankpatel9896@gmail.com

D. Mehta
e-mail: darshanmehta2490@gmail.com

P. V. Timbadiya et al. (eds.), *Climate Change Impact on Water Resources*, Lecture Notes in Civil Engineering 313, https://doi.org/10.1007/978-981-19-8524-9_20

Keywords Drought · Innovative trend analysis (ITA) · Rainfall · SPI

1 Introduction

Based on the Intergovernmental Panel on climate change, environment is mainly affected by the increasing population, increasing industrialization, usage of pesticides and fertilizers in agricultural field, depletion of ozone layer, etc. So, the rainfall pattern and rainfall scenario may also be changed and affected largely. To avoid this thing, different studies and different measurements are required to study. For both climatology and hydrology, trend analysis is an essential area of research interest for examining climate change scenarios and improving the efficiency of current water resources and their influence on climate change. The long-term fluctuation in precipitation, temperature, humidity, evaporation, wind speed, and other meteorological factors is referred to as climatic variability for an area. Climate change can have a significant impact on hydrometeorological variables as rainfall, temperature, and evaporation variability. Many academics and organizations have researched trends in meteorological, hydrological, and climatological variables using various approaches [7–9, 12, 28].

Different parametric and non-parametric statistical methods have been used in many researches and studies to achieve daily, monthly, and annual trends of various parameters such as temperature, precipitation, dissolved oxygen, biological oxygen demand, and chemical oxygen demand [3, 10, 22, 23].

For trend detection of a precipitation variable, different methods and different methodologies are used in different countries. Basically, MK test, ITA method, and Sen's slope method are very important techniques which are used for the trend analysis detection of precipitation. Turkes [28] used MK test for the monthly precipitation trend analysis in the Turkey. Partal and Kahya [18] used MK test and Sen's slope test for the annual and monthly precipitation trend analysis in Nigeria.

Sen introduced an innovative trend analysis (ITA) method in 2012–2014, which has been used for detecting trends in environmental, hydrological, and meteorological variables (e.g., Ay and Kisi [1]; Kisi [11]; Onyutha [17]; Tabari and Willems [26]). Martnez-Austria et al. [14] used data linear adjustment, Spearman's test, and ITA to examine temperature and heat wave trends in Northwest Mexico, and all of the studies revealed the existence of a heating process with increasing maximum temperature. The Mann–Kendall test, linear regression model, and innovative trend analysis were also used by several researchers to investigate the change in monthly and annual river flows. The results were similar for all three ways. Furthermore, the study discovered a strong link between Mann–Kendall test markers and innovative trend analysis. The ITA approach was used to examine the temporal trend in seasonal and yearly rainfall time series data. In this study, a high-quality monthly dataset of one rain gauge with 30 years of monitoring was used to investigate the temporal rainfall variability in the Mindhola River Basin. The purpose of this study was to analyze and determine the importance of a prospective trend of variables, such as rainfall, over the Mindhola

River Basin in Gujarat's Bardoli District. The study's goal is to look into the rainfall variability in the Mindhola River Basin. The trend analysis for rainfall was done on a monthly, seasonal, and annual basis in this study, using data from 1990 to 2020. We employed innovative trend analysis (ITA) for rainfall variability in the Mindhola River Basin in this study. The ITA approach could discover some trends that the MK test would miss. This test was used to determine the magnitude and direction of a current trend over time [21]. The ITA technique allows for the detection of the impact of low, medium, and high values in detected trends while also overcoming several issues such as the time series' independent structure, normalcy of the distribution, and data length.

These changes in the climate variability may cause the changes in the flood and drought condition scenario. The present scenario due to uneven and non-uniform precipitation may cause flood and drought condition, so the analysis of this condition is required. Researchers commonly utilize the departure analysis of rainfall (D percent), Rainfall Anomaly Index (RAI), and Standardized Precipitation Index (SPI) are the well-known methodologies used for the study of drought using the rainfall patterns [27]. The Standardized Precipitation Index (SPI) offers various advantages over other indices, including its ease of use and adaptability. Positive SPI numbers imply a normal state to a wet state, while negative values suggest a normal state to a dry state. To calculate several drought parameters, SPI can be calculated across a wide range of time intervals and for a variety of water variables, including soil moisture, groundwater, and so on [25].

2 Study Area and Data Sources

Bardoli is a part of the Surat District in the state of Gujarat. Bardoli is the historical city which is situated in the western part of the country in Gujarat State occupying the area of 196,024 km^2. Bardoli is situated at latitudes 21.1255° N and longitudes 73.1122° E. There is only one Mindhola River which is in the area. The Mindhola River's origin is from Doswada (Songadh), and its length is about 105 km and flows into the Tokarva village in the Ground. The total catchment area of the Mindhola River is 1518 km^2. Geographically, Bardoli is the urban area. The surface elevation of the Bardoli is about 22 m above the Mean Sea Level (MSL). Hydrologic data at gauging site of Mindhola River are procured by the Nasa Power Data Access. As the study includes only rainfall data from period of January 1, 1990, to January 1, 2021 (30 years). Many researchers use time series (precipitation, temperature, etc.) of different record lengths (30, 40, 50, 75, 100, 135 years, etc.) to trend in the innovative trend analysis method. I analyzed it. Is it appropriate to use any length, and due to the unavailability of more data, only 30 years' data are used for the research. In the state of Gujarat, there are 19 manual observatories, 33 automatic weather stations, 66 automatic rain gauges, nine agro automatic weather stations, and four higher air observatories. The rain gauge station is located on the Mindhola River in the Bardoli area which is shown in Fig. 1.

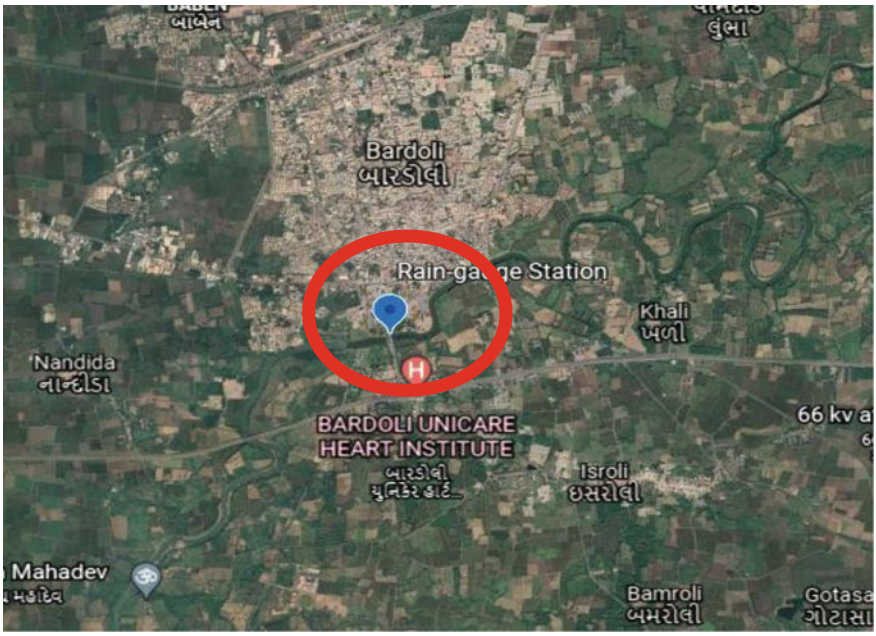

Fig. 1 Study area: rain gauge station. *Source* Google earth images

3 Methodology

3.1 Innovative Trend Analysis

Annual and seasonal rainfall trends were studied using the ITA approach. In innovative trend analysis approach, all the data are divided into two different time series, namely, first series and second series and then arrange into an ascending order. In a two-dimensional Cartesian coordinate system, the first sub-series is placed on the horizontal axis (x-axis) and the second sub-series is placed on the vertical axis (y-axis). The points in the scatter plot are collected on the 1:1 line if the two sub-series are equal, indicating no trend. If the points are above the 1:1 line, then we can say that time series has an increasing trend, and if the points accumulate below the 1:1 line, it is assumed that the time series has a falling trend. If the values of the time series are covered directly on the 1:1 line, then we can say that there is no trend and the data are best fit to the particular area. The horizontal or vertical distance from the 1:1 line is the absolute value of the difference between a point's y and x values. The magnitude of a rising or declining trend is indicated by the difference. As a result, it can be used to determine a trend, with average differences indicating a time series' overall tendency. The average discrepancies between two time series that may have different magnitudes must be normalized before they can be compared. Because the first sub-series is used to detect change, the trend indicator is calculated by dividing

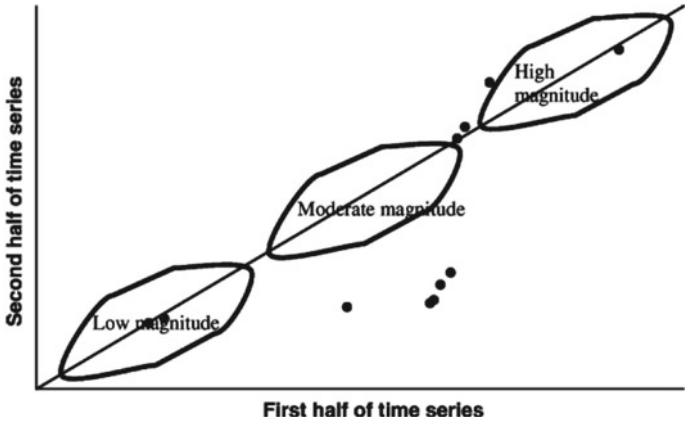

Fig. 2 Graphical representation of innovative trend analysis. *Source* Zakwan and Ahmad [34]

the average difference by the average of the first sub-series. The indicator is multiplied by ten to obtain the same scale as the Mann–Kendall test and linear regression analysis, allowing for direct comparison. The ITA indicator is then written as follows:

$$D = \frac{1}{n}\sum_{i=1}^{n}\frac{10(y_i - x_i)}{\overline{x}},$$

where D is the trend indicator, with a positive value indicating an increasing trend and a negative value indicating a falling trend; n is the number of observations in each sub-series, and x is the first sub-series' average. Innovative trend analysis gives the analysis of hydrological data in the magnitude manner whether other method cannot give the monotonic trend because sometimes hydrological events have different magnitude, so the trend may also differ due to the monotonic magnitude. So, it is helpful in trend analysis using the graphical manner. Figure 2 shows the graphical representation of the ITA.

In this study, we apply this methodology in the RStudio software which gives the easy representation and speedy result. After getting the data, we are applying these data into the RStudio software, and then, we are applying different tasks they give the direct graphical representation of the daily, monthly, seasonal graphical representation of the different trend analysis.

4 Drought Analysis Using Standardized Precipitation Index:

The departure analysis of rainfall (D percent), Rainfall Anomaly Index (RAI), and Standardized Precipitation Index (SPI) approaches are among the most important and

Table 1 SPI value classification

SPI values	Rainfall regime
≥ 2.00	Extremely wet
1.50–1.99	Very wet
1.00–1.49	Moderately wet
-0.99–0.99	Near normal
-1.00 to − 1.49	Moderately dry
-1.50 to − 1.99	Severely dry
≤ -2.00	Extremely dry

Source Hayes et al. [6]

extensively used tools for analyzing droughts based on rainfall. The Standardized Precipitation Index (SPI) approach was utilized to analyze the drought in this study. Among the different drought indices, the SPI is the most frequent meteorological drought index. Standardized Precipitation Index gives the long-term rainfall statistics to identify the drought condition in the respective area as three-month SPI, six-month SPI, nine-month SPI, and twelve-month SPI. Because of its statistical precision and intrinsic probabilistic character, the SPI approach is widely used to assess droughts around the world [16]. Drought is defined as a period in which the SPI value is constantly negative or less than (− 1) and ends when the SPI value is positive. The intensity of the drought is determined by the ratio of the magnitude of the drought to its duration, and the severity of the drought can be determined using Table 1 [6]. The SPI values are obtained using the RStudio software, and the drought idea is derived from the graphical depiction of the SPI numbers (see Table 1). SPI values can be obtained directly from the RStudio software, which is highly handy for obtaining SPI readings. Also, in RStudio, we can directly obtain the SPI values' graphical representation so that it is very easy and simple method for the drought analysis. In RStudio software trend change SPEI index, these two are important packages which are widely used for the trend analysis and the graphical representation of the trend. SPI values are found out on the bases of the 3 months, 9 months and on the annual bases of 12 months. In this study, we are using the SPI 12 value for the drought analysis because drought is analyzed on a yearly basis of the precipitation.

5 Results and Discussions

5.1 Variation in the Precipitation

5.1.1 Monthly Variation in Precipitation

Figure 3 shows the monthly fluctuation in precipitation in the Bardoli region. June, July, August, and September are the months with the most precipitation. The results

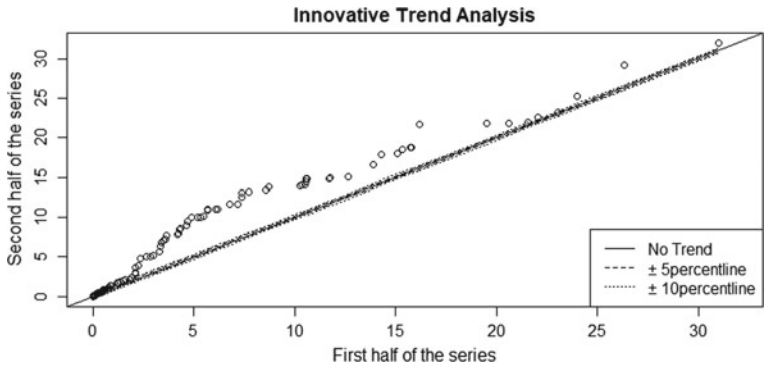

Fig. 3 Monthly variation in precipitation

demonstrate that precipitation in the entire region is growing monotonically. The monthly precipitation statistics are the best fit for the Bardoli region, according to the trend line. The rise in light precipitation is most noticeable, whereas the decrease in heavy precipitation is most noticeable. As a result, the reduction in total precipitation is primarily due to a reduction in heavy precipitation. The rise in precipitation is due primarily to an increase in light and low precipitation or weak precipitation.

5.2 Seasonal Variation in the Precipitation

Figure 4 shows the seasonal variation in the precipitation in the Bardoli region. Precipitation is mainly concentrated in the monsoon period or we can say that in the month of the June, July, August, and September (spring). Also, the trend line shows that the seasonal precipitation values are best fit for the Bardoli region. According to the trend sometimes in the monsoon period, the precipitation concentration becomes very high because it is directly depending on the seasonal heavy precipitation or due to the flood condition in the river basin area. This trend is increasing trend or best fit to the seasonal precipitation values for the Bardoli region. During the monsoon season, the variation trend of the precipitation is similar to that of the annual trend.

5.3 Annual Variation in the Precipitation

Figure 5 shows the annual variation in the precipitation in the Bardoli region. Precipitation is mainly concentrated due to the light and heavy precipitations. But, due to the present scenario, the heavy precipitation may decrease due to climate variability and increase in the light precipitation for longer time due to that in present scenario,

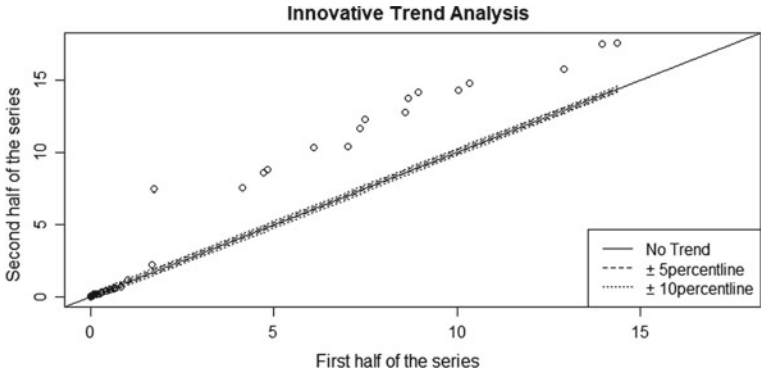

Fig. 4 Seasonal variation in the precipitation

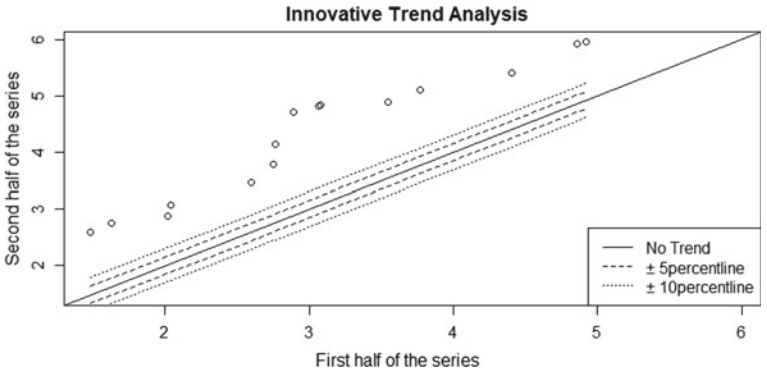

Fig. 5 Annual variation in the precipitation

the trend is in monotonic increasing nature. The increase in regional annual precipitation is primarily due to an increase in light precipitation, whereas the decline in regional annual precipitation is primarily due to a decrease in heavy precipitation.

5.4 Overall Trends in Precipitation

As we know that the precipitation is directly depended on the various factors, among them climate is very important factor. Precipitation trend or variability is shown that for Bardoli region, the trend of precipitation is almost similar or fit to the annual average precipitation or it cannot generate the any drought conditions. Rainfall trend analysis is vital because it helps policymakers make decisions on agricultural patterns, displaying dates, road development, and providing drinking water to urban and rural areas. The annual fluctuation trend of total precipitation acquired using the

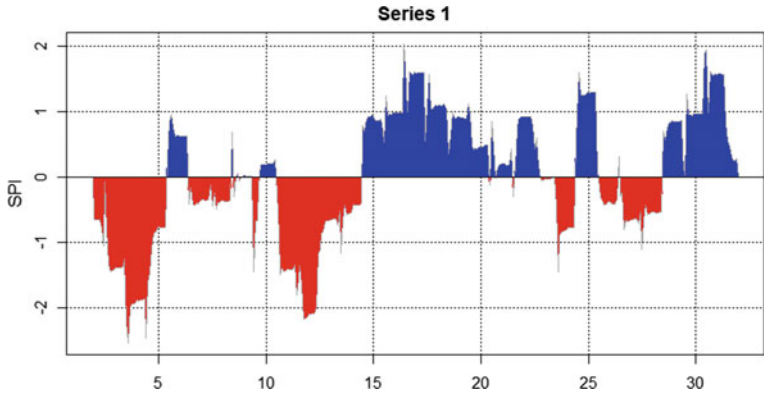

Fig. 6 Drought analysis graph for SPI 12

innovative trend analysis method is similar to that reported in prior research using other methodologies [30]. According to a study, the Bardoli region is not afflicted by severe drought in the current scenario or at this time.

5.4.1 Drought Analysis Using SPI Values

Figure 6 shows that in the earlier stage, the drought condition occurs in the Bardoli region after that the conditions may be improved and it shows that there is no drought condition in the present scenario. From result, we can say that up to 1995, the moderately dry or severely dry conditions occur. After that, from 1996 to 1998, area is affected by the normal regime condition; after 1998, condition may change at some extent; and up to year 2000, region is stay in normal condition. After that, up to year 2004, the condition of drought is moderate. After 2005, the conditions of region are moderately wet up to year 2013. After 2013, the region may be affected by the normal drought condition up to year 2018. After year 2018, the graph shows that the condition may improve and region may lie in the moderately dry condition. Out of 30 drought events, four years are recorded with the severely dry years, five years are recorded with moderately dry years, seven years are recorded near normal dry years, and remaining fourteen years are recorded as the moderately wet years, so there is no possibility of the drought (refer table of SPI value classification).

6 Conclusions

- In this study, we are carried out the analysis of the precipitation trend of Bardoli region precipitation between the year 1990 and 2020 (30 years) and analyze the drought condition using Standardized Precipitation Index of the twelve months

or annual data based on the precipitation values which shows the following conclusion.

- From the study, overall trends of the station are in monotonic increasing nature or somehow it is best fit for the Bardoli region conditions.
- The trend of the annual precipitation in the Bardoli region may also in the monotonic increasing nature. The seasonal trends of precipitation show that the contributions of the different types of extreme precipitation vary by season.
- The monthly trends of precipitation show that the contribution of the regional and weak precipitation is responsible for the increasing or decreasing trend of the precipitation. As per the study and analysis for the Bardoli region, the monthly trend of precipitation is increasing, and after the monsoon period, it shows the best fit to the trend line.
- Results of Standardized Precipitation Index show that at present time, Bardoli region lies in the normal conditions or in the moderately wet condition. The study's findings provide a thorough understanding of precipitation changes in the Bardoli region, which will aid policymakers and managers in managing water resources in the face of changing climatic circumstances.
- Water resources' managers should implement methods to adapt to different locations in the context of global warming because of the regional variability in precipitation trends. The result gained from this work may be very valuable for the management of water resources in designing the proposed mitigation strategies to minimize the consequences of drought.

References

1. Ay M, Kisi O (2015) Investigation of trend analysis of monthly total precipitation by an innovative method. Theoret Appl Climatol 120(3):617–629
2. Caloiero T (2020) Evaluation of rainfall trends in the South Island of New Zealand through the innovative trend analysis (ITA). Theoret Appl Climatol 139(1):493–504
3. Duhan D, Pandey A, Gahalaut KPS, Pandey RP (2013) Spatial and temporal variability in maximum, minimum and mean air temperatures at Madhya Pradesh in central India. Competes Rendus Geosci 345(1):3–21
4. Ghosh KG (2018) Analysis of rainfall trends and its spatial patterns during the last century over the Gangetic West Bengal, Eastern India. J Geovisualization Spatial Anal 2(2):1–18
5. Hasan Z, Akhter S, Kabir A (2014) Analysis of rainfall trends in the South-east Bangladesh. J Environ 3(4):51–56
6. Hayes MJ (2000) Revisiting the SPI: clarifying the process
7. Hirsch RM, Slack JR (1984) A nonparametric trend test for seasonal data with serial dependence. Water Resour Res 20(6):727–732
8. Kahya E, Kalaycı S (2004) Trend analysis of streamflow in Turkey. J Hydrol 289(1–4):128–144
9. Kalayci S, Kahya E (1998) Detection of water quality trends in the rivers of the Susurluk basin. Turk J Eng Environ Sci 22(6):503–514
10. Kisi O, Ay M (2014) Comparison of Mann-Kendall and innovative trend method for water quality parameters of the Kizilirmak River, Turkey. J Hydrol 513:362–375
11. Kisi O (2015) An innovative method for trend analysis of monthly pan evaporations. J Hydrol 527:1123–1129

12. Libiseller C, Grimvall A (2002) Performance of partial Mann–Kendall tests for trend detection in the presence of covariates. Environmetrics Official J Int Environmetrics Soc 13(1):71–84
13. Malik A, Kumar A, Guhathakurta P, Kisi O (2019) Spatial-temporal trend analysis of seasonal and annual rainfall (1966–2015) using innovative trend analysis method with significance test. Arab J Geosci 12(10):1–23
14. Martinez-Austria PF, Bandala ER, Patiño-Gómez C (2016) Temperature and heat wave trends in northwest Mexico. Phys Chem Earth Parts A/B/C 91:20–26
15. Mehta D, Yadav SM (2021) An analysis of rainfall variability and drought over Barmer District of Rajasthan: Northwest India. Water Supply
16. Mohammed R, Scholz M (2019) Climate variability impact on the spatiotemporal characteristics of drought and Aridity in arid and semi-arid regions. Water Resour Manage 33(15):5015–5033
17. Onyutha C, Willems P (2015) Spatial and temporal variability of rainfall in the Nile Basin. Hydrol Earth Syst Sci 19(5), 2227–2246
18. Partal T, Kahya E (2006) Trend analysis in Turkish precipitation data. Hydrol Process Int J 20(9):2011–2026
19. Sa'adi Z, Shahid S, Ismail T, Chung ES, Wang XJ (2019) Trends analysis of rainfall and rainfall extremes in Sarawak, Malaysia using modified Mann–Kendall test. Meteorol Atmosph Phys 131(3):263–277
20. Sah S, Singh RN, Chaturvedi G, Das B (2021) Trends, variability, and teleconnections of long-term rainfall in the Terai region of India. Theoret Appl Climatol 143(1):291–307
21. Salinger MJ, Mullan AB (1999) New Zealand climate: temperature and precipitation variations and their links with atmospheric circulation 1930–1994. Int J Climatol J R Meteorol Soc 19(10):1049–1071
22. Şen Z (2012) Innovative trend analysis methodology. J Hydrol Eng 17(9):1042–1046
23. Şen Z (2014) Trend identification simulation and application. J Hydrol Eng 19(3):635–642
24. Singh RN, Sah S, Das B, Vishnoi L, Pathak H (2021) Spatio-temporal trends and variability of rainfall in Maharashtra, India: Analysis of 118 years. Theoret Appl Climatol 143(3):883–900
25. Shah R, Bharadiya N, Manekar V (2015) Drought index computation using standardized precipitation index (SPI) method for Surat District, Gujarat. Aquatic Procedia 4:1243–1249
26. Tabari H, Taye MT, Willems P (2015) Statistical assessment of precipitation trends in the upper Blue Nile River basin. Stoch Env Res Risk Assess 29(7):1751–1761
27. Thomas J, Prasannakumar V (2016) Temporal analysis of rainfall (1871–2012) and drought characteristics over a tropical monsoon-dominated State (Kerala) of India. J Hydrol 534:266–280
28. Türkeş M (1996) Spatial and temporal analysis of annual rainfall variations in Turkey. Int J Climatol J R Meteorol Soc 16(9):1057–1076
29. Umran Komuscu A (1999) Using the SPI to analyze spatial and temporal patterns of drought in Turkey. Drought Network News (1994–2001):49
30. Wang P, Xie D, Zhou Y, Youhao E, Zhu Q (2014) Estimation of net primary productivity using a process-based model in Gansu Province, Northwest China. Environ Earth Sci 71(2):647–658
31. Wang Y, Zhang Q, Singh VP (2016) Spatiotemporal patterns of precipitation regimes in the Huai River basin, China, and possible relations with ENSO events. Nat Hazards 82(3):2167–2185
32. Wu H, Qian H (2017) Innovative trend analysis of annual and seasonal rainfall and extreme values in Shaanxi, China, since the 1950s. Int J Climatol 37(5):2582–2592
33. Yang H, Xiao H, Guo C, Sun Y, Gao R (2020) Innovative trend analysis of annual and seasonal precipitation in Ningxia, China. Atmosph Oceanic Sci Lett 13(4):308–315
34. Zakwan M, Ahmad Z (2021) Trend analysis of hydrological parameters of Ganga River. Arab J Geosci 14(3):1–15

Trend Analysis of Drought Events Over the Sirohi District in Western Rajasthan of India

Darshan J. Mehta and S. M. Yadav

Abstract The present study aims to assess the drought trends, seasonal and annual rainfall patterns at multiple time scales using Mann–Kendall and Sen's slope estimator over the Sirohi district of western Rajasthan, India, as this district is experiencing severe drought conditions due to a lack of annual rainfall and high variability. The Standardized Precipitation Index (SPI) is used to assess the drought pattern in the Sirohi district on monthly, seasonal, and annual time scales. The monthly time scales of SPI-3, SPI-6, SPI-9, and SPI-12, as well as the seasonal time scales of winter, pre-monsoon, southwest monsoon, and post-monsoon, are used to estimate drought using SPI for 102 years (1901–2002). The long-term series of monthly rainfall data from 33 stations from 1901 to 2021 (120 years) is used for this purpose. The spatial variation of positive and negative trends, as well as the findings of the trend analysis at different time scales, has been worked out. The drought pattern will be shown by analyzing SPI time series trends at each station in the study region. Drought trend analysis based on the SPI is proven to be more sensitive to different time scales. The findings show that rainfall in the study region is decreasing insignificantly throughout the winter, pre-monsoon, and s-w monsoon seasons. In addition, the result shows that all the time scales are capable of detecting rainfall regimes in the study region. This sort of drought regional trend analysis might aid the Sirohi district administration's decision-makers in planning and managing existing water

D. J. Mehta (✉)
Department of Civil Engineering, Sardar Vallabhbhai National Institute of Technology Surat, Surat 395007, India
e-mail: darshanmehta2490@gmail.com

S. M. Yadav
Department of Civil Engineering Department, Dr. S. & S. S. Ghandhy Government Engineering College, Surat, India

P. V. Timbadiya et al. (eds.), *Climate Change Impact on Water Resources*, Lecture Notes in Civil Engineering 313, https://doi.org/10.1007/978-981-19-8524-9_21

resources to fulfill the demands of agricultural and drinking water for the people in the study area.

Keywords Drought · Mann–Kendall test · Rainfall · Rajasthan · Sen's slope estimator

Rainfall is an important component of the hydrological cycle, and its variability on temporal and spatial scales is crucial from both scientific and socioeconomic perspectives [1, 2]. Long-term rainfall patterns are affected by global climate change, reducing water availability and increasing the risk of severe drought and flooding. During the monsoon season (June–August), high instantaneous rainfall may cause a water shortage during the non-monsoon season [3]. Trend analysis is a method for determining the spatial variation and temporal changes in various climate parameters. This is a critical issue for a country like India, which has an agro-based economy that is heavily reliant on rainfall due to the monsoon. As a result, any change in that phase of the year has the potential to devastate the country's agricultural conditions and thereby the economy. In comparison to global climate variability, India's climate change is too high. It has also emphasized the importance of determining whether the trend is rising or falling. Natural calamities such as drought and flooding may be caused by changes in the most important climatological parameter, rainfall [4, 5].

According to the Intergovernmental Panel on Climate Change (IPCC, 2007), studies to detect climate change and its impact on various sectors are urgently needed due to the impact of climate change on cropping patterns and also on land production which increases the risk of hunger and water scarcity, rapid melting of glaciers, and decreased river flows. Climate change is expected to reduce freshwater availability in many Indian river basins [6, 7]. The hydrological cycle and the pattern of stream flows will be affected by changes in rainfall as a result of global warming.

Carbon dioxide, a greenhouse gas, reached a global atmospheric concentration of 400 parts per million in 2014, up from 280 parts per million in pre-industrial times. In addition, the global atmospheric concentrations of methane and nitrogen oxides, two other important GHGs, have increased significantly. Increased anthropogenic activities are constantly affecting the earth's climate system, resulting in increased greenhouse gas levels in the atmosphere and thus climate change.

Climate changes have a significant effect on the magnitude and variability of rainfall as well as the temperature at various levels of spatial scale such as local, national, regional, continental, and global [8, 9]. The increasing trend of precipitation and temperature in the twentieth century is likely to continue in the twenty-first century. Global warming produces more evaporation from oceans (WMO, 2019) and intensifies the magnitude–frequency of extreme rainfall events [10].

The M–K test [11] is a recurrently and extensively applied non-parametric test for time series trend analysis. Recently, [12] suggested a new method (ITA) for the trend analysis of such variables across the globe. Several scholars have used together the M–K and ITA methods to examine the time series data of hydrometeorological

variables. Although several studies were conducted on rainfall trends over the Indian region, none of them had shown a strong increase or decrease trend in any time scale of rainfall for the entire region [8, 13].

Droughts are environmental disasters that are very destructive, destroying a huge area of land and causings significant economic damages [14]. Droughts are determined by a shortfall in the supply of water for a long time period, owing to the region's consistently below-average precipitation. These situations are compounded by meteorological factors such as increasing temperatures or high winds intensifying [15]. Droughts are a regular occurrence in all climate systems and can happen anywhere in the world, including in the desert and the rainforest [16]. The most expensive environmental threat is drought, and it has significant and frequent effects on many different economic sectors and people [17]. The impact of drought is more severe on the food and agricultural sector. Drought is a severe natural occurrence that has far-reaching effects on the socioeconomic, agricultural, and environmental areas [18].

These extreme climate changes increase the intensity of rainfall within shorter periods, thereby promoting drought and excessive rainfall to occur simultaneously [17, 18]. Any change in annual rainfall in the area puts a strain on annual average streamflow, which has implications for water resource development project planning and design [19]. Droughts decrease the primary productivity [20], streamflow, runoff, surface and groundwater resources [9], electricity production [21] and increase the rate of tree mortality and wildfires [6]. The Standardized Precipitation Index (SPI) is the most widely accepted index that only uses precipitation as input data [20]. The reason for its wide range of acceptance is its simplicity. It is also used to evaluate the performances of new indices. In the end, large economical losses occur due to droughts in particular regions. In India, many regions are facing droughts due to climate change and other factors. Rajasthan is one of the highly drought-prone regions of India. The purpose of the study was to analyze the trend of rainfall and identify drought events using the SPI method on monthly time scales as well as on seasonal time scales in the Sirohi district of Rajasthan.

1 Study Area and Data Source

Sirohi district is selected as a study area. Sirohi district is located in the southern part of Rajasthan. It is bounded by Pali district in the North direction, Udaipur district in the East direction, Gujarat state in the South direction, and Jalor in the western border. Sirohi is located between 24° 19′ 34.7″ to 25° 17′ 21.54″ north latitude and 72° 13′ 52.86″ to 73° 10′ 44.57″ seast longitude (See Fig. 1). It covers a 5139.1 km^2 area in Rajasthan. Sirohi district is made up of 467 towns and villages, of which five are block headquarters as well. The total population of the district as per Census 2011 is 8,50,804. The overall climatic condition of the district is semi-arid which remains dry and is partially sub-humid for the most part of the year. The summer season is from March to June month. The maximum average temperature in the

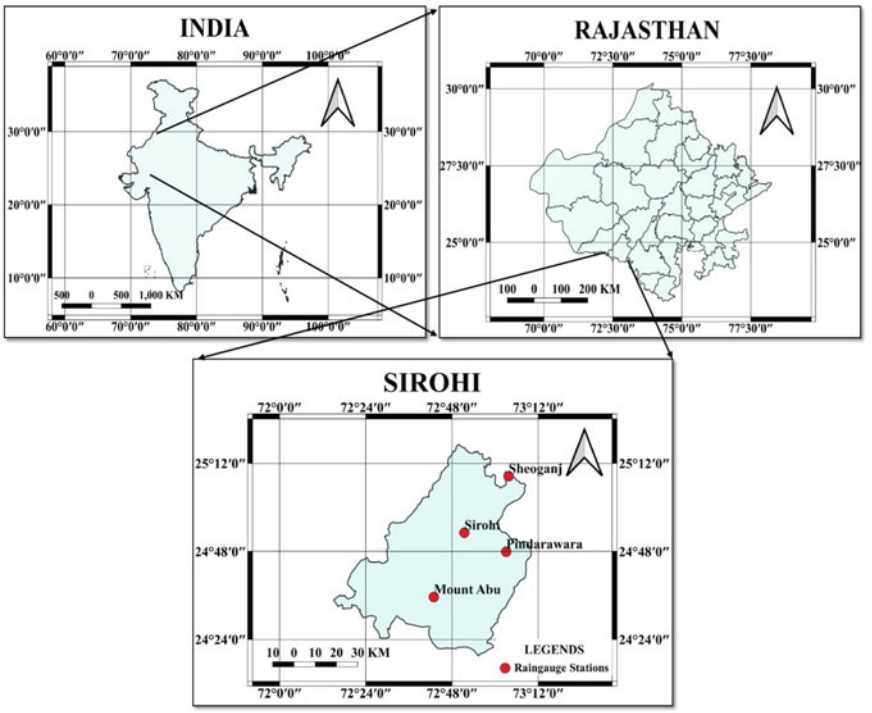

Fig. 1 Location of Sirohi district, Rajasthan

summer season is more than 47 °C. The average rainfall of Sirohi is 741.1 mm. The winter season is very cold which extends from the month of November to February. The minimum average temperature in Sirohi during winter is 23 °C. There is a large temperature difference which is observed between day and night times as well as between two seasons. So, it needs to be in consideration for the study. The majorly affected meteorological parameter on drought events is precipitation. For this study, monthly precipitation data of the Sirohi district are collected for the years 1901–2021. These monthly precipitation data are collected from the India Water Portal website. One can also collect precipitation data in daily, monthly, and yearly format from India-Water Resources Information System (India-WRIS).

2 Methodology

The first part of this study focuses on rainfall trend analysis for 120 years (1901–2021), while the second part focuses on meteorological drought using SPI for 102 years (1901–2002). Sirohi district is located in Rajasthan's semi-arid region, where the monsoon is the only source of climatic seasonality. As a result, rainfall

is used for climate change studies based on the hydrological year (June–May). As per Indian Metrological Department (IMD), there are four climatic seasons: south-west (s-w) monsoon (June–September), post-monsoon (October–December), winter (January–February), and pre-monsoon (March–May). The gradual change in the pattern of precipitation time series is investigated using the M–K test (statistical non-parametric test), and Sen's slope estimator is used to estimate the magnitude of the trend.

2.1 Trend Analysis Using M–K Test

This test is used to determine the seasonal and annual precipitation trends in the Sirohi district [11]. The rainfall trend analysis was carried out using Eqs. 1 and 2.

$$S = \sum_{i=1}^{n-1} \sum_{j=i+1}^{n} \operatorname{sign}\left(x_j - x_i\right), \tag{1}$$

$$\operatorname{sign}\left(x_i - x_j\right) = \begin{cases} -1; \left(x_j - x_i\right) < 0 \\ 1; \left(x_j - x_i\right) > 0 \\ 0; \left(x_j - x_i\right) = 0 \end{cases}. \tag{2}$$

The mean of S is $E[S] = 0$, and Eq. 3 can be used to compute the variance $\rho 2$.

$$\rho 2 = \left\{ n(n-1)(2n+5) - \sum_{j=1}^{p} tj(tj-1)(2tj+5) \right\} / 18 \tag{3}$$

$$Z = \begin{cases} \frac{S-1}{\rho} \\ 0 \\ \frac{S+1}{\rho} \end{cases} \tag{4}$$

The S (statistic) is closely related to Kendall's τ as given in Eq. 5:

$$\tau = \frac{S}{D}, \tag{5}$$

where D is the number of possible pairs of observations from a total of n observations and Z is the standard normal variate; increasing (decreasing) Z values indicate rising (falling) trends. When $|Z| > Z1\text{-}/2$ and a significant trend in the time series occurs, the null hypothesis is rejected. All of the results are evaluated at a significance level of $= 0.05$.

In this study, hypothesis testing was performed at a significance level of 5%, and in a two-tailed test, with the null hypothesis being that there is no trend in the time

series. The alternative hypothesis states that the time series reveals a significantly increasing/decreasing trend. The level of significance selected includes effective of rejecting the null hypothesis when it is true. As a result, five data points are likely to be rejected at a 5% significance level for a dataset of 100.

2.2 Sen's Slope Estimator Method

The slope estimator developed by [12] is a method for calculating change per unit of time. This is a non-parametric robust tool for determining monotonic trends in hydrologic time series [22, 23]. The Sen's slope estimator, which is carried out by Eq. 6, was used to estimate the slope of n pairs of data points:

$$\text{Sen}'ss\ \text{Slope}(\beta) = \text{median}\left[\frac{X_i - X_j}{(i-j)}\right];\ j < i. \tag{6}$$

2.3 Drought Analysis Using SPI Method

[20] created the SPI, where the probability of precipitation depends on the probability that the measured precipitation (x) will be translated into an index over a different time scale (3, 6, 12, 24, and 48 months).

The long-term rainfall history for each area over the requested time is a key factor in the SPI estimate [1, 2]. The long-term precipitation data are transformed into a probability distribution, which is then normalized using a probability distribution function (i.e., a function that is converted into a normal distribution) so that the mean SPI for the position and desired time is zero [2]. A gamma probability density function for a specific precipitation frequency distribution for a single station is matched by the SPI model. The alpha and beta parameters of the gamma probability density function are calculated for each month of the year, each season, and each important time scale (3 months, 12 months, 48 months, etc.) [1]. Using the distributed parameters, the cumulative probability of a recorded precipitation event for the specified month and time scale for the particular station is then calculated.

Drought is considered to have occurred when the SPI values are continually negative and reach (−1) or less, and it ends when the SPI becomes positive [20]. Drought magnitude is defined as the positive sum of the SPI for all months of drought events. Drought intensity is determined by the ratio of drought magnitude to duration, and severity of drought may be assessed using [1] classification (see Table 1). In this study, we have calculated SPI using the DrinC program for 102 years (1901–2002), which is a drought indices calculator.

Table 1 Rainfall regime classification based on SPI standard ranges

Value of SPI	Rainfall regime classifications
≥ 2.00	Extremely wet
1.50–1.99	Very wet
1.00–1.49	Moderately wet
−0.99–0.99	Near normal
−1.00–−1.49	Moderately dry
−1.50–−1.99	Severely dry
≤ −2.00	Extremely dry

Source Hayes et al. [3]

3 Results and Discussions

3.1 Rainfall Trend Analysis

Precipitation time series is analyzed for trends on a monthly, seasonal, and annual scale. The Mann–Kendall test was used to carry out a detailed trend analysis of the average (winter, pre-monsoon, s-w monsoon, and post-monsoon) and extreme annual daily precipitation for the Sirohi district from 1901 to 2021. Sen's slope estimator was also estimated. Identification of precipitation trends for various groups with significant effects: High precipitation causes flooding, whereas low precipitation causes drought.

Trend analysis of the Sirohi district was detected and revealed that a positive trend of rainfall was observed only for post-monsoon with the value of Z_{mk} is 0.002, whereas negative trend was reported for winter, pre-monsoon, S-W monsoon, and annual with Z_{mk} values being −0.131, −0.065, −0.037, and −0.036, respectively. A significant decreasing trend is reported for winter at a 5% significance level. It is observed that there is no trend in some of the months. Sen's slope results are also in agreement with the M–K test results. The summary of both tests is shown in Table 2. Figures 2 and 3 show an annual and seasonal graphical representations of long-term M–K test results.

3.2 Standardized Precipitation Index

To calculate 3-month SPI, months of January–March, months of April–June, months of July–September, and months of October–December were considered. A time series is plotted in Fig. 4 for all four time frames of 3-month SPI. The calculated values of SPI for the study time span reveal 82 drought conditions among all four time frames of 3 months (October–December, January–March, April–June, and July–September). Out of these 82 drought conditions, nine events were found to be extremely dry and

Table 2 Results of the M–K test for rainfall trend data 1901–2021

Rainfall period	Kendall's tau	Trend interpretation	Mann–Kendall test *P*-value	Sen's slope	Test interpretation
January	−0.080	Decreasing trend	0.218	0	There is no trend
February	−0.136	Decreasing trend	0.039	0	There is no trend
March	−0.040	Decreasing trend	0.553	0	There is no trend
April	0.101	Increasing trend	0.118	0	There is no trend
May	−0.056	Decreasing trend	0.370	−0.003	Insignificant decreasing trend
June	0.062	Increasing trend	0.314	0.112	Insignificant increasing trend
July	−0.013	Decreasing trend	0.828	−0.083	Insignificant decreasing trend
August	−0.054	Decreasing trend	0.381	−0.405	Insignificant decreasing trend
September	0.037	Increasing trend	0.554	0.091	Insignificant increasing trend
October	−0.012	Decreasing trend	0.844	0	There is no trend
November	−0.007	Decreasing trend	0.921	0	There is no trend
December	−0.107	Decreasing trend	0.111	0	There is no trend
Winter	−0.131	Decreasing trend	0.036	−0.01	Significant decreasing trend
Pre-monsoon	−0.065	Decreasing trend	0.292	−0.019	Insignificant decreasing trend
S-W monsoon	−0.037	Decreasing trend	0.544	−0.444	Insignificant decreasing trend
Post-monsoon	0.002	Increasing trend	0.971	0	There is no trend
Annual	−0.036	Decreasing trend	0.563	−0.477	Insignificant decreasing trend

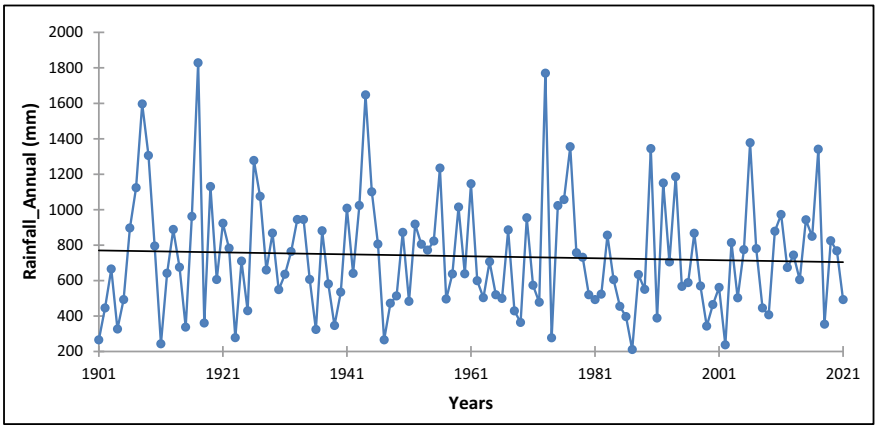

Fig. 2 Long-term trend of annual rainfall (1901–2021) over Sirohi district

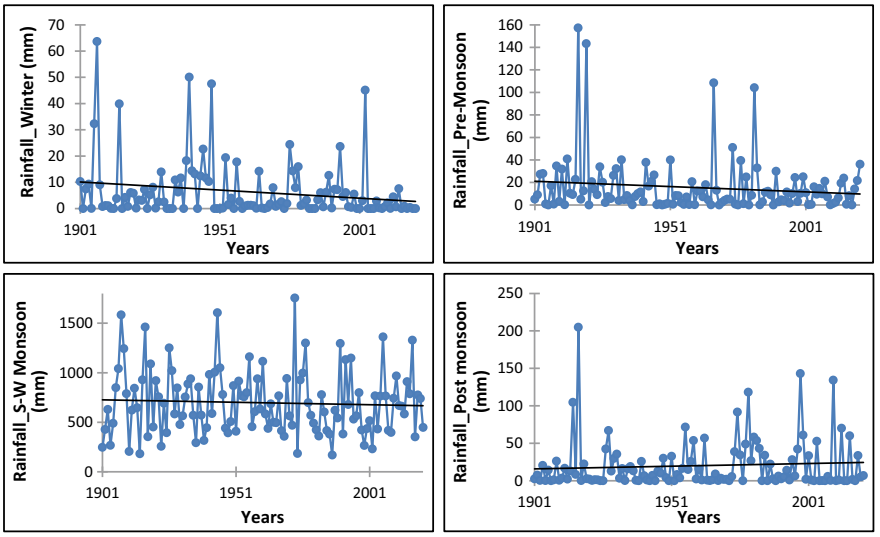

Fig. 3 Long-term trend of rainfall during **a** winter, **b** pre-monsoon, **c** southwest monsoon, and **d** post-monsoon for 1901–2021 over the Sirohi district

the other nine scenarios were found to be severely dry, while remaining 69 drought events were found moderately dry. The same analogy was employed to analyze intermediate drought events for 6-month and 9-month SPI. For the calculation of 6-month SPI, the months of October–March and months of April–September were considered. A time series is plotted in Fig. 5 for two time frames of 6-month SPI. A rainfall regime classification based on the value of SPI is shown in Table 1. According to the classification, 56 drought events were observed during the study time span. Out

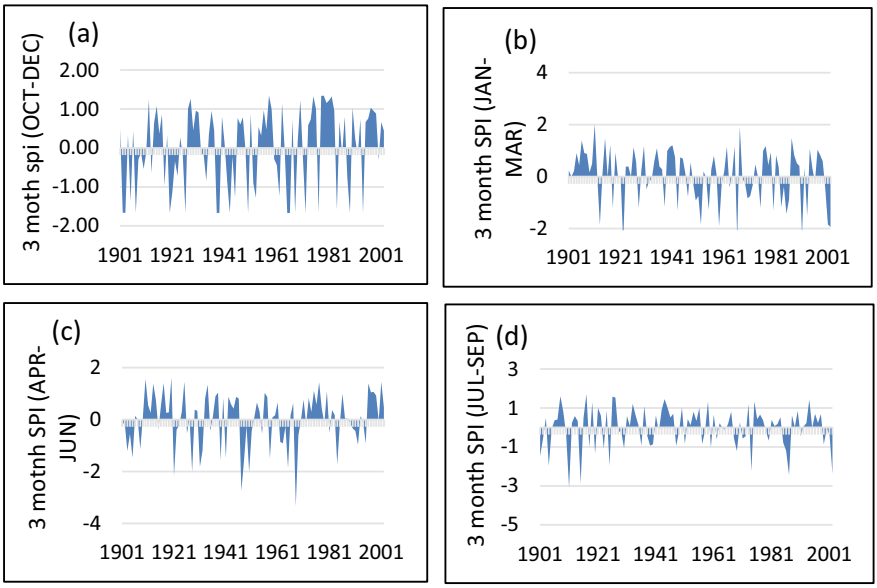

Fig. 4 Standardized Precipitation Index (SPI) of 3-month time frame for **a** October–December, **b** January–March, **c** April–June, and **d** July–September over Sirohi district

of these 56 drought conditions, 16 events were found extremely dry, other 16 events found to be severely dry, and remaining 24 events were found moderately dry. To determine 9-month SPI, months of October–June were considered and a time series is plotted in Fig. 6. According to the rainfall regime classification, 28 drought events were observed, out of which nine events were found extremely dry, seven events found severely dry, and 12 events found moderately dry. Figure 7 shows a time series plot and its drought characteristics for long-term drought events for 12-month SPI (October–September). From the value of 12-month SPI, 24 drought events were found, out of which six events were extremely dry, eight events were severely dry, and ten events were moderately dry.

4 Conclusions

Temporal variation analysis results show drought events in the Sirohi district. The results reveal that maximum stations are showing mild drought conditions and very few severe and extreme drought events. Rainfall data statistics also revealed that there were only seasonal variations of time series patterns, but no long-term drought trend was observed. During the observed 24 years, 12 drought years have been observed in the district. There were eight severe drought years, namely, 1986, 1987, 1989, 1991, 1995, 1996, 1998, and 1999, with average annual rainfalls 66.8%, 87.0%,

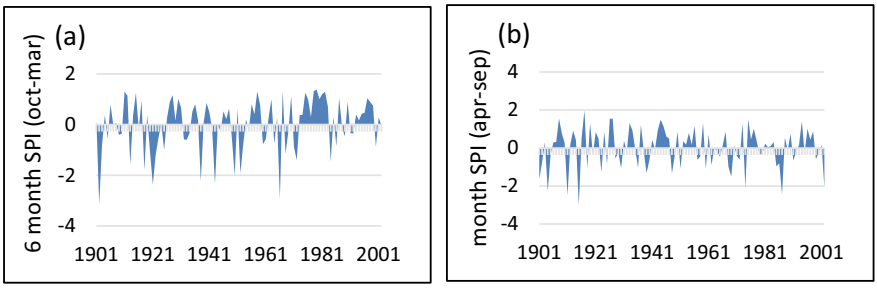

Fig. 5 Standardized Precipitation Index (SPI) of 6-month time frame for **a** October–March, **b** April–September over Sirohi district

Fig. 6 Standardized Precipitation Index (SPI) for 9-month time frame for October–June over Sirohi district

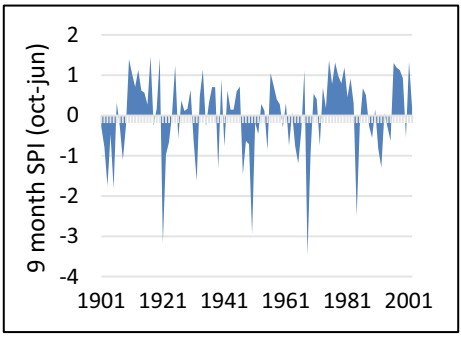

Fig. 7 Standardized Precipitation Index (SPI) for 12-month time frame for October–September over Sirohi district

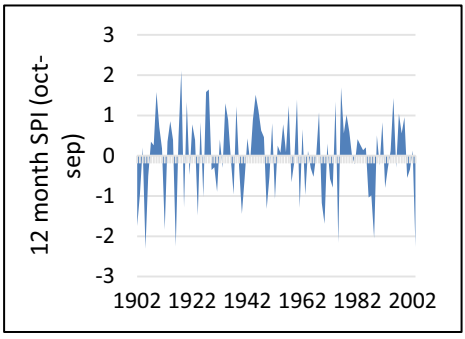

58.7%, 67.4%, 64.2%, 60.9%, 65.4%, and 69.7% below average, respectively. 1990, 1993, 1997, and 2002 were the four moderate drought years, with an average annual rainfall below average by 44.3, 27.5, 45.7, and 28.3%, respectively. The findings of the present study can be very beneficial in designing the drought mitigation strategies that have been recommended.

References

1. Mehta D, Yadav SM (2021) An analysis of rainfall variability and drought over Barmer District of Rajasthan, Northwest India. Water Supply 21(5):2505–2517. https://doi.org/10.2166/ws.2021.053
2. Mehta D, Yadav SM (2022) Temporal analysis of rainfall and drought characteristics over Jalore District of S-W Rajasthan. Water Pract Technol 17(1):254–267. https://doi.org/10.2166/wpt.2021.114
3. Hayes MJ, Svoboda MD, Wiihite DA, Vanyarkho OV (1999) Monitoring the 1996 drought using the standardized precipitation index. Bull Am Meteor Soc 80(3):429–438
4. Abramowitz M, Stegun IA, Miller D (1965) Handbook of mathematical functions with formulas, graphs and mathematical tables (National Bureau of Standards Applied Mathematics Series No. 55)
5. Chelu A (2019) A typology of indices for drought assessment. Air and Water—Components of the Environment. Cluj-Napoca, Romania, pp 77–90
6. Allen CD, Macalady AK, Chenchouni H, Bachelet D, McDowell N, Vennetier M, Cobb N (2010) A global overview of drought and heat-induced tree mortality reveals emerging climate change risks for forests. Forest Ecol Manage 259(4, SI):660–684. https://doi.org/10.1016/j.foreco.2009.09.001
7. Ciais P, Reichstein M, Viovy N, Granier A, Ogée J, Allard V, Valentini R (2005) Europe-wide reduction in primary productivity caused by the heat and drought in 2003. Nature 437(7058):529–533. https://doi.org/10.1038/nature03972
8. Perera A, Mudannayake SD, Azamathulla HM, Rathnayake U (2020) Recent climatic trends in Trinidad and Tobago, West Indies. Asia-Pacific J Sci Technol 25(02):1–11
9. Smakhtin VU (2001) Low flow hydrology: a review. J Hydrol 240(3–4):147–186. https://doi.org/10.1016/S0022-1694(00)00340-1
10. Heim RR (2002) A review of twentieth-century drought indices used in the United States. Bull Am Meteor Soc 83(8):1149–1165
11. Mann HB (1945) Nonparametric tests against trend. Econometrica: J Econom Soc 2(3):245–259
12. Sen PK (1968) Estimates of the regression coefficient based on Kendall's tau. J Am Stat Assoc 63(324):1379–1389
13. Perera A, Rathnayake US, Azamathulla HM (2020) Comparison of different artificial neural network (ANN) training algorithms to predict atmospheric temperature in Tabuk, Saudi Arabia. MAUSAM: Quart J Meteorol Hydrol Geophys 71(2):551–560
14. Mehta D, Yadav SM (2020) Long-term trend analysis of climate variables for arid and semi-arid regions of an Indian State Rajasthan. Int J Hydrol Sci Technol Indersci Publ. https://doi.org/10.1504/IJHST.2020.10033400
15. Mishra AK, Singh VP (2010) A review of drought concepts. J Hydrol 391(1–2):204–216. https://doi.org/10.1016/j.jhydrol.2010.07.012
16. Katz RW, Glantz MH (1986) Anatomy of a rainfall index. Monthly Weather Rev. https://doi.org/10.1175/1520-0493(1986)114<0764:AOARI>2.0.CO;2
17. Kallis G (2008) Droughts. Annu Rev Environ Resour 33:85–118. https://doi.org/10.1146/annurev.environ.33.081307.123117
18. Mehta D, Yadav SM (2021) Analysis of long-term rainfall trends in Rajasthan, India. In: Jha R, Singh VP, Singh V, Roy LB, Thendiyath R (eds) Climate change impacts on water resources. Water Science and Technology Library, vol 98. Springer, Cham. https://doi.org/10.1007/978-3-030-64202-0_26
19. Khaniya B, Priyantha HG, Baduge N, Azamathulla HM, Rathnayake U (2020) Impact of climate variability on hydropower generation: a case study from Sri Lanka. ISH J Hydraulic Eng 26(3):301–309
20. McKee TB, Doesken NJ, Kleist J (1993) The relationship of drought frequency and duration to time scales. In: Proceedings of the 8th conference on applied climatology, pp 179–184. citeulike-article-id:10490403

21. Van Vliet MTH, Sheffield J, Wiberg D, Wood EF (2016) Impacts of recent drought and warm years on water resources and electricity supply worldwide. Environ Res Lett 11(12). https://doi.org/10.1088/17489326/11/12/124021
22. Mohammed S, Alsafadi K, Mohammad S, Mousavi N (2019) Drought trends in Syria from 1900 to 2015. In: Proceedings of the 4th international congress of developing agriculture, natural resources, environment and tourism of Iran, Tabriz Islamic Art University In cooperation with Shiraz University and Yasouj University, Tabriz, Iran, vol 14
23. Mokhtarzad M, Eskandari F, Vanjani NJ, Arabasadi A (2017) Drought forecasting by ANN, ANFIS, and SVM and comparison of the models. Environ Earth Sci 76(21):1–10
24. Shah R, Bharadiya N, Manekar V (2015) Drought index computation using standardized precipitation index (SPI) method for Surat District, Gujarat. Aquatic Proc 4:1243–1249

Statistical Analysis of Precipitation Over Kota (India) from 1981 to 2020

Kuldeep, Sohil Sisodiya, and Anil. K. Mathur

Abstract Variation in precipitation amounts and distribution patterns leads to changes in general atmospheric circulation, cloud cover, surface albedo, and concentrations of air pollutants in the context of climatic variability. Industrial, residential, and agricultural water demands largely depend on rainfall. Even rainfall variability significantly affects people's livelihood. This study evaluates the temporal variation in rainfall for the Kota district of Rajasthan state in India. Eight rainfall monitoring stations were utilised to collect precipitation data for 40 years (1981–2020). Trend analysis has been performed for monthly, seasonal, and annual rainfall series with the help of Mann–Kendall (non-parametric) and linear regression (parametric) trend tests. Standardised rainfall anomaly and wetness index were estimated to determine the excess in total annual rainfall. The monthly distribution of precipitation is contrasted with the help of the precipitation concentration index. Both non-parametric and parametric trend tests estimate an increasing trend in precipitation for February, March, June, July, August, and September months, reflecting an increase in the total annual precipitation for the research area. The analysis of precipitation data shows a very high inter and intra variability in annual rainfall (C.V. = 169.45). A very high non-uniformity of rain is observed from the analysis of PCI. The maximum concentration of precipitation (~84.50) took place in monsoon months. Annual rainfall has significantly increased over the last four decades, indicating

Kuldeep (✉) · S. Sisodiya · Anil. K. Mathur
Department of Civil Engineering, University Department, Rajasthan Technical University, Kota, Rajasthan 324010, India
e-mail: kuldeep.kamboj44@rtu.ac.in

S. Sisodiya
e-mail: ssisodiya.npiu.ce@rtu.ac.in

Anil. K. Mathur
e-mail: akmathur@rtu.ac.in

P. V. Timbadiya et al. (eds.), *Climate Change Impact on Water Resources*, Lecture Notes in Civil Engineering 313, https://doi.org/10.1007/978-981-19-8524-9_22

the need for proper rainwater management and utilisation plans to take maximum benefits shortly.

Keywords Trend analysis · Mann–Kendall trend test · Standardised rainfall anomaly · Wetness index · Precipitation concentration index

1 Introduction

The biggest challenge facing humanity in the twenty-first century is worldwide climate change and its severe consequences on the environment. Climate change is directly linked with variations in rainfall patterns, hydrological cycle, moisture content, melting of ice, extreme conditions, and the frequency and intensity of extreme events [1].

Increased emission of greenhouse gases (CO_2, CH_4, N_2O, and halocarbons) has been the leading cause of global warming since the 1950s. Global warming is responsible for the rise in the mean temperature of the earth's surface, leading to climate change [2]. All the important sectors, such as ecological, biological, meteorological, and socio-economic, are directly or indirectly affected by global climate change [3]. Hence, it is a point of attention in research worldwide. The long-term variation in rainfall trends is analysed regularly to estimate the significant impact of climate change. Quantitative analysis of temporal rainfall distribution for a region is crucial for hydraulic structure modelling, hydrological modelling, surface water modelling, flood forecasting, agriculture modelling, groundwater modelling, evaporation modelling, crops scheduling, etc. [4, 5].

India is situated in a tropical monsoon zone and receives almost 80% of annual rainfall in June, July, August, and September due to the Southwest monsoon with more significant spatiotemporal variability [6, 7]. Several studies have been conducted in different parts of the world on rainfall variability for various purposes in the literature, but almost negligible studies have been available for Kota.

This paper examines the trends for annual, seasonal, and monthly rainfall series for Rajasthan (India) Kota district (1981–2020) using the Mann–Kendall (non-parametric) trend test and linear regression (parametric) trend test. Standardised rainfall anomaly and wetness index are estimated to determine the excess in total annual rainfall. The monthly distribution of precipitation is contrasted with the help of the precipitation concentration index (PCI). The coefficient of variation measures the dispersion of rains.

2 Study Area and Data Source

Kota is the south-eastern district of Rajasthan state, India, and its geographical area lies between 75° 37′ and 77° 26′ longitude and 24° 25′ and 25° 51′ latitude. The

maximum width and length of Kota are 54 km (east to west) and 153 km (north to south), respectively. The geographical area of the Kota district is 5217 km^2 and has shaped like Dumber [8]. The population of Kota district as per the census of 2011 was 1,951,014 [9]. The total number of registered vehicles was 885,737 in 2020 as per the Rajasthan Transport department [10]. The total number of industrial areas and industrial units were 19 and 12,908, respectively, as per the MSME report, 2015 [11].

Rainfall data were collected for 40 years (1981–2020) from eight rainfall monitoring stations daily, and these monitoring stations, along with the study area, are shown in Fig. 1. The GPS coordinates of each monitoring station are tabulated in Table 1. The total rainfalls reading during the observation period for all the monitoring stations was 116,880, i.e., 14,610 readings for each sampling location. Each year is categorised into three seasons: Summer (March, April, May, and June), rainy (July, August, September, and October), and Winter (January, February, November, and December) [12].

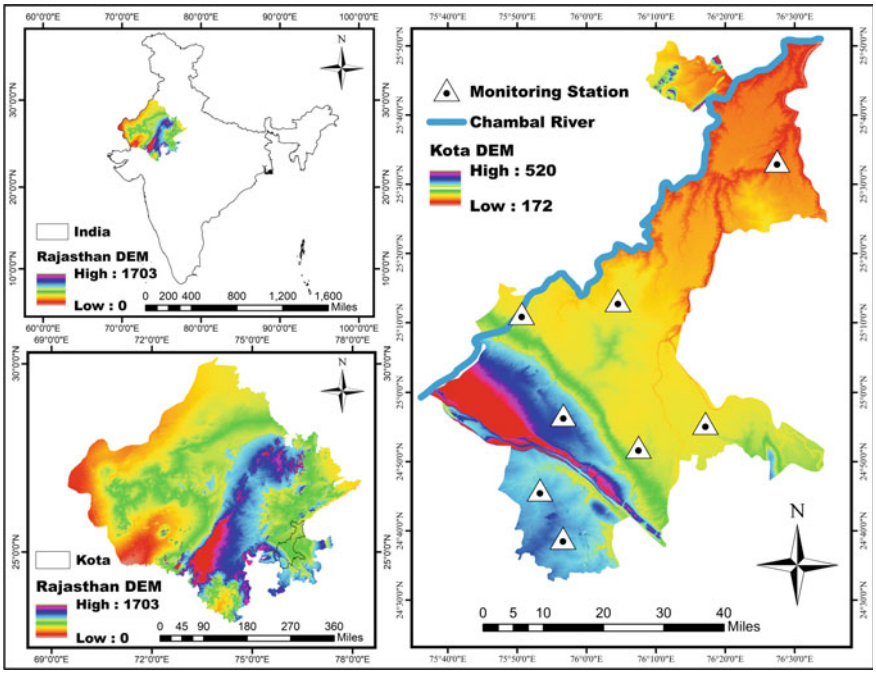

Fig. 1 Area of interest for study along with rainfall monitoring station

Table 1 GPS coordinates for precipitation monitoring station at Kota district, Rajasthan

Code	Station	Longitude	Latitude
MS-1	Digod	76.075	25.220
MS-2	Ladpura	75.844	25.188
MS-3	Pipalda	76.457	25.556
MS-4	Ramganjmandi	75.943	24.649
MS-5	Sangod	76.285	24.925
MS-6	Mandana	75.944	24.945
MS-7	Kanwas	76.124	24.868
MS-8	Chechat	75.888	24.765

3 Trend Analysis and Precipitation Indices

3.1 Trend Analysis

It has been performed for annual, seasonal, and monthly rainfall series using the linear regression trend test (parametric) and the non-parametric trend test (Mann–Kendall test).

3.1.1 Linear Regression Trend Analysis

Linear regression trend test is computed to define the extent of the linear relationship between precipitation (dependent variable) and time (independent variable). It predicts the value of rainfall concerning time. The regression equation is as follows [13]:

$$Y = ax + b \tag{1}$$

where a is the slope of the line and b is the intercept.

3.1.2 Mann–Kendall Trend Analysis

The null hypothesis and alternative hypothesis are tested against each other in Mann–Kendall test. The null hypothesis supposes no trend in precipitation-time data series, while the alternative hypothesis assumes a trend. The following equations govern Mann–Kendall test [14]:

$$R = \sum_{K=1}^{n-1} \sum_{L=K+1}^{n} \text{sign}(X_L - X_K) \tag{2}$$

$$\text{sign}(T_L - T_K) = \left\{ \begin{array}{ll} 1 & \text{if } X_L - X_K > 0 \\ 0 & \text{if } X_L - X_K = 0 \\ -1 & \text{if } X_L - X_K < 0 \end{array} \right\} \tag{3}$$

The variance for the R-statistic can be calculated through Shreepada Devi et al. [16]:

$$\sigma^2 = \frac{[(2n+5)(n-1)n)}{18} \tag{4}$$

The standard test is defined by Kumar et al. [15]:

$$Z_R = \left\{ \begin{array}{c} \frac{R-1}{\sigma} \text{ for } R > 0 \\ 0 \text{ for } R = 0 \\ \frac{R+1}{\sigma} \text{ for} R < 0 \end{array} \right\} \tag{5}$$

3.2 Normal Annual Rainfall (NAR)

The 30-year consecutive rainfall series average is termed as normal annual rainfall. The rainfall series for the present study is categorised into monthly, seasonal, and yearly precipitation-time data series. The up-gradation of normal annual rainfall takes place after every 10 years, and its trend was predicted. Normal annual rainfall is calculated through the following equation [14]:

$$\text{NAR} = \frac{\sum_{i=1}^{30} P_i}{30} \tag{6}$$

where P_i Denotes the rainfall that occurred in the ith year.

3.3 Precipitation Concentration Index (PCI)

It defines the non-uniformity and uniformity of precipitation over a given period. The highest PCI's value denotes a more significant non-uniformity of precipitation. The following equation is used to calculate PCI's value:

$$\text{PCI} = \frac{\sum_{i=1}^{12} P_i^2}{\left(\sum_{i=1}^{12} P_i\right)^2} * 100 \tag{7}$$

Table 2 Categorisation of PCI and SRA values

PCI	Rainfall category	SRA	Drought severity
< 10	Uniform precipitation distribution	< −1.65	Extreme
11–15	Moderate precipitation concentration	−1.65 to −1.28	Severe
16–20	High precipitation concentration	−1.28 to −0.84	Moderate
> 20	Very high precipitation concentration	> −0.84	No drought

The PCI values are characterised into the following categories, as shown in Table 2.

3.4 Standardised Rainfall Anomaly (SRA)

Drought severity is expressed through standardised rainfall anomalies. The most negligible SRA's value denotes the maximum possibility of draught. The following equation is used to calculate SRA's values:

$$\text{SRA} = \frac{\left(P_i - \overline{P}_i\right)}{S} \tag{8}$$

where S = standard deviation of rainfall time series and P_i = the rainfall in the ith year.

The SRA's values are characterised into the following categories, as shown in Table 2.

3.5 Wetness Index ($\mathbf{W_i}$)

The precipitation ratio for a given year over the mean annual precipitation is the index of wetness and expressed on a percentage basis.

$$W_i(\%) = \frac{\text{Precipitation in a particular year at a place}}{\text{Normal Annual precipitation}} * 100 \tag{9}$$

A value less than 100 of the wetness index denotes a rainfall deficiency equivalent to the deficit from 100, i.e., Rainfall Deficiency = 100 – Wetness Index. Rainfall deficiency is categorised into large deficiency (30–45%), serious deficiency (45–60%), and the disastrous deficiency (> 60%).

3.6 Coefficient of Variation (C.V.)

The coefficient of variation measures the dispersion of precipitation. It is used to determine the reliability of an average and provide a basis for controlling the variability. It can be calculated through the following equation:

$$\text{C.V.}(\%) = \frac{\text{The standard deviation of precipitation}}{\text{Average Precipitation}} * 100 \quad (10)$$

3.7 Dependable Rainfall

The data of rainfall-time series should be arranged in descending order and then ranked accordingly to determine dependable rainfall. The dependable rainfall is calculated for 50, 75, and 90% dependency in this research work. It can be calculated through the following equation:

$$\text{Precipitation Occurrence } (\%) = \left(\frac{\text{Rank}}{\text{Total number of observations}}\right) * 100 \quad (11)$$

4 Results and Discussions

The maximum, minimum, and average precipitation on a monthly, seasonal and annual basis, along with standard deviation, is shown in Table 3. The intra-annual rainfall variability (PCI) is evaluated for the entire data set (1981–2020). PCI lies between 22.97 and 52.15, indicating a very high non-uniformity of rainfall in each year, i.e., a very high concentration of rainfall in a particular part of a year. Monsoon average and percentage are computed to identify the reason behind more significant non-uniformity.

Precipitation indices are tabulated in Table 4. It is found that the southeast monsoon, which takes place in the rainy season (July, August, September, and October) every year responsible for 62.50–97.37% of the total rainfall of a year. On average, monsoon rainfall contributed nearly 84.50% of the total rainfall and explained the large PCI values.

Significant monthly rainfall variability has been observed. The average coefficient of variation was 169.45, while maximum variability in precipitation was seen in December (285.51) and minimum variability in precipitation was obtained for August (47.62). The overall coefficient of variation and PCI values are very high and indicate significant inter- and intra-annual variations in the precipitation.

Table 3 The maximum, minimum, and average precipitation in millimetres along with standard deviation

Sr. No.	Period	Average	Maximum	Minimum	Standard deviation
1	January	4.76	32.38	0.00	8.45
2	February	5.45	39.04	0.00	10.56
3	March	3.30	46.00	0.00	8.31
4	April	4.20	38.25	0.00	8.15
5	May	8.37	82.20	0.00	18.52
6	June	83.17	475.50	2.09	81.80
7	July	257.43	653.12	18.53	123.73
8	August	273.72	636.54	49.59	130.36
9	September	98.08	308.25	6.75	68.02
10	October	20.26	161.56	0.00	38.85
11	November	6.00	72.60	0.00	15.28
12	December	3.19	50.14	0.00	9.11
13	Winter	4.85	25.96	0.00	5.69
14	Summer	24.76	119.25	3.54	20.27
15	Rainy	162.37	312.31	64.84	48.53
16	Annual	63.99	112.98	32.47	18.14

Table 4 Precipitation Indices along with annual total and average rainfall

Precipitation indices	Average	Maximum	Minimum
Total	767.94	1355.76	389.6
Average	63.99	112.98	32.46667
PCI	31.96	52.15	22.96774
Monsoon average	649.49	1249.26	259.36
Monsoon percentage	84.50	97.37	62.50
Coefficient of variation	169.45	285.51	47.62
SRA	2.65	7.82	−0.57
Wetness index	102.13	180.31	51.81

Normal annual rainfall based on the average of 30 consecutive years was 60.68 mm and 64.64 mm for 1981–2010 and 1991–2020, respectively. Standardised rainfall anomaly was calculated to determine interannual variability of rainfall. The SAR value ranged from −0.57 (2002, the driest year) to 7.81 (2008, the Wettest year). The average value of SRA is greater than −0.84, avoiding any possibility of drought.

Analysis of the wetness index revealed that 2019 was the wettest year (W_i = 180.31), while 2002 was the driest year (W_i = 51.81) due to the amount of rainfall that took place in these years. The rainfall observed in 2002 and 2019 were 389.6 (Lowest) and 1355.76 (Highest) mm, respectively. Rainfall dependability is critical

Table 5 Trend test statistics along with rainfall dependability

Time	Kendall's tau	Slope	Rainfall dependability		
			50%	75%	90%
January	−0.127	−0.089	0.125	0	0
February	0.060	0.047	0	0	0
March	0.040	0.166	0	0	0
April	−0.080	0.010	0.66	0	0
May	−0.072	−0.027	1.42	0.42	0
June	0.162	1.658	63.25	35.1	19.31
July	0.124	0.61	244.88	190.04	123.18
August	0.034	0.97	256.75	180.85	134.23
September	0.006	0.41	87.85	48.34	15.52
October	−0.247	−1.06	3	0	0
November	0.018	−0.257	0	0	0
December	0.071	−0.103	0	0	0
Total	0.032	0.194	751.35	652.55	545,375

to maintaining sustainable use of water. Hence, dependable rainfall (90, 75, and 50%) for other months has been calculated and shown in Table 5. June, July, August, and September are the southwest monsoon months when maximum precipitation occurs and is available to complete water demands in the remaining months. An inspection of Table 5 reveals significant positive trends exist for precipitation over the previous four decades (1981–2020). A substantial increase in monsoon rainfall reflects the possible impact of climate change.

The slope of regression analysis for precipitation illustrates the falling and rising trends of precipitation at different time intervals; rising and falling values specify the trends of increased and decreased rainfall, respectively. In January, May, October, November, and December, the slope of the precipitation data series is falling, i.e., a reduction in the monthly rainfall in respective months. The most negative slope, −1.06, was obtained for August. The slope of precipitation for the remaining months shows rising trends; the rising slope had the highest value of 1.65 in June. Rainfall trends (1981–2020) are tabulated in Table 6 and graphically presented in Figs. 2 and 3.

Table 6 Precipitation trends analysis obtained through linear regression over four decades

Month	1981–90	1991–00	2001–10	2011–20
January	Decremental	Decremental	Decremental	Decremental
February	Incremental	Incremental	Decremental	Decremental
March	Decremental	Decremental	Incremental	Incremental
April	Decremental	Decremental	Incremental	Incremental
May	Decremental	Incremental	Decremental	Decremental
June	Incremental	Incremental	Incremental	Decremental
July	Decremental	Incremental	Incremental	Decremental
August	Decremental	Decremental	Decremental	Decremental
September	Decremental	Incremental	Incremental	Incremental
October	Incremental	Decremental	Incremental	Decremental
November	Decremental	Decremental	Incremental	Incremental
December	Incremental	Incremental	Incremental	Decremental

5 Conclusions

The following conclusions are derived from this study:

- Different aspects of water resources planning and management rely on the rainfall occurring in a given region. This study has been made to determine the variation in temporal presentation for the Kota district in Rajasthan, India.
- Rainfall trend analysis has been performed for monthly, seasonal, and annual precipitation using linear regression (parametric) and Mann–Kendall (non-parametric) trend test for the duration of 1981–2020. For a particular year, excessive rainfall in the research area was determined using a wetness index and standardised rainfall anomaly.
- The monthly distribution of precipitation was calculated through the precipitation concentration index. A very high non-uniformity has been observed in rainfall distribution. Almost 85% of total annual rainfall is contributed through a southeast monsoon in the rainy season.
- Mann–Kendall and regression analyses test predict increasing trends for February, March, June, July, August, and September. As an outcome, total annual precipitation exhibits a positive trend.
- Over the last four decades (1981–2020), a significant increase in total precipitation was observed, highlighting greater water availability in the Kota that needs development and restoration of water reservoirs, proper rainwater harvesting, and a drainage management program to avoid the risk of flood.

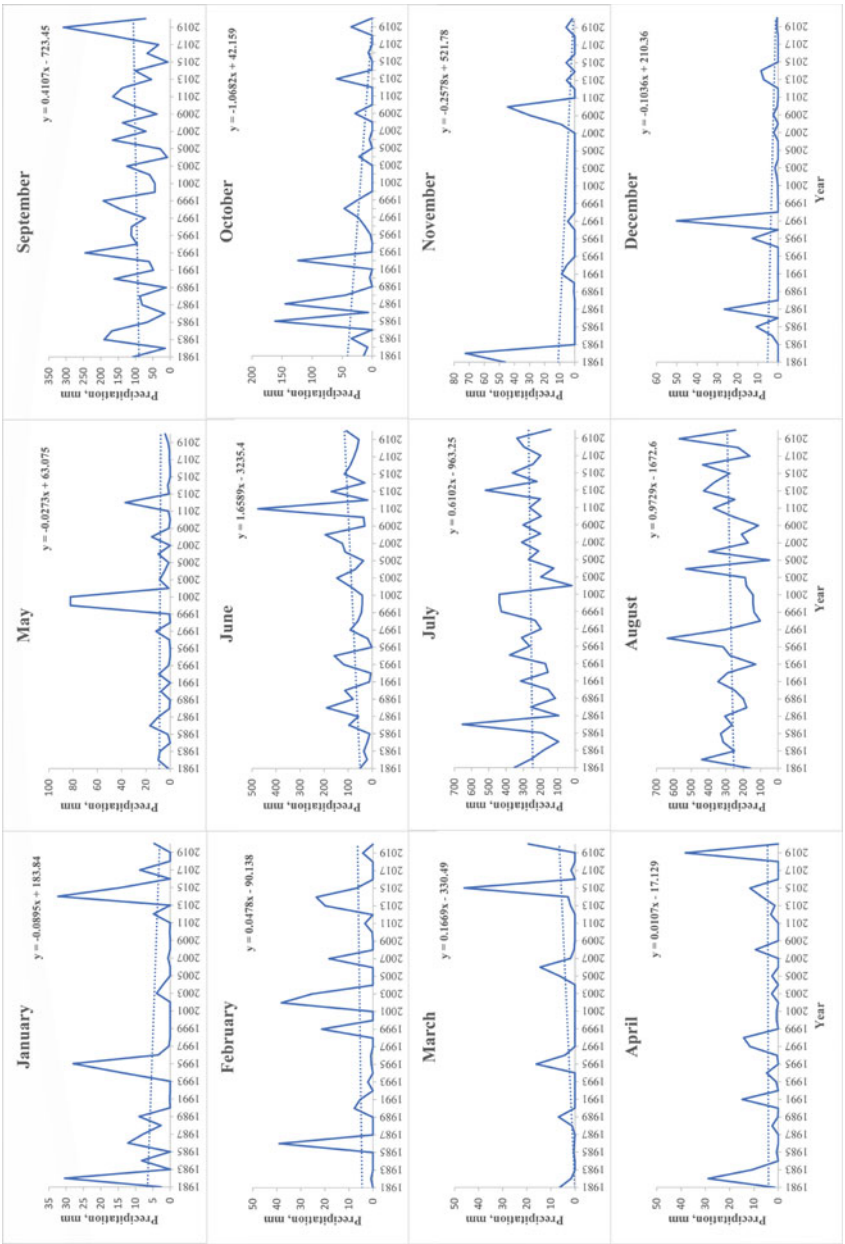

Fig. 2 Variation in the monthly, seasonal, and annual rainfall trends from 1981 to 2020

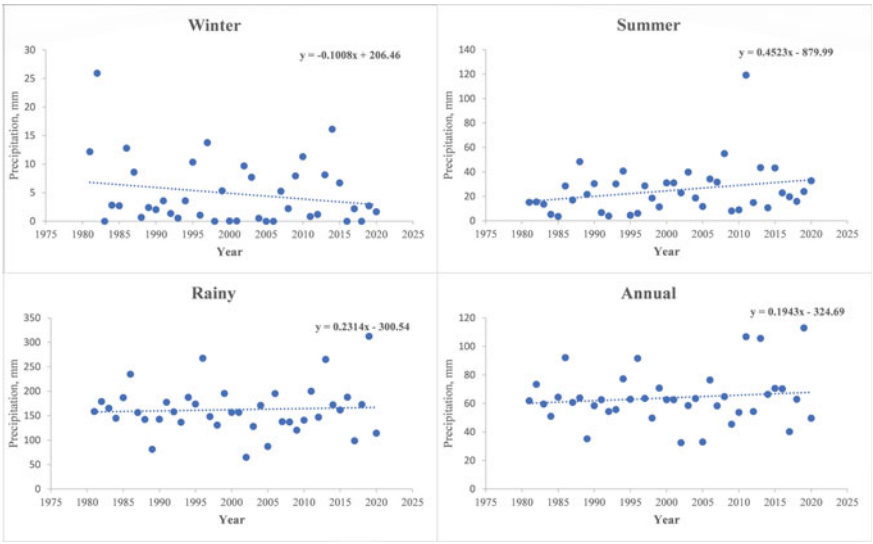

Fig. 3 Seasonal and annual rainfall trends from 1981 to 2020

Acknowledgements The authors acknowledge the financial support received from University Department, Rajasthan Technical University, Kota-324010, Rajasthan, India, to carry out the present work. The authors are also thankful to the Water Resources Department, Government of Rajasthan, India, for providing the necessary data to conduct the present study.

Conflict of Interest The authors declare that they don't have any conflict of interest.

Data Statement The data utilised in this research work are freely available and provided to anyone if needed.

References

1. Pradhan RK et al (2018) Changes of precipitation regime and its indices over Rajasthan state of India: impact of climate change scenarios experiments. Clim Dyn 52:3405–3420. https://doi.org/10.1007/s00382-018-4334-9
2. Caloiero T, Ferrari RCE (2018) Analysis of monthly rainfall trend in Calabria (Southern Italy). Appl Statist 2(11), 629:1–9. https://doi.org/10.3390/proceedings2110629
3. Devi S et al (2017) Spatial and temporal trends of precipitation and temperature for the MPUAT service area, Rajasthan, India. IOSR J Agric Veterin Sci 10(07):15–20. https://doi.org/10.9790/2380-1007011520
4. Deoli V, Rana S (2019) Seasonal trend analysis in rainfall and temperature for Udaipur District of Rajasthan, vol 14, issue (2), pp 312–319. https://doi.org/10.12944/CWE.14.2.15
5. Li XN et al (2017) Multi-timescale analysis of rainfall in Karst in Guizhou, China. IOP Conf Ser Earth Environ Sci 82(1):1–7. https://doi.org/10.1088/1755-1315/82/1/012051

6. Meena HM et al (2019) Trends and homogeneity of monthly, seasonal, and annual rainfall over arid region of Rajasthan, India. Theor Appl Climatol 136:795–811. https://doi.org/10.1007/s00704-018-2510-9
7. Singh B et al (2012) Probability analysis for estimation of annual one day maximum rainfall of Jhalarapatan Area of Rajasthan, India. Plant Arch 12(2):1093–1100
8. Kuldeep, Sisodiya S, Mathur AK (2020) Comparative assessment of noise models for Kota city. Mater Today Proc (xxxx):1–7. https://doi.org/10.1016/j.matpr.2020.09.513
9. Kuldeep et al (2019) Spatio-temporal variability of precipitation and temperature in Hadoti region, Rajasthan (India). Taru J Sustain Technol Comp 1(1):35–44. https://doi.org/10.47974/TJSTC.010.2019.v01i01
10. Kuldeep et al (2021) Noise vulnerability assessment at 78 dB (A) for Kota City, In: Baredar PV, Tangellapalli S, Solanki CS (eds) Advances in clean energy technologies. Springer Proceedings in Energy. Springer, Singapore, pp 1147–1159. https://doi.org/10.1007/978-981-16-0235-1_89
11. Kamboj K et al (2022) Assessment and spatial distribution mapping of criteria pollutants. Water Air Soil Poll 233:82:1:15. https://doi.org/10.1007/s11270-022-05522-y
12. Singh B et al (2014) Analysis of rainfall data for storage and irrigation planning in humid south-eastern plain of Rajasthan in India. J Appl Nat Sci 6(1):214–219. https://doi.org/10.31018/jans.v6i1.403
13. Meshram SG et al (2017) Statistical evaluation of rainfall time series in concurrence with agriculture and water resources of Ken River basin. Central India (1901–2010), no. Ipcc 2007 134(1):1231–1243. https://doi.org/10.1007/s00704-017-2335-y
14. Zakwan M, Ara Z (2019) Statistical analysis of rainfall in Bihar. Sustain Water Resour Manage 5(4):1781–1789. https://doi.org/10.1007/s40899-019-00340-3
15. Pradhan RK, Sharma D, Panda SK, Dubey SK, Sharma A (2019) Changes of precipitation regime and its indices over Rajasthan state of India: impact of climate change scenarios experiments Climate Dynamics 52(5-6):3405–3420 https://doi.org/10.1007/s00382-018-4334-9
16. Shreepada D, Purohit RC, Bhakar SR, Lakhawat SS (2017) Spatial and temporal trends of precipitation and temperature for the MPUAT service area Rajasthan India IOSR Journal of Agriculture and Veterinary Science 10(07):15–20 https://doi.org/10.9790/2380https://doi.org/10.9790/2380-100701https://doi.org/10.9790/2380-1007011520

Trend Analysis of Long-Term Rainfall Data Series

Sharad K. Jain

Abstract This paper presents some interesting results of trend analysis of long-term rainfall data series. The long-term precipitation data series for India the period 1871–2016, published in 2017 by Kothawale and Rajeevan, were used. Mann–Kendall, Sen's Innovative Trend Analysis Method and Wavelet Decomposition were used to analyze the data. While MK test showed no trend in any of the series used, (Sen in J Hydrol Eng, 2012) method revealed trends in different ranges of the data. Further, the wavelet decomposed series helped identify the periods of high variabilities in the various components of data series. Additional insights provided by these methods could be of immense value in identifying the likely future behavior of the data and the implications for water management.

Keywords Trend analysis · Rainfall · Mann–Kendall test · Innovative method · Wavelet decomposition

1 Introduction

Recent times have seen significant warming of atmosphere. Intergovernmental Panel on Climate Change (IPCC) has recently released the Report of Working Group I covering the physical science basis for the 6th Assessment Report (AR6). This report categorically states that the atmosphere, ocean, and land have warmed up. As per IPCC, the human-caused increase in global surface temperature from 1850–1900 to 2010–2019 is about 1.07 °C [8].

S. K. Jain (✉)
Civil Engineering Department, IIT Roorkee, Roorkee 247667, India
e-mail: sharad.jain@ce.iitr.ac.in

P. V. Timbadiya et al. (eds.), *Climate Change Impact on Water Resources*, Lecture Notes in Civil Engineering 313, https://doi.org/10.1007/978-981-19-8524-9_23

In the fourth assessment report, [15] had noted that there is a 'notable lack of geographical balance in the data and literature on observed changes, with marked scarcity in developing countries'. Although data availability has improved in various parts of the world over time since better instruments are being deployed and advanced techniques including remote sensing are being used to collect data. Further, more efforts are underway to analyze the data and share the outcome. Nevertheless, much more progress is still needed on both the fronts to overcome the lack of data and comprehensive analysis.

Among the different climatic variables, precipitation is perhaps the most important for hydrologists and water managers and it directly influences almost all the water related processes in a catchment. Therefore, analysis of trends in rainfall data is of immense interest to hydrologists, meteorologists, and all those whose interest lies in climate change and its impacts. With this background, the aim of the current paper is to analyze trends in observed long-term rainfall data series for India by using a range of conventional and new methods. Utility of new insights, revealed by the advanced, for water resources management has also been discussed.

2 Trend Analysis of Hydrologic Data

Trend analysis of a hydrologic time series involves finding two things: the magnitude of trend and how significant it is statistically. In view of the importance of the topic, it has attracted attention of a large number of researchers, as evidenced by numerous publications, including reviews, emerging from numerous studies. Kundzewicz [11] and Sonali and Nagesh Kumar [27] have provided detailed discussion on the trend detection methods for hydro-meteorological data. Some of the noteworthy studies on rainfall (RF) trends in India include.

Some past studies had found no clear trend in average annual RF over India [12, 26] although the regions of significant long-term rainfall changes were reported by Kumar et al. [4], Dash et al. [12] and Kumar and Jain (2010) [13]. Ramesh and Goswami [23] found falling trends in early and late monsoon RF and the number of rainy days over India for the period 1951–2003. Kumar et al. [12] did not detect significant trend for annual, seasonal, and monthly rainfalls on All India scale for RF data for 1871–2005. Guhathakurta and Rajeevan [14] analyzed a RF series created by using data of 1476 rain gauge stations for the period 1901–2003 and found significant falling and increasing trend for different sub-divisions. Pal and Al-Tabbaa [17] reported falling trends in the monsoon and spring RF and increasing trends in winter and autumn RFs over the country for the period 1954–2003. Kumar and Jain [13] examined trends seasonal RF over various river basins of India.

Broadly, two methods are used to calculate the magnitude of trend in a time series: regression analysis which is a parametric method or the Sen's estimator method [24] which is a non-parametric method. Both these methods assume that the time series of (hydrologic) data has a linear trend. In regression analysis, time is the independent variable and the hydrologic data is the dependent variable. In some studies, in place

of the hydrologic data, anomalies or the series of deviations from the mean, are used. In regression, the following a linear equation is fitted to the data:

$$y = at + b \tag{1}$$

where b is the intercept and a is a coefficient representing trend or slope. The parameters a and b are determined by method of least-squares. Note that slope of the line provides the rate of change (rise/fall) in the values of the variable.

Sen's estimator has been used extensively to compute the magnitude of trend in hydro-meteorological time series [9, 19]. In Sen's method, first slopes (T_i) of all data pairs are calculated by

$$T_i = \frac{x_j - x_k}{j - k} \quad \text{for } i = 1, 2, \ldots, N \tag{2}$$

where x_j and x_k are the values of variable at time j and k, respectively, such that $j > k$. The median value of the N values of T_i is the Sen's slope, computed as

$$\beta = \begin{cases} T_{\frac{N+1}{2}} & N \text{ is odd} \\ \frac{1}{2}\left(T_{\frac{N}{2}} + T_{\frac{N+2}{2}}\right) & N \text{ is even} \end{cases} \tag{3}$$

A positive value of β indicates a rising trend whereas negative value is an indicator of falling trend in the data series.

3 Significance of Trend

To find out the statistical significance of trend in the data series, Mann–Kendall (MK) test is employed [3, 6]. MK test is a non-parametric test. It checks the validity of the null hypothesis of no trend against the alternative hypothesis that an increasing or decreasing trend exists. MK test is helpful in detecting deterministic trends. We note that the MK test makes only very few assumptions: the potential trend in the data may be linear or nonlinear. The test does not make any assumption about the underlying statistical distribution.

It is known that the MK test is not robust when the series has high autocorrelation and in such cases, false positive trend is likely to be identified. If a series is positively autocorrelated, it is quite likely that the series may be detected as having a trend while it may not be present. Conversely, in a negatively autocorrelated series, the trend may remain undetected. This performance also depends on the length of the sample and also on the magnitude of the trend to be identified. In autocorrelated series, pre-whitening is applied to remove autocorrelation but, of course, it may also bias the Mann–Kendall test result.

4 Sen's Innovative Trend Analysis Method

This method uses the concept that if two time series, having similar statistical properties are plotted against each other, they will follow a straight line with 45° slope or 1:1 line irrespective of their underlying distributions, length, and serial correlation [25]. If all the data from the two series fall on the 45° line, it means that the time series do not have any trend. An important feature of such graphs is that data get sorted in order of magnitude along the 45° line. This idea can be implemented for trend detection by diving a long time series in two equal parts and plotting the first half against the second half. Scatter of the data points about the 1:1 or 45° line indicates rising or falling monotonic trends, respectively [27]. If the points are scattered on either side of the 45° line, it indicates the presence of non-monotonic rising or falling trend in time series at different temporal scales.

[25] also reported that if the cluster of the points is closer to the 1:1 line, it shows the presence of weaker trend magnitude. If the plot of data points appears along a straight line which is parallel to 1:1 line, the time series is likely to have a monotonic trend.

4.1 Wavelet Decomposition Method

Wavelets are becoming an increasingly useful and popular tool for analysis of time series data. A wave is a real-valued function, defined over the entire real axis. Value of a wave function oscillates about zero and the amplitude of the oscillations are nearly the same over the entire range. A wavelet is 'smaller' than a wave in the sense that a wavelet has a finite magnitude over some finite interval and is zero or close to zero beyond this interval.

For a function $\psi(.)$ to be called a wavelet, it should satisfy three conditions: (a) $\psi(.)$ must integrate to 0; (b) $\psi^2(.)$ must integrate to 1; and (c) $\psi(.)$ must be 'admissible' [20].

Wavelet transform (WT) is a technique for analysis of time–frequency characteristics of a time series. WT can be classified in two main groups–continuous (CWT) and discrete (DWT). Compared to CWT, DWT is a simpler process that provides useful outputs. DWT commonly uses dyadic calculations where the wavelet coefficients can be calculated by Eq. (4) [19, 22]:

$$W_\psi(a,b) = \frac{1}{2^{\alpha/2}} \sum_{t=0}^{N-1} x(t)\psi\left(\frac{t}{2^a} - b\right) \tag{4}$$

where ψ is the mother wavelet, a and b represent the amount of dilation (scale factor) and translation of the wavelet, respectively.

In the wavelet method, first, the decomposition level is determined. If data are decomposed in unnecessary details, lots of data are generated which may not help

with analysis. The level to which data decomposed also depends upon the mother wavelet used. The following equation to compute the maximum decomposition level, L, was suggested by de Artigas et al. [5]:

$$L = \log_2[n/(2v - 1)] \tag{5}$$

where n is the number of data points and v represents the number of vanishing moments of a Daubechies (db) wavelet. Studies suggest that for annual and seasonal data series, 3 levels of decomposition are adequate [18] for the commonly used wavelets (db6–db10). For trend analysis, smoother db wavelets (db5–db10) are commonly applied on the annual and seasonal time series [18]. Smoother wavelets are also preferred in the present study because the trends in hydro-meteorological data are likely to be gradual due to slowly changing nature of the deriving processes. de Artigas et al. [5] used the mean relative error (MRE) to identify the smooth mother wavelet and the extension mode of db wavelets. MRE can be computed as:

$$\text{MRE} = \frac{1}{n}\sum_{j=1}^{n}\frac{|a_j - x_j|}{|x_j|} \tag{6}$$

where x_j is the original variable, and a_j is the approximate value of x_j.

5 Data Used

This study has used long-term precipitation data for India. These data were published in a report by Kothawale and Rajeevan [10]. This report had compiled area weighted rainfall time series for the whole India and 5 homogeneous regions. The data series were constructed from the data of fixed and a network of 306 rain gauge stations, the stations were well-distributed over India and covered the period 1871–2016.

Here, I am reporting the results of analysis carried out on the All India annual and seasonal data.

6 Preliminary Data Processing

Precipitation data series for 146 years (1871–2016) for the whole India as well as four seasons, Winter (JF), Summer (MAM), Monsoon (JJAS), and Post-monsoon (OND) were analyzed to detect trends. Figure 1 shows the time series of annual rainfall. The series shows a very slow falling trend which is not statistically significant.

Summary statistical properties of the data are shown in Table 1. Among the seasons, monsoon season accounts for about 78% of the annual rainfall whereas only about 2% of the annual rainfall occurs in the winters. Interestingly, the monsoon

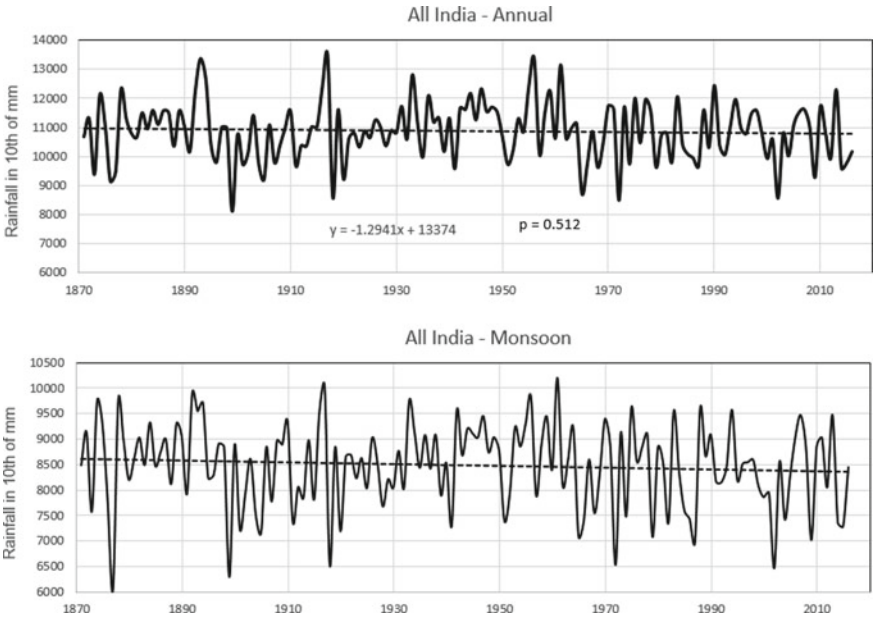

Fig. 1 Time series of All India annual and monsoon season rainfall

season rainfall has the smallest variability and the winters the highest, as evidenced by the coefficient of variation.

Next, autocorrelations were computed for each of the four seasonal and annual precipitation data series. Autocorrelations were computed for lag-1 to lag-12 and the correlograms for the annual RF has been plotted in Fig. 2. To determine whether the

Table 1 Summary statistical properties of the data used

Parameter	Winters (JF)	Summer (MAM)	Monsoon (JJAS)	Post-monsoon (OND)	Annual
Average rainfall (10th of mm)	232.04	943.95	8481.62	1201.45	10,859.09
Standard deviation (10th of mm)	116.25	205.47	834.52	345.61	1013.68
Coeff. of variation	0.501	0.218	0.098	0.288	0.093
Minimum value (10th of mm)	30	552	6040	501	8109
Maximum value (10th of mm)	611	1665	10,202	2099	13,470
Correlation at lag-1	0.025	−0.077	−0.091	0.132	−0.009

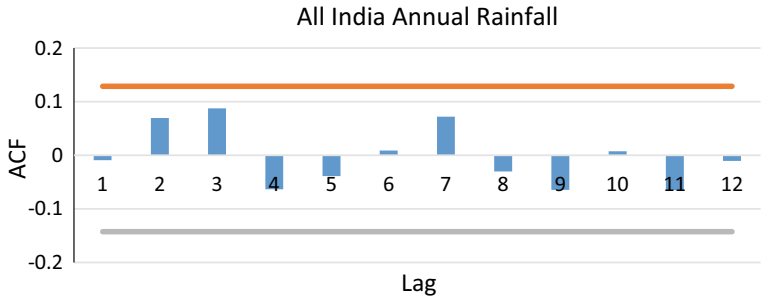

Fig. 2 Autocorrelation plot for All India annual rainfall for lag-1 to lag-12

autocorrelation coefficients are significant or not, the limits are computed by Eq. (7) [1]:

$$\frac{\left\{-1-1.645\sqrt{(n-2)}\right\}}{n-1} \leq R \leq \frac{\left\{-1+1.645\sqrt{(n-2)}\right\}}{n-1} \tag{7}$$

If the autocorrelation coefficients are within the interval computed by Eq. (7), one can assume that the series does not display a significant autocorrelation. It is noticed that for the annual rainfall, all the autocorrelations are well within the limits (−0.1430 to 0.1292) given by Eq. 7. Hence, we can assume that the data series do not have a significant autocorrelation.

6.1 Mann–Kendall Test and Sen's Slope Estimation

The MK test was performed on the annual series and the data series of three seasons. Trends were examined at 5% significance level in a two-tailed test for which the standard value of Z is ±1.96. No trend was found in the data of All India and in any of the seasons and the Z values were all within the interval −1.96 to +1.96. Further, the Sen's slope was also computed as shown in Table 2.

Table 2 Trend, MK Z-value, and Sen's slope for All India–Annual and seasonal rainfall series

Time scale	Trend and Z-value		Sen's slope
	Trend	Z-value	
All India–Annual	No trend	−0.5755	34.8750
All India—March, April, May	No trend	0.7526	6.6389
All India—June, July, August, September	No trend	−1.2854	8.300
All India—October, November, December	No trend	0.5714	33.333

6.2 Sen's [25] Innovative Trend Analysis Method

The innovative trend analysis method developed by Sen [25] and described earlier was used to find trend in the All India rainfall data series. In Fig. 3, RF data for All India have been partitioned in two parts and plotted as scatter diagram: *X*-axis has data series from 1871 to 1943 and data series for 1944–2016 is plotted on *Y*-axis. To interpret and understand the trend, data have been qualitatively divided in three segments–low, medium, and high. The limits of the ranges are varying with the season since the magnitude of rainfalls are different in different seasons.

Four graphs have been presented here: All India–annual rainfall; seasonal rainfalls for March, April, and May (MAM); June, July, August, and September (JJAS); and October, November, and December (OND). The interpretation of the graphs is summarized in Table 3. Broadly, in each case, three distinct trends are seen in three ranges of data, demarcated by rectangular boxes.

For All India RF, in the lower ranges (8000–10,000 mm), all the data fall above the 45° line implying that in the second half (1944–2016), RF show strong increasing trend compared to the first half. In higher range (12,000–14,000 mm), all the data fall below the 45° line showing a declining trend in this range. In the mid-range, data are

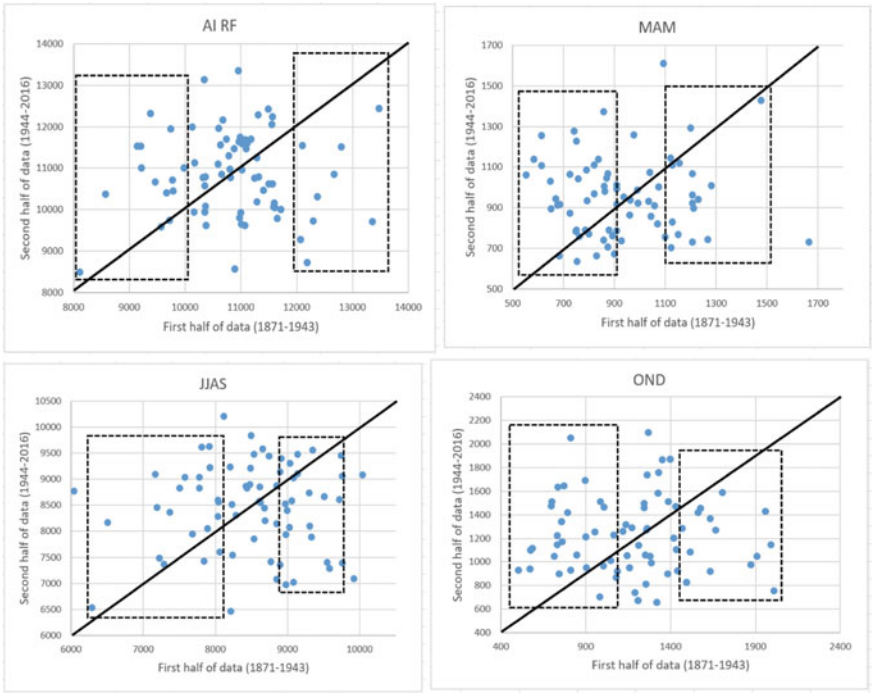

Fig. 3 Identification of trend in annual and seasonal series by use of [25] innovative trend analysis method

Table 3 Trends in All India and seasonal rainfalls

Time scale	Trend in		
	Lower range	Mid-range	High range
All India—Annual	Strong increasing trend	Mixed trend with bias toward increase	Falling trend
All India—March, April, May	Strong increasing trend	Falling trend	Falling trend
All India—June, July, August, September	Strong increasing trend	Mixed trend with bias toward increase	Falling trend
All India—October, November, December	Strong increasing trend	Mixed trend	Falling trend

nearly evenly distributed around the 45° line. When the data points are away from the 45° line, it indicates stronger trends [25]. Interpretation on similar lines were made for the data of seasonal RFs and the outcomes are summarized in Table 3.

As seen from the Table 3, in the lower ranges of RF values, strong increasing trend was noticed in the data for All India and the three seasons. Conversely, the data for All India and the three seasons show a falling trend. In the mid-range, mixed or falling trends were observed. One can conclude form this table that at the national scale, RFs in India will have lesser variability in future if the observed trends continue. It is also likely that in future, at the All India scale, lower values of RFs will likely increase and the higher values will fall. Note that this interpretation is not applicable to RF intensities which are expected to increase.

A comparison of these results with the MK test brings out the utility of [25] innovative Trend Analysis Method. While the MK method did not detect any trend in the RF data series, the [25] method was able to reveal trends in various ranges of the data series. However, Serinaldi et al. [29] have raised concerns about this method, noting that this method suffers from many theoretical inconsistencies. Hence, the outcomes of this method should be viewed with caution.

6.3 Results of Wavelet Decomposition for Trend Analysis

A variety of wavelet forms have been developed and are used in studies, e.g., the Haar wavelet, the Daubechies wavelet. Here, the Daubechies (db) wavelet was employed since it is one of the most commonly used mother wavelets for analysis of hydro-meteorological data [18] and is said to be 'smooth'. Smooth wavelets were employed here since the trends in rainfall series are expected to be slow. Among the different forms of the Daubechies wavelet, db5 to db10 [18] were used in this study. The annual and seasonal time series were decomposed into approximate and detailed components. Each series was decomposed in one approximate (A3) and three detailed components (D1, D2, D3). A detailed component represents dyadic fluctuations at 2^n level; here n is the level of the detailed component. For annual or seasonal series, D1,

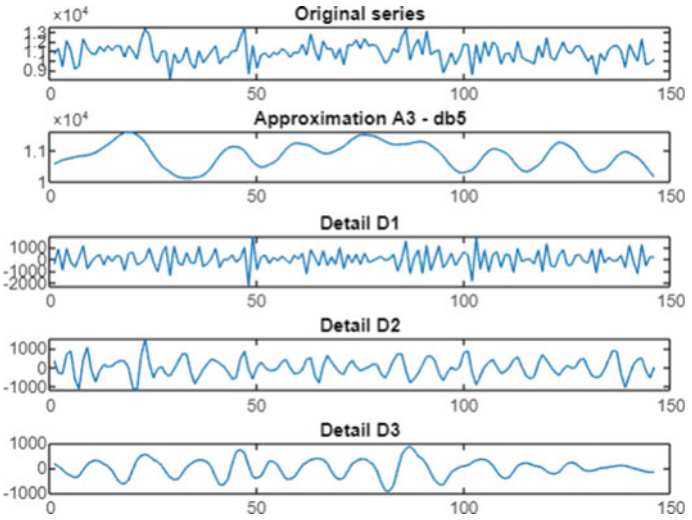

Fig. 4 Plot of original All India RF series and its components

D2 and D3 represent 2^1 year (or 2 year), 2^2 year (or 4 year), and 2^3 year (or 8 year) period, respectively. Further, as evident from Fig. 4, the approximate component of transformation (A3 in this case) is a slowly varying component of the time series.

To select among the best Daubechies wavelet from the group db5 to db10, the mean relative error (MRE) criterion was employed. The computed values of MRE are given in Table 4; minimum values of MRE for a particular data set are shown in bold numbers.

The results of MRE calculations show that the db9 wavelet had the lowest value of MRE for All India annual RF whereas the db5, db7, and db9 had the lowest MRE values for data of pre-monsoon, monsoon, and post-monsoon seasons.

Figure 4 shows the results of multi-resolution analysis (MRA) for time series of RF following the Daubechies wavelet transform. The top-most curve shows the original RF data series while the other four curves show the approximate and detailed components. The second graph in Fig. 4 shows the approximate component of the

Table 4 Computed values of MRE for All India and seasonal data series

Time scale	MRE for					
	db5	db6	db7	db8	db9	db10
All India—Annual	0.0685	0.0693	0.0680	0.0695	**0.0675**	0.0695
All India—March, April, May	**0.1721**	0.1728	0.1725	0.1723	0.1730	0.1723
All India—June, July, August, September	0.0771	9.0780	**0.0769**	0.0777	0.0771	0.0776
All India—October, November, December	0.2323	0.2321	0.2321	0.2325	**0.2318**	0.2333

series, which is the portion of RF that is attributable to averages on a scale of 16 years. Very slow variation over a rather narrow range is seen for this component. Next three graphs are the detailed series, D1, D2, and D3. Since an MRA is an additive decomposition, the sum of the components will yield the exact values of the original data.

Examination of the wavelet components helps in better appreciation of variabilities. For example, the periods of high variabilities can be easily demarcated in the approximate series A3: between years 40 to 75 and between years 102 till the end. The MRA enables to identify some localized features of data that are of interest. For example, in the plot of the original RF data series (Fig. 4), short stretches of decreased variability can be identified: between years 18 to 32 and years 73 to 100. At shorter time scales, detailed D1 series shows high variabilities around year 50 and year 100; detailed D2 series shows high variabilities around year 20 and year 100; and detailed D3 series shows high variabilities around year 80 to 85. Of course, some of these variabilities can be seen in the original time series but the MRA has vividly highlighted these features.

In addition to the results presented in Table 4, MK test was performed and Z value was computed for A3, A3 + D1 and A3 + D1 + D2 series. Based on Z values, A3 series for monsoon season, and all the three series for post-monsoon seasons had statistically significant trend.

7 Conclusions

This paper presents results of trend analysis of observed long-term rainfall data series for India. Results of MK test showed no trend in the series of All India RF and RF for three seasons–pre-monsoon, monsoon, and post-monsoon. However, [25] innovative trend analysis method revealed trends in various ranges of the data series. Lastly, multi-resolution analysis of the wavelet decomposed series highlighted periods of high variabilities in the approximate and detailed series. It also showed that some of the decomposed data series had statistically significant trend whereas the original data did not show such trends in MK test. In the series generated by wavelet decomposition, the approximate series may be considered to represent 'climate' and the detailed 'weather'. More research is needed to understand the implications of these findings and how these can be harnessed for better water management. Since the approximate component of All India monsoon series has a declining trend, there is good possibility that the entire series may show similar trend in future. Impact of falling rainfalls on the GDP of India and livelihood would be significant and would be important for planners.

Changes in precipitation features, its average levels and ranges are important in planning adaptation programs and associated challenges. Precipitation trends are indicators of forthcoming changes in the hydrologic cycle in terms of variabilities and uncertainties and are helpful in preparing future projections. They also influence

availability of surface and ground water, and probabilities of floods and droughts in future.

References

1. Araghi M, Mousavi Baygi J, Adamowski J, Malard D, Nalley SM, Hasheminia (2015) Using wavelet transforms to estimate surface temperature trends and dominant periodicities in Iran based on gridded reanalysis data. Atmos Res 155:52–72
2. Bayazit M, Önöz B (2007) To prewhiten and not to prewhiten in trend analysis? Hydrol Sci J 52(4):611–624
3. Burn DH, Cunderlik JM, Pietroniro A (2004) Hydrological trends and variability in the Liard river basin. Hydrol Sci J 49:53–67
4. Dash SK, Jenamani RK, Kalsi SR, Panda SK (2007) Some evidence of climate change in twentieth-century India. Clim Change 85:299–321
5. de Artigas MZ, Elias AG, de Campra PF (2006) Discrete wavelet analysis to assess long-term trends in geomagnetic activity. Phys Chem Earth Parts A/B/C 31(1–3):77–80. https://doi.org/10.1016/j.pce.2005.03.009
6. Douglas EM, Vogel RM, Knoll CN (2000) Trends in flood and low flows in the United States: impact of spatial correlation. J Hydrol 240:90–105
7. Goswami BN, Venugopal V, Sengupta D, Madhusoodanam MS, Xavier PK (2006) Increasing trends of extreme rain events over India in a warming environment. Science 314:1442–1445
8. IPCC (2021) Summary for Policymakers. In: Masson-Delmotte V, Zhai P, Pirani A, Connors SL, Péan C, Berger S, Caud N, Chen Y, Goldfarb L, Gomis MI, Huang M, Leitzell K, Lonnoy E, Matthews JBR, Maycock TK, Waterfield T, Yelekçi O, Yu R, Zhou B (eds) Climate change 2021: the physical science basis. Contribution of Working Group I to the Sixth Assessment Report of the Intergovernmental Panel on Climate Change. Cambridge University Press In Press
9. Jain SK, Kumar V, Saharia M (2013) Analysis of rainfall and temperature trends in North-East India. Int J Climatol 33:968–978
10. Kothawale DR, Rajeevan M (2017) Monthly, seasonal and annual rainfall time series for All-India, homogeneous regions and meteorological subdivisions: 1871–2016. Research Report No. RR-138. Indian Institute of Tropical Meteorology (IITM), Pune, India
11. Kundzewicz ZW, Robson AJ (2004) Change detection in hydrological records—a review of the methodology. Hydrol Sci J 49(1):7–19
12. Kumar V, Jain SK, Singh Y (2010) Analysis of long-term rainfall trends in India. Hydrol Sci J 55(4):484–496
13. Kumar V, Jain SK (2010) Trends in rainfall amount and number of rainy days in river basins of India (1951–2004). Hydrol Res 42(4):290–306
14. Guhathakurta P, Rajeevan M (2008) Trends in the rainfall pattern over India. Int J Climatol 28(11):1453–1469
15. IPCC (2007) Climate change 2007: impacts, adaptation and vulnerability. In: Parry ML, Canziani OF, Palutikof JP, van der Linden PJ, Hanson CE (eds) Contribution of Working Group II to the Fourth Assessment Report of the Intergovernmental Panel on Climate Change. Cambridge University Press, Cambridge, UK, p 976
16. Önöz B, Bayazit M (2011) Block bootstrap for Mann-Kendall trend test of serially dependent data. Hydrol Process. https://doi.org/10.1002/hyp.8438
17. Pal I, Al-Tabbaa A (2010) Assessing seasonal precipitation trends in India using parametric and non-parametric statistical techniques. Theoret Appl Climatol. https://doi.org/10.1007/s00704-010-0277-8
18. Pandey BK, Tiwari H, Khare D (2017) Trend analysis using discrete wavelet transform (DWT) for long-term precipitation (1851–2006) over India. Hydrol Sci J 62(13):2187–2208

19. Partal T, Kahya E (2006) Trend analysis in Turkish precipitation data. Hydrol Process 20:2011–2026
20. Percival DB, Wang M, Ovesrland JE (2004) An introduction to wavelet analysis with applications to vegetation time series. Commun Ecol 5(1):19–30
21. Pettitt AN (1979) A non-parametric approach to the change point problem. J Appl Stat 28(2):126–135
22. Kristina P, Gilja G, Kunštek D (2017) An overview of the applications of wavelet transform for discharge and suspended sediment analysis. Tehnički vjesnik 24(5):1561–1569
23. Ramesh KV, Goswami P (2007) The shrinking Indian summer monsoon. Research Report RR CM 0709, CSIR Centre for Mathematical Modelling and Computer Simulation, Bengaluru
24. Sen PK (1968) Estimates of the regression coefficient based on Kendall's tau. J Am Stat Assoc 63:1379–1389
25. Sen Z (2012) An innovative trend analysis methodology. J Hydrol Eng. https://doi.org/10.1061/(ASCE)HE.1943-5584
26. Sinha Ray KC, De US (2003) Climate change in India as evidenced from instrumental records. WMO Bulletin 52(1):53–59
27. Sonali P, Nagesh Kumar D (2013) Review of trend detection methods and their application to detect temperature changes in India. J Hydrol 476:212–227
28. Yue S, Hashino M (2003) Long term trends of annual and monthly precipitation in Japan. J Am Water Resour 39(3):587–596
29. Serinaldi, Francesco, Fateh Chebana, and Chris G. Kilsby (2020). Dissecting innovative trend analysis. Stochastic Environmental Research and Risk Assessment, 34:733–754, https://doi.org/10.1007/s00477-020-01797.

Spatio-Temporal Variability and Trend Analysis of Changing Rainfall Patterns Over Upper Bhima Sub-Basin, Maharashtra, India

D. S. Londhe, Y. B. Katpatal, and M. S. Mukesh

Abstract The objective of the research is to use spatio-temporal variability and trend analysis to examine how the rainfall pattern is changing in the Upper Bhima Sub-basin of Maharashtra, India. To achieve this objective, rainfall data was analyzed for monsoon and annual timescale using CHRS precipitation data. The study considered five agro-climatic zones viz. Western ghat zone, Transition zone I, Transition zone II, Water scarcity zone and Assured rainfall zone within the watershed. This work analyses the pattern, distribution and trend behavior of rainfall for the period from 1983 to 2018. Since more than 85% of precipitation occurs during monsoon, the analysis has been performed for monsoon season and annual average precipitation data. Statistical summary like the mean, standard deviation and coefficient of variation and inferential statistics like linear regression and standardized anomaly were utilized for the analysis. The Mann–Kendall non-parametric test is used to analyze the trend of precipitation in different agro-climatic zones and the Sen's slope estimator is used to analyze magnitude of the trend. Spatial variation of the rainfall is analyzed and studied in geographical information system (GIS) environment. The effect of changing climate and regional environment on the spatial and temporal variation of rainfall is clearly noticeable in this study. Climate change strongly affects the agriculture activities where irrigation mainly depends on monsoon precipitation. Hence, policymakers and stakeholders should give importance to proper design and adopting area specific approaches to reduce the adverse effects on crop production at regional level. Rainwater harvesting and advancement in present irrigation facilities could be taken as best possible options in the areas having scarce and more inconsistent rainfall.

D. S. Londhe (✉) · Y. B. Katpatal · M. S. Mukesh
Department of Civil Engineering, Visvesvaraya National Institute of Technology, Nagpur 440010, India
e-mail: digambarlondhe@students.vnit.ac.in

P. V. Timbadiya et al. (eds.), *Climate Change Impact on Water Resources*, Lecture Notes in Civil Engineering 313, https://doi.org/10.1007/978-981-19-8524-9_24

Keywords Upper Bhima sub-basin · Spatio-temporal variation · Trend analysis · Mann–Kendall test · Sen's slope

1 Introduction

Precipitation has a significant impact on economic development of the regional environment by maintaining physical sustainability in hydrological cycle and water resource. Precipitation is a variable climatic parameter in hydrological cycle. Spatial and temporal changes and long term fluctuations in precipitation affects the water storage of the region [1, 2]. Hydrological cycle is affected due to rise in anthropogenic activities in the natural environment.

In recent years, agricultural growth and patterns is severely affected due to decrease in precipitation and its irregular behavior. Many research studies have been done to investigate the variability, distribution and trend behavior of rainfall at global, regional and at watershed level [3–8]. Amount of precipitation controls the groundwater availability and surface soil moisture which plays a significant role in many agricultural activities [9]. Pattern behavior of the rainfall has been interconnected to physical climatology.

Crop selection is primarily depends upon the total rainfall occurred in that area. Crop production also affects due to the uneven cropping patterns and farmer's lack of knowledge in the field of meteorological parameters and climatology. Precipitation trend analysis particularly at regional level will be beneficial to farmers as well as commercial and physical planners and policy makers. The possible future hydro-climatic changes at regional level can be predicted by analyzing the past trends.

In this study, the changing characteristics of rainfall using spatio-temporal variability and trend behavior over Upper Bhima Sub-basin, Maharashtra, India has been analyzed. The study considered five agro-climatic zones viz. Western ghat zone (WGZ), Transition zone I (TR1), Transition zone II (TR2), Water scarcity zone (WSZ) and Assured rainfall zone (ARZ) within the sub-basin. The analysis has been done for monsoon season and annual average precipitation data since more than 85% of precipitation occurs during monsoon.

2 Materials and Methods

2.1 Study Area: Upper Bhima Sub-Basin

The Upper Bhima sub-basin is situated between latitude 17.18 N to 19.24 N and longitude 73.20 E to 76.15 E (Fig. 1). Total area of the Upper Bhima sub-basin is 46,066 km^2. Elevation in the Western ghat zone reaches up to 1472 m from 160 m in the eastern parts of sub-basin [10]. The study area includes five agro-climatic

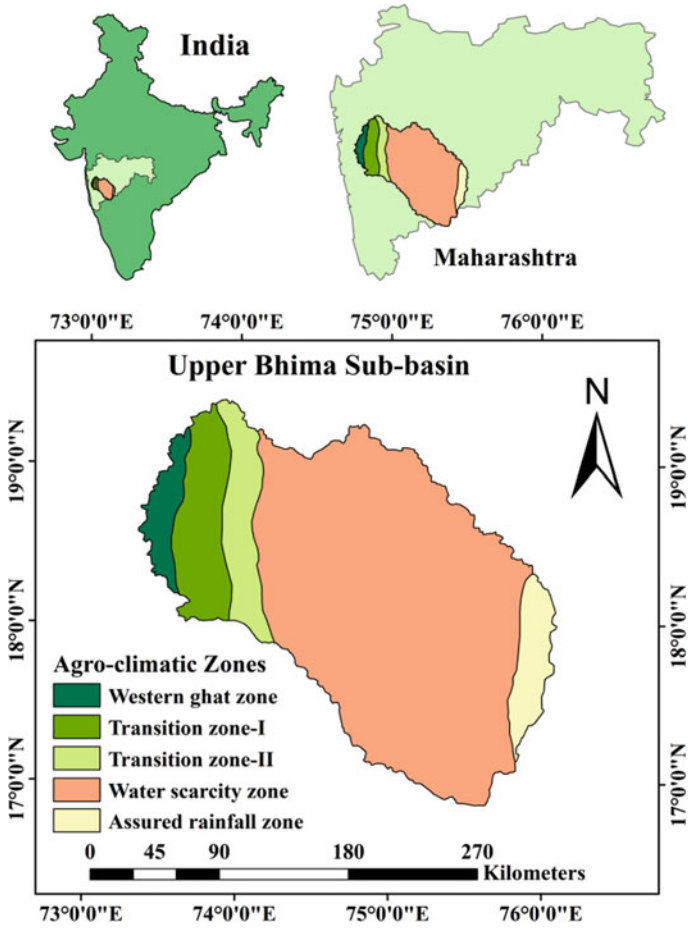

Fig. 1 Location map of study area

zones namely Western ghat zone (WGZ), Transition zone I (TR1), Transition zone II (TR2), Water scarcity zone (WSZ) and Assured rainfall zone (ARZ) within the sub-basin. Location map of the Upper Bhima sub-basin and its agro-climatic zones are shown in Fig. 1.

2.2 Precipitation Data

Precipitation data is obtained from Climate Forecast System Reanalysis (CFSR) developed at NOAA-NCEP [11] and Center for Hydrometeorology and Remote Sensing (CHRS). The spatial resolution of CFSR data is 0.350 and available from

1979 to present. CHRS rainfall data is available from 1983 to present. Also, the Global Precipitation Climatology Project (GPCP) precipitation data product is used. GPCP Version 3 (GPCP V3.1) product is homogeneous precipitation data extracted using advanced merging techniques.

The statistical summary for the region was calculated using precipitation data. Based on the obtained daily precipitation data, annual average and monsoon rainfall, standard deviation and coefficient of variation (CV) were calculated. The CV of yearly rainfall data indicates the climate risk which signifies potential fluctuations in crop production [12].

2.3 Mann–Kendall Test (MK) and Sen's Slope Estimator

The non-parametric Mann–Kendall (MK) test [13, 14] is used to study the precipitation trends and the Sen's slope estimator [15] is used to study the magnitude of that trend. The MK test is used to analyze the annual rainfall and monsoon rainfall. Tests have been considered at 5% significance level, i.e., significance levels at $\alpha = 0.05$ is considered for which $Z = 1.96$. MK test is applied to identify the trend in different climatological and hydrological time series. The MK test statistic S and standard normal test statistic Z were calculated as:

$$S = \sum_{i=1}^{N-1} \sum_{j=i+1}^{N} \operatorname{sgn}\left(X_j - X_i\right) \tag{1}$$

where N is total number of data samples;

X_i and X_j are time series observed data.

The σ statistic is approximately normally distributed which is calculated using mean and variance as:

$$\sigma^2 = \frac{n(n-1)(2n+5)}{18} \tag{2}$$

The standardized normal deviate Z statistics is calculated as:

$$Z = \begin{cases} \frac{s-1}{\sigma} & \text{if } s > 0; \\ 0 & \text{if } s = 0; \\ \frac{s+1}{\sigma} & \text{if } s < 0 \end{cases} \tag{3}$$

The positive Z value indicates increasing trends and negative Z value indicates decreasing trends. It is important to analyze the results of MK trend test and quantify the magnitude of the trend of time series data. Magnitude of the trend has been quantified by using the Sen's slope estimator [15]. In the present study, the annual and monsoon rainfall data time series was analyzed.

$$T_i = \frac{X_j - X_k}{j - k} \quad \text{for } i = 1, 2, \ldots N \quad (j > k) \tag{4}$$

where T_i is Sen's Slope, X_j and X_k are observational at time j and k, respectively, and the median of observation values of T_i is represented as Sen's estimator of slope given as:

$$Q_{\text{median}} = \begin{cases} T_{\frac{(N+1)}{2}} & \text{if } N \text{ is odd;} \\ \frac{T_{\frac{N}{2}} + T_{\frac{(N+2)}{2}}}{2} & \text{if } N \text{ is even} \end{cases} \tag{5}$$

The value of Q_{median} replicates the data trend direction and its value indicates the magnitude of slope of the trend.

2.4 Standard Deviation (S) and Coefficient of Variation (CV)

$$\text{Standard Deviation, } S = \sqrt{\frac{\sum_{i=1}^{n}(x - \overline{x})}{n}} \tag{6}$$

where S is standard deviation and n is total number of variables.

The Coefficient of Variation (CV) is an expression used to convert the standard deviation into % of the mean. CV shows the rainfall variation for annual and monsoon rainfall in study area.

$$\text{Coefficient of Variation, CV} = \frac{S}{x} \times 100 \tag{7}$$

3 Results and Discussion

3.1 Long Term Mean Monthly Rainfall Distribution

On the basis of 35 years average monthly, monsoon and annual rainfall has been estimated for all the five agro-climatic zones. Long term mean monthly and annual rainfall distribution from 1983 to 2018 is summarized in Table 1. Upper Bhima sub-basin receives maximum amount of rainfall in June, July, August and September, i.e., in monsoon period. The maximum average annual rainfall occurs in WGZ and TR1 which is 1380.12 mm and 1359.97 mm, respectively, while minimum rainfall occurs in ARZ and WSZ which is 1204.41 mm and 974.47 mm, respectively. The location of WSZ and ARZ in study area is located as rainfall shadow area of WGZ and TR1. June, July, August and September months are considered for the Monsoon period.

Table 1 Long term mean monthly and annual rainfall (mm) distribution in Agro-climatic zones (1983–2018)

	Jan.	Feb.	Mar.	Apr.	May	Jun.	Jul.
WGZ	2.48	1.89	8.00	5.95	29.76	256.37	418.58
TR1	2.89	2.37	8.40	5.39	27.98	254.37	414.40
TR2	2.32	1.91	10.14	7.36	27.32	224.67	402.02
WSZ	2.89	2.53	10.86	14.60	35.84	191.39	337.61
ARZ	2.34	2.69	10.08	16.12	36.86	155.58	232.54
	Aug.	Sept.	Oct.	Nov.	Dec.	Annual	
WGZ	293.28	229.92	103.00	25.38	5.51	1380.12	
TR1	287.99	226.04	100.50	24.16	5.48	1359.97	
TR2	293.82	232.64	95.54	22.05	5.33	1325.11	
WSZ	276.00	217.49	92.01	17.87	5.32	1204.41	
ARZ	216.49	192.65	89.09	14.44	5.59	974.47	

3.2 Temporal Variation and Trends of Rainfall

Temporal variation of the annual rainfall for the period from 1983 to 2018 is shown in Fig. 2. The lowest average annual rainfall was recorded in WGZ (870.31 mm) and TR1 (868.69 mm) in 2012 and for TR2 (820.69 mm), WSZ (748.15) and ARZ (654.61) lowest rainfall occurred in 2018. The highest average annual rainfall was recorded in WGZ (1856.55 mm) and TR1 (1846.78 mm) in 2006 and TR2 (1780.51 mm) and WSZ (1618.51 mm) in 2016 and ARZ (1396.47 mm) in 1988. The line chart shown in Fig. 2 also reveals that WSZ and ARZ receive lowest rainfall and WSZ and TR1 receives highest rainfall in the study area.

The linear regression analysis indicate the decreasing trend at the rate of −7.0793 mm/year, −4.9842 mm/year, −7.0336 mm/year, −8.7423 mm/year and −4.6402 mm/year for WGZ, TR1, TR2, WSZ and ARZ, respectively.

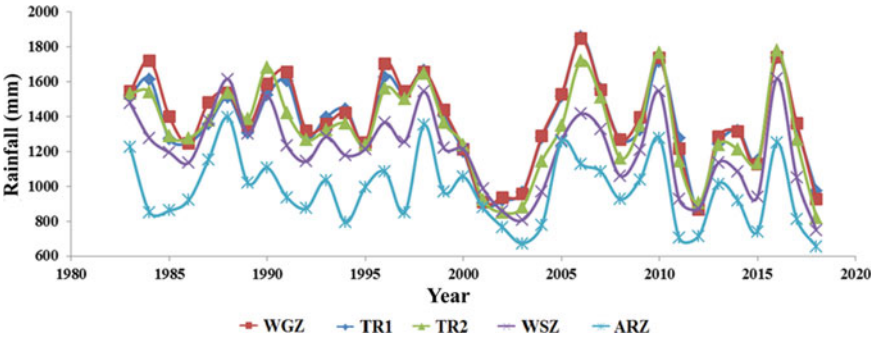

Fig. 2 Temporal variation of rainfall (1983–2018)

Table 2 Standard deviation, coefficient of variation, MK Test Statistic and Sen's slope analysis of monsoon and annual rainfall (at 5% significance level)

Agro-climatic zones	Monsoon rainfall			
	Standard deviation	Coefficient of variation (%)	MK test statistic	Sen's slope
WGZ	210.577	21.7	−2.25	−7.937
TR1	201.687	21.1	−1.95	−6.595
TR2	190.431	20.7	−2.27	−7.447
WSZ	157.5	19.6	−2.85	−7.912
ARZ	134.557	22.3	−1.81	−4.045
Annual rainfall				
WGZ	256.4355	18.6	**−1.39**	−6.888
TR1	244.2656	18.0	**−1.11**	−4.624
TR2	254.4257	19.2	**−1.33**	−7.16
WSZ	227.5544	18.9	−2.55	−9.89
ARZ	196.2324	20.1	−1.51	−5.323

Bold values in table indicate statistically significant values

The statistical parameters like standard deviation, coefficient of variation, MK test statistics and Sen's slope are illustrated in Table 2. From the results shown in Table 2, the results of MK test showed a statistically significant downward trend in annual and monsoon rainfall. The results also revealed a significant downward trend in WGZ, TR1 and TR2 zones and non-significant downward trend in WSZ and ARZ at 95% significant level for annual rainfall over the years.

The results of Sen's slope estimator identifies the maximum rate of average decrease is in WGZ for monsoon rainfall (−7.937 mm/year) and WSZ for annual rainfall (−9.89 mm/year) in the study area.

The higher CV value indicates higher variability of the sample data. The results indicate that CV is higher in ARZ as compared to other zones for both monsoon and annual rainfall which are 22.3% and 20.1%, respectively. The higher CV value in this zone denotes the region's irregular and inter-annual changing rainfall patterns. Lowest CV for monsoon rainfall is in WSZ (19.6%) and for annual rainfall is in TR1 (18.0%).

3.3 Spatial Variation of Rainfall

The regional level climatic parameters affect the global climatic conditions. Unique geographical features that control regional level environment are locations and proximity to water bodies, arid and semi-arid areas, forests, land use land cover classes, lakes, rivers, urban heat islands, etc.

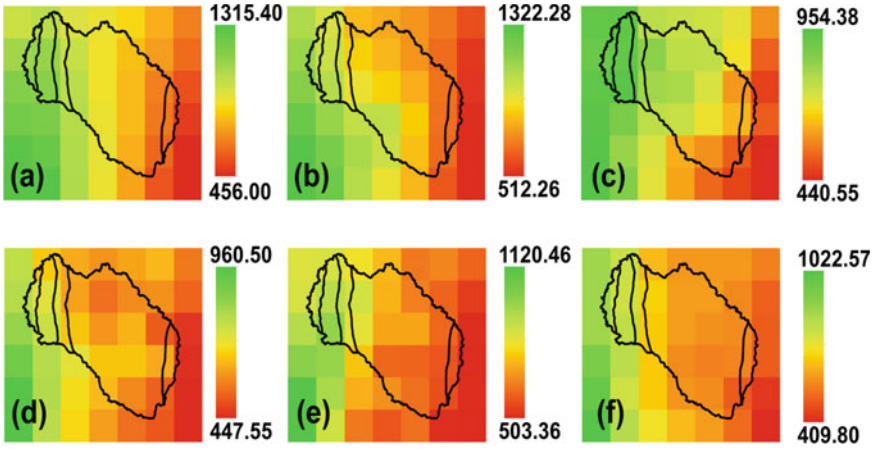

Fig. 3 Spatial variation of rainfall (mm/year) over Upper Bhima Sub-basin for **a** 1983–1990; **b** 1991–1995; **c** 1996–2000; **d** 2001–2005; **e** 2006–2010; **f** 2011–2018

Spatial variation of rainfall (mm/year) over Upper Bhima Sub-basin is shown in Fig. 3. The average annual rainfall values are divided into sub-periods from 1983 to 1990, 1991–1995, 1996–2000, 2001–2005, 2006–2010 and 2011 to 2018. The year 2001 to 2005 and 2010 to 2018 are received lowest rainfall while 1983–1990, 1991–1995 and 2006–2010 received higher rainfall. Spatial distribution clearly indicates that the WGZ, TR1 and TR2 receive higher rainfall as compared to WSZ and ARZ which are rainfall shadow zone.

3.4 Deviation in Rainfall from Mean

It is said to be inadequate or excessive rainfall for the year when annual rainfall deviates from the average rainfall of the tested years. The deviation of rainfall from average rainfall over the study area for annual timescale and for monsoon rainfall is shown in Fig. 4a and Fig. 4b, respectively. During the study period of 35 years (1983–2018), 17 years recorded below average annual rainfall (Fig. 4a) and 19 years recorded below average monsoon rainfall (Fig. 4b). The study of deviation of rainfall from mean is analyzed for annual timescale and also for monsoon rainfall only.

There are irregular short periods of dry phases at the initial study period. Regular negative deviation from mean, i.e., deficient rainfall has been observed from 2000. First dry period is during 1985 and 1986 which receives 45.188 mm and 82.432 mm deficit rainfall than mean rainfall, respectively. The major continuous dry period is during 2000 to 2005 and 2011 to 2015. This is also ascertained by the results shown in spatial variation of the annual average rainfall for 2001–2005 (Fig. 3d) and 2011–2018 (Fig. 3f) as it evident. Deficit rainfall value during 2000 to 2005 reaches up to 392.818 mm and during 2011 to 2015, deficit rainfall reaches up to 403.118 mm. The

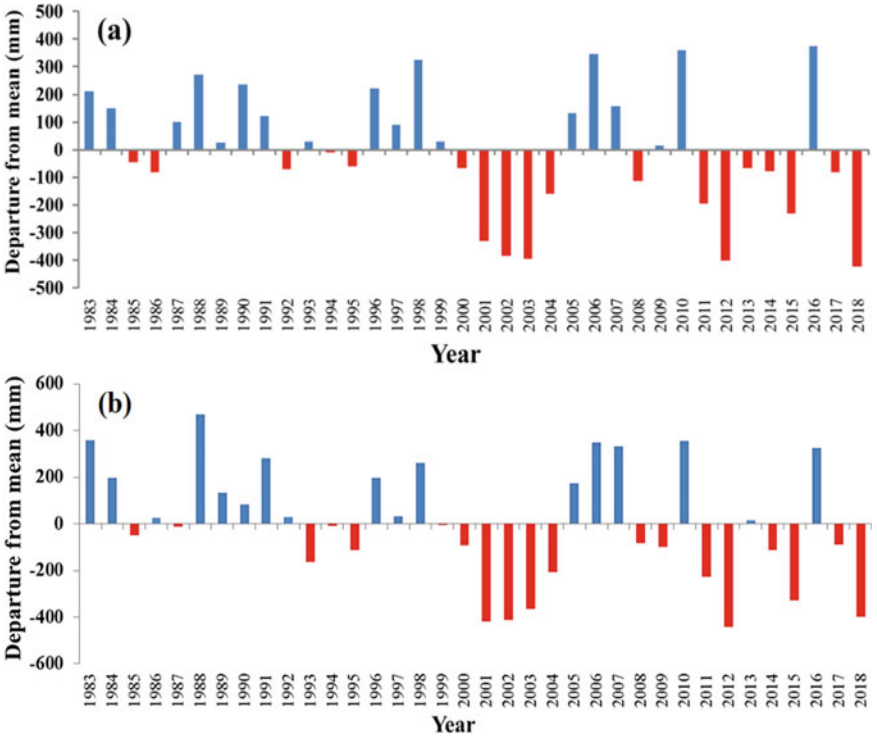

Fig. 4 Rainfall deviation from mean over the study area for **a** annual average rainfall and **b** monsoon rainfall

maximum negative deviation occurs in 2018 which is 424.314 mm and maximum positive deviation occurs in 2016 which is 376.412 mm.

The results of the deviation of rainfall from mean during years 1986, 1987, 1992, 1993, 1999, 2009 and 2013 for monsoon and annual period showing contrasting results which indicates that the amount and period of rainfall is altered in these years. The average negative deviation is of −177.459 mm and average positive deviation is 177.458 mm for annual rainfall while average negative deviation is of −190.561 mm and average positive deviation is 212.981 mm for monsoon rainfall.

4 Conclusions

The analysis was carried out to study the rainfall distribution, variation and trend of rainfall over five agro-climatic zones in Upper Bhima sub-basin for 1983–2018 (35 years). The MK non-parametric test was used to analyze the trend and Sen's slope estimator was used to analyze the magnitude of the trend in rainfall data. A declining trend of rainfall was observed in all five zones for monsoon rainfall and

annual rainfall data. The monsoon rainfall (June–September) contributes 85.50% in annual rainfall. The ARZ has highest coefficient of variation for both monsoon rainfall and annual rainfall which are 22.3% and 20.1%, respectively. WSZ and ARZ receive lowest rainfall (1204.41 mm/year and 974.47 mm/year) and WGZ and TR1 receives highest rainfall (1380.12 mm/year and 1359.97 mm/year).

MK non-parametric test and Sen's slope estimator also identifies the decreasing trend in monsoon and annual rainfall. Deviation from the mean rainfall results are also showing the major dry phases in the rainfall are occurred in period 2000–2004 and 2011–2018. These distractions and change in patterns and irregularities in the rainfall are due to changes in the weather and climate at regional level.

The areas having high CV must balance it by developing new dams, reservoirs and other irrigation facilities which will improve crop production in that area. The research studies on rainfall trend analysis and its spatio-temporal variation at regional level can be beneficial for the planning of agricultural activities and management of water resources available.

References

1. Juan-Carlos A, Brian HL (2009) Spatio-temporal rainfall patterns in Southern South America. Int J Climatol 29:2106–2120
2. Chahine MT (1992) The hydrological cycle and its influence on climate. Nature 359:373–380
3. Krishnakumar KN, Prasada Rao GSLHV, Gopakumar CS (2008) Rainfall trends in twentieth century over Kerala, India. Atmos Environ 43:1940–1944
4. Bothale RV, Katpatal YB (2014) Spatial and statistical clustering based regionalization of precipitation and trend identification in Pranhita catchment. India. IJIRSET-Int J Innov Res Sci Eng Technol 3(5):12557–12567
5. Bothale RV, Katpatal YB (2016) Trends and anomalies in extreme climate indices and influence of El Niño and La Niña over Pranhita catchment in Godavari Basin, India. J Hydrol Eng 21(2):05015023. https://doi.org/10.1061/(ASCE)HE.1943-5584.0001283
6. Buba LF, Kura NU, Dakagan JB (2017) Spatiotemporal trend analysis of changing rainfall characteristics in Guinea Savanna of Nigeria. Model Earth Syst Environ 3(3):1081–1090
7. Biswas B, Jadhav RS, Tikone N (2019) Rainfall distribution and trend analysis for upper Godavari basin, India, from 100 years record (1911–2010). J Indian Soc Rem Sens 47(10):1781–1792
8. Mekonen AA, Berlie AB (2020) Spatiotemporal variability and trends of rainfall and temperature in the Northeastern Highlands of Ethiopia. Model Earth Syst Environ 6(1):285–300
9. Gupta M, Srivastava PK, Islam T, Ishak AMB (2014) Evaluation of TRMM rainfall for soil moisture prediction in a subtropical climate. Environ Earth Sci 71:4421–4431
10. DRAFT report, Upper Bhima Sub basin, K-5 Bhima Sub Basin available at http://www.indiawris.nrsc.gov.in/Publications/BasinReports/KrishnaBasin.pdf
11. Dile YT, Srinivasan R (2014) Evaluation of CFSR climate data for hydrologic prediction in data-scarce watersheds: an application in the Blue Nile River Basin. JAWRA J American Water Resour Assoc 50(5):1226–1241
12. Sushant S, Balasubramani K, Kumaraswamy K (2015) Environmental management of river basin ecosystems, pp. 21–42. https://doi.org/10.1007/978-3-319-13425-3

13. Mann HB (1945) Nonparametric tests against trend. Econometrica 13:245–259
14. Kendall MG (1946) The advanced theory of statistics, 2nd edn. Charles Griffin, London, p 521
15. Sen PK (1968) Estimates of the regression coefficient based on Kendall's tau. J Am Stat Assoc 63:1379–1389

A Non-parametric Study on the Precipitation Trend in the Upper Brahmaputra River Basin, India

Shehnaj Ahmed Pathan, Subhrajyoti Deb, and Briti Sundar Sil

Abstract The Majuli Island, due to its geographical location and topography, is under constant risk of rainfall-driven flash floods in the Brahmaputra River, which cause colossal damages to life and properties almost yearly. In this view, a study on the temporal variations in precipitation at the local scale is necessary for mitigating such flood hazards. The annual and seasonal rainfall trends in the region of the upper Brahmaputra River basin up to Majuli River Island, India, are investigated in this study using a 0.25° × 0.25° resolution gridded precipitation dataset for the period 1979–2014 obtained from Climate Forecast System Reanalysis (CFSR) database. This study aims to find out the precipitation trend's direction and magnitude and the precipitation time series trend using the non-parametric Mann–Kendall trend test and Sen's slope estimator. The annual precipitation trend shows no negative or positive statistically significant trend in the study area. In contrast, the winter season has shown an increasing trend (which is not statistically significant at a 0.05 level of significance. Interestingly the monsoon season revealed a significant trend with Sen's slope values of 1.78 mm/year from 1998 to 2014. This study's findings may benefit other researchers and play a significant role in flood control and flood management in this area.

Keywords Precipitation · Brahmaputra basin · Mann–Kendell test · Sen's estimator test · Majuli River Island

S. A. Pathan (✉) · B. S. Sil
Department of Civil Engineering, National Institute of Technology, Silchar 788010, India
e-mail: shehnajpathan9@gmail.com

S. Deb
Department of Civil Engineering, ICFAI University, Tripura 799210, India
e-mail: subhrajyotideb@iutripura.edu.in

P. V. Timbadiya et al. (eds.), *Climate Change Impact on Water Resources*, Lecture Notes in Civil Engineering 313, https://doi.org/10.1007/978-981-19-8524-9_25

1 Introduction

Hydrologists say flood occurs due to a stationary, independent, and identically distributed random process [1]. However, growing evidence of trends and long-term variability in the stream flow can be seen at several timescales [2]. Porporato and Ridolfi [3] showed that a weak trend might strongly influence the probability of flood exceedance. Precipitation is one of the essential hydro-meteorological factors. Changes in rainfall can cause a flood, drought, stream flow, agricultural productivity, soil erosion, etc. These spatial and temporal precipitation trends are essential for watershed management planners. The rainfall received in a watershed is crucial in calculating stream flow, soil erosion, and floods. Global climate change can affect long-term precipitation variability, water availability, and water scarcity occurrences of droughts and floods. In India, the increase in annual floods in the upper Brahmaputra River basin provides a key example of such a concern. The dynamics of the river Brahmaputra and the extreme floods are due to the snowmelts during the summer and spring seasons and the large-scale climate patterns [4]. Some scholars researched the variations and trends in temperature and rainfall around the world [5–11]. Using 75 rain gauge sites in North Carolina, Boyles and Raman [12] forecasted precipitation and temperature trends on seasonal and yearly scales from 1949 to 1998. Raziei et al. [13] looked at the temporal changes in yearly rainfall in central and east Iran from 1965 to 2000 and found no evidence of climate change throughout that period. Kumar et al. [14] utilized the modified Mann–Kendall (MK) test and Sen's slope (SS) to observe annual precipitation spatial and temporal changes in 78 sub-districts (Tehsils) over 30 years from 1981 to 2020. Annual and southwest monsoon rainfalls show an upward tendency over time. Annual and southwest monsoon rains are found increasing in all of the tehsils. Numerous statistical approaches have been developed and deployed to detect trends and shifts in hydro-meteorological variables [15–18]. There are two numerous statistical methods (parametric and non-parametric) generally used by researchers. Out of these two methods, the non-parametric method is preferred over parametric methods [19].

The significance of trends in precipitation time series is quantified by using the most commonly used non-parametric Mann–Kendall (MK) statistical test [20, 21]. The MK test cannot determine the quantity of the trend's magnitude. For this purpose, the researchers use another non-parametric approach referred to as Sen's slope (SS) to compute the slope or magnitude of the trend [22]. Due to its geo-ecological instability, tactical position in the southern Himalayan land and international borders, transboundary water bodies, and fragile social economy, the Indian part of the upper Brahmaputra River basin is highly vulnerable to climate change. The research area is sub-tropical, and the terrain pattern and geomorphology change fast from one location to the next. As a result, a trend analysis study for the upper Brahmaputra River basin in India, up to Majuli Island, is taken, using precipitation as a meteorological variable for ten gauging stations scattered throughout the watershed. The primary goal of this study is to estimate the trend of a meteorological variable using the Mann–Kendall (MK) statistical test and Sen's slope (SS) estimator and identify

possible changes on an annual and seasonal basis. The study's findings will contribute to a better understanding of regional hydrologic behavior in the study area over the last several decades.

2 Study Area and Data Source

2.1 Upper Brahmaputra River Basin

This study has been conducted in the upper Brahmaputra River basin, India, downstream of Majuli River Island. The study area lies between 25° N to 30° N and 92°30′ E to 97°30′ E in northeastern India (Fig. 1). This study area covers Nagaland, Arunachal Pradesh, and Assam, India. The total area of the study area is approximately 103,459 km^2. The Brahmaputra River rises in the Himalayan Mountains and flows east through southern China into eastern India [23]. The upper part of the watershed receives snowmelt discharge before it enters India [24]. The land slopes are towards the downward direction from the north to the south, containing the Himalayan region on the north side. High seasonal flow, sediment transport, and channel configuration characterize the basin [25]. The geography of the watershed is characterized by the alpine mountain system of the Himalayas and the tropical monsoon climate. The southwest monsoon is responsible for causing the bulk of rainfall, which is heavy annual rainfall over the plain areas, followed by moderate rain in hilly regions [26]. Variation of rainfall is seasonal. This study area has a wide spatial variation of temperatures that range from negative values as a minimum in the Himalayan region to a maximum of 35–39 °C during summer in the plain areas. Figure 1 depicts a map of the study area's location.

2.2 Data Used

The precipitation datasets of ten stations across the study area are analyzed from 1979 to 2014. Daily precipitation data for 36 years is collected from the Climate Forecast System Reanalysis (CFSR) database. The stations are S-1, S-2, S-3, S-4, S-5, S-6, S-7, S-8, S-9, and S-10. Figure 2 shows all rain gauge stations, including Brahmaputra River streams. Each station's precipitation on a seasonal and annual scale is calculated by averaging the daily values. Table 1 shows the details of all the stations within the study area.

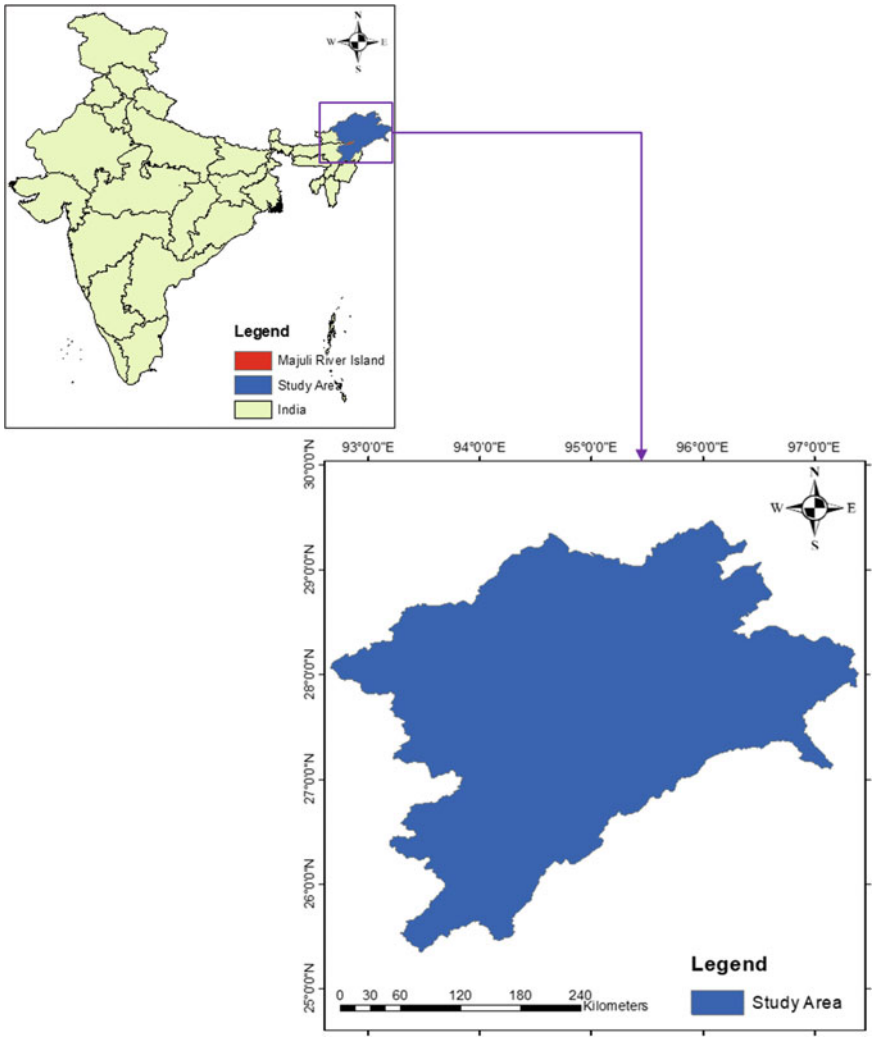

Fig. 1 Location map of the study area

3 Methodology

Trend analysis provides information on the weather variables that can be used for future forecasting. Many techniques for analyzing heterogeneous data series have been developed by researchers and can be used appropriately to analyze weather data [27, 28]. Generally, there are two types of trend analysis for hydrologic time series, i.e., parametric and non-parametric methods. The data in the non-parametric method is independent of its distribution, whereas the data in the parametric method must be dependent and normally distributed.

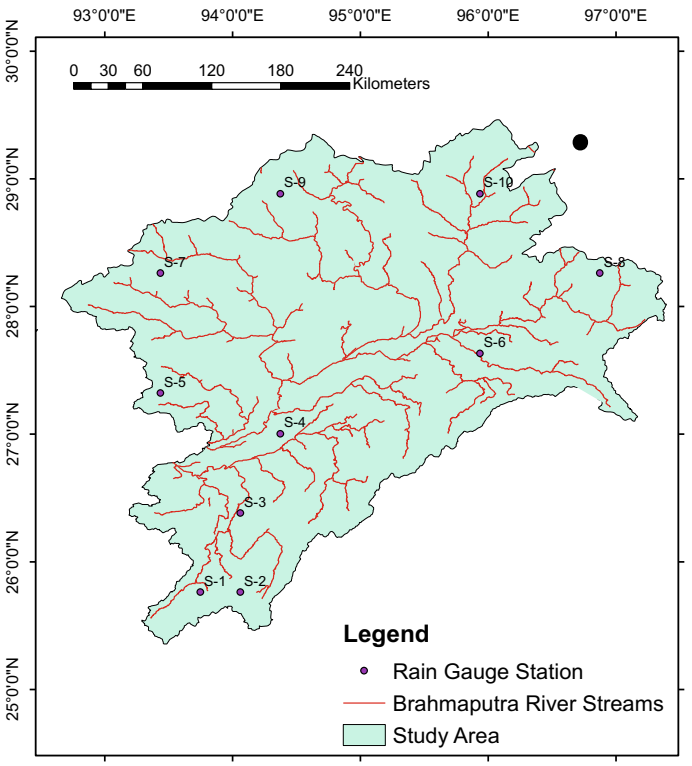

Fig. 2 Rain gauge station map showing Brahmaputra River streams

Table 1 Physical overview of the rainfall stations

Sl. No.	State	Station	Latitude	Longitude	Altitude (m)
1	Nagaland	S-1	25.76	93.75	560
2	Nagaland	S-2	25.76	94.06	958
3	Assam	S-3	26.38	94.06	194
4	Assam	S-4	27.00	94.38	78
5	Arunachal Pradesh	S-5	27.32	93.44	1620
6	Arunachal Pradesh	S-6	27.63	95.94	156
7	Arunachal Pradesh	S-7	28.26	93.44	3213
8	Arunachal Pradesh	S-8	28.26	96.88	3996
9	Arunachal Pradesh	S-9	28.88	94.38	3347
10	Arunachal Pradesh	S-10	28.88	96.25	3795

3.1 Selection of Input Parameters

Mann–Kendall [20, 21] and Sen's slope estimator are two popular non-parametric methods discussed in this paper [22]. The MK test is a non-parametric test for detecting trend in a time series. The MK test can detect trend in a time series in such a way that the distribution of the time series has no effect on the results. Before applying this test, one has to make sure that the data series is free of any kind of serial correlation. The test statistics is calculated as

$$S = \sum_{i=1}^{n-1} \sum_{j+1}^{n} \text{sign}\left(x_j - x_i\right) \tag{1}$$

where n denotes the number of records, x_i and x_j represent the data values in time series i and $j(j > i)$, respectively, and in Eq. (2), sgn $\left(x_j - x_i\right)$ denotes sign function as

$$\text{sign}\left(x_j - x_i\right) = \begin{cases} +1, & \text{if}\left(x_j - x_i\right) > 0 \\ 0, & \text{if}\left(x_j - x_i\right) = 0 \\ -1, & \text{if}\left(x_j - x_i\right) < 0 \end{cases} \tag{2}$$

The variance is computed as

$$\text{VS} = \frac{n(n-1)(2n+5)\sum_{k=1}^{m} t_k(t_k-1)(2t_k+5)}{18} \tag{3}$$

In Eq. (3), n denotes the total number of data points, m the number of coupled groups, and t_k denotes the number of ties of extent k. A tied group is a collection of sample data with the same value. When there are more than ten data points ($n > 10$), the standard normal test statistic Z_S is calculated using Eq. (4):

$$Z_S = \begin{cases} \frac{S-1}{V\sqrt{S}}, & \text{if } S > 0 \\ 0, & \text{if } S = 0 \\ \frac{S+1}{V\sqrt{S}}, & \text{if } S < 0 \end{cases} \tag{4}$$

Positive Z_S values indicate increasing trends, while negative Z_S values indicate decreasing trends. Trends are tested at the α significance level. The null hypothesis is rejected when $|Z_S| > Z_{1-\frac{\alpha}{2}}$, and a significant trend exists in the time series $Z_{1-\frac{\alpha}{2}}$ is obtained from the standard normal distribution table. The MK test is used in this analysis to determine whether a trend in the precipitation time series is statistically significant at significance levels of $\alpha = 0.01$ (or 99% confidence intervals) and $\alpha = 0.05$ (or 95% confidence intervals). The null hypothesis of no trend is rejected at the 5 and 1% significance level if $|Z_S| > 1.96$ and $|Z_S| > 2.576$, respectively.

The Sen's slope (SS) test is non-parametric regression analysis and estimates whether y values increase or decrease over the period. This test is used to determine

the magnitude of the trend in a hydro-meteorological time series. The test computes the difference in signs between observed and estimated data. Furthermore, it is used to determine whether or not a trend exists in the datasets. The test's advantage is that missing values are allowed here, and the data do not fit into any specific distribution. It also allows a value to be less than, greater than, or equal to a new value, data independence, and the time series to remain constant in the original and transformed units. From Sen's equation, a parameter called slope estimator Q_i is also used [22]. Q_i defines the median of all possible pair combinations for the entire set of data points. Positive values of Q_i indicate 'upward trend' (increasing values with time), while negative values indicate 'downward trend' (decreasing value with time) [29]. Here, the slope of the trend (Q_i) is calculated as

$$Q_i = \frac{(x_j - x_k)}{j - k} \tag{5}$$

where $i = 1, 2, \ldots, N$. The terms x_j and x_i indicate data values at time j and $k(j > k)$, respectively.

The median of these N values of Q_i is represented as Sen's estimator of the slope. Sen's estimator is calculated as

$$Q_{\text{med}} = \begin{cases} Q_{N+2/2} & \text{If } N \text{ appears to be odd} \\ Q_{N/2} + Q_{(N+2)/2} & \text{If } N \text{ appears to be even} \end{cases} \tag{6}$$

Q_{med} indicates the slope and gradient of the data trend. The significance level of Q_{med} should be chosen specifically to avoid zero median slopes, and then the non-parametric test can be used to obtain the true slope. When Q_{med} is positive, it indicates an upward or increasing trend and vice versa in the case of negative value [30].

4 Results and Discussions

The precipitation data is derived from ten gauging stations located throughout the basin, each with a consistent dataset and a long enough time span. The Mann–Kendall test (MK) and Sen's slope (SS) yield seasonal and annual trend analyses, shown in Tables 2, 3 and 4. Sen's slope estimator value, denoted by a star (*) in their respective tables, indicates a significant trend. For the two-sided test, the level of significance is set at 0.05. Based on this significance level, normalized Z_S statistic value greater than or less than 0 indicates an upward or downward trend, respectively.

First of all, MK and Sen's slope (SS) tests are done for maximum precipitation in the time series 1979–2014 for both annual and seasonal cycles, along with the Z-statistics and magnitude of the trend (Table 2). All tests are considered at a 5% level of significance. The only positive significant trends are found in the annual

Table 2 Mann–Kendall test and Sen's Slope estimator test results for P_{max} during 1979–2014

Station	Test statistics	Trends				
		Winter (Dec–Feb)	Pre-monsoon (Mar–May)	Monsoon (Jun–Aug)	Post-monsoon (Sep–Nov)	Annual
S-1	Z_S	1.78	1.43	3.19*	1.73	1.72
	Q_{med}	0.021	0.016	0.028*	0.005	0.003
S-2	Z_S	1.72	1.52	3.40*	3.62	1.07
	Q_{med}	0.015	0.012*	0.070*	0.028	0.001
S-3	Z_S	1.50	1.50	1.82*	2.68	0.90*
	Q_{med}	0.015	0.011	0.027*	0.024	0.046
S-4	Z_S	2.33	2.56	4.46*	2.79	1.01
	Q_{med}	0.031	0.043	0.036*	0.032	0.003
S-5	Z_S	1.74	1.65	2.89	1.96	1.01
	Q_{med}	0.011	0.017	0.074	0.072	0.007
S-6	Z_S	2.43	0.87	2.73	2.59	1.02
	Q_{med}	0.028	0.004	0.012	0.023	0.008
S-7	Z_S	2.46	1.63	3.38	3.12	1.46
	Q_{med}	0.031	0.017	0.052	0.028	0.009
S-8	Z_S	1.86	1.56	4.46*	3.45	0.19
	Q_{med}	0.063	0.017	0.087*	0.075	0.004
S-9	Z_S	1.60	1.20	3.02*	2.09	1.20*
	Q_{med}	0.035	0.001	0.080*	0.076	0.071*
S-10	Z_S	2.17*	1.56	3.38	1.14	0.31
	Q_{med}	0.023*	0.011	0.030	0.078	0.073

Z_S standard normal test statistics; Q_{med} SS estimator, (*) significant trend at 0.05 level of significance

and seasonal rainfall data. As seen in Table 3, the significant increasing trends are found in all seasons except the post-monsoon season. The monsoon time series for the entire study area shows significantly increasing trends except for S-5, S-6, S-7, and S-10, which exhibit no significant trend. The stations RS-3 and RS-9 show a slight change in trend with a magnitude of 0.90 mm/year and 0.071 mm/year in case of annual rainfall. Only S-10 shows a significant change of 0.023 mm/year in the winter season, whereas no negative trend is found in maximum precipitation (P_{max}) at any station.

The results of the MK and SS tests for minimum precipitation are presented in Table 3. The *Z*-statistics for minimum precipitation (P_{min}) in the time series for annual and seasonal cycles is done along with the magnitude of the trend. A positive trend is identified using the MK test in the annual and seasonal rainfall data. The results show significant increasing trends which are found in monsoon rainfall time series for the entire study area except for S-5, S-6, and S-7, which exhibit a significantly increasing

Table 3 Mann–Kendall test and Sen's Slope estimator test results for P_{min} during 1979–2014

Station	Test statistics	Trends				
		Winter (Dec-Feb)	Pre-monsoon (Mar-May)	Monsoon (Jun-Aug)	Post-monsoon (Sep-Nov)	Annual
S-1	Z_S	1.48	1.56	3.45*	1.57	1.44
	Q_{med}	0.041	0.023	0.058*	0.005	0.045
S-2	Z_S	0.52	1.68	3.45*	3.65	1.02
	Q_{med}	0.025	0.036	0.056*	0.008	0.014
S-3	Z_S	2.50	1.63	4.78*	2.35	0.25
	Q_{med}	0.005	0.003	0.032*	0.008	0.074
S-4	Z_S	2.77	2.96	4.62*	2.74	1.73
	Q_{med}	0.042	0.055	0.086*	0.036	0.058
S-5	Z_S	0.44	1.60	3.35	1.95	2.44
	Q_{med}	0.002	0.005	0.005	0.014	0.033
S-6	Z_S	2.85*	0.56	2.53	2.35	1.65
	Q_{med}	0.054*	0.009	0.057	0.007	0.015
S-7	Z_S	2.45	1.53	3.33	3.74	1.35
	Q_{med}	0.022	0.036	0.038	0.045	0.052
S-8	Z_S	1.86	1.60	4.63*	3.02	0.02
	Q_{med}	0.034	0.070	0.089*	0.074	0.035
S-9	Z_S	1.63	1.41	3.97*	2.35	1.47
	Q_{med}	0.003	0.032	0.035*	0.025	0.023
S-10	Z_S	2.98*	1.75	3.74*	1.85	0.33
	Q_{med}	0.003*	0.005	0.002*	0.0052	0.025

Z_S standard normal test statistics; Q_{med} SS estimator, (*) significant trend at 0.05 level of significance

trend. In the winter season, only two stations S-6 and S-10 show a significant trend in minimum precipitation at 0.054 and 0.003 mm/year. In contrast, no negative trends are found in minimum precipitation (P_{min}) at any station.

In Table 4, the MK test and the Z-statistics results reveal the trend in the time series for annual and seasonal cycles for average precipitation (P_{avg}) with the magnitude of the trend (SS). Both positive and negative trends are found for average rainfall in the annual and seasonal rainfall data. A significant increase in trends is found in monsoon rainfall time series for the stations S-2, S-3, S-7, and S-9, which exhibit a significantly increasing trend with values of 1.048 mm/year, 0.912 mm/year, 1.114 mm/year, and 0.774 mm/year, respectively. Five stations, S-2, S-3, S-4, S-7, and S-9, show significant negative precipitation trends in the post-monsoon season with magnitudes of −0.932 mm/year, −0.874 mm/year, −0.702 mm/year, −0.896 mm/year, and −0.86 mm/year, respectively. The precipitation during the winter, pre-monsoon, and annual seasons shows no significant trend change in all stations.

Table 4 Mann–Kendall test and Sen's Slope test results for P_{avg} during 1979–2014

Station	Test statistics	Trends				
		Winter (Dec–Feb)	Pre-monsoon (Mar–May)	Monsoon (Jun–Aug)	Post-monsoon (Sep–Nov)	Annual
S-1	Z_S	0.56	0.15	3.36	1.02	1.53
	Q_{med}	0.035	0.033	1.255	0.841	0.325
S-2	Z_S	0.54	0.73	3.52*	−1.35	1.53
	Q_{med}	0.014	0.168	1.048*	−0.932	0.350
S-3	Z_S	0.36	0.26	4.67*	−1.02	1.68
	Q_{med}	0.036	0.155	0.912*	−0.874	0.850
S-4	Z_S	0.74	0.25	4.02	−0.75	1.58
	Q_{med}	0.098	0.192	1.73	−0.702	0.865
S-5	Z_S	0.73	0.89	3.15	0.56	0.53
	Q_{med}	0.041	0.328	1.165	0.530	0.587
S-6	Z_S	0.96	0.28	1.72	0.46	0.005
	Q_{med}	0.053	0.320	1.350	0.325	0.535
S-7	Z_S	0.25	0.015	3.45*	−1.14	1.57
	Q_{med}	0.046	0.065	1.114*	−0.896	0.74
S-8	Z_S	0.35	0.55	1.32	0.66	1.007
	Q_{med}	0.045	0.038	1.053	0.356	1.6
S-9	Z_S	0.75	0.97	4.35*	−1.63	0.75
	Q_{med}	0.035	0.539	0.774*	−0.86	0.002
S-10	Z_S	0.36	0.19	0.35	1.36	1.05
	Q_{med}	0.095	0.118	0.463	0.958	0.430

Z_S standard normal test statistics; Q_{med} SS estimator, (*) significant trend at 0.05 level of significance

5 Conclusions

Precipitation trend analysis is a prerequisite for rainfall forecasting of any region, and the results of trend analysis are helpful in determining the probable maximum precipitation (PMP) maps. The annual and seasonal rainfall trends in 36 years of (1979–2014) data series in the region of the upper Brahmaputra River basin up to Majuli River Island, India, are investigated in this paper. Precipitation data totaling ten meteorological stations are applied to the non-parametric Mann–Kendall test, Sen's slope test to analyze the precipitation trends. The major conclusions derived from the study are listed below:

- MK and Sen's slope tests are useful for significant trend detection and trend magnitude analysis, and these tests provided valuable results for the selected study area.

- The monsoon precipitation series is found to be increasing trends in the majority of the stations. The majority of the stations have shown statistically significant trends in all the minimum, maximum, and average precipitation conditions.
- The trend in the pre-monsoon season is showing no clear pattern in all the minimum, maximum, and average rainfall series. No variation in the rain is expected in hilly regions of the study area.
- The bulk of the upper Brahmaputra area is identified as an increasing trend in the monsoon season for the period 1979–2014.

References

1. Bobee B, Ashkar F (1991) The gamma family and derived distributions applied in hydrology. Water Resources Publications
2. Baldwin CK, Lall U (1999) Seasonality of streamflow: the upper Mississippi River. Water Resour Res 35(4):1143–1154
3. Porporato A, Ridolfi L (1998) Influence of weak trends on exceedance probability. Stoch Hydrol Hydraul 12(1):1–14
4. Singh P, Jain SK (2002) Snow and glacier melt in the Satluj River at Bhakra Dam in the western Himalayan region. Hydrol Sci J 47(1):93–106
5. Price C, Michaelides S, Pashiardis S, Alpert P (1999) Long term changes in diurnal temperature range in Cyprus. Atmos Res 51(2):85–98
6. Ventura F, Pisa PR, Ardizzoni E (2002) Temperature and precipitation trends in Bologna (Italy) from 1952 to 1999. Atmos Res 61(3):203–214
7. Partal T, Kahya E (2006) Trend analysis in Turkish precipitation data. Hydrol Process Int J 20(9):2011–2026
8. Kampata JM, Parida BP, Moalafhi DB (2008) Trend analysis of rainfall in the headstreams of the Zambezi River Basin in Zambia. Phys Chem Earth Parts A/B/C 33(8–13):621–625
9. Krishnakumar KN, Rao GP, Gopakumar CS (2009) Rainfall trends in twentieth century over Kerala, India. Atmos Environ 43(11):1940–1944
10. de la Casa A, Nasello O (2010) Breakpoints in annual rainfall trends in Córdoba, Argentina. Atmos Res 95(4):419–427
11. Sayyad RS, Dakhore KK, Phad SV (2019) Analysis of rainfall trend of Parbhani, Maharshtra using Mann-Kendall test. Econometrica 13:245–259
12. Boyles PR, Raman S (2003) Analysis of climate trends in North Carolina (1949–1998). Environ Int 29:263–275
13. Raziei T, Arasteh PD, Saghafian B (2005, May) Annual rainfall trend in arid and semi-arid regions of Iran. In: ICID 21st European regional conference, pp 15–19
14. Kumar A, Giri RK, Taloor AK, Singh AK (2021) Rainfall trend, variability and changes over the state of Punjab, India 1981–2020: a geospatial approach. Rem Sens Appl Soc Environ 23:100595
15. Modarres R, da Silva VDPR (2007) Rainfall trends in arid and semi-arid regions of Iran. J Arid Environ 70(2):344–355
16. Tabari H, Somee BS, Zadeh MR (2011) Testing for long-term trends in climatic variables in Iran. Atmos Res 100(1):132–140
17. Martinez CJ, Maleski JJ, Miller MF (2012) Trends in precipitation and temperature in Florida, USA. J Hydrol 452:259–281
18. Jha MK, Singh AK (2013) Trend analysis of extreme runoff events in major river basins of Peninsular Malaysia. Int J Water 7(1–2):142–158

19. Sonali P, Kumar DN (2013) Review of trend detection methods and their application to detect temperature changes in India. J Hydrol 476:212–227
20. Mann HB (1945) Non-parametric tests against trend. Econom J Econom Soc 245–259
21. Kendall MG (1975) Rank correlation methods. Charles Griffin Book Series, p 202
22. Sen PK (1968) Estimates of the regression coefficient based on Kendall's tau. J Am Stat Assoc 63(324):1379–1389
23. Nepal S, Shrestha AB (2015) Impact of climate change on the hydrological regime of the Indus, Ganges and Brahmaputra river basins: a review of the literature. Int J Water Resour Dev 31(2):201–218
24. Singh UK, Kumar B (2018) Climate change impacts on hydrology and water resources of Indian River Basins. Curr World Environ 13(1):32
25. Goswami DC (1985) Brahmaputra River, Assam, India: physiography, basin denudation, and channel aggradation. Water Resour Res 21(7):959–978
26. Deka RL, Mahanta C, Pathak H, Nath KK, Das S (2013) Trends and fluctuations of rainfall regime in the Brahmaputra and Barak basins of Assam, India. Theor Appl Climatol 114(1):61–71
27. Aguilar E, Auer I, Brunet M, Peterson TC, Wieringa J (2003) Guidance on metadata and homogenization. Wmo Td 1186:1–53
28. Costa AC, Soares A (2009) Homogenization of climate data: review and new perspectives using geostatistics. Math Geosci 41(3):291–305
29. Karpouzos D, Kavalieratou S, Babajimopoulos C (2010) Trend analysis of precipitation data in Pieria Region (Greece). European Water 30:31–40
30. Babar SF, Ramesh H (2013) Analysis of south west monsoon rainfall trend using statistical techniques over Nethravathi basin. Int J Adv Technol Civ Eng 2:130–136

A Spatio-temporal Analysis of Rainfall Trends and Variability Due to Changing Climate in the Central Zone of Himachal Pradesh, India

Suman Kumari and Vijay Shankar

Abstract The drastic change in precipitation as a result of climate change is altering the pattern of stream flows and demands, as well as the spatial and temporal distribution of runoff, soil moisture, and groundwater reserves leading to hazardous events like landslides, floods, drought, etc. Trend analysis has proved to be a potential tool by providing useful information on the possibility of changes of rainfall trends in future. The current study uses the Statistical Downscaling Model-Decision Centric (SDSM-DC) and GIS to evaluate the imminent regional and temporal variations in rainfall caused by various climatic conditions. The study area considered for this study is central zone of Himachal Pradesh. To evaluate rainfall patterns and their reactions to climate variability, seven rainfall stations in the study area were selected. The study concludes that the changing climate has resulted in a significant change in precipitation patterns when compared to previous climatic conditions. Numerous natural hazards, including floods, landslides, cloudbursts, etc., are occurring in the area as a result of the rate of change in seasonal and yearly precipitation over the years as indicated by precipitation trends. Changes in the pattern and an increase in pre-monsoon precipitation are additional significant impacts of climate change.

Keywords Rainfall · Climate change · Trends · Variability · SDSM-DC

S. Kumari (✉) · V. Shankar
Department of Civil Engineering, National Institute of Technology Hamirpur, Hamirpur, Himachal Pradesh 177005, India
e-mail: kumarisuman1993@gmail.com

P. V. Timbadiya et al. (eds.), *Climate Change Impact on Water Resources*, Lecture Notes in Civil Engineering 313, https://doi.org/10.1007/978-981-19-8524-9_26

1 Introduction

Precipitation is a vital part of the hydrologic cycle that gets altered considerably with the varying climatic conditions. Climate change has had a substantial impact on the frequency and intensity of precipitation across the globe [1–5]. The study of current susceptibility and current climate variability is the first step towards future climate change adaptation [6]. Spatial and temporal variability of rainfall is a significant factor in water resources planning and management, hydrological modelling, agriculture planning, forecasting, and mitigation of natural hazards such as floods, drought, landslides, and cloud burst. Several recent studies conducted to examine extreme rainfall patterns found significant variation in rainfall events throughout India [7–11].

Globally, it is common practice to utilise general circulation models (GCMs) to analyse how climate change may affect extreme precipitation situations in future. The GCMs, however, lack the resolution needed to provide accurate climatic projections at the temporal and spatial scales required for hydrological assessments [12]. Downscaling strategies can be used to bridge the gap between local and regional climates (predictor and predictand) [13]. There are numerous downscaling methods which are often categorised into statistical and dynamical approaches [14], and statistical approaches are the least computationally demanding. GCMs and downscaling techniques have improved throughout time, increasing their usability for end users looking to study the effects of climate change. To find connections between meteorological variables and the outputs of large-scale GCMs, several statistical downscaling methods have been created, including transfer functions, weather typing approach, and SDSM.

The Statistical Downscaling Model-Decision Centric (SDSM-DC) is a simple programme for constructing future climatic data sets from GCM data using statistical downscaling. It may also be used as a decision support system (DSS) to create believable weather series. The SDSM-DC is a transfer function-based model that represents local weather through seven primary processes, including quality control and data processing, predictor variables screening, model calibration, weather creation, and statistic generation [15]. This software can also be used to complete data gaps in data-scarce locations to better understand regional climate systems [16].

As trend analysis aids in the investigation of the general pattern of change in rainfall, particularly at temporal and spatial scales; it is important to have detailed rainfall characteristics at the regional level for improved disaster management and water resource management planning. In the context of regional variations in rainfall, studies on the trend and variability at regional scale of different parts of Indian states are scarce, and Himachal Pradesh is no exception. Hence, an attempt has been made to investigate the present climate change scenario and its impact on extreme precipitation occurrences in the central zone of Himachal Pradesh. The first objective of present study is to assess the variation in the monthly and annual rainfall trends for the selected seven stations of the study area using SDSM-DC Model. The second objective of the study is to establish the influence of climate change on rainfall trends in the study area.

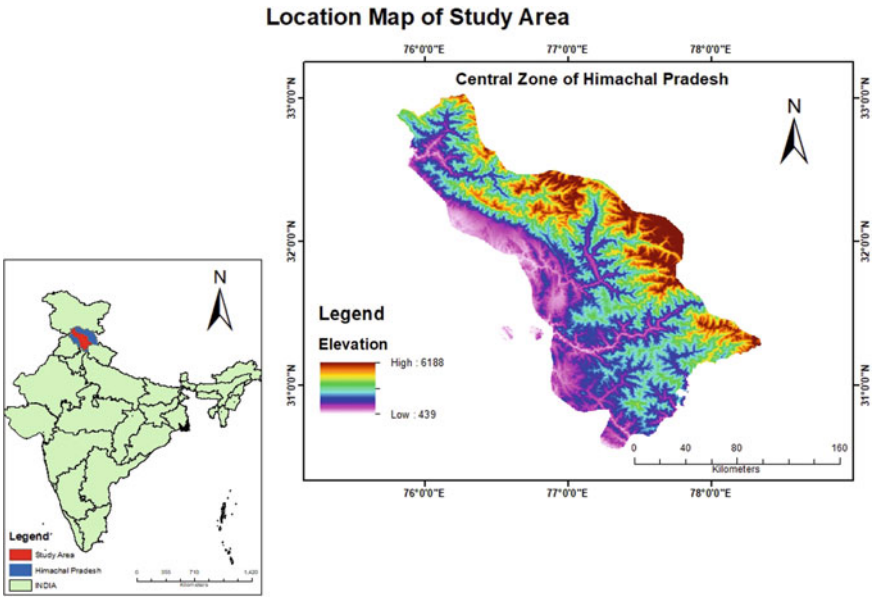

Fig. 1 Location map of study area

2 Data and Methodology

2.1 Study Area and Data

2.1.1 Study Area

Himachal Pradesh is a hilly state that is located close to the Western Himalayan Region. The Western Himalayan Region is located in latitudes between 30°22′44″ and 33°12′40″ N and longitudes between 75° 45′55″ and 79°04′20″ E. The state is divided into four agro-climatic zones based on its elevation above mean sea level (msl), which ranges from 240 to 7000 m. For the purpose of the current investigations, the central portion of the state, which is comprised of both mid hills sub-humid and high hills temperate wet agro-climate zones, will serve as the study area. The study covers a total area of 13,881 km^2, which is equivalent to 24.94% of the overall geographical area of the state (55,650 km^2). Figure 1 presents a map illustrating the location of the research area.

2.1.2 Data Collection

Information on daily precipitation for the seven chosen stations in the study area was acquired from the Global Historical Climatology Network (GHCN) database

Table 1 Details of selected stations

S. No.	Station	District	Latitude (°N)	Longitude (°E)	Elevation (m)
1	Arki	Solan	31°09′	76°57′	1130
2	Banjar	Kullu	31°38′	77°20′	1520
3	Chowari	Chamba	32°27′	76°01′	716
4	Karsog	Mandi	31°23′	77°12′	1347
5	Palampur	Kangra	32°08′	76°32′	1217
6	Renuka	Sirmaur	30°40′	77°30′	690
7	Shimla	Shimla	31°06′	77°10′	2202

and the Indian Meteorological Department (IMD), Pune. The stations were chosen to be evenly spread among the two zones, with each district encompassing at least one big precipitation station. The exact locations of the selected stations, as well as their elevations, are listed in Table 1.

The time frame of the study is limited to the years 1951–2015, broken up into two segments of thirty years each (e.g. 1951–1980 and 1981–2015). The World Meteorological Organization recommends a normal baseline period of thirty years to examine climate change [17]. The global atmospheric variables from two grid boxes, i.e. BOX 30 N 77.5 E and BOX 32.5 N 77.5 E, were taken from the National Centre for Environmental Prediction (NCEP) data set.

2.2 Downscaling Using SDSM-DC

In statistical downscaling, links are formed and empirically quantified between small-scale observed predictands and large-scale atmospheric predictors [16]. Wilby et al. [18] created SDSM as a decision support tool for evaluating the impacts of local climate change through downscaling. The statistical downscaling method is a combination of SWG and MLR approaches [19] which has been used in the present study.

In this study, climate data were downscaled and synthesised using Statistical Downscaling Model-Decision Centric (SDSM-DC) Model Version 5.3. The model's four primary functions are predictor screening, model calibration, a weather-generating function, and modelling of projections for future climatic scenarios. In addition, it has the ability to perform fundamental analytical tests, statistical analysis, and graphical depiction of climate data. We need two different kinds of daily time series data in order to create the SDSM model. The first is a daily time series of NCEP predictors, while the second is a daily collection of observed predictands. In both directions, the gridded NCEP reanalysis outputs had a $2.5° \times 2.5°$ spatial resolution. As a result, the atmospheric domain was retained for downscaling, and stations were selected for the study to ensure that the station boundaries matched those of the NCEP reanalysis data [20]. To generate regression parameters, the calibration and

screening processes of the NCEP predictors are followed by regression-based statistical correlatives between them. The relationships between NCEP reanalysis data and observed precipitation are used to identify potential predictors in the research area.

The most important phase of statistical downscaling is screening of global atmospheric variables. For regression-based downscaling, it is essential to identify empirical connections between gridded predictors like airflow velocity, mean sea level pressure, etc., and local scale predictands like precipitation [18, 21]. Using the SDSM "Screen Variables" operation, the potential predictors for each station were discovered and downscaling models were created based on entire period consistency. These data were used to create a statistical connection between the observed station data and the significant atmospheric variables from the NCEP reanalysis. For the years 1951 to 2015, a total of 32 distinct predictor variables were acquired from the SDSM website (https://www.sdsm.org.uk/).

Following the selection of prospective predictors, numerous regression equations were generated by combining the predictand, predictor, and model calibration functions to generate a transfer function file in the common parameter file format (*.PAR). For precipitation downscaling, the model type was changed to monthly in order to create regression equations. Either an unconditional process or a conditional process is used to describe the model structure. Precipitation was chosen as the dependent variable in this study because the model process relied on intermediates between regional forcing and local weather, such as the possibility of a rainy day. In accordance with the data that were readily available, the observed historical data sets for the years 1951–1980 were split into two distinct groups: the calibration procedure used the data from the years 1951–1965, while the validation process used the data from the years 1966–1980. These divisions were made for the period of 1951–1980. The NCEP predictors and the calibrated model were used to generate twenty different precipitation ensembles, and the mean value of all of the precipitation ensembles was the one that was used for the study.

The SDSM model was checked against the observed data for the years 1976–1980. Calibration of the variables at each of the stations was accomplished through the use of a consistent method. The standard error and variance percentages for each type of regression model that uses monthly, seasonal, or annual averages are addressed in order to assess the effectiveness of SDSM when calibrating. This is done so that annual, seasonal, and monthly averages can be differentiated [21]. A statistical metric called the percentage of explained variance shows how closely daily variations in the predictand are related to predictor variables. While explained variance for diverse variables, like precipitation, is typically less than 40%, it can exceed 70% for homogeneous variables like temperature [18]. The model is validated using statistical analysis.

Table 2 Performance indicators of SDSM model calibration

Station	Precipitation	
	Explained variance (EV)	Standard error (SE)
Arki	21.8	0.34
Banjar	9.4	0.41
Chowari	25.8	0.35
Karsog	16.7	0.34
Palampur	17.6	0.41
Renuka	28.83	0.32
Shimla	30.8	0.37

3 Results and Discussions

3.1 Performance Evaluation of SDSM During Calibration

To evaluate the outputs for each month and simulating daily data series, the monthly model was chosen. The data that were collected over the course of 30 years and the potential predictors were split into two time periods. Because of the significance of their relationships with the observed precipitation over the course of the full 30-year period, the consistent prospective factors were chosen for consideration (1951–1980). The standard error (SE) and the proportional explained variance (EV) are performance indicators that are used during the calibration process to evaluate the model's performance. When measured against the results of earlier research conducted by [18, 21], the mean percentage of EV ranged from 9 to 30%, which is an amount that may be regarded satisfactory. Table 2 shows that Shimla had the highest percentage EV (30.8%) and Banjar had the lowest percentage EV (9.4%), respectively, for precipitation. These results can be found in Shimla and Banjar.

3.2 Comparison of Observed and Modelled Precipitation

In order to develop and model daily synthetic data in compliance with the standards established by SDSM, the weather generator was utilised. The calibration output (*.PAR file) and available NCEP global atmospheric variables were used as inputs for the simulation. The "Weather Generator" function, which displays the connection between precipitation and important atmospheric factors, was employed for two things during the research. It was first utilised to enable output comparisons between observed and simulated models, as well as to evaluate a calibrated model (using observed data) by producing simulated data series for prior climatic periods (baseline period 1961–1990). Second, it was utilised to generate synthetic time series for the

second climate period, which encompasses the current climatic state from 1988 to 2018, and these time series were then statistically analysed.

In order to assess the differences between the two climatic periods covered by the study, the projected changes in precipitation variables such as mean and cumulative monthly precipitation are compared to observed (1951–1980) and modelled (1986–2015) precipitation (Fig. 2).

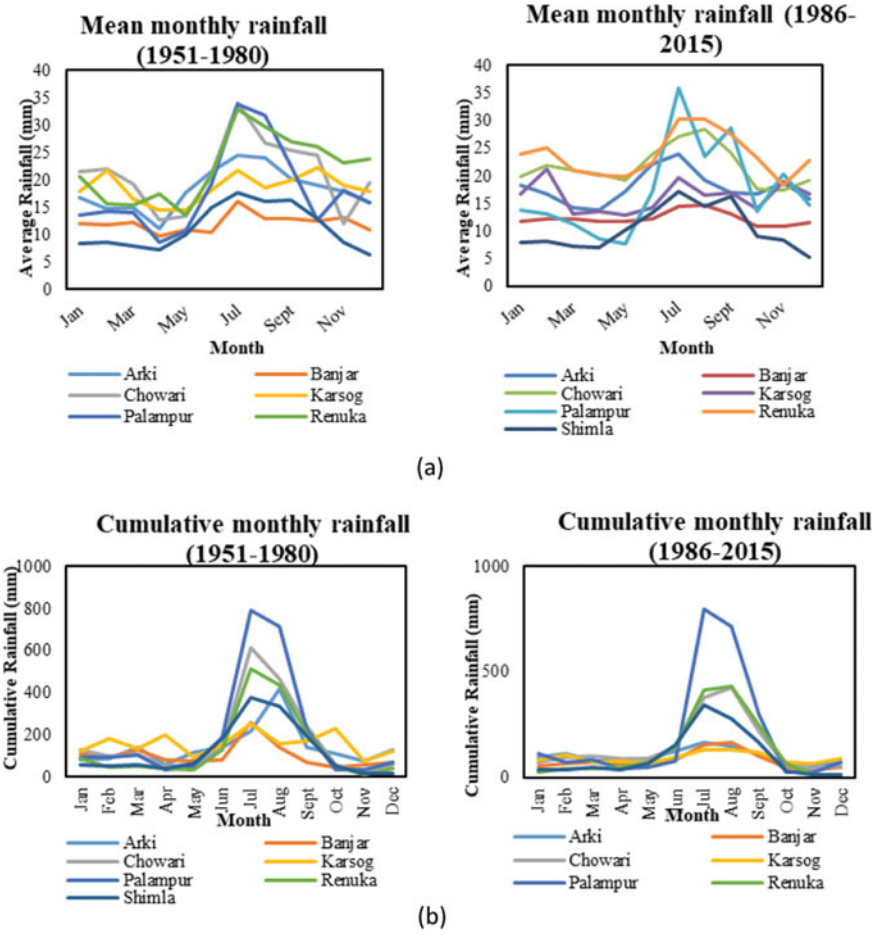

Fig. 2 Graphs comparing observed and predicted precipitation for **a** mean monthly rainfall and **b** cumulative monthly rainfall for all stations

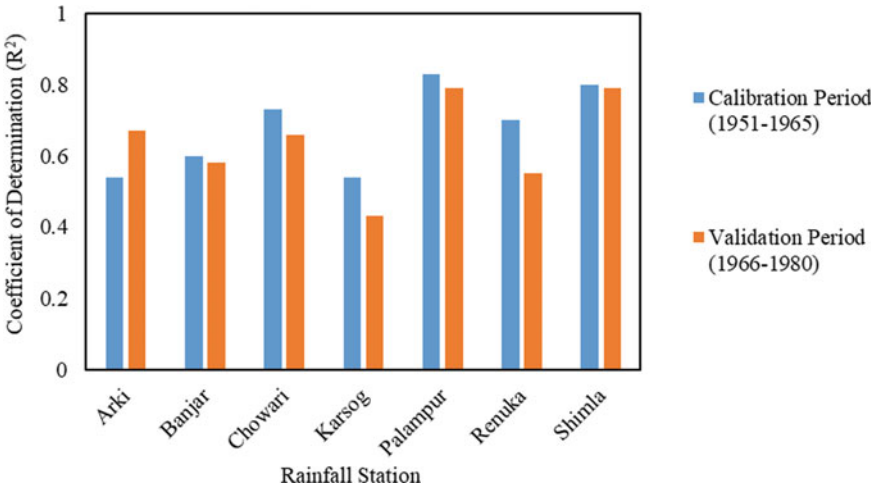

Fig. 3 Performance evaluation indicators of SDSM for model calibration (1951–1965) and validation (1966–1980)

3.3 Validation of SDSM Model

To validate SDSM, a set of synthetic meteorological data series for the testing period was constructed using NCEP predictors (1966–1980). The average of these ensembles was used to calibrate the model using the observed weather data saved for training (1951–1965). In order to evaluate the quantitative performance of the downscaling model, the average monthly precipitation (Avg) and coefficient of determination (R^2) of model simulations were compared to those of observations. Figure 3 depicts the evaluation results from the calibration and validation processes. The results show that the model performs well in Palampur and Shimla but poorly in Banjar and Karsog.

3.4 Annual Trends of Projected Climatic Variables

All of the stations' climate trends from the past (1951–1980) and the present (1986–2015) were projected by comparing the yearly changes for the two, thirty-year time periods. The meteorological variable, i.e. precipitation, was divided into two time periods for analysis: 1951–1980 and 1986–2015, hereafter referred to as the 1970s and 2000s, respectively. The comparison between the climate factors of the past and those of the present may be seen in the analysis that was conducted for the baseline period of 1951–1980. Based on the fluctuating rate of growth or decrease in yearly monsoon rainfall over the two eras, the results are to be interpreted. Despite the fact that precipitation is a heterogeneous parameter and does not produce predictable

effects. The analysis's findings are depicted in Fig. 4 together with the unique shifting trends in each station's rainfall during the annual monsoon.

When the two climate periods are compared, it is clear that there is a downward tendency in the total annual rainfall for both times, with the exception of Chowari, which exhibits an upward trend in the total annual rainfall. The current climate period has seen a decrease in yearly rainfall for all of the stations; however, the rate of decrease in rainfall has varied quite a little from station to station. There is a discernible upward trend in Chowari's average annual precipitation, and the current rate of growth is higher than it ever has been in the region's history (Fig. 4c).

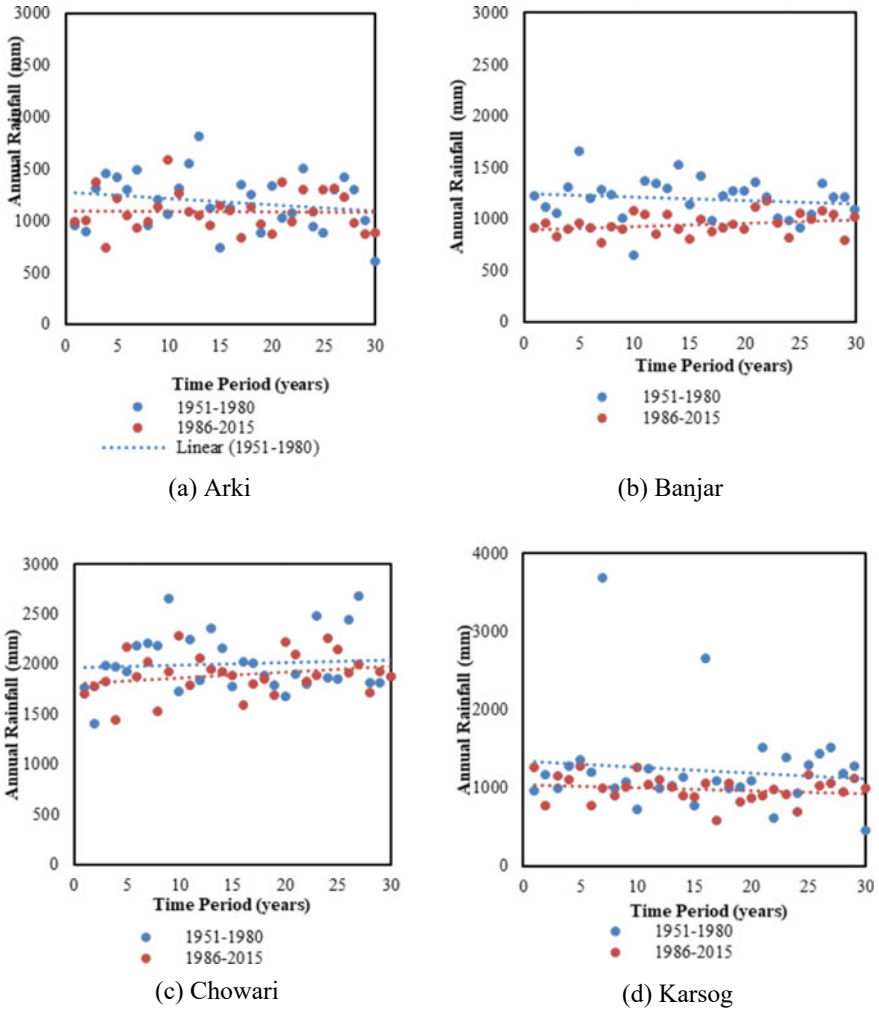

Fig. 4 Annual rainfall trends for observed (1951–1980) and modelled (1986–2015) climatic periods

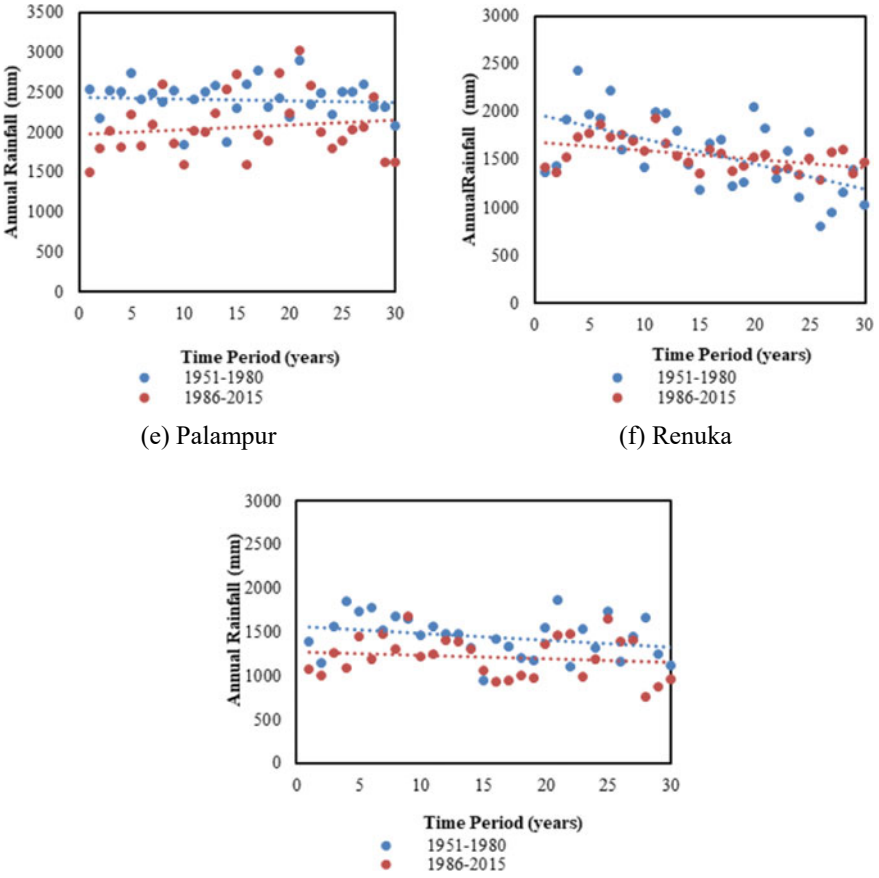

Fig. 4 (continued)

The model projections for Palampur and Renuka indicate that, despite the declining patterns of precipitation between the two time periods, the pace of decrease has moved to a rising or stable rate (Fig. 4e, f). As indicated by the trend lines, Shimla's results are comparable, albeit the rate of decline has slowed in the light of current circumstances (Fig. 4g). Climate change may be responsible for a shift in annual precipitation rates in the 2000s compared to the 1970s.

4 Conclusions

The present study employs the Statistical Downscaling Model-Decision Centric (SDSM-DC) as the downscaling model and aims to simulate rainfall utilising weather

generation in order to analyse rainfall trends in the central zone of Himachal Pradesh from 1980 to 2015. The following conclusions are derived from the study:

- According to the results of downscaling and trend projections, climate change has resulted in a shift in precipitation patterns relative to historical climatic circumstances.
- The peak monsoon rainfall for Palampur has increased, as evidenced by the station's increasing cumulative rainfall. A large increase in the yearly precipitation rate over time is indicative of an increased trend in the amount of precipitation at these stations.
- Furthermore, pre-monsoon precipitation has increased, leading in extended wet periods at sites such as Arki, Chowari, Renuka, and Shimla.
- A noteworthy observation based on the rate of change in annual precipitation throughout time is that precipitation trends are changing and, as a result, at a detectable rate.
- A shift in pattern and greater pre-monsoon precipitation are two other prominent effects of climate change.
- The investigation of precipitation trends over these years reveals that seasonal patterns have changed as a result of changes in climatic conditions, and maximum annual rainfall in the study area has increased.

References

1. Lupikasza E (2010) Spatial and temporal variability of extreme precipitation in Poland in the period 1951–2006. Int J Climatol J R Meteorol Soc 30(7):991–1007
2. Pingale SM, Khare D, Jat MK, Adamowski J (2014) Spatial and temporal trends of mean and extreme rainfall and temperature for the 33 urban centers of the arid and semi-arid state of Rajasthan, India. Atmos Res 138:73–90
3. Goyal MK (2014) Statistical analysis of long term trends of rainfall during 1901–2002 at Assam, India. Water Resour Manage 28(6):1501–1515
4. Chaithong T, Soralump S, Pungsuwan D, Komori D (2017) Assessing the effect of predicted climate change on slope stability in northern Thailand: a case of Doi Pui. Int J GEOMATE 13(38):38–48
5. Kumar D, Bhattacharjya RK (2021) Change in rainfall patterns in the hilly region of Uttarakhand due to the impact of climate change. Appl Environ Res 43(1):1–13
6. IPCC (2014) Climate change 2014: synthesis report. Contribution of working groups I, II and III to the Fifth assessment report of the Intergovernmental Panel on Climate Change [Core Writing Team, Pachauri RK, Meyer LA (eds)]. IPCC, Geneva, Switzerland, p 151
7. Ghosh S, Luniya V, Gupta A (2009) Trend analysis of Indian summer monsoon rainfall at different spatial scales. Atmos Sci Lett 10(4):285–290
8. Guhathakurta P, Sreejith OP, Menon PA (2011) Impact of climate change on extreme rainfall events and flood risk in India. J Earth Syst Sci 120(3):359–373
9. Mondal A, Khare D, Kundu S (2015) Spatial and temporal analysis of rainfall and temperature trend of India. Theoret Appl Climatol 122(1):143–158
10. Joshi R, Verma KS (2020) Understanding the effect of climate change on temperature and precipitation in Sirmaur district of Himachal Pradesh. Int J Curr Microbiol App Sci 9(10):918–928

11. Tirkey N, Parhi PK, Lohani AK, Chandniha SK (2021) Analysis of precipitation variability over Satluj Basin, Himachal Pradesh, India: 1901–2013. J Water Clim Change 12(1):127–135
12. Herath SM, Sarukkalige PR, Nguyen VTV (2016) A spatial temporal downscaling approach to development of IDF relations for Perth airport region in the context of climate change. Hydrol Sci J 61(11):2061–2070
13. Benestad RE, Chen D, Hanssen-Bauer I (2008) Empirical-statistical downscaling. World Scientific Publishing Company
14. Maraun D, Wetterhall F, Ireson AM, Chandler RE, Kendon EJ, Widmann M, Brienen S, Rust HW, Sauter T, Themeßl M, Venema VKC, Chun KP, Goodess CM, Jones RG, Onof C, Vrac M, Thiele-Eich I (2010) Precipitation downscaling under climate change: recent developments to bridge the gap between dynamical models and the end user. Rev Geophys 48(3)
15. Fowler HJ, Blenkinsop S, Tebaldi C (2007) Linking climate change modelling to impacts studies: recent advances in downscaling techniques for hydrological modelling. Int J Climatol J R Meteorol Soc 27(12):1547–1578
16. Wilby RL, Dawson CW, Murphy C, Connor PO, Hawkins E (2014) The statistical downscaling model-decision centric (SDSM-DC): conceptual basis and applications. Climate Res 61(3):259–276
17. Arguez A, Vose RS (2011) The definition of the standard WMO climate normal: the key to deriving alternative climate normals. Bull Am Meteor Soc 92(6):699–704
18. Wilby RL, Dawson CW, Barrow EM (2002) SDSM—a decision support tool for the assessment of regional climate change impacts. Environ Model Softw 17(2):145–157
19. Li Z, Liu WZ, Zhang XC, Zheng FL (2009) Impacts of land use change and climate variability on hydrology in an agricultural catchment on the Loess Plateau of China. J Hydrol 377(1–2):35–42
20. Sachindra DA, Huang F, Barton A, Perera BJC (2014) Statistical downscaling of general circulation model outputs to precipitation—part 1: calibration and validation. Int J Climatol 34(11):3264–3281
21. Huang J, Zhang J, Zhang Z, Xu C, Wang B, Yao J (2011) Estimation of future precipitation change in the Yangtze River basin by using statistical downscaling method. Stoch Env Res Risk Assess 25(6):781–792

Trend Analysis of Hourly Rainfall Indices in Savitri River Basin, India

E. S. Namitha, V. Jothiprakash, and Bellie Sivakumar

Abstract Adequate knowledge of the temporal variations of extreme rainfall events is key to modeling and forecasting extreme hydrologic events (e.g., floods) and for undertaking water-related emergency measures and management strategies. In this study, the temporal variations of extreme hourly rainfall events are examined using trend analysis on rainfall indices. The extreme indices are developed based on hourly monsoon (July to September) rainfall data (from 2000 to 2010) collected from five rain gauges in the Savitri River basin, Maharashtra, India. Commonly used Mann-Kendall and Sen's slope tests are employed in this study to identify the trends. The indices are representing the total rainy hours, the maximum value of 1-h rainfall, and the hourly distribution of rainfall in a day. To obtain the hourly distribution in a day, a day is divided into six time periods, each with a length of four hours (early morning from 02:00 a.m. to 06:00 a.m., morning from 06:00 a.m. to 10:00 a.m., afternoon from 10:00 a.m. to 02:00 p.m., evening from 02:00 p.m. to 06:00 p.m., late evening from 06:00 p.m. to 10:00 p.m., and night from 10:00 p.m. to 02:00 a.m.). The hourly rainfall trend analysis shows that the total rainy hours and the maximum hourly rainfall show an increasing trend during July and September. The trend of rainfall occurring from early morning to night increases during September. However, during July, rainfall occurring from morning to night shows an increasing trend for most of

E. S. Namitha (✉) · V. Jothiprakash · B. Sivakumar
Department of Civil Engineering, Indian Institute of Technology Bombay, Mumbai 400076, India
e-mail: namithaelza@gmail.com

V. Jothiprakash
e-mail: vprakash@iitb.ac.in

B. Sivakumar
e-mail: b.sivakumar@iitb.ac.in

P. V. Timbadiya et al. (eds.), *Climate Change Impact on Water Resources*, Lecture Notes in Civil Engineering 313, https://doi.org/10.1007/978-981-19-8524-9_27

the stations. But during August, the hourly rainfall occurring in a day is showing no clear pattern in the basin.

Keywords Hourly rainfall indices · Mann-Kendall test · Sen's slope test · Savitri River basin

1 Introduction

Trend analysis is widely used to evaluate the variability of hydrometeorological variables, before more detailed modeling and prediction analyses are performed on them. The commonly used trend detection techniques are Sen's slope test, Mann-Kendall (MK) test, and Modified Mann-Kendall test [1–5]. Many studies have carried out trend analysis for hydrometeorological data observed in river basins in India. Such studies have addressed the long-term trend of rainfall, runoff, temperature, potential evapotranspiration, relative humidity, and sunshine duration, among others [6–11]. Some studies have used certain indices developed for the extreme conditions of hydrologic events and performed trend analysis on those indices to identify the nature of variability of the extreme hydrologic conditions [12–14]. The importance of temporal analysis of extreme hydrologic events is increasingly realized at the current time, because of climate change and its effect on water availability.

In this study, temporal variation of hourly rainfall events from the Savitri River basin, India is analyzed using indices. The indices represent the total rainy hours, the maximum value of 1-h rainfall, and the hourly distribution of rainfall in a day. The rainfall observed during the monsoon season (July–September) over the period 2000–2010 is used here for the temporal analysis. The temporal variation is examined using trend analysis. Two trend test are employed: MK test and Sen's slope test.

2 Study Area and Data Used

2.1 Savitri River Basin

The Savitri River basin is one of the west flowing river basins in India. It completely lies in the Raigad district of Maharashtra, India, within the global coordinates of 17°50′ N to 18°20′ N and 73°07′ E to 73°41′ E (Fig. 1). The basin has a total area of 2262.42 km^2. In this study, the Shuttle Radar Topographic Mission (SRTM) Digital Elevation Model (DEM) is used for the delineation of the study area. The elevation varies from 0 to 1403 m above mean sea level**.** The Savitri River originates from the Mahabaleshwar plateau and flows down for a length of 95.1 km to join the Arabian Sea at Bankot Creek. In the downstream, the Kal River, the Ghandari River, and the Kundalika River join the Savitri River. These tributaries have a length of 45.5 km, 20.9 km, and 58.7 km, respectively.

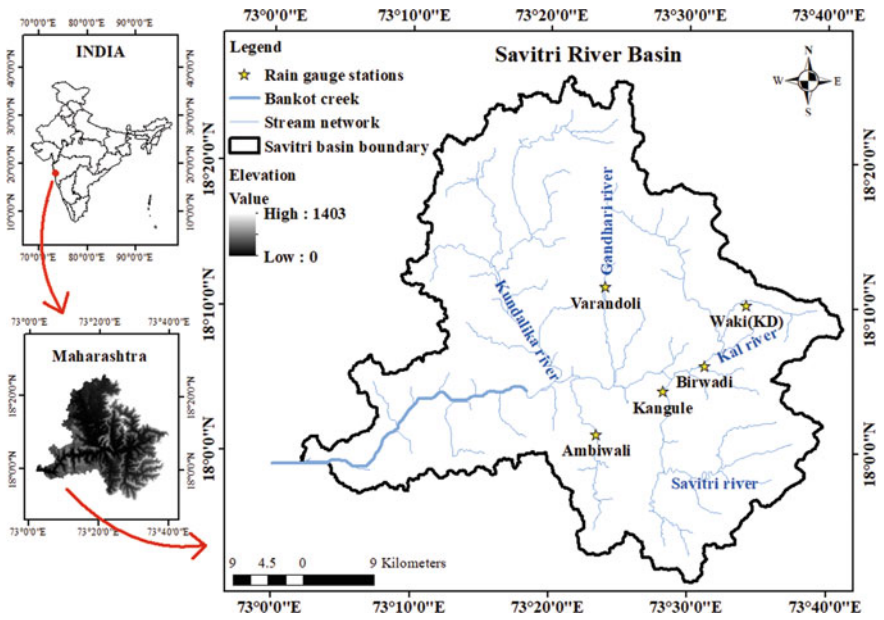

Fig. 1 Savitri River basin location and the position of rain gauge stations

The southwest monsoon (June–September) and orographic rainfall is the main source of the rivers in the study area [15]. The locations of the rain gauge stations namely Ambiwali, Kangule, Birwadi, Varandoli, and Waki (KD) in the basin are shown in Fig. 1.

2.2 Data Used

The hourly rainfall data available during the (Southwest) monsoon season over the period 2000–2010 for the study area are collected from the Hydrology Project, Nasik, India. The rain gauges in the study area are located at Ambiwali, Kangule, Birwadi, Varandoli, and Waki (KD). The rainfall data collected from these stations have few

Table 1 Details and statistics of rain gauges in Savitri River basin

Station	Elevation (m)	μ (mm)	σ (mm)	α	β	Max (mm)	Min (mm)
Ambiwali	14	0.96	3.04	6.70	72.70	78.00	0.00
Kangule	20	1.08	3.22	6.30	64.22	82.50	0.00
Birwadi	33	1.19	3.28	6.39	85.66	112.80	0.00
Varandoli	51	1.29	3.52	5.25	43.10	78.00	0.00
Waki (KD)	103	1.28	3.23	4.90	35.99	60.00	0.00

μ—mean, σ—standard deviation, α—skewness, β—kurtosis, Max—maximum, and Min—minimum

missing points in the period, and these are filled with the inverse distance weighting (IDW) method [16]. Table 1 presents some basic statistics of the rainfall data from these stations. The rain gauges are not evenly distributed in the study area. They are more concentrated on the eastern side of the basin, and there are no gauges toward the western side.

As seen from Table 1, the mean value of the hourly rainfall series for the monsoon season varies from 0.96 mm (Ambiwali) to 1.29 mm (Waki (KD)) and the standard deviation varies from 3.04 mm (Ambiwali) to 3.52 mm (Varandoli). The hourly maximum value of rainfall in a day varies from 72.7 mm (Ambiwali) to 112.8 mm (Waki (KD)). The hourly monsoon rainfall series in all the stations is positively skewed and has high kurtosis. There is a large difference between the mean hourly rainfall value and the maximum amount of rainfall for all the stations. This shows the high variation in the amount of rainfall received in the study area.

3 Methodology

The methodology adopted for the temporal analysis of the rainfall data in this study is shown as a flow chart in Fig. 2. Trend analysis shows the general nature of the variation of the variable under consideration. In this study, the commonly used MK test and Sen's slope test are used to analyze the trend. The trend analysis is performed at a significance level of 5%. The MK test gives the significance of trend, and this non-parametric test can be applied to non-homogeneous data as well. The test gives the significance of the trend by checking the null hypothesis that there is no trend in the series and the alternate hypothesis is taken as there is a trend in the series. The parameter, S, is calculated [17] using the following formula:

$$S = \sum_{n=1}^{N-1} \sum_{m=n+1}^{N} \operatorname{sgn}(x_m - x_n) \tag{1}$$

$$\begin{aligned} \operatorname{sgn}(x_m - x_n) &= 1 \text{ if } (x_m - x_n) > 0 \\ &= 0 \text{ if } (x_m - x_n) = 0 \\ &= -1 \text{ if } (x_m - x_n) < 0 \end{aligned} \tag{2}$$

where N is the total number of data points, x_m and x_n are the data points where $m > n$.

When the data is independent and uniformly distributed, the average and variance of S is given as

$$E(S) = 0 \tag{3}$$

$$\operatorname{var}(S) = \frac{N(N-1)(2N+5) - \sum_{i=1}^{j} l_i(l_i-1)(2l_i+5)}{18} \tag{4}$$

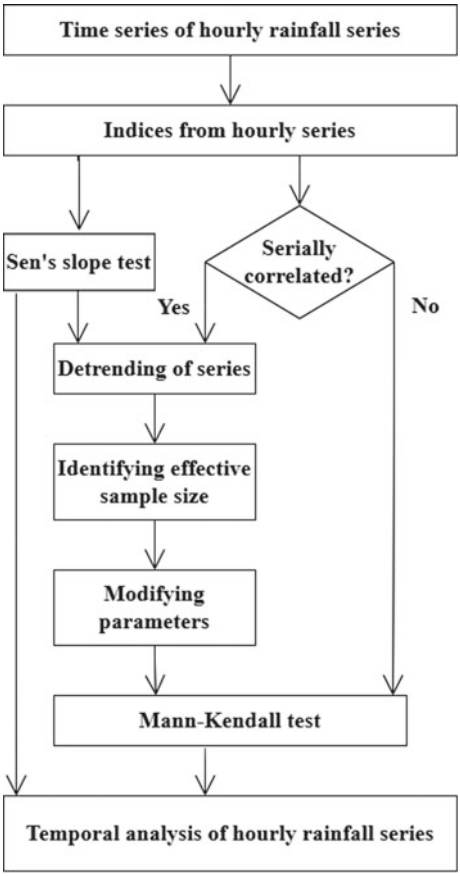

Fig. 2 Flow chart of the methodology adopted in this study

where j is the number of ties which resulted from similar consequent values in time series and l_i is the number of data points in the ith tied group.

The test statistics (Z) is found as shown below

$$\begin{aligned} Z &= \frac{S-1}{\sqrt{\text{var}(S)}} \text{ if } S > 0 \\ &= 0 \text{ if } S = 0 \\ &= \frac{S+1}{\sqrt{\text{var}(S)}} \text{ if } S < 0 \end{aligned} \tag{5}$$

The positive Z value indicates an increasing trend, whereas the negative Z indicates a decreasing trend. The magnitude of the trend is significant when the critical standard normal deviate value (1.96) is less than the test statistics (Z). As a prerequisite for the MK test, the series should be checked for the independency of values. Therefore, the serial correlation of each series is checked, and if it is correlated, prewhitening needs

to be carried out to remove the correlation. The effectiveness of the prewhitening procedure in removing the correlation has been a topic of concern. In this study, the MK test is done by using effective sample size (ESS) approach [18] to reduce the effect of serial correlation. It begins with detrending the series as follows:

$$x_t' = x_t - \beta \tag{6}$$

where x_t' is the data point in detrended series at time t, x_t is the data point in series at time t, and β is the trend identified by Sen's slope test.

The Sen's slope test gives the direction of the trend. It identifies the direction of trend by using the slope of all the data point pairs in the time series [19] as shown below

$$\beta = \text{median}\left(\frac{x_m - x_n}{m - n}\right) \tag{7}$$

The positive β indicates increasing nature of trend, and negative β indicates decreasing nature of trend. After detrending using Sen's slope value, ESS is identified. Then, the MK test is performed by using modified variance [18], which is estimated by using the following formula:

$$\text{var}(S)^* = \text{var}(S)\frac{N}{N^*} \tag{8}$$

where N is the actual sample size and N^* is the ESS.

The following section discusses the application of trend test on the indices for the hourly rainfall from study area and the results obtained. There are 8 indices in total, and definition of each index is presented in Table 2. The first index, PRCPHR indicates the total rainy hours in each month. Second index, R1HR represents the maximum value of 1-h rainfall during a month.

The next set of indices are formed to identify the hourly distribution of rainfall in a day. For this, a day is divided into six time periods with four hours each in it, like early morning from 02:00 a.m. to 06:00 a.m. (RELMG), morning from 06:00 a.m. to 10:00 a.m. (RMRNG), afternoon from 10:00 a.m. to 02:00 p.m. (RAFNN), evening from 02:00 p.m. to 06:00 p.m. (REVNG), late evening from 06:00 p.m. to 10:00 p.m. (RLTEV), and night from 10:00 p.m. to 02:00 a.m. (RNGHT).

4 Results and Discussion

The hourly rainfall data collected from the five rain gauges in the study area are used to develop the indices in order to understand the trend of hourly rainfall. The results of the trend analysis on the hourly rainfall indices are given in Fig. 3. The first index, PRCPHR indicates the total rainy hours in each month. On an average, Ambiwali, Kangule, Varandoli, Birwadi, and Waki (KD) are receiving rainfall for 310, 351,

Table 2 List and definitions of indices used

Indicator	Indicator name	Description	Unit
PRCPHR	Total rainy hours	Total rainy hours in a month	h
R1HR	Maximum hourly rainfall	Monthly 1-h maximum rainfall	mm
RELMG	Rainfall amount during early morning	Monthly total rainfall in a day from 02:00 a.m. to 06:00 a.m	mm
RMRNG	Rainfall amount during morning	Monthly total rainfall in a day from 06:00 a.m. to 10:00 a.m	mm
RAFNN	Rainfall amount during afternoon	Monthly total rainfall in a day from 10:00 a.m. to 02:00 p.m	mm
REVNG	Rainfall amount during evening	Monthly total rainfall in a day from 02:00 p.m. to 06:00 p.m	mm
RLTEV	Rainfall amount during late evening	Monthly total rainfall in a day from 06:00 p.m. to 10:00 p.m	mm
RNGHT	Rainfall amount during night	Monthly total rainfall in a day from 10:00 p.m. to 02:00 a.m	mm

401, 376, and 433 h, respectively, during July, whereas during August, the total rainy hours is 291, 325, 367, 344, and 400 h at Ambiwali, Kangule, Varandoli, Birwadi, and Waki (KD), respectively. The rainy hours during September varies among the five stations from 138 to 169 h during September. More rainy hours is observed during July month and least during September month. The Waki (KD) and Varandoli stations which are lying at higher elevation and close to mountain area experiences more rainy hours than the low lying and far from mountain stations like Kangule and Birwadi. Because stations which are lying close to mountain region receives more orographic precipitation than the far away stations. All the stations show an increasing trend for PRCPHR during July and September. Among the increasing trends during September, the Varandoli ($Z = 2$), Birwadi ($Z = 2.18$), and Waki (KD) ($Z = 2.08$) stations are showing significant increase. The trend of PRCPHR during August month is decreasing for all stations except the Ambiwali station.

The second index, maximum value of 1-h rainfall (R1HR) during July is 30 mm, 30 mm, 30 mm, 32 mm, and 31 mm at Ambiwali, Kangule, Varandoli, Birwadi, and Waki (KD), respectively. But during August, the R1HR at Ambiwali, Kangule, Varandoli, Birwadi, and Waki (KD) is 27 mm, 28 mm, 24 mm, 29 mm, and 24 mm, respectively. During September month, the 1-h maximum rainfall value varies from 33 mm (Birwadi) to 21 mm (Waki (KD)). The Birwadi station is experiencing more R1HR during the three months. The increased rainy hours and more magnitude of rainfall at Birwadi station might result in more flood events in the Kal River (where Birwadi station is located). During September, all the five stations are showing an increasing trend for R1HR. The majority of the stations (three out of five) show an increasing trend for R1HR during July and August.

The amount of rainfall received during each period in a day and its trend over time are analyzed using the six indices. The trends of these indices are shown in

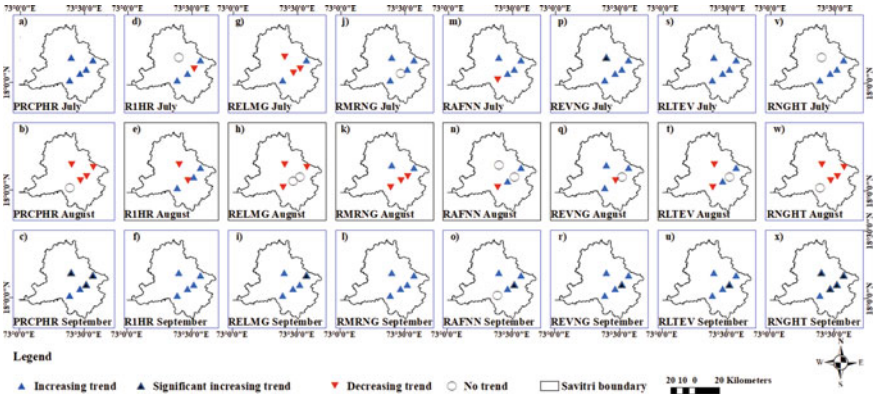

Fig. 3 Trend analysis results for the hourly rainfall index: **a–c** PRCPHR, **d–f** R1HR, **g–i** RELMG, **j–l** RMRNG, **m–o** RAFNN, **p–r** REVNG, **s–u** RLTEV, and **v–x** RNGHT

Fig. 3. The total amount of rainfall received during early morning hours varies from 144 mm (Ambiwali) to 217 mm (Waki (KD)), 117 mm (Ambiwali) to 185 mm (Waki (KD)), and 38 mm (Varandoli) to 50 mm (Waki (KD)) for July, August, and September month, respectively. The index, RELMG shows a decreasing trend for the majority of stations during July and August. During September, however, all the stations show an increasing trend. The Waki (KD) station shows a significant increase during September with a Z value of 2.

During July, August, and September, the value of index RMRNG varies between stations from 152 mm (Ambiwali) to 235 mm (Birwadi), 100 mm (Ambiwali) to 173 mm (Birwadi), and 29 mm (Ambiwali) to 53 mm (Varandoli), respectively. The total rainfall received in the morning shows an increasing trend for four stations during July and all the stations during September. But during August, Varandoli and Waki (KD) are only showing an increasing trend, remaining stations are showing decreasing trend.

The total amount of rainfall received during afternoon hours varies from 225 mm (Waki (KD)) to 248 mm (Birwadi) during July, whereas during August and September, it varies from 145 mm (Ambiwali) to 234 mm (Birwadi), and 45 mm (Waki (KD)) to 61 mm (Birwadi), respectively. The RAFNN shows an increasing trend for all the stations except Ambiwali during July and September. The Ambiwali station is showing a decreasing trend for RAFNN during July and no trend during September. The increasing trend at Birwadi ($Z = 2.14$) is significant during September. But during August, RAFNN is showing no trend at Varandoli and Birwadi stations, increasing trend for Kangule and Waki (KD) stations and decreasing trend for Ambiwali station.

The REVNG, which indicates the total amount of rainfall received during the evening time, varies from 217 mm (Ambiwali) to 289 mm (Birwadi), 153 mm (Ambiwali) to 263 mm (Waki (KD)), and 75 mm (Ambiwali) to 138 mm (Birwadi) during July, August, and September month, respectively. The REVNG shows an increasing trend for all the five stations during July and September. But during August, all stations except Kangule (decreasing trend) and Birwadi (no trend) are showing an

increasing trend. Among these, there is a significant increase at Varandoli ($Z = 2.09$) during July and Birwadi ($Z = 2.32$) during September.

During July, August, and September, the index RLTEV varies from 151 mm (Ambiwali) to 237 mm (Waki (KD)), 117 mm (Ambiwali) to 208 mm (Waki (KD)), and 47 mm (Ambiwali) to 106 mm (Waki (KD)), respectively. The amount of rainfall received during late evening hours has an increasing trend for all the stations during July and September. The Birwadi station shows a significant increase during September with a Z value of 1.97. But during August month, Ambiwali and Varandoli are showing a decreasing trend, Kangule and Waki (KD) are showing an increasing trend, and Birwadi is showing no trend.

The total amount of rainfall received during night hours varies from 142 mm (Ambiwali) to 195 mm (Waki (KD)), 122 mm (Ambiwali) to 165 mm (Birwadi), and 33 mm (Ambiwali) to 58 mm (Waki (KD)), for July, August, and September, respectively. The RNGHT shows an increasing trend for all station except Varandoli (no trend) during July. All stations except Ambiwali (no trend) station are showing a decreasing trend for RNGHT during August. But during September, all the five stations show an increasing trend for RNGHT, with a significant trend shown by Kangule ($Z = 2.18$), Birwadi ($Z = 2.83$), Varandoli ($Z = 2.38$), and Waki (KD) ($Z = 2.04$). For all the five stations, rainfall received mainly during afternoon, evening, and late evening hours during the monsoon season. This may be due to the high temperature, high evaporation, and long sunshine duration during these hours in the basin. The trend analysis of hourly rainfall series for different periods in a day shows that the rainfall during the morning, afternoon, evening, late evening, and night hours shows an increasing trend for majority of stations during July, whereas during August, there is no clear pattern of trend for the hourly rainfall in the basin. All the stations in the area show an increasing trend for rainfall received from early morning to night during September.

5 Conclusions

This study performed trend analysis of the hourly rainfall in the Savitri River basin during the monsoon period. The trend analysis was done on the indices developed for the hourly rainfall series. The results show an increase in the number of rainy hours during July and September. The maximum value of 1-h rainfall shows an increasing trend during monsoon period. During July, most of the rainfall occurs from morning to night, during August there is no clear pattern, whereas during September, most rainfall occurs from early morning to night. These results are very much useful for the planning and management of water resource related problems in the area, such as irrigation, water distribution, water storage by dams, and disaster management, among others. The present study can serve as an important initial step for developing hydrological models for the study area, with elaborate studies for flood flow in the future.

Acknowledgements The authors are thankful to the Hydrology Project (HP), Nasik for providing the hydrometeorological data in the Savitri basin. The data can be procured from HP by directly contacting them.

References

1. Gavrilov MB, Tošić I, Marković SB, Unkašević M, Petrović P (2016) Analysis of annual and seasonal temperature trends using the Mann-Kendall test in Vojvodina, Serbia. Q J Hung Meteorol Serv 120(2):183–198
2. Soro GE, Noufé D, Bi TAG, Shorohou B (2016) Trend analysis for extreme rainfall at sub-daily and daily timescales in Côte d'Ivoire. Climate 4:37. https://doi.org/10.3390/cli4030037
3. Sreelash K, Sharma RK, Gayathri JA, Upendra B, Maya K, Padmalal D (2018) Impact of rainfall variability on river hydrology: a case study of Southern Western Ghats, India. J Geol Soc India 92:548–554
4. Umar DA, Ramli MF, Aris AZ, Jamil NR, Abdulkareem JH (2018) Runoff irregularities, trends, and variations in tropical semi-arid river catchment. J Hydrol Reg Stud 19:335–348
5. Deng Y, Cao G, Jiang W, Wu J, Li Z, Wang X (2020) Spatiotemporal changes in heavy precipitation events in the Beijing-Tianjin-Hebei region revealed by hourly meteorological station observations. Theoret Appl Climatol. https://doi.org/10.1007/s00704-020-03198-0
6. Singh P, Kumar V, Thomas T, Arora M (2008) Changes in rainfall and relative humidity in river basins in northwest and central India. Hydrol Process 22:2982–2992. https://doi.org/10.1002/hyp.6871
7. Jaswal AK (2009) Sunshine duration climatology and trends in association with other climatic factors over India for 1970–2006. Mausam 60(4):437–454
8. Deshpande NR, Kulkarni A, Kumar KK (2012) Characteristic features of hourly rainfall in India. Int J Climatol 32:1730–1744. https://doi.org/10.1002/joc.2375
9. Gupta PK, Chauhan S, Oza MP (2016) Modelling surface run-off and trends analysis over India. J Earth Syst Sci 125(6):1089–1102. https://doi.org/10.1007/s12040-016-0720-z
10. Sonali P, Kumar DN (2016) Spatio-temporal variability of temperature and potential evapotranspiration over India. J Water Clim Change 7(4):810–822. https://doi.org/10.2166/wcc.2016.230
11. Chandniha SK, Meshram SG, Adamowski JF, Meshram C (2017) Trend analysis of precipitation in Jharkhand state, India: investigating precipitation variability in Jharkhand state. Theoret Appl Climatol 130:261–274. https://doi.org/10.1007/s00704-016-1875-x
12. Ali H, Mishra V, Pai DS (2014) Observed and projected urban extreme rainfall events in India. J Geophys Res Atmos 119(12):12621–12641. https://doi.org/10.1002/2014JD022264
13. Deshpande NR, Kothawaleb DR, Kulkarnic A (2016) Changes in climate extremes over major river basins of India. Int J Climatol 36:4548–4559
14. Sharma PJ, Loliyana VD, Resmi SR, Timbadiya PV, Patel PL (2018) Spatiotemporal trends in extreme rainfall and temperature indices over Upper Tapi Basin, India. Theoret Appl Climatol 134:1329–1354. https://doi.org/10.1007/s00704-017-2343-y
15. Gharde KD, Mahesh K, Singh PK, Mittal HK (2015) Geomorphometric analysis and prioritization of sub catchments of Savitri basin in Konkan region of Maharashtra, India using GIS technique. Int J Civil Eng 4(2):1–18
16. Lam NS (1983) Spatial interpolation methods: a review. Am Cartographer 10(2):129–149
17. Kendall MG (ed) (1975) Rank correlation methods. Charles Griffin, London
18. Yue S, Wang CY (2004) The Mann-Kendall test modified by effective sample size to detect trend in serially correlated hydrological series. Water Resour Manage 18:201–218
19. Sen PK (1968) Estimation of regression coefficient based on Kendall's test. J Am Stat Assoc 63(324):1379–1389

Precipitation and Stream flow Trends for Swarna River Watershed, Karnataka, India.

K. T. Nagamani, S. S. Chethana, and T. N. Bhagwat

Abstract Analysing the spatiotemporal distribution of precipitation patterns and their effects on flash floods in moist, humid environments is crucial for determining the situation and offering suitable adaptation strategies. In addition to trend analysis and homogeneity tests, the climate variability under expected flash floods was analysed using the coefficient of variation, number of wet days, precipitation concentration index, and predicted maximum precipitation, while the flash flood magnitude index and flood magnitude ratio were used to determine streamflow episodes. A case study basin for humid climatic conditions has been proposed as the Swarna River basin in the western region of Udupi, which suffers high levels of climate fluctuation due to flash floods. Precipitation patterns were increasing from the headwaters of the Swarna River basin to the downstream. According to the findings of the homogeneity tests carried out by Pettitt, SNHT, Buishand, and Von Neumann, there is no appreciable variation between the pre- and post-alteration points in the mean of the precipitation.

Keywords Precipitation trends · Flash floods · Mann-Kendall test · Flash flood magnitude index

K. T. Nagamani (✉)
Department of Civil Engineering, Dayananda Sagar College of Engineering Bangalore, Bangalore 560078, India
e-mail: nagamanikt-cvl@dayanandasagar.edu

S. S. Chethana · T. N. Bhagwat
Department of Civil Engineering, University BDT College of Engineering Davanagere, Davanagere 577004, India

P. V. Timbadiya et al. (eds.), *Climate Change Impact on Water Resources*, Lecture Notes in Civil Engineering 313, https://doi.org/10.1007/978-981-19-8524-9_28

1 Introduction

The identification and comprehension of changes in a rainfall-runoff process at the basin scale depend on trend analysis of hydro-meteorological data. Climate variability and their detection are expected to have an impact on ecological sustainability as well as land usage, land cover, and water resources [1, 2]. Flash flood frequency and severity changes in river flow with other hydro-meteorological phenomena that have a direct impact on the environment include an increase or decrease in precipitation [3, 4]. One of the main indications of climate change is changes in rainfall pattern and intensity at very local levels [5]. Extreme precipitation and discharge patterns throughout time and space can have a negative impact on tropical river basins, where agriculture, the economy, and wildlife are all threatened by the significant spatiotemporal variability in the precipitation and any shift in the mean precipitation pattern [6]. In addition to altering the environment of Western Ghats ecosystems that are biodiversity hotspots, high intensity precipitation for extended periods of time and changes in land use/land cover also contribute to landslides because of frequent flash floods [7, 8]. The risk of frequent flash floods in low lying places is increased based on the spatial distribution of rainfall intensity and the geomorphological characteristics of the basin, as well as the precipitation in river basins with orographic intensification [5, 9]. Usually shorter than six hours, a flash flood occurs when there is heavy or severe rainfall for a short period of time [10].

Flash floods are excessive flows that overwhelm the water-carrying capacity of a river channel, lake, pond, reservoir, drainage system, dam, or any other water body and cause areas outside of the water body to get inundated. This runoff volume, if managed well, is anticipated to satisfy the basin's water deficit and assist in preventing negative effects from intra-basin water transfers, particularly in coastal river basins of peninsular India [11, 12]. Flash floods are very brief-duration events in relation to the geomorphological aspects of the basin, involving the strengthening of orography and the dispersion of rainfall intensity events over space and time [13]. As a result, such basins present a challenge for mitigating efforts. Small streams are affected by flash floods, which are associated with brief but intense rainfall events and are particularly common in tropical river basins. With even modest rainfall posing a major risk of flooding in tropical river basins with high watershed gradient, the problem is only anticipated to get worse as a changing climate brings about more catastrophic rainfall events [14, 15]. Therefore, the current work's goal is to research patterns in precipitation in river basins.

The goals of this research are (1) analysis of the regional and temporal trends of rainfall during flash floods and (2) examine the tropical basin's precipitation patterns and their relationship to the occurrence of flash floods.

2 Study Area and Data Source

2.1 Swarna River Basin (SRB)

The Swarna River originates in Udupi, flows across western India at an elevation of 1100 m above mean sea level, then joins the Madisal River after travelling about 80 km along the coast before emptying its water into the Arabian Sea. The tributaries of this river are situated between latitudes 13°13′ and 13°48′ north and 74°62′ and 75°19′ east. The SRB has a total size of about 789.33 km^2, and its height varies from 0 to 1208 m above sea level. The river travels a distance of 61.05 km before meeting the sea. Mulikar, Ajekar, Karkala, Puttige, Kervashe, and Udupi are rain gauge stations that are situated in the basin. At Yennehole, river discharge is measured (Fig. 1 and Table 1). Red lateritic soil, gneiss, alluvium, and colluvium deposits can be found on the river banks and seashores of the basin. The humid subtropical climate of SRB spans a variety of ecological and climatic regions. River has a mean discharge of 2516.98 m^3/s and a maximum discharge of 1069.32 m^3/s, respectively. The range of annual precipitation is 3465 mm to 7751 mm. The Swarna River flow regime has significant seasonal flow changes, with the highest discharge occurs during the monsoon season, which runs from June to September. In January, the temperature varies from 21.7 °C to 32.4 °C (April). The highest average monthly wind speed ranges from 7.2 to 9.6 km/h.

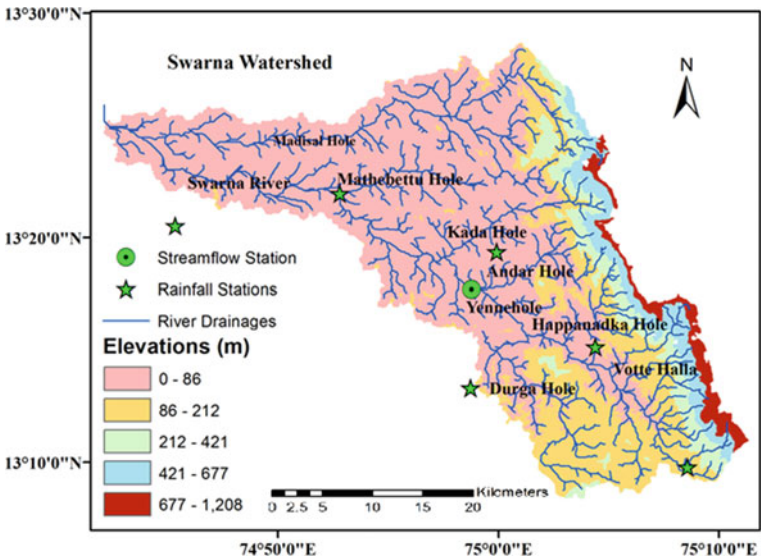

Fig. 1 Location of the research area's meteorological stations

Table 1 Latitude, longitude, yearly daily rainfall, average annual rainfall, and distance from Kodibengre are included in the station addresses

Rain gauge station	Latitude	Longitude	Altitude (m)	Average annual daily rainfall (mm)	Average annual rainfall (mm)	Distance from Kodibengre (km)
Puttige	13°21′59.02″ N	74°52′48.67″ E	315	17	4175.165	67.9
Udupi	13°20′31.75″ N	74°45′19.94″ E	380	15	3712.17	40
Kervashe	13°19′22.38″ N	74°59′55.38″ E	700	22	5397.225	60.9
Ajekar	13°15′9.98″ N	75° 4′23.83″ E	502	19	4788.62	50.3
Mulikar	13° 9′47.75″ N	75° 8′34.22″ E	970	23	5753.025	97
Karkala	13°13′20.36″ N	74°58′44.45″ E	782	18	4421.23	50.5

3 Data Used

The daily precipitation totals from six meteorological stations and the daily discharge from one gauging station for the time periods of 1998–2017 and 1989–2017, respectively, were collected as climate data for this study. The stations are dispersed both inside and outside the SRB and range in height from 0 to 1208 msl (Fig. 1 and Table 1). The directorate of statistics and economics as well as India WRIS has provided the data. From the USGS Earth Explorer, digital elevation models were acquired. ArcGIS 10.5 has been used for delineating the river and the basin, shaping the Thiessen network, and projecting rain gauge stations. For the homogeneity test, XLSTAT, a user-friendly statistical software add-in for Microsoft Excel, was utilised.

3.1 Rainfall Analysis and Stream Flow Analysis

Numerous techniques, which may typically be divided into variability and trend analysis, have been proposed to test meteorological data. The coefficient of variation (CV), number of rainy days, maximum precipitation that is likely to occur, and precipitation concentration index are the earlier tests that are used for the precipitation (PCI). R-Studio software has been used to conduct the latter, which is often done with non-parametric trend analysis for regular climate data [16, 17]. The discharge data, flash flood magnitude ratio, and flash flood magnitude index are used in the test.

CV and PCI have been used to estimate the variability of precipitation. To evaluate the irregularity of precipitation, the CV has been taken into account. Great CV values suggest large variability and vice versa. Equation calculates the coefficient (1)

$$\mathrm{CV} = \frac{\sigma}{\mu} \tag{1}$$

The standard deviation, the average amount of precipitation, and the coefficient of variation are all written as CV. The amount of precipitation variability can be categorised as low (CV 20), moderate (20 CV 30), and high (CV > 30). PCI is employed to look into the seasonal (monsoon) and yearly variation of precipitation. Equation provides the formula for PCI annual in Eq. (2) [18].

$$\mathrm{PCI} = \frac{\sum_{i=1}^{12} p_i^2}{(\sum_{i=1}^{12} p_i)^2} * 100 \tag{2}$$

Pi denotes the month's rainfall total. Low, moderate, and very high precipitation concentrations are the three categories under which the PCI is categorised. The following are the various PCI ranges: PCI < 10, 11 < PCI < 15, 16 < PCI < 20, and PCI > 21, respectively. To determine the initial moisture content of the impacted watershed, the number of wet days was employed, and it was influenced by rainfall characteristics, including spatial extent, length, and intensity, topography, land use, and soil types [15, 19].

In order to calculate the likely maximum flood, PMP was utilised. Uncertainty of the PMP values estimated by the Hershfield technique [20]. The link established by Eq. (3).

$$X_{\mathrm{PMP}} = \ddot{X} + K_m * \sigma_n \tag{3}$$

The frequency factor is km.

Equation shows how to compute the FFMI from annual peak discharge (4).

$$\mathrm{FFMI} = \frac{X^2}{N-1} \tag{4}$$

where $X = X_m - M$, $X_m =$ annual peak discharge, mean discharge on a yearly basis, and number of record years. The flood magnitude ratio has been used to estimate the annual peak discharge. Equation can be used to get it (5)

$$M = \frac{Q_p}{Q_a} \tag{5}$$

where Q_a is the annualised discharge. The yearly maximum discharge is Q_p.

According to the respective ranges of $Z > 0.84$, $Z > 1.65$, $1.28 > Z > 1.65$, and $0.84 > Z > 1.28$, the classifications of flash flood severity are extreme, severe, moderate,

and no flash flood. To ascertain if the climatic time series had a monotonically dropping or growing trend, the non-parametric Mann-Kendall (MK) test was used. Though the trend may or may not be linear, a monotonic growing or decreasing trend depicts the variable as rising or falling steadily over the span of time. To examine the homogeneity of the climatic indices, the following tests were used: Pettitt's, Standard Normal Homogeneity (SNHT), Buishand's test, and von Neumann's test [17, 21]. The SNHT, Pettitt, and Buishand tests look for to determine the breaking point, hop in the time series. The SNHT is sensitive to breaks at the beginning and end of the time series, whereas the Pettitt test and the Buishand test are more sensitive to detecting breaks in the time series' middle. Recognising the differences between the upstream and downstream using a flash flood magnitude index parameter that relates annual peak discharge to mean annual flow. For long-term peak rainfall, the flood magnitude ratio has been used.

4 Results and Discussions

4.1 Homogeneity Test

To assess the homogeneity of the annual precipitation data set, the Pettitt test, Standard Normal Homogeneity test (SNHT), and Buishand test were utilised. In each homogeneity test, the null hypothesis (H0) is accepted if the estimated p-value is larger than the value at the 5% level of significance, and it is rejected, otherwise, according to test statistics.

Since the results from the annual series of six rain gauge locations are homogeneous and the estimated p-value is higher than the value at a threshold of significance of 5%, the null hypothesis (H0) is accepted (Table 2).

Table 2 Results of homogeneity test in Swarna River basin for annual precipitation

Rain gauge stations	Petti's test	SNHT	Buishand test
Karkala	0.536	0.607	0.646
Ajekar	0.267	0.221	0.431
Mulikar	0.074	0.071	0.115
Udupi	0.32	0.501	0.467
Puttige	0.231	0.206	0.284
Kervashe	0.511	0.326	0.544

Homogeneous at 5% significance level

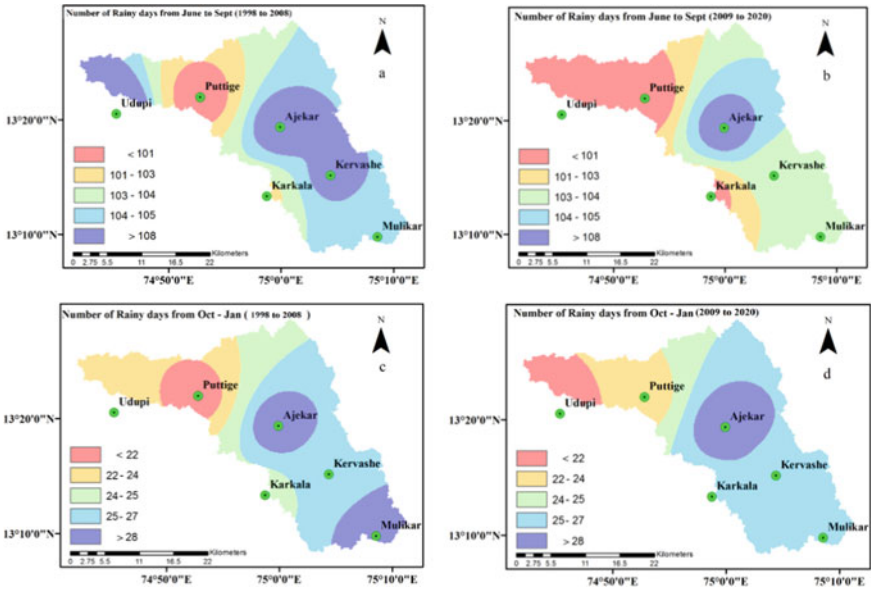

Fig. 2 Spatial map depicting the number of wet days for the **a** first decade from June to September, **b** the second decade from June to September, **c** the first decade from October to January, and **d** the second decade from October to January

4.2 Number of Rainy Days

Because they occur farther away from the ocean and have a much higher moisture content in terms of quantity, extreme rainfall events cause more damage than early monsoon events. The total amount of rain that falls should be influenced by the increase in rainy days over the course of the year or a season. The goal of this analysis is related to climate change and the prevalence of flash floods.

The results of the classified spatial maps of the number of rainy days from June to September of the first and second decades (Fig. 2a, b) demonstrate how many days it has rained increases as the volume of rain increases and vice versa in the first decade and second decade (Fig. 2c, d) from October to January. The number of rainy days has increased near Ajekar and Kervashe stations, which increases the probability of flooding. Submergence suggests that it is imminent, but there is also a greater chance that flash floods may occur.

4.3 Coefficient of Variation

The coefficient of variation is a statistical measure of how much the data points vary from the mean value. The coefficient of variation is calculated for six rain gauge

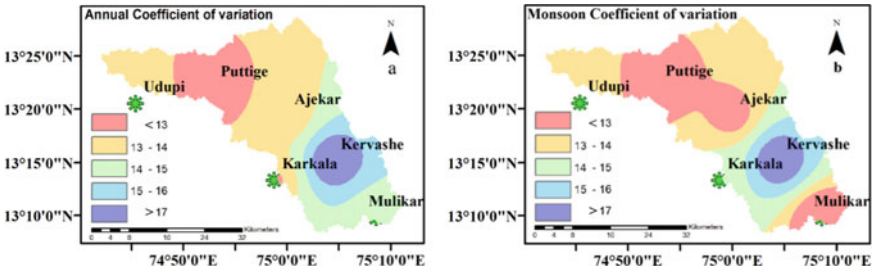

Fig. 3 **a** Annual rainfall and **b** monsoon rainfall: spatial patterns of coefficient of variation

stations for both the yearly and monsoon seasons in order to analyse the spatial pattern variability (fluctuation) of precipitation over the research area.

The catchment scale has been used to evaluate the yearly and monsoon coefficient of variation. For annual and monsoon rainfall, ranges of coefficient of variations between 13% and > 17% are referred to as fairly variable (16–24%) (Fig. 3a, b). In this research area, where there has been a lot of rainfall, the highest and lowest coefficients of variation values have been recorded in Kervashe and Puttige, respectively. Due to the flash flood, extreme events are expected in Kervashe.

4.4 Precipitation Concentration Index (PCI)

For the purpose of measuring the relative distribution of precipitation over a research area, the precipitation concentration index is offered. Based on yearly (Jan to Dec) and monsoon (June to Sept) precipitation distributions, APCI and SPCI are distributed, respectively.

The graph clearly highlights the variation of 1-day PMP values at different stations. The.

maximum PMP is found in Bhola district and the maximum value is 811 mm. The second.

highest PMP value is seen in Sandwip with a PMP value of 721 mm. Srimangal, the.

wettest place in the country has a one-day PMP of 663 mm. On the other hand, Barishal,

Bogra, Jessore, Rajshahi, Rangpur, and Madaripur have the PMP values below 300 mm.

and the lowest value 262 mm is observed in the Rajshahi. It should be noted that Rajshahi.

is the driest region of Bangladesh. Therefore, a low value of mean annual maximum.

rainfall might be contributed towards a lower PMP. It is observed that the maximum.

PMP is found over the northeastern, parts of southern and the southeastern regions of.

Bangladesh. Though Sylhet is situated near Cherapunji of Shillong plateau which.

receives the highest rainfall in the world, it is interesting to note that the PMP obtained in.

this location is only 386 mm. However, this may indicate that the intensity of 1-day.

rainfall is low but rather uniform here.

Determine how daily precipitation in a location changes throughout the year and season using spatial maps for the precipitation concentration index (during the monsoon season) will vary, as these extremes will be close to flash flood events. Figure 4a, b, which illustrates the monsoon rainfall, shows the dominance of high irregularity in precipitation distribution in the first decade and second decade, according to assessments of the annual precipitation concentration index (Fig. 4c, d).

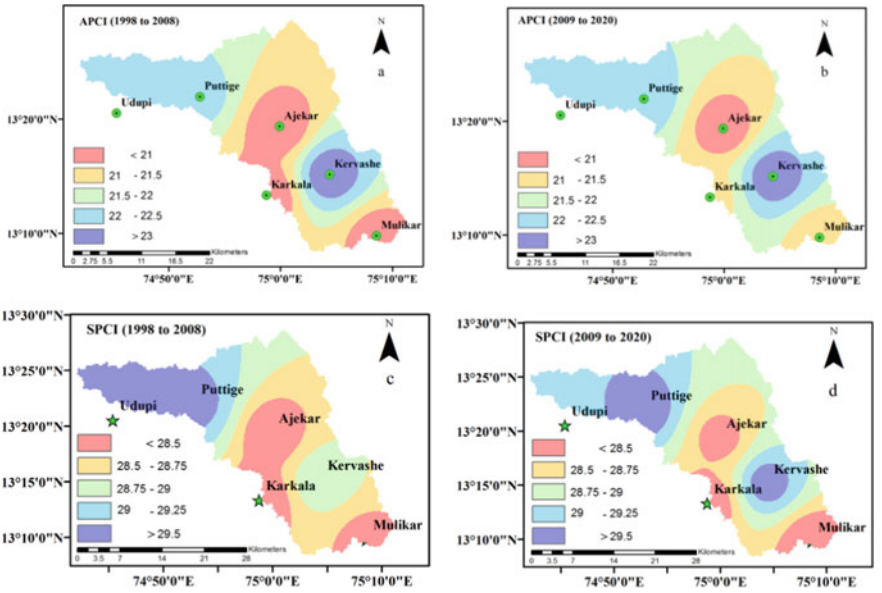

Fig. 4 Seasonal precipitation concentration index for **a** first decade from June to September, **b** the second decade from June to September, **c** the first decade from October to January, and **d** the second decade from October to January

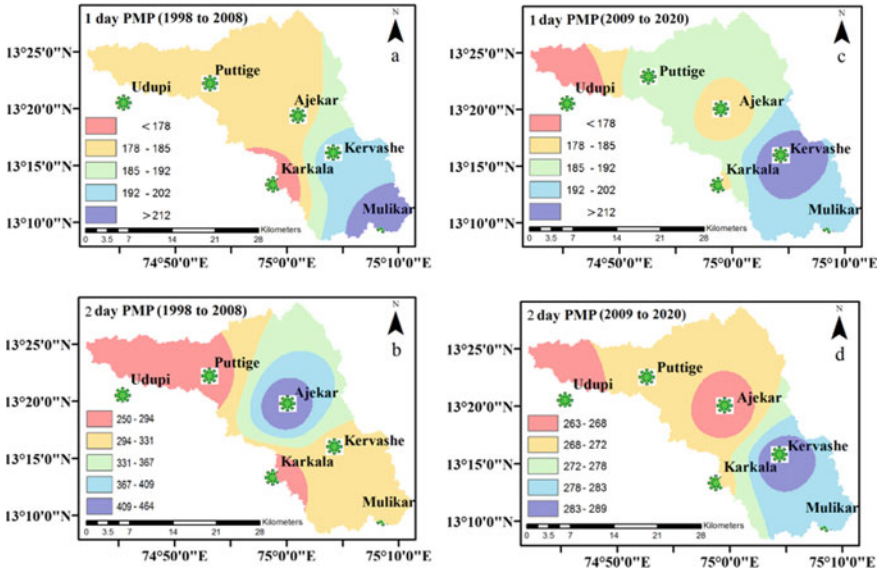

Fig. 5 Spatial patterns for **a** first decade of 1 day PMP, **b** second decade of 1 day PMP, **c** first decade of 2 day PMP, and **d** second decade of 2 day PMP

4.5 Probable Maximum Precipitation

For high-hazard hydrological structures like flood control dams on the upstream side, estimates for the probable maximum flood (PMF) are utilised in the planning, design, and risk assessment. The PMF is the maximum depth of precipitation that is physically feasible across a given size storm region at a specific geographic location during a specific time of the year for a given period.

Figure 5a, b shows the spatial distribution of 1 day PMP for the first decade and second decade, and Fig. 5, 5d shows the spatial distribution of 2 day PMP for the first decade and second decade. These findings demonstrate that the research area's upstream region has higher elevations and more precipitation and indicated a substantial future increase of maximum flash flood occurred in comparison with downstream areas.

4.6 Trend Analysis

Statistics are utilised to determine using the Mann-Kendall (MK) test, whether interest variable has been increasing or decreasing over time between 1998 and 2017. Each 5-year average of the Sen's slope, Mann-Kendall trend, and *P*-value listed in Table 3.

Table 3 Statistical properties of the precipitation variables of MK test for 5-year average

Year	Karkala			Ajekar			Mulikar			Kervashe			Puttige			Udupi		
	Z	*S*	*P*	*Z*	*S*	*P*	*Z*	*S*	*P*	*Z*	*S*	*P*	*Z*	*S*	*P*	*Z*	*S*	*P*
Annual precipitation																		
1998–2002	−1.29	−4.80	0.22	−1.43	−5.20	0.18	−0.88	−3.60	0.39	−1.02	−4.00	0.35	−1.43	−5.20	0.18	−1.43	−5.20	0.18
2003–2008	−1.43	−5.20	0.18	−0.88	−3.60	0.39	−0.88	−3.60	0.43	−1.24	−4.60	0.27	−1.02	−4.00	0.35	−.09	−4.00	0.36
2009–2013	−0.62	−2.60	0.61	−0.75	−3.20	0.48	−0.82	−3.20	0.53	−0.34	−1.60	0.76	−0.75	−3.20	0.48	−0.88	−3.60	0.43
2014–2020	−1.15	−4.40	0.31	−1.09	−4.00	0.36	−0.75	−3.20	0.48	−0.88	−3.60	0.39	−1.09	−4.00	0.36	−1.22	−4.40	0.32
Seasonal precipitation																		
1998–2002	0.82	12.80	0.43	0.75	11.80	0.49	0.94	14.60	0.37	0.80	12.60	0.44	0.75	11.60	0.46	0.52	8.40	0.63
2003–2008	0.64	10.20	0.53	0.82	12.80	0.42	0.57	9.20	0.58	0.53	8.60	0.61	0.82	12.80	0.43	0.88	13.60	0.39
2009–2013	0.96	14.80	0.39	1.02	15.80	0.35	1.02	15.80	0.37	0.90	13.60	0.41	0.93	14.40	0.37	1.00	15.40	0.33
2014–2020	1.04	16.00	0.32	0.96	15.00	0.35	1.00	15.40	0.32	1.28	19.60	0.21	0.98	15.20	0.36	0.74	11.60	0.49

Note Z Mann Kendell trend, *S* Sen's slope, *P* significance level

Table 4 Statistical properties of the stream flow variables of MK test for 5-year average

Year	Annual			Monsoon		
	Z	S	P	Z	S	P
1989–1993	0.14	0.60	0.79	1.22	18.20	0.25
1994–1998	−0.14	−0.80	0.89	0.87	13.60	0.39
1999–2003	−0.27	−1.60	0.79	1.04	16.20	0.31
2004–2008	−0.07	−0.40	0.95	1.09	16.80	0.29
2009–2013	0.00	0.00	0.89	1.03	16.00	0.32
2014–2020	0.00	0.00	0.87	1.10	16.75	0.30

The precipitation trend of annual and monsoon precipitation series was examined using a Mann-Kendall (MK) and Sens slope test. Sen's slope, the *P*-value, and the results of the MK test are shown in Table 3. A monsoon's increasing tendency is shown by a positive value of "*S*" during the past 20 years, while a downward trend is indicated by a negative value (annual). On the other hand, the declining trend is not significant, while the increasing trend is significant at the monsoon level of significance (annually). The anticipated *p*-value at the 5% level of significance is higher than the value. Both annual and monsoon data are acceptable for the null hypothesis (H_0). The monsoon season demonstrates that flash floods cause the areas to get swamped.

With a Sen's slope magnitude, the monsoon has a strong positive tendency that is significantly increasing. This upward trend is a result of the stream's immediate reaction to the abrupt rise in water levels brought on by heavy rains at the start of the monsoon season. At a 5% threshold of significance, estimated p-value exceeds the α-value, accepts the null hypothesis (H_0), because monsoon season's climate variability and the drop in yearly (Table 4).

4.7 Flash Flood Magnitude Index (FFMI)

It shows that the Swarna River's downstream region no longer has the ability to carry the former amount of monsoon flash flood surge. It is determined using the five-year average of the annual peak discharge.

Average discharge to the highest value is $Y = 0.039X^{1.8569}$, and it indicates high degree of deviation with a correlation coefficient of 0.99. Average FFMI for Swarna River is 0.335 which is substantially higher than the average worldwide 0.278 (Fig. 6).

4.8 Flash Flood Magnitude Ratio

It is helpful to know the frequent flash flood events within the study area.

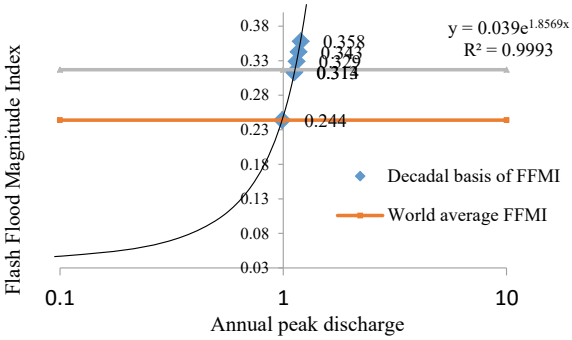

Fig. 6 Graph of annual peak discharge versus flash magnitude index

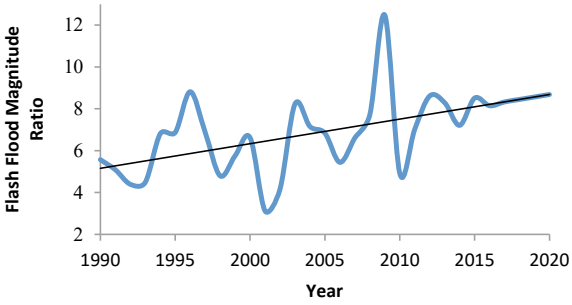

Fig. 7 Scatter plots demonstrating the connection between annual peak rainfall versus FFMR

The association between flood magnitude ratio and year is used to observe and display (Fig. 7). In comparison with other years, the year 2009 had a high magnitude of flash flood. An increasing trend in the scatter plot of the annual peak rainfall versus flood magnitude ratio suggests for sure that there will be more flash floods in the coming years.

5 Conclusions

The following conclusions are derived from the foregoing study:

- Homogeneity test analysis would provide a good picture of the long-term variations of the climate variables. At a significance level of 5%, the results of the experiments carried out by Pettitt, SNHT, Buishand, and von Neumann showed that there is no detectable fluctuation in the mean of the flash flood.
- Compared to the yearly precipitation concentration index, the monsoon seasonal precipitation concentration index exhibits a more pronounced irregularity in the distribution of precipitation. The number of rainy days indicates that the monsoon season's extremely saturated soil state.

- The monsoon's coefficient of variation fluctuates a lot. It suggests that the trends in monsoon precipitation are growing (positive).
- A decade-scale upstream catchment (Kervashe) has increases in 1 and 2 day PMP, which enhances the likelihood of a flash flood.
- In the monsoon season, six rain gauge stations were approved at the 5% level of significance and were statistically significant ($p > 0.05$).
- Analyses of meteorological precipitation trends showed how the increasing frequency of flash floods is influenced by climate variability. Despite the lack of clear changing trends in the regional dispersion of the climatic data, the mean annual and monsoon seasonal precipitation reveal broad growing or decreasing patterns.
- Climate change and precipitation fluctuation allowed for highly precise predictions of annual, seasonal, and peak discharge characteristics. Additionally, the hydrological model's improvement will undoubtedly increase the probability exceedance's accuracy.
- Rainfall rises as return periods lengthen and an anticipated flash flood upstream. Further supported by, flash flood magnitude index is 0.335 which is much greater than world average.
- The likelihood of future flash floods is anticipated based on their magnitude ratio.

Acknowledgements Data that was given by the Central Water Commission (CWC) and the India Meteorological Department (IMD) for our project. This work is being done at the Visvesvaraya Technological University's BDT College of Engineering in Davanagere, a constituent college of the Research Center, Department of Studies in Civil Engineering.

References

1. Mohammed R, Scholz M (2019) Climate variability impact on the spatiotemporal characteristics of drought and aridity in arid and semi-arid regions. Water Resour Manage 33:5015–5033
2. Islam HMT, Islam ARMT, Abdullah-Al-Mahabub M, Shahid S, Tasnuva A, Kamruzzaman M, Hu Z, Elbetagi A, Kabir MM, Salam MA, Ibrahim SM (2021) Spatiotemporal changes and modulations of extreme climatic indices in monsoon-dominated climate region linkage with large scale atmospheric oscillation. Atmos Res 264:105840
3. Chauluka F, Singh S, Kumar R (2021) Rainfall and streamflow trends of Thuchila River, Southern Malawi. Mater Today Proc 34(3):846–855
4. Wang N, Lombardo L, Toni M, Cheng W, Guo L, Xiong J (2021) Spatiotemporal clustering of flash floods in a changing climate (China, 1950–2015). Nat Hazards Earth Syst Sci 21:2109–2124
5. Zhai X, Guo L, Zhang Y (2021) Flash flood type identification and simulation based on flash flood behaviour indices in China. Sci China Earth Sci 64:1140–1154
6. Nkunzimana A, Bi S, Jiang T, Wu W, Abro MI (2019) Spatiotemporal variation of rainfall and occurrence of extreme events over Burundi during 1960 to 2010. Arab J Geosci 12:176
7. Ezaz GT, Zhang K, Li X, Shalehy HM, Hossain MA, Liu L (2021) Spatio temporal changes of precipitation extremes in Bangladesh during 1987–2017 and their connections. Global Planet Change 208:103712

8. Mahmood MI, Elagib NA, Horn F, Saad SAG (2017) Lessons learned from Khartoum flash flood impacts: an integrated assessment. Sci Total Environ, 1031–1045
9. Gopalakrishnan T, Hasan MK, Haque ATMS, Jayasinghe SL, Kumar L (2019) Sustainability of coastal agriculture under climate change. Sustainability 11:7200
10. Marchi L, Borga M, Preciso E, Gaume E (2010) Characterisation of selected extreme flash floods in Europe and implications for flood risk management. J Hydrol 394(1–2):118–133
11. Jenifer MA, Jha MK (2021) Assessment of precipitation trends and its implications in the semi-arid region of Southern India. Environ Challenges 5:100269
12. Wei L, Hu K, Hu X (2018) Rainfall occurrence and its relation to flood damage in China from 2000 to 2015. J Mt Sci 15:2492–2504
13. Hoyos CD, Ceballos LI, Perez JS, Sepulveda J, Lopez SM, Zuluaga MD, Velasquez N, Herrera L, Hernandez O, Guzman G, Zapata M (2019) Hydro meteorological conditions leading to the 2015 Salgar flash flood: lessons for vulnerable regions in tropical complex terrain. Nat Hazard 19:2635–2665
14. Zhang KX, Yao YL, Qian XQ, Wang JJ (2019) Various characteristics of precipitation concentration index and its cause analysis in China between 1960 and 2016. Int J Climatol 39(12):4648–4658
15. Grillakis MG, Koutroulis AG, Komma J, Tsanis IK, Wagner W, Bloschl G (2016) Initial soil moisture effects on flash flood generation—a comparison between basins of contrasting hydro-climatic conditions. J Hydrol 541:206–217
16. Duhan D, Pandey A (2013) Statistical analysis of long term spatial and temporal trends of precipitation during 1901–2002 at Madhya Pradesh, India. Atmos Resour 122:136–149
17. Tabari H, Taalaee PH (2011) Analysis of trend in temperature data in arid and semi-arid regions of Iran. Global Planet Change 79(2):1–10
18. Asfaw A, Simane B, Hassen A, Bantider A (2018) Variability and time series trend analysis of rainfall and temperature in north Central Ethiopia: a case study in Woleka sub-basin. Weather Climate Extremes 19:29–41
19. Komma J, Bloschl G, Reszler C (2008) Soil moisture updating by Ensemble Kalman Filtering in real-time flood forecasting. J Hydrol 357:228–242
20. Afzali-Gorouh Z, Bakhtiari B, Qaderi K (2018) Probable maximum precipitation estimation in a humid climate. Nat Hazard 18:3109–3119
21. Zahumensky I (2004) Guidelines on quality control procedures for data from automatic weather stations. World Meteorological Organization Geneva. https://www.wmo.int/pages/prog/www/IMOP/meetings/Surface/ETSTMT1_Geneva2004/Doc6.1(2).pdf

Assessment of Crop Water Requirement in the Context of Climate Change

Jitendra Sharma, M. K. Choudhary, and R. K. Jaiswal

Abstract Climate change is influencing and will continue to affect essential natural resources, such as water. Its effect on agriculture is usually considered as one of the most serious challenges in water resource management. In this study, the bias-corrected future climate data from the global climate model (GCM), ACCESS-ESM1.5, has been used to estimate the monthly crop water requirement for paddy in the Seonath sub-basin, Chhattisgarh State, India. The bias-corrected outputs of the ACCESS-ESM1.5 GCM model and projection of the future temperature and rainfall were done for two Shared Socioeconomic Pathway (SSP) scenarios, namely the SSP370 and SSP 585. Further, the future crop water requirement was calculated for the SSP370 and SSP585 scenarios using the CROPWAT model for the period of 2015–2099 with three future periods (FP) 2015–2045, 2046–2075, and 2076–2099. The reference evapotranspiration ET_o was calculated using ET_o calculator given by FAO. The results indicate rising in temperature and rainfall over future periods when compared to the base period (1981–2014). The annual average temperature has been projected to increase by 2.07 °C and 2.61 °C from 2015 to 2099, when compared to the base period for the SSP 370 and SSP 585 scenarios, respectively. The annual average rainfall has been projected to increase from 1207.7 mm in the base period to 1441.1 mm and 1400.1 mm for SSP 370 and SSP 585 scenarios. The average reference evapotranspiration (ET_o) values showed an increase from 4.54 mm/day to

J. Sharma (✉) · M. K. Choudhary
Department of Civil Engineering, Maulana Azad National Institute of Technology Bhopal, Bhopal 462003, India
e-mail: jitendrasharma447@gmail.com

M. K. Choudhary
e-mail: mkchoudhary@manit.ac.in

R. K. Jaiswal
National Institute of Hydrology Regional Center, Bhopal 462004, India

P. V. Timbadiya et al. (eds.), *Climate Change Impact on Water Resources*, Lecture Notes in Civil Engineering 313, https://doi.org/10.1007/978-981-19-8524-9_29

4.61 mm/day and 4.72 mm/day for SSP 370 and SSP 585 scenarios, respectively. The average annual crop water requirements (CWRs) showed an increase of 17.01% and 18.45% for the SSP 370 and SSP 585 scenarios. For optimal irrigation planning, projected deviation in required values can be used in the culturable command area of the Seonath sub-basin.

Keywords Crop water requirements · Climate change · Reference evapotranspiration · Shared socioeconomic pathway · CROPWAT

1 Introduction

Climate change is affecting and will continue to affect important natural resources, such as water. It is widely believed that the impact of climate change on agriculture has become one of the major issues in water resources management. The available water resource would be altered by a change in rainfall pattern and rate of evaporation. Further, higher evapotranspiration would result in a greater amount of irrigation and crop water demand. The climate of a region has a strong influence on irrigation demand [1]. Climate change is expected to raise or decrease the demand for irrigation water on a regional and global scale in the future. Rainfall patterns, solar radiation, relative humidity, temperature, and wind speed are just a few of the climatic variables that influence a region's irrigation water requirements and agricultural production [2]. Hence, there is a need to study the long-term change in the key climatic variables which affect the ET/crop water requirement. This study focuses on quantifying future crop water requirements using different scenarios and GCM on a long-term basis.

In a nutshell, the climate is commonly referred to as average weather. To be more specific, the statistical definition of associated numbers in terms of mean and variation over time spans varies between months to thousands or millions of years. According to the World Meteorological Organization (WMO), the traditional duration for averaging these parameters is 30 years. Temperature, precipitation, and wind are often significant surface variables. The climate system, including a statistical overview, is referred to as the climate in the broader context (IPCC).

The IPCC requested that the scientific community establishes a new set of scenarios to aid future climate change assessments due to the need for fresh scenarios (IPCC, 2007). Time series of emissions and amounts of greenhouse gas emissions (GHGs), aerosol, and chemically active gases, as well as land use and land cover, are included in the scenarios. The term "representative" refers to the fact that each RCP shows only one of many possible scenarios for achieving the desired radiative forcing properties. The term "pathway" highlights the importance of long-term concentration levels as well as the path that leads to them throughout time. Climate projections are provided for four representative concentration pathways (RCPs), namely RCP 2.6, 4.5, 6.0, and 8.5-W m^{-2}, for the years up to 2100, as per the Intergovernmental Panel on Climate Change's fifth edition (AR5). Any changes or uncertainties in long-term

rainfall patterns have an impact on agriculture, as well as an increase in the frequency of floods and droughts on a regional scale [3].

Temperature fluctuations have a strong link to evapotranspiration (ET) losses, resulting in changes in irrigation requirements. Rising temperatures resulted in an increase in expected evapotranspiration in the future at Aleltu agriculture locations in Ethiopia, according to the outputs of various global climate model ensembles under the RCP 4.5 and RCP 8.5 emission scenarios [4]. The month-wise crop water requirement of the primary crops cultivated in the Jayakwadi command area was computed using downscaled (SDSM) future climate datasets from the general circulation model (GCM), CanESM2. The CanESM2 general circulation model was statistically downscaled to predict future temperature and rainfall for two representative concentration pathways (RCPs) scenarios, which are RCP 4.5 (low emission) and RCP 8.5 (high emission). In addition, projected irrigation requirements for 2011–2100 were calculated using the RCP 4.5 and 8.5 scenarios [5].

A group of international climatologists, economists, and energy system modelers has recently released a series of new "pathways" that look at how world culture, demographics, and economics might change over the next century. They are known as "Shared Socioeconomic Pathways (SSP)" as a group. These SSPs are currently being used as an essential input for the most recent GCM and RCM models, including in the IPCC's sixth assessment report scheduled in 2020–21. They are still being used to figure out how social decisions can influence greenhouse gas emissions. Researchers from various modeling groups around the world started designing new scenarios in the late 2000s to see how the world could adapt for the rest of the twenty-first century. A group was given the task of forecasting how socioeconomic conditions would change over the following century. The rate of technical innovation, population increase, economic development, education, and urbanization are all factors to consider. These "Shared Socioeconomic Pathways" (SSPs) analyze five distinct scenarios as to how the world can develop in the omission of climate change policy, as well as how varying levels of its mitigation might be obtained when RCP mitigation objectives are coupled with different SSPs. Estimating the water demand of crops is one of the most essential criteria for crop planning on the field and the design of any irrigation schemes [6]. Understanding how changes in climate affects crop water demand is critical for solving future food security and water resource sustainability concerns [7]. Water is the most valuable input and a primary factor of agricultural output. Irrigation water has supported farmers in increasing crop production by reducing their reliance on rainfall patterns, raising average crop production while lowering inter-annual variability since the start of plant cultivation over 10,000 years ago [8]. Increasing mean temperature above a threshold level will cause a reduction in the yield of various crops. The grain yield of rice is predicted to decrease by 10%, with each 1 °C increase in the temperature above 32 °C [9].

The IPCC's fourth assessment report (AR4) states that direct observation of changes in sea level, snow cover, and temperature in the northern hemisphere from 1850 to the present proves beyond a shadow of a doubt that global warming is occurring. Since 1750, the concentration of CO_2 in the atmosphere has risen by 31%.

According to climate change scenarios, the impact of climate change on paddy irrigation demands in Sri Lanka revealed a 13–23% increase in rice irrigation water demand [10]. The regional circulation model research community is at a critical crossroads, transitioning from a period dominated through the usage of hydrostatic atmospheric model for specific engrossment problems to one dominated by the use of extremely high-resolution CPRCMs, possibly combined with another part of the climate change and simulated as part of a global climate model [11].

Numerous research has been done to investigate the effects of climate change on reference evapotranspiration (ET_o) and crop water requirements at the local and basin levels, according to the literature. However, no extensive research addressing the calculation of future irrigation requirements at the command area level under SSP scenarios has been done in India. The current study explores the impact of climate change on future crop water requirements in the Seonath command area, situated in Chhattisgarh, India, utilizing bias-corrected GCM outputs for the SSP 370 and SSP 585 scenarios. The demand variability assessments can be utilized to make irrigation planning and modeling strategies for the Seonath command area in the future.

2 Materials and Methods

2.1 Study Area

Seonath River basin is the most extended tributary basin of the Mahanadi River basin of 30,860 km^2 catchment area from which Seonath basin containing 25% of the Mahanadi basin's area. For this study, 12,404 km^2 area of Seonath basin have been considered. The river basin stretches over 380 km. It starts in the village of Panabaras in Rajanandgaon and flows three districts in Chhattisgarh: Rajanandgaon, Durg, and Bilaspur. The basin is located between 20°16 N and 22°41 N latitudes and 80°25 E and 82°35 E longitudes. Arpa, Tandula, Kharun, Agar, Hamp, and Maniyari streams are its major tributaries. The basin is 329 m above sea level, with low and maximum elevations of 234 m and 887 m, respectively. This basin comes under the drought prone area.

A sub-humid climate prevails throughout the river basin. The basin's annual rainfall ranges from 1005 to 1255 mm. The majority of the rain falls within three months (July–September). During the monsoon season, there is a lot of humidity. For the hottest month of May, the average daily maximum temperature ranges from 42 to 45 °C. During the winter, the temperature ranges from 10 to 25 °C. The predominant occupation of the people in this area is agriculture. Approximately 76% of the basin area is under cultivation. The monsoon season (Kharif) lasts from mid-June to October, while the post-monsoon (Rabi) season lasts from November to mid-April. The most important crop is rice, which accounts for 94% of the farmed basin. Wheat, summer paddy, pulses, and oilseeds are grown during the Rabi season. The primary crops are Kharif rice, summer paddy, and wheat, which cover an area

of around 22,680 km^2, or 98% of the basin. The basin's soil types are sandy clay, which accounts for 72.2% of the basin's surface area, followed by silt loam, 17.3% of the basin area. The major urban centers in the basin are Raipur and Durg. Seonath basin, because of its rich mineral reserve and adequate power resource, has a favorable industrialized ambiance. In the present study, the paddy crop considers for the estimation of CWR.

2.2 Dataset

Crop data for the paddy crop in the irrigated area and its growing pattern for the Seonath region were taken from the website of State Data Center (SDC), Department of Water Resources, Raipur, Chhattisgarh. SDC, Raipur, and FAO Irrigation and Drainage Paper No. 56 defined crop data, including crop coefficient (Kc), development stages, sowing, and harvesting dates, root zone depth (m), for the selected region [12]. For the period 1981–2014, the National Institute of Hydrology (NIH) regional center Bhopal provided daily gridded observed temperature and rainfall data with a $0.25° \times 0.25°$ resolution. The data includes the minimum and maximum temperatures, as well as daily rainfall levels. Future climate change predictions were developed using the Australian Community Climate and Earth-System Simulator (ACCESS). The purpose of ACCESS-ESM1.5 was to allow Australia to participate in the Coupled Model Intercomparison Project Phase 6 (CMIP6) with an Earth System Model version. The approximate spatial resolution in latitude and longitude is $1.25° \times 1.875°$. The ACCESS-ESM-1.5 projection under the SSP 370 and 585 scenarios for the period 2015–2099 was also obtained from the CMIP6-GCMs [13]. The bias-corrected GCM outputs are used in this study. For this study, a 34-year baseline period was considered, spanning the years from 1981 to 2014. The index map of the Seonath sub-basin is shown in Fig. 1.

2.3 CROPWAT Model

In this study, the CROPWAT8.0 model was used to estimate the future crop water requirement of the Seonath sub-basin. The crop water requirements (CWR) of paddy in the research region were determined using the CROPWAT 8.0 software and the CLIMWAT 2.0 tool. The CROPWAT model is designed to provide a realistic technique for doing typical calculations for ET_o, crop water requirements, agricultural irrigation requirements, and, more specifically, irrigation scheme design and management [14]. The Penman-Monteith approach of the Food and Agriculture Organization (FAO) and the United States Department of Agriculture soil conservation service method are mentioned in FAO Irrigation and Drainage Paper No. 56. The ETo was estimated using the Penman-Monteith equation for future climate conditions, as shown in Eq. 1.

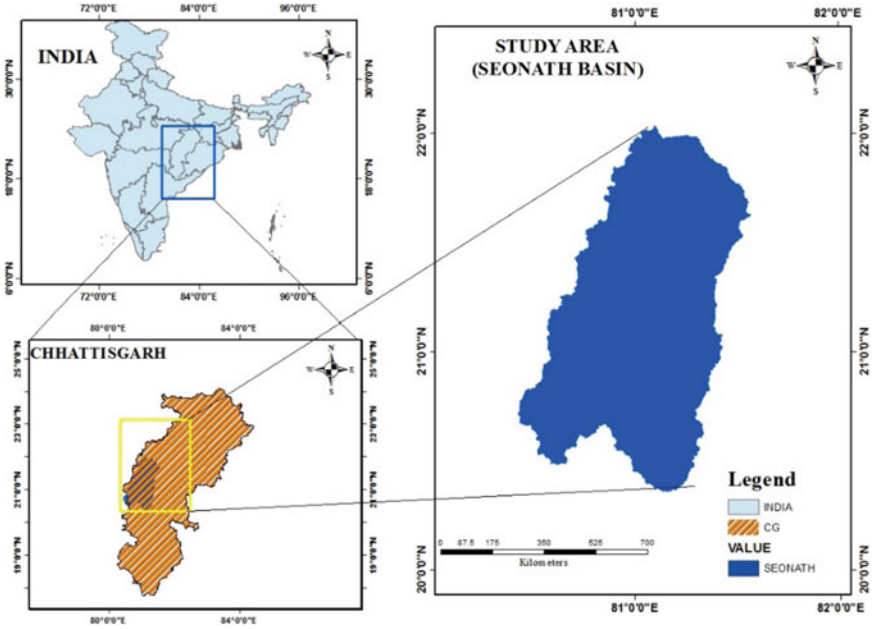

Fig. 1 Index map of Seonath sub-basin

$$\mathrm{ET_o} = \frac{0.408\Delta(R_\mathrm{n} - G) + \left(\gamma \frac{900}{T+273} u_2 (e_\mathrm{s} - e_\mathrm{a})\right)}{\Delta + \gamma(1 + .34u_2)} \tag{1}$$

where $\mathrm{ET_o}$ is the reference evapotranspiration (mm/day), G is the soil heat flux density (MJ $\mathrm{m^{-2}}$ $\mathrm{day^{-1}}$), R_n is the net radiation at the surface (MJ $\mathrm{m^{-2}}$ $\mathrm{day^{-1}}$), γ is the psychrometric constant (kPa $\mathrm{°C^{-1}}$), T is the average daily air temperature at 2 m height (°C), u_2 is the wind speed at 2 m height (m/s), Δ is the slope of vapor pressure curve (kPa/C), e_s is the saturation vapor pressure, e_a is the actual vapor pressure (kPa), and $e_\mathrm{s} - e_\mathrm{a}$ is the net vapor pressure (kPa). The reference evapotranspiration ($\mathrm{ET_o}$) was the important parameter used to measure crop evapotranspiration ($\mathrm{ET_c}$). Under normal circumstances, the $\mathrm{ET_c}$ is estimated from $\mathrm{ET_o}$ and the crop coefficient (K_c) using Eq. 2.

$$\mathrm{ET_c} = \mathrm{ET_o} \times K_\mathrm{c} \tag{2}$$

The seasonal CWR was estimated by combining the daily $\mathrm{ET_c}$ values determined for several crop growth phases. For the SSP 370 and SSP 585 scenarios, the CROPWAT8.0 model was used to calculate the future CWR of the Paddy crop. Figure 2 shows a flow chart illustrating the process for estimating future CWR using the CROPWAT model. The projected climatic variables were utilized as input into the CROPWAT8.0 model to estimate future irrigation demand in this study. Wind speed, relative humidity, and daylight hours were supposed to be constant during the study period. The $\mathrm{ET_o}$ calculator was used to calculate the reference evapotranspiration using simulated temperature and precipitation data.

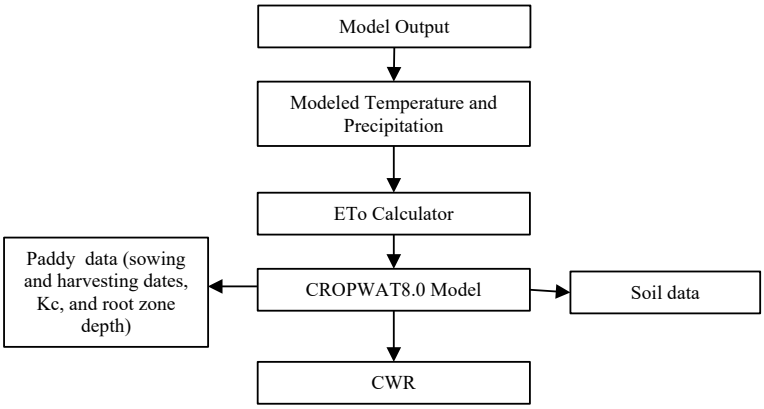

Fig. 2 Flow chart illustrating the process for estimating future CWR using CROPWAT model

2.4 ET_o Calculator

In the ET_o calculator program, the FAO Penman-Monteith equation is utilized to determine the ET_o reference evapotranspiration from meteorological data. Climate data will be managed on a daily, 10 daily, and monthly basis by the software. The information can be provided in several units and analyzed using generally used climate parameters. As a result, ET_o is a climatic variable that can be estimated with the help of weather data. ET_o is a measurement of the atmosphere's evaporation intensity at a specific place and time of year, taking into account crop characteristics and soil conditions. The FAO Penman-Monteith equation is used to estimate the ET_o reference evapotranspiration from meteorological data in the ET_o calculator program. FAO picked this technique as the reference because it is physically orientated, closely mimics grass ET_o at the examined site and specifically includes both physiological and aerodynamic characteristics. The inputs of the ET_o calculator are temperature, relative humidity, vapor pressure, sunshine duration, wind speed, and radiation. Suppose wind speed, humidity, or radiation data are not available for a specific day, ten-day, or month. In that case, the software will estimate the missing meteorological data using the information listed in the corresponding boxes (missing wind speed, air humidity, or radiation data).

3 Results and Discussions

In this study, the bias-corrected future climate data from the global climate model (GCM), ACCESS-ESM1.5, has been used to estimate the monthly CWR of the crop (paddy) in the Seonath sub-basin, Chhattisgarh State, India. The bias-corrected GCM outputs of the ACCESS-ESM1.5 and estimation of the future temperature and

rainfall were done for two Shared Socioeconomic Pathway (SSP) scenarios, namely the SSP370 and SSP 585. Further, the future crop water requirement was calculated for the SSP370 and SSP585 scenarios using the CROPWAT model for the period of 2015–2099 with three future periods (FP) 2015–2045, 2046–2075, and 2076–2099. The reference evapotranspiration ET_o was estimated using ET_o calculator given by FAO. The projected deviations in required values can be utilized to plan irrigation in the Seonath sub-culturable basin's command area.

3.1 *Variation of* T_{max} *and* T_{min}

The model produced a future climatic scenario up to the year 2099 with three phases (2015–2045), (2046–2075), and (2076–2100). The differences in SSP scenarios were detected when the anticipated temperature and rainfall data were compared to the base period (1981–2014) data.

Figure 3 shows the ACCESS-ESM1.5 predicted average monthly maximum (T_{max}) and minimum temperature (T_{min}) for the SSP370 and SSP585 scenarios from 2015 to 2099. The estimated maximum temperature (T_{max}) and minimum temperature (T_{min}) for both scenarios also indicated an increasing trend, as shown in Fig. 3. The results showed that by the 2099s, the annual mean maximum temperature (T_{max}) will have increased by 1.56 °C and 2.18 °C, respectively, for the SSP 370 and SSP 585 scenarios. However, the forecasted rise in the annual minimum temperature (T_{min}) for SSP 370 and SSP 585 scenarios was larger, with values of 2.56 °C and 3.22 °C, respectively. The average monthly temperature for both situations increased with time, as shown in the graph. Annual average temperatures are predicted to increase by 2.07 °C and 2.61 °C, for SSP 370 and SSP 585 scenarios, respectively, from 2015 to 2099 when compared to the baseline period.

3.2 *Simulation of Reference Evapotranspiration*

Using bias-corrected climatic parameters, the ET_o calculator and the CROPWAT model were used to estimate reference evapotranspiration (ET_o) fluctuations for future scenarios. Because of its extensive application for all crops, the FAO Penman-Monteith equation is used in the ET_o calculator and CROPWAT model for future ETo estimation [15]. Climatic parameters such as maximum and minimum temperatures define the ET_o value unaffected by crop properties. Using the estimated monthly mean of the modeled daily data series of maximum temperature (T_{max}), minimum temperature (T_{min}), and rainfall, the CROPWAT model was utilized to forecast future demands [16]. The ETo calculator was updated with the simulated climatic data, and future ET_o values were calculated for both the SSP 370 and SSP 585 scenarios. For both SSP scenarios, the variation in ET_o from 2015 to 2099 is shown in Fig. 4.

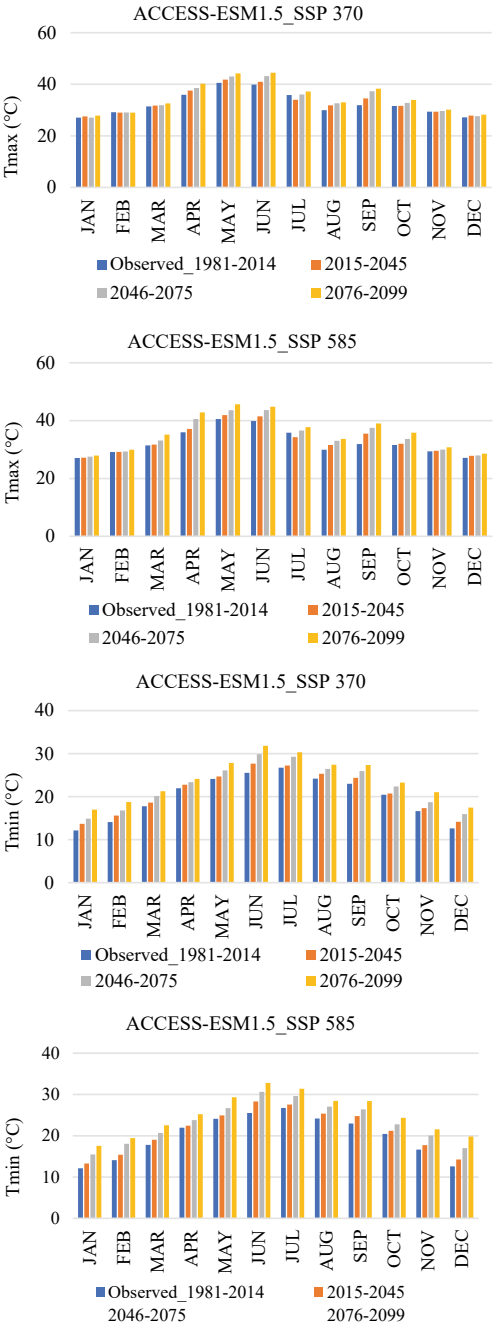

Fig. 3 Average monthly variation in the projected maximum (T_{max}) and minimum (T_{min}) temperature for SSP 370 and SSP 585 scenarios

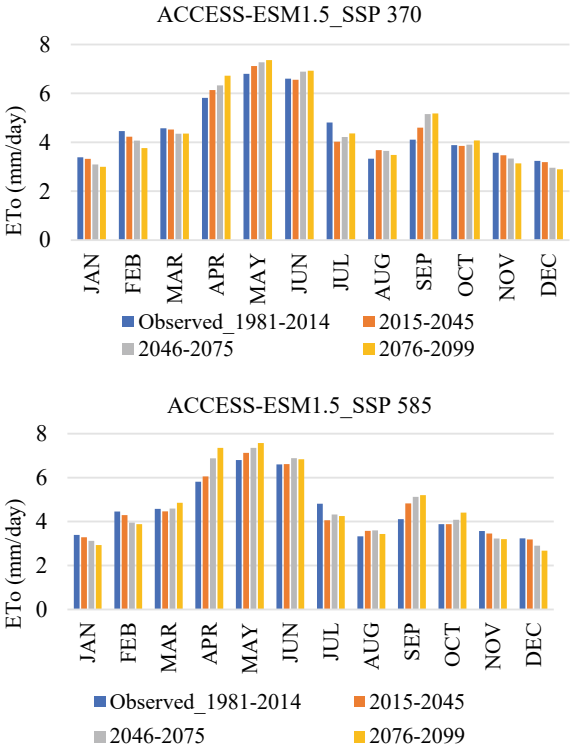

Fig. 4 Average daily variation of reference evapotranspiration (ET_o) under SSP 370 and SSP 585 scenarios

For both SSP scenarios, the monthly reference evapotranspiration values revealed a rising tendency in the future, especially from April to October. For the SSP 370 and SSP 585 scenarios, the highest increase in monthly ET_o by 2099 was expected in May, with monthly increases of 0.57 mm/day and 0.78 mm/day, respectively. The highest ET_o was recorded in May for all SSP scenarios, while the lowest ET_o was recorded in December. The expected (T_{max}) and (T_{min}) values have increased, resulting in rising trend in the future ET_o values as calculated by the model. This increasing trend in projected ET_o may result in increased crop water requirements in the future. Using the climatic parameters acquired, the CROPWAT model was utilized to simulate crop water requirements for future situations.

3.3 Variation of Rainfall

The annual average precipitation increased in the SSP370 scenario, with the greatest value of 1734.58 mm over the period 2076–2099. For the SSP 370 and SSP585 scenarios, the average rainfall is projected to increase by 19.41% and 15.92%, respectively, from 2015 to 2099. The SSP 370 and SSP 585 scenarios, the annual average

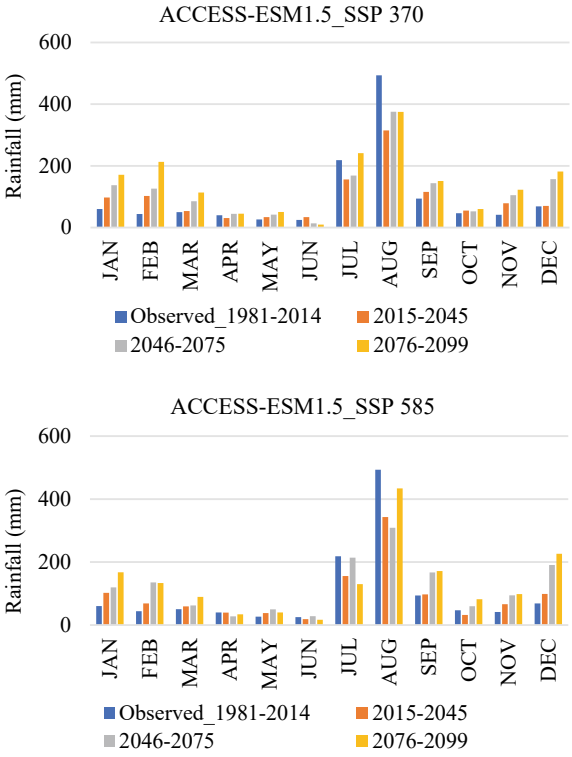

Fig. 5 Average monthly variation of rainfall under SSP 370 and SSP 585 scenarios

precipitation is expected to rise from 1207.7 mm in the baseline period to 1441.1 mm and 1400.1 mm, respectively. The rate of evapotranspiration increases as the temperature rises, which can harm healthy vegetation. Under the SSP scenarios, both temperature and rainfall are expected to increase in the Seonath sub-basin, as per the study. The variation in monthly rainfall is shown in Fig. 5.

3.4 Simulation of Crop Water Requirement

The CROPWAT 8.0 model was adopted to estimate crop water requirements (CWR) for paddy crops in the Seonath sub-basin, and the change in crop water demands for the SSP370 and 585 scenarios were studied. For the Kharif season, agricultural irrigation requirements were determined. The crop coefficient (K_c) determines crop evapotranspiration (ET_c) at various stages of crop growth. For future crop water requirements estimation, the crop data were included in the CROPWAT8.0 model. Figure 6 shows the CWR for paddy crop with the SSP370 and SSP585 scenarios, respectively. As shown in the figures, the CWR for the paddy showed a considerable increase during the entire base period. The annual CWR of paddy shows an

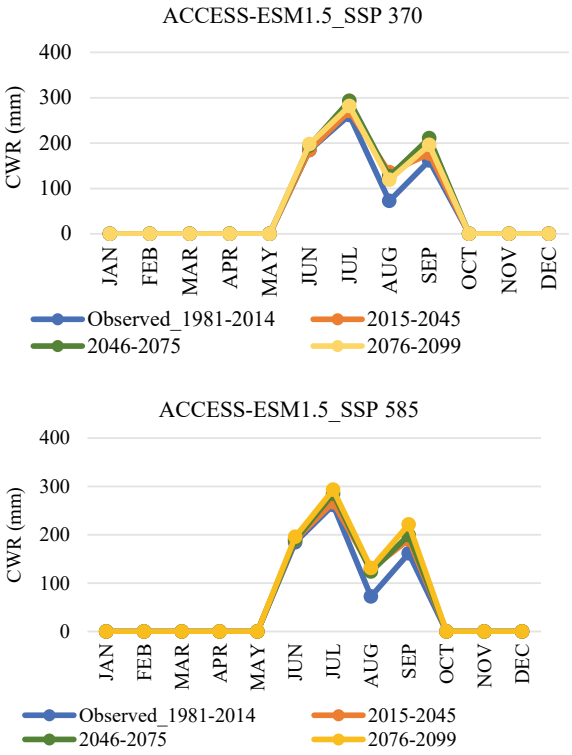

Fig. 6 Crop water requirement of paddy crop in the Seonath sub-basin for the SSP 370 and 585 scenarios

increase of 17.01% and 18.45% by the 2100s for the SSP 370 and SSP 585 scenarios, respectively.

The rise in irrigation water requirement is due to an uneven tendency in the expected precipitation (this is one of the reasons) for the Kharif season's future scenarios. The findings show that, despite an increasing variation in projected annual rainfall, rainfall during the Kharif season will not be sufficient to meet crop water demands due to increased evaporation and transpiration losses. Figure 6 represents the monthly deviation in total crop water requirements for the various SSP scenarios. The projected irrigation demand values for the Kharif months (June to October) indicate a significant rise.

4 Conclusions

This research predicts the future crop water requirement for the Seonath sub-basin, Chhattisgarh, India, under different climate scenarios (SSP). The future bias-corrected GCM outputs were used as an input for the ET_o calculator for the calculation of reference evapotranspiration (ET_o), and the outputs were utilized as an input

for the CROPWAT8.0 model. The results showed that for the various IPCC SSP scenarios, there would be a rise in temperature and rainfall. The reference evapotranspiration, which was simulated for the years 2015–2099, also revealed a rise in the future. May was the month with the highest forecasted temperature and reference evapotranspiration. The paddy crop's future crop water demands have been shown to be significantly increased. The crop water demands for the paddy crop in the SSP 580 scenarios were higher than the demands in the SSP 370 scenario from 2076 to 2099. In this study, the reference evapotranspiration showed a rising trend under the SSP 370 and 585 scenarios. For the forecasted future scenarios, the precipitation in the Seonath sub-basin area is not expected to decrease due to rising temperatures**.** As the temperature rises, the reference evapotranspiration values rise as well, resulting in a large demand for water will require in the future. The future crop water requirements (CWRs) for the paddy crop have been examined in this study.

Acknowledgements I am thankful to the National Institute of Hydrology (NIH), regional center, Bhopal, and MANIT Bhopal for providing the necessary data and continuous support for this study.

References

1. Tukimat NN, Harun S, Shahid S (2017) Modelling irrigation water demand in a tropical paddy cultivated area in the context of climate change. J Water Resour Plan Manage 143:05017003
2. Rehana S, Mujumdar PP (2012) Regional impacts of climate change on irrigation water demands. Hydrol Process
3. Jain SK, Kumar V (2012) Trend analysis of rainfall and temperature data for India. Curr Sci 102:37–49
4. Yadeta D, Kebede A, Tessema N (2020) Potential evapotranspiration models evaluation, modeling, and projection under climate scenarios, Kesem sub-basin, Awash River basin, Ethiopia. Model Earth Syst Environ
5. Sunil A, Deepthi B, Mirajkar AB, Adarsh S (2020) Modeling future irrigation water demands in the context of climate change: a case study of Jayakwadi command area, India. Model Earth Syst Environ
6. Dhamge NR, Badar AM, Baiswarey NZ (2008) Crop water requirement by modified Penman method using HYMOS. ISH J Hydraulics Eng 14:28–42
7. Zhou T, Wu P, Sun S, Li X, Wang Y, Luan X (2017) Impact of future climate change on regional crop water requirement: a case study of Hetao irrigation district, China. Water 9:429
8. Fischer G, Tubiello FN, van Velthuizen H, Wiberg DA (2007) Climate change impacts on irrigation water requirements: effects of mitigation, 1990–2080. Technol Forecast Soc Chang 74(7):1083–1107
9. Lu S, Bai X, Li W, Wang N (2019) Impacts of climate change on water resources and grain production. Technol Forecast Soc Change 143(November 2018):76–84
10. De Silva CS, Weatherhead EK, Knox JW, Rodriguez-Diaz JA (2007) Predicting the impacts of climate change—a case study of paddy irrigation water requirements in Sri Lanka. Agric Water Manag 93(1–2):19–29
11. Giorgi F (2019) Thirty years of regional climate modeling: where are we and where are we going next? J Geophys Res Atmos 124(11):5696–5723
12. Allen RG, Smith M, Pereira LS, Raes D, Wright JL (2001) Revised FAO procedures for calculating evapotranspiration: irrigation and drainage paper no. 56 with testing in Idaho. In: Watershed management and operations management

13. Ziehn T, Chamberlain MA, Law RM, Lenton A, Bodman RW, Dix M, Stevens L, Wang Y-P, Srbinovsky J (2020) The Australian earth system model: ACCESS-ESM1.5. J S Hemisphere Earth Syst Sci 70(1):193
14. Allen RG, Pereira LS, Rase D, Smith XM (1998) Crop evapotranspiration. Guidelines for computing crop water requirements. Irrig. & Drain. Paper 56 Food and Agricultural Organisation, Rome, p 293
15. Ashofteh P, Haddad O, Marino M (2015) Risk analysis of water demand for agricultural crops under climate change. J Hydrol Eng
16. Sharma J, Choudhary MK, Jaiswal RK (2021) Effect of climate change on crop water requirement using CROPWAT—a review. In: Proceeding of "international conference on water and environment" (ICWE-2021), March 22–23, 2021, organized by Department of Civil Engineering MANIT, Bhopal (M.P.), India

Climate Change Impact on Future Reference Evapotranspiration and Crop Evapotranspiration for Maize in Sehore District of Madhya Pradesh

A. Balvanshi and H. L. Tiwari

Abstract The FAO CROPWAT tool was utilised to estimate the future reference evapotranspiration and maize crop evapotranspiration for years 2030, 2060 and 2090 under RCP scenarios 2.6 and 8.5 for Sehore district of Madhya Pradesh, India. The statistically downscaled GCM CanESM2 climate model projections were used as input to the CROPWAT for prediction of future reference and crop evapotranspiration data. The values of constants viz. $K_c$initial, $K_c$mid and $K_c$end were fixed to 0.5, 1.15 and 0.6, respectively, as per the FAO-56 for maize crop. In the Sehore region, the ET_0 and ET_c values for RCP 2.6 were calculated to be in range of (400.5–512) mm and (430.5–448.4) mm, respectively, during years 2030, 2060 and 2090, while the ET_0 and ET_c values for RCP 8.5 were found out to be (466–740.5) mm and (440.5–492.5) mm, respectively, during years 2030, 2060 and 2090, respectively. The RCP scenario 8.5 is the worst case scenario in which the reference evapotranspiration as well as crop water requirement for maize crop has been showing high demands of water. The results of this work can be utilised for proper irrigation scheduling for the maize crop and thereby reducing the agricultural risks due to climate change.

Keywords CROPWAT · Reference evapotranspiration (ET_0) · Crop evapotranspiration (ET_c) · General circulation model · Maize

A. Balvanshi (✉)
Department of Civil Engineering, National Institute of Technology Goa, Farmagudi, Ponda 403401, India
e-mail: abalvanshi@nitgoa.ac.in

H. L. Tiwari
Department of Civil Engineering, Maulana Azad National Institute of Technology Bhopal, Bhopal 462051, India

P. V. Timbadiya et al. (eds.), *Climate Change Impact on Water Resources*, Lecture Notes in Civil Engineering 313, https://doi.org/10.1007/978-981-19-8524-9_30

1 Introduction

Maize is one of the major crops grown at a large scale in Central India with high yield production [1]. Based on the yield and productivity of maize at a large scale in Madhya Pradesh, it is therefore important to conduct climate change studies to avoid agriculture crisis in future.

The GCMs serve as a simplified representation of the climate system and are effective tools for identifying climate change's effects [2]. Climatic projections are to be considered as competent technique to put up the possible future situations under specified emission scenarios [3, 4].

There are several applications for the reference evapotranspiration (ET_0) which is a significant agrometeorological parameter. Extensive research has been looked at how reference evapotranspiration may be affected by climate change (ET_0) [5]. The term "reference evapotranspiration" (ET_0) refers to the water that is lost to the atmosphere by evaporation and transpiration from a surface covered in green grass that is 8–12 cm tall, actively developing and totally shading the ground. This ETo can be used to calculate the crop evapotranspiration by using a crop coefficient (K_c) value (ET_c) [6].

Scheduling irrigations to fulfil the crop's water use requirements and for best crop production requires the adoption of an exact or precise volume of water and the proper timing of application [7, 8]. Estimation of crop water requirements (ETc) is one of the main components used in irrigation planning, design and operation [9, 10]. Using nine years of climate data (2005–2013) from the Halali dam command area in Vidisha district of Madhya Pradesh state, India, [11] did a case study on assessing the irrigation water requirements and irrigation scheduling of wheat crop for Rabi season. Reference crop evaporation was computed using meteorological data, including temperature, relative humidity and sunshine hours, which were gathered from the Vidisha district meteorological station. The FAO Technical Paper "Irrigation and Drainage Paper No. 24" provided the crop coefficient K_c value according to the stages of crop growth. Due to the recurrence of rainfall, it was discovered that the overall crop water need for wheat was 209.7 mm. The ET_0 and ET_c of wheat and maize for 16 locations were determined by [10] using identical methods. A study to ascertain the ET_0 and ET_c of wheat and maize for 16 sites in Gujarat was carried out by [10] using identical methods. The findings showed that the mean daily (ETo) fluctuates between 4.2 and 7.6 mm/day over the winter season (Nov 15 to March 13).

Keeping in view the economic importance of maize production in Central India, the present study was conducted employing the FAO—CROPWAT tool and CANESM2 climate model to determine the impact of climate change on evapotranspiration of maize crop for the Sehore district of Madhya Pradesh. The per cent change in ET_0 and ET_c values of maize was calculated and depicted in Tables 1 and 2 ahead.

Table 1 Change in reference evapotranspiration (mm)

Region/district	Average ET_0 (2000–2015)	ET_0 year 2030		ET_0 year 2060		ET_0 year 2090	
		RCP 2.6	RCP 8.5	RCP 2.6	RCP 8.5	RCP 2.6	RCP 8.5
Sehore		400.5	466	428	596.5	512	740.5
% change in future ET_0 compared to average ET_0 (2000–15)	396.14	1.1	17.63	8.04	50.57	29.24	86.92

Table 2 Change in crop evapotranspiration—maize crop (mm)

Region/district	Average ET_c (2000–2015)	ET_c year 2030		ET_c year 2060		ET_c year 2090	
		RCP 2.6	RCP 8.5	RCP 2.6	RCP 8.5	RCP 2.6	RCP 8.5
Sehore		430.5	440.5	440.5	475	448.4	492.5
% change in future ET_c compared to average ET_c (2000–15)	430	0.11	2.44	2.44	10.46	4.27	14.53

2 Material and Methods

The present study has been carried out for one of the highly agricultural rich district of Madhya Pradesh, namely Sehore. The study region (Fig. 1) is the Sehore district located at 23.2050° N latitudes 77.085° E longitudes in Madhya Pradesh which comes under Vindhyachal Range in the middle of Malwa region.

Geographically, the district has been separated into the Narmada basin, Chambal basin and Betwa basin based on the valleys produced by the major rivers. The district encompasses an area of 6578 km^2 having average precipitation of 1217.7 mm. The area has coverage of black cotton soil under hydrologic soil group D that exhibits high potential runoff. The principal crops sown in the Sehore district are Wheat, Rice, Jawar, Maize and Soyabean.

In this research work, FAO CROPWAT model was employed to estimate the reference evapotranspiration and the maize crop evapotranspiration. The Penman-Monteith equation [12] was adopted to calculate reference crop evapotranspiration in the CROPWAT tool. CROPWAT 8.0 was developed by Food and Agriculture Organization (FAO), Italy. This support system (model) works out the reference evapotranspiration, crop water requirement and irrigation requirement. CROPWAT 8.0 uses the FAO Penman-Monteith method for calculation of reference crop evapotranspiration [12].

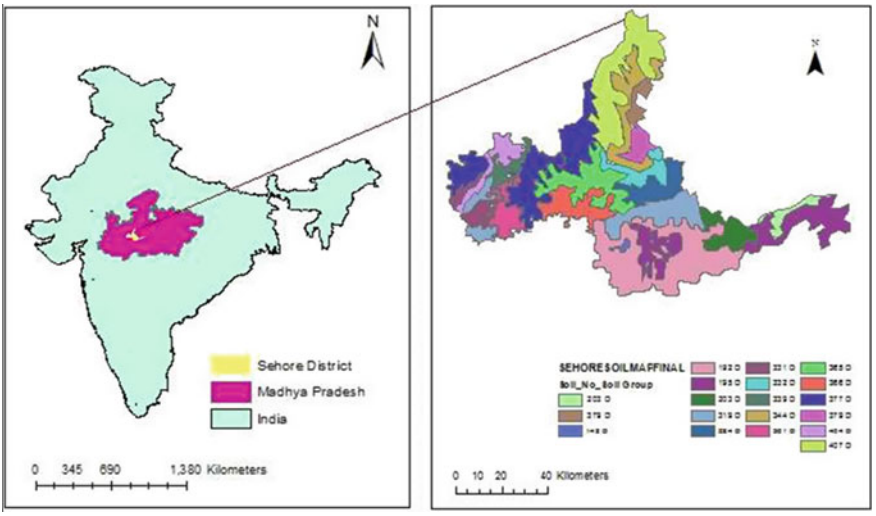

Fig. 1 Index map of study area

A Windows-based computer programme called CROPWAT 8.0 is used to determine how much irrigation and water crops need based on information about the soil, the environment and the crops themselves. The application also enables the creation of irrigation schedules for various management scenarios and the estimation of scheme water supply for various crop configurations. The CROPWAT 8.0 can be used to gauge crop performance under both irrigated and rainfed situations, as well as to assess farmers' irrigation methods. The two FAO papers from the Irrigation and Drainage Series, No. 56, "Crop Evapotranspiration—Guidelines for computing crop water requirements," and No. 33, "Yield response to water," served as the foundation for the calculation methods utilised in CROPWAT 8.0. The CROPWAT uses FAO Penman-Monteith formula for computation of evapotranspiration for reference crop.

The $K_c$initial, $K_c$mid and $K_c$end were fixed to 0.50, 1.15 and 0.60, respectively, as per FAO-56 for maize crop in the CROPWAT tool. The sowing date was kept constant to be 24 June with total crop period of 125 days. The historic meteorological data was used from year 2000 to 2015 to calculate ET_o and ET_c. The historic ET_o and ET_c was averaged and was used in comparison with the future ET_o and ET_c. For computing future values of ET_o and ET_c data from the CROPWAT model, statistically downscaled GCM CanESM2 (grid size 2.790 × 2.812, Canadian Centre for Environment and Climate change, Canada) was employed with future projections RCP 2.6 and RCP 8.5 for the years 2030, 2060 and 2090. One major impact of future climate change is variation in demand of region's ET_0 and ET_c. The increase in the demands of water required makes it necessary to conduct a prior study so that proper planning and adaptation policies can be made for the farmers which will help to reduce the agricultural risks.

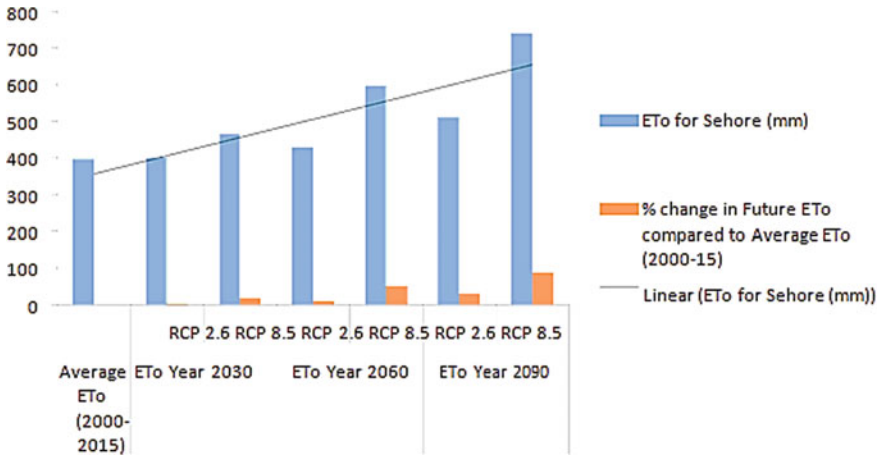

Fig. 2 Comparison of average historic ET_0 with future ET_0 for Sehore district

3 Results and Discussions

The future ET_0 and ET_c values for the years 2030, 2060 and 2090 under emission scenarios RCP 2.6 and 8.5 were estimated using FAO CROPWAT and CANESM2 climate model. The future ET_0 and ET_c maize for Sehore district was compared to the average ET_0 and ET_c during the period (2000–15 years) (Refer Tables 1 and 2).

Figure 2 and Table 1 showcase the clear increase in the reference evapotranspiration values from the historic to the future periods. The ET_0 values for RCP 2.6 showed a small increase of 1.1% for the year 2030, but for years 2060 and 2090, ET_0 value depicted an increase up to 29.24%. However, the ET_0 values for RCP 8.5 showed high increase up to 86.92%.

Figure 3 and Table 2 portray the clear increase in the evapotranspiration values of maize crop from the historic to the future periods. In the Sehore district of Central India, the ET_c values for RCP 2.6 showed a small increase of 0.11% for the year 2030, but for years 2060 and 2090, ET_c value depicted an increase up to 10.46%. However, the ET_c values for RCP 8.5 showed highest increase up to 14.53%.

The negative effect of climate change was found on the Sehore district which is profound in the reference evapotranspiration and maize crop evapotranspiration. The year 2090 can be assumed to have the highest vulnerability for maize under RCP 8.5 scenario.

4 Conclusions

It can be concluded that the future climate at Sehore region could lead to increase in the reference evapotranspiration and crop evapotranspiration of maize crop. The

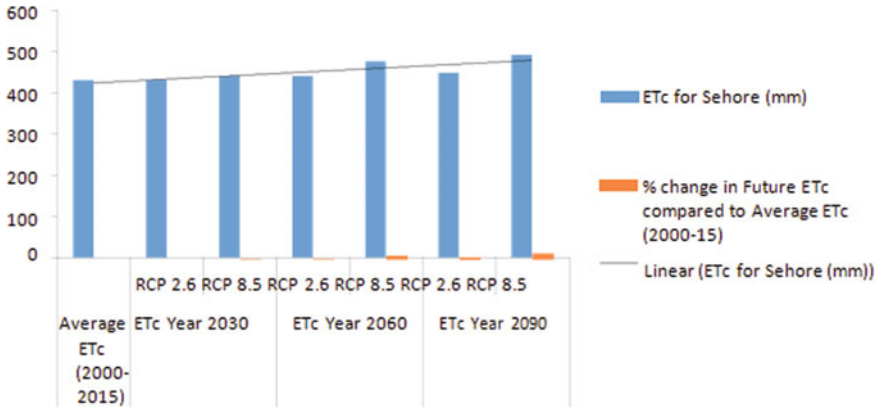

Fig. 3 Comparison of average historic ET_c maize with future ET_c maize for Sehore district

maximum increase in ET_o and ET_c values was found to be for the year 2090 under RCP scenario 8.5 for both regions indicating high demands of water. It was also concluded that the FAO CROPWAT model can be applied to other crops as well as in other regions to estimate the future changes in ET_o and ET_c and accordingly proper irrigation and cropping strategies can be formulated for the farmers that will help decrease the agricultural risks due to change in climate.

References

1. Agricultural Statistics at a Glance (2017) Directorate of economics and statistics. Department of agriculture and cooperation, Government of India
2. Johnson FM, Sharma A (2009) Measurement of GCM skill in predicting variables relevant for hydro climatological assessments. J Clim 22:4373–4382
3. Suppiah R, Hennessy KJ, Whetton PH (2007) Australian climate change projections derived from simulations performed for the IPCC 4th assessment report. Aust Meteorol Mag 56:131–152
4. Solomon S, Qin D, Manning M et al (eds) (2007) IPCC summary for policymakers. Climate change The physical science basis. Contribution of working group I to the fourth assessment report of the intergovernmental panel on climate change. Cambridge University Press, Cambridge, pp 1–18
5. Patel HR, Lunagaria MM, Karande BI, Yadav SB, Shah AV, Sood VK, Pandey V (2015) Climate change and its impact on major crops in Gujarat. J Agrometeorol 17(2):190–193
6. Doorenbos J, Pruitt WO (1975) Guidelines for predicting crop water requirements, Irrigation and Drainage Paper 2. FAO of the United Nations, Rome, p 179
7. Balvanshi A, Tiwari HL (2018) Analysis of GCMs for prediction of precipitation for Hoshangabad region of Madhya Pradesh. J Agrometeorol 20(4):302–304
8. Balvanshi A, Tiwari HL (2019) Scenario of climate change and its impacts. Int J Recent Technol Eng 8(1):2601–2604
9. Rowshon MK, Amin MSM, Mojid M, Yaji M (2013) Estimated evapotranspiration of rice based on pan evaporation as a surrogate to lysimeter measurement. Paddy Water Environ 13(4):356–364

10. Mehta R, Pandey V (2015) Reference evapotranspiration (ET_0) and crop water requirement (ET_c) of wheat and maize in Gujarat. J Agrometeorol 17(1):107–113
11. Pandram V, Choudhary MK (2015) Crop water requirement estimation by using CROPWAT model: a case study of Halali Dam Command Area, Vidisha District, Madhya Pradesh, India. Int J Eng Manage Res 5(3):553–557
12. Allen RG, Pereira LS, Raes D, Smith M (1998) Crop evapotranspiration: guidelines for computing crop water requirements. Irrigation and Drainage Paper 56 Food and Agriculture Organization of the United Nations, Rome

Impact of Climate Change on Crop Water Requirement: A Case Study of Amreli District

Swinal Chaudhari and Falguni Parekh

Abstract Climate can be demarcated as the weather condition, which has been measured over a long period of time. Climate change studies reveal that it will affect the water requirement of different crops. Consider this as a major effect on agriculture, a study was taken to know the climate change impact on the water requirement of crops cultivated in the area of Amreli district, Gujarat. For this study, meteorological data (maximum temperature, minimum temperature, precipitation, relative humidity, wind velocity, and solar radiation) of periods 2001–2020 are used. Future meteorological parameters were predicted for the period of 2031–2090 using a ClimGen weather generator. Results of generated future climatological data are showing increasing and decreasing trend, but overall climatic data shows increasing trend for the future years till 2090. These results show that climatological parameters are changing in upcoming years. Crop evapotranspiration (ET_c) was determined with the help of CROPWAT 8.0 using daily climatological parameters for generated weather data, and then, the water requirement of different crops was determined. The clear effect of climatological parameters on the water requirement crops of Rabi and Kharif was identified in results. To meet the increasing demand of water, water resources should be increased by increase in water level and doing water conservation efficiently. Farmers should also be motivated to use different methods for irrigation as sprinkler and drip irrigation systems according to the requirement of crops instead of using flooding methods.

Keywords Climate change · Crop water requirement · ClimGen · CROPWAT · Evapotranspiration

S. Chaudhari · F. Parekh (✉)
Water Resources Engineering and Management Institute, Faculty of Technology and Engineering, The Maharaja Sayajirao University of Baroda, Samiala 391410, India
e-mail: fpparekh-wremi@msubaroda.ac.in

P. V. Timbadiya et al. (eds.), *Climate Change Impact on Water Resources*, Lecture Notes in Civil Engineering 313, https://doi.org/10.1007/978-981-19-8524-9_31

1 Introduction

Climate can be demarcated as the weather condition, which has been measured over a long period of time. In the world, India is the largest producer of jute and pulses and also the second-largest producer of sugarcane, rice, groundnut, wheat, cotton, vegetables, and fruit crops. The report of the IPCC of the Working Group **II** shows the effects of climate changes which is on key sectors as water, food, industry, settlement and society, and health. The effect of climate change on agriculture production will be one of the major factors which influence the future food security of human's on the earth.

By keeping in view the significance of climate change, a study is carried out to fulfill the following objectives:

- To make a definite examination of the fluctuation of different meteorological boundaries over the district dependent on long-term recorded data.
- To identify the month-to-month and occasional patterns of meteorological parameters.
- Generate the various meteorological parameters based on the historical available data.
- To study the effects of generated meteorological factors on the water requirement of different crops.

Present study is conducted to know the effects of climate change on the crop water requirement in Amreli district.

Gondaliya and Khasiya [1] conducted a study to evaluate the climate change over a period of time worked out at Amreli district and its impact on crop yield and crop water requirement. The Fourth Assessment Report (AR4) of the United Nations Intergovernmental Panel on Climate Change (IPCC) [2] was published in 2007 and is the fourth in a series of reports intended to assess scientific, technical and socio-economic information concerning climate change, its potential effects, and options for adaptation and mitigation. Krishna Kumar et al. [3] presents an analysis of crop–climate relationships for India, using historic production statistics for major crops. Parekh and Prajapati [4] carried out the study to assess the impact of climate change on crop water requirement for the crops grown in the Sukhi command area of Vadodara district, Gujarat. All crops in study area show considerable increase in water requirement for future scenarios generated. Pathak et al. [5] concluded that most irrigated areas in India would require more water around 2025 and global net irrigation requirements would increase relative to the situation without climate change by 3.5–5% by 2025 and 6–8% by 2075. The effect of climate change on water resources may be mitigated through better water harvesting through the creation of micro-storage facilities in watersheds. Semenov et al. [6] presented paper to test and compare 2 commonly-used weather generators, namely WGEN and LARS-WG, at 18 sites in the USA, Europe and Asia, chosen to represent a range of climates. Pandey et al. [7] analyzed climatic data of various stations of Gujarat to ascertain the climatic change/variability in the state and its likely impact on crop production using crop models.

2 Study Area and Data Source

Amreli lies at 21.603176° N and 71.222084° E in India at 119 m (391 ft) above sea level. The district conquers an area of around 6760 km^2. Amreli district is allocated into eleven tehsils known as Amreli, Dhari, Khamba, Rajula, Babra, Jagrabad, Kunkavav, Lathi, Lilia, and Kundla. It has 616 villages and as per census 2011, population in Amreli district is 1513614. It is bounded by the southwest Bhavnagar district in the east, Rajkot district in the north, the Junagarh district in the west, and the Arabian Sea in the south. Entire Gujarat is divided into the seven sub agro-climatic zones like Southern Gujarat, Middle Gujarat, North Gujarat, Southern Hills, North-West Arid, North Saurashtra, and South Saurashtra in which Amreli is located in the North Gujarat agro-climatic zone of Gujarat state.

In the district, as per the land use data available for 2006–07, the area under forest land is around 360 km. The land which is not available for cultivation is 70,300 ha and either uncultivated or excluding fallow land is 66,200 ha. The whole land is about 16,300 ha. The net area sown is 550,400 ha, the area shown more than once is 45,100 ha. And the total area for cultivation is 595,500 ha. The cropping intensity in the Amreli district is 108.19%. The net area which is irrigated by canals is 7700 ha. The net area irrigated by different sources like surface water and groundwater is 177,900 ha. The percentage of net area irrigated in the Amreli is 32.32%. Total gross cropped area in Amreli is around 595,500 ha. And the total gross irrigated area is 211,300 ha. The net irrigated area is about 177,900 ha. And the irrigation intensity is 118.77%. The crops are cultivated in Kharif and Rabi in both seasons. The main Kharif crops are groundnut and sorghum. Wheat and pulses are Rabi crops. The main crop, cotton, is spread in different cropping seasons such as Kharif and Rabi seasons. Figure 1a shows index map of study area, and Fig. 1b shows index map of crops sown in Gujarat.

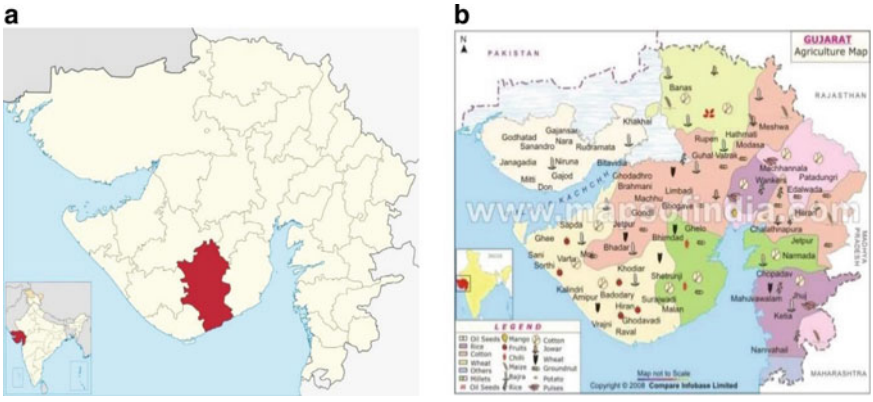

Fig. 1 **a** Index map of study area. **b** Index map of crops sown in Gujarat

2.1 Data Collection

The basic data required to generate the future meteorological parameters like maximum and minimum temperature, relative humidity, precipitation, etc. Study involves different climatological parameters which were obtained from the State Water Data Center of Gujarat, Gandhinagar, which contain the information of climatological parameters for the period of 2001–2010.

3 Methodology

Methodology is divided in two parts to get desired results for crop water requirement. First part includes generation of future climate data, and second part includes calculation of crop water requirements for the generated future climatic data.

Future meteorological parameters are generated using ClimGen weather generator. ClimGen is based on the apparently "design scaling" method of synthesizing geographic environmental change data for a given global mean temperature change. ClimGen calculates meteorological parameters such as daily maximum and minimum temperatures, as well as precipitation, using either daily weather data or monthly summaries, if available. It uses a Weibull distribution to generate precipitation The Weibull distribution is easier to parameterize, describes well the distribution of precipitation amounts and can be simplified for applications to conditions with minimum data. In ClimGen, all generation parameters are calculated for each site of interest. The advantage is that ClimGen can be applied to any world location with enough information to parameterize the program. ClimGen uses quadratic spline functions chosen to ensure that the average of the daily values is continuous across month boundaries, and that the first derivative of the function is continuous across month boundaries.

To generate crop water requirement for generated climatological parameter, CROPWAT software is used. In order to calculate reference evapotranspiration (ET_o), using the Penman-Monteith method, monthly mean data are required, including maximum and minimum temperatures (°C), sunshine hours (h), wind speed (m/s), and relative humidity (%).

For calculation of crop water requirement, K_c values are used for all the crops. Crop coefficient for Kharif and Rabi crops is taken from FAO 56 and approximate planting date. Monthly K_c values are calculated for Rabi and Kharif crops. Finally, crop according ET_c is estimated by multiplying K_c with ET_o.

ET_c is measured crop evapotranspiration (mm/dec), K_c is crop coefficient, and ET_o is reference evapotranspiration (mm/dec).

3.1 Selection of Input Parameters

Meteorological data like maximum temperature, minimum temperature, precipitation, relative humidity, wind velocity, and solar radiation during the period of 2001–2010 are used for generation of future meteorological data. For calculation of C.W.R of Kharif and Rabi crops, K_c (crop coefficient) value is identified.

4 Results and Discussions

4.1 Trend of Climatological Parameters

The maximum and minimum temperature is showing increasing trend till the year 2090, and it is increasing at the rate of 0.0122 as shown in Figs. 2 and 3. Average precipitation of an area is increasing at the rate of 0.0054 as shown in Fig. 4. Average solar radiation is also increasing at the rate of 0.0022 as shown in Fig. 5. Results of wind velocity of Amreli district is decreasing in all decades. The wind velocity is decreasing at the rate of 0.0049 rate in all the decades as shown in Fig. 6. Wind velocity of Amreli is decreasing from 6.1 to 5.1 m/s till 2064, and then, it is again increasing from 5.2 to 5.4 m/s during the period of 2081–90. It is showing increasing and decreasing trend as shown in Fig. 2.

Increase in temperature, evapotranspiration, variable rainfall patterns, increase in solar radiation and interaction of other meteorological parameters may have negative effects on crop water requirement.

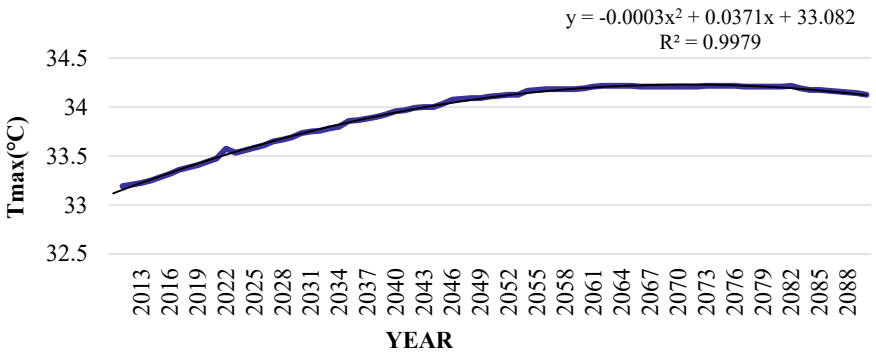

Fig. 2 Trend of average maximum temperature in Amreli district, T_{max} (°C)

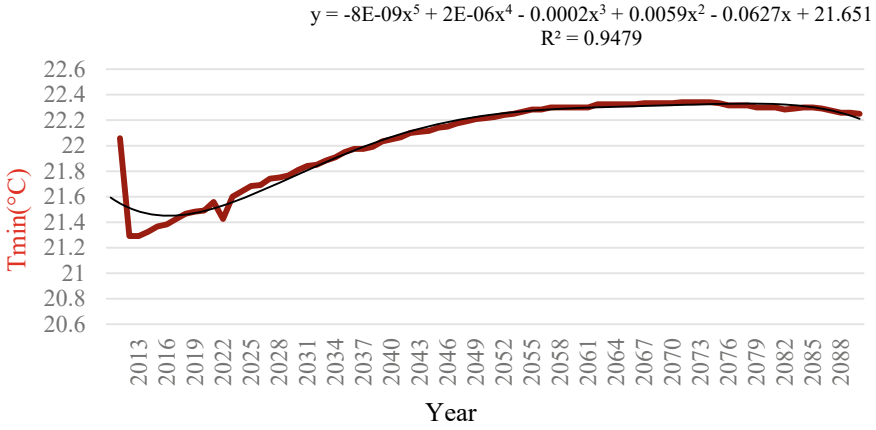

Fig. 3 Trend of average minimum temperature in Amreli district T_{min} (°C)

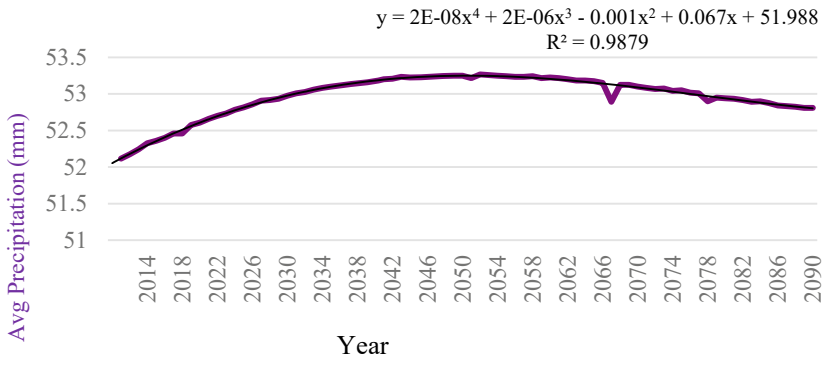

Fig. 4 Trend of average precipitation in Amreli district (mm)

Fig. 5 Trend of average solar radiation in Amreli district (kwh/m^2)

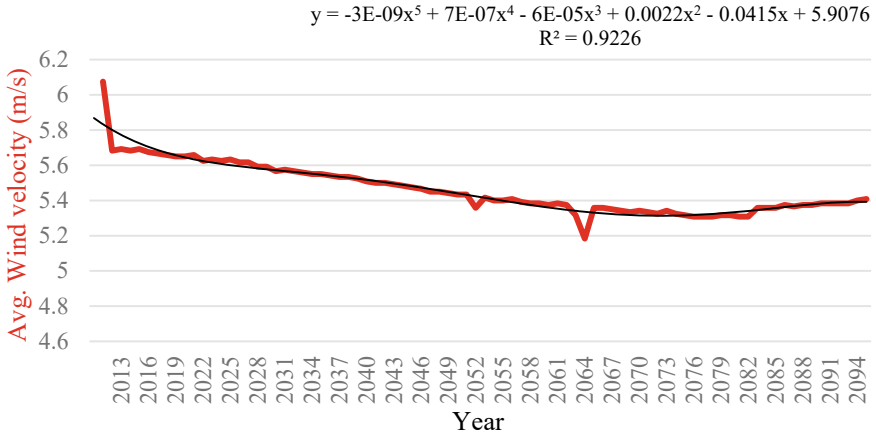

Fig. 6 Trend of average wind velocity in Amreli district in (m/s)

4.2 Crop Water Requirement

Effects show that the water requirement of cotton (Kharif) is increasing in all future years compare to the base year, whereas crop water requirement of cotton Rabi is decreasing in all future years compare to the base year. Crop water requirement for all other crops such as winter wheat, sorghum, pulses, and groundnut is increasing in the future decades compare to the year. Crop water requirement of vegetables (Rabi) is increasing in the future years compare to the base year (2001), whereas for vegetables (Kharif), it is increasing in all future years compare to the base year. Table 1 and Fig. 7 show crop water requirement of various crops grown in Amreli decade wise (mm/dec).

Percentage increment in CWR of different crops grown in Amreli district (mm/dec) is presented in Table 2. It is observed that maximum percentage increment is there in last decade (2081–90). Trend of percentage increment in crop water requirement is increasing trend for all crops accept cotton (Rabi). Percentage increment in CWR varies from 1.4 to 7.55%

5 Conclusions

The above results for different crops in Amreli state that climate change is affecting to the water requirement of all Kharif crops and Rabi crops. Water requirement for cotton, winter wheat, pulses, groundnut, and vegetables is increasing from 0.1 to 2.5% for crops in Amreli district, which means water demand of the crops is increasing throughout the years from 2031 to 2090.

Table 1 Crop water requirement of various crops grown in Amreli decade wise (mm/dec)

Crop/year	2001–2010	2011–2020	2021–2030	2031–2040	2041–2050	2051–2060	2061–2070	2071–2080	2081–2090
	Crop water requirement in mm								
Cotton Kharif	742	779	786	786	789	791	794	795	798
Cotton Rabi	1124	970	996	996	1001	1003	1003	1103	1004
Winter wheat	629	663	681	681	685	686	687	687	686
Sorghum	310	317	316	316	317	318	321	322	323
Pulses	424	408	421	421	423	425	425	425	427
Rabi veg	350	345	353	353	357	359	359	359	360
Kharif veg	333	348	448	348	349	350	352	353	354
Groundnut	497	475	475	475	477	478	481	482	484

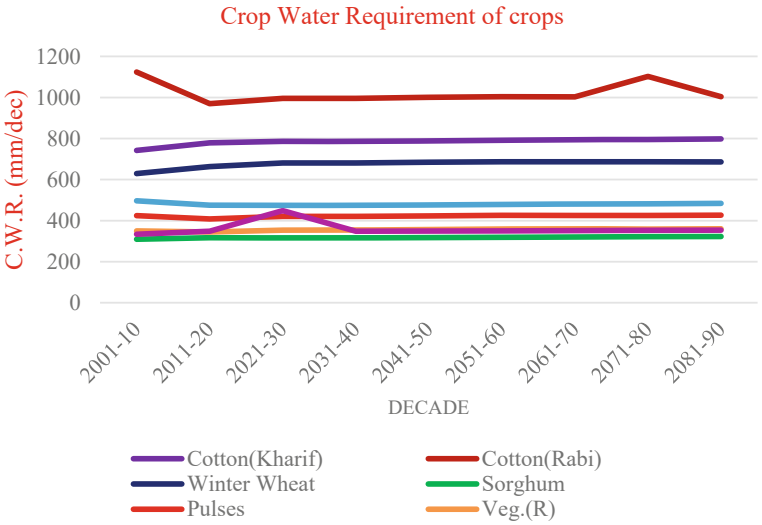

Fig. 7 Crop water requirement of various crops grown in Amreli district (mm/dec)

To meet the need for increased water demand and yield, overall water resources should be increased, such as by increasing water levels in water resources, which can be done effectively through conservation practices and farmers, should be motivated as well. They can use various irrigation systems depending on the water needs of crops, such as sprinkler irrigation systems and drip irrigation systems instead of flooding methods. It needs to understand that water needs to be harvested in a manner that is used systematically and efficient manner to get optimum utilization.

The flood water of monsoon needs to be stored and utilized during the period of its shortage for domestic purpose, industrial purpose, etc. To meet the future demand, various strategy and approaches should be used in industries and in irrigation systems.

Table 2 Percentage increment in CWR of different crops (mm/dec)

Crop/Year	2001–2010	2011–2020	2021–2030	2031–2040	2041–2050	2051–2060	2061–2070	2071–2080	2081–2090
Cotton Kharif	0	4.65	5.95	5.93	6.35	6.62	7.06	7.22	7.55
Cotton Rabi	0	−11.5	−9.79	−9.2	−8.71	−8.48	−8.49	−8.54	−8.47
Winter wheat	0	5.44	7.57	8.18	8.88	9.11	9.19	9.14	9.07
Sorghum	0	2.34	2.67	2.04	2.52	2.79	3.5	3.83	4.24
Pulses	0	−2.86	−0.58	0.083	0.58	1.14	1.11	1.02	1.44
Rabi veg	0	−0.85	1.67	2.28	2.8	3.38	3.38	3.32	3.72
Kharif veg	0	4.4	4.71	4.49	4.74	4.98	4.98	5.75	6.11
Groundnut	0	2.63	2.99	2.51	2.94	3.2	3.84	4.08	4.48

Acknowledgements The authors acknowledge the support received from Water Resources Engineering and Management Institute (WREMI). The authors are also thankful to State Water Data Center (SWDC) for providing necessary data to conduct the present study.

References

1. Gondaliya PN, Khasiya RB (2013) Effect of climate change on crops—a case study of Amreli district. Indian J Res 2(7)
2. IPCC AR4 (Intergovernmental Panel on Climate Change Fourth Assessment Report), IPCC (2007): Climate change
3. Krishna Kumar K, Rupa Kumar K, Ashrit RG, Deshpande NR, Hansen JW (2004) Climate impacts on Indian agriculture. Int J Climatol 24:1375–1393
4. Parekh FP, Prajapati KP (2013) Climate change impacts on crop water requirement for Sukhi reservoir project. Int J Innov Res Sci Eng Technol 2(9):4685–4692
5. Pathak S, Pramanik P, Khanna M, Kumar A (2014) Climate change and water availability in Indian agriculture: impacts and adaptation. Indian J Agric Sci
6. Semenov MA, Brooks RJ, Barrow EM, Richardson CW (1998) Comparison of the WGEN and LARS-WG stochastic weather generators for diverse climates. Climate Res 10(2):95–107
7. Pandey V et al (2009) Impact analysis of climate change on different crops in Gujarat, India. In: SPRS archives XXXVIII-8/W3 workshop proceedings, pp 118–123

Development of Intensity–Duration–Frequency Curves for Surat City Incorporating Daily Data

Pallavi Patarot and S. M. Yadav

Abstract One of the most important hydrologic tools used in design of hydraulic and water resource projects and flood control structures in urban areas by hydraulic engineers is the intensity–duration–frequency (IDF). IDF curves are the representation of relationship between duration, intensity and return period (frequency) of rainfall, which are obtained from a series of analysis of observed rainfall data. In most part of India, short duration rainfall is scarce and only daily rainfall data are available. In such case, it is required to convert the daily rainfall data into hourly using India Metrological Department (IMD) formulas. Assessing the adverse effects of climate change and adapting to them is one way to reduce vulnerability caused, specifically confronting city floods. Since, the rainfall IDF curves are used in the design of water resources projects, in order to have safe and economically stable hydraulic structures. In the present study, the rainfall data of 119 years (1901–2020) were collected from IMD. The aim of this study is to obtain IDF curves having durations of 15 min, 30 min, 45 min, 1 h, 2 h and 3 h for the Surat city. The maximum rainfall intensity curves of different durations like 15 min, 30 min, 45 min, 1 h, 2 h and 3 h are derived from daily rainfall data using IMD formula. It was found that rainfall intensity of 60 mm/h can be used in the design of water resources project and an equation is obtained which can be used to compute daily maximum intensity at any given return period. The developed curves are useful for planning and design of urban storm water and water conservation measures for the Surat city.

P. Patarot (✉) · S. M. Yadav
Department of Civil Engineering, Sardar Vallabhbhai National Institute of Technology Surat, Surat 395007, India
e-mail: p20wr014@ced.svnit.ac.in

S. M. Yadav
e-mail: smy@ced.svnit.ac.in

P. V. Timbadiya et al. (eds.), *Climate Change Impact on Water Resources*, Lecture Notes in Civil Engineering 313, https://doi.org/10.1007/978-981-19-8524-9_32

Keywords IMD formula · Short duration · Data scarcity

1 Introduction

The relationship between intensity, duration and frequency of rainfall obtained from rainfall depth data is nothing but intensity–duration–frequency curves (IDF). The two variables that define rainfall are magnitude and frequency, also known as precipitation regime. The extent of rain is the total precipitation that occurred in mm at a particular time. In contrast, the frequency of rainfall is associated with the probability articulated by the return period. And hence, rainfall intensity is directly proportional to the return period and inversely proportional to the rainfall duration.

Zope et al. [1] developed IDF curves for Mumbai city by Kothyari and Garde's method, IDF curves by probability distribution for annual maximum rainfall and modified Kothyari and Garde's method had been observed that for the 100-year return period, it was found that the IDF curves developed by using equation given by Kothyari and Garde does not show the proper results in the recently changing hydrologic conditions for the Mumbai city. Sun et al. [2] developed IDF curves using remote sensed data and developed Bartlett-Lewis rectangular pulses (BLRP) model for Singapore and the results where validated using station data, a good correlation was found [3]. Indicated future warmer climate of world due to increasing trend in rainfall and intensity and also developed climate models, including global climate models (GCMs), regional climate models (RCMs) and convection-permitting models (CPMs) [4]. The average intensities of the annual largest storms and corresponding storm durations rather than obtaining the annual maximum average intensity for specific durations and thus the intensity-duration data do not comply with the definition of the IDF curves. Sherif et al. [5] the spatial and temporal rainfall characteristics of UAE were derived using IDF curves. The country was divided into four different climatic regions, and the IDF curves of these four regions were used for comparisons. The results obtained from the study was used in dam design and possible occurrence of flash flood. Wolcott et al. [6] rainfall data of 55 years were analyzed and IDF curves where developed to check whether it is required to update the existing IDF curves, but it was found the though there is increasing trend in the rainfall depth due to climate change and it was concluded that there is no need to update as the maximum rainfall intensity did not change for large scale. de Paola et al. [7] IDF curves for three cities of Africa were developed using Gumbel method of probability distribution which was used to estimate the contingent influence of climate change on the IDF curves. Mahdi and Mohamedmeki [8] developed an equation for IDF curve for Bagdad city, and the equation was derived using three statistical methods, those are Gumbel distribution, log Person III and log normal distribution as the induvial equation derived from each of these statical method was not satisfactory. IDF curves for Canada was developed by Nguyen and Asce n.d. using three statistical models a spatial–temporal statistical downscaling, statistical downscaling method and multisite SD though the data scarcity was there the model gave satisfactory results. Gutierrez-Lopez et al. [9] used empirical approach to establish the IDF curves for the Mexico City for 50 years to observe the climate change effect.

Various hydraulic engineers use IDF curves to analyze water resource projects; therefore, reviewing, updating and analyzing rainfall characteristics is one of the essential aspects. One of the first steps in designing a drainage system is determining the duration and intensity of a rainfall event. IDF curve is used for this process. It is computed by considering the average rainfall intensity for a given area over a given period. They help assess the potential duration of an event.

2 Study Area and Data Collection

2.1 Surat City

Surat city, (21°10′ N 72°50′ E) in the western state of Gujarat, is located at the mouth of the Tapi River close to Arabian Sea (Fig. 1) with a total area of 474.2 km^2 and of 13 m elevation from MSL. The climate in the city of Surat is tropical, and in monsoon season, the rainfall is abundant about 1100–1200 mm per year. The monsoon season begins late in June, and it falls under seismic III zone.

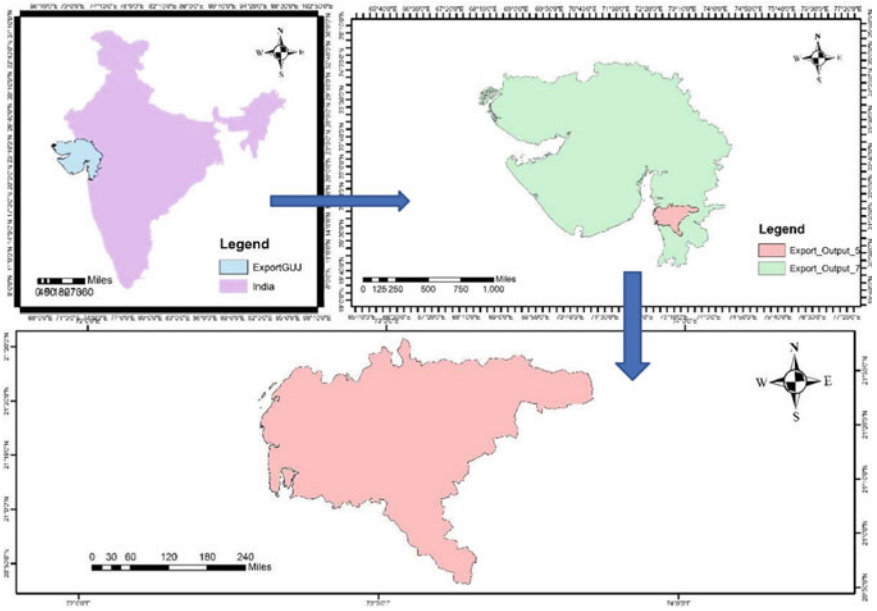

Fig. 1 Index map Surat city (*source* Created in Arc-GIS)

2.2 Data Collection

The daily cumulative rainfall using IMD grid data of size 0.25° × 0.25° of Surat city for 119 years, i.e., from 1991 to 2020 for the entire year (Jan to Dec) from India water resources information system (https://indiawris.gov.in/wris/#/rainfall) was obtained.

3 Methodology

After collection of annual rainfall data, the maximum rainfall in a year was selected. The 24-h rainfall depth was converted to 15-min, 30-min, 45-min, 1-h, 2-h and 3-h rainfall depth using IMD equation (Table 1)

$$R_t = R_{24}(t/24)^n \tag{1}$$

$$I = R_t/t \tag{2}$$

where

R_t required rainfall depth in mm for duration
R_{24} daily rainfall depth (mm)
t required duration (h)
n exponential constant = 1/3
I intensity of rainfall in mm/h.

Gumbel [10] introduced the theory of extremes by looking at the distribution of the greatest and smallest values in repeated samples. Due to its suitability for modeling maximum data, the Gumbel theory is the most often utilized distribution for IDF analysis. It is simple and should only be used in dire circumstances (maximum data or peak rainfalls). The following equation can be used to calculate the design rainfall depth for a particular period [11]

$$K_t = (Y_t - Y_n)/S_n \tag{3}$$

$$Y_t = L_n(L_n(T/T - 1)) \tag{4}$$

$$X_t = \text{mean} + (\text{STD} * K_t) \tag{5}$$

where

STD standard deviation,
K_t frequency factor,
Y_n reduced mean in Gumbel extreme value distribution,

Table 1 Maximum rainfall depth calculated from the year 1901 to 2020

Year	Max rainfall	Year	Max rainfall	Year	Max rainfall	Year	Max rainfall	Year	Max rainfall
1901	68.2	1925	113.82	1949	69.99	1973	123.72	1997	90.69
1902	205.44	1926	124.5	1950	92.4	1974	31.19	1998	213.96
1903	119.96	1927	55.57	1951	69.76	1975	88.41	1999	117.8
1904	150.2	1928	57.29	1952	73.35	1976	174.95	2000	62.74
1905	143.65	1929	215.64	1953	116.52	1977	128.39	2001	130.13
1906	83.74	1930	121.09	1954	143.55	1978	84.3	2002	117.97
1907	95.39	1931	149.65	1955	62.74	1979	112.48	2003	103.15
1908	198.13	1932	114.83	1956	116.4	1980	48.69	2004	242.91
1909	198.13	1933	128.26	1957	73.81	1981	120.27	2005	142.11
1910	76.15	1934	128.26	1958	131	1982	112.6	2006	190.78
1911	95.56	1935	79.1	1959	95.2	1983	100.49	2007	190.05
1912	101.96	1936	59.91	1960	54.78	1984	122.59	2008	116.23
1913	116.59	1937	164.92	1961	73.7	1985	110.13	2009	93.65
1914	114.15	1938	113.92	1962	51.41	1986	92.15	2010	73.18
1915	83.74	1939	159.09	1963	141.6	1987	48.69	2011	64.83
1916	87.63	1940	133.47	1964	152.59	1988	168.04	2012	104.54
1917	108.57	1941	315.86	1965	152.59	1989	56.21	2013	121.44
1918	66.31	1942	173.76	1966	120.51	1990	132.31	2014	104.79
1919	118.37	1943	70.53	1967	92.8	1991	69.77	2015	82.05
1920	96.76	1944	113.46	1968	210.56	1992	185.36	2016	82.16
1921	131.5	1945	349.15	1969	102.41	1993	113.85	2017	72.08
1922	94.21	1946	172.5	1970	247.15	1994	149.3	2018	89.64
1923	168.25	1947	100.59	1971	74.32	1995	125.96	2019	178.34
1924	140.72	1948	42.22	1972	76.14	1996	125.96	2020	111.61

S_n reduced standard deviation in Gumbel extreme value distribution = mean in Gumbel extreme value distribution,
T return period.

The above obtained rainfall depth data are arranged from highest to lowest to assign rank, and the exceedance probability is calculated (Appendix 1).

$$P = 1/T = \text{Rank}/m + 1 \tag{6}$$

where

P exceedance probability
T time period
m total number of observation.

Meanwhile the rainfall intensities for the time period obtained are calculated by dividing the rainfall depth by time in hours. Intensity in arithmetic scale is plotted against return period in the log scale.

4 Results and Discussion

A detailed investigation of rainfall intensity curve was carried out for Surat city, and succeeding results were obtained (Figs. 1 and 2). The maximum rainfall occurred in a particular year for 24 h was selected. The same was converted to different duration depth using Eq. (1), and the corresponding intensity was found and plotted against the return period. The maximum rainfall intensity observed for 1 in 100 return period for 15 min, 30 min, 45 min, 1 h, 2 h ad 3 h duration is 240.2 mm, 173.24 mm, 132.105 mm, 109.97 mm, 69.28 mm and 52.86 mm per hour. These values of intensity are obtained from the IDF curves of respective duration (Figs. 3 and 4; Tables 2 and 3).

5 Conclusions

The following conclusions are derived from the preceding study. Equation $54.787 * \mathrm{LN}(x) + 64.93$ obtained from the plot can be used to compute maximum daily intensity at any given return period. This equation obtains maximum intensity rainfall for various return periods (x). The maximum rainfall intensity observed for 1 in 100 return period for 15 min, 30 min, 45 min, 1 h, 2 h and 3 h duration is

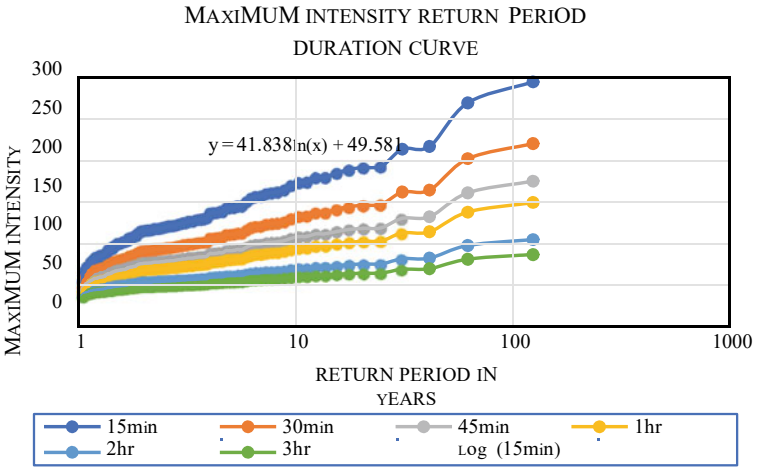

Fig. 2 Resultant IDF curves for Surat city plotted as return period versus maximum intensity

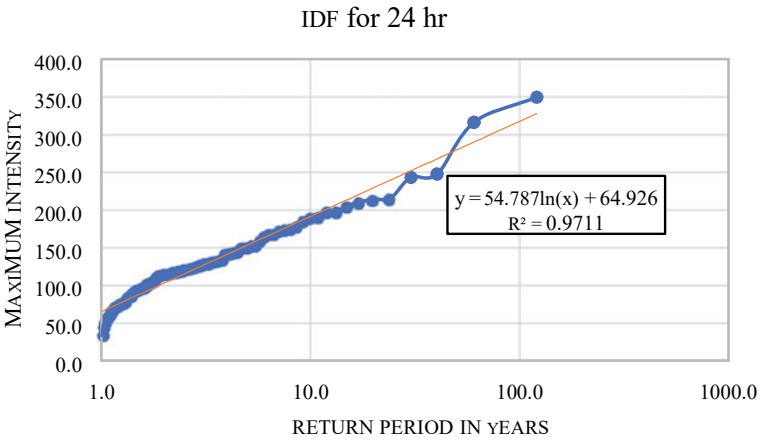

Fig. 3 Resultant IDF curve (24 h) for Surat city plotted as return period versus maximum intensity

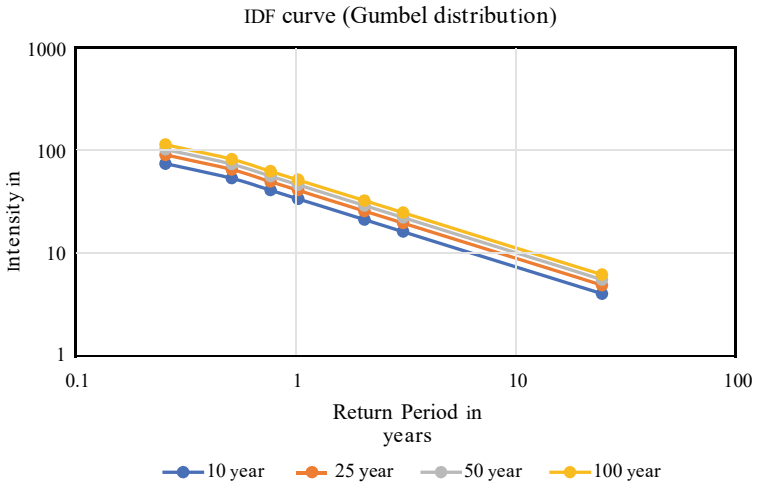

Fig. 4 IDF curve through Gumbel distribution

240.2 mm, 173.24 mm, 132.105 mm, 109.97 mm, 69.28 mm and 52.86 mm per hour. These values of intensity are obtained from the IDF curves of respective duration. The empirical formula slightly overestimated the value of maximum intensity rainfall compared to the Gumbel distribution.

Table 2 Calculated rainfall values with respect to duration and return period in terms of empirical formula

Time (min)	10 years (mm/h)	25 years (mm/h)	50 years (mm/h)	100 years (mm/h)
15	145.9166	184.2523	213.2522	242.2521
30	105.1529	132.7791	153.6775	174.5759
45	80.24718	101.3301	117.2787	133.2274
60	66.2443	83.64833	96.81396	109.9796
120	41.73043	52.69385	60.98736	69.28086
180	31.8459	40.21256	46.54168	52.87081
1440	191.0777	241.2785	279.254	317.2295

Table 3 Calculated rainfall values with respect to duration and return period in terms of Gumbel distribution

Time (T) (min)	10 years (mm/h)	25 years (mm/h)	50 years (mm/h)	100 years (mm/h)
0.25	146.2927	177.5259	200.6964	223.6958
0.5	105.4251	127.9331	144.6308	161.2052
0.75	80.4544	97.6312	110.3739	123.0226
1	66.41364	80.59278	91.11167	101.5529
2	41.83797	50.77027	57.39676	63.97432
3	31.92835	38.74497	43.80192	48.82154
24	7.982087	9.686242	10.95048	12.20539

Acknowledgements I express my sincere gratitude to co-author Dr. Sanjay Yadav for his constant guidance and support. The authors are grateful to IMD and India WRIS for providing required data for the present analysis.

Appendix 1: Intensities Corresponding to Time and Return Period

S. No.	Return period	15 min	30 min	45 min	1 h	2 h	3 h	24 h
1	121.0	266.6	192.1	146.6	121.0	76.3	58.2	349.2
2	60.5	241.2	173.8	132.7	109.5	69.0	52.6	315.9
3	40.3	188.7	136.0	103.8	85.7	54.0	41.2	247.2
4	30.3	185.5	133.7	102.0	84.2	53.1	40.5	242.9
5	24.2	164.7	118.7	90.6	74.8	47.1	35.9	215.6
6	20.2	163.4	117.7	89.9	74.2	46.7	35.7	214.0

(continued)

(continued)

S. No.	Return period	15 min	30 min	45 min	1 h	2 h	3 h	24 h
7	17.3	160.8	115.9	88.4	73.0	46.0	35.1	210.6
8	15.1	156.9	113.1	86.3	71.2	44.9	34.2	205.4
9	13.4	151.3	109.0	83.2	68.7	43.3	33.0	198.1
10	12.1	151.3	109.0	83.2	68.7	43.3	33.0	198.1
11	11.0	145.7	105.0	80.1	66.1	41.7	31.8	190.8
12	10.1	145.1	104.6	79.8	65.9	41.5	31.7	190.1
13	9.3	141.6	102.0	77.8	64.3	40.5	30.9	185.4
14	8.6	136.2	98.1	74.9	61.8	38.9	29.7	178.3
15	8.1	133.6	96.3	73.5	60.7	38.2	29.2	175.0
16	7.6	132.7	95.6	73.0	60.2	37.9	29.0	173.8
17	7.1	131.7	94.9	72.4	59.8	37.7	28.8	172.5
18	6.7	128.5	92.6	70.7	58.3	36.7	28.0	168.3
19	6.4	128.3	92.5	70.6	58.3	36.7	28.0	168.0
20	6.1	125.9	90.8	69.3	57.2	36.0	27.5	164.9
21	5.8	121.5	87.6	66.8	55.2	34.7	26.5	159.1
22	5.5	116.5	84.0	64.1	52.9	33.3	25.4	152.6
23	5.3	116.5	84.0	64.1	52.9	33.3	25.4	152.6
24	5.0	114.7	82.7	63.1	52.1	32.8	25.0	150.2
25	4.8	114.3	82.4	62.8	51.9	32.7	24.9	149.7
26	4.7	114.0	82.2	62.7	51.8	32.6	24.9	149.3
27	4.5	109.7	79.1	60.3	49.8	31.4	23.9	143.7
28	4.3	109.6	79.0	60.3	49.8	31.4	23.9	143.6
29	4.2	108.5	78.2	59.7	49.3	31.0	23.7	142.1
30	4.0	108.1	77.9	59.5	49.1	30.9	23.6	141.6
31	3.9	107.5	77.4	59.1	48.8	30.7	23.5	140.7
32	3.8	101.9	73.5	56.1	46.3	29.1	22.2	133.5
33	3.7	101.0	72.8	55.6	45.9	28.9	22.1	132.3
34	3.6	100.4	72.4	55.2	45.6	28.7	21.9	131.5
35	3.5	100.0	72.1	55.0	45.4	28.6	21.8	131.0
36	3.4	99.4	71.6	54.7	45.1	28.4	21.7	130.1
37	3.3	98.0	70.7	53.9	44.5	28.0	21.4	128.4
38	3.2	97.9	70.6	53.9	44.5	28.0	21.4	128.3
39	3.1	97.9	70.6	53.9	44.5	28.0	21.4	128.3
40	3.03	96.19	69.32	52.90	43.67	27.51	20.99	125.96
41	2.95	96.19	69.32	52.90	43.67	27.51	20.99	125.96
42	2.88	95.07	68.51	52.29	43.16	27.19	20.75	124.50
43	2.81	94.48	68.09	51.96	42.89	27.02	20.62	123.72

(continued)

(continued)

S. No.	Return period	15 min	30 min	45 min	1 h	2 h	3 h	24 h
44	2.75	93.62	67.46	51.48	42.50	26.77	20.43	122.59
45	2.69	92.74	66.83	51.00	42.10	26.52	20.24	121.44
46	2.63	92.47	66.64	50.85	41.98	26.45	20.18	121.09
47	2.57	92.03	66.32	50.61	41.78	26.32	20.09	120.51
48	2.52	91.84	66.19	50.51	41.70	26.27	20.05	120.27
49	2.47	91.61	66.02	50.38	41.59	26.20	19.99	119.96
50	2.42	90.39	65.14	49.71	41.04	25.85	19.73	118.37
51	2.37	90.09	64.92	49.54	40.90	25.76	19.66	117.97
52	2.33	89.96	64.83	49.47	40.84	25.73	19.63	117.80
53	2.28	89.03	64.16	48.96	40.42	25.46	19.43	116.59
54	2.24	88.98	64.12	48.94	40.40	25.45	19.42	116.52
55	2.20	88.89	64.06	48.88	40.35	25.42	19.40	116.40
56	2.16	88.76	63.96	48.81	40.29	25.38	19.37	116.23
57	2.12	87.69	63.19	48.23	39.81	25.08	19.14	114.83
58	2.09	87.17	62.82	47.94	39.57	24.93	19.03	114.15
59	2.05	87.00	62.69	47.84	39.49	24.88	18.99	113.92
60	2.02	86.94	62.65	47.81	39.47	24.86	18.98	113.85
61	1.98	86.92	62.64	47.80	39.46	24.86	18.97	113.82
62	1.95	86.64	62.44	47.65	39.33	24.78	18.91	113.46
63	1.92	85.99	61.97	47.29	39.04	24.59	18.77	112.60
64	1.89	85.90	61.90	47.24	38.99	24.57	18.75	112.48
65	1.86	85.23	61.42	46.87	38.69	24.38	18.60	111.61
66	1.83	84.10	60.61	46.25	38.18	24.05	18.36	110.13
67	1.81	82.91	59.75	45.60	37.64	23.71	18.10	108.57
68	1.78	80.02	57.67	44.01	36.33	22.89	17.47	104.79
69	1.75	79.83	57.53	43.90	36.24	22.83	17.42	104.54
70	1.73	78.77	56.77	43.32	35.76	22.53	17.19	103.15
71	1.70	78.21	56.36	43.01	35.50	22.37	17.07	102.41
72	1.56	79.96	57.62	43.97	36.30	22.87	17.45	104.71
73	1.52	79.46	57.26	43.70	36.07	22.72	17.34	104.05
74	1.48	78.95	56.89	43.42	35.84	22.58	17.23	103.38
75	1.44	78.44	56.53	43.14	35.61	22.43	17.12	102.72
76	1.40	77.94	56.17	42.86	35.38	22.29	17.01	102.06
77	1.35	77.43	55.80	42.58	35.15	22.15	16.90	101.40
78	1.31	76.93	55.44	42.31	34.92	22.00	16.79	100.74
79	1.27	76.42	55.07	42.03	34.69	21.86	16.68	100.08
80	1.23	75.92	54.71	41.75	34.46	21.71	16.57	99.41

(continued)

(continued)

S. No.	Return period	15 min	30 min	45 min	1 h	2 h	3 h	24 h
81	1.19	75.41	54.34	41.47	34.24	21.57	16.46	98.75
82	1.15	74.91	53.98	41.19	34.01	21.42	16.35	98.09
83	1.5	70.4	50.7	38.7	31.9	20.1	15.4	92.2
84	1.4	69.3	49.9	38.1	31.4	19.8	15.1	90.7
85	1.4	68.5	49.3	37.6	31.1	19.6	14.9	89.6
86	1.4	67.5	48.7	37.1	30.7	19.3	14.7	88.4
87	1.4	66.9	48.2	36.8	30.4	19.1	14.6	87.6
88	1.4	64.4	46.4	35.4	29.2	18.4	14.1	84.3
89	1.4	63.9	46.1	35.2	29.0	18.3	14.0	83.7
90	1.3	63.9	46.1	35.2	29.0	18.3	14.0	83.7
91	1.3	62.7	45.2	34.5	28.5	17.9	13.7	82.2
92	1.3	62.7	45.2	34.5	28.4	17.9	13.7	82.1
93	1.3	60.4	43.5	33.2	27.4	17.3	13.2	79.1
94	1.3	58.2	41.9	32.0	26.4	16.6	12.7	76.2
95	1.3	58.1	41.9	32.0	26.4	16.6	12.7	76.1
96	1.3	56.8	40.9	31.2	25.8	16.2	12.4	74.3
97	1.2	56.4	40.6	31.0	25.6	16.1	12.3	73.8
98	1.2	56.3	40.6	31.0	25.6	16.1	12.3	73.7
99	1.2	56.0	40.4	30.8	25.4	16.0	12.2	73.4
100	1.2	55.9	40.3	30.7	25.4	16.0	12.2	73.2
101	1.2	55.0	39.7	30.3	25.0	15.7	12.0	72.1
102	1.2	53.9	38.8	29.6	24.5	15.4	11.8	70.5
103	1.2	53.4	38.5	29.4	24.3	15.3	11.7	70.0
104	1.2	53.3	38.4	29.3	24.2	15.2	11.6	69.8
105	1.2	53.3	38.4	29.3	24.2	15.2	11.6	69.8
106	1.1	52.1	37.5	28.6	23.6	14.9	11.4	68.2
107	1.1	50.6	36.5	27.8	23.0	14.5	11.1	66.3
108	1.1	49.5	35.7	27.2	22.5	14.2	10.8	64.8
109	1.1	47.9	34.5	26.3	21.8	13.7	10.5	62.7
110	1.1	47.9	34.5	26.3	21.8	13.7	10.5	62.7
111	1.1	45.8	33.0	25.2	20.8	13.1	10.0	59.9
112	1.1	43.7	31.5	24.1	19.9	12.5	9.5	57.3
113	1.1	42.9	30.9	23.6	19.5	12.3	9.4	56.2
114	1.1	42.4	30.6	23.3	19.3	12.1	9.3	55.6
115	1.1	41.8	30.1	23.0	19.0	12.0	9.1	54.8
116	1.0	39.3	28.3	21.6	17.8	11.2	8.6	51.4
117	1.0	37.2	26.8	20.4	16.9	10.6	8.1	48.7

(continued)

(continued)

S. No.	Return period	15 min	30 min	45 min	1 h	2 h	3 h	24 h
118	1.0	37.2	26.8	20.4	16.9	10.6	8.1	48.7
119	1.0	32.2	23.2	17.7	14.6	9.2	7.0	42.2
120	1.0	23.8	17.2	13.1	10.8	6.8	5.2	31.2

References

1. Zope PE, Jothiprakash V (2016) Development of rainfall intensity duration frequency curves for Mumbai City, India. J Water Resource Prot, 11
2. Sun, Y., Wendi, D., Kim, D. E., & Liong, S. Y. (2019). Deriving intensity–duration–frequency (IDF) curves using downscaled in situ rainfall assimilated with remote sensing data. Geoscience Letters, 6, 1–12.
3. Martel J-l, Brissette F, Picher L (2018) Climate change and rainfall intensity duration curves: review of science and guidelines for adaptation. ASCE, p 18
4. Singh V, Zhang L (2007) Discussion of IDF curves using the frank Archimedean copula. ASCE, p 5
5. Sherif M, Chowdhury R, Shetty A (2014) Rainfall and intensity-duration-frequency (IDF) curves in the United Arab Emirates. In: World environmental and water resources congress 2014, pp 2316–2325
6. Wolcott SB, Mroz M, Basile J (2009) Application of northeast regional climate center research results for the purpose of evaluating and updating intensity-duration-frequency (IDF) curves—case study: Rochester, New York. In: World environmental and water resources congress 2009: Great
7. de Paola F, & Topa ME (2014) Intensity-duration-frequency rainfall curves for data series and climate projection in African series. Springer Open J, 18
8. Mahadi and Mohammedmeki (2020) Analysis of rainfall-duration-duration curves for Baghdad city. IOP Conf Ser: Mater Sci Eng, 10
9. Gutierrez-Lopez A, Jimenez Hernandez SB, Escalante Sandoval C (2019) Physical parameterization of IDF curves based on short-duration storms. Water 11(9):1813
10. Gumbel, E. J. (1958). Disarmament and clandestine rearmament under the Weimar Republic. In Inspection for Disarmament (pp. 203–219). Columbia University Press.
11. Chow, V. T. (1953). Frequency analysis of hydrologic data with special application to rainfall intensities. University of Illinois. Engineering Experiment Station. Bulletin; no. 414.
12. Campos JNB, de Carvalho Studart TM (2020) On rainfall intensity-duration-frequency curves, partial-area affect and the rational method: theory and engineering practice. Water, 11
13. Daniel D, Sanjay S (2019) Rainfall patterns and implications for runoff and groundwater recharge. ASCE, p 7
14. Dourte D, Shukla S, Singh P, Haman D (2013) Rainfall intensity-duration-frequency relationships for Andhra Pradesh, India: changing rainfall patterns and implications for runoff and groundwater recharge. J Hydrol Eng 18(3):324–330.
15. Ibrahim Deger H, Ishak MY (2019) Rainfall intensity duration curve analysis for the city Gazaintep. In: International civil engineering and architecture conference, p 8
16. Lee T, Son C, Kim M, Lee S, Yoon S (2020) Climate change adaptation to extreme rainfall events on a local scale in Namyangju, South Korea. J Hydrol Eng 25(5):05020005
17. Link GA, Watkins Jr DW, Johnson DL (2000) Mapping spatial variation in rainfall intensity-duration-frequency estimates using a geographical information system. In: Building partnerships, pp 1–10

18. Porras PJ Sr, Porras PJ Jr (2001) New perspective on rainfall frequency curves. J Hydrol Eng 6(1):82–85
19. Thanh V (2020) Development of new methods for methods for updating IDF curves in Canada in the context of climate change. In: World environment and water resources congress 2020, p 15
20. Yabin S, Dadiyorto W, Dong Eon K, Shie-Yui L (2019) Deriving intensity–duration–frequency (IDF) curves using downscaled in situ rainfall assimilated with remote sensing data. Geosci Lett, 12
21. Zhu J (2012) Impact of climate change on extreme rainfall across the United States. ASCE, p 15

Generation of Intensity–Duration–Frequency Curve for Tezpur, Assam

Priyanshu Kashyap Hazarika, Ananya Swargiary, Gautam Sonowal, and Anurag Sharma

Abstract Calculating rainfall intensity–duration–frequency curve (IDF curve) is a pre-requisite in water resource engineering for the development, management and planning of hydraulic infrastructures such as barrages, spillways and for various engineering projects against design floods. The objective of this study is to develop an IDF curve relationship for Tezpur, Assam for a short duration of 15 years which will be helpful for the design of drainage work like storm sewers, culverts, etc. In this study, the rainfall data of 15 years, i.e., from 2007 to 2021 has been collected from the Water Resource Department of Tezpur. Firstly, the peak annual daily rainfall was found out and then, Gumbel, log-normal and normal distributions have been used to calculate probable maximum rainfall intensity for a return period of 2, 10, 25, 50, 75 and 100 years from the maximum annual rainfall. The other objective of this study is to compare the IDF curves derive from these three distributions and is to find the best IDF curve for Tezpur. For Gumbel's analysis, the value of reduced mean and reduced standard deviation has been taken as 0.5128 and 1.0206, respectively, for 15 numbers of sample sizes. The data trend illustrates that as duration increases,

P. K. Hazarika (✉) · A. Swargiary · G. Sonowal
Department of Civil Engineering, Central Institute of Technology, Kokrajhar, , Kokrajhar 783370, India
e-mail: b18ce223@cit.ac.in

A. Swargiary
e-mail: b18ce201@cit.ac.in

G. Sonowal
e-mail: b18ce220@cit.ac.in

A. Sharma
Department of Civil Engineering, National Institute of Technology, Rourkela, Rourkela 769008, India
e-mail: sharmaan@nitrkl.ac.in

P. V. Timbadiya et al. (eds.), *Climate Change Impact on Water Resources*, Lecture Notes in Civil Engineering 313, https://doi.org/10.1007/978-981-19-8524-9_33

the intensity value declines and that rainfall increases with length for a particular duration as return period increases, intensity tends to increase. It is also observed that log-normal distribution gives the lowest variation for different return periods. The derived IDF curve model can be further used for flood forecasting.

Keywords Intensity–duration–frequency curve · Gumbel distribution · Normal distribution function · Log-normal distribution

1 Introduction

The amount of rainfall received by an area impacts its weather conditions which is responsible for causing floods as well as droughts. Correct characterization of magnitude and frequency of rainfall may be helpful to control such extreme weather conditions. This may also help with disaster management. Calculating rainfall intensity–duration–frequency curve (IDF curve) is useful in the field of water resource engineering, public safety, various civil engineering projects against design floods, drainage design and operation, river discharge studies, etc. The magnitude of severe rainfall occurrences for specific return periods (e.g., 2-to 100-year) and storm durations are also summarized by intensity–duration–frequency (IDF) curves (e.g., 5 min to 24 h), which a common component of hydrological infrastructure designs and other engineering applications [1]. The amount of historical rainfall data collected is directly proportional to the accuracy of the curve derived.

Intensity–duration–frequency curves give the relationship between the intensity of precipitation and the duration of storm for a given return period. The IDF curves are created for a certain location and return period. It is a curve in which return period serves as the third parameter while duration, intensity and ordinate serve as the abscissa [2]. The likelihood that a certain average rainfall intensity will occur within a specific time period is shown graphically by the rainfall intensity–duration–frequency (IDF) curve [3]. Intensity–duration–frequency (IDF) curves need to be reviewed and updated for future climatic scenarios since rainfall characteristics are frequently utilized to build water infrastructure [4]. Climate change has affected rainfall pattern of areas to a great extent. Therefore, unless the IDFs are revised to reflect future climatic trends, those IDFs produced in accordance with historical climatic circumstances are not applicable to future climatic conditions [5, 6]. A Mediterranean area study showed that studies on extreme rainfall of shorter duration will increase in the future in spite of changes in increment of precipitation [7]. This may help to track the changes in climatic conditions for a short duration and its impact on rainfall. Information about rainfall intensity, duration and return periods—the inverse of the chance of exceeding—is crucial in the field of hydrology. The ability to predict significant precipitation occurrences of varying intensities is also of great importance since it is necessary for the construction of many hydraulic facilities, such as flood detention reservoirs and sewage systems, which control storm runoff. [8].

Precipitation magnitude is different for various locations. Numerous research [9, 10] have been conducted to identify relationships between various regions of the world so that IDF curve applications can be used in a variety of fields. In a country like India, precipitation mostly occurs in the form of rain. So, it is very much essential to study the pattern of rainfall to interpret floods and droughts. But, in developing countries like India, IDF curve relationships have not been derived accurately for many regions or have not developed at all. The reasons may be lack of proper rainfall data, fund or exposure.

2 Study Area and Data Source

2.1 Tezpur

Tezpur is called the cultural capital of Assam. It is the sub-division of Sonitpur district which is known for its mythical history. This city is located on the northern bank of the mighty Brahmaputra river; 180 km from Guwahati, Assam. This city is related to so much ancient history, for example, there was a great mythical war which happened in Tezpur between the lord Shiva and Krishna. Tezpur is situated between 26.6528° to 26.691° N and 92.725° to 92.860° E, of the eastern longitudes with the GPS coordinates 26°39′4.3848″ N and 92°47′1.7268″ E with an area of 40 km^2 and bounded by Rangapara in the north, Jamugurihat in the east, Dhekiajuli in the west and Nagaon in the south. We have seen that the Tezpur area climatically comes under sub-tropical monsoon. The average temperature of this area is 21 °C in summer and 10 °C in winter. The Tezpur is situated on the northern bank of Brahmaputra which is dotted with a range of lower hills and hillocks like Agnigarh, Auguri, Bamuni hills with the semi-deciduous forests. Along with these lower hills and hillocks, Tezpur city is also decorated with some different geometric shapes in low-lying areas which are abandoned channels of the River Jia Bharali. With the density of 2600 persons/km^2, the total population of this beautiful city is 1.03 lakhs as per the 2011 census.

The Water Resource Department in Tezpur provided daily rainfall data for the study's purposes from the period 2007–2021, which were used to create the intensity–duration–frequency curve (Fig. 1).

2.2 Data Used

For this study, daily rainfall data of Tezpur was collected from Tezpur Water Resource Department from the year 2007 to 2021. The daily rainfall data was analyzed to find the maximum daily rainfall data for every month. To reduce the variability in the daily rainfall data, it was measured daily at exactly 08:30 a.m. With the help of this data, intensity–duration–frequency curves were generated for our study area.

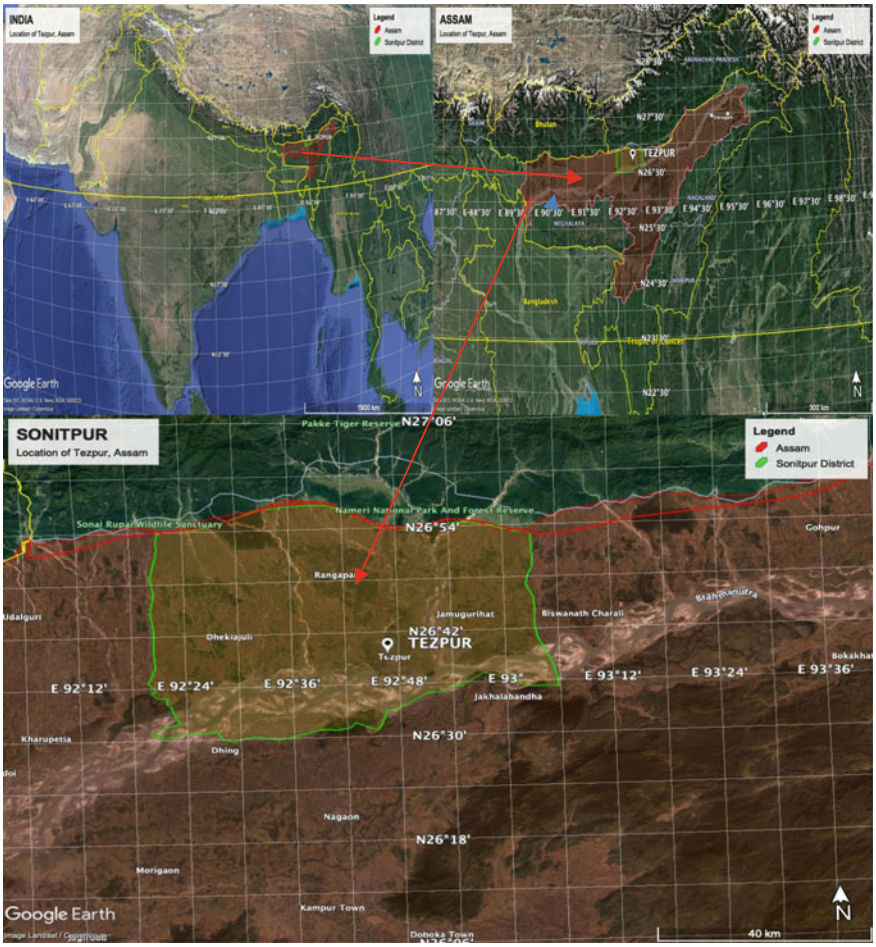

Fig. 1 Index map of study area

2.3 Methods Used

2.3.1 Estimation of Short-Duration Rainfall

In order to estimate rainfall values for various durations, such as 5 min, 10 min, 15 min, 30 min, 60 min, 120 min, 720 min and 1440 min, the Indian Meteorological Department (IMD) utilizes an empirical reduction formula (1). Using daily rainfall data of Tezpur city and the IMD empirical reduction formula, it was discovered that this formula provides the most accurate short-duration rainfall estimation.

$$P_t = P_{24}\sqrt[3]{\frac{t}{24}} \tag{1}$$

where P_t is the required rainfall depth in mm at t hour duration, P_{24} is the daily rainfall in mm and t is the duration of rainfall for which the rainfall depth is required in minute.

Now by using the following three theoretical probability distribution functions, i.e., Gumbel's extreme value distribution, normal distribution, log-normal distribution rainfall (mm) and then rainfall intensity (mm/h) of different return period (2 years, 10 years, 25 years, 50 years, 75 years and 100 years) is found out. These three are the most commonly used distribution functions to develop the IDF curves from the data of rainfall of the study area.

2.3.2 Gumbel's Extreme Value Distribution (GEV)

The most popular frequency or probability distribution function that may be used to various hydrological investigations is known as the general equation of hydrologic frequency analysis (GEV), and it can be expressed as (2).

The magnitude (X_T) of a hydrological event can be represented as the arithmetic mean ($\overline{x}$) plus frequency factor (K_t) into standard deviation (σ_{n-1})

$$X_T = \overline{x} + K_t \sigma_{n-1} \tag{2}$$

where

X_T value of variate X of a random hydrological series with return period

K_t frequency factor expressed as $\frac{Y_T - Y_N}{S_N}$.

$_{n-1}$ standard deviation of sample size $N = \left[\frac{1}{N-1}\sum_{i=1}^{N}(x_i - \overline{x})^2\right]^{1/2}$.

Y_T reduced variate which is a function of return period T and is given by $\mathrm{YT} = -\left[\ln\left\{\ln\frac{T}{T-1}\right\}\right]$

Y_N reduced mean, a function of sample size N and equal to 0.5424 for sample size 15.

S_N reduced standard deviation, a function of sample size N and equal to 1.1363 for sample size 15.

2.3.3 Normal Distribution Function

Normal (Gaussian) distribution is one of the most prominent continuous probability distribution functions in statistics. For obtaining the rainfall intensities for specified return period (2, 10, 25, 50, 75 and 100 years) and numerous calculations must be made for each storm period, e.g., this approach also calculates rainfall intensities like other methods. Following is the equation to determine P_T (in mm) using a specified time period T (in years) and specified duration (t):

$$P_T = \overline{P} + K_T S \tag{3}$$

Here, K_T is the frequency factor and is equal to z for both log-normal and normal distributions. z can be calculated by

$$z = w - \frac{2.515517 + 0.802853w + 0.010328w^2}{1 + 1.432788w + 0.189269w^2 + 0.001308w^3} \tag{4}$$

Here, w is given as

$$w = \ln\left(\frac{1}{p^2}\right)^{\frac{1}{2}} \tag{5}$$

In the above equation, p is the probability of occurrence in a specified return period and is given as

$$\mathrm{p} = \frac{1}{T} \tag{6}$$

For the case $p > 0.5$, the value of p is substituted by $1 - p$ in Eq. (5) and z gives a negative value. In the Eq. (3),

$\overline{P}$ arithmetic average of rainfall records obtained for a single time period.
S standard deviation.

After calculating the precipitation, the rainfall intensities I (in mm/h) corresponding to a particular return period T are calculated which is necessarily developing IDF:

$$I_t = \frac{P_T}{t}$$

Here, t represents the duration in hour.

The above procedure was followed and uses to calculate the rainfall intensities for eight durations and six return periods.

2.3.4 Log-Normal Distribution

Similar to the normal method, the log-normal method with the interference of logarithm variables can be used to calculate the frequency of precipitation. The logarithmically converted data is used to calculate the average precipitation and the standard deviation.

$$P^* = \log(P_i)$$

$$\overline{P^*} = \frac{1}{n}\sum_{i=1}^{n} P_i^*$$

$$S^* = \left[\frac{1}{n-1}\sum_{i=1}^{n}\left(P^* - \overline{P}^*\right)^2\right]^{1/2}$$

The frequency precipitation is calculated as

$$P_T^* = \overline{P}^* + K_T S^*$$

The intensity can be calculated by

$$I_t = \frac{P_T}{t}$$

Here, P_T is the antilogarithm of P^* calculated by equation.

3 Results and Discussions

There are three different methods used to obtain the IDF curves which link the relationship between duration of rainfall (in min.), intensity (in mm/h) and return period (in years). The deductions made were summarized in Tables 2, 3 and 4. In Table 1, the return intervals are described as frequency factor K_T for different probability distribution functions.

The intensity of rainfall and the return durations are directly proportional to each other as seen in Figs. 2, 3, 4, 5, 6 and 7, which represents the IDF curves that is the summation of all the three methods, if the return period increases, the intensity was also seen increasing for a particular duration of storm. It is observed from the graph that intensity of rainfall and the duration of storm are inversely proportional to each other in every three cases. The intensity–duration–frequency curve is a graphical representation of the connection between rainfall intensity and duration. The flood hydrographs for various design floods may be calculated using the rainfall intensity measured for various periods. The intensity duration curve shows that Gumbel distribution gives highest rainfall intensity values for higher return periods between the

Table 1 Value of frequency factor for different return periods

Probability distribution function	Frequency factor, K_T					
	Return period (years)					
	2	10	25	50	75	100
Gumbel distribution	−0.154	1.503	2.337	2.956	3.316	3.571
Normal distribution	0.000199	1.282059	1.751386	2.054509	2.217132	2.327114
Log-normal distribution	0.000199	1.282059	1.751386	2.054509	2.217132	2.327114

Table 2 Calculation of frequency intensity values for different duration and return periods using Gumbel's distribution

Duration (h)	Intensity values (mm/h) for return period of					
	2 years	10 years	25 years	50 years	75 years	100 years
0.08333	148.00485	225.188747	264.036342	292.855707	309.606620	321.462274
0.16667	93.237217	141.860020	166.332471	184.487533	195.039948	202.508541
0.25	71.153313	108.259457	126.935433	140.790338	148.843337	154.542941
0.5	44.823778	68.1991848	79.9643121	88.6923556	93.7654272	97.3559526
1	28.237211	42.9627942	50.3743600	55.8726829	59.0685177	61.3304070
2	17.788328	27.0648644	31.7338582	35.1975846	37.2108344	38.6357354
12	5.3872563	8.19668708	9.61070789	10.6597093	11.2694289	11.7009650
24	3.3937588	5.16358929	6.054366592	6.715196076	7.099295366	7.371146098

Table 3 Calculation of frequency intensity values for different duration and return periods using normal distribution

Duration (h)	Intensity values (mm/h) for return period of					
	2 years	10 years	25 years	50 years	75 years	100 years
0.08333	156.99206	208.611920	237.112870	250.981819	258.394467	263.462127
0.16667	98.8987999	131.417274	149.371747	158.108637	162.778313	165.970739
0.25	75.4739100	100.290150	113.991978	120.659473	124.223102	126.659379
0.5	47.5455840	63.1788358	71.8104463	76.0107050	78.2556509	79.7904091
1	29.9518410	39.800172	45.2377464	47.8837436	49.2979709	50.2648080
2	18.8684775	25.072537	28.4979945	30.1648682	31.0557756	31.6648448
12	5.71438317	7.5933040	8.63071544	9.13553388	9.40534824	9.58980694
24	3.59983582	4.78348182	5.437010032	5.755025724	5.924998116	6.041199818

Table 4 Calculation of frequency intensity values for different duration and return periods using log-normal distribution

Duration (h)	Intensity values (mm/h) for return period of					
	2 years	10 years	25 years	50 years	75 years	100 years
0.08333	151.834916	211.706464	239.105485	258.637253	269.799811	277.605294
0.16667	95.6499209	133.366600	150.626887	162.931119	169.963084	174.880226
0.25	72.9945514	101.777764	114.949829	124.339715	129.706109	133.458591
0.5	45.9836858	64.1159741	72.4138546	78.3291123	81.7097284	84.0736439
1	28.9679069	40.3905327	45.6178698	49.3442487	51.4739034	52.9630769
2	18.24863784	25.4444412	28.7374572	31.0849288	32.4265272	33.3646477
12	5.52666260	7.705936343	8.70323756	9.41417738	9.82048506	10.1045980
24	3.48157828	4.854434319	5.48269453	5.93055843	6.18651616	6.365496093

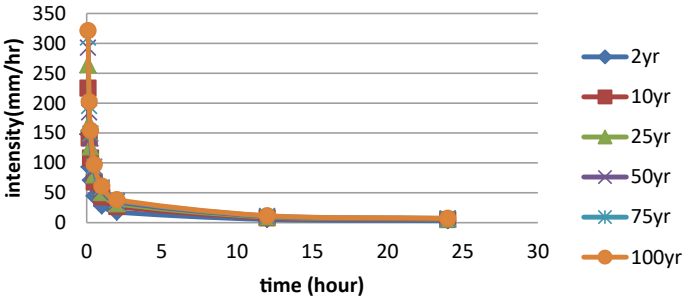

Fig. 2 IDF curve in arithmetic scale using Gumbel's distribution

Fig. 3 IDF curve in log scale using Gumbel's distribution

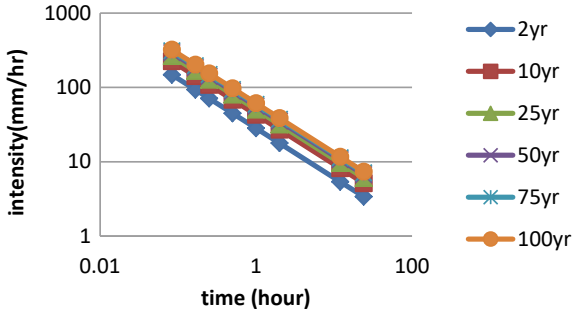

three and the values deduced from the other two methods are nearly close to each other. The frequency precipitation value was also found higher in Gumbel's method. As the sample size is small, so the log-normal distribution gives the least variation in the IDF curve. The graphs of Gumbel's distribution, log-normal distribution and normal distribution were plotted in both arithmetic and logarithmic scale. The estimated IDF relationships may also be utilized as useful information for the region's development and maintenance of hydraulic infrastructures. By assessing extreme weather scenarios like floods, these statistical approaches play a significant role in enabling the adoption of appropriate mitigation measures to reduce the risk of loss of life and property. Therefore, the evaluation of the heaviest precipitation occurrences provides guidance for a variety of civil engineering tasks, such as reservoir management, flood forecasts and hydraulic structure designs.

4 Conclusions

The aim of the study is to develop the IDF curve of Tezpur to calculate the intensity of rainfall using the specific storm duration and return period by using the daily

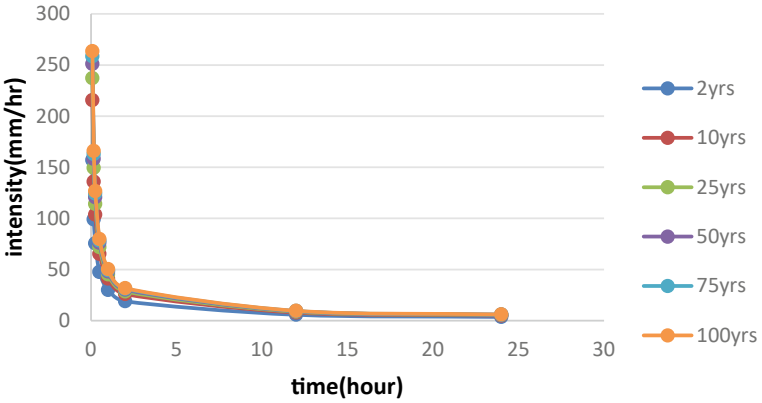

Fig. 4 IDF curve in arithmetic scale using normal distribution

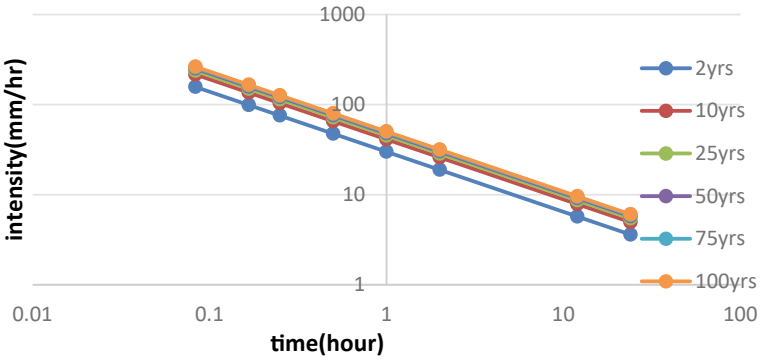

Fig. 5 IDF curve in log scale using normal distribution

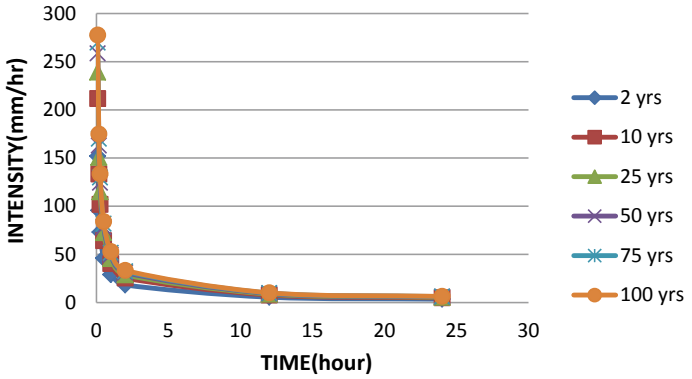

Fig. 6 IDF curve in arithmetic scale using log-normal distribution

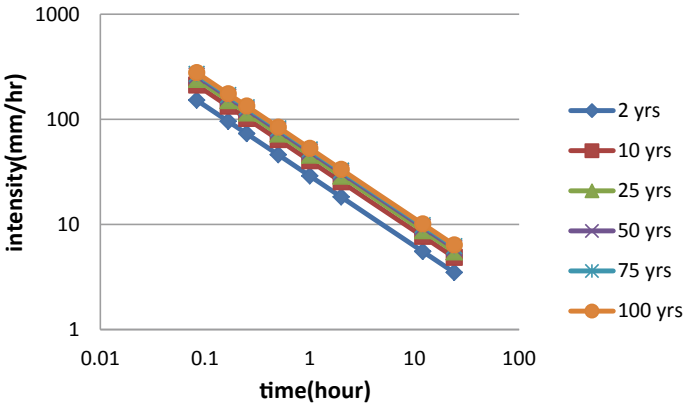

Fig. 7 IDF curve in log scale using log-normal distribution

rainfall data from Tezpur Water Resource Department till August 2021. The following conclusions have been derived from this study.

- Out of the three distribution methods, the Gumbel distribution method gives the highest rainfall intensity values for high return periods among the three.
- The rainfall intensity value obtained from normal and log-normal distributions are nearly close to each other.
- The floods with higher return period were severe when compared to that of lower return period.
- The graphs would be more appropriate and distinct if more than 30 years data are used.
- The rainfall intensities obtained for different durations can be used to calculate the flood hydrographs for different design floods.

Acknowledgements The authors would like to acknowledge the Water Resource Department of Tezpur, Government of India (GoI) for providing the necessary data which was required for this research.

References

1. Willems P (2000) Compound intensity/duration/frequency-relationships of extreme precipitation for two seasons and two storm types. J Hydrol 233(1–4):189–205
2. Aron G, Wall DJ, White EL, Dunn CN (1987) Regional rainfall intensity-duration-frequency curves for Pennsylvania 1. JAWRA J Am Water Resour Assoc 23(3):479–485
3. Dupont B, Allen DL (1999) Revision of the rainfall-intensity duration curves for the commonwealth of Kentucky (No. KTC-00-18). University of Kentucky Transportation Center
4. Mirhosseini G, Srivastava P, Stefanova L (2013) The impact of climate change on rainfall intensity–duration–frequency (IDF) curves in Alabama. Reg Environ Change 13(1):25–33

5. Mailhot A, Duchesne S (2010) Design criteria of urban drainage infrastructures under climate change. J Water Resour Plan Manag 136(2):201–208
6. Guo Y (2006) Updating rainfall IDF relationships to maintain urban drainage design standards. J Hydrol Eng 11(5):506–509
7. Rodríguez R, Navarro X, Casas MC, Ribalaygua J, Russo B, Pouget L, Redaño A (2014) Influence of climate change on IDF curves for the metropolitan area of Barcelona (Spain). Int J Climatol 34(3):643–654
8. Agarwal S, Kumar S (2019) Applicability of SWMM for semi urban catchment flood modeling using extreme rainfall events. Int J Recent Technol Eng 8(2):245–251
9. Mailhot A, Duchesne S, Caya D, Talbot G (2007) Assessment of future change in intensity–duration–frequency (IDF) curves for Southern Quebec using the Canadian Regional Climate Model (CRCM). J Hydrol 347(1–2):197–210
10. De Paola F, Giugni M, Topa ME, Bucchignani E (2014) Intensity-duration-frequency (IDF) rainfall curves, for data series and climate projection in African cities. Springerplus 3(1):1–18

Intercomparison of MoM, MLM and LMO Estimators of Probability Distributions for Assessment of Extreme Rainfall

N. Vivekanandan, C. Srishailam, and R. G. Patil

Abstract Assessment of extreme rainfall is needed to be carried out to prevent floods and droughts and applied to the studies on water resources projects. This can be done by extreme value analysis (EVA) that consists of fitting probability distributions to the annual 1-day maximum rainfall (AMR) series. This paper presents a study on EVA of rainfall for Pune and Vadgaon Maval sites using method of moments, maximum likelihood method and L-moments (LMO) estimators of log normal, extreme value type-1 (EV1), generalized extreme value (GEV) and generalized Pareto distributions. The evaluation of probability distributions adopted in EVA is made by goodness-of-fit (viz., Chi-square and Kolmogorov–Smirnov) tests, D-index and fitted curves of the estimated rainfall. On the basis of the results obtained from the study, it is found that EV1 (LMO) is better suited for rainfall estimation for Pune whereas GEV (LMO) for Vadgaon Maval.

Keywords Chi-square · D-index · Extreme value type-1 · Generalized extreme value · Kolmogorov–Smirnov · L-moments · Rainfall

1 Introduction

Rainfall is one of the most important parameters in hydrological studies, and its occurrence and distribution is erratic, temporal and spatial variations in nature. Determination of annual 1-day maximum rainfall for a given return period would enhance the management of water resources applications as well as the effective utilization

N. Vivekanandan (✉) · C. Srishailam · R. G. Patil
Central Water and Power Research Station, Pune, Maharashtra 411024, India
e-mail: vivek.n@cwprs.gov.in

P. V. Timbadiya et al. (eds.), *Climate Change Impact on Water Resources*, Lecture Notes in Civil Engineering 313, https://doi.org/10.1007/978-981-19-8524-9_34

of water resources. Probability and frequency analysis of rainfall data enables us to determine the expected rainfall at various chances. Such information can also be used to prevent floods and droughts and applied to planning and designing of water resources related to engineering such as reservoir design, flood control work and soil and water conservation planning. Depending on design-life of structure, extreme (i.e. 1-day maximum) rainfall with a given return period is used [15]. This can be carried out by extreme value analysis (EVA) that involves fitting probability distribution to the annual 1-day maximum rainfall (AMR) series.

Out of number of available probability distributions, the 2-parameter log normal (LN2), extreme value type-1 (EV1), generalized extreme value (GEV) and generalized Pareto (GP) distributions are widely applied in EVA [11–13] and hence used in this paper. The parameters of the distributions are determined by method of moments (MoM), maximum likelihood method (MLM) and L-moments (LMO) and also used for estimation of rainfall.

Esteves [6] applied EV1 for estimation of extreme rainfall for different rain-gauge stations in southeast UK. Rasel and Hossain [10] estimated the rainfall intensities at seven divisions in Bangladesh using EV1 and developed the intensity–duration–frequency curves. By using EV1 distribution, the maximum rainfall at Bamenda mountain region, Cameroon was estimated by Afungang and Bateira [1]. Study by Arvind et al. [2] indicated that EV1 is better suited for analysing the annual and monthly rainfall for Musiri region, Tiruchirappalli. Esberto [5] determined the best fit frequency distribution of rainfall patterns for event forecasting in order to address potential disasters. Baghel et al. [3] stated that LN2 and EV1 are the best fit distributions to estimate the rainfall for Udaipur district. Vivekanandan and Srishailam [15] compared the EVA results of rainfall of Anakapalli, Kasimkota, Parvada and Atchutapuram by adopting EV1, LN2 and log Pearson type-3 distributions. However, it is very difficult to evaluate the best fit distribution when number of distributions adopted in EVA. This can be done by using goodness-of-fit (GoF) (viz., Chi-square (χ^2) and Kolmogorov–Smirnov (*KS*)) tests, *D-index* and fitted curves of the estimated rainfall [14]. The procedures adopted in EVA of rainfall, evaluation of EVA results using GoF and diagnostic tests, and discussion on the results is briefly described with an illustrative example in the following sections.

2 Methodology

The cumulative distribution function (CDF) and quantile estimator of probability distributions adopted in EVA are presented in Table 1. The empirical equations used in determining the parameters of the distributions are presented in Table 2 [9]. The terms λ_1, λ_2 and λ_3 [7, 8] are defined as first, second and third LMOs that can be determined Eq. (1) and are given by

$$\lambda_1 = b_0,\ \lambda_2 = 2b_1 - b_0 \ \text{ and } \ \lambda_3 = 6b_2 - 6b_1 + b_0 \tag{1}$$

wherein λ_{r+1} is the $r+1$th LMO, which is defined by

$$\lambda_{r+1} = \sum_{k=0}^{r} \frac{(-1)^{r-k}(r+k)!}{(k!)^2(r-k)!} b_k \tag{2}$$

wherein b_k is an unbiased estimator and given by

$$b_k = N^{-1} \sum_{i=k+1}^{N} \frac{(i-1)(i-2)\ldots(i-k)}{(N-1)(N-2)\ldots(N-k)} x(i) \tag{3}$$

where $x(i)$ is the observed data of ith sample and N the total number of samples.

Table 1 CDF and quantile estimator of LN2, EV1, GEV and GP distributions

Distribution	CDF	Quantile estimator ($x(T)$)
LN2 ($\mu(y)$, $\sigma(y)$)	$F(y) = \varphi\left(\frac{y-\mu(y)}{\sigma(y)}\right)$ and $y = \ln(x)$	$x(T) = \exp(\mu(y) + K(T)\sigma(y))$
EV1 (ξ, α)	$F(x) = e^{-e^{-\left(\frac{x-\xi}{\alpha}\right)}}$, $\alpha > 0$	$x(T) = \xi + \alpha[-\ln(-\ln(1-(1/T)))]$
GEV (ξ, α, β)	$F(x) = e^{-\left(1-\frac{\beta(x-\xi)}{\alpha}\right)^{1/\beta}}$, $\alpha > 0$, $\beta > 0$	$x(T) = \xi + \frac{\alpha[1-(-\ln(1-(1/T)))^{\beta}]}{\beta}$
GP (ξ, α, β)	$F(x) = 1 - \left(1 - \frac{\beta(x-\xi)}{\alpha}\right)^{1/\beta}$, $\alpha > 0$, $\beta > 0$	$x(T) = \xi + \frac{\alpha(1-(1-(1/T)))^{\beta})}{\beta}$
Wherein		
ξ	Location parameter	
α	Scale parameter	
β	Shape parameter	
τ_3	L-skewness (λ_3/λ_2)	
T	Return period (in year)	
$F(x)$	*CDF* of a variable x	
$F(y)$	*CDF* of a variable $y = \ln(x)$	
$K(T)$	Frequency factor (K) of a return period (T) corresponding to coefficient of skewness (CS), say CS = 0.0 for LN2	
$x(T)$	Estimated rainfall (x) for a return period (T)	
$\phi(\ldots)$	*CDF* of standard normal distribution	
$\mu(x)$	Average (μ) of observed data (x)	
$\sigma(x)$	Standard deviation (σ) of observed data (x)	
$\mu(y)$	Average (μ) of logarithmic series ($y = \ln(x)$) of observed data	
$\sigma(y)$	Standard deviation (σ) of logarithmic series of observed data	

A relation between F and T is given by F (or $F(x)$) $= 1 - 1/T$

Table 2 Empirical equations used in determining the parameters of distributions

Distribution	Parameters of the distribution		
	MoM	MLM	LMO
LN2	$\mu(y) =$ $\frac{1}{N}\sum_{i=1}^{N} y(i) - \frac{1}{2N}\sum_{i=1}^{N} y(i)^2 + \frac{1}{2}\left(\frac{1}{N}\sum_{i=1}^{N} y(i)\right)^2$ $\sigma(y) = \left[\frac{1}{N}\sum_{i=1}^{N} y(i)^2 - 2\left(\frac{1}{N}\sum_{i=1}^{N} y(i)\right)\right]^{1/2}$ Where $y(i) = \ln(x(i))$	$\mu(y) = \frac{1}{N}\sum_{i=1}^{N} y(i)$ $\sigma(y) = \left(\frac{1}{N}\sum_{i=1}^{N} (y(i) - \mu(y))^2\right)^{1/2}$	$\alpha = \lambda_1 = b_0 = \frac{1}{N}\sum_{i=1}^{N} y(i)$ $\lambda_2 = 2b_1 - b_0 = \hat{\beta}/\sqrt{\pi}$ wherein $b_1 = \frac{1}{N(N-1)}\sum_{i=2}^{N} (i-1)y(i)$
EV1	$\xi = \mu(x) - (0.5772157)\alpha$ $\alpha = \left(\frac{\sqrt{6}}{\pi}\right)\sigma(x)$	$\xi = -\alpha \ln\left[\sum_{i=1}^{N} \exp\left(-x(i)/\alpha\right)\Big/ N\right]$ $\alpha = \mu(x) -$ $\left[\sum_{i=1}^{N} x(i)\exp\left(-x(i)/\alpha\right)\Big/ \sum_{i=1}^{N} \exp(-x(i)/\alpha)\right]$	$\xi = \lambda_1 - (0.5772157)\alpha$ $\alpha = \frac{\lambda_2}{\ln(2)}$
GEV	$\mu(x) = \xi + \frac{\alpha(1-\Gamma(1+\beta))}{\beta}$ $\sigma(x) = \frac{\alpha}{\beta}\left(\Gamma(1+2\beta) - \Gamma(1+\beta)^2\right)^{1/2}$CS = $(\text{sign}\,\beta)\frac{\Gamma(1+3\beta)+3\Gamma(1+\beta)(1+2\beta)-2\Gamma^3(1+\beta)}{\{\Gamma(1+\beta)-\Gamma^2(1+\beta)\}^{1/2}}$	Can be determined by using modified Newton-Raphson algorithm	$z = (2/(3+\tau_3)) - (\ln(2)/\ln(3))$ $\tau_3 = (2(1-3^{-\beta})/(1-2^{-\beta})) - 3\alpha =$ $(\lambda_2\beta)/(1-2^{-\beta})\Gamma(1+\beta)$ $\xi = \lambda_1 + (\alpha(\Gamma(1+\beta)-1)/\beta)$ $\beta = 7.817740z + 2.930462z^2$ $+ 13.641492z^3 + 17.206675z^4$

(continued)

Table 2 (continued)

Distribution	Parameters of the distribution		
	MoM	MLM	LMO
GP	$\mu(x) = \xi + (\alpha/(1+\beta))$ $\sigma(x) = \left[\alpha^2/(1+2\beta)(1+\beta)^2\right]^{1/2}$ $\mathrm{CS} = 2(1-\beta)(1+2\beta)^{1/2}/(1+3\beta)$	$\sum_{i=1}^{N} \frac{(x(i)-\xi)/\alpha}{1-(\beta(x(i)-\xi)/\alpha)} = \frac{N}{1-\beta}$ $\sum_{i=1}^{N} \ln[1-(\beta(x(i)-\xi)/\alpha)] = -N\beta$ $\xi \leq$ lowest value of $x(i)$	$\xi = \lambda_1 - (\alpha/(1+\beta))$ $\beta = (1-3\tau_3)/(\tau_3+1)$ $\alpha = (1+\beta)(2+\beta)\lambda_2$

2.1 Goodness-of-Fit Tests

In this paper, the probability distributions adopted in EVA are evaluated by using GoF tests (viz., χ^2 and *KS*). The mathematical expressions of GoF tests [16] are as follows:

χ^2 statistic is defined by

$$\chi^2 = \sum_{j=1}^{NC} \frac{\left(O_j(x) - E_j(x)\right)^2}{E_j(x)} \tag{4}$$

where $O_j(x)$ is the observed frequency value (x) for jth class, $E_j(x)$ the expected frequency value (x) for jth class and NC the number of frequency classes [4]. The acceptance region of χ^2 statistic at the desired significance level (η) is given by $\chi^2_C \leq \chi^2_{1-\eta,\,\mathrm{NC}-m-1}$. Here, m denotes the number of parameters of distribution and χ^2_C is the computed value of χ^2 statistic by the distribution.

KS statistic is defined by

$$KS = \underset{i=1}{\overset{N}{\mathrm{Max}}} |F_e(x(i)) - F_c(x(i))| \tag{5}$$

where $x(i)$ is the observed data (x) for ith sample, $F_e(x(i)) = r/(N+1)$ the empirical CDF of $x(i)$ of ith sample, 'r' the rank assigned to a sample values arranged in ascending order $(x(1) < x(2) < \ldots..x(N))$ and $F_c(x(i))$ the computed CDF of $x(i)$ of ith sample.

Test criteria: If the GoF tests statistic values computed by the distribution are not greater than its theoretical values at the desired level of significance, then the distribution is acceptable for EVA at that level.

2.2 Diagnostic Test

In addition to GoF tests, *D-index* test is applied for the selection of most suitable distribution [14] for rainfall estimation, which is given by

$$D\text{-}index = (1/\mu(x)) \sum_{i=1}^{6} \left| x(i) - x(i)^* \right| \tag{6}$$

Here, $x(i)$ $(i = 1$ to $6)$ and $x(i)^*$ are the six highest observed and the corresponding estimated values of ith sample. The distribution with least *D-index* is considered as better suited for rainfall estimation.

3 Application

This paper details a study on comparison of four probability distributions (viz., LN2, EV1, GEV and GP) applied in EVA of rainfall for Pune and Vadgaon Maval sites. The index map of the study area with locations of the rain-gauge stations is presented in Fig. 1. The AMR series of Pune and Vadgaon Maval was extracted from the daily rainfall data observed at the respective sites during the period 1901 to 2017 and also used for EVA. From the scrutiny of the daily rainfall data of Pune, it is observed that there is no missing data and hence, the entire data series is used in EVA. For Vadgaon Maval, it is found that the data for the intermittent period during the years 1966, 1967 and 1972 are found to be missing. However, by considering the importance on hydrological aspects of the study region, the data for the missing years are ignored and also not considered in EVA. Table 3 gives the descriptive statistics of AMR.

From Table 3, it is observed that the higher moments (*CS* and *CK*) of AMR series have different behaviours for Pune when compared to Vadgaon Maval. Also, from Table 3, it is found that the *CV* of the AMR series of Pune and Vadgaon Maval is noted to be about 35.2% and 41.9%, respectively.

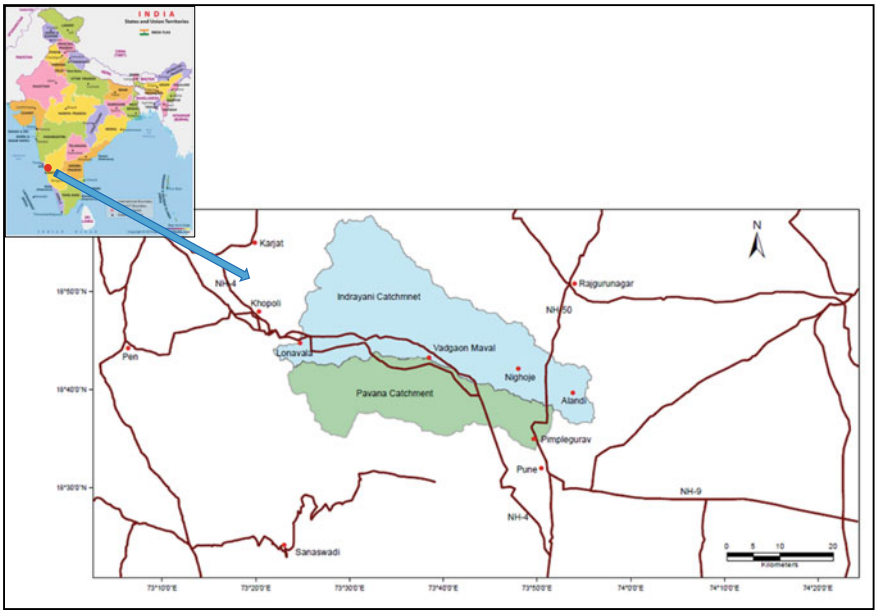

Fig. 1 Index map of the study area with locations of rain-gauge stations

Table 3 Descriptive statistics of AMR series

Site	Average (mm)	Standard deviation (mm)	Coefficient of skewness (CS)	Coefficient of Kurtosis (CK)	Minimum (mm)	Maximum (mm)
Pune	74.2 (4.249)	26.1 (0.343)	1.010 (−0.042)	1.694 (−0.014)	28.5 (3.350)	181.1 (5.199)
Vadgaon Maval	102.5 (4.556)	42.9 (0.377)	1.420 (0.472)	2.143 (−0.188)	47.2 (3.854)	253.0 (5.533)

Number given within brackets indicates a descriptive statistic of logarithmic value of AMR

4 Results and Discussions

By applying the EVA procedures, as described above, a computer code was developed and used for rainfall estimation. The EVA results of rainfall obtained from four probability distributions (viz., LN2, EV1, GEV and GP) for Pune and Vadgaon Maval sites are presented in the following sections.

4.1 Extreme Value Analysis of Rainfall

The estimators of the parameters of LN2, EV1, GEV and GP distributions were determined by MoM, MLM and LMO and are further used for rainfall estimation. Tables 4 and 5 present the 1-day maximum rainfall estimates for different return periods for Pune and Vadgaon Maval, respectively, whereas the EVA plots are shown in Fig. 2a, b.

The EVA results of rainfall showed that the estimated rainfall by EV1 (LMO) for Pune and GEV (LMO) for Vadgaon Maval are higher than those values of other distributions for return periods above 200-year. Also, the EVA results showed that no appreciable difference between the estimated rainfall using EV1 (MLM) and EV1 (LMO). From Fig. 2a, b, it is noticed that the fitted lines using LN2 and EV1 are linear, while GEV curves are exponentially upward and GP curves are exponentially downward.

4.2 Analysis of Results Based on GoF Tests

In the present study, the number of frequency classes (*NC*) is considered as thirteen and accordingly the degree of freedom (NC – m − 1) is considered as ten for GEV and GP whereas eleven for LN2 and EV1 while computing the χ^2 statistic values. By using the information, the GoF tests statistic values were computed for Pune and Vadgaon Maval and are given in Table 6. The theoretical values of χ^2 statistic at 5%

Table 4 1-day maximum rainfall given by LN2, EV1, GEV and GP for Pune

Distribution	Method	1-day maximum rainfall (mm) for a return period (in year)									
		2	5	10	20	25	50	100	200	500	1000
LN2	MoM	70.0	93.3	108.4	122.7	127.2	141.1	154.8	168.5	186.8	200.8
	MLM	70.0	93.4	108.6	123.0	127.5	141.5	155.3	169.2	187.7	201.8
	LMO	70.0	93.6	109.0	123.5	128.1	142.3	156.3	170.3	189.1	203.4
EV1	MoM	70.0	93.0	108.2	122.9	127.5	141.8	156.0	170.1	188.8	202.9
	MLM	70.0	93.2	108.6	123.4	128.1	142.5	156.9	171.2	190.0	204.2
	LMO	69.9	93.2	108.7	123.5	128.2	142.6	157.0	171.3	190.2	204.4
GEV	MoM	70.3	93.5	108.5	122.7	127.1	140.7	154.0	167.0	183.8	196.3
	MLM	70.1	93.2	108.3	122.6	127.2	141.0	154.6	168.1	185.7	198.8
	LMO	70.1	93.4	108.6	123.2	127.8	141.8	155.6	169.3	187.2	200.6
GP	MoM	67.8	95.4	112.3	126.3	130.3	141.3	150.4	158.0	166.1	171.0
	MLM	71.2	100.2	117.9	132.6	136.8	148.3	157.9	165.9	174.4	179.6
	LMO	69.4	97.2	112.0	122.8	125.7	132.9	138.3	142.2	145.9	147.8

Table 5 1-day maximum rainfall given by LN2, EV1, GEV and GP for Vadgaon Maval

Distribution	Method	1-day maximum rainfall (mm) for a return period (in year)									
		2	5	10	20	25	50	100	200	500	1000
LN2	MoM	94.6	132.6	158.3	183.1	191.1	215.8	240.8	266.2	300.5	327.3
	MLM	95.2	130.6	154.0	176.5	183.7	205.9	228.1	250.5	280.6	303.8
	LMO	95.2	130.8	154.5	177.3	184.5	207.0	229.4	252.1	282.7	306.3
EV1	MoM	95.5	133.4	158.5	182.6	190.2	213.8	237.2	260.4	291.1	314.4
	MLM	94.9	128.1	150.1	171.2	177.8	198.4	218.9	239.2	266.1	286.4
	LMO	95.7	132.6	157.1	180.5	188.0	210.9	233.6	256.3	286.2	308.8
GEV	MoM	94.6	131.8	157.4	182.8	191.0	216.8	243.2	270.3	307.3	336.3
	MLM	93.0	126.9	151.2	176.0	184.2	210.5	238.2	267.5	309.0	342.5
	LMO	92.0	128.3	156.0	185.8	196.0	229.7	266.9	308.2	370.0	422.9
GP	MoM	90.4	133.3	162.6	189.4	197.6	221.5	243.4	263.5	287.4	303.8
	MLM	101.7	149.9	182.9	213.1	222.2	249.1	273.8	296.4	323.4	341.8
	LMO	90.6	133.6	162.7	189.0	196.9	220.0	240.9	259.9	282.2	297.3

significance level with reference to the degree of freedom are observed as 18.307 for GEV and GP whereas 19.675 for LN2 and EV1. Likewise, the theoretical values of *KS* statistic at 5% level of significance with reference to the number of samples considered in EVA are observed as 0.126 for Pune and 0.127 for Vadgaon Maval.

Based on GoF tests results, the observations drawn from the study were summarized and are given as below.

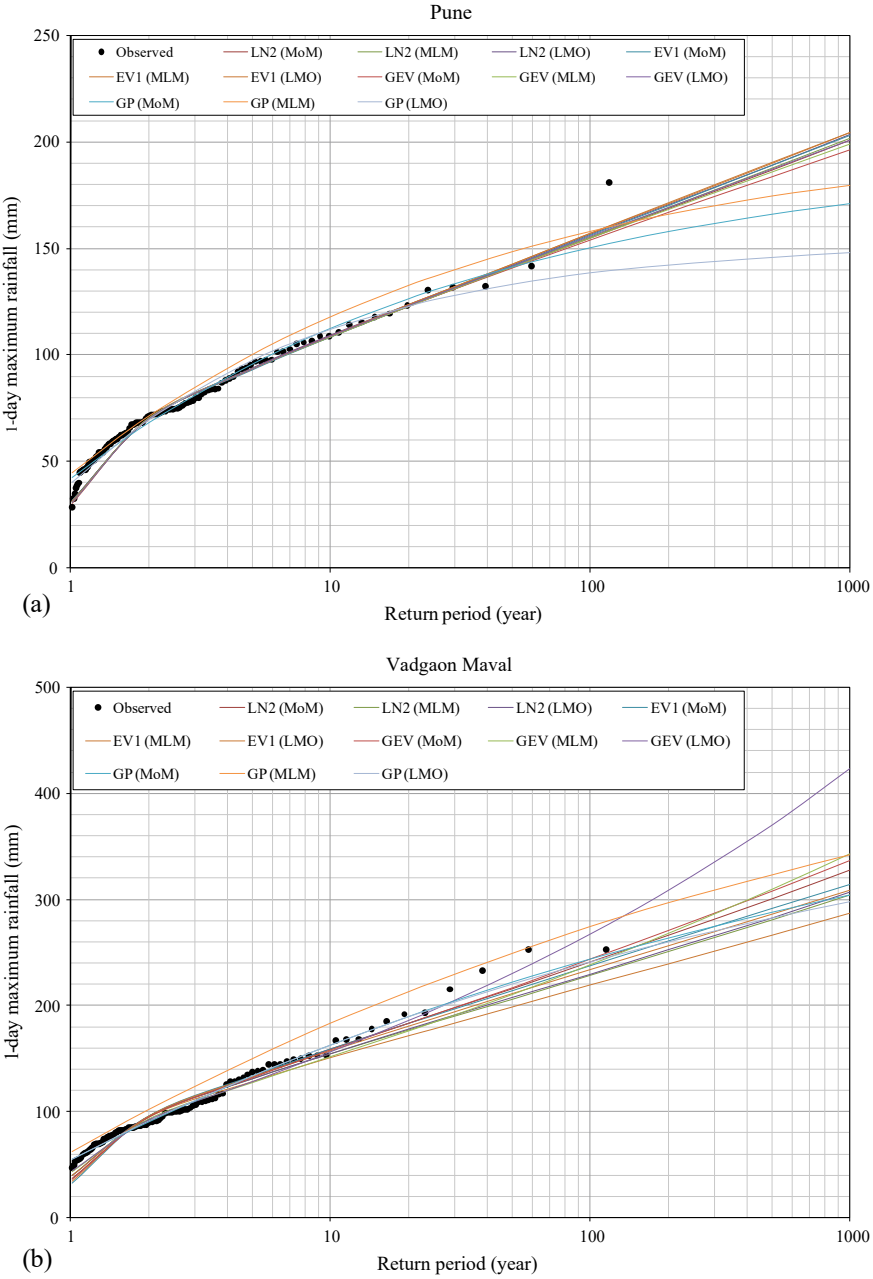

Fig. 2 Observed and estimated 1-day maximum rainfall for different return periods for Pune and Vadgaon Maval

Table 6 Computed values of GoF and diagnostic tests statistic by LN2, EV1, GEV and GP

Distribution	Method	Computed values of GoF and diagnostic tests					
		Pune			Vadgaon Maval		
		χ^2	KS	D-index	χ^2	KS	D-index
LN2	MoM	7.555	0.038	0.490	19.421	0.070	0.980
	MLM	7.555	0.038	0.481	19.421	0.070	1.509
	LMO	7.558	0.039	0.465	19.427	0.071	1.448
EV1	MoM	6.222	0.039	0.481	20.789	0.079	1.079
	MLM	7.010	0.039	0.465	19.235	0.080	1.911
	LMO	7.778	0.040	0.464	17.368	0.082	1.235
GEV	MoM	8.444	0.036	0.497	18.965	0.071	0.941
	MLM	8.013	0.036	0.494	12.807	0.057	1.309
	LMO	7.556	0.037	0.477	6.649	0.043	0.745
GP	MoM	10.222	0.381	0.554	16.000	0.152	0.696
	MLM	9.778	0.311	0.872	15.545	0.147	0.884
	LMO	9.333	0.240	0.824	15.089	0.141	0.755

- χ^2 test results supported the LN2, EV1, GEV and GP distributions for rainfall estimation for Pune.
- χ^2 test results did not support the EV1 (MoM) and GEV (MoM) for estimation of rainfall for Vadgaon Maval.
- *KS* test results did not support the use of GP for EVA of rainfall for Pune and Vadgaon Maval.

4.3 Analysis of Results Based on Diagnostic Test

In addition to GoF tests, a diagnostic test using *D-index* is applied for identifying the best suitable distribution for rainfall estimation. Table 6 presents the *D-index* values of LN2, EV1, GEV and GP for Pune and Vadgaon Maval. From Table 6, it is noted that EV1 (LMO) for Pune and GP (MoM) for Vadgaon Maval are having minimum *D-index* when compared with those values of other distributions adopted in EVA.

4.4 Selection of Probability Distribution

The best fit for estimation of rainfall was re-assessed by using the fitted lines of the estimated rainfall together with *D-index* values.

- *D-index* values showed that EV1 (LMO) for Pune and GP (MoM) for Vadgaon Maval could be used for rainfall estimation.

- As described earlier, the MoM estimators provide less accurate results when compared with those values of MLM and LMO. Moreover, *KS* test results did not support the applicability of GP (MoM) for estimation of rainfall for Vadgaon Maval. By considering these facts, for Vadgaon Maval, the *D-index* value obtained from GP is not considered in selection of best fit distribution.
- In the light of the above, it is identified that *D-index* of GEV (LMO) is the second minimum next to GP (MoM) for Vadgaon Maval.
- However, on the basis of qualitative assessment on EVA plots of rainfall together with *D-index* values, it is identified that EV1 (LMO) is better suited for rainfall estimation for Pune while GEV (LMO) for Vadgaon Maval. The plots of observed and estimated 1-day maximum rainfall with 95% confidence limits by the selected distribution for Pune and Vadgaon Maval sites are presented in Fig. 3a, b.
- From Fig. 3a, it is noted that the AMR varies between 70.0 and 150.0 mm observed at Pune during the period 1901 to 2017 is falling within confidence limits of the rainfall given by EV1 (LMO).
- From Fig. 3b, it can be seen that the AMR varies from 85.0 to 260.0 mm observed at Vadgaon Maval during the period 1901 to 2017 (except for the years 1966, 1967 and 1972 that are found to be missing) is falling within confidence limits of the rainfall given by GEV (LMO).

5 Conclusions

The paper presented a study on comparison of EVA results of rainfall given by MoM, MLM and LMO estimators of LN2, EV1, GEV and GP distributions for Pune and Vadgaon. The selection of best fit distribution for estimation of rainfall was made through GoF tests, *D-index* and fitted curves of the estimated rainfall. Based on EVA results, the following conclusions were drawn from the study:

- χ^2 test results supported the LN2, EV1, GEV and GP distributions adopted in EVA of rainfall for Pune.
- χ^2 test results did not accept the use of EV1 (MoM) and GEV (MoM) for EVA of rainfall for Vadgaon Maval.
- The *KS test* results did not support the use of GP for EVA of rainfall for Pune and Vadgaon Maval.
- The qualitative assessment of EVA results with *D-index* indicated the EV1 (LMO) is better suited for rainfall estimation for Pune while GEV (LMO) for Vadgaon Maval.

The study suggested that the estimated rainfall for return period beyond 500-year may be cautiously used due to uncertainty in the higher order return periods while designing the hydraulic structures in the respective sites.

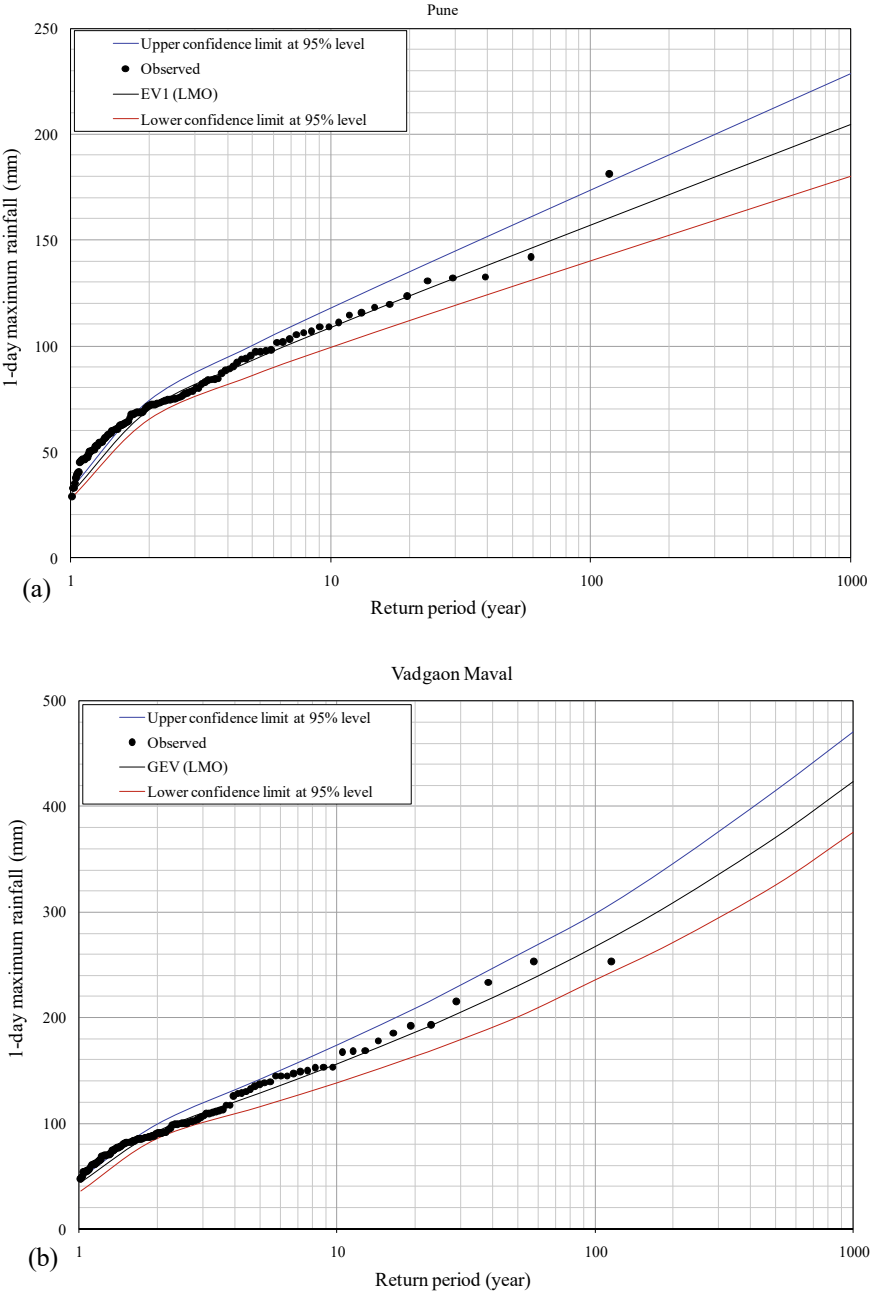

Fig. 3 Plots of the estimated 1-day maximum rainfall with confidence limits and observed AMR for Pune and Vadgaon Maval

Acknowledgements The authors are grateful to Dr. K.S. Kangara, Director and Shri A.K. Agarwal, Scientist-E (Retired), Central Water and Power Research Station, Pune for encouragement and guidance during conduct of the studies and also for giving permission to publish this paper.

References

1. Afungang R, Bateira C (2016) Statistical modelling of extreme rainfall, return periods and associated hazards in the Bamenda Mountain, NW Cameroon. Geogr Spat Plan J 1(9):5–19. https://doi.org/10.17127/got/2016.9.001
2. Arvind G, Kumar PA, GirishKarthi S, Suribabu CR (2017) Statistical analysis of 30 years rainfall data: a case study. Proc IOP Conf Ser Earth Environ Sci. https://doi.org/10.1088/1755-1315/80/1/012067
3. Baghel H, Mittal HK, Singh PK, Yadav KK, Jain S (2019) Frequency analysis of rainfall data using probability distribution models. Int J Curr Microbiol Appl Sci 8(6):1390–1396. https://doi.org/10.20546/ijcmas.2019.806.168
4. Charles Annis PE (2009) Goodness-of-fit tests for statistical distributions
5. Esberto MDP (2018) Probability distribution fitting of rainfall patterns in Philippine regions for effective risk management. Environ Ecol Res 6(3):178–186. https://doi.org/10.13189/eer.2018.060305
6. Esteves LS (2013) Consequences to flood management of using different probability distributions to estimate extreme rainfall. J Environ Manage 115(1):98–105. https://doi.org/10.1016/j.jenvman.2012.11.013
7. Hosking JRM, Wallis JR (1993) Some statistics useful in regional frequency analysis. Water Resour Res 29(2):271–281. https://doi.org/10.1029/92WR01980
8. Hosking JRM (1990) L-moments: analysis and estimation of distributions using linear combinations of order statistics. R Stat Soc (Ser B) 52(1):105–124. https://www.jstor.org/stable/2345653
9. Rao AR, Hamed KH (2000) Flood frequency analysis. CRC Publications, New York, USA
10. Rasel M, Hossain SM (2015) Development of rainfall intensity duration frequency equations and curves for seven divisions in Bangladesh. Int J Sci Eng Res 6(5):96–101
11. Sasireka K, Suribabu CR and Neelakantan TR (2019) Extreme rainfall return periods using Gumbel and Gamma distributions. Int J Recent Technol Eng 8(4):27–29. https://doi.org/10.35940/ijrte.D1007.1284S219
12. Sharma NK, Sharma S (2019) Frequency analysis of rainfall data of Dharamshala region. Int J Sci Res 8(2):886–892. https://www.ijsr.net/get_abstract.php?paper_id=ART20195211
13. Tank G, Dongre P, Obi Reddy GP, Sen P (2021) Rainfall trend analysis—a review. Int Res J Eng Technol 8(4):4028–4030
14. Vivekanandan N (2020) A comparative study on Gumbel and LP3 probability distributions for estimation of extreme rainfall. Int J Water Resour Eng 6(1):21–33
15. Vivekanandan N, Srishailam C (2020) Selection of best fit probability distribution for extreme value analysis of rainfall. CBIP Water Energy Int 63(10):13–19
16. Zhang J (2002) Powerful goodness-of-fit tests based on the likelihood ratio. J R Stat Soc 64(2):281–294. https://doi.org/10.1111/1467-9868.00337

Development of a Fog Index to Study Relationships Between Fog and Climate Variables

Rakshit Paurwal, Shivam Tripathi, and Arnab Bhattacharya

Abstract Most of the existing studies on the long-term correlation between fog and climate variables have considered fog visibility and fog duration data for analysis. The use of fog duration in terms of number of fog days has suffered from the lack of a universally accepted definition of a fog day. Additionally, fog duration fails to quantify fog intensity. While fog visibility data can be used to quantify fog intensity for short-term analysis, their non-additive nature and high variability over a short period of time render them unsuitable for long-term analysis. In this study, a fog index based on the extinction of light intensity governed by Beer's Law is developed. The index is defined as the ratio of the energy attenuated by a fog event with a given visibility to the energy attenuated by the same fog event with the visibility assumed to be zero. The additive nature of the index allows quantification of the fog intensity over any time window. The index was found to be bounded and independent of the choice of unit systems. Furthermore, the index can be employed for studying the relationship between long-term fog conditions and climate variables such as soil moisture, sea-level and surface pressure, near surface and sea-surface temperature. The developed index is applied to understand fog phenomenon in north India and explore its linkages with local meteorological parameters at seasonal scale.

R. Paurwal (✉) · S. Tripathi
Department of Civil Engineering, Indian Institute of Technology Kanpur, Kanpur, UP 208016, India
e-mail: rakshup@iitk.ac.in

S. Tripathi
e-mail: shiva@iitk.ac.in

A. Bhattacharya
Department of Computer Science and Engineering, Indian Institute of Technology Kanpur, Kanpur, UP 208016, India
e-mail: arnabb@cse.iitk.ac.in

P. V. Timbadiya et al. (eds.), *Climate Change Impact on Water Resources*, Lecture Notes in Civil Engineering 313, https://doi.org/10.1007/978-981-19-8524-9_35

Keywords Fog index · Beer's Law · Climate variables

1 Introduction

Fog is characterised by the suspension of extremely small droplets of water and occasionally ice which results in the reduction of horizontal visibility to less than 1000 m [1]. Since fog plays a disruptive role in aviation and transport sectors [2], it has become a topic of scientific interest. Fog is affected by a number of variables such as local air temperature, humidity and atmospheric stability [3]; hence, it is imperative to understand the impact that such variables might have on fog occurrence.

Visibility serves as an indicator of fog [4] and has been used in several studies to study fog occurrence. However, the non-additive nature and high variability of visibility make it unfit as an indicator of fog intensity for long-term analysis. Fog duration in terms of the number of fog days has also suffered from the lack of a standardised definition of a fog day. Hu et al. [5] considered a day to be a fog day if fog was observed at any of the four times (02:00, 08:00, 14:00, 20:00 local time), whereas Kutty et al. [2] considered the same if fog was observed at any point of time and for any duration during the day. The objectives of the present study are to (1) develop a fog index that could provide a quantitative estimate of fog and (2) analyse the relationship between local meteorological parameters and fog.

2 Study Area and Data

2.1 Study Area

Lucknow city located in the state of Uttar Pradesh, India has been considered in the study. The collected data pertains to the data recorded at Chaudhary Charan Singh International Airport weather station (Lat: 26.7606 N; Lon: 80.8893 E).

2.2 Data

Half-hourly METAR reports corresponding to a period of 27 years (1995–2021) were obtained from the India Automated Surface Observing Systems (ASOSs) Network dataset hosted on Iowa Environmental Mesonet (IEM) server. The variables for which the records were obtained are 2 m air temperature, 2 m dew-point temperature, relative humidity and visibility. The data from 2 January 2011 to 22 August 2011 (233 days) were missing from the records. Rainfall values for the same period were obtained

from IMD, which maintains rainfall records over the Indian landmass at a spatial resolution of 0.25° × 0.25° and a temporal resolution of 1 day [6].

3 Methodology

3.1 Development of Fog Index

The fog index is based on Beer's Law for atmosphere. Beer's Law for atmosphere is defined as

$$T(x) = \frac{P(x)}{P(0)} = e^{-\sigma x} \tag{1}$$

where $T(x)$ is the transmittance at a distance 'x' from the light source, $P(x)$ is the power at a distance 'x', $P(0)$ is the power of the light source and σ is the extinction coefficient. The relationship between extinction coefficient and visual range (visibility) is based on Koschmieder's Law [7] which is given as

$$\text{Visibility} = \frac{-\ln\ \varepsilon}{\sigma} \tag{2}$$

where ε represents the pilot contrast threshold fixed at 0.05 [7]. An integral component of the fog index is the fog event which is defined as the duration during which the visibility remains below 1 km. The fog index of an event is defined as the ratio of the energy attenuated by the fog event with a given visibility to the energy attenuated by the same fog event with the visibility assumed to be zero. Mathematically, it can be represented as

$$\text{Fog Index} = \frac{\sum_{i=1}^{n}\{P(0)\}\left\{1 - e^{-\sigma_i x_i}\right\}\{t_i\}}{\sum_{i=1}^{n}\{P(0)\}\{1 - e^{-\sigma_{1i} x_i}\}\{t_i\}} = \frac{\sum_{i=1}^{n}\{1 - e^{-\sigma_i x_i}\}\{t_i\}}{\sum_{i=1}^{n}\{1 - e^{-\sigma_{1i} x_i}\}\{t_i\}} \tag{3}$$

where i is the ith sub-duration in a fog event, n is the number of sub-durations in the fog event, $P(0)$ is the power of the light source, σ_i is the average extinction coefficient existing during the ith sub-duration of the fog event obtained by using the average visibility during the same period, σ_{1i} is the average extinction coefficient existing during the ith sub-duration of the fog event obtained by assuming zero visibility during the same period and x_i is the distance over which the energy extinction occurs (extinction length). For calculation purposes, the value of σ_{1i} was obtained by assuming visibility to be very close to zero in Eq. (2). An attempt was made to constrain the value of extinction length (x_i) so as to eliminate user subjectivity in selecting the value of extinction length for the calculation of the index. Thus, a new parameter known as apparent extinction length was formulated to be used in place of extinction length. Apparent extinction length was defined as the length in a 1 km

long horizontal column over which apparent attenuation of light energy takes place. The column length was taken as 1 km to conform to the standard definition of fog in terms of visibility given by WMO. Mathematically, it can be represented as

$$\text{Apparent extinction length (km)} = 1\ \text{km} - \text{Visibility (km)} \tag{4a}$$

or

$$\text{Apparent extinction length (m)} = 1000\ \text{m} - \text{Visibility (m)} \tag{4b}$$

depending on the choice of unit system. For example, if for a given fog event or a sub-duration of a fog event, the average visibility is observed to be 0.350 km, the apparent extinction length for the fog event would be 1 km − 0.350 km = 0.650 km. For time windows with visibility > 1 km, no energy was assumed to be attenuated; thus, they were not considered for fog index. The calculation of fog index for a fog event is illustrated below. Table 1 shows hypothetical half-hourly visibility observations recorded at a station. It can be seen that a fog event begins at 07:30 local time (LT) on 1 Jan 2019 when the visibility is first recorded to be below 1 km and ends at 08:30 LT on 1 Jan 2019 when the visibility is last recorded to be below 1 km. Thus, the fog event occurs for 1 h between 07:30 LT and 08:30 LT, since it is during this period that the visibility remains below 1 km. Table 2 shows calculations of average visibility, average extinction coefficient and apparent extinction length for each sub-duration of the fog event. The fog index for the fog event has been calculated using Eq. (3).

Using Eq. (3), fog index was obtained as 0.68.

Table 1 Visibility observations

Date and (local) time of observation	Visibility (in km)
01/01/2019 07:00	1.2
01/01/2019 07:30	0.8
01/01/2019 08:00	0.6
01/01/2019 08:30	0.9
01/01/2019 09:00	1.1

Table 2 Components of fog index

Sub-duration	Avg. visibility (km)	Avg. extinction coefficient (km^{-1})	Apparent extinction length (km)
07:30–08:00	0.7	4.28	0.3
08:00–08:30	0.75	4	0.25

3.2 Analysis of the Relationship Between Climate Variables and Fog

For each year, the winter season consists of November and December months of the same year and January and February months of the succeeding year. Thus, the winter season of 2018 would include November and December of 2018 and January and February of 2019. The monsoon season for the year is defined as June, July, August, September (JJAS) months of the year. The fog index was calculated for each year using the visibility data pertaining to the winter months of the year. Thus, a single value of the fog index was obtained for the winter season (NDJF) of each year. Average daily air temperature, average daily maximum and minimum air temperature, average dew-point temperature, average daily maximum and minimum dew-point temperature, average daily relative humidity and average daily maximum and minimum relative humidity were obtained for the monsoon months (JJAS) and winter months (NDJF). The seasonal rainfall during a season was obtained by calculating the cumulative rainfall during the season. Since the visibility and meteorological data for 233 days in 2011 (2 January 2011 to 22 Aug 2011) were missing, the analysis could not be performed for 2010 and 2011. There were no missing values for any other years. Correlation between fog index and the climate variables was calculated using the Pearson correlation coefficient. A separate analysis was conducted using the number of fog days in the winter season. The definition for fog day was derived from the study conducted by Kutty et al. [2], which mentions that a day is considered to be a fog day if fog is observed at any point of time and for any duration during the day. Visibility threshold of 1 km as per WMO was used to indicate fog.

4 Results

Figure 1 shows the fog index values for the winter months (NDJF) from 1995 to 2020. A substantial number of years (14) exhibit a high fog index (> 0.75), indicating that the winter months in Lucknow exhibit intense fog, which is in agreement with the fact that the North Indian states experience thick and widespread fog during winter months [8]. Furthermore, the index values follow an overall decreasing trend with occasional peaks indicating that the fog intensity in Lucknow has been decreasing on an annual basis. Figure 2 shows the number of fog days during the winter months (NDJF) in Lucknow. A decreasing trend with lower values was observed up to 2007, however, relatively higher number of fog days were observed from 2008 onwards. An increasing trend for the same was observed from 2017 onwards.

Table 3 shows the Pearson correlation coefficient values of fog index for NDJF (winter) season and the climate variables for two different seasons, JJAS (A) and NDJF (B). It is observed that variables such as average daily maximum air temperature, average daily minimum air temperature, average daily dew point temperature, average daily minimum dew point temperature, average daily maximum relative

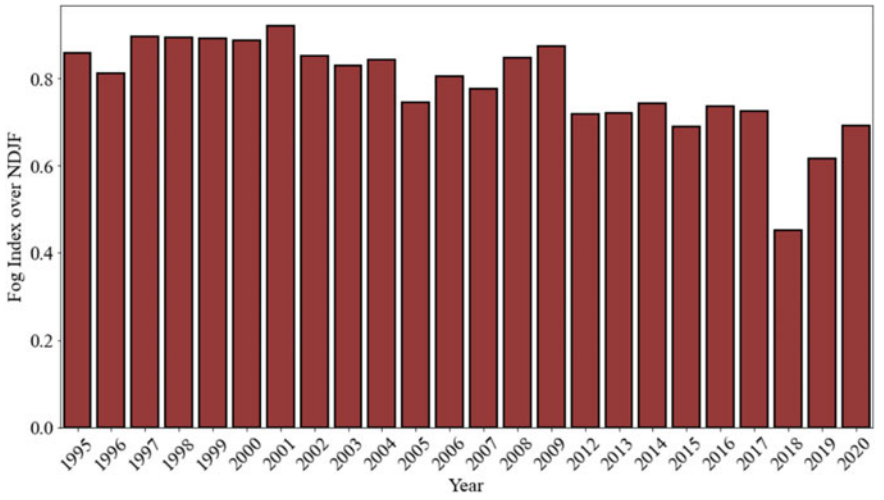

Fig. 1 Fog index values for winter season (NDJF) at Lucknow

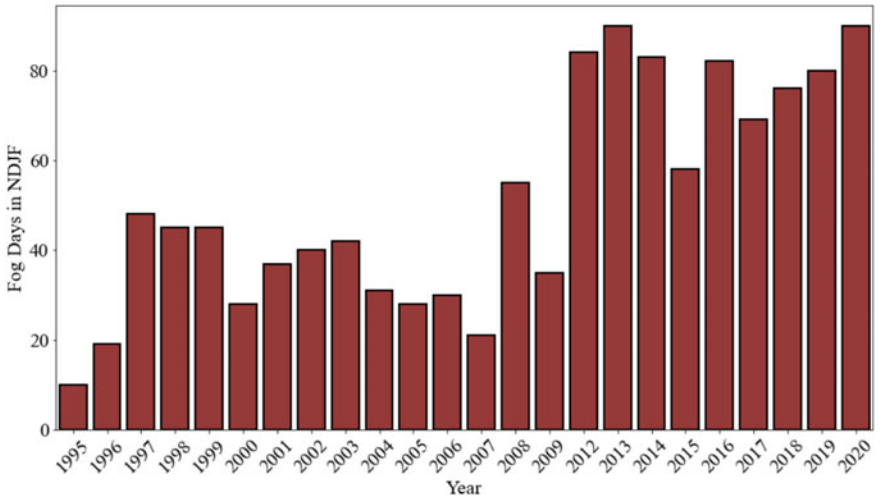

Fig. 2 Plot of fog days for winter season (NDJF) at Lucknow

humidity and rainfall show positive and negative correlation with fog index depending on the season over which they are considered.

Since the magnitudes of correlation values were less than 0.1 for most of the variables for NDJF, only the variables corresponding to JJAS were used for further analysis. Scatter plots with regression lines were plotted for fog index values over NDJF against average daily minimum air temperature, average daily maximum dew point temperature, average daily minimum relative humidity and rainfall over JJAS.

Table 3 Correlation of fog index for NDJF with variables for (A) JJAS and (B) NDJF

Variable	A	B
Average daily air temperature (in °C)	−0.39	−0.01
Average daily maximum air temperature (in °C)	−0.34	0.05
Average daily minimum air temperature (in °C)	−0.48*	0.17
Average daily dew point temperature (in °C)	−0.18	0.03
Average daily maximum dew point temperature (in °C)	−0.32	−0.07
Average daily minimum dew point temperature (in °C)	−0.10	0.08
Average daily relative humidity (in %)	0.19	0.06
Average daily maximum relative humidity (in %)	0.12	−0.13
Average daily minimum relative humidity (in %)	0.25	0.14
Rainfall (in mm)	−0.15	0.05

* Denotes statistically significant correlation at 5% significance level

Figures 3, 4, 5 and 6 show the scatter plots of fog index against the variables average daily minimum air temperature, average daily maximum dew point temperature, average daily minimum relative humidity and rainfall, respectively. Out of the four variables, fog index shows the maximum magnitude of correlation with average daily minimum air temperature. The variation of fog index with rainfall shows no clear trend and is clustered.

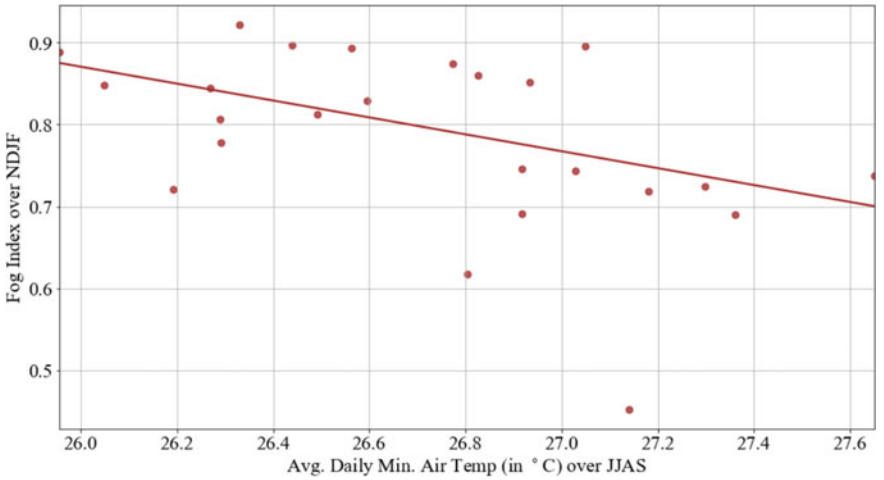

Fig. 3 Fog index versus avg. daily min. air temp. (correlation $= -0.48$)

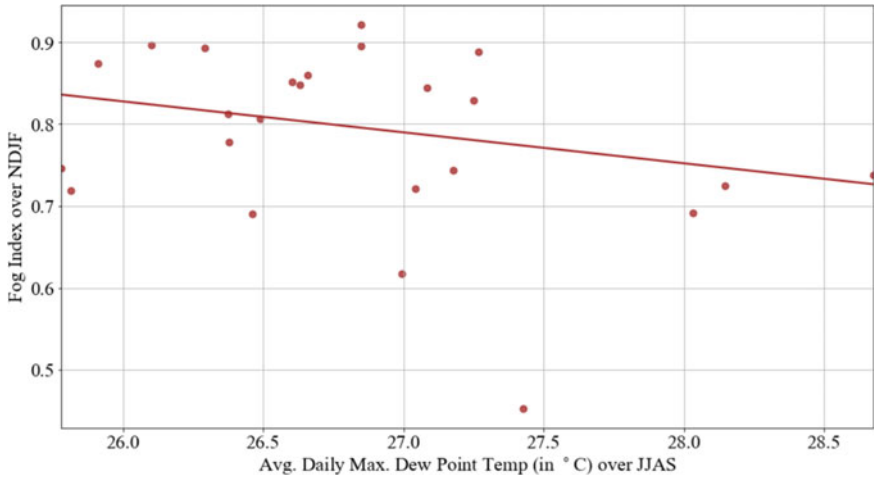

Fig. 4 Fog index versus avg. daily max. dew point temp. (correlation $= -0.32$)

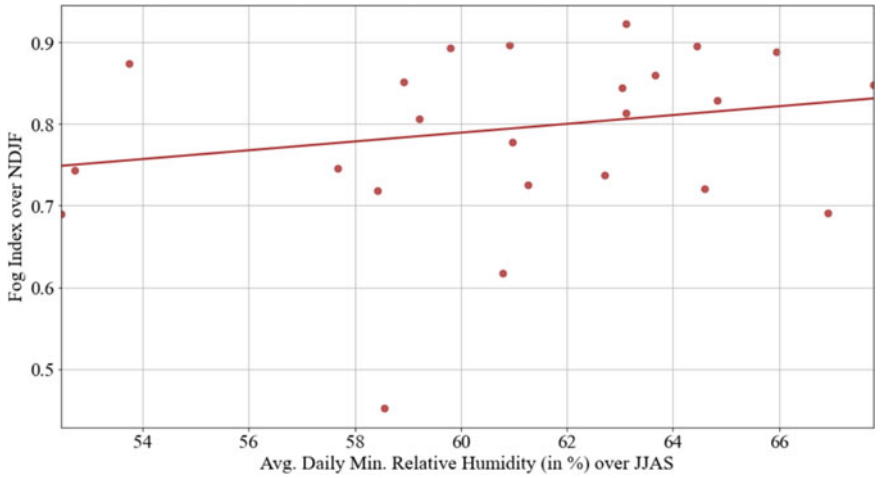

Fig. 5 Fog index versus avg. daily min. rel. humidity (correlation = 0.25)

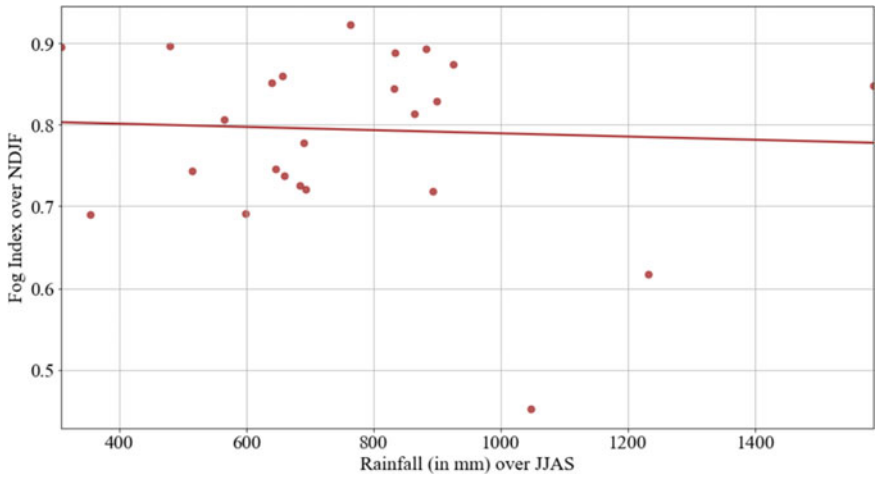

Fig. 6 Fog index versus rainfall (correlation = −0.15)

5 Conclusions

The additive nature of the fog index allowed for the quantification of fog intensity over a seasonal scale. Analysis of the fog index values showed that although most of the years prior to 2012 exhibited a high fog index value of at least 0.75, in the recent years (2012 onwards), the fog index has been decreasing for Lucknow. Furthermore, correlation analysis indicated that the climate variables during JJAS were correlated to a higher degree (in terms of magnitude) with the fog index than the climate variables during NDJF. Amongst the variables pertaining to JJAS, the average daily minimum air temperature had the highest negative correlation (−0.48) and the average daily minimum relative humidity had the highest positive correlation (0.25) with fog index. The fog index quantifies fog intensity and does not consider fog duration; thus, additional work is required to make the fog index inclusive of fog duration. Further study is required to explore the linkages of fog index with large-scale climate variables such as soil moisture, sea-level pressure and sea-surface temperature.

Acknowledgements The authors would like to express sincere thanks to Fog Prediction Group—IIT Kanpur (https://fog.iitk.ac.in/). The financial support provided by the Ministry of Education under the Scheme for Transformational and Advanced Research in Sciences (MoE/STARS-1/261) is also duly acknowledged.

References

1. World Meteorological Organization (1992) International meteorological vocabulary, 2nd edn. WMO, Geneva
2. Kutty SG, Agnihotri G, Dimri AP, Gultepe I (2019) Fog occurrence and associated meteorological factors over Kempegowda International Airport, India. Pure Appl Geophys 176(5):2179–2190
3. Sachweh M, Koepke P (1995) Radiation fog and urban climate. Geophys Res Lett 22:1073–1076
4. Sawaisarje G, Khare P, Shirke S, Deepakumar S, Narkhede NM (2014) Study of winter fog over Indian subcontinent: climatological perspectives. Mausam 65(1):19–28
5. Hu S, Zhang W, Turner AG et al (2020) How does El Niño-southern oscillation affect winter fog frequency over eastern China? Clim Dyn 54(1–2):1043–1056
6. Pai DS, Latha Sridhar, Rajeevan M, Sreejith OP, Satbhai NS, Mukhopadhyay B (2014) Development of a new high spatial resolution (0.25° × 0.25°) Long period (1901–2010) daily gridded rainfall data set over India and its comparison with existing data sets over the region. MAUSAM 65(1):1–18
7. Tai H, Zhuang Z, Jiang L, Sun D (2017) Visibility measurement in an atmospheric environment simulation chamber. Curr Opt Photonics 1(3):186–195
8. Ghude SD, Bhat GS, Prabhakaran T, Jenamani RK, Chate DM, Safai PD et al (2017) Winter fog experiment over the Indo-Gangetic plains of India. Curr Sci 112(4):767–784

Regionalization of Multiplicative Random Cascade Model Parameter for Awash River Basin, Ethiopia

Ashenafi Dabesa and Shivam Tripathi

Abstract Data on fine-resolution precipitation are necessary for the design of hydraulic structures, the estimation of rainfall erosivity, and the assessment of urban hydrological climate change. In Ethiopia, precipitation data are typically available on a daily or monthly basis. The number of weather stations equipped with automatic gauges for measuring precipitation rates is small. Therefore, a scientific approach is required to disaggregate existing coarser resolution rainfall data to finer resolution. It is also necessary to regionalize the developed disaggregation models to simulate sub-hourly rainfall data across a wide region. The multiplicative cascade models appear to be interesting instruments for simulating fine-resolution rainfall because of its connection to the multifractal theory. Thus, the study aims to regionalize random cascade model (RCM) parameters and analyze their potential and limitations. The newly developed regional models are tested on rainfall data of Awash River Basin in Ethiopia. The models demonstrated acceptable accuracy in simulating the sub-hourly rainfall, demonstrating the potential of parameter regionalization.

Keywords Parameter regionalization · Rainfall disaggregation · Random cascade model · Statistical moment scaling

A. Dabesa (✉) · S. Tripathi
Department of Civil Engineering, Indian Institute of Technology Kanpur, Kanpur 208016, India
e-mail: ashenafi@iitk.ac.in

S. Tripathi
e-mail: shiva@iitk.ac.in

P. V. Timbadiya et al. (eds.), *Climate Change Impact on Water Resources*, Lecture Notes in Civil Engineering 313, https://doi.org/10.1007/978-981-19-8524-9_36

1 Introduction

A high resolution of precipitation time series data is essential for the design of hydraulic structures, the estimation of rainfall erosivity, and the assessment of urban hydrological climate change. To efficiently design hydrological structures such as dams, bridges, and culverts, water resources engineers need to use high temporal resolution data to assess the frequency and magnitude of extreme hydrological events. Rainfall data at a high level of resolution can be obtained from satellite products or from automatic gauges, which can measure precipitation rate at a high temporal resolution. While satellite products provide high-resolution rainfall data, they are not easy to obtain anywhere and anytime for a low price [1]. A modest number of automated gauges for measuring high-resolution precipitation rates are available at meteorological stations. A scientific technique is thus required to obtain fine-resolution data by employing already-existing coarse-resolution information.

Disaggregating rainfall data from coarser temporal scales into smaller temporal scales may be done in a number of different ways, and the literature provides a variety of these approaches. The uniform model [2] and point process stochastic models such as Neyman-Scott or Bartlett-Lewis [3] can be mentioned. Both have their own drawbacks. Uniform model has limitation to represent rainfall variability [2], whereas Neyman-Scott or Bartlett-Lewis [3] has limitations in reproducing extreme value distributions and preserving correlation structures of rainfall sequences [4, 5].

The multiplicative cascade models introduced first by Yaglom [6], is one of the most promising of the various modeling approaches. Based on their ability to preserve mass in disaggregation, these models are divided into two types. A canonical model which preserves mass on the average, and a microcanonical model preserves mass exactly in disaggregation. Until the desired time resolution is achieved, the model iteratively fragments the rainfall volume in a coarser time scale into smaller discrete time intervals of rainfall volumes. The model was tested both for spatial and temporal rainfall disaggregation [7, 8].

The process of estimating the parameters for the RMC models requires fine-resolution rainfall data. In order to evaluate the scale-invariance theory and develop a disaggregation model, we also need rainfall data with a high resolution. The parameters of canonical models, for instance, are determined by fitting the Mandelbrot-Kahane-Peyriere (MKP) function to the sample moment scaling relationship, which requires high-resolution rainfall data. For the microcanonical model (e.g., beta model), which is based on the distribution of the breakdown coefficients, fine-resolution data on rainfall are required. The model parameter can be obtained from the coarse-resolution data, which can then be extrapolated to a fine-resolution scale assuming scale invariance. But in the study, the scale showed a break as we moved from a very coarse scale to a very fine scale [9]. This makes applying the RMC model in areas lacking fine-resolution data very difficult. Our study proposes regionalization of model parameters based on climate similarities so that the model can be used in areas lacking fine-resolution rainfall data. In areas with similar climates, rainfall distributions are also expected to be similar [10], indicating that the scale characteristics of rainfall at stations in similar climate regions are likely to be similar. Therefore, this study aims to evaluate the performance of both RMC models, the canonical and

microcanonical models, when the parameters calibrated at other station in similar regions are used to disaggregate rainfall at a different stations in similar region.

2 Methodology

2.1 Study Area (Awash River Basin)

The study area covers an area of 110,000 km [11], which is located between latitudes 8°30′ N and 12°00′ N, and longitudes 38°05′ E and 43°25′ E (Fig. 1). Climate conditions over most of the study area are characterized by arid and semi-arid conditions, with average annual precipitation ranging from 160 to 1600 mm and average annual temperature ranging from 20.8 to 29 °C. The elevation of the basin may be seen in Fig. 1, which shows that it ranges from 259 to 4055 m. It is anticipated that the basin has a total flow capacity of 4.9 billion cubic meters [12]. The multiplicative discrete random cascade (MDRC) model parameter was validated and calibrated using the 13 class 1 stations that are located inside the basin. Each of these stations has a record resolution of 15 min.

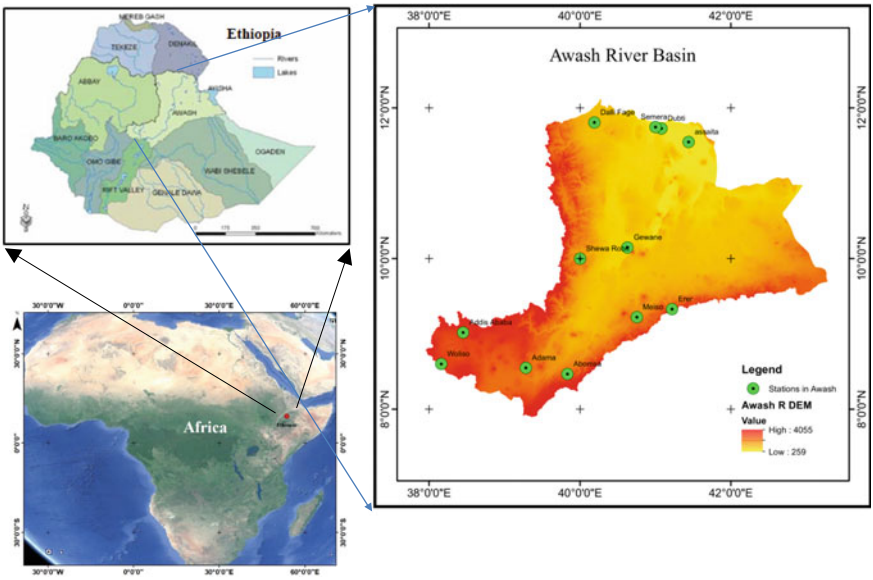

Fig. 1 Awash River Basin's location and digital elevation model

2.2 Multiplicative Random Cascade Model

The multifractal theory, which states that the structure of an entity may be deduced from its component pieces, serves as the foundation for the multiple random cascade disaggregation approaches. According to the scale-invariance hypothesis [13], two things are considered to be self-similar if it is possible to break them up into smaller versions of themselves. The cascade model falls within the umbrella of the stochastic model's group [14].

2.2.1 The Canonical Model

Through an iterative segmentation technique, the intensity of the rainfall at a coarse time scale is broken down into two or more sub-intervals. These sub-intervals are determined by the branching number b. A method of partitioning that may be used to fragment data is specified by a set of weights that is referred to as a cascade generator [15]. When the level n of the cascade is taken into consideration, together with the fact that the number of accessible sub-intervals is b^n, the equivalent dimensionless temporal duration scale for the cascade may be defined as $\lambda_n = b^{-n}$.

According to the Molnar and Burlando's [16], the corresponding mass $\mu_n(\Delta_i)$ for an integer in the range of 1 to n in the subdivided interval Δ_i in the cascade level n is given by

$$\mu_n(\Delta_i) = m_0 \times \lambda_n \times \prod_{j-1}^{n} W_j(i) \tag{1}$$

where

m_0: is the initial volume of the rainfall at coarser time scale.

2.3 Moment Scaling

The estimate of sample moments is required in order to calculate W given a set of rainfall data. The following is a description of the moments of the order q:

$$M_n(q) = \sum_{i=1}^{b^n} \mu_n^q\left(\Delta_n^i\right) \tag{2}$$

where q is the moment order ($q \geq 0$). It is reasonable to anticipate that the sample moments will eventually converge to the ensemble moments as the value of n continues to rise. The MKP function is used to show how the scaling behavior follows a log–log-linear function [13, 17].

Table 1 Canonical models and associated MKP function

Canonical models	$\chi(q)$ MKP function
Log-Poisson beta model $W = B \times Z$ $P(B = 0) = 1 - b^{-\beta}$ & $P\left(B = b^{\beta}\right) = b^{-\beta}$ $Z = A\beta^{N}$ $P(N = M) = \frac{c^m e^{-c}}{m!}$	$\chi(q) = (\beta - 1) \times (1 - q) + \frac{c \times (q \times (1-\beta)+) - (\beta^q - 1)}{\ln b}$
Log-Normal beta model $W = B \times Y$ $P(B = 0) = 1 - b^{-\beta}$ & $P\left(B = b^{\beta}\right) = b^{-\beta}$ $Y = b^{\gamma + \sigma X}$ where X is normal $N(0, 1)$	$\chi(q) = (\beta - 1) \times (q - 1) + \frac{\sigma^2 \times \ln b \times (q^2 - q)}{2}$

$$\chi_b(q) = 1 - q + \log_b E(W^q) \tag{3}$$

The scaling of the sample moments is obtained by calculating (q), and afterward, the parameters of the cascade model can be derived by assuming a distribution for the cascade generator W. The canonical models that were utilized in this research are presented in Table 1, and they are the log-Normal beta model and the log-Poisson beta model. The methods that are employed to estimate the probability distribution functions that represent W and the models' approaches to the conservation of mass are different in each of these models [7].

2.3.1 Microcanonical Model

The results of the MDRC model (microcanonical) validate the hypothesis that the mass of the disaggregated product does not change during the process of disaggregation. It is possible to fit an independent probability distribution function to the weights of each successive level of the cascade [16]. The weights are summed up to one at the end of each stage of the disaggregation process to ensure that the mass is preserved throughout the whole procedure. The assumption is made that the weights are independent variables that all follow the same distribution. In order to ensure that the aforementioned criteria is met at level n throughout each and every subdivision into b sub-intervals, the following equation must be established.

$$\sum_{k=1}^{b} W_n(b(i-1)+k) = 1 \text{ for } i = 1, 2, \ldots, b^{n-1} \tag{4}$$

The term "breakdown coefficients" can also be used to refer to these weights. The weights in the model are permitted to vary between 0 and 1, so that it may accurately represent the intermittent nature of rainfall. Calculations are performed to determine the corresponding rainfall quantities R_1 and R_2 at the lower level of disaggregation, along with their respective weights W_1 and W_2. These calculations are based on each level of disaggregation and each nonzero rainfall volume R.

$$W_i = \frac{R_\lambda}{R_{\lambda-1}} \tag{5}$$

The levels of the cascade are represented by the symbol λ. P_{01} and α are the names of two parameters that may be found in the microcanonical model. These parameters are associated with the intermittency and variability of the generator W, respectively. The chance that the disaggregated mass will fall within one of the sub-intervals is denoted by the variable P_{01}, which has the following definition:

$$P_{01} = p(W_1 = 0) + p(W_1 = 1) \tag{6}$$

Another possibility comes when the total amount of rainfall is broken up into its constituent sub-intervals. Within the confines of this situation, it is expected that the cascade generator would behave in accordance with a certain probability distribution function. In order to accurately portray the symmetric disaggregation of the weights, we made use of an asymmetric beta distribution function that consisted of a single parameter denoted by α [16].

$$f(w) = \frac{1}{B(\alpha)} w^{\alpha-1}(1-w)^{\alpha-1} \tag{7}$$

2.4 Regionalization

In this study, the Awash River Basin was regionalized based on a study by Beyene et al. [10]. Climate proximity was used to group the stations in the basin. As a result, groups of sites that approximately satisfy the homogeneity condition were formed. Three variables that influence rainfall variability are selected for performing regionalization—elevation of the stations, geographical location, and mean monthly maximum rainfall depth derived from sub-hourly data. K-means clustering algorithm is used for finding homogenous regions in terms of three selected variables. For more details, readers are referred to Beyene et al. [10].

Table 2 Chosen stations in each region

Parameters	Log-Poisson beta					
	Region 1		Region 2		Region 3	
	Addis Ababa	Woliso	Meiso	Dallifage	Elidar	Dubuty
c	0.67	0.67	0.82	0.82	0.5	0.5
Beta (β)	0.6	0.6	0.67	0.67	0.68	0.68
Parameters	Log-Normal beta					
	Region 1		Region 2		Region 3	
	Addis Ababa	Woliso	Meiso	Dallifage	Elidar	Dubuty
c	0.2	0.2	0.14	0.14	0.12	0.12
Beta (β)	0.6	0.6	0.68	0.68	0.66	0.66

3 Result and Discussion

3.1 Canonical Model

Using the procedure mentioned in Ashenafi and Tripathi [18], the parameters of the model were estimated. Several canonical models have been compared in the previous work of Ashenafi and Tripathi [18], with the log-Normal beta and log-Poisson beta models showing promising results for the Awash River Basin. Consequently, these models are selected for regionalization. In each region, two stations are selected based on their equivalency and the availability of data. A parameter calibrated at one station is used at another station in the region to disaggregate the daily rainfall data. We then evaluate the model's performance in the other station based on its ability to preserve the mean, standard deviation, and intermittency of the observed rainfall data. Table 2 shows the calibrated parameters and the selected stations.

3.1.1 Rainfall Depth, Distributions, and Intermittency

When generating rainfall data at 45-min intervals based on daily rainfall measurements, the models must first be examined to see whether or not they are able to maintain the total rainfall depth throughout all time scales. This is solely a test for the canonical models since the microcanonical models, by virtue of their formulation, perfectly retain the total rainfall depth in disaggregation. The results of the simulated mean, standard deviation, and intermittency for the log-Normal beta and log-Poisson beta model are presented in Figs. 2 and 3, respectively. These results are presented for each validation station in each region. The mean, intermittency, and standard deviations were determined from 100 realizations and compared with the observed 45-min mean and standard deviation and intermittency.

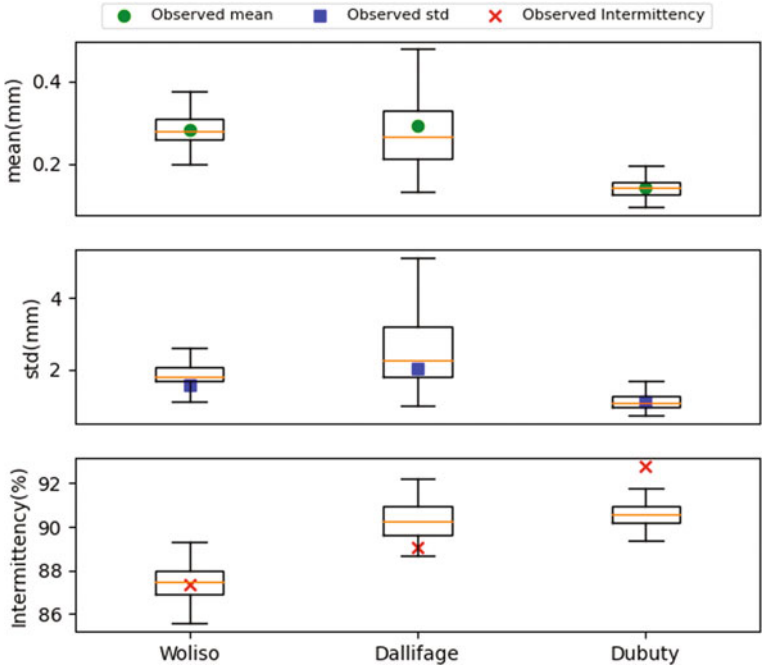

Fig. 2 Simulated 45-min precipitation mean, standard deviation, and intermittency for log-Normal beta model 100 simulation

The regionalized log-Poisson beta and log-Normal beta models were able to accurately replicate the depth (mean) variability and intermittency of the observed 45-minute rainfall at all stations, with the exception of Dubuty. However, both models underestimated the intermittency at the Dubuty station in Region 3. The cause of this underestimation may be linked to rainfall mechanisms in the area, but additional investigation is necessary. The next study will explore this issue further and build upon this research's findings.

3.1.2 Microcanonical Model

Similar procedure is followed here for the evaluation of model regionalization for the microcanonical model. To see the performance evaluation of the test station in the region, the parameters (P_{01} and α) obtained from the station mentioned in Table 2 were applied. The result of standard deviation and intermittency of the 45-min simulated and observed data at station in each region is presented in Table 3.

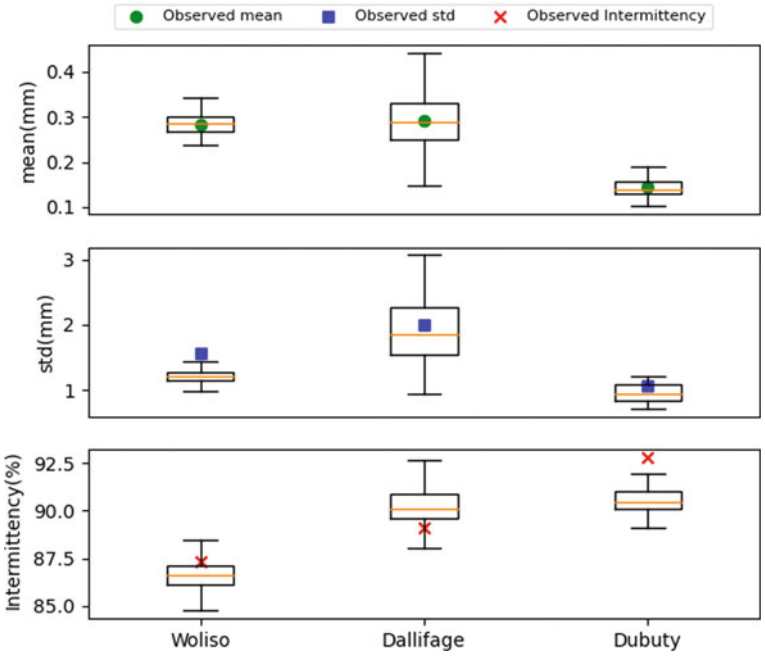

Fig. 3 Simulated 45-min precipitation mean, standard deviation, and intermittency for log-Poisson beta model 100 simulation

Table 3 Result of microcanonical model in the selected station in the region

Performance parameter	Region 1		Region 2		Region 3	
	Woliso (using parameters of Addis Ababa)		Dallifage (using parameters of Meiso)		Duppty (using parameters of Elidar)	
	Observed	Simulated	Observed	Simulated	Observed	Simulated
Standard deviation (STD) (mm)	0.98	0.98	0.93	0.97	0.33	0.34
Intermittency (%)	95	94	97.7	97.4	98.75	98.27

4 Summary and Conclusion

A regionalization analysis for the parameters of the random cascade models is presented. The regional models are applied to disaggregate daily rainfall to 45-min rainfall at gauging stations in Awash River Basin, Ethiopia. The basin is divided into three homogeneous regions. The performance of regionalization is tested by transferring the parameters of disaggregation models learned at one station to another (test) station in the same region. The beta distribution for the microcanonical model and the log-Normal beta and the log-Poisson beta distributions for the canonical

model are studied. Both the microcanonical and canonical models using parameters acquired from a station in the same region represented both the variation in the sub-hourly rainfall and the dry percentage of the observed 45-min rainfall, as shown by the results.

References

1. Pluntke T, Jatho N, Kurbjuhn C et al (2010) Use of past precipitation data for regionalisation of hourly rainfall in the low mountain ranges of Saxony, Germany. Nat Hazards Earth Syst Sci 10:353–370
2. Ormsbee LE (1989) Rainfall disaggregation model for continuous hydrologic modeling. J Hydraul Eng 115:507–525. https://doi.org/10.1061/(ASCE)0733-9429(1989)115:4(507)
3. Rodriguez-Iturbe I, Cox DR, Isham V (1987) Some models for rainfall based on stochastic point processes. Proc R Soc Lond A. Math Phys Sci, pp 269–288
4. Northrop PJ, Stone TM (2005) A point process model for rainfall with truncated Gaussian rain cells. Department of Statistical Science, University College London, London, pp 1–15
5. Alem AM, Tilahun SA, Moges MA et al (1985) A regional hourly maximum rainfall extraction method for part of Upper Blue Nile Basin, Ethiopia. In: Extreme hydrology and climate variability. Elsevier, pp 93–102
6. Yaglom AM (1966) The influence of fluctuations in energy dissipation on the shape of turbulence characteristics in the inertial interval. Sov Phys Dokl 11
7. McIntyre N, Shi M, Onof C (2016) Incorporating parameter dependencies into temporal downscaling of extreme rainfall using a random cascade approach. J Hydrol 542:896–912. https://doi.org/10.1016/j.jhydrol.2016.09.057
8. Over TM (1995) Modeling space-time rainfall at the mesoscale using random cascades. University of Colorado at Boulder
9. Gaume E, Mouhous N, Andrieu H (2007) Rainfall stochastic disaggregation models: calibration and validation of a multiplicative cascade model. Adv Water Resour 30:1301–1319
10. Beyene TD, Moges MA, Tilahun SA (2018) Development of Rainfall disaggregation model in the Awash River Basin, Ethiopia. In: International conference on advances of science and technology, pp 50–64
11. Taddese G, Sonder K, Peden D (2009) The water of the Awash River basin: a future challenge to Ethiopia. ILRI, Addis Ababa
12. Berhanu B, Seleshi Y, Melesse AM (2014) Surface water and groundwater resources of Ethiopia: potentials and challenges of water resources development. In: Nile River Basin. Springer, pp 97–117
13. Mandelbrot BB (1974) Intermittent turbulence in self-similar cascades: divergence of high moments and dimension of the carrier. J Fluid Mech 62:331–358
14. McIntyre N, Bárdossy A (2017) Using probable maximum precipitation to bound the disaggregation of rainfall. Water 9:496
15. Olsson J (1998) Evaluation of a scaling cascade model for temporal rain-fall disaggregation. Hydrol earth Syst Sci 2:19–30
16. Molnar P, Burlando P (2005) Preservation of rainfall properties in stochastic disaggregation by a simple random cascade model. Atmos Res 77:137–151
17. Kahane J-P, Peyriere J (1976) Sur certaines martingales de Benoit Mandelbrot. Adv Math (N Y) 22:131–145
18. Ashenafi D, Tripathi S (2022) Evaluation of rainfall disaggregation models for the Awash River Basin, Ethiopia, pp 247–265. https://doi.org/10.1007/978-981-19-0304-5_19